

Cell Press Selections

Reprint Compendium

Tumor Immune Microenvironment

The Roles and Regulation of Immune Cells in Cancer



CellPress
www.cell.com

CSTIMBETHYL2019



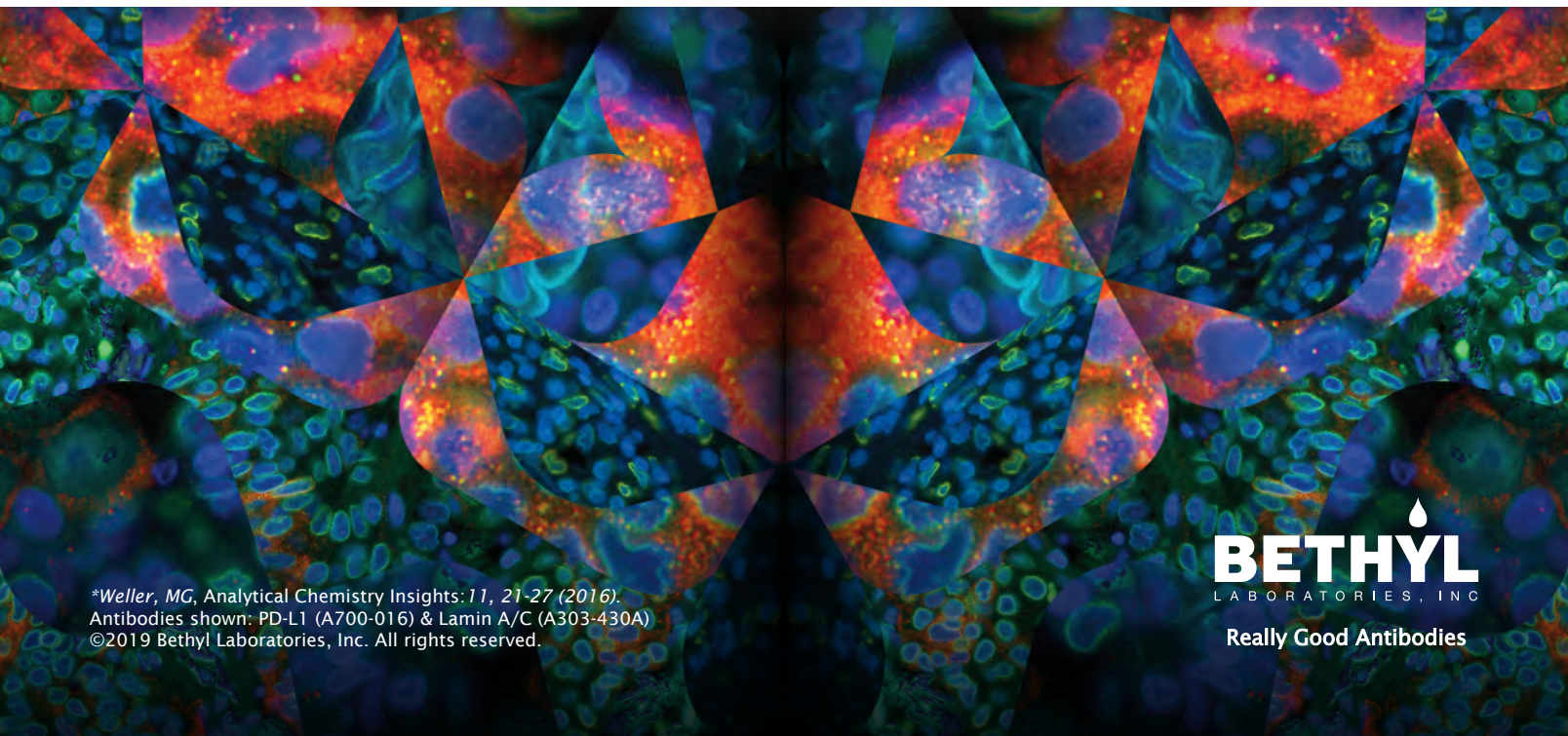


Brilliant visualization

See the difference to make big breakthroughs
in your tumor microenvironment research

In the world of next generation immuno-oncology research, having confidence in your immunoassay results is vital. Unfortunately, 75% of antibodies in today's market are non-specific or simply do not work at all.* That's why at Bethyl, we manufacture and validate every antibody on-site to ensure target specificity and sensitivity. More than 10,000 independent citations over the past 15 years have proven that our antibodies will function as designed in your assay — and we offer a 100% guarantee. Work with Bethyl to bring your discovery into full focus.

See our data at bethyl.com/immuno-oncology



*Weller, MG, Analytical Chemistry Insights: 11, 21-27 (2016).
Antibodies shown: PD-L1 (A700-016) & Lamin A/C (A303-430A)
©2019 Bethyl Laboratories, Inc. All rights reserved.

**BETHYL**
LABORATORIES, INC

Really Good Antibodies

Foreword

The tumor microenvironment is complex, and immune cells are critical components that play a central role in modulating cancer progression. Because immune cells are highly diverse and plastic, they possess multifaceted functions in cancer, ranging from tumor-suppressive to pro-tumor activities. The tumor immune microenvironment also varies substantially between and within cancer types. Comprehensively elucidating the immune landscape of cancer and the underlying regulatory mechanisms may improve the utility of current immunotherapies and facilitate the discovery of more effective cancer therapies. The reviews and research in this *Cell Press Selection* offer a snapshot of the latest advances in this rapidly evolving field.

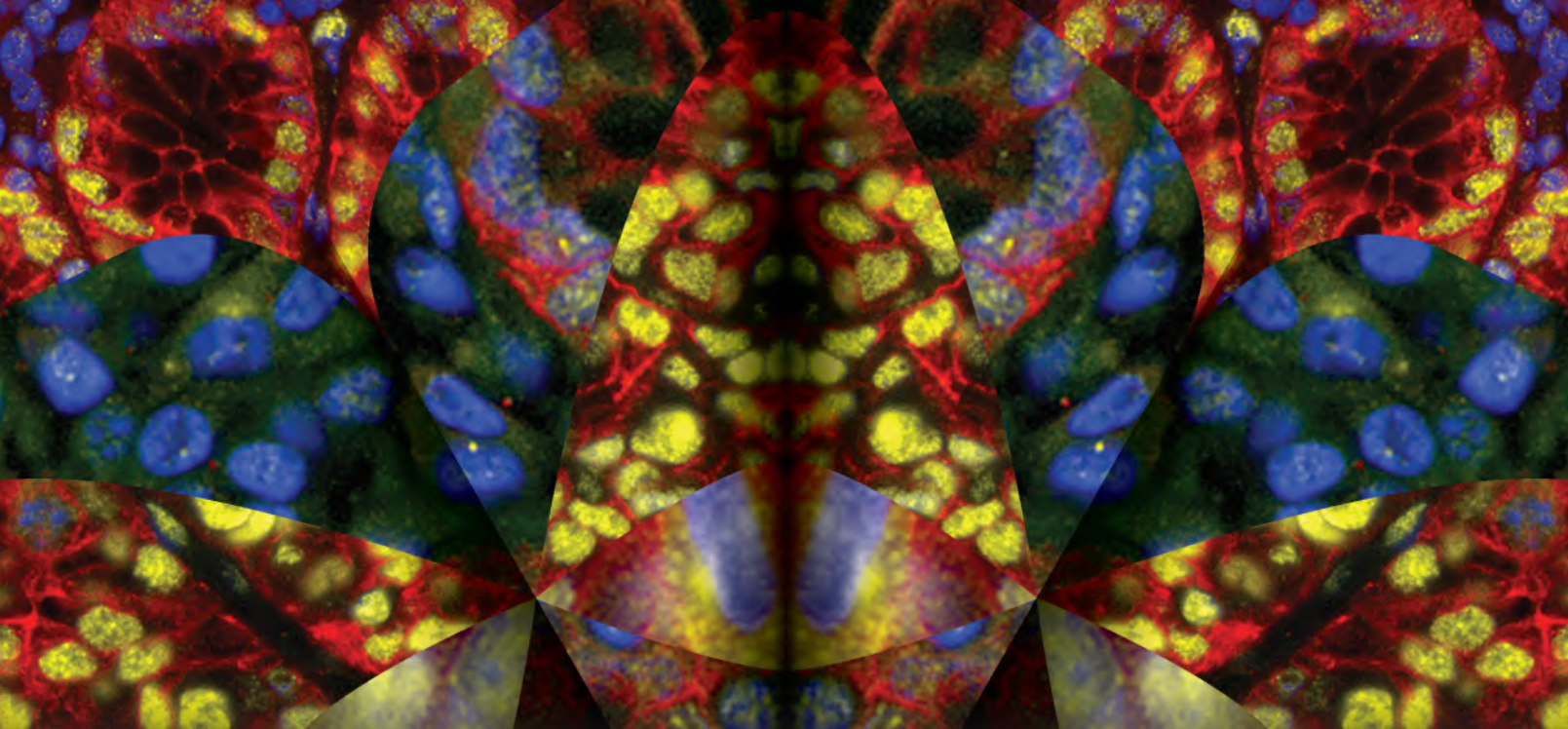
As research into the tumor immune microenvironment progresses, the key cellular players and biological pathways involved in shaping the immune landscape are being revealed. Cancer genomic and transcriptomic datasets and single-cell analyses provide a comprehensive view of the immune composition of primary and metastatic cancer. Mechanistic studies are uncovering cancer-cell-intrinsic and -extrinsic processes that regulate immune cell infiltration and function. The articles compiled in this reprint collection showcase the current progress in these areas—from analyses of tumor immune landscapes to define immune subtypes and investigate the impact of the immune microenvironment on metastatic evolution, to studies that mechanistically dissect the crosstalk between cancer and immune cells. The biological insights coming out of these studies provide opportunities for therapeutic and biomarker development.

These articles represent only a small portion of the exciting research Cell Press has published on the tumor immune microenvironment. We hope you'll visit www.cell.com on a regular basis to keep up with the latest cancer biology and tumor immunology research.

Finally, we are grateful for the support of Bethyl Labs, who helped to make the publication of this collection possible.

Harmony Turk
Scientific Editor, *Cancer Cell*

For more information about Cell Press Selections:
Gordon Sheffield
Program Director, Cell Press Selections
g.sheffield@cell.com
617-386-2189

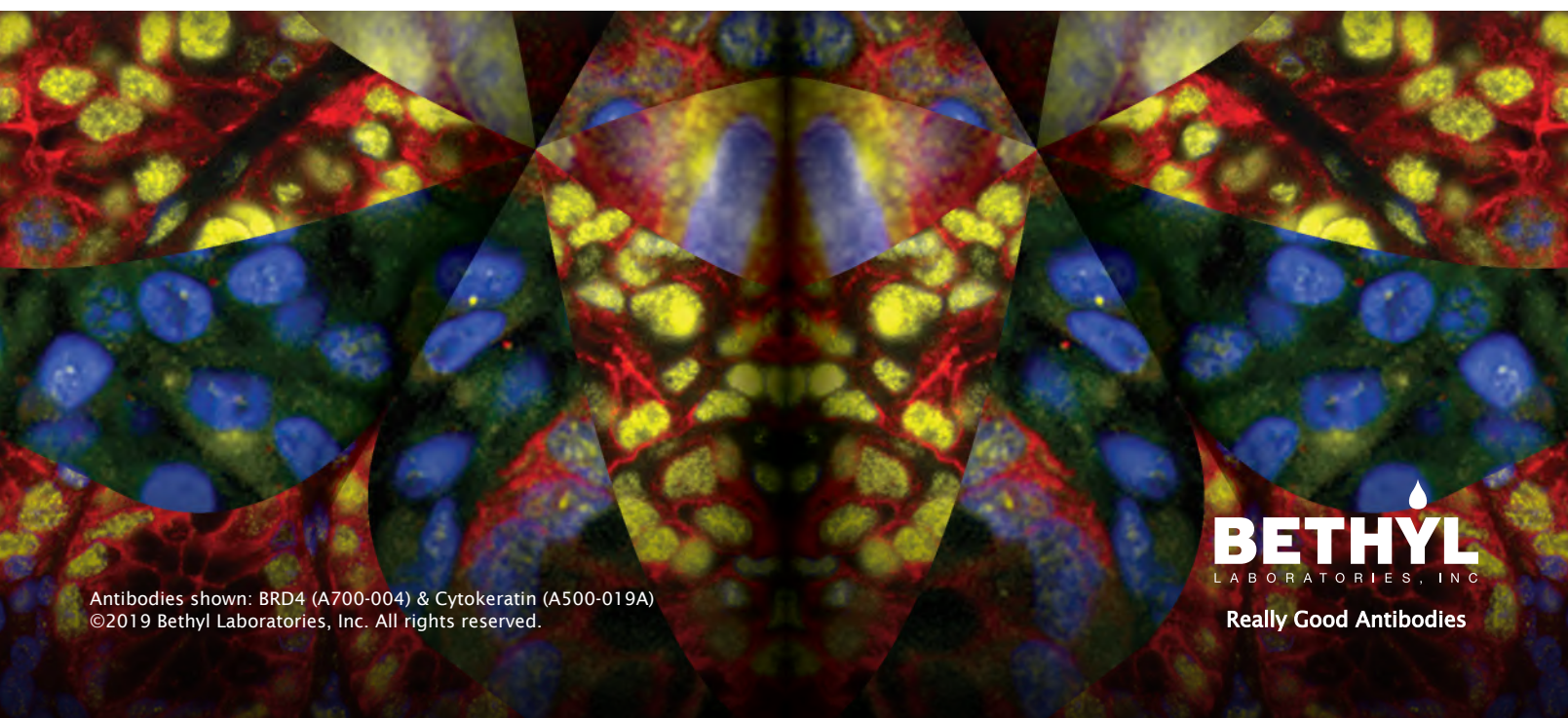


Dazzling synergy

Partner for success with custom recombinant rabbit
monoclonal antibody contracts

Bethyl is not your typical custom contract partner. We believe the best results start with dedicated teams that take each project from start to finish. We believe in on-site manufacturing and validation. We believe that binding to a desired target is not enough, it must also be highly-specific. And most importantly, we believe in your vision. That means highly customizable workflows combined with a CRO/CMO approach to each project that makes your goals our goals. Work with Bethyl to bring your discovery into full focus.

Learn more at bethyl.com/contract



Antibodies shown: BRD4 (A700-004) & Cytokeratin (A500-019A)
©2019 Bethyl Laboratories, Inc. All rights reserved.


BETHYL
LABORATORIES, INC
Really Good Antibodies

Tumor Immune Microenvironment

The Roles and Regulation of Immune Cells in Cancer

Reviews and Perspectives

T Cell Dysfunction in Cancer

Daniela S. Thommen and Ton N. Schumacher

Immunomodulation of Tumor Vessels: It Takes Two to Tango

Anna Johansson-Percival, Bo He, and Ruth Ganss

The Role of Type 1 Conventional Dendritic Cells in Cancer Immunity

Jan P. Böttcher and Caetano Reis e Sousa

Articles and Resources

Complement C5a Fosters Squamous Carcinogenesis and Limits T Cell Response to Chemotherapy

Terry R. Medler, Dhaarini Murugan, Wesley Horton, Sushil Kumar, Tiziana Cotechini, Alexandra M. Forsyth, Patrick Leyshock, Justin J. Leitenberger, Molly Kulesz-Martin, Adam A. Margolin, Zena Werb, and Lisa M. Coussens

Evolution of Metastases in Space and Time under Immune Selection

Mihaela Angelova, Bernhard Mlecnik, Angela Vasaturo, Gabriela Bindea, Tessa Fredriksen, Lucie Lafontaine, Bénédicte Buttard, Erwan Morgand, Daniela Bruni, Anne Jouret-Mourin, Catherine Hubert, Alex Kartheuser, Yves Humblet, Michele Ceccarelli, Najeeb Syed, Francesco M. Marincola, Davide Bedognetti, Marc Van den Eynde, and Jérôme Galon

Extrinsic Phagocyte-Dependent STING Signaling Dictates the Immunogenicity of Dying Cells

Jeonghyun Ahn, Tianli Xia, Ailem Rabasa Capote, Dillon Betancourt, and Glen N. Barber

Fibrinogen-like Protein 1 Is a Major Immune Inhibitory Ligand of LAG-3

Jun Wang, Miguel F. Sanmamed, Ila Datar, Tina Tianjiao Su, Lan Ji, Jingwei Sun, Ling Chen, Yusheng Chen, Gefeng Zhu, Weiwei Yin, Linghua Zheng, Ting Zhou, Ti Badri, Sheng Yao, Shu Zhu, Agedi Boto, Mario Sznol, Ignacio Melero, Dario A.A. Vignali, Kurt Schalper, and Lieping Chen

The Lineage-Defining Transcription Factors SOX2 and NKX2-1 Determine Lung Cancer Cell Fate and Shape the Tumor Immune Microenvironment

Gurkan Mollaoglu, Alex Jones, Sarah J. Wait, Anandaroop Mukhopadhyay, Sangmin Jeong, Rahul Arya, Soledad A. Camolotto, Timothy L. Mosbrugger, Chris J. Stubben, Christopher J. Conley, Arjun Bhutkar, Jeffery M. Vahrenkamp, Kristofer C. Berrett, Melissa H. Cessna, Thomas E. Lane, Benjamin L. Witt, Mohamed E. Salama, Jason Gertz, Kevin B. Jones, Eric L. Snyder, and Trudy G. Oliver

Mitophagy in Intestinal Epithelial Cells Triggers Adaptive Immunity during Tumorigenesis

Paul K. Ziegler, Julia Bollrath, Charles K. Pallangyo, Takaji Matsutani, Özge Canli, Tiago De Oliveira, Michaela A. Diamanti, Nina Müller, Jaba Gamrekelashvili, Tracy Putoczki, David Horst, Arun K. Mankan, Meryem G. Öner, Susanna Müller, Josef Müller-Höcker, Thomas Kirchner, Julia Slotta-Huspenina, M. Mark Taketo, Thomas Reinheckel, Stefan Dröse, Andrew C. Lerner, Winfried S. Wels, Matthias Ernst, Tim F. Greten, Melek C. Arkan, Thomas Korn, Dagmar Wirth, and Florian R. Greten

The Immune Landscape of Cancer

Vésteinn Thorsson, David L. Gibbs, Scott D. Brown, Denise Wolf, Dante S. Bortone, Tai-Hsien Ou Yang, Eduard Porta-Pardo, Galen F. Gao, Christopher L. Plaisier, James A. Eddy, Elad Ziv, Aedin C. Culhane, Evan O. Paull, I.K. Ashok Sivakumar, Andrew J. Gentles, Raunaq Malhotra, Farshad Farshidfar, Antonio Colaprico, Joel S. Parker, Lisle E. Mose, Nam Sy Vo, Jianfang Liu, Yuexin Liu, Janet Rader, Varsha Dhankani, Sheila M. Reynolds, Reanne Bowlby, Andrea Califano, Andrew D. Cherniack, Dimitris Anastassiou, Davide Bedognetti, Arvind Rao, Ken Chen, Alexander Krasnitz, Hai Hu, Tathiane M. Malta, Houtan Noushmehr, Chandra Sekhar Pedamallu, Susan Bullman, Akinyemi I. Ojesina, Andrew Lamb, Wanding Zhou, Hui Shen, Toni K. Choueiri, John N. Weinstein, Justin Guinney, Joel Saltz, Robert A. Holt, Charles E. Rabkin, The Cancer Genome Atlas Research Network, Alexander J. Lazar, Jonathan S. Serody, Elizabeth G. Demicco, Mary L. Disis, Benjamin G. Vincent, and Ilya Shmulevich



On the Cover: An artistic 3D rendering of a T cell attacking a tumor. Image courtesy of Enot Poloskun/iStock. Cover design by Kip Lyall.

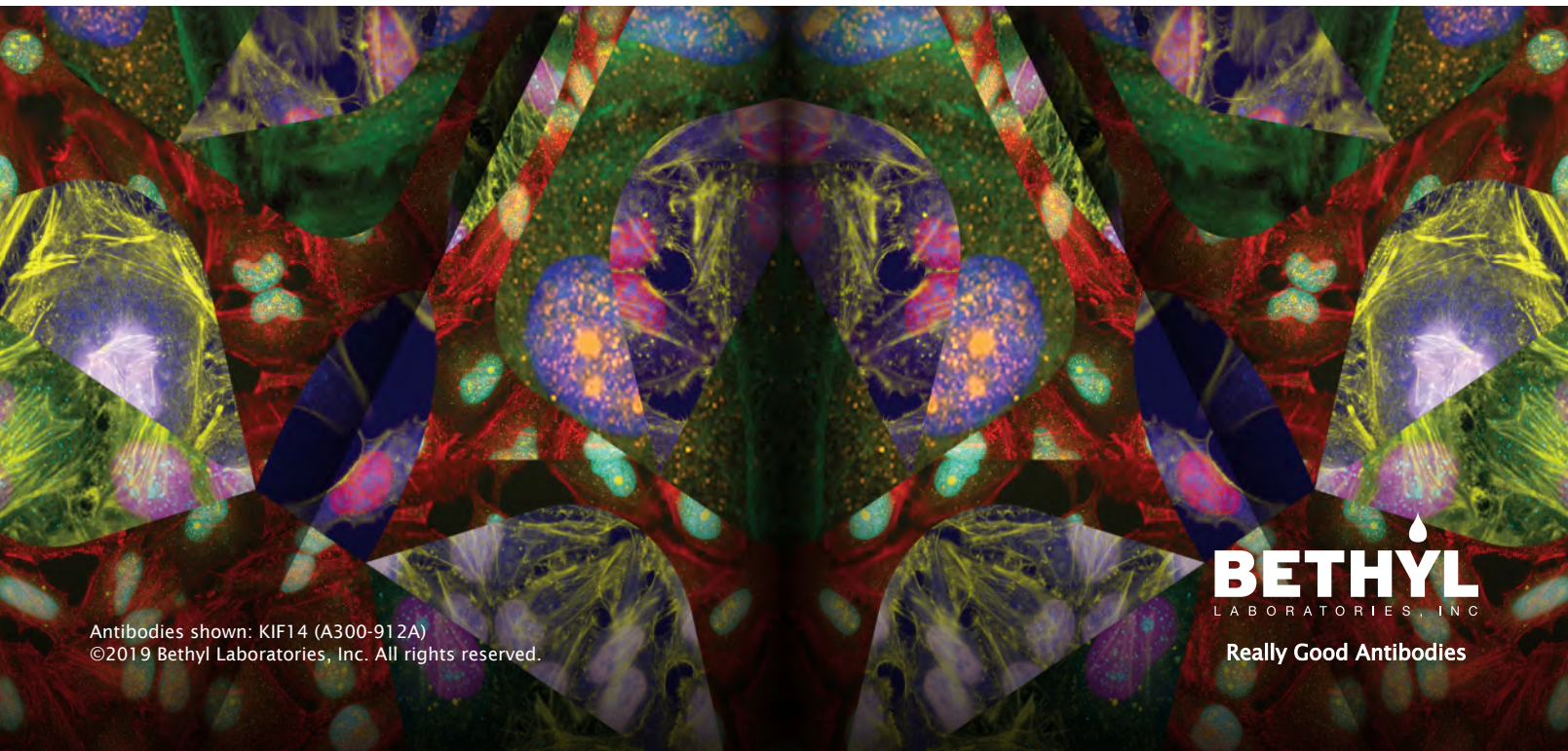


Full-spectrum scalability

Raise the bar on reliability with high-quality antibodies in bulk

When scaling up, consistency counts. For more than 45 years, Bethyl has manufactured and validated all bulk antibodies in-house to exacting standards, ensuring reliable results. And that means every one of our nearly 10,000 catalog products are available in large-scale formats. From antiserum generation to large-scale conjugation, our proven process controls enable the scaling and customization of products based on your needs. Work with Bethyl to bring your discovery into full focus.

See our data at bethyl.com/bulkabs



Antibodies shown: KIF14 (A300-912A)
©2019 Bethyl Laboratories, Inc. All rights reserved.

**BETHYL**
LABORATORIES, INC

Really Good Antibodies

ARE YOUR ANTIBODIES WORKING HARD, OR HARDLY WORKING?

75%

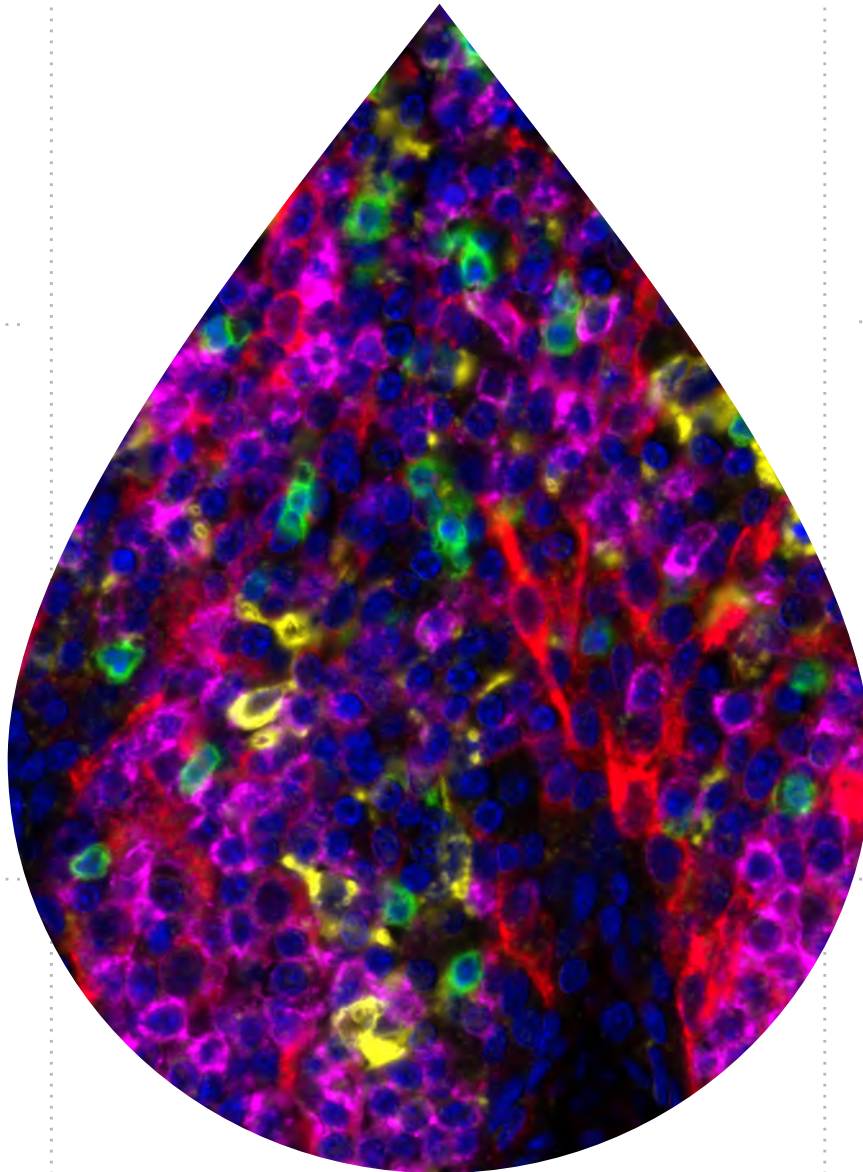
OF MANUFACTURED
ANTIBODIES ARE
NON-SPECIFIC OR DID
NOT WORK AT ALL*



EVERY ANTIBODY THAT
BETHYL SELLS IS
MANUFACTURED TO
EXACTING STANDARDS
ON SITE IN
MONTGOMERY, TX

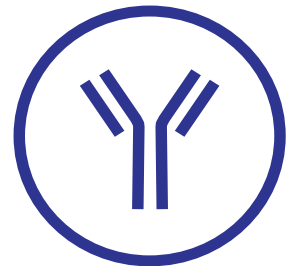
TARGETING OVER
3,300

PROTEINS AND 1,300
SECONDARY ANTIBODIES



\$350

MILLION
IS WASTED ANNUALLY ON
BIOMEDICAL RESEARCH
BECAUSE POOR QUALITY
MATERIALS LEAD TO
FALSE RESULTS**



QUALIFIED
ANTIBODIES
MADE IN THE USA
VALIDATED IN THE USA

40+

YEARS OF
EXPERIENCE

OF CATALOG &
CUSTOM ANTIBODY
PRODUCTION SERVICES

Bethyl is dedicated to improving lives by supporting scientific discovery through its qualified polyclonal and recombinant rabbit monoclonal antibody products and ELISA kits. Our antibodies have been manufactured and validated on-site by our scientists to ensure target specificity and sensitivity. If a product doesn't meet our standards, it doesn't leave our facility and every antibody sold is backed with a 100% guarantee to provide confidence in your results. **We put a lot in every drop.**

BETHYL
LABORATORIES, INC

Really Good Antibodies

FIND OUT MORE AT BETHYL.COM/VALIDATION

T Cell Dysfunction in Cancer

Daniela S. Thommen^{1,*} and Ton N. Schumacher¹¹Division of Molecular Oncology and Immunology, Oncode Institute, The Netherlands Cancer Institute, Amsterdam, The Netherlands

*Correspondence: d.thommen@nki.nl

<https://doi.org/10.1016/j.ccell.2018.03.012>

Therapeutic reinvigoration of tumor-specific T cells has greatly improved clinical outcome in cancer. Nevertheless, many patients still do not achieve durable benefit. Recent evidence from studies in murine and human cancer suggest that intratumoral T cells display a broad spectrum of (dys-)functional states, shaped by the multifaceted suppressive signals that occur within the tumor microenvironment. Here we discuss the current understanding of T cell dysfunction in cancer, the value of novel technologies to dissect such dysfunction at the single cell level, and how our emerging understanding of T cell dysfunction may be utilized to develop personalized strategies to restore antitumor immunity.

Introduction

Tumors harbor genetic alterations resulting from DNA damage, e.g., due to exposure to UV light, tobacco smoke, or deficiencies in DNA repair (Alexandrov et al., 2013; Stephens et al., 2009). These alterations distinguish cancer cells from normal cells, thereby frequently prompting the induction of tumor-reactive T cell responses in both mouse models and cancer patients (Castle et al., 2012; Matsushita et al., 2012; Robbins et al., 2013; van Rooij et al., 2013). While the presence of tumor-infiltrating lymphocytes (TILs), and in particular CD8⁺ T cells, is a positive prognostic marker in multiple solid tumors (Fridman et al., 2012), these cells fail to effectively eliminate cancer cells (Boon et al., 2006). One reason for this failed immune control is the curtailing of effector functions of infiltrating T cells by a broad spectrum of immunosuppressive mechanisms that are present in the tumor microenvironment (TME) (Chen and Mellman, 2013; Mellman et al., 2011; Schreiber et al., 2011). Among these mechanisms, the upregulation of programmed cell death-1 (PD-1) on T cells has emerged as a major marker of T cell dysfunction. The altered functional state of PD-1⁺ T cells, termed T cell exhaustion, has originally been described and most extensively studied in murine models of chronic lymphocytic choriomeningitis virus (LCMV) infection (Wherry et al., 2007; Zajac et al., 1998), but ample evidence for it has also been obtained in human infection and cancer (Ahmadzadeh et al., 2009; Baitsch et al., 2011; Day et al., 2006; Trautmann et al., 2006).

The successful reinvigoration of T cell function by blockade of PD-1, or its ligand PD-L1, highlights the importance of the PD-1/PD-L1 axis in T cell dysfunction (Day et al., 2006). In line with this, antibodies targeting PD-1/PD-L1 have shown impressive activity in multiple cancer types, including melanoma (Robert et al., 2014, 2015), non-small-cell lung cancer (NSCLC) (Borghaei et al., 2015; Brahmer et al., 2015; Fehrenbacher et al., 2016), renal cancer (RCC) (Motzer et al., 2015), urothelial cancer (Balar et al., 2017; Rosenberg et al., 2016), and head and neck squamous cell cancer (HNSCC) (Seiwert et al., 2016). While the objective response rates between 15% and 34% that were observed in these studies signify a clear improvement in patient outcome, the majority of patients still do not respond or do not achieve durable responses to this therapy. Lack of (durable) response is thought to be explained at least in part by the activity of other inhibitory pathways in T cells. Specifically, a simultaneous

expression of different inhibitory receptors, so-called immune checkpoints, has been observed on a fraction of T cells and increases with progressive dysfunction (Thommen et al., 2015; Wherry, 2011). Furthermore, it has been found that T cells can differentiate into an exhausted state even in the absence of PD-1 (Legat et al., 2013; Odorizzi et al., 2015). Direct evidence for the role of these additional pathways comes from the observation that T cell subsets expressing certain immune checkpoint combinations display synergistic responses to immunotherapy combinations, compared with anti-PD-1 monotherapy (Fourcade et al., 2010; Sakuishi et al., 2010). As the intratumoral T cell pool is exposed to many distinct immunosuppressive mechanisms, a broad spectrum of dysfunctional T cell states may be expected. Importantly, these states can also be expected to partially diverge from the dysfunctional state of T cells in chronic viral infections, as the microenvironment in tumors will only show a partial overlap with that of chronically infected sites (Figure 1).

In this perspective, we review the hallmarks of exhausted T cells in cancer and in chronic viral infection. A better understanding of intratumoral T cell dysfunction should be of value from a fundamental biological perspective, should allow improved patient stratification, and should offer novel avenues for the restoration of intratumoral T cell activity.

Characteristics of Intratumoral T Cell Dysfunction Hallmarks of Exhausted T Cells in Chronic Viral Infection and Cancer

Prolonged exposure of T cells to their cognate antigen results in T cell receptor (TCR) signals that lead to elevated and sustained expression of inhibitory receptors on these cells. In addition, T cells enter a state of dysfunction that is characterized by a hierarchical loss of effector functions and proliferation, as well as distinct transcriptional and metabolic changes. This dysfunctional state was initially described for antigen-specific T cells in chronic murine LCMV infection (Wherry et al., 2007), but a similar state has also been observed in T cells in cancers (Baitsch et al., 2011). Comparison of gene expression profiles derived from T cells in human or murine tumors with those from chronic viral infections has revealed that exhausted T cells in both conditions share many phenotypic and functional characteristics. Of these characteristics, the upregulation of immune checkpoints has



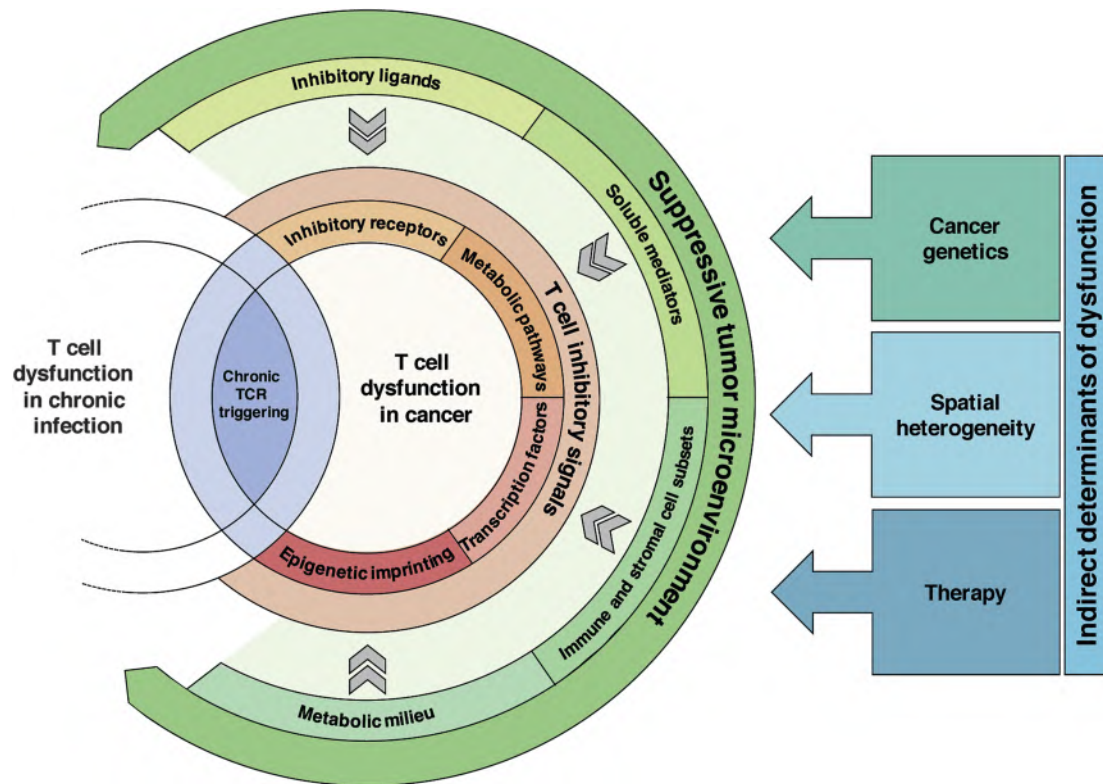


Figure 1. Drivers of T Cell Dysfunction in Cancer

Dysfunctional T cells in cancer share core exhaustion features with dysfunctional T cells in chronic infection that are at least partially driven by chronic TCR stimulation. The consequences of chronic TCR signaling are further modulated by a multitude of immunosuppressive signals in the TME, including inhibitory ligands, suppressive soluble mediators, cell subsets, and metabolic factors. Strength of these different signals is determined by parameters such as the specific mutations in the cancer cells, spatial gradients in tumor composition, and therapy-induced alterations in the TME. Collectively, the immunosuppressive signals in the TME shape the (dys-)functional state of intratumoral T cells by influencing the expression of inhibitory receptors, changing metabolic pathways, modifying the epigenetic state, and altering their transcription factor profiles.

been described as one of the hallmarks of T cell exhaustion (Wherry et al., 2007). While transient expression of PD-1 is a characteristic of normal T cell activation, persistent antigen exposure induces a sustained expression of PD-1, which characterizes—and possibly drives—T cell dysfunction (Ahmadzadeh et al., 2009; Baitsch et al., 2011; Wherry, 2011). In addition to PD-1, dysfunctional T cells have been shown to overexpress other inhibitory receptors, including T cell immunoglobulin and mucin domain-3 protein (Tim-3), Lymphocyte-activation gene 3 (Lag-3), Cytotoxic T lymphocyte antigen-4 (CTLA-4), and T cell immunoglobulin and ITIM domain (TIGIT) (Blackburn et al., 2009; Kuchroo et al., 2014). The fraction of T cells that simultaneously express these receptors—and that often also exhibit a high expression level of PD-1—increases during progressive dysfunction, as defined by the gradual loss of effector functions (Blackburn et al., 2008; Schreiner et al., 2016). Analysis of the pattern of inhibitory receptor co-expression on T cells in both chronic hepatitis B virus infection and cancer has revealed a hierarchical expression of these receptors, dominated by the expression of PD-1 (Bensch et al., 2014; Thommen et al., 2015).

A second feature of exhausted T cells in chronic viral infection is the progressive loss of effector functions, including the secretion of interleukin (IL)-2, tumor necrosis factor (TNF) α , interferon (IFN) γ , and β -chemokines (Wherry et al., 2007). Several studies

have demonstrated that tumor-infiltrating CD8⁺ T lymphocytes are also impaired in their production of effector cytokines (Baitsch et al., 2011; Zippelius et al., 2004) in, among others, melanoma (Ahmadzadeh et al., 2009), NSCLC (Thommen et al., 2015), HNSCC (Li et al., 2016), gastric cancer (Lu et al., 2017), and ovarian cancer (Matsuzaki et al., 2010).

Finally, exhausted T cells in chronic LCMV infection display a particular gene expression profile that is distinct from that of naive, effector, or memory T cells and that, in addition to changes in inhibitory receptor expression and cytokine production, encompasses alterations in transcription factor expression and in pathways involved in chemotaxis, migration, and metabolism (Wherry et al., 2007). The transcriptional profile of CD8⁺ T cells directed against the Melan-A/MART-1 melanoma antigen isolated from melanoma metastases after vaccination largely overlaps with the exhaustion signature derived from CD8⁺ T cells during chronic LCMV infection, and contains similar alterations in processes involved in immune response, cell migration, signaling, metabolism, cell cycle, and DNA repair (Baitsch et al., 2011).

Phenotypic and Transcriptional Differences between Dysfunctional T Cells in Cancer and Chronic Viral Infection

Based on the observation that T cells derived from human tumors and chronic viral infection share a number of phenotypic,

transcriptional, and functional characteristics, initial studies assumed that the exhausted state of tumor-reactive T cells would be similar to that of virus-specific T cells in chronic infections. More recent work that provides an in-depth analysis of intratumoral T cell dysfunction, however, leads to a model in which the exhaustion signatures during chronic infection and cancer do exhibit clear differences. In particular, whereas the upregulation of inhibitory receptors is seen in both situations, the relative expression of distinct inhibitory receptors appears to differ between tumor- and virus-specific T cells. Specifically, the expression of KLRG-1, CD160, Lag-3, and CTLA-4 varies between melanoma- and EBV-specific T cells, indicating that the upregulation of inhibitory receptors might be context-dependent (Baitsch et al., 2011, 2012).

Transcriptional profiling of T cells in chronic infection has revealed a set of transcription factors that is altered in expression compared with non-exhausted T cells, and thus has been associated with exhaustion (Wherry et al., 2007). While further studies have suggested involvement of a broad number of transcription factors, including NFAT, Eomes, T-bet, Blimp-1, BATF, FoxO1, VHL, and c-Maf, a master regulator that initiates and controls the process of dysfunction has not yet been found (Agnellini et al., 2007; Doedens et al., 2013; Giordano et al., 2015; Kao et al., 2011; Paley et al., 2012; Quigley et al., 2010; Shin et al., 2009; Staron et al., 2014). The understanding of gene regulation in dysfunctional T cells is further complicated by the fact that many of these transcription factors act in a context-specific manner, with a different function in exhausted T cells than in non-exhausted effector or memory T cell subsets (Kao et al., 2011; Paley et al., 2012; Quigley et al., 2010; Shin et al., 2009). One prominent example of this is formed by the T-box transcription factors T-bet and Eomesodermin (Eomes). While T-bet controls normal effector differentiation of CD8⁺ and CD4⁺ T cells, it also regulates the non-terminally exhausted progenitor pool in chronic LCMV infection by repressing the expression of PD-1 and other inhibitory receptors. Eomes, in contrast, regulates the protein expression needed for memory formation following acute infection, but is also expressed by the terminally exhausted T cell pool in chronic infection, contributing to the upregulation of inhibitory receptors seen in these cells (Banerjee et al., 2010; Intlekofer et al., 2005; Paley et al., 2012; Zhou et al., 2010). Importantly, while these two transcription factors thus show a reciprocal expression pattern in chronic viral infections, this is different from what is observed in tumor-specific dysfunctional T cells. In the latter situation, T cells do not display high Eomes expression, but rather show both reduced T-bet and Eomes expression over the course of tumor progression, as recently described in a murine liver cancer model (Schieteringer et al., 2016). Thus, the role of these two transcription factors in T cell dysfunction may differ between chronic viral infection and tumor outgrowth. It will be of particular interest to assess whether the unresponsiveness to PD-1 blockade that is observed for Eomes^{hi} PD-1^{hi} T cells in chronic infection is also present in highly dysfunctional intratumoral T cells, with their lower level of Eomes expression.

The identification of transcriptional pathways that mediate T cell dysfunction is complicated by the fact that the gene signatures of exhausted T cells show a fair degree of overlap with those of recently activated T cells, consistent with the critical

role of TCR signaling in driving both states (Doering et al., 2012; Tirosh et al., 2016). This overlap is also reflected by the large number of immune checkpoints present on exhausted T cells that are transiently expressed during T cell activation, a process that may be interpreted as a protection mechanism against overstimulation (Anderson et al., 2016). Network analysis of exhausted LCMV-specific T cells has, however, revealed that the connectivity patterns of key transcriptional regulators are different between exhausted and memory T cells (Doering et al., 2012). Recent work from the Anderson group described a distinct gene module for dysfunction in murine tumor models that could be separated from that of T cell activation (Singer et al., 2016), and single cell RNA sequencing of intratumoral T cells indicated that these two gene modules are mutually exclusive. Expression of metallothioneins, which regulate intracellular zinc availability, and several zinc-finger transcription factors were highly increased in dysfunctional CD8⁺ TILs, and targeted deletion of metallothionein 1 and 2 could improve T cell functionality and restore antitumor immunity. Of note, PD-1 and Tim-3 expression remained unchanged upon metallothionein-deletion, indicating that inhibitory receptor expression can be uncoupled from other aspects of T cell dysfunction, and was more likely to reflect T cell activation in this setting.

Tumors are complex ecosystems, defined by the interplay of a large number of cellular and soluble components. Whereas TILs share the core exhaustion signature of virus-specific T cells driven by the persistent antigen exposure, their phenotypic and transcriptional profile is additionally shaped by cell-intrinsic and -extrinsic immunosuppressive factors in the TME that will partially differ from those at sites of chronic infection. These immunosuppressive mechanisms include (1) the expression of inhibitory receptors and their ligands; (2) the recruitment of immunosuppressive cell populations such as regulatory T cells (Tregs) and myeloid-derived suppressor cells; (3) direct repression of T cell function via secretion of suppressive cytokines such as IL-10 and TGFβ; (4) direct repression of T cell function via production of metabolites, including adenosine, prostaglandins, and lactate; (5) production of suppressive compounds and enzymes, including nitric oxide synthase, reactive oxygen species and indoleamine-2,3 dioxygenase (IDO); and (6) physiological changes in the TME such as hypoxia, low pH, and the deprivation of nutrients, such as glucose or amino acids (Fridman et al., 2017; Gajewski et al., 2013; Speiser et al., 2016; Zarour, 2016). In the next section, we focus on the role of metabolic factors in T cell dysfunction. For an overview of other immunosuppressive mechanisms in the TME, we refer to the excellent reviews mentioned above.

Impact of the Tumor Metabolism and Genetics on Dysfunctional TIL States

Following TCR triggering, T cells undergo profound metabolic changes to meet the bio-energetic demands associated with cellular proliferation and effector differentiation. Whereas naive T cells largely rely on oxidative phosphorylation (OXPHOS), they switch to the use of aerobic glycolysis upon antigen stimulation, to generate the required ATP (Chang et al., 2013; Pearce and Pearce, 2013). During memory formation, T cells revert back to the use of OXPHOS and become increasingly dependent on mitochondrial fatty acid oxidation (van der Windt et al., 2013; van der Windt and Pearce, 2012). In dysfunctional T cells, the

link between antigenic stimulation, and metabolic pathway activation appears altered. In chronic LCMV infection, profound changes in genes related to metabolic pathways have been observed (Wherry et al., 2007). Of note, metabolic dysfunction of virus-specific T cells already develops during the first weeks of infection, before a major loss in effector functions occurs. These bio-energetic alterations include a reduction in glucose uptake and use, dysregulation of mitochondrial energetics, as well as the upregulation of anabolic pathways. Furthermore, it has been shown that PD-1 contributes to these early glycolytic and mitochondrial changes, as PD-1 deficient T cells do not undergo these metabolic changes in the murine LCMV model, and as the key metabolic regulator PPAR-gamma coactivator 1 α (PGC-1 α) is repressed by PD-1 triggering (Bengsch et al., 2016). Similar observations have been made in a murine tumor model, where enforced expression of PGC-1 α led to reprogramming of tumor-specific T cells and improvement of metabolic and effector function (Scharping et al., 2016). While these metabolic changes have been observed in both tumor- and virus-specific T cells, comparison of T cells reactive to the same antigen in either a murine chronic infection model or cancer model revealed a persistent loss of mitochondrial function and mass that was specific to T cells that resided at the tumor site. These mitochondrial alterations were also observed in human CD8⁺ TILs in HNSCC tumors (Scharping et al., 2016; Siska et al., 2017).

To generate the energy required to exert effector functions, T cells are highly dependent on the availability of nutrients within their microenvironment (Scharping et al., 2016). T cells that fail to upregulate metabolic pathways upon activation, or that are activated under nutrient-poor conditions, have been described to acquire a hypo-responsive phenotype that cannot be reverted by subsequent stimulation (Zheng et al., 2009). The metabolic landscape of tumors is in large part determined by the energetics of cancer cells, because of their high bio-energetic demands for proliferation. The increased utilization of glycolysis and OXPHOS by tumor cells leads to a depletion of essential nutrients, as well as the accumulation of immunosuppressive metabolites such as lactic acid (Vander Heiden et al., 2009). This creates an environment with low glucose, low amino acids, low oxygen, and low pH, which are all considered metabolic checkpoints (Kato et al., 2013; Martinez-Otschoorn et al., 2017; Scharping and Delgoffe, 2016; Wilson and Hay, 2011). Hence, the functionality of T cells will not only be affected by their intrinsic metabolic alterations, but also by the unfavorable metabolic milieu within the TME.

In line with this model, low glucose availability in the TME has been shown to render CD8⁺ T cells less capable of controlling tumor growth in a mouse sarcoma model (Chang et al., 2015). Similar findings in a mouse melanoma model indicated a role for the glycolytic metabolite phosphoenolpyruvate (PEP) in sustaining Ca²⁺-NFAT signaling and T cell effector function (Ho et al., 2015). PEP levels are decreased in exhausted T cells, and overexpression of phosphoenolpyruvate carboxykinase (PCK1) to increase PEP production can restore effector functions in CD8⁺ T cells via metabolic reprogramming. Blockade of the immune checkpoints CTLA-4, PD-1, and PD-L1 in a mouse tumor model has been shown to restore glucose availability in the TME as well as to increase glucose uptake, and to reinstate effector functions in CD8⁺ TILs (Chang et al.,

2015). Moreover, this study provided evidence to suggest that PD-L1 blockade may not only target the metabolism of T cells, but also that of tumor cells by directly dampening glucose uptake and glycolysis in the latter. On a more general note, efforts to reduce the metabolic activity of tumor cells may be of potential interest, as an indirect strategy to increase the amount of glucose that can be utilized by T cells.

In addition to glucose, the supply of certain amino acids also impacts the effector functions of intratumoral T cells. First, glutamine is essential for T cell activation and differentiation, but is also often depleted from the TME due to its use as primary fuel for tumor cells (Altman et al., 2016; Carr et al., 2010). Second, tryptophan is lacking in some TMEs due to the secretion of the tryptophan metabolizing enzyme IDO by tumor cells and suppressive immune cells, also leading to an increase in its immunosuppressive catabolite kynurenine (Platten et al., 2012). Kynurenine accumulation in turn promotes the generation of regulatory T cells (Julliard et al., 2014). Third, arginase secretion by myeloid cells leads to depletion of the arginine that is required for T cell activation and proliferation (Lind, 2004; Munder et al., 2009). Next to amino acid deprivation, the pH changes and the loss of cytosolic NAD⁺ regeneration induced by the lactic acid that is generated as a waste product of tumor cell glycolysis further inhibit T cell function and cytokine production (Choi et al., 2013). In addition, tumor-derived lactic acid has also been shown to induce apoptosis of naive T cells via loss of FAK family-interacting protein of 200 kDa (FIP200), which may further support the ability of tumors to evade immune control (Xia et al., 2017). Neutralization of acidic components in the TME has been shown to boost antitumor immunity in animal models (Pilon-Thomas et al., 2016).

Another metabolic parameter that is closely linked with the above discussed characteristics of the TME is hypoxia. During rapid tumor growth, areas that lack sufficient perfusion develop. The resulting limitation in oxygen availability impacts T cell metabolism, by reducing energy production via OXPHOS and inducing an increased dependency on glycolysis. In different studies, hypoxia has been shown to both increase and impair T cell responses. On the one hand, data from murine chronic infections and tumor models suggest that cytotoxicity of T cells may be enhanced under conditions of hypoxia, leading to more efficient virus and tumor control (Doedens et al., 2013; Gropper et al., 2017). On the other hand, hypoxia induces increased expression and activity of the transcription factor hypoxia-inducible factor 1 α (HIF-1 α), which promotes the expression of inhibitory receptors on T cells (Doedens et al., 2013), and leads to a reduction in T cell effector functions (Fischer et al., 2007). These seemingly contradictory findings may be explained by a model in which the outcome of hypoxia is determined by the presence or absence of other metabolic checkpoints. In particular the lack of glucose in the TME may restrict the functionality of T cells that rely on glycolysis in an oxygen-low milieu (a detailed review of this topic is provided by Zhang and Ertl, 2016).

Recent studies have provided evidence that classical immune checkpoints can interact with metabolic checkpoints. For instance, the inhibitory receptor CTLA-4 on T cells competes with CD28 for B7 ligands and thereby suppresses the CD28-mediated T cell costimulation that is essential to increase T cell

Performance of single cell technologies in T cell dysfunction profiling

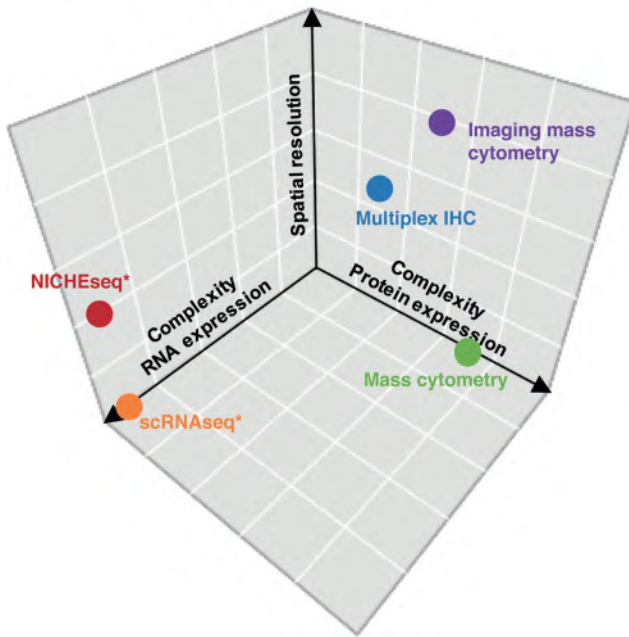


Figure 2. Comparison of Single Cell Technologies to Dissect Intratumoral T Cell Dysfunction

Technologies that assess T cell dysfunction at the single cell level are required to describe the heterogeneity of functional states within the TME. Current single cell technologies differ in the complexity and spatial resolution they provide. Ability to provide multiparametric information with respect to RNA and protein expression, and ability to provide spatial information are depicted for the indicated technologies. Asterisks indicate technologies that also provide TCR sequence information and may be combined with functional testing to evaluate tumor reactivity.

glucose uptake and metabolism (Frauwirth et al., 2002; Parry et al., 2005). Moreover, CTLA-4 ligation has been shown to inhibit mTOR signaling via recruitment of protein phosphatase 2A (PP2A) and subsequent Akt dephosphorylation (Teft et al., 2009; Wlodarchak and Xing, 2016). Activation of PI3K, Akt, and mTOR regulates the switch to anabolic metabolism and subsequent aerobic glycolysis via transcription factors including Myc and HIF-1 (MacIver et al., 2013; Wang et al., 2011). Furthermore, Akt and mTOR are also inhibited by PD-1 ligation (Chemnitz et al., 2004; Wu et al., 2001).

The genetic alterations that cancer cells acquire during tumor development have been shown to sculpt the TME. Such sculpting can either involve repression of T cell recruitment to the tumor site (Nagarsheth et al., 2017; Peng et al., 2015) or inhibition of the functionality of T cells at that site. For instance, activation of the Wnt- β -catenin signaling pathway in melanoma has been found to reduce the recruitment of antigen-presenting cells, particularly CD103⁺ dendritic cells (DCs). This not only promotes T cell exclusion from the tumor, but also limits the priming and activation of the few T cells that do manage to infiltrate (Spranger et al., 2015). Antitumor T cell responses can also be suppressed by cytokines such as IL-1 and VEGF that are highly abundant in tumors with BRAF mutations (Khalili et al., 2012). In addition, BRAF mutations lead to constitutive activation of the MEK-MAPK

pathway, thereby suppressing OXPHOS and enhancing glycolysis (Hall et al., 2013; Haq et al., 2013). Loss of PTEN correlated with reduced T cell-mediated tumor cell killing and effector cytokine secretion. Of note, melanoma patients with tumors that display PTEN loss showed a significantly lower reduction in tumor burden upon PD-1 treatment (Peng et al., 2016). Finally, a recent study investigating longitudinal biopsies of melanoma patients under CTLA-4 and PD-1 blockade observed that, while response to PD-1 blockade was associated with increased expression of genes related to cytotoxicity, antigen processing, and IFN γ signaling, therapy resistance correlated with increased VEGFA expression (Chen et al., 2016). VEGF secretion has been found to affect T cell functionality both directly and indirectly, via suppression of DC maturation and recruitment of suppressive cell populations (Gabrilovich et al., 1998; Terme et al., 2013).

Taken together, an increasing amount of evidence has been obtained indicating that intratumoral T cells can adopt a spectrum of dysfunctional states, sculpted by TCR triggering in the context of different micro-environmental factors, such as engagement of inhibitory receptors, presence of immunosuppressive cytokines, and cell populations, as well as metabolic factors. The observation of a series of distinct dysfunctional states provides a strong rationale for the development of individually tailored therapeutic strategies to restore the function of the intratumoral T cell population.

Novel Technologies to Describe T Cell Dysfunction at the Single Cell Level

Capturing T Cell States by Mass Cytometry and Single Cell Sequencing

While the (dys-)functional states of intratumoral T cells show differences between tumors, T cell infiltrates within individual tumors are also highly heterogeneous. This heterogeneity occurs along at least three axes: (1) heterogeneity with respect to the conventional T cell subsets (e.g., CD8⁺, CD4⁺ Th₁, Th₂, Th₁₇, Tregs, $\gamma\delta$ T cells), (2) heterogeneity with respect to the degree and type of dysfunction of T cells in a given subset, and (3) heterogeneity with respect to the capacity of the TCR of an individual cell to recognize tumor antigen. Because of this heterogeneity, the spectrum of T cell states in a tumor can only be captured appropriately by analyses at the single cell level. Immunologists realized the value of single cell-based analyses long ago, as shown by the development of immunohistochemistry and in particular flow cytometry. These more traditional approaches have over the past few years been complemented by novel approaches that allow one to determine individual cell states of immune cells, stromal cells, and malignant cells in human cancers, such as mass cytometry, single cell sequencing, and highly multiplexed single cell imaging (Figure 2). Mass cytometry allows for quantification of more than 50 readouts at the single cell level by combining metal isotope-labeled antibodies with mass spectrometry-based detection (Bandura et al., 2009; Ornatsky et al., 2010). One drawback of this method is that data are only obtained on a pre-defined set of parameters, thereby precluding completely unbiased analyses. In addition, unlike flow cytometry, isolation of viable cells for downstream (functional) analysis is precluded. Single cell sequencing has the advantage of being truly unbiased. As a downside, the low RNA content of T cells presently precludes the identification of the full transcriptome

of cells, and heterogeneity with respect to transcripts that are present at lower levels may be difficult to identify (Chevrier et al., 2017). In addition, heterogeneity at the level of protein translation or protein turnover will be missed.

Recent work describes the use of these technologies to obtain an in-depth characterization of tumor ecosystems in different cancer types, including breast cancer (Chung et al., 2017), RCC (Chevrier et al., 2017), NSCLC (Lavin et al., 2017), and HCC (Zheng et al., 2017). Single cell sequencing of 11 breast cancer patients revealed three clusters of immune cells: T cells displaying either an exhausted or regulatory phenotype, B cells, and macrophages with mostly an M2 differentiation profile (Chung et al., 2017). Several T cell subclusters could be identified, distinguished by naive, costimulatory, cytotoxic, regulatory, or exhaustion signatures. PD-1 expression was modest in all clusters, but expression of other immune checkpoints such as TIGIT or Lag-3 was observed more frequently, suggesting that these alternative pathways might be important in this tumor type.

A study using single cell mass cytometry compared immune infiltrates in 32 NSCLCs with matched adjacent normal tissue and peripheral blood. Tumors displayed increased numbers of Tregs and decreased numbers of cytolytic T cells compared to normal tissue. PD-1 was expressed on a subset of CD8⁺ and CD4⁺ T cells. In addition, changes in the distribution of myeloid cells between tumors, normal lung tissue and peripheral blood were observed (Lavin et al., 2017). A second study, describing the in-depth profiling of immune infiltrates in 73 patients with clear cell RCC by mass cytometry led to the identification of 22 T cell phenotypes and 17 tumor-associated macrophage phenotypes (Chevrier et al., 2017). Among the T cell clusters, seven different clusters of CD8⁺ T cells that expressed PD-1 were observed. Of note, the co-expression of other inhibitory receptors including Tim-3 and CTLA-4, as well as the expression of costimulatory or proliferation markers, varied greatly between these clusters, which are therefore likely to reflect distinct (dys-)functional states. In patients harboring large numbers of T cell clusters expressing high levels of PD-1 and a marker profile corresponding to intermediate to highly exhausted TILs, other T cell subsets with little or no PD-1 expression were absent, suggesting mutually exclusive T cell states. Furthermore, correlation analyses of the frequencies for each immune cell cluster of each individual tumor were used to unravel relationships between different immune cell subsets. These analyses demonstrated that the presence of a highly exhausted T cell cluster strongly correlated with the presence of both regulatory T cells and PD-L1 and PD-L2 expressing macrophages, indicating that this technology allows the identification of connectivity between cell populations in the TME.

Single cell RNA sequencing of tumor material from 19 melanoma patients yielded profiles of tumor, immune, stromal, and endothelial cells (Tirosh et al., 2016). Intratumoral T cell clusters displayed gene signatures associated with cytotoxicity and T cell exhaustion, suggesting an activation-dependent exhaustion program, as described previously (Fuertes Marraco et al., 2015; Wherry et al., 2007). In line with the data discussed in the previous section, also an activation-independent exhaustion program could be derived. This program was used to further subdivide T cells into “high-exhaustion” and “low-exhaustion” cells, relative to their expression of cytotoxicity genes. Compar-

ison of these high- and low-exhaustion signatures allowed the definition of a core exhaustion signature that consistently identified high-exhaustion cells in most tumors, as well as additional genes that showed variable expression across tumor samples, conceivably reflecting distinct influences of the TME, or treatment-induced effects.

A major advantage of single cell sequencing in the analysis of T cell dysfunction is its truly unbiased nature, making it possible to detect novel markers that are associated with the exhausted T cell state. A recent example of this is the discovery of LAYN as a marker of dysfunctional CD8⁺ T cells and Tregs in HCC (Zheng et al., 2017). Phenotypic and functional analyses indicated that the expression of LAYN was mutually exclusive with LAG-3 on CD8⁺ T cells and that overexpression of LAYN impaired IFN γ secretion. Another gene that has repetitively been found to be expressed in exhausted intratumoral T cell clusters, but not in gene expression data from chronic viral infections, is *CXCL13* (Baitsch et al., 2011; Tirosh et al., 2016; Zheng et al., 2017). *CXCL13* is a chemokine that is critically involved in the recruitment of B cells to lymph nodes and in the formation of germinal centers (Ansel et al., 2000). While its secretion by CD4⁺ follicular helper T cells has been well described (Crotty, 2011; Kroenke et al., 2012), its role in intratumoral CD8⁺ T cells is presently unknown.

The combined analysis of transcriptional profiles and TCR sequences of individual cells was recently used to investigate clonal relationships between distinct T cell clusters (Zheng et al., 2017). Comparison of tumor, adjacent normal liver tissue, and blood samples from six patients with HCC revealed a preferential enrichment of two T cell subsets with gene signatures associated with exhausted CD8⁺ T cells and Tregs in tumor samples. TCR analysis demonstrated a clonal expansion of T cells in these subsets. Pseudotime state transition analysis provided evidence that CD8⁺ T cells progress from naive via effector memory differentiation to a cytotoxic and finally exhausted T cell state. This conclusion was also supported by sharing of TCRs between the effector memory and cytotoxic T cell clusters, and between the cytotoxic and exhausted T cell clusters. In contrast, CD4⁺ T helper cells appeared to initially progress from a naive to a T helper cell state and then diverged into either a cytotoxic or exhausted T cell state, with very limited sharing of TCR sequences between the two populations. The use of this type of technology that provides detailed information on the transcriptional or phenotypic profile of distinct T cell states, together with the identification of the TCRs they carry, should greatly increase our understanding of the conditions under which dysfunctional T cell populations develop and which cell states they occupy.

Coupling T Cell State to Tumor Recognition Potential

One of the main limitations of the technologies discussed above is that these approaches do not allow one to couple cell state to the intrinsic capacity of a cell to recognize tumor. To develop novel therapeutic strategies to restore antitumor immunity, it is not only important to achieve a better understanding of the (dys-)functional states that T cells assume, but also how particular dysfunctional states and intrinsic tumor reactivity are connected. Put differently, the functional states of specifically those T cells that carry a tumor-reactive TCR are of most interest, as reactivation of those cells can be expected to have the most

profound impact on tumor control. At least four different strategies are currently being developed to address this question. First, peptide-MHC (pMHC) multimers have over the past years been widely used to quantify the effects of cancer immunotherapy on T cell responses to defined antigens (e.g., Kvistborg et al., 2012; van Rooij et al., 2013). The combination of MHC multimer staining with mass cytometry or with single cell sequencing analysis forms a logical next step. Indeed, recent data obtained by mass cytometry of MHC multimer-labeled cells demonstrate feasibility and reveal that intratumoral T cells with the same epitope specificity can display substantial heterogeneity (Fehlings et al., 2017).

As a second strategy to understand tumor reactivity, intratumoral T cells may be expanded to subsequently assess their reactivity, either by co-culture with autologous tumor material (Muul et al., 1987; Topalian et al., 1989; Tran et al., 2008), or by using high-throughput platforms that incorporate tumor-specific epitopes of an individual patient (Gros et al., 2016). With the caveat that proliferative and functional potential may be influenced by T cell exhaustion state, the parallel testing of expanded T cells that are sorted on the basis of phenotypic markers makes it possible to couple T cell differentiation state to tumor reactivity. This approach was successfully used to demonstrate the superior tumor recognition capacity of PD-1⁺ compared with PD-1⁻ T cells in tumors and peripheral blood of melanoma patients (Gros et al., 2014, 2016). In this approach, the markers used to separate T cell subsets need to be chosen in advance, thereby limiting its value to the analysis of small lists of “usual suspects.” A third approach that does not suffer from this limitation would be to link single cell sequencing data and tumor recognition data by TCR analysis. The identification of TCR sequences in single cell sequencing data allows one to couple the specific state of an intratumoral T cell to the TCR expressed by this cell (Zheng et al., 2017). T cells from the same tumor may conceivably be expanded *ex vivo* and assessed for tumor reactivity. TCR analysis of those T cells that show or lack tumor reactivity would then enable one to couple tumor recognition potential within a specific cell state, based on the matching of TCR sequences.

A limitation of the above two approaches may be that the functional and proliferative capacity of tumor-infiltrating T cells could be impaired due to their exhausted state, thereby skewing the detection of tumor reactivity in the expanded T cell population. The transfer of TCR $\alpha\beta$ gene pairs identified by single cell TCR sequencing from tumor material into healthy donor peripheral blood T cells overcomes this issue and allows the analysis of tumor reactivity of intratumoral TCR repertoires in a truly unbiased manner. Coupling of this approach with single cell transcriptome analysis should form a fourth and fully unambiguous approach to link tumor recognition potential of a T cell to its transcriptional state. An interesting goal of all these analyses will be to develop algorithms to predict tumor reactivity of T cells with high precision, without any requirement for functional testing.

Spatial Analysis of T Cell States

Signals derived from immune checkpoint ligands on cancer cells, stromal cells, or other immune cells that surround tumor-infiltrating T cells, as well as local gradients of pH, oxygen levels, or suppressive soluble factors, may provide a spatial component to the intratumoral heterogeneity of T cell states. A recent study in melanoma revealed that, rather than the numbers of intratu-

mor CD8⁺ T cells, the localization of these cells within the tumor was predictive of response to PD-1 blockade (Tumeh et al., 2014). The same study also observed a predictive effect of PD-1 expression in pretreatment biopsies, if PD-1⁺ T cells colocalized with PD-L1 expressing cells at the invasive margin. The impact of spatial distribution of intratumoral lymphocyte populations on clinical outcome, and particularly their colocalization with other cell subsets has also been described in other studies. Localization of CD8⁺ T cells, but not CD4⁺ or total T cells in proximity to cancer cells correlated with a better overall survival in pancreatic adenocarcinoma (Carstens et al., 2017). Similar findings have been obtained in breast cancer (Heindl et al., 2015; Yuan et al., 2012). Further evidence for the significance of the spatial organization of (PD-1⁺) lymphocytic infiltrates is provided by recent studies that analyze tertiary lymphoid structures (TLS) in cancer. TLS are present in the large majority of NSCLC, colorectal or ovarian cancers (Di Caro et al., 2014; Goc et al., 2014; Kroeger et al., 2016) and comprise a T cell zone harboring (mostly follicular helper) T cells and DCs, as well as a follicular zone containing B cells, similar to secondary follicles in lymph nodes. The occurrence of TLS is often associated with a favorable prognosis (Dieu-Nosjean et al., 2008; Sautes-Fridman et al., 2016) and frequently correlates with high overall T cell infiltration and lower macrophage infiltration (Lavin et al., 2017; Poschke et al., 2016). T cells in NSCLC tumors harboring many TLS display a more biased TCR repertoire (Zhu et al., 2015), either hinting at a possible role of these structures in promoting clonal expansion of T cells, or at a role of clonally expanded T cells in TLS formation. The former explanation would be consistent with a model in which TLS act as centers where primary or secondary antitumor responses are generated (Fridman et al., 2012). It will be of major interest to investigate how the presence of TLS may have an impact on T cell dysfunction and the response to immunotherapy.

In view of the emerging evidence for a spatial component to T cell heterogeneity, strategies that allow spatial analyses of the T cell state will become increasingly important. Two approaches that have recently been developed—highly multiplexed single cell imaging and single cell sequencing of spatial niches—may be employed to address this question. Immunohistochemistry is commonly used to evaluate the expression of a marker at the single cell level, and to assess the localization of cells carrying this marker within a tissue. The development of multiplex immunofluorescence platforms and novel imaging technologies allow for the detection and quantification of multiple markers on a single cell, or of the spatial organization of cells expressing different markers. While multiplex immunofluorescence imaging is currently limited to the combination of a handful of markers, recent work using imaging mass cytometry demonstrated the simultaneous analysis of 32 parameters in human breast cancer samples (Giesen et al., 2014). Of note, this analysis could not only be used to identify cell populations, but also to detect cell-cell interactions based on protein phosphorylation levels, as well as to distinguish hypoxic and normoxic areas by analysis of gradients of carbonic anhydrase IX.

As a second approach to describe cell states in different niches, Amit and colleagues recently developed technology that combines photoactivatable fluorescent markers, two-photon microscopy, and single cell sequencing, termed NICHE-seq (Medaglia

et al., 2017). *In situ* two-photon irradiation of transgenic mice expressing a photoactivatable fluorescent reporter allowed the identification of cells located at specific tissue regions based on the fluorescent signal that was induced by light exposure. Cells from irradiated and non-irradiated regions could then be sorted and subjected to single cell sequencing, thereby allowing the comparison of transcriptional profiles of cells at specific locations. Development of a similar technology applicable to human material will be of interest.

T Cell Dysfunction and Cancer Immunotherapy Heterogeneity of the PD-1 Expressing T Cell Pool

While the efficacy of antibodies targeting the PD-1/PD-L1 axis has been impressively demonstrated in multiple cancer types, the majority of patients still does not experience durable responses to this therapy. The mechanisms underlying this lack of responsiveness are highly multifactorial (Blank et al., 2016). While in some patients, lack of response to PD-1/PD-L1 blockade can be explained by a scarcity of antigens or by mutations in the antigen-presentation machinery, in part of the patient population lack of responsiveness will likely be due to T cell dysfunction that is not reversible by the sole blockade of the PD-1/PD-L1 axis. For this reason, a better understanding of the relationship between intratumoral T cell state and response to checkpoint blockade forms a major priority.

Evidence from chronic murine infection models indicates that the PD-1 positive CD8⁺ T cell pool consists of different subpopulations, and that the potential of reinvigoration by PD-1 blockade differs between CD8⁺ T cell subpopulations that are characterized by distinct expression levels of PD-1 (Blackburn et al., 2008). Specifically, in chronic murine LCMV infection, two subsets of exhausted PD-1⁺ T cells with distinct responses to PD-1/PD-L1 blockade have been identified. Whereas T cells with high expression of the transcription factor T-bet and intermediate expression of PD-1 (T-bet^{hi} PD-1^{int}) can be reinvigorated by *in vivo* blockade with anti-PD-L1, terminally differentiated T cells with high Eomes and high PD-1 expression (Eomes^{hi} PD-1^{hi}) do not respond (Blackburn et al., 2008; Paley et al., 2012). It is thought that T-bet^{hi} PD-1^{int} T cells represent a progenitor T cell subset, that proliferates in response to persisting antigen exposure, and ultimately gives rise to Eomes^{hi} PD-1^{hi} progeny (Paley et al., 2012). The latter cells, which are also characterized by high expression of other inhibitory receptors and loss of cytokine production, accumulate due to the persistent antigen stimulation during ongoing infection. Of note, Eomes^{hi} PD-1^{hi} cells do retain their cytotoxic function, suggesting that while these cells might not be able to completely eliminate the virus, they may play a role in the partial viral control seen during chronic infection.

Two recent studies on chronic LCMV infection identified two PD-1⁺ antigen-specific T cell populations that differ in their expression of CXCR5 (He et al., 2016; Im et al., 2016). CXCR5 is a chemokine receptor that is normally expressed on B cells and CD4⁺ follicular helper cells, but that has also been described on a CD8⁺ T cell subset in a murine model of systemic lupus erythematoses (Kim et al., 2010). The CXCR5-positive and -negative PD-1⁺ subsets seen in LCMV infection also differ in their expression of other receptors, with higher expression of costimulatory molecules and lower levels of inhibitory receptors on

CXCR5⁺ T cells than on CXCR5⁻ T cells. Of note, also PD-1 expression levels differ between the two populations with an intermediate PD-1 level on CXCR5⁺ T cells and high PD-1 levels on CXCR5⁻ T cells (Im et al., 2016). The two subsets vary in their functional capacities, with CXCR5⁺PD-1^{int} T cells secreting higher levels of effector cytokines upon restimulation, compared with the CXCR5⁻PD-1^{hi} cells (He et al., 2016). Interestingly, in this model, only the CXCR5⁺PD-1^{int} subset migrates to and resides in lymphoid tissues, and can be reactivated by PD-1 blockade (He et al., 2016; Im et al., 2016). A similar effect has been observed in dysfunctional CD8⁺ T cells that co-express PD-1 and the transcription factor Tcf1, which also plays an essential role in the generation of the CXCR5⁺PD-1^{int} subset (Im et al., 2016; Utzschneider et al., 2016). While now firmly established in models of chronic viral infection, it is presently unclear whether the same dichotomy between PD-1 high and low cells might be observed in cancer.

The presence or absence of PD-1 has previously been employed as a strategy to identify tumor-specific T cells in murine cancer and human melanoma and NSCLC (Fernandez-Poma et al., 2017; Gros et al., 2014; McGranahan et al., 2016; Pasetto et al., 2016). However, recent data suggest it will be even more informative to look at the level of PD-1 expression. Specifically, by using co-transfer of tumor-specific and virus-specific T cells in a murine cancer model it was shown that also T cells reactive to viral antigens infiltrate tumor lesions. While the latter cells express PD-1 at low to intermediate levels and retain their functionality, many of the tumor antigen-specific TILs that are found in the same tumors, express high levels of PD-1 and are dysfunctional (Erkes et al., 2017). On a related note, total CD8⁺ T cells with high PD-1 expression from patients with chronic lymphocytic leukemia display a global dysfunction, which is absent in the CMV-specific T cells that express PD-1 at a lower level (te Raa et al., 2014). Thus, PD-1 expression is not always indicative of dysfunction, and the presence of PD-1 positive virus- or other non-tumor-specific T cells in cancers might reduce the value of global PD-1 expression as a biomarker. At present, it is unclear whether the PD-1^{int} or PD-1^{hi} subset could be a positive or negative predictor of response to anti-PD-1/anti-PD-L1 therapy. While on the one hand tumor reactivity may be enriched in PD-1^{hi} T cells, on the other hand these cells display a highly exhausted state in human cancers (see below) and may be dysfunctional “beyond repair,” as suggested by observations in models of chronic infection (Blackburn et al., 2008; Paley et al., 2012). Additionally, the use of PD-1 as a marker for tumor-specific T cells may be further complicated by the fact that PD-1 expression cannot only be induced by TCR signaling, but also by other factors such as IL-10 (Sun et al., 2015) and TGF-β (Park et al., 2016).

Reactivation of Dysfunctional T Cells by Immunotherapy Combinations

As mentioned above, in addition to PD-1, dysfunctional CD8⁺ T cells also show (increased) expression of other inhibitory receptors including CTLA-4, Tim-3, Lag-3, and TIGIT, which can bind to their respective ligands expressed by antigen-presenting cells and tumor cells in the TME, thereby potentially impeding T cell functions (Ahmadzadeh et al., 2009; Fourcade et al., 2010; Sakuishi et al., 2010). Co-expression of PD-1 and Lag-3 has been observed on both virus- and tumor antigen-specific

T cells (Grosso et al., 2009; Matsuzaki et al., 2010; Wherry et al., 2007). Of note, T cells expressing both receptors are more impaired in effector functions, such as TNF and IFN γ secretion, compared with single positive cells. Simultaneous blockade of PD-1 and Lag-3 has been shown to improve T cell responses in chronic infection models and tumor models, compared with anti-PD-1 monotherapy (Blackburn et al., 2009; Matsuzaki et al., 2010), and Lag-3 targeting agents are currently being tested in clinical studies. By the same token, Tim-3 has been shown to be expressed on a subset of PD-1⁺ NY-ESO-1-specific T cells in advanced melanoma and gastric cancer. Of note, T cells that co-express PD-1 and Tim-3 have substantially higher PD-1 levels and are more dysfunctional than cells with either single or no detectable expression of these receptors (Fourcade et al., 2010; Li et al., 2016; Lu et al., 2017). A study in HNSCC observed that *in vitro* single-agent PD-1 blockade exerts its effect on PD-1^{int} Tim-3⁻ T cells, but not on PD-1^{hi} Tim-3⁺ T cells (Li et al., 2016), in line with the previously discussed reactivation of PD-1^{int} T cells that co-express CXCR5 by PD-1 blockade in chronic LCMV infection (He et al., 2016; Im et al., 2016). While the effect of dual PD-1/Tim-3 blockade was not addressed in this work, other studies have suggested that the simultaneous blockade of these two receptors might have additive effects in the reactivation of antigen-specific T cells in chronic infection and cancer *in vitro* and *in vivo* (Fourcade et al., 2010; Jin et al., 2010; Lu et al., 2017; Sakuishi et al., 2010). Another inhibitory receptor that is frequently co-expressed with PD-1 is TIGIT, which competes with the costimulatory molecule CD226 for the same ligand, the poliovirus receptor (PVR, CD155) (Bottino et al., 2003; Chauvin et al., 2015). In addition, TIGIT has also been described to bind with lower affinity to CD112 (PVRL2), as well as to disrupt the costimulatory function of CD226 by cis-binding (Johnston et al., 2014; Yu et al., 2009), but the functional impact of these interactions is still unclear. While TIGIT⁺ CD8⁺ TILs that co-express PD-1, Tim-3, and Lag-3 show a highly dysfunctional phenotype in murine cancer models (Kurtulus et al., 2015), TIGIT expression by itself does not appear to distinguish PD-1⁺ T cell subsets with different degrees of dysfunction in melanoma patients. Nevertheless, combined blockade of PD-1 and TIGIT on CD8⁺ TILs cultured in the presence of autologous tumor did show an additive effect in restoring effector functions (Chauvin et al., 2015).

The most prominent example of combined immune checkpoint blockade that has also reached clinical practice, is the dual blockade of PD-1 and CTLA-4. In contrast to PD-1, which inhibits T cell function by interfering with T cell signaling, CTLA-4 competes with CD28 for binding to CD80/CD86 and thereby inhibits T cell function (Krummel and Allison, 1995; Walunas et al., 2011). The CTLA-4 targeting agent ipilimumab was the first checkpoint inhibitor to demonstrate an improvement in overall survival in patients with advanced melanoma (Hodi et al., 2010; Robert et al., 2011). Treatment of melanoma patients with anti-CTLA-4 leads to a significant broadening of melanoma-reactive T cell responses in peripheral blood, suggesting that at least part of its effect occurs through enhanced T cell priming (Kvistborg et al., 2014). CTLA-4 blockade has also been suggested to target regulatory T cells by either functional inhibition or depletion of this subset (Duraiswamy et al., 2013; Simpson et al., 2013). Together, these observations indicate that the syn-

ergistic effect of anti-CTLA-4 and anti-PD-1 in clinical trials (Larkin et al., 2015; Wolchok et al., 2013) is unlikely to occur through the simultaneous targeting of inhibitory molecules on the same cell.

In addition to inhibitory receptors, PD-1⁺ cells can also express costimulatory molecules such as CD28, which is critical during the activation of naive T cells and enhances cytokine secretion (Bour-Jordan et al., 2011; Watts, 2010). Recently, it was demonstrated that PD-1/PD-L1 signaling suppresses T cell functionality via inactivation of CD28 signaling rather than TCR signaling (Hui et al., 2017). Furthermore, the effect of PD-1 blockade was abrogated by conditional gene deletion of CD28 in a mouse model of chronic infection (Kamphorst et al., 2017), indicating that the CD28/B7 pathway may play a crucial role in the efficacy of anti-PD-1 treatment. CD28, among other costimulatory molecules such as ICOS, is also expressed on the LCMV-specific CXCR5⁺ PD-1^{int} T cells that mediate response to PD-1 therapy in mouse models (Im et al., 2016).

A synergistic effect of combined targeting of inhibitory and costimulatory molecules in reinvigorating tumor-specific T cells has been implied in other studies. CD137 (or 4-1BB) is a member of the TNFR family that is expressed on recently activated T cells (Pollok et al., 1993). Combination of PD-1 blockade with agonistic anti-CD137 antibodies increases tumor control in murine models, while also enhancing T cell reactivity to tumor antigens as well as effector/memory T cell formation (Chen et al., 2015; Wei et al., 2013, 2014). OX40 is another TNFR family member that is expressed on activated CD4⁺ T cells and, at lower levels, also on CD8⁺ T cells after recent TCR engagement (Croft, 2010). OX40 agonists have been shown to promote antitumor immunity in immunogenic mouse tumor models, while failing to exert tumor control in poorly immunogenic tumor models (Kjaergaard et al., 2000; Weinberg et al., 2000). Conceptually, the combination of OX40 agonists with therapies targeting inhibitory receptors on T cells would be an attractive approach to reactivate dysfunctional T cells in such tumors. However, recent data suggest that addition of PD-1 blockade to an OX40 agonist in a vaccination setting can actually abrogate the antitumor effect of OX40 monotherapy, by reducing TIL infiltration and enhancing activation-induced cell death of tumor-reactive CD8⁺ T cells (Shrimali et al., 2017). It is difficult to predict whether a similar deleterious effect would also take place in human cancer, in which T cell priming may have occurred many years before. However, the data do highlight that it will be crucial to investigate the timing of different immunotherapeutic interventions, to avoid similar negative effects due to T cell overstimulation. As a second word of caution, positive clinical data on immunotherapy combinations are presently still limited, and it is unclear whether the encouraging data obtained in *in vitro* and *in vivo* models will be recapitulated in cancer patients. Over the next few years, the results from ongoing early clinical trials that investigate antibodies targeting many of these inhibitory and costimulatory molecules—including additional targets such as GITR, ICOS, and CD27—as monotherapies or in combination with anti-PD-1/PD-L1, should reveal how these agents should be combined and which dysfunctional states might best be targeted by them.

Epigenetic Imprinting of Dysfunction

An additional T cell-intrinsic parameter that may influence the efficacy of immunotherapeutic intervention is the durability of

reinvigoration of dysfunctional T cells upon therapy. Observations from chronic viral infection indicate a prominent role for differences in methylation of *PDCD1* (encoding PD-1) in sustaining dysfunction. While the PD-1 transcriptional regulatory region is only transiently demethylated in activated T cells, it remains demethylated in exhausted T cells, resulting in prolonged expression of PD-1 (Ahn et al., 2016; Youngblood et al., 2011, 2013). This altered methylation pattern is maintained even after viral clearance to undetectable levels. Recent work reported the existence of low avidity T cell clones within the Melan-A-specific TIL population in human melanoma that are unable to express PD-1 due to continued methylation of the *PDCD1* promoter even upon TCR stimulation. In contrast, antigen-specific T cells of high functional avidity within the same TIL population did express PD-1, thereby confirming a link between the strength of TCR signaling, modification of the *PDCD1* locus, and PD-1 expression (Simon et al., 2016). When Melan-A-specific TILs were expanded *in vitro* in the presence of anti-PD-1 antibodies, the T cell repertoire was skewed toward higher avidity T cell clonotypes. In addition to the sustained demethylation of *PDCD1*, dysfunctional T cells also progressively acquire *de novo* methylation of genes associated with effector functions during both infections and tumor development, which could not be reverted by PD-1 blockade (Ghoneim et al., 2017). Of note, blockade of these exhaustion-associated methylation programs increased T cell responses and tumor control upon PD-1 blockade in murine tumor models.

On a related note, several reports have recently demonstrated that dysfunctional T cells display specific alterations in chromatin accessibility. Part of this chromatin remodeling is likely driven by the initial antigen stimulation as based on the overlap in chromatin accessibility patterns among effector, memory, and exhausted T cells (Scott-Browne et al., 2016). This notion is further supported by the observation that a fixed state of dysfunction was only induced in tumor-specific T cells, when tumor-specific and bystander T cells were co-transferred in a murine liver cancer model (Schietinger et al., 2016). Thus, micro-environmental factors were not sufficient to induce this fixed exhausted state by themselves, but appear to shape the effects of TCR triggering on intratumoral T cells. Next to the chromatin remodeling patterns that are shared with effector and memory T cells, dysfunctional T cells also display changes in chromatin accessible regions that are specific to these cells. For instance, exhausted T cells in chronic LCMV infection showed additional accessible regions in the *PDCD1* locus and lacked several open regions in the *IFNG* locus that were present in functional T cells (Pauken et al., 2016; Sen et al., 2016). Of note, many of these accessible regions specific to the exhausted state are retained after anti-PD-1 treatment, indicating that this therapy only induces minor epigenetic remodeling (Pauken et al., 2016). In line with this observation, exhausted virus-specific T cells that have regained effector functions upon PD-L1 blockade could not undergo memory development after viral antigen clearance and became dysfunctional again when the infection persisted. A similar observation was made in a murine tumor model, in which both tumor antigen-specific and bystander T cells were adoptively transferred and gene expression as well as chromatin accessibility were compared (Mognol et al., 2017). Only tumor-specific T cells acquired characteristics of dysfunction and, while displaying improved effector functions upon treatment with anti-

PD-L1 therapy, these cells showed only very limited alterations in chromatin accessibility patterns.

Interestingly, the imprinting of this epigenetic state already starts early during exhaustion, as T cells from premalignant lesions harbor many of the alterations found in exhausted T cells in late-stage tumors or metastases in a murine liver cancer model (Schietinger et al., 2016). This progression from mild exhaustion in early tumor lesions to more severe exhaustion in advanced tumors is reflected by two distinct chromatin states. Whereas the chromatin state of early dysfunctional TILs still displays some plasticity and can be reprogrammed by PD-1/PD-L1 blockade, the later state is fixed and cannot be altered by anti-PD-1 therapy (Philip et al., 2017). Strikingly, the chromatin accessibility state of PD-1^{hi} CD8⁺ TILs from human NSCLC was largely overlapping with that of murine late-stage TILs. Hence, also in human tumors PD-1/PD-L1 blockade might only induce transcriptional rewiring due to increased binding of transcription factors to accessible chromatin regions in the more severely dysfunctional T cells, rather than a change in chromatin accessibility patterns themselves. *In vitro* treatment with histone deacetylase inhibitors has been shown to lead to significantly improved effector functions and memory transition in adoptively transferred exhausted LCMV clone 13-specific T cells (Zhang et al., 2014). Whether this effect is observed on all exhausted T cells and leads to a durable reinvigoration of these cells in combination with PD-1 blockade needs to be further investigated.

Therapy-Induced Resistance and T Cell Dysfunction

Cancer immunotherapy-induced resistance can in some patients be explained by tumor-intrinsic alterations, such as defects in the antigen-presentation machinery or inactivation of the IFN γ signaling pathway (Patel et al., 2017; Restifo et al., 1996; Zaretsky et al., 2016). In addition, therapy-induced changes in the functional state of TILs have been suggested to form a cause of resistance to both targeted treatments and immunotherapy. For instance, genomic and non-genomic alterations evolving in BRAF-mutated melanoma upon treatment with MAPK inhibitors co-developed with dysfunction of CD8⁺ T cells in a subset of resistant tumors. Of note, this often correlated with an enhanced expression of an inflammation signature associated with M2 macrophages that are known to antagonize T cell recruitment and effector function (Hugo et al., 2015). Direct evidence that these changes play a major role in the observed resistance is however currently lacking. Upon adoptive transfer of MART-1 TCR-transduced T cells in patients with advanced melanoma, a change in the functional phenotype of the T cells has been observed at the time of relapse (Ma et al., 2013). Specifically, TCR-transgenic T cells either completely lost their initial cytotoxic activity or acquired a distinct functional profile with secretion of inflammatory cytokines, but lack of cytotoxicity.

Therapy-induced reinvigoration of tumor-specific T cell responses may be expected to in some cases induce the further development of T cell dysfunction. In particular, the IFN γ secretion that occurs as a consequence of T cell reactivation may induce immunosuppressive counterbalance mechanisms (Figure 1). In addition, the IFN γ -induced increase in MHC expression could also increase the TCR signal that contributes to T cell dysfunction. Recent evidence from a study comparing longitudinal samples from immunocompetent versus immunodeficient murine colon cancer models indicated that immune pressure on tumor cells induced two major tumor escape mechanisms that

involved the accumulation of immunosuppressive cell populations, such as Tregs, and the increased expression of multiple inhibitory receptors on T cells (Efremova et al., 2018). The upregulation of alternative immune checkpoints has also been postulated as a possible resistance mechanism upon anti-PD-1 therapy. Data from HNSCC indicated that PD-1 blockade of TILs *in vitro* as well as in a murine tumor model led to upregulation of Tim-3. Of note, combined blockade of both receptors significantly increased antitumor activity in this model (Shayan et al., 2017). Another study described increased TIGIT expression on NY-ESO-1-specific CD8⁺ T cells upon PD-1 blockade *in vitro* (Chauvin et al., 2015). Upregulation of multiple alternative immune checkpoints including Tim-3, Lag-3, and CTLA-4 upon anti-PD-1 resistance was also observed in a murine lung cancer model (Koyama et al., 2016). Direct evidence of whether this expression of alternative immune checkpoints truly represents a mechanism of resistance, or simply reflects a more activated state of these T cells upon reinvigoration by immunotherapy, is difficult to obtain. However, support for the former model comes from work that assessed resistance to CTLA-4 blockade and radiation in a murine melanoma model (Benci et al., 2016). In these experiments, therapy resistance was accompanied by expression of multiple inhibitory receptor ligands on tumor cells and high inhibitory receptor expression on T cells. While triple or quadruple immune checkpoint blockade combinations were necessary to significantly improve treatment response in resistant tumors, knockout of tumor type I and/or II interferon signaling allowed for response to anti-PD-1 or anti-CTLA-4 monotherapy. To evaluate whether alterations in the dysfunctional state are also important in mediating immunotherapy resistance in cancer patients, studies comparing monotherapy and combination therapy at the start of treatment versus the moment of resistance will be of value.

Conclusions

Dysfunctional tumor-specific T cells display a broad spectrum of cell states that are induced by persistent TCR triggering, but that are additionally influenced by T cell-intrinsic and -extrinsic factors. While traits of their core exhaustion signature are shared with T cells in chronic viral infection, intratumoral T cell dysfunction is further sculpted by the multifaceted immunosuppressive processes ongoing in the TME, which can be expected to deviate from those present at chronically infected sites (Figure 1). This leads to heterogeneous (dys-)functional states between and within tumors, shaped by inhibitory and costimulatory signals from immune, stromal, and cancer cells, but also by gradients of suppressive soluble mediators, metabolic factors, and hypoxia. In order to restore antitumor immunity, an understanding of the processes that drive and maintain these different dysfunctional T cell states is essential. Novel technologies that allow characterization of these cells at the single cell level, in combination with assessment of tumor reactivity and spatial organization within the tumor, will be of value to achieve this goal and thereby support the development of personalized therapeutic strategies to target dysfunctional T cells.

ACKNOWLEDGMENTS

This work was supported by a Swiss National Science Foundation grant (P300PB_164755/1) to D.S.T. and ERC AdG SENSIT to T.N.S.

REFERENCES

- Agnellini, P., Wolint, P., Rehr, M., Cahenzli, J., Karrer, U., and Oxenius, A. (2007). Impaired NFAT nuclear translocation results in split exhaustion of virus-specific CD8⁺ T cell functions during chronic viral infection. *Proc. Natl. Acad. Sci. USA* *104*, 4565–4570.
- Ahmadzadeh, M., Johnson, L.A., Heemskerck, B., Wunderlich, J.R., Dudley, M.E., White, D.E., and Rosenberg, S.A. (2009). Tumor antigen-specific CD8 T cells infiltrating the tumor express high levels of PD-1 and are functionally impaired. *Blood* *114*, 1537–1544.
- Ahn, E., Youngblood, B., Lee, J., Lee, J., Sarkar, S., and Ahmed, R. (2016). Demethylation of the PD-1 promoter is imprinted during the effector phase of CD8 T cell exhaustion. *J. Virol.* *90*, 8934–8946.
- Alexandrov, L.B., Nik-Zainal, S., Wedge, D.C., Aparicio, S.A., Behjati, S., Biankin, A.V., Bignell, G.R., Bolli, N., Borg, A., Borresen-Dale, A.L., et al. (2013). Signatures of mutational processes in human cancer. *Nature* *500*, 415–421.
- Altman, B.J., Stine, Z.E., and Dang, C.V. (2016). From Krebs to clinic: glutamine metabolism to cancer therapy. *Nat. Rev. Cancer* *16*, 749.
- Anderson, A.C., Joller, N., and Kuchroo, V.K. (2016). Lag-3, Tim-3, and TIGIT: Co-inhibitory receptors with specialized functions in immune regulation. *Immunity* *44*, 989–1004.
- Ansel, K.M., Ngo, V.N., Hyman, P.L., Luther, S.A., Forster, R., Sedgwick, J.D., Browning, J.L., Lipp, M., and Cyster, J.G. (2000). A chemokine-driven positive feedback loop organizes lymphoid follicles. *Nature* *406*, 309–314.
- Baitsch, L., Baumgaertner, P., Devevre, E., Raghav, S.K., Legat, A., Barba, L., Wieckowski, S., Bouzourene, H., Deplancke, B., Romero, P., et al. (2011). Exhaustion of tumor-specific CD8(+) T cells in metastases from melanoma patients. *J. Clin. Invest.* *121*, 2350–2360.
- Baitsch, L., Legat, A., Barba, L., Fuertes Marraco, S.A., Rivals, J.P., Baumgaertner, P., Christiansen-Jucht, C., Bouzourene, H., Rimoldi, D., Pircher, H., et al. (2012). Extended co-expression of inhibitory receptors by human CD8 T-cells depending on differentiation, antigen-specificity and anatomical localization. *PLoS One* *7*, e30852.
- Balar, A.V., Galsky, M.D., Rosenberg, J.E., Powles, T., Petrylak, D.P., Bellmunt, J., Loriot, Y., Necchi, A., Hoffman-Censits, J., Perez-Gracia, J.L., et al. (2017). Atezolizumab as first-line treatment in cisplatin-ineligible patients with locally advanced and metastatic urothelial carcinoma: a single-arm, multi-centre, phase 2 trial. *Lancet* *389*, 67–76.
- Bandura, D.R., Baranov, V.I., Ornatsky, O.I., Antonov, A., Kinach, R., Lou, X., Pavlov, S., Vorobiev, S., Dick, J.E., and Tanner, S.D. (2009). Mass cytometry: technique for real time single cell multitarget immunoassay based on inductively coupled plasma time-of-flight mass spectrometry. *Anal. Chem.* *81*, 6813–6822.
- Banerjee, A., Gordon, S.M., Intlekofer, A.M., Paley, M.A., Mooney, E.C., Lindsten, T., Wherry, E.J., and Reiner, S.L. (2010). Cutting edge: the transcription factor eomesodermin enables CD8⁺ T cells to compete for the memory cell niche. *J. Immunol.* *185*, 4988–4992.
- Benci, J.L., Xu, B., Qiu, Y., Wu, T.J., Dada, H., Twyman-Saint Victor, C., Cuculo, L., Lee, D.S.M., Pauken, K.E., Huang, A.C., et al. (2016). Tumor interferon signaling regulates a multigenic resistance program to immune checkpoint blockade. *Cell* *167*, 1540–1554.e12.
- Bensch, B., Johnson, A.L., Kurachi, M., Odorizzi, P.M., Pauken, K.E., Attanasio, J., Stelekati, E., McLane, L.M., Paley, M.A., Delgoffe, G.M., and Wherry, E.J. (2016). Bioenergetic insufficiencies due to metabolic alterations regulated by the inhibitory receptor PD-1 are an early driver of CD8(+) T cell exhaustion. *Immunity* *45*, 358–373.
- Bensch, B., Martin, B., and Thimme, R. (2014). Restoration of HBV-specific CD8⁺ T cell function by PD-1 blockade in inactive carrier patients is linked to T cell differentiation. *J. Hepatol.* *61*, 1212–1219.
- Blackburn, S.D., Shin, H., Freeman, G.J., and Wherry, E.J. (2008). Selective expansion of a subset of exhausted CD8 T cells by alphaPD-L1 blockade. *Proc. Natl. Acad. Sci. USA* *105*, 15016–15021.
- Blackburn, S.D., Shin, H., Haining, W.N., Zou, T., Workman, C.J., Polley, A., Betts, M.R., Freeman, G.J., Vignali, D.A., and Wherry, E.J. (2009). Coregulation of CD8⁺ T cell exhaustion by multiple inhibitory receptors during chronic viral infection. *Nat. Immunol.* *10*, 29–37.

- Blank, C.U., Haanen, J.B., Ribas, A., and Schumacher, T.N. (2016). CANCER IMMUNOLOGY. The “cancer immunogram”. *Science* 352, 658–660.
- Boon, T., Coulie, P.G., Van den Eynde, B.J., and van der Bruggen, P. (2006). Human T cell responses against melanoma. *Annu. Rev. Immunol.* 24, 175–208.
- Borghaei, H., Paz-Ares, L., Horn, L., Spigel, D.R., Steins, M., Ready, N.E., Chow, L.Q., Vokes, E.E., Felip, E., Holgado, E., et al. (2015). Nivolumab versus docetaxel in advanced nonsquamous non-small-cell lung cancer. *N. Engl. J. Med.* 373, 1627–1639.
- Bottino, C., Castriconi, R., Pende, D., Rivera, P., Nanni, M., Carnemolla, B., Cantoni, C., Grassi, J., Marcenaro, S., Reymond, N., et al. (2003). Identification of PVR (CD155) and Nectin-2 (CD112) as cell surface ligands for the human DNAM-1 (CD226) activating molecule. *J. Exp. Med.* 198, 557–567.
- Bour-Jordan, H., Esensten, J.H., Martinez-Llordella, M., Penaranda, C., Stumpf, M., and Bluestone, J.A. (2011). Intrinsic and extrinsic control of peripheral T-cell tolerance by costimulatory molecules of the CD28/B7 family. *Immunol. Rev.* 241, 180–205.
- Brahmer, J., Reckamp, K.L., Baas, P., Crino, L., Eberhardt, W.E., Poddubskaya, E., Antonia, S., Pluzanski, A., Vokes, E.E., Holgado, E., et al. (2015). Nivolumab versus docetaxel in advanced squamous-cell non-small-cell lung cancer. *N. Engl. J. Med.* 373, 123–135.
- Carr, E.L., Kelman, A., Wu, G.S., Gopaul, R., Senkevitch, E., Aghvanyan, A., Turay, A.M., and Frauwrith, K.A. (2010). Glutamine uptake and metabolism are coordinately regulated by ERK/MAPK during T lymphocyte activation. *J. Immunol.* 185, 1037–1044.
- Carstens, J.L., Correa de Sampaio, P., Yang, D., Barua, S., Wang, H., Rao, A., Allison, J.P., LeBleu, V.S., and Kalluri, R. (2017). Spatial computation of intratumoral T cells correlates with survival of patients with pancreatic cancer. *Nat. Commun.* 8, 15095.
- Castle, J.C., Kreiter, S., Diekmann, J., Lower, M., van de Roemer, N., de Graaf, J., Selmi, A., Diken, M., Boegel, S., Paret, C., et al. (2012). Exploiting the mutanome for tumor vaccination. *Cancer Res.* 72, 1081–1091.
- Chang, C.H., Curtis, J.D., Maggi, L.B., Jr., Faubert, B., Villarino, A.V., O’Sullivan, D., Huang, S.C., van der Windt, G.J., Blagih, J., Qiu, J., et al. (2013). Posttranscriptional control of T cell effector function by aerobic glycolysis. *Cell* 153, 1239–1251.
- Chang, C.H., Qiu, J., O’Sullivan, D., Buck, M.D., Noguchi, T., Curtis, J.D., Chen, Q., Gindin, M., Gubin, M.M., van der Windt, G.J., et al. (2015). Metabolic competition in the tumor microenvironment is a driver of cancer progression. *Cell* 162, 1229–1241.
- Chauvin, J.M., Pagliano, O., Fourcade, J., Sun, Z., Wang, H., Sander, C., Kirkwood, J.M., Chen, T.H., Maurer, M., Korman, A.J., and Zarour, H.M. (2015). TIGIT and PD-1 impair tumor antigen-specific CD8(+) T cells in melanoma patients. *J. Clin. Invest.* 125, 2046–2058.
- Chemnitz, J.M., Parry, R.V., Nichols, K.E., June, C.H., and Riley, J.L. (2004). SHP-1 and SHP-2 associate with immunoreceptor tyrosine-based switch motif of programmed death 1 upon primary human T cell stimulation, but only receptor ligation prevents T cell activation. *J. Immunol.* 173, 945–954.
- Chen, D.S., and Mellman, I. (2013). Oncology meets immunology: the cancer-immunity cycle. *Immunity* 39, 1–10.
- Chen, P.L., Roh, W., Reuben, A., Cooper, Z.A., Spencer, C.N., Prieto, P.A., Miller, J.P., Bassett, R.L., Gopalakrishnan, V., Wani, K., et al. (2016). Analysis of immune signatures in longitudinal tumor samples yields insight into biomarkers of response and mechanisms of resistance to immune checkpoint blockade. *Cancer Discov.* 6, 827–837.
- Chen, S., Lee, L.F., Fisher, T.S., Jessen, B., Elliott, M., Evering, W., Logronio, K., Tu, G.H., Tsaparikos, K., Li, X., et al. (2015). Combination of 4-1BB agonist and PD-1 antagonist promotes antitumor effector/memory CD8 T cells in a poorly immunogenic tumor model. *Cancer Immunol. Res.* 3, 149–160.
- Chevrier, S., Levine, J.H., Zanotelli, V.R.T., Silina, K., Schulz, D., Bacac, M., Ries, C.H., Ailles, L., Jewett, M.A.S., Moch, H., et al. (2017). An immune atlas of clear cell renal cell carcinoma. *Cell* 169, 736–749.e18.
- Choi, S.Y., Collins, C.C., Gout, P.W., and Wang, Y. (2013). Cancer-generated lactic acid: a regulatory, immunosuppressive metabolite? *J. Pathol.* 230, 350–355.
- Chung, W., Eum, H.H., Lee, H.O., Lee, K.M., Lee, H.B., Kim, K.T., Ryu, H.S., Kim, S., Lee, J.E., Park, Y.H., et al. (2017). Single-cell RNA-seq enables comprehensive tumour and immune cell profiling in primary breast cancer. *Nat. Commun.* 8, 15081.
- Croft, M. (2010). Control of immunity by the TNFR-related molecule OX40 (CD134). *Annu. Rev. Immunol.* 28, 57–78.
- Crotty, S. (2011). Follicular helper CD4 T cells (TFH). *Annu. Rev. Immunol.* 29, 621–663.
- Day, C.L., Kaufmann, D.E., Kiepiela, P., Brown, J.A., Moodley, E.S., Reddy, S., Mackey, E.W., Miller, J.D., Leslie, A.J., DePierres, C., et al. (2006). PD-1 expression on HIV-specific T cells is associated with T-cell exhaustion and disease progression. *Nature* 443, 350–354.
- Di Caro, G., Bergomas, F., Grizzi, F., Doni, A., Bianchi, P., Malesci, A., Laghi, L., Allavena, P., Mantovani, A., and Marchesi, F. (2014). Occurrence of tertiary lymphoid tissue is associated with T-cell infiltration and predicts better prognosis in early-stage colorectal cancers. *Clin. Cancer Res.* 20, 2147–2158.
- Dieu-Nosjean, M.C., Antoine, M., Danel, C., Heudes, D., Wislez, M., Poulot, V., Rabbe, N., Laurans, L., Tartour, E., de Chaisemartin, L., et al. (2008). Long-term survival for patients with non-small-cell lung cancer with intratumoral lymphoid structures. *J. Clin. Oncol.* 26, 4410–4417.
- Doedens, A.L., Phan, A.T., Stradner, M.H., Fujimoto, J.K., Nguyen, J.V., Yang, E., Johnson, R.S., and Goldrath, A.W. (2013). Hypoxia-inducible factors enhance the effector responses of CD8(+) T cells to persistent antigen. *Nat. Immunol.* 14, 1173–1182.
- Doering, T.A., Crawford, A., Angelosanto, J.M., Paley, M.A., Ziegler, C.G., and Wherry, E.J. (2012). Network analysis reveals centrally connected genes and pathways involved in CD8+ T cell exhaustion versus memory. *Immunity* 37, 1130–1144.
- Duraiswamy, J., Kaluza, K.M., Freeman, G.J., and Coukos, G. (2013). Dual blockade of PD-1 and CTLA-4 combined with tumor vaccine effectively restores T-cell rejection function in tumors. *Cancer Res.* 73, 3591–3603.
- Efremova, M., Rieder, D., Klepsch, V., Charoentong, P., Finotello, F., Hackl, H., Hermann-Kleiter, N., Lower, M., Baier, G., Krogsdam, A., and Trajanoski, Z. (2018). Targeting immune checkpoints potentiates immunoeediting and changes the dynamics of tumor evolution. *Nat. Commun.* 9, 32.
- Erkes, D.A., Smith, C.J., Wilski, N.A., Caldeira-Dantas, S., Mohgbeli, T., and Snyder, C.M. (2017). Virus-specific CD8+ T cells infiltrate melanoma lesions and retain function independently of pd-1 expression. *J. Immunol.* 198, 2979–2988.
- Fehlings, M., Simoni, Y., Penny, H.L., Becht, E., Loh, C.Y., Gubin, M.M., Ward, J.P., Wong, S.C., Schreiber, R.D., and Newell, E.W. (2017). Checkpoint blockade immunotherapy reshapes the high-dimensional phenotypic heterogeneity of murine intratumoural neoantigen-specific CD8(+) T cells. *Nat. Commun.* 8, 562.
- Fehrenbacher, L., Spira, A., Ballinger, M., Kowanzet, M., Vansteenkiste, J., Mazieres, J., Park, K., Smith, D., Ardal-Cortes, A., Lewanski, C., et al. (2016). Atezolizumab versus docetaxel for patients with previously treated non-small-cell lung cancer (POPLAR): a multicentre, open-label, phase 2 randomised controlled trial. *Lancet* 387, 1837–1846.
- Fernandez-Poma, S.M., Salas-Benito, D., Lozano, T., Casares, N., Riezu-Boj, J.I., Mancheno, U., Elizalde, E., Alighani, D., Zubeldia, N., Otano, I., et al. (2017). Expansion of tumor-infiltrating CD8+ T cells expressing PD-1 improves the efficacy of adoptive T-cell therapy. *Cancer Res.* 77, 3672–3684.
- Fischer, K., Hoffmann, P., Voelkl, S., Meidenbauer, N., Ammer, J., Edinger, M., Gottfried, E., Schwarz, S., Rothe, G., Hoves, S., et al. (2007). Inhibitory effect of tumor cell-derived lactic acid on human T cells. *Blood* 109, 3812–3819.
- Fourcade, J., Sun, Z., Benallaoua, M., Guillaume, P., Luescher, I.F., Sander, C., Kirkwood, J.M., Kuchroo, V., and Zarour, H.M. (2010). Upregulation of Tim-3 and PD-1 expression is associated with tumor antigen-specific CD8+ T cell dysfunction in melanoma patients. *J. Exp. Med.* 207, 2175–2186.
- Frauwrith, K.A., Riley, J.L., Harris, M.H., Parry, R.V., Rathmell, J.C., Plas, D.R., Elstrom, R.L., June, C.H., and Thompson, C.B. (2002). The CD28 signaling pathway regulates glucose metabolism. *Immunity* 16, 769–777.
- Fridman, W.H., Pages, F., Sautes-Fridman, C., and Galon, J. (2012). The immune contexture in human tumours: impact on clinical outcome. *Nat. Rev. Cancer* 12, 298–306.

- Fridman, W.H., Zitvogel, L., Sautes-Fridman, C., and Kroemer, G. (2017). The immune contexture in cancer prognosis and treatment. *Nat. Rev. Clin. Oncol.* *14*, 717–734.
- Fuertes Marraco, S.A., Neubert, N.J., Verdeil, G., and Speiser, D.E. (2015). Inhibitory receptors beyond T cell exhaustion. *Front. Immunol.* *6*, 310.
- Gabrilovich, D., Ishida, T., Oyama, T., Ran, S., Kravtsov, V., Nadaf, S., and Corbone, D.P. (1998). Vascular endothelial growth factor inhibits the development of dendritic cells and dramatically affects the differentiation of multiple hematopoietic lineages in vivo. *Blood* *92*, 4150–4166.
- Gajewski, T.F., Schreiber, H., and Fu, Y.X. (2013). Innate and adaptive immune cells in the tumor microenvironment. *Nat. Immunol.* *14*, 1014–1022.
- Ghoneim, H.E., Fan, Y., Moustaki, A., Abdelsamed, H.A., Dash, P., Dogra, P., Carter, R., Awad, W., Neale, G., Thomas, P.G., and Youngblood, B. (2017). De novo epigenetic programs inhibit PD-1 blockade-mediated T cell rejuvenation. *Cell* *170*, 142–157.e19.
- Giesen, C., Wang, H.A., Schapiro, D., Zivanovic, N., Jacobs, A., Hattendorf, B., Schuffler, P.J., Grolimund, D., Buhmann, J.M., Brandt, S., et al. (2014). Highly multiplexed imaging of tumor tissues with subcellular resolution by mass cytometry. *Nat. Methods* *11*, 417–422.
- Giordano, M., Henin, C., Maurizio, J., Imbratta, C., Bourdely, P., Buferne, M., Baitsch, L., Vanhille, L., Sieweke, M.H., Speiser, D.E., et al. (2015). Molecular profiling of CD8 T cells in autochthonous melanoma identifies Maf as driver of exhaustion. *EMBO J.* *34*, 2042–2058.
- Goc, J., Germain, C., Vo-Bourgais, T.K., Lupo, A., Klein, C., Knockaert, S., de Chaisemartin, L., Ouakrim, H., Becht, E., Alifano, M., et al. (2014). Dendritic cells in tumor-associated tertiary lymphoid structures signal a Th1 cytotoxic immune contexture and license the positive prognostic value of infiltrating CD8+ T cells. *Cancer Res.* *74*, 705–715.
- Gropper, Y., Feferman, T., Shalit, T., Salame, T.M., Porat, Z., and Shakhar, G. (2017). Culturing CTLs under hypoxic conditions enhances their cytotoxicity and improves their anti-tumor function. *Cell Rep.* *20*, 2547–2555.
- Gros, A., Parkhurst, M.R., Tran, E., Pasetto, A., Robbins, P.F., Ilyas, S., Prickett, T.D., Gartner, J.J., Crystal, J.S., Roberts, I.M., et al. (2016). Prospective identification of neoantigen-specific lymphocytes in the peripheral blood of melanoma patients. *Nat. Med.* *22*, 433–438.
- Gros, A., Robbins, P.F., Yao, X., Li, Y.F., Turcotte, S., Tran, E., Wunderlich, J.R., Mixon, A., Farid, S., Dudley, M.E., et al. (2014). PD-1 identifies the patient-specific CD8(+) tumor-reactive repertoire infiltrating human tumors. *J. Clin. Invest.* *124*, 2246–2259.
- Grosso, J.F., Goldberg, M.V., Getnet, D., Bruno, T.C., Yen, H.R., Pyle, K.J., Hipkiss, E., Vignali, D.A., Pardoll, D.M., and Drake, C.G. (2009). Functionally distinct LAG-3 and PD-1 subsets on activated and chronically stimulated CD8 T cells. *J. Immunol.* *182*, 6659–6669.
- Hall, A., Meyle, K.D., Lange, M.K., Klima, M., Sanderhoff, M., Dahl, C., Abildgaard, C., Thorup, K., Moghimi, S.M., Jensen, P.B., et al. (2013). Dysfunctional oxidative phosphorylation makes malignant melanoma cells addicted to glycolysis driven by the (V600E)BRAF oncogene. *Oncotarget* *4*, 584–599.
- Haq, R., Shoag, J., Andreu-Perez, P., Yokoyama, S., Edelman, H., Rowe, G.C., Frederick, D.T., Hurley, A.D., Nellore, A., Kung, A.L., et al. (2013). Oncogenic BRAF regulates oxidative metabolism via PGC1alpha and MITF. *Cancer Cell* *23*, 302–315.
- He, R., Hou, S., Liu, C., Zhang, A., Bai, Q., Han, M., Yang, Y., Wei, G., Shen, T., Yang, X., et al. (2016). Follicular CXCR5-expressing CD8+ T cells curtail chronic viral infection. *Nature* *537*, 412–428.
- Heindl, A., Nawaz, S., and Yuan, Y. (2015). Mapping spatial heterogeneity in the tumor microenvironment: a new era for digital pathology. *Lab. Invest.* *95*, 377–384.
- Ho, P.C., Bihuniak, J.D., Macintyre, A.N., Staron, M., Liu, X., Amezquita, R., Tsui, Y.C., Cui, G., Micevic, G., Perales, J.C., et al. (2015). Phosphoenolpyruvate is a metabolic checkpoint of anti-tumor T cell responses. *Cell* *162*, 1217–1228.
- Hodi, F.S., O'Day, S.J., McDermott, D.F., Weber, R.W., Sosman, J.A., Haanen, J.B., Gonzalez, R., Robert, C., Schadendorf, D., Hassel, J.C., et al. (2010). Improved survival with ipilimumab in patients with metastatic melanoma. *N. Engl. J. Med.* *363*, 711–723.
- Hugo, W., Shi, H., Sun, L., Piva, M., Song, C., Kong, X., Moriceau, G., Hong, A., Dahlman, K.B., Johnson, D.B., et al. (2015). Non-genomic and immune evolution of melanoma acquiring MAPKi resistance. *Cell* *162*, 1271–1285.
- Hui, E., Cheung, J., Zhu, J., Su, X., Taylor, M.J., Wallweber, H.A., Sasmal, D.K., Huang, J., Kim, J.M., Mellman, I., and Vale, R.D. (2017). T cell costimulatory receptor CD28 is a primary target for PD-1-mediated inhibition. *Science* *355*, 1428–1433.
- Im, S.J., Hashimoto, M., Gerner, M.Y., Lee, J., Kissick, H.T., Burger, M.C., Shan, Q., Hale, J.S., Lee, J., Nasti, T.H., et al. (2016). Defining CD8+ T cells that provide the proliferative burst after PD-1 therapy. *Nature* *537*, 417–421.
- Intlekofer, A.M., Takemoto, N., Wherry, E.J., Longworth, S.A., Northrup, J.T., Palanivel, V.R., Mullen, A.C., Gasink, C.R., Kaech, S.M., Miller, J.D., et al. (2005). Effector and memory CD8+ T cell fate coupled by T-bet and eomesodermin. *Nat. Immunol.* *6*, 1236–1244.
- Jin, H.T., Anderson, A.C., Tan, W.G., West, E.E., Ha, S.J., Araki, K., Freeman, G.J., Kuchroo, V.K., and Ahmed, R. (2010). Cooperation of Tim-3 and PD-1 in CD8 T-cell exhaustion during chronic viral infection. *Proc. Natl. Acad. Sci. USA* *107*, 14733–14738.
- Johnston, R.J., Comps-Agrar, L., Hackney, J., Yu, X., Huseni, M., Yang, Y., Park, S., Javinal, V., Chiu, H., Irving, B., et al. (2014). The immunoreceptor TIGIT regulates antitumor and antiviral CD8(+) T cell effector function. *Cancer Cell* *26*, 923–937.
- Julliard, W., Fechner, J.H., and Mezrich, J.D. (2014). The aryl hydrocarbon receptor meets immunology: friend or foe? A little of both. *Front. Immunol.* *5*, 458.
- Kamphorst, A.O., Wieland, A., Nasti, T., Yang, S., Zhang, R., Barber, D.L., Konieczny, B.T., Daugherty, C.Z., Koenig, L., Yu, K., et al. (2017). Rescue of exhausted CD8 T cells by PD-1-targeted therapies is CD28-dependent. *Science* *355*, 1423–1427.
- Kao, C., Oestreich, K.J., Paley, M.A., Crawford, A., Angelosanto, J.M., Ali, M.A., Intlekofer, A.M., Boss, J.M., Reiner, S.L., Weinmann, A.S., and Wherry, E.J. (2011). Transcription factor T-bet represses expression of the inhibitory receptor PD-1 and sustains virus-specific CD8+ T cell responses during chronic infection. *Nat. Immunol.* *12*, 663–671.
- Kato, Y., Ozawa, S., Miyamoto, C., Maehata, Y., Suzuki, A., Maeda, T., and Baba, Y. (2013). Acidic extracellular microenvironment and cancer. *Cancer Cell Int.* *13*, 89.
- Khalili, J.S., Liu, S., Rodriguez-Cruz, T.G., Whittington, M., Wardell, S., Liu, C., Zhang, M., Cooper, Z.A., Frederick, D.T., Li, Y., et al. (2012). Oncogenic BRAF(V600E) promotes stromal cell-mediated immunosuppression via induction of interleukin-1 in melanoma. *Clin. Cancer Res.* *18*, 5329–5340.
- Kim, H.J., Verbinnen, B., Tang, X., Lu, L., and Cantor, H. (2010). Inhibition of follicular T-helper cells by CD8(+) regulatory T cells is essential for self tolerance. *Nature* *467*, 328–332.
- Kjaergaard, J., Tanaka, J., Kim, J.A., Rothchild, K., Weinberg, A., and Shu, S. (2000). Therapeutic efficacy of OX-40 receptor antibody depends on tumor immunogenicity and anatomic site of tumor growth. *Cancer Res.* *60*, 5514–5521.
- Koyama, S., Akbay, E.A., Li, Y.Y., Herter-Sprrie, G.S., Buczkowski, K.A., Richards, W.G., Gandhi, L., Redig, A.J., Rodig, S.J., Asahina, H., et al. (2016). Adaptive resistance to therapeutic PD-1 blockade is associated with upregulation of alternative immune checkpoints. *Nat. Commun.* *7*, 10501.
- Kroeger, D.R., Milne, K., and Nelson, B.H. (2016). Tumor-infiltrating plasma cells are associated with tertiary lymphoid structures, cytolytic T-cell responses, and superior prognosis in ovarian cancer. *Clin. Cancer Res.* *22*, 3005–3015.
- Kronke, M.A., Eto, D., Locci, M., Cho, M., Davidson, T., Haddad, E.K., and Crotty, S. (2012). Bcl6 and Maf cooperate to instruct human follicular helper CD4 T cell differentiation. *J. Immunol.* *188*, 3734–3744.
- Krummel, M.F., and Allison, J.P. (1995). CD28 and CTLA-4 have opposing effects on the response of T cells to stimulation. *J. Exp. Med.* *182*, 459–465.
- Kuchroo, V.K., Anderson, A.C., and Petrovas, C. (2014). Coinhibitory receptors and CD8 T cell exhaustion in chronic infections. *Curr. Opin. HIV AIDS* *9*, 439–445.

- Kurtulus, S., Sakuishi, K., Ngjow, S.F., Joller, N., Tan, D.J., Teng, M.W., Smyth, M.J., Kuchroo, V.K., and Anderson, A.C. (2015). TIGIT predominantly regulates the immune response via regulatory T cells. *J. Clin. Invest.* **125**, 4053–4062.
- Kvistborg, P., Philips, D., Kelderman, S., Hageman, L., Ottensmeier, C., Joseph-Pietras, D., Welters, M.J., van der Burg, S., Kapiteijn, E., Michielin, O., et al. (2014). Anti-CTLA-4 therapy broadens the melanoma-reactive CD8+ T cell response. *Sci. Transl. Med.* **6**, 254ra128.
- Kvistborg, P., Shu, C.J., Heemskerck, B., Fankhauser, M., Thru, C.A., Toebes, M., van Rooij, N., Linnemann, C., van Buuren, M.M., Urbanus, J.H., et al. (2012). TIL therapy broadens the tumor-reactive CD8(+) T cell compartment in melanoma patients. *Oncoimmunology* **1**, 409–418.
- Larkin, J., Chiarion-Sileni, V., Gonzalez, R., Grob, J.J., Cowey, C.L., Lao, C.D., Schadendorf, D., Dummer, R., Smylie, M., Rutkowski, P., et al. (2015). Combined nivolumab and ipilimumab or monotherapy in untreated melanoma. *N. Engl. J. Med.* **373**, 23–34.
- Lavin, Y., Kobayashi, S., Leader, A., Amir, E.D., Elefant, N., Bigenwald, C., Remark, R., Sweeney, R., Becker, C.D., Levine, J.H., et al. (2017). Innate immune landscape in early lung adenocarcinoma by paired single-cell analyses. *Cell* **169**, 750–765.e17.
- Legat, A., Speiser, D.E., Pircher, H., Zehn, D., and Furtak, S.A. (2013). Inhibitory receptor expression depends more dominantly on differentiation and activation than “exhaustion” of human CD8 T cells. *Front. Immunol.* **4**, 455.
- Li, J., Shayan, G., Avery, L., Jie, H.B., Gildener-Leapman, N., Schmitt, N., Lu, B.F., Kane, L.P., and Ferris, R.L. (2016). Tumor-infiltrating Tim-3+ T cells proliferate avidly except when PD-1 is co-expressed: evidence for intracellular cross talk. *Oncoimmunology* **5**, e1200778.
- Lind, D.S. (2004). Arginine and cancer. *J. Nutr.* **134**, 2837S–2841S, discussion 2853S.
- Lu, X., Yang, L., Yao, D., Wu, X., Li, J., Liu, X., Deng, L., Huang, C., Wang, Y., Li, D., and Liu, J. (2017). Tumor antigen-specific CD8+ T cells are negatively regulated by PD-1 and Tim-3 in human gastric cancer. *Cell. Immunol.* **313**, 43–51.
- Ma, C., Cheung, A.F., Chodon, T., Koya, R.C., Wu, Z., Ng, C., Avramis, E., Cochran, A.J., Witte, O.N., Baltimore, D., et al. (2013). Multifunctional T-cell analyses to study response and progression in adoptive cell transfer immunotherapy. *Cancer Discov.* **3**, 418–429.
- MacIver, N.J., Michalek, R.D., and Rathmell, J.C. (2013). Metabolic regulation of T lymphocytes. *Annu. Rev. Immunol.* **31**, 259–283.
- Martinez-Outschoorn, U.E., Peiris-Pages, M., Pestell, R.G., Sotgia, F., and Lisanti, M.P. (2017). Cancer metabolism: a therapeutic perspective. *Nat. Rev. Clin. Oncol.* **14**, 11–31.
- Matsushita, H., Vesely, M.D., Koboldt, D.C., Rickert, C.G., Uppaluri, R., Magrini, V.J., Arthur, C.D., White, J.M., Chen, Y.S., Shea, L.K., et al. (2012). Cancer exome analysis reveals a T-cell-dependent mechanism of cancer immunoeediting. *Nature* **482**, 400–404.
- Matsuzaki, J., Gnjatich, S., Mhawech-Fauceglia, P., Beck, A., Miller, A., Tsuji, T., Eppolito, C., Qian, F., Lele, S., Shrikant, P., et al. (2010). Tumor-infiltrating NY-ESO-1-specific CD8+ T cells are negatively regulated by LAG-3 and PD-1 in human ovarian cancer. *Proc. Natl. Acad. Sci. USA* **107**, 7875–7880.
- McGranahan, N., Furness, A.J., Rosenthal, R., Ramskov, S., Lyngaa, R., Saini, S.K., Jamal-Hanjani, M., Wilson, G.A., Birkbak, N.J., Hiley, C.T., et al. (2016). Clonal neoantigens elicit T cell immunoreactivity and sensitivity to immune checkpoint blockade. *Science* **351**, 1463–1469.
- Medaglia, C., Giladi, A., Stoler-Barak, L., De Giovanni, M., Salame, T.M., Biram, A., David, E., Li, H., Iannacone, M., Shulman, Z., and Amit, I. (2017). Spatial reconstruction of immune niches by combining photoactivatable reporters and scRNA-seq. *Science* **358**, 1622–1626.
- Mellman, I., Coukos, G., and Dranoff, G. (2011). Cancer immunotherapy comes of age. *Nature* **480**, 480–489.
- Mognol, G.P., Spreafico, R., Wong, V., Scott-Browne, J.P., Togher, S., Hoffmann, A., Hogan, P.G., Rao, A., and Trifari, S. (2017). Exhaustion-associated regulatory regions in CD8(+) tumor-infiltrating T cells. *Proc. Natl. Acad. Sci. USA* **114**, E2776–E2785.
- Motzer, R.J., Escudier, B., McDermott, D.F., George, S., Hammers, H.J., Srinivas, S., Tykodi, S.S., Sosman, J.A., Procopio, G., Plimack, E.R., et al. (2015). Nivolumab versus everolimus in advanced renal-cell carcinoma. *N. Engl. J. Med.* **373**, 1803–1813.
- Munder, M., Choi, B.S., Rogers, M., and Kropf, P. (2009). L-arginine deprivation impairs Leishmania major-specific T-cell responses. *Eur. J. Immunol.* **39**, 2161–2172.
- Muul, L.M., Spiess, P.J., Director, E.P., and Rosenberg, S.A. (1987). Identification of specific cytolytic immune responses against autologous tumor in humans bearing malignant melanoma. *J. Immunol.* **138**, 989–995.
- Nagarsheth, N., Wicha, M.S., and Zou, W. (2017). Chemokines in the cancer microenvironment and their relevance in cancer immunotherapy. *Nat. Rev. Immunol.* **17**, 559–572.
- Odorizzi, P.M., Pauken, K.E., Paley, M.A., Sharpe, A., and Wherry, E.J. (2015). Genetic absence of PD-1 promotes accumulation of terminally differentiated exhausted CD8+ T cells. *J. Exp. Med.* **212**, 1125–1137.
- Ornatsky, O., Bandura, D., Baranov, V., Nitz, M., Winnik, M.A., and Tanner, S. (2010). Highly multiparametric analysis by mass cytometry. *J. Immunol. Methods* **361**, 1–20.
- Paley, M.A., Kroy, D.C., Odorizzi, P.M., Johnnidis, J.B., Dolfi, D.V., Barnett, B.E., Bikoff, E.K., Robertson, E.J., Lauer, G.M., Reiner, S.L., and Wherry, E.J. (2012). Progenitor and terminal subsets of CD8+ T cells cooperate to contain chronic viral infection. *Science* **338**, 1220–1225.
- Park, B.V., Freeman, Z.T., Ghasemzadeh, A., Chattergoon, M.A., Rutebemberwa, A., Steigner, J., Winter, M.E., Huynh, T.V., Sebald, S.M., Lee, S.J., et al. (2016). TGFbeta1-mediated SMAD3 enhances PD-1 expression on antigen-specific T cells in cancer. *Cancer Discov.* **6**, 1366–1381.
- Parry, R.V., Chemnitz, J.M., Frauwirth, K.A., Lanfranco, A.R., Braunstein, I., Kobayashi, S.V., Linsley, P.S., Thompson, C.B., and Riley, J.L. (2005). CTLA-4 and PD-1 receptors inhibit T-cell activation by distinct mechanisms. *Mol. Cell. Biol.* **25**, 9543–9553.
- Pasetto, A., Gros, A., Robbins, P.F., Deniger, D.C., Prickett, T.D., Matus-Niodemos, R., Douek, D.C., Howie, B., Robins, H., Parkhurst, M.R., et al. (2016). Tumor- and neoantigen-reactive T-cell receptors can be identified based on their frequency in fresh tumor. *Cancer Immunol. Res.* **4**, 734–743.
- Patel, S.J., Sanjana, N.E., Kishton, R.J., Eidzadeh, A., Vodnala, S.K., Cam, M., Gartner, J.J., Jia, L., Steinberg, S.M., Yamamoto, T.N., et al. (2017). Identification of essential genes for cancer immunotherapy. *Nature* **548**, 537–542.
- Pauken, K.E., Sammons, M.A., Odorizzi, P.M., Manne, S., Godec, J., Khan, O., Drake, A.M., Chen, Z., Sen, D.R., Kurachi, M., et al. (2016). Epigenetic stability of exhausted T cells limits durability of reinvigoration by PD-1 blockade. *Science* **354**, 1160–1165.
- Pearce, E.L., and Pearce, E.J. (2013). Metabolic pathways in immune cell activation and quiescence. *Immunity* **38**, 633–643.
- Peng, D., Kryczek, I., Nagarsheth, N., Zhao, L., Wei, S., Wang, W., Sun, Y., Zhao, E., Vatan, L., Szeliga, W., et al. (2015). Epigenetic silencing of TH1-type chemokines shapes tumour immunity and immunotherapy. *Nature* **527**, 249–253.
- Peng, W., Chen, J.Q., Liu, C., Malu, S., Creasy, C., Tetzlaff, M.T., Xu, C., McKenzie, J.A., Zhang, C., Liang, X., et al. (2016). Loss of PTEN promotes resistance to T cell-mediated immunotherapy. *Cancer Discov.* **6**, 202–216.
- Philip, M., Fairchild, L., Sun, L., Horste, E.L., Camara, S., Shakiba, M., Scott, A.C., Viale, A., Lauer, P., Merghoub, T., et al. (2017). Chromatin states define tumour-specific T cell dysfunction and reprogramming. *Nature* **545**, 452–456.
- Pilon-Thomas, S., Kodumudi, K.N., El-Kenawi, A.E., Russell, S., Weber, A.M., Luddy, K., Damaghi, M., Wojtkowiak, J.W., Mule, J.J., Ibrahim-Hashim, A., and Gillies, R.J. (2016). Neutralization of tumor acidity improves antitumor responses to immunotherapy. *Cancer Res.* **76**, 1381–1390.
- Platten, M., Wick, W., and Van den Eynde, B.J. (2012). Tryptophan catabolism in cancer: beyond IDO and tryptophan depletion. *Cancer Res.* **72**, 5435–5440.
- Pollok, K.E., Kim, Y.J., Zhou, Z., Hurtado, J., Kim, K.K., Pickard, R.T., and Kwon, B.S. (1993). Inducible T cell antigen 4-1BB. Analysis of expression and function. *J. Immunol.* **150**, 771–781.
- Poschke, I., Faryna, M., Bergmann, F., Flossdorf, M., Lauenstein, C., Hermes, J., Hinz, U., Hank, T., Ehrenberg, R., Volkmar, M., et al. (2016). Identification of a tumor-reactive T-cell repertoire in the immune infiltrate of patients

with resectable pancreatic ductal adenocarcinoma. *Oncoimmunology* 5, e1240859.

Quigley, M., Pereyra, F., Nilsson, B., Porichis, F., Fonseca, C., Eichbaum, Q., Julg, B., Jesneck, J.L., Brosnahan, K., Imam, S., et al. (2010). Transcriptional analysis of HIV-specific CD8⁺ T cells shows that PD-1 inhibits T cell function by upregulating BATF. *Nat. Med.* 16, 1147–1151.

Restifo, N.P., Marincola, F.M., Kawakami, Y., Taubenberger, J., Yannelli, J.R., and Rosenberg, S.A. (1996). Loss of functional beta 2-microglobulin in metastatic melanomas from five patients receiving immunotherapy. *J. Natl. Cancer Inst.* 88, 100–108.

Robbins, P.F., Lu, Y.C., El-Gamil, M., Li, Y.F., Gross, C., Gartner, J., Lin, J.C., Teer, J.K., Clifton, P., Tycksen, E., et al. (2013). Mining exomic sequencing data to identify mutated antigens recognized by adoptively transferred tumor-reactive T cells. *Nat. Med.* 19, 747–752.

Robert, C., Long, G.V., Brady, B., Dutriaux, C., Maio, M., Mortier, L., Hassel, J.C., Rutkowski, P., McNeil, C., Kalinka-Warzocha, E., et al. (2015). Nivolumab in previously untreated melanoma without BRAF mutation. *N. Engl. J. Med.* 372, 320–330.

Robert, C., Ribas, A., Wolchok, J.D., Hodi, F.S., Hamid, O., Kefford, R., Weber, J.S., Joshua, A.M., Hwu, W.J., Gangadhar, T.C., et al. (2014). Anti-programmed-death-receptor-1 treatment with pembrolizumab in ipilimumab-refractory advanced melanoma: a randomised dose-comparison cohort of a phase 1 trial. *Lancet* 384, 1109–1117.

Robert, C., Thomas, L., Bondarenko, I., O'Day, S., Weber, J., Garbe, C., Lebbe, C., Baurain, J.F., Testori, A., Grob, J.J., et al. (2011). Ipilimumab plus dacarbazine for previously untreated metastatic melanoma. *N. Engl. J. Med.* 364, 2517–2526.

Rosenberg, J.E., Hoffman-Censits, J., Powles, T., van der Heijden, M.S., Balar, A.V., Necchi, A., Dawson, N., O'Donnell, P.H., Balmanoukian, A., Loriot, Y., et al. (2016). Atezolizumab in patients with locally advanced and metastatic urothelial carcinoma who have progressed following treatment with platinum-based chemotherapy: a single-arm, multicentre, phase 2 trial. *Lancet* 387, 1909–1920.

Sakuishi, K., Apetoh, L., Sullivan, J.M., Blazar, B.R., Kuchroo, V.K., and Anderson, A.C. (2010). Targeting Tim-3 and PD-1 pathways to reverse T cell exhaustion and restore anti-tumor immunity. *J. Exp. Med.* 207, 2187–2194.

Sautes-Fridman, C., Lawand, M., Giraldo, N.A., Kaplon, H., Germain, C., Fridman, W.H., and Dieu-Nosjean, M.C. (2016). Tertiary lymphoid structures in cancers: prognostic value, regulation, and manipulation for therapeutic intervention. *Front. Immunol.* 7, 407.

Scharping, N.E., and Delgoffe, G.M. (2016). Tumor microenvironment metabolism: a new checkpoint for anti-tumor immunity. *Vaccines (Basel)* 4, E46.

Scharping, N.E., Menk, A.V., Moreci, R.S., Whetstone, R.D., Dadey, R.E., Watkins, S.C., Ferris, R.L., and Delgoffe, G.M. (2016). The tumor microenvironment represses T cell mitochondrial biogenesis to drive intratumoral T cell metabolic insufficiency and dysfunction. *Immunity* 45, 701–703.

Schietinger, A., Philip, M., Krisnawan, V.E., Chiu, E.Y., Delrow, J.J., Basom, R.S., Lauer, P., Brockstedt, D.G., Knoblaugh, S.E., Hammerling, G.J., et al. (2016). Tumor-specific T cell dysfunction is a dynamic antigen-driven differentiation program initiated early during tumorigenesis. *Immunity* 45, 389–401.

Schreiber, R.D., Old, L.J., and Smyth, M.J. (2011). Cancer immunoediting: integrating immunity's roles in cancer suppression and promotion. *Science* 331, 1565–1570.

Schreiner, J., Thommen, D.S., Herzig, P., Bacac, M., Klein, C., Roller, A., Belousov, A., Levitsky, V., Savic, S., Moersig, W., et al. (2016). Expression of inhibitory receptors on intratumoral T cells modulates the activity of a T cell-bispecific antibody targeting folate receptor. *Oncoimmunology* 5, e1062969.

Scott-Brown, J.P., Lopez-Moyado, I.F., Trifari, S., Wong, V., Chavez, L., Rao, A., and Pereira, R.M. (2016). Dynamic changes in chromatin accessibility occur in CD8⁺ T cells responding to viral infection. *Immunity* 45, 1327–1340.

Seiwert, T.Y., Burtneis, B., Mehra, R., Weiss, J., Berger, R., Eder, J.P., Heath, K., McClanahan, T., Lunceford, J., Gause, C., et al. (2016). Safety and clinical activity of pembrolizumab for treatment of recurrent or metastatic squamous cell carcinoma of the head and neck (KEYNOTE-012): an open-label, multicentre, phase 1b trial. *Lancet Oncol.* 17, 956–965.

Sen, D.R., Kaminski, J., Barnitz, R.A., Kurachi, M., Gerdemann, U., Yates, K.B., Tsao, H.W., Godec, J., LaFleur, M.W., Brown, F.D., et al. (2016). The epigenetic landscape of T cell exhaustion. *Science* 354, 1165–1169.

Shayan, G., Srivastava, R., Li, J., Schmitt, N., Kane, L.P., and Ferris, R.L. (2017). Adaptive resistance to anti-PD1 therapy by Tim-3 upregulation is mediated by the PI3K-Akt pathway in head and neck cancer. *Oncoimmunology* 6, e1261779.

Shin, H., Blackburn, S.D., Intlekofer, A.M., Kao, C., Angelosanto, J.M., Reiner, S.L., and Wherry, E.J. (2009). A role for the transcriptional repressor Blimp-1 in CD8⁺ T cell exhaustion during chronic viral infection. *Immunity* 31, 309–320.

Shrimali, R.K., Ahmad, S., Verma, V., Zeng, P., Ananth, S., Gaur, P., Gittelman, R.M., Yusko, E., Sanders, C., Robins, H., et al. (2017). Concurrent PD-1 blockade negates the effects of OX40 agonist antibody in combination immunotherapy through inducing T-cell apoptosis. *Cancer Immunol. Res.* 5, 755–766.

Simon, S., Vignard, V., Florenceau, L., Dreno, B., Khammari, A., Lang, F., and Labarriere, N. (2016). PD-1 expression conditions T cell avidity within an antigen-specific repertoire. *Oncoimmunology* 5, e1104448.

Simpson, T.R., Li, F., Montalvo-Ortiz, W., Sepulveda, M.A., Bergerhoff, K., Arce, F., Roddie, C., Henry, J.Y., Yagita, H., Wolchok, J.D., et al. (2013). Fc-dependent depletion of tumor-infiltrating regulatory T cells co-defines the efficacy of anti-CTLA-4 therapy against melanoma. *J. Exp. Med.* 210, 1695–1710.

Singer, M., Wang, C., Cong, L., Marjanovic, N.D., Kowalczyk, M.S., Zhang, H., Nyman, J., Sakuishi, K., Kurtulus, S., Gennert, D., et al. (2016). A distinct gene module for dysfunction uncoupled from activation in tumor-infiltrating T cells. *Cell* 166, 1500–1511.e9.

Siska, P.J., Beckermann, K.E., Mason, F.M., Andrejeva, G., Greenplate, A.R., Sendor, A.B., Chiang, Y.J., Corona, A.L., Gemta, L.F., Vincent, B.G., et al. (2017). Mitochondrial dysregulation and glycolytic insufficiency functionally impair CD8 T cells infiltrating human renal cell carcinoma. *JCI Insight* 2, 93411.

Speiser, D.E., Ho, P.C., and Verdeil, G. (2016). Regulatory circuits of T cell function in cancer. *Nat. Rev. Immunol.* 16, 599–611.

Spranger, S., Bao, R., and Gajewski, T.F. (2015). Melanoma-intrinsic beta-catenin signalling prevents anti-tumour immunity. *Nature* 523, 231–235.

Staron, M.M., Gray, S.M., Marshall, H.D., Parish, I.A., Chen, J.H., Perry, C.J., Cui, G., Li, M.O., and Kaech, S.M. (2014). The transcription factor FoxO1 sustains expression of the inhibitory receptor PD-1 and survival of antiviral CD8⁺ T cells during chronic infection. *Immunity* 41, 802–814.

Stephens, P.J., McBride, D.J., Lin, M.L., Varela, I., Pleasance, E.D., Simpson, J.T., Stebbings, L.A., Leroy, C., Edkins, S., Mudie, L.J., et al. (2009). Complex landscapes of somatic rearrangement in human breast cancer genomes. *Nature* 462, 1005–1010.

Sun, Z., Fourcade, J., Pagliano, O., Chauvin, J.M., Sander, C., Kirkwood, J.M., and Zarour, H.M. (2015). IL-10 and PD-1 cooperate to limit the activity of tumor-specific CD8⁺ T cells. *Cancer Res.* 75, 1635–1644.

te Raa, G.D., Pascutti, M.F., Garcia-Vallejo, J.J., Reinen, E., Remmerswaal, E.B., ten Berge, I.J., van Lier, R.A., Eldering, E., van Oers, M.H., Tonino, S.H., and Kater, A.P. (2014). CMV-specific CD8⁺ T-cell function is not impaired in chronic lymphocytic leukemia. *Blood* 123, 717–724.

Teft, W.A., Chau, T.A., and Madrenas, J. (2009). Structure-Function analysis of the CTLA-4 interaction with PP2A. *BMC Immunol.* 10, 23.

Terme, M., Pernot, S., Marcheteau, E., Sandoval, F., Benhamouda, N., Colussi, O., Dubreuil, O., Carpentier, A.F., Tartour, E., and Taieb, J. (2013). VEGFA-VEGFR pathway blockade inhibits tumor-induced regulatory T-cell proliferation in colorectal cancer. *Cancer Res.* 73, 539–549.

Thommen, D.S., Schreiner, J., Muller, P., Herzig, P., Roller, A., Belousov, A., Umama, P., Pisa, P., Klein, C., Bacac, M., et al. (2015). Progression of lung cancer is associated with increased dysfunction of T cells defined by co-expression of multiple inhibitory receptors. *Cancer Immunol. Res.* 3, 1344–1355.

Tirosh, I., Izar, B., Prakadan, S.M., Wadsworth, M.H., 2nd, Treacy, D., Trombetta, J.J., Rotem, A., Rodman, C., Lian, C., Murphy, G., et al. (2016). Dissecting the multicellular ecosystem of metastatic melanoma by single-cell RNA-seq. *Science* 352, 189–196.

- Topalian, S.L., Solomon, D., and Rosenberg, S.A. (1989). Tumor-specific cytotoxicity by lymphocytes infiltrating human melanomas. *J. Immunol.* **142**, 3714–3725.
- Tran, K.Q., Zhou, J., Durflinger, K.H., Langhan, M.M., Shelton, T.E., Wunderlich, J.R., Robbins, P.F., Rosenberg, S.A., and Dudley, M.E. (2008). Minimally cultured tumor-infiltrating lymphocytes display optimal characteristics for adoptive cell therapy. *J. Immunother.* **31**, 742–751.
- Trautmann, L., Janbazian, L., Chomont, N., Said, E.A., Gimmig, S., Bessette, B., Boulassel, M.R., Delwart, E., Sepulveda, H., Balderas, R.S., et al. (2006). Upregulation of PD-1 expression on HIV-specific CD8⁺ T cells leads to reversible immune dysfunction. *Nat. Med.* **12**, 1198–1202.
- Tumeh, P.C., Harview, C.L., Yearley, J.H., Shintaku, I.P., Taylor, E.J., Robert, L., Chmielowski, B., Spasic, M., Henry, G., Ciobanu, V., et al. (2014). PD-1 blockade induces responses by inhibiting adaptive immune resistance. *Nature* **515**, 568–571.
- Utzschneider, D.T., Charmoy, M., Chennupati, V., Pousse, L., Ferreira, D.P., Calderon-Copete, S., Danilo, M., Alfei, F., Hofmann, M., Wieland, D., et al. (2016). T cell factor 1-expressing memory-like CD8⁺ T cells sustain the immune response to chronic viral infections. *Immunity* **45**, 415–427.
- van der Windt, G.J., O'Sullivan, D., Everts, B., Huang, S.C., Buck, M.D., Curtis, J.D., Chang, C.H., Smith, A.M., Ai, T., Faubert, B., et al. (2013). CD8 memory T cells have a bioenergetic advantage that underlies their rapid recall ability. *Proc. Natl. Acad. Sci. USA* **110**, 14336–14341.
- van der Windt, G.J., and Pearce, E.L. (2012). Metabolic switching and fuel choice during T-cell differentiation and memory development. *Immunol. Rev.* **249**, 27–42.
- van Rooij, N., van Buuren, M.M., Philips, D., Velds, A., Toebes, M., Heemskerck, B., van Dijk, L.J., Behjati, S., Hilkmann, H., El Atmioui, D., et al. (2013). Tumor exome analysis reveals neoantigen-specific T-cell reactivity in an ipilimumab-responsive melanoma. *J. Clin. Oncol.* **31**, e439–442.
- Vander Heiden, M.G., Cantley, L.C., and Thompson, C.B. (2009). Understanding the Warburg effect: the metabolic requirements of cell proliferation. *Science* **324**, 1029–1033.
- Walunas, T.L., Lenschow, D.J., Bakker, C.Y., Linsley, P.S., Freeman, G.J., Green, J.M., Thompson, C.B., and Bluestone, J.A. (2011). Pillars article: CTLA-4 can function as a negative regulator of T cell activation. *Immunity* **1994**, 1: 405–413. *J. Immunol.* **187**, 3466–3474.
- Wang, R., Dillon, C.P., Shi, L.Z., Milasta, S., Carter, R., Finkelstein, D., McCormick, L.L., Fitzgerald, P., Chi, H., Munger, J., and Green, D.R. (2011). The transcription factor Myc controls metabolic reprogramming upon T lymphocyte activation. *Immunity* **35**, 871–882.
- Watts, T.H. (2010). Staying alive: T cell costimulation, CD28, and Bcl-xL. *J. Immunol.* **185**, 3785–3787.
- Wei, H., Zhao, L., Hellstrom, I., Hellstrom, K.E., and Guo, Y. (2014). Dual targeting of CD137 co-stimulatory and PD-1 co-inhibitory molecules for ovarian cancer immunotherapy. *Oncotarget* **3**, e28248.
- Wei, H., Zhao, L., Li, W., Fan, K., Qian, W., Hou, S., Wang, H., Dai, M., Hellstrom, I., Hellstrom, K.E., and Guo, Y. (2013). Combinatorial PD-1 blockade and CD137 activation has therapeutic efficacy in murine cancer models and synergizes with cisplatin. *PLoS One* **8**, e84927.
- Weinberg, A.D., Rivera, M.M., Prell, R., Morris, A., Ramstad, T., Vetto, J.T., Urba, W.J., Alford, G., Bunce, C., and Shields, J. (2000). Engagement of the OX-40 receptor in vivo enhances antitumor immunity. *J. Immunol.* **164**, 2160–2169.
- Wherry, E.J. (2011). T cell exhaustion. *Nat. Immunol.* **12**, 492–499.
- Wherry, E.J., Ha, S.J., Kaeck, S.M., Haining, W.N., Sarkar, S., Kalia, V., Subramaniam, S., Blattman, J.N., Barber, D.L., and Ahmed, R. (2007). Molecular signature of CD8⁺ T cell exhaustion during chronic viral infection. *Immunity* **27**, 670–684.
- Wilson, W.R., and Hay, M.P. (2011). Targeting hypoxia in cancer therapy. *Nat. Rev. Cancer* **11**, 393–410.
- Wlodarchak, N., and Xing, Y. (2016). PP2A as a master regulator of the cell cycle. *Crit. Rev. Biochem. Mol. Biol.* **51**, 162–184.
- Wolchok, J.D., Kluger, H., Callahan, M.K., Postow, M.A., Rizvi, N.A., Lesokhin, A.M., Segal, N.H., Ariyan, C.E., Gordon, R.A., Reed, K., et al. (2013). Nivolumab plus ipilimumab in advanced melanoma. *N. Engl. J. Med.* **369**, 122–133.
- Wu, C.J., O'Rourke, D.M., Feng, G.S., Johnson, G.R., Wang, Q., and Greene, M.I. (2001). The tyrosine phosphatase SHP-2 is required for mediating phosphatidylinositol 3-kinase/Akt activation by growth factors. *Oncogene* **20**, 6018–6025.
- Xia, H., Wang, W., Crespo, J., Kryczek, I., Li, W., Wei, S., Bian, Z., Maj, T., He, M., Liu, R.J., et al. (2017). Suppression of FIP200 and autophagy by tumor-derived lactate promotes naive T cell apoptosis and affects tumor immunity. *Sci. Immunol.* **2**, eaan4631.
- Youngblood, B., Noto, A., Porichis, F., Akondy, R.S., Ndhlovu, Z.M., Austin, J.W., Bordi, R., Procopio, F.A., Miura, T., Allen, T.M., et al. (2013). Cutting edge: prolonged exposure to HIV reinforces a poised epigenetic program for PD-1 expression in virus-specific CD8 T cells. *J. Immunol.* **191**, 540–544.
- Youngblood, B., Oestreich, K.J., Ha, S.J., Duraiswamy, J., Akondy, R.S., West, E.E., Wei, Z., Lu, P., Austin, J.W., Riley, J.L., et al. (2011). Chronic virus infection enforces demethylation of the locus that encodes PD-1 in antigen-specific CD8⁺ T cells. *Immunity* **35**, 400–412.
- Yu, X., Harden, K., Gonzalez, L.C., Francesco, M., Chiang, E., Irving, B., Tom, I., Ivelja, S., Refino, C.J., Clark, H., et al. (2009). The surface protein TIGIT suppresses T cell activation by promoting the generation of mature immunoregulatory dendritic cells. *Nat. Immunol.* **10**, 48–57.
- Yuan, Y., Failmezger, H., Rueda, O.M., Ali, H.R., Graf, S., Chin, S.F., Schwarz, R.F., Curtis, C., Dunning, M.J., Bardwell, H., et al. (2012). Quantitative image analysis of cellular heterogeneity in breast tumors complements genomic profiling. *Sci. Transl. Med.* **4**, 157ra143.
- Zajac, A.J., Blattman, J.N., Murali-Krishna, K., Sourdive, D.J., Suresh, M., Altman, J.D., and Ahmed, R. (1998). Viral immune evasion due to persistence of activated T cells without effector function. *J. Exp. Med.* **188**, 2205–2213.
- Zaretsky, J.M., Garcia-Diaz, A., Shin, D.S., Escuin-Ordinas, H., Hugo, W., Hu-Lieskovan, S., Torrejon, D.Y., Abril-Rodriguez, G., Sandoval, S., Barthly, L., et al. (2016). Mutations associated with acquired resistance to PD-1 blockade in melanoma. *N. Engl. J. Med.* **375**, 819–829.
- Zarour, H.M. (2016). Reversing T-cell dysfunction and exhaustion in cancer. *Clin. Cancer Res.* **22**, 1856–1864.
- Zhang, F., Zhou, X., DiSpirito, J.R., Wang, C., Wang, Y., and Shen, H. (2014). Epigenetic manipulation restores functions of defective CD8⁺ T cells from chronic viral infection. *Mol. Ther.* **22**, 1698–1706.
- Zhang, Y., and Ertl, H.C. (2016). Starved and asphyxiated: how can CD8⁺ T cells within a tumor microenvironment prevent tumor progression. *Front. Immunol.* **7**, 32.
- Zheng, C., Zheng, L., Yoo, J.K., Guo, H., Zhang, Y., Guo, X., Kang, B., Hu, R., Huang, J.Y., Zhang, Q., et al. (2017). Landscape of infiltrating T cells in liver cancer revealed by single-cell sequencing. *Cell* **169**, 1342–1356.e16.
- Zheng, Y., Delgoffe, G.M., Meyer, C.F., Chan, W., and Powell, J.D. (2009). Anergic T cells are metabolically anergic. *J. Immunol.* **183**, 6095–6101.
- Zhou, X., Yu, S., Zhao, D.M., Harty, J.T., Badovinac, V.P., and Xue, H.H. (2010). Differentiation and persistence of memory CD8⁺ T cells depend on T cell factor 1. *Immunity* **33**, 229–240.
- Zhu, W., Germain, C., Liu, Z., Sebastian, Y., Devi, P., Knockaert, S., Brohawn, P., Lehmann, K., Damotte, D., Validire, P., et al. (2015). A high density of tertiary lymphoid structure B cells in lung tumors is associated with increased CD4⁺ T cell receptor repertoire clonality. *Oncotarget* **4**, e1051922.
- Zippelius, A., Batard, P., Rubio-Godoy, V., Biolley, G., Lienard, D., Lejeune, F., Rimoldi, D., Guillaume, P., Meidenbauer, N., Mackensen, A., et al. (2004). Effector function of human tumor-specific CD8 T cells in melanoma lesions: a state of local functional tolerance. *Cancer Res.* **64**, 2865–2873.

Review

Immunomodulation of Tumor Vessels: It Takes Two to Tango

Anna Johansson-Percival,¹ Bo He,¹ and Ruth Ganss^{1,*}

The density of intratumoral CD8⁺ T cells predicts patient survival and responsiveness to immunotherapy. Effector T cell infiltration in turn is controlled by the tumor vasculature which co-evolves together with an immune-suppressive environment. At the T cell-vascular interface, endothelial cells actively suppress T cell trafficking and function. Conversely, forced activation, normalization, and differentiation of tumor vessels into high endothelial venule entrance portals for lymphocytes can facilitate T cell extravasation. Emerging evidence demonstrates that this process is not exclusively controlled by the endothelium. Indeed, tumor vasculature and CD4⁺ and/or CD8⁺ T cells may regulate each other: increasing local effector T cell numbers or re-invigorating pre-existing T cells via immune checkpoint blockade can directly affect the vasculature. A deeper understanding of the orchestration and duration of this reciprocal relationship may help shape the design of future immunotherapies.

Coevolution of Cancer, Angiogenic Blood Vessels, and Immunity

Cancer-associated stroma is rich in support cells, including blood vessels, and a diverse spectrum of innate and adaptive immune cells. Stroma coevolves with malignant cells and generates a microenvironment of factors and cytokines, which sustains tumor growth and suppresses the immune response against the cancer. For instance, the formation of new blood vessels, a process called angiogenesis, is initiated by the increasing metabolic demands of the expanding tumor. Low oxygen levels and proangiogenic factors such as vascular endothelial growth factor (VEGF) are major drivers of angiogenesis [1]. Consequently, excessive vessel proliferation in the tumor environment profoundly changes the biology and function of endothelial cells as gate keepers and immune regulators [2]. Together with abnormal **pericyte** (see Glossary) vessel coverage and a defective basement membrane, this results in a dysfunctional, leaky tumor vasculature that directly or indirectly contributes to the tumor's intrinsic immune-suppressive environment [3]. Blocking Vegf in solid tumors of murine cancer models has profound immune-enhancing effects, by repolarizing, for instance, macrophages into an immune-stimulating phenotype and inducing dendritic cell maturation [4]. This provides the rationale for combined antiangiogenesis and immune-enhancing therapies to treat tumors such as advanced melanoma [5]. In addition, low-dose anti-Vegf therapy can, at least temporarily, restore **vessel patency** and tumor perfusion in a process called **vessel normalization** [6]. Reversing blood vessel abnormalities with low-dose anti-Vegf therapy can alleviate **tumor hypoxia** and also enhance anticancer immunity, demonstrating that the state of tumor vasculature and the immune microenvironment are intricately linked [7]. The role of myeloid cells in angiogenic programming has been extensively reviewed [1,4]. In this review, we focus on recent insights into the reciprocal control of tumor vessels and adaptive immunity, in particular CD4⁺ and CD8⁺ T cells. These new findings highlight, to our knowledge, unrecognized roles of effector T cells in modulating their own migration across the tumor vascular barrier, reducing angiogenesis and

Highlights

Effector CD4⁺ and CD8⁺ T cells are key drivers of combined antiangiogenesis and checkpoint blockade immunotherapies in solid cancers.

Reciprocal interactions between the tumor endothelium and effector CD8⁺ T cells can regulate T cell migration across the tumor vascular barrier.

Mutual and self-amplifying regulation of tumor vessel normalization can be mediated by effector T cells.

Effector CD8⁺ T cells are key players in IFN γ -mediated vessel regression.

Effector CD4⁺ and CD8⁺ T cells can mediate therapeutic induction of high endothelial venules in certain solid cancers.

¹The Harry Perkins Institute of Medical Research, Centre for Medical Research, The University of Western Australia, Nedlands, Western Australia 6009, Australia

*Correspondence: ganss@perkins.uwa.edu.au (R. Ganss).

stimulating antitumor immunity in a self-amplifying loop at the vessel wall. These new findings may be key in improving the design of more effective future anticancer immunotherapies.

T Cell Trafficking at the Vascular Interface

With anticancer immunotherapy coming-of-age, the question on how to deliver immune effector cells in sufficient numbers across the vascular barrier is more important than ever. Endothelial cells play an exquisite role in controlling immune cell entry into healthy and pathological tissue in a process that involves defined sets of chemokines and adhesion molecules [8] (Figure 1, Key Figure). Naïve lymphocytes patrol the body by circulating from the blood to secondary lymphatic organs and back into the blood. Most naïve lymphocytes and memory T cells enter lymph nodes through **high endothelial venules (HEVs)**, a specialized endothelium with a 'high' cuboidal morphology and a unique set of adhesion molecules, so-called peripheral node addressins (PNAd), which bind L-selectin⁺ T cells [9]. Mammalian HEVs are also decorated with the chemokine CCL21, which selectively facilitates CCR7⁺ T cell entry [10]. Secondary lymphatic organs provide the appropriate environment for T cells to encounter cognate antigens on antigen-presenting cells. Once primed, CXCR3⁺ effector T cells are guided by chemokines, such as CXCL9 and CXCL10, to sites of infection and inflammation, and migrate across inflamed postcapillary venules in order to perform their immune functions [10]. During this process, T cells first tether to the endothelium under shear stress in circulation, rolling along E- and P-selectin positive endothelial cells on the inflamed endothelium, becoming activated by specific endothelial chemokines, and expressing lymphocyte function-associated antigen-1 (LFA-1), which enables firm adhesion to intercellular adhesion molecule (ICAM-1) or vascular adhesion molecule (VCAM-1) on endothelial cells; this finally allows the transmigration (or diapedesis) of T lymphocytes through the leaky endothelium [11]. Chronically inflamed tissue further supports T cell influx by differentiating endothelial cells into HEVs [12]. Tissue-resident HEVs, together with infiltrating T and B cells, form clusters resembling lymph nodes, so-called **tertiary lymph node structures (TLS)**, and can further perpetuate inflammation [12]. HEVs and TLS can also arise spontaneously in some human cancers, where they are often associated with a better prognosis [13] (Box 1).

Box 1. Spontaneous HEV Formation in Cancer

A growing number of studies have reported spontaneous assembly of TLS in human cancers, most notably in melanoma, colorectal, breast, and non-small cell lung cancers [13]. While it is still debated how these structures form, spontaneous HEVs and TLS in cancer can directly correlate with the degree of endogenous effector cell infiltration, indicating that T cells may play a critical role in this process. For instance, in human breast cancer, **CD4⁺ T follicular helper cells (Tfh)** (not normally found in cancers) have been located in TLS and associated with a T cell-rich environment, along with improved responsiveness to chemotherapy and overall survival of patients [75]. A critical role of CD8⁺ effector T cells in the formation of HEV⁺ lymph node-like structures has also been demonstrated in murine melanoma and lung cancer models [72]. In these tumors, a low-level lymphocyte infiltrate can trigger PNAd- and Ccl21-expression on blood vessels; this in turn can enable further tumor infiltration by naïve CD8⁺ T cells and their intratumoral differentiation into effector T cells [72]. Mechanistically, HEVs and TLS neogenesis can be induced by lymphotoxin (LT) α / β -LT β receptor (LT β R) signaling [76], or by effector T cell-derived Tnf α and LT α , which engage stromal Tnf receptors, thus bypassing LT β R signaling [72,65]. A strong correlation between TLS formation in human breast cancer and **LIGHT** expression also suggests a potential role of LIGHT in intratumoral TLS neogenesis in humans [77]. Various studies suggest that intratumoral rather than peripheral location of TLS [78,79], as well as reciprocal regulation of endothelial cells and infiltrating T cells during TLS neogenesis may be crucial parameters for tumor growth control [67]. Whether spontaneous TLS are active sites of antitumor immunity is still not clear and may be dependent on tumor type [80]. Moreover, while spontaneous TLS may enable T cell recruitment from the periphery and facilitate interactions with dendritic cells, the mere existence of HEVs or TLS in cancer is unlikely to activate robust antitumor immune responses. This will depend on tumor antigenicity [72], the presence of immune inhibitory cells such as T regs, the inflammatory microenvironment, and the presence of tumor-antigen presenting dendritic cells, among other factors [65,80].

Glossary

Angiopoietin 2: vascular growth factor that binds the endothelial-specific receptor tyrosine kinase 2 (TIE2) and can promote pathological angiogenesis.

Anthracyclines: chemotherapeutic agents, including doxorubicin, which inhibit DNA and RNA synthesis, preventing the replication of fast-growing cancer cells.

Autochthonous vasculature: blood vessels found in an organ from which they originate (e.g., a tissue-specific cancer type).

CD4⁺ T follicular helper cells (Tfh): subset of CD4⁺ helper T cells required to regulate B cell differentiation in peripheral lymphatic organs.

CD40/CD40L: CD40 is a co-stimulatory molecule expressed on antigen presenting cells and in tumor stroma. CD40L is primarily expressed on activated T cells.

CD73: membrane-bound nucleotidase catalyzing the hydrolysis of extracellular AMP into adenosine (expressed on lymphocytes, endothelial, and epithelial cells). It participates in the regulation of endothelial cell barrier function and homeostasis, as well as protection from ischemia.

Chimeric antigen receptor (CAR) T cells: T cells engineered to express chimeric antigen receptors that are specific for certain cancer types.

CpG-ODN: synthetic reagent comprising immunostimulatory oligodeoxynucleotides (ODNs) with cytosine-guanine-rich (CpG) motifs and a phosphothioate-stabilized backbone. It mimics bacterial DNA and is a potent immune adjuvant which activates TLR9.

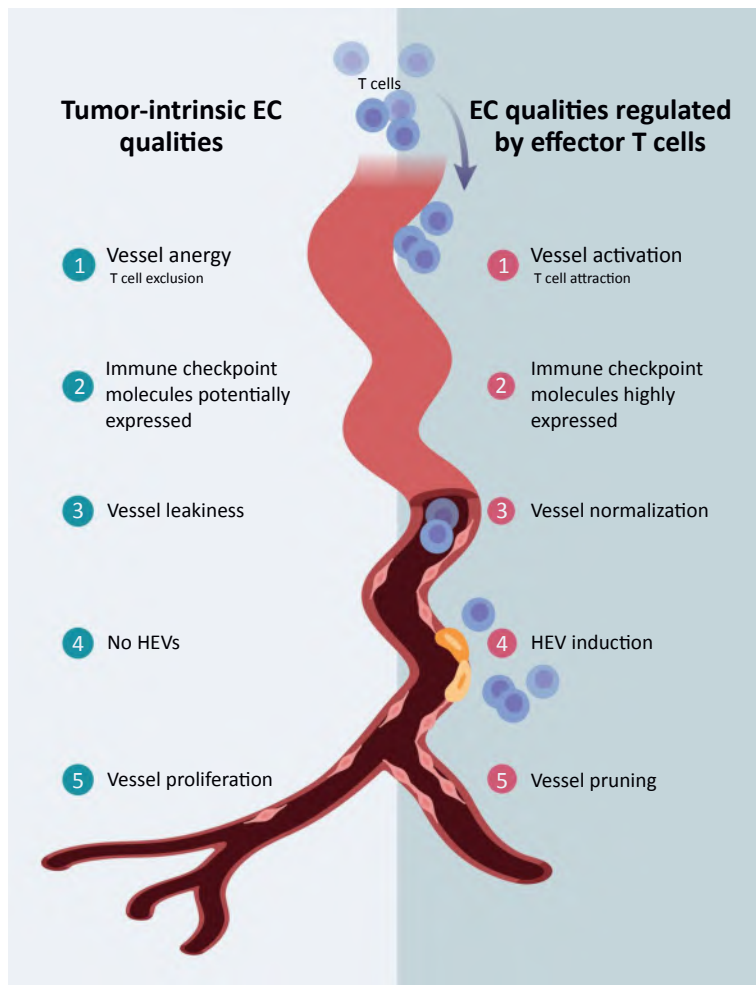
Endothelial anergy: tolerance mechanism in which the state of the endothelium prevents T cell capture and transmigration.

Endothelial cell complement system: consists of proteins (components) produced by the endothelium in response to inflammatory factors, which act as modulators of inflammation and immune responses.

High endothelial venules (HEVs): a specialized form of endothelial cells expressing peripheral node addressins (Ad) and facilitating

Key Figure

Model for the Reciprocal Regulation of Tumor Vessels and Effector T Cells



Trends in Immunology

Figure 1. Tumor-intrinsic features of endothelial cells (EC) include the lack of effector T cell attraction and transmigration, potential expression of immune inhibitory molecules such as programmed cell death ligand-1 (PD-L1), vascular leakiness for plasma molecules, lack of high endothelial venules (HEVs), and sustained vessel proliferation in a hypoxic and immunosuppressive environment. Recent work has demonstrated a role of CD4⁺ and CD8⁺ effector T cells in vessel activation and T cell transmigration in lung tumor models [48]; substantial upregulation of immune checkpoint molecules such as PD-L1 in mouse models of melanoma, fibrosarcoma, pancreatic neuroendocrine, and breast cancers [36,37,39]; vessel normalization resulting in improved barrier function in mouse breast cancer [56]; HEV induction and formation of tertiary lymph node structures (TLS) in murine pancreatic neuroendocrine tumors, breast cancers, and glioblastoma [36,53,71]; as well as vessel pruning in mouse fibrosarcomas [59]. Created with ©BioRender.io.

lymphocyte trafficking in lymph nodes, chronically inflamed tissue, and in some cancers.

Immune checkpoint molecules: molecules that either promote or inhibit T cell activation. Blockade of inhibitory immune checkpoint molecules (immune checkpoint therapy), such as CTLA-4 and PD-1, has enabled antitumor immunity in certain cancer types.

Light/LIGHT (TNFSF14): transmembrane glycoprotein of the TNF super family. LIGHT binds to herpes virus entry mediator and LTβR.

Low dose per fraction radiation: lower dose of radiation treatment compared with standard radiation therapy, divided into a number of treatment sessions called fractions.

Neoantigen load: number of cancer-derived, mutated peptides predicted to bind to class I or II MHC molecules for productive antigen presentation.

Patient-derived tumor xenograft (PDX): cancer models where tissue or cells from a patient's cancer are implanted into an immunodeficient mouse.

Pericyte: contractile perivascular or mural cell lining the endothelial cells of small blood vessels.

Programmed cell death ligand-1 (PD-L1): surface receptor that binds to PD-1 and is part of the group of immune checkpoint inhibitors. PD-L1 can be overexpressed on cancer or stromal cells. Anti-PD-L1 antibodies have been approved to treat certain cancer types.

Prostaglandins: bioactive lipid compounds synthesized by cyclooxygenases (COX). Prostaglandins (e.g., PGE₂) have a wide range of biological effects associated with inflammation and cancer.

Regulator of G protein signaling 5 (Rgs5): member of the regulator of G protein signaling family, hydrolyzes GTP and controls G protein-coupled receptor signaling. Can be highly expressed in tumor pericytes.

Regulatory T cells (T regs): CD4⁺ T cells that express the transcription factor FoxP3, maintain immune tolerance to self-antigens, prevent autoimmunity, and can also suppress antitumor immune responses.

How effector T cell extravasation into solid cancers is orchestrated and what signaling cues remain functional in a growth factor-saturated environment, is still largely unresolved. However, T cell adhesion to tumor endothelium appears to be compromised [14,15]. For instance, intravital microscopy of a mouse model of pancreatic neuroendocrine tumors has shown diminished leukocyte adhesion with malignancy, coinciding with the first structural abnormalities observed, including tumor vessel dilation [14]. Moreover, cytotoxic CD8⁺ effector T cell interactions at the tumor vascular interface are low in multiple murine solid cancer models such as melanoma, colon, and pancreatic neuroendocrine cancers, relative to controls [15]. Indeed, angiogenic endothelial cells play an active role in restricting capture and transmigration of T cell populations into solid tumors, for instance, by reducing vessel activation and upregulating **immune checkpoint molecules** such as **programmed cell death ligand-1 (PD-L1)** [16,17]. Such features of an angiogenic vasculature may present potential therapeutic target approaches for the treatment of solid cancers (Figure 1).

Tumor Vasculature and Chemokines

Once activated, chemokine receptors such as CXCR3 and CCR5 are upregulated on effector T cells, which are attracted into inflamed tissues by their corresponding ligands, interferon γ (IFN γ)-inducible CXCL9, CXCL10, and CCL3, CCL4, CCL5, respectively [18]. For the transition from rolling to firm adhesion, endothelial cells must be decorated with sufficient chemokines to promote high-affinity T cell binding [18]. Given the diverse set of chemokines and cognate receptors, a recent study has shown a unique role of CXCR3 receptor-signaling in CD8⁺ T cell trafficking into mouse and human melanoma. Specifically, *Cxcr3* gene deletion or pharmaceutical blockade of *Cxcr3* signaling has been reported to abolish adhesion and transmigration of adoptively transferred effector CD8⁺ effector T cells in mice [19]. Homing of human CD8⁺ T cells into melanoma **xenografts** was equally impaired when the function of CXCR3 was inhibited using anti-CXCR3 blocking antibodies [19]. Moreover, there is clear evidence that chemokines such as CXCL10 can regulate effector T cell trafficking in solid cancers, and furthermore, the release of biologically active chemokines can be upregulated with specific therapeutic treatments [20–22]. For instance, **anthracyclines** are chemotherapeutic agents which can induce intratumoral Cxcl10 protein expression in mouse models of fibrosarcoma by triggering production of type I interferons in cancer cells; this, in turn, contributes to boosting anticancer innate and adaptive immunity [20]. Preventing *in vivo* degradation of Cxcl10 pharmacologically in B16F10 melanoma tumors could improve *Cxcr3*-dependent CD8⁺ T cell infiltration into tumors and increase survival following anti-PD-1 and anti-CTLA-4 checkpoint therapy [21]. Aiming to improve effector T cell antitumor activity, strategies are being employed to engineer **chimeric antigen receptor (CAR) T cells** that structurally include chemokine receptors, such as CCR2, to enhance trafficking into CCL2-secreting human malignant pleural mesotheliomas [23], although the actual success of these CAR-T cell variants remains to be determined. Indeed, secretion of chemokines by multiple cell types and pleiotropic effects in the tumor environment make their therapeutic use challenging. For instance, CCL5, when produced by CD4⁺ and CD8⁺ T lymphocytes in human metastatic colorectal cancer, can engage with CCR5 tumor-promoting monocytes, activating these cells and contributing to reduced survival outcomes [24]. Hypoxia-associated chemokines, such as Ccl22 and Ccl28, can selectively attract **regulatory T cells (T regs)**, which suppress tumor-specific T cell immunity, promote tumor tolerance, and stimulate tumor growth in mouse xenograft models of human ovarian cancer [25,26]. Nevertheless, chemokines such as Cxcl9 and Cxcl10 have been shown to be beneficial in the tumor microenvironment by inhibiting angiogenesis in irradiated murine pancreatic neuroendocrine cancer, and by increasing CD8⁺ T cell influx in a murine model of lung cancer following myeloid cell depletion [27,28]. Therefore, the shared expression of the chemokine receptor CXCR3 by endothelial cells and activated effector CD8⁺ T cells may enable synergistic

RIP-Tag: genetically modified mouse model where the SV40 Large T antigen (Tag) is expressed under the transcriptional control of the rat insulin gene promoter (RIP). Mice develop highly angiogenic pancreatic neuroendocrine tumors.

Stimulator of interferon gene (STING): receptor that senses both exogenous and endogenous cytosolic cyclic dinucleotides and induces type I interferon and proinflammatory cytokine responses.

Tertiary lymph node structure (TLS): arise in chronically inflamed or cancerous tissues. They resemble peripheral lymph nodes, contain HEVs, and comprise T and B cells zones.

Toll-like receptor (TLR)/TLR9: Toll-like receptors sense microorganisms and play a role in innate immune responses to pathogens. TLR9 senses DNA in bacteria and triggers a proinflammatory response. TLR9 agonists such as CpG-ODN are used as adjuvants in cancer treatment.

Tumor hypoxia: low oxygen concentration in certain areas of solid cancers.

Type 1T helper (Th1 cells): a subtype of CD4⁺ helper T cells that predominantly produce cytokines such as IL-2 and IFN γ .

Vessel normalization: transformation of abnormal cancer blood vessels into more anatomically organized, tighter, and functional structures.

Vessel patency: degree of unobstructed blood flow in a blood vessel.

Vessel pruning: physiological regression of a subset of microvessels within a growing vasculature.

Xenograft: tumor graft taken from a donor of one species (e.g., human) and transplanted into a recipient of another species (e.g., immunodeficient mouse).

effects of chemokines such as CXCL9 and CXCL10 on tumor angiogenesis and lymphocyte infiltration. This is relevant as these pathways could be potentially exploited therapeutically [29].

Endothelial Anergy and T Cell Exclusion

Once activated, CD4⁺ and CD8⁺ T cells are captured at the vessel wall, and productive lymphocyte integrin interactions with endothelial adhesion molecules are required for transmigration. However, in an angiogenic environment with high expression of VEGF and other growth factors, endothelial ICAM-1 and VCAM-1 expression is subdued, leading to a state of **endothelial anergy**, where lymphocyte–endothelial interactions remain unproductive, as observed in murine and human cancers [16,30,31]. In addition to ‘neglect’ by the endothelium, active cell contact-dependent mechanisms can occur to either deactivate or even kill incoming effector T cells, thus fostering biased transmigration of immune-suppressive T regs [32]. For instance, in mouse models of melanoma, ovarian, colon, and renal cancers, Vegf and **prostaglandins** are prominent factors shown to induce CD95 (FasL) expression on angiogenic blood vessels, leading in turn to apoptosis (programmed cell death) of activated anticancer CD8⁺ T cells [32]. In contrast, T regs are protected by higher expression of antiapoptotic genes, such as *Bcl2* and *Bclxl*, and these cells can selectively migrate into tumors [32]. Consequently, treatment of a murine ovarian cancer model with vessel remodeling agents, such as Vegf blocking antibodies and/or aspirin, can also increase effector T cell infiltration [32]. Furthermore, adenosine receptors and the adenosine-producing enzyme **CD73** (expressed on endothelial cells), are important regulators of angiogenesis and lymphocyte trafficking [33]. Upregulation of CD73 on tumor vessels can limit effector T cell homing, whereas selective inhibition via a pharmacological inhibitor or anti-CD73 antibodies can restore efficacy of adoptive T cell therapy, and can also impair angiogenesis as evidenced from multiple mouse tumor models, including breast cancer [34,35]. In addition, upregulation of negative regulators of T cell activation (inhibitory checkpoint receptors), such as PD-L1 on endothelial cells, has been shown to correlate with poor patient prognosis in several human cancers, including melanoma [17], and although the mechanism for this remains to be elucidated, it is possible that endothelial cell-mediated impairment of anticancer T cell infiltration and function may be involved [36,37]. Of note, currently, the single most important predictor for responsiveness to PD-1/PD-L1 checkpoint blockade therapy in metastatic melanoma patients appears to be the density and close proximity of PD-1 expressing CD8⁺ T cells with PD-L1 signals in the tumor environment; this may indicate that pre-existing CD8⁺ T cells are required for checkpoint inhibition to be effective in killing human cancer cells [38]. Similarly, pre-existing, tumor-infiltrating CD8⁺ T cells in murine colon cancer are a prerequisite for achieving successful PD-L1 blockade [39], highlighting the need for immunotherapies that enable adequate T cell trafficking into solid tumors. Thus, one way to increase anticancer therapeutic efficacy may be to overcome endothelial anergy, which can restrict T cell accumulation in the vicinity of cancer cells, thus resulting in T cell exclusion.

Reactivating Tumor Endothelia to Improve T Cell Infiltration

Endothelial anergy can be considered a reversible state (Figure 1). For instance, it has been extensively studied in a mouse model of spontaneous pancreatic neuroendocrine tumors (**RIP-Tag**). The **autochthonous vasculature** in this highly angiogenic cancer acts as a barrier for spontaneous or adoptively transferred, tumor-reactive T cells, thus resembling T cell-poor human cancers [14,27]. In this model, multiple strategies have been developed to ‘inflammate’ the inert endothelium, which in turn supports T cell transmigration and effector function. This has included performing tumor irradiation at a non-tumorcidal dose in RIP-Tag mice; this in turn can induce Icam-1/Vcam-1 expression on endothelial cells concomitant with an upregulation of macrophage-derived Cxcl9 and Cxcl10 [27,40]. Of clinical relevance, synergies between local

radiation and immunotherapy are being actively pursued in multiple human cancers, including melanoma, head and neck, and liver cancers, not least because of the notion that **low dose per fraction radiation** might be effective in stimulating effector T cell recruitment and diapedesis into tumor sites [41,42]. Another strategy has been to exploit inflammatory stimulators such as **Toll-like receptors (TLRs)** or the **stimulator of interferon genes (STING)**, which can activate endothelial cells directly or indirectly via innate immune cells [43,44]. For instance, the **TLR9** ligand **CpG-ODN** can be taken up by tumor-resident macrophages; this in turn can induce strong expression of endothelial adhesion molecules such as Icam-1 and Vcam-1, thus rendering tumors such as RIP-Tag and B16 melanoma permissive for infiltration by adoptively transferred effector T cells in mice [43,44]. CpG-ODN has also been shown *ex vivo* to directly induce ICAM-1 and E-selectin expression on human umbilical cord endothelial cells in an NF κ B-dependent pathway [45]. In the B16F10 melanoma mouse model, STING activation by intratumoral injection of cyclic dinucleotide GMP-AMP has been reported to prime endothelial cells to produce type I interferon, preceding the spontaneous infiltration of dendritic cells and CD8⁺ T cells, which can, in turn, be further activated by anti-CTLA-4 and anti-PD-1 antibodies to enhance antitumor immunity and delay tumor growth [46]. Based on their actions on solid tumors, as well as on endothelial and immune cells when delivered intratumorally, the efficacies of TLR9 agonists and STING ligands, in combination with immunotherapy (anti-PD-1), are currently under clinical investigation for metastatic melanoma (e.g., Phase I NCT02521870 at clinicaltrials.gov) and other advanced solid cancers (e.g., Phase I NCT03010176 at clinicaltrials.gov), respectively. While combining endothelial activators and adaptive immune stimulators is an attractive concept, intratumoral delivery, toxicity, and pleiotropic effects in the tumor environment pose significant challenges. To more specifically modulate the endothelium in mice, selected inflammatory stimulators or cytokines, such as I κ B γ , Tnf α , or **Light**, might be directly targeted to the tumor endothelium utilizing specific antibodies or peptides [47] (Box 2). Recently, a critical role of T cells in promoting their own migration into mouse lung tumors was demonstrated [48]. This infiltration was accompanied by the upregulation of **endothelial cell complement components** through the action of **type 1 T helper (Th1)** cytokines I κ B γ and Tnf α , which in turn increased Icam-1/Vcam-1 expression on endothelial cells, thus leading to activated anticancer effector CD8⁺ T cell extravasation [48] (Figure 1). Endothelial complement activation requires high numbers of adoptively transferred, activated effector CD8⁺ T cells [48]. Accordingly, in the absence of effector T cells, complement activation has been reported to lead to tumor-promoting macrophage recruitment in a sarcoma mouse model [49], underscoring the need for local effector cells to reach a critical threshold of infiltration for tumor growth control.

Vessel Normalization and Antitumor Immunity

Hierarchical blood vessel organization, a hallmark of normal tissue vasculature, is lost in tumors. Nevertheless, the tumor vascular bed, like normal tissue, consists of endothelial cells, basement membrane, pericytes, and perivascular immune cells. Thus, activation of the tumor endothelium is often accompanied by substantial remodeling and reprogramming of the entire vascular bed, which can result in a more structured or normalized tumor vasculature [50]. Of clinical relevance, using low-dose anti-Vegf therapy in murine breast cancer models or specific vascular targeting of cytokines such as Tnf α or Light in murine pancreatic neuroendocrine tumors, shows that therapeutically induced vessel normalization can increase vascular barrier function and tumor perfusion and can potentially improve the outcome of immunotherapies (Figure 1) [7,50,51]. This concept was first demonstrated in the mouse cancer model where genetic deletion of the **regulator of G protein signaling 5 (Rgs5)** enforced pericyte maturation and improved pericyte/endothelial cell alignment, thus leading to a marked reduction in vessel leakiness and tumor hypoxia, which in turn increased CD8⁺ effector T cell influx. This

Box 2. Specific Targeting of Inflammatory Factors to Tumor Vessels

To mitigate systemic immune-mediated toxicity, peptide or antibody fusion compounds can be used as carrier molecules to specifically deliver payloads to tumor blood vessels. VTPs can bind to the abnormal, highly angiogenic vasculature in tumors, but not in normal tissue [47]. Specific vascular delivery of immune modulatory compounds can potentially activate endothelial cells, perivascular macrophages, and T cells and thus amplify signals at the vessel walls. As proof-of-concept, this has been shown in diverse murine tumor models with payload delivery of biologics such as CpG-ODN, **CD40** agonists, $\text{I}\text{f}\text{n}\gamma$, $\text{Tn}\text{f}\alpha$, and Light [81,82,50,83,51]. Vascular effects of these compounds are unique, highly dose-dependent, and dynamic [81,82,50,83,51]. Most compounds induce vessel death at high doses or prolonged exposure [50,83]. Of note, $\text{I}\text{f}\text{n}\gamma$, a major $\text{C}\text{D}4^+$ and $\text{C}\text{D}8^+$ T cell effector molecule, can exert angiostatic properties at low doses, but surprisingly, can also inhibit antitumor immunity at higher doses in mouse models of pancreatic neuroendocrine cancer and B16F1 melanoma [50,62]. Upregulation of endothelial adhesion molecules is a feature shared by the biologics listed above when applied at low physiological doses. This, in turn, can increase $\text{C}\text{D}8^+$ effector T cell extravasation following adoptive T cell transfer or via certain anticancer immunotherapies such as via CpG-ODN or dendritic cell vaccination strategies in mouse models of pancreatic neuroendocrine cancers or melanoma, respectively [81,83]. Moreover, $\text{Tn}\text{f}\alpha$ and Light can activate endothelial cells and simultaneously normalize the vascular bed, which can further increase tumor access by preactivated T cells in the RIP-Tag mouse model of pancreatic neuroendocrine tumors [50,51]. Only vascular delivery of CpG-ODN or Light, however, can prime endogenous antitumor immunity, as evidenced by spontaneous $\text{C}\text{D}8^+$ T cell infiltration and growth control; this might most likely occur by stimulating perivascular innate immune cells in highly angiogenic RIP-Tag tumors, resulting in signal diversification at the vessel wall and subsequent secretion of T cell chemoattractants, although this remains to be investigated [84]. Light, but not $\text{Tn}\text{f}\alpha$, also induces HEVs and TLS on a background of normalized vessels in mouse models of pancreatic neuroendocrine and lung cancers [50,53] (see below). These studies suggest that the extent of anticancer immune responses may be linked to the capacity of vascular targeting compounds to modulate the entire vascular niche, and to also attract effector $\text{C}\text{D}8^+$ T cells.

suggested that *Rgs5* played a major role in controlling aberrant angiogenic vessel remodeling and effector T cell penetration into RIP-Tag tumors [52]. The list of factors that can normalize tumor blood vessels and support adaptive antitumor immunity is steadily growing [6]. Mechanistically, vessel normalization re-establishes endothelial barrier integrity, and this can also be achieved by increasing **VE-cadherin** mRNA or protein expression [53,54]. Moreover, vessel normalization can involve activation of endothelia with local cytokine delivery [50] (Box 2), triggering pericyte maturation and/or reprogramming tumor-resident macrophages to secrete factors such as $\text{Tg}\text{f}\beta$, which can then induce vessel maturation, as shown in RIP-Tag mice [51]. It is important to highlight that these vascular changes are not necessarily independent events but might occur simultaneously or consecutively to stimulate effector T cell attraction, transmigration, and function within the tumor environment.

The relative contribution of a normalized vasculature to alleviating immune suppression, following anti-VEGF therapy, for instance, remains unclear. However, based on encouraging preclinical data, combinatorial therapy of VEGF inhibition (bevacizumab) with checkpoint blockade (anti-PD-L1) is being trialed in Phase III studies in renal cell carcinoma (e.g., Phase III NCT02420821 at clinicaltrials.gov) [55]. There is now evidence that a normalized tumor vasculature can naturally arise in human cancers such as breast tumors in association with a pre-existing Th1 profile [56]; this is intriguing because normalized tumor vessels have so far mainly been observed and characterized in mouse cancer models. Moreover, it is possible that checkpoint inhibitors such as anti-CTLA-4 and anti-PD-1 could indirectly contribute to achieving a normalized vasculature by increasing effector T cells locally [56]. This hypothesis is supported by functional data demonstrating that breast tumors grown orthotopically in $\text{C}\text{D}4^+$ T cell-deficient mice, generated by deletion of the *Cd4* gene, harbor more abnormal, anergic and hyperpermeable blood vessels relative to wild type controls [56]. Moreover, anti-CTLA-4 and anti-PD-1 checkpoint blockade in $\text{C}\text{D}4^+$ T cell-competent animals can normalize vessels by increasing pericyte coverage and reducing vascular leakiness, suggesting that activated $\text{C}\text{D}4^+$ T cells may play a major role in this process [56]. Furthermore, when implanted into immune-deficient athymic nude mice, **patient-derived tumor xenografts (PDX)** display a hypoxic

phenotype harboring more leaky blood vessels than their freshly resected counterparts [56]. In addition, hypoxia in the tumor can be alleviated upon adoptive transfer of human Th1 cells, which also suggests that effector CD4⁺ T cell–endothelial interactions may normalize tumor vessels, stimulating, in turn, extravasation of effector cells in a positive feedback loop [56] (Figure 1). This may partially explain the observation that having pre-existing T cell infiltrates in close vicinity to tumor blood vessels can lead to therapeutic benefits and synergistic effects of vessel normalization and T cell activation that contribute to combating a neoplastic mass.

The Yin and Yang of IFN γ at the T Cell–Vascular Interface

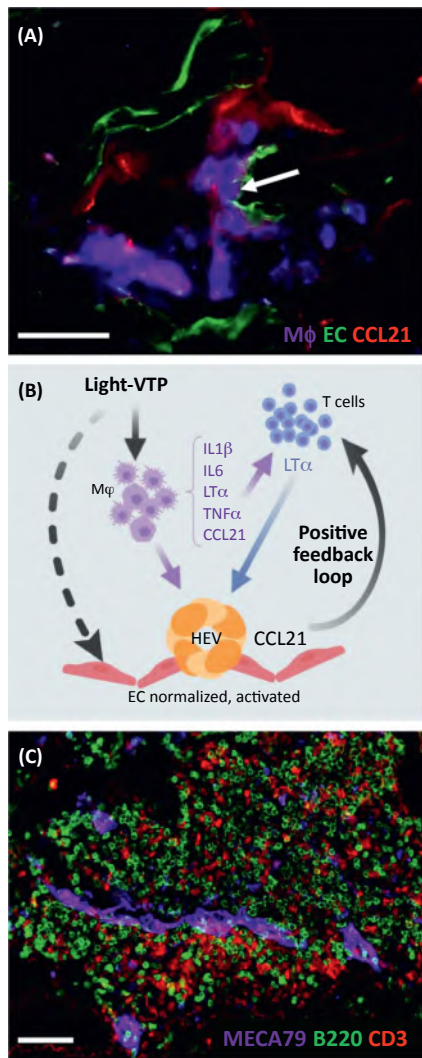
IFN γ is a key cytokine produced by Th1 cells and, amongst multiple other effects, induces expression of the angiostatic chemokines CXCL9 and CXCL10, upregulates endothelial cell ICAM-1, and induces T cell migration [56,57]. In a mouse model of methylcholanthrene-induced fibrosarcoma, helper CD4⁺ T cells were shown to play an essential role in the effector phase of the antitumor immune response; they produced Ifn γ , which in turn inhibited angiogenesis in a process that, as shown in *Ifn γ R*-deficient mice, depended on the expression of Ifn γ R on nonhematopoietic stromal cells [58]. Accordingly, Ifn γ R expression in tumor endothelial cells, but not in other stromal components, was shown to be sufficient to trigger Ifn γ -induced tumor cell necrosis and mass regression in a model of fibrosarcoma implanted in *Ifn γ* - and *Ifn γ R*-deficient transgenic mice, but which selectively expressed *Ifn γ R* in endothelial cells [59]. Indeed, Ifn γ , produced by engineered tumor cells or adoptively transferred effector CD8⁺ T cells, can induce potent antiangiogenic and antitumor effects. Specifically, in one study, chronic exposure to Ifn γ for 5 days in the tumor endothelium of mouse fibrosarcomas *in vivo* led to a controlled regression of blood vessels resembling physiological vascular remodeling [59] (Figure 1). Moreover, perivascular infiltration of Ifn γ -producing tumor antigen-specific T cells directly correlated with vascular remodeling processes preceding vessel regression [60]. Of note, Ifn γ and CD40L-producing Th1 cells have also been deemed crucial players in tumor vessel normalization, and this is interesting because their normalization effect was further increased upon anti-CTLA-4 and anti-PD-1 checkpoint blockade, even when orthotopic breast tumors were grown in the absence of CD8⁺ T cells in *Cd8* gene-deficient mice. This, in turn, demonstrated an exclusive and crucial role of CD4⁺ effector T cells in vessel normalization [56]. Furthermore, genetic pericyte depletion in mice carrying orthotopic mammary tumors reduced Th1 cell intratumor influx relative to wild type controls. In contrast, Th1 adoptive transfer improved pericyte coverage and increased overall immune cell penetration into tumor parenchyma relative to wild type breast cancers [56]. Thus, there appears to be a certain level of reciprocal control between Th1 cell migration and vessel normalization [56], although further studies are needed to better elucidate this process. The importance of CD4⁺ T cells in antitumor immunity is underscored by findings indicating that tumor penetration can be enabled by pharmacological Tgf β signaling blockade using Galunisertib (a TGF β receptor I inhibitor) in advanced murine colorectal cancer, concomitant with the presence of a Th1 effector phenotype, and that these may be required for successful anti-PD-1 checkpoint inhibitor treatments [61]. At a first glance, the role of IFN γ in vessel normalization and **pruning** appears somewhat paradoxical. However, intratumoral Ifn γ effects on tumor vasculature vary with Ifn γ dose and exposure time [50,62] and might induce dynamic rather than static vascular changes. Similar dose-dependent biological effects have been observed with anti-VEGF treatment in solid cancers. For example, low dose anti-Vegf therapy can induce temporary vessel normalization in murine breast cancer but can also ultimately lead to vessel pruning and vessel death [63]. Moreover, following Vegf or dual **angiopoietin 2**/Vegf inhibition in murine neuroendocrine pancreatic, metastatic breast, and melanoma tumors, Ifn γ secreted by activated CD8⁺ effector T cells can induce PD-L1 upregulation on endothelial cells, thus limiting overall tumor control by inducing immunosuppression [36,37]. However, paradoxically, this adaptive immune

resistance can also sensitize tumors to immune checkpoint inhibition via anti-PD-1 antibodies in melanoma and breast cancer models, thus providing further support for contemplating combined vascular and immune targeting strategies in the treatment of solid cancers [37]. Much like anti-VEGF therapy, the multiple facets of IFN γ treatment in the tumor microenvironment underscore the importance of mechanistic insights when designing IFN γ -inducing immunotherapies.

Therapeutic Induction of HEVs in Cancer: A Reciprocal Regulation of HEVs and Adaptive Immunity

Thus far, vessel normalization strategies in preclinical models have been mainly exploited in the context of preactivated effector T cells. However, since **neoantigens** are detectable in most solid cancers [64], it is prudent to speculate that remodeling of the vascular interface may also facilitate spontaneous antitumor immune cell influx. Taking vessel normalization one step further, HEVs (the entrance portals for naïve lymphocytes into peripheral lymph nodes) can be therapeutically induced in murine cancers such as neuroendocrine pancreatic tumors, breast cancers, and glioblastomas by stimulating lymphotoxin β receptor (LT β R) in the tumor microenvironment [36,53]. This process, similar to vessel normalization induced by adoptively transferred Th1 cells in breast cancer [56], requires reciprocal interactions between the tumor endothelium and infiltrating T cells [53] (Figure 1). For instance, in a mouse model of carcinogen-induced fibrosarcoma, T reg depletion increased numbers, proliferation, and activation of Tnf α -producing intratumoral CD8⁺ T cells, which then induced the formation of intratumoral HEVs; it was surmised that this process supported further effector T cell diapedesis in a self-amplifying loop [65,66]. In this context, the formation of HEVs was dependent on TnfR signaling since blockade of TnfR with TnfRII.Ig, anti-Tnf antibodies, or via anti-LT α treatment reduced HEVs specifically in fibrosarcomas, but not in secondary lymph nodes [65].

In the RIP-Tag mouse cancer model, targeting the TNF superfamily member Light specifically to tumor vessels using vascular targeting peptides (VTPs) (small linear peptide sequences specifically binding abnormal, angiogenic tumor vessels) initiated a cascade of events that involved perivascular macrophages and CD4⁺ and CD8⁺ T cells, leading to vessel normalization, HEV differentiation, and TLS formation (Figure 2) [53]. Intratumoral HEVs could then attract a higher number of naïve CD4⁺ and CD8⁺ T cells into tumors compared with HEV-negative cancers, which were sparsely infiltrated. While this alone was not curative in the RIP-Tag mouse model, the therapeutic potential of intratumoral TLS was vastly improved in combination with anti-CTLA-4 and anti-PD-1 immune checkpoint inhibition and/or antitumor vaccination [53]. In these studies, vessel normalization enabled initial T cell migration deep into the tumor parenchyma, where the cells played an essential part in inducing HEV differentiation and attraction of more T cells in a positive feedback loop [53] (Figure 2). Similar interrelationships between a normalized vasculature, T cells, and intratumoral lymph nodes have been observed clinically. For instance, in human pancreatic cancer, spontaneous TLS are surrounded by abundant capillaries displaying a normalized phenotype with high pericyte coverage, and which have been associated with a better prognosis in these patients [67]. Mechanistically different, albeit conceptually similar, anti-Vegf therapy, when combined with anti-PD-L1 blockade in murine pancreatic and breast cancers, can also induce normalized vessels, HEVs, and increased numbers of activated cytotoxic T cells in the tumor microenvironment relative to untreated tumors [36]. Similar to spontaneous HEV formation in cancer (Box 1), the ability of endothelial cells to differentiate into HEVs in these mouse models is directly linked to the degree of T cell infiltration [36,53] and further suggests a reciprocal regulation of vascular phenotype and adaptive immune function. In tumors where anti-Vegf/anti-PD-L1 therapy failed to increase effector T cell numbers, such as in glioblastoma, additional stimulation with anti-LT β R agonistic



Trends in Immunology

Figure 2. Tertiary Lymph Node Structure (TLS) Induction in Murine Pancreatic Neuroendocrine Cancers Can Trigger a Self-Amplifying Loop Involving Macrophages, Endothelial, and CD4⁺ or CD8⁺ T Cells. (A) Representative immunohistochemistry micrograph image depicting a cluster (arrow) of vascular structures (CD31, green) and perivascular macrophages (CD68, purple), decorated with the lymphoid tissue chemokine Ccl21 (red), which forms in pancreatic neuroendocrine RIP-Tag tumors after targeting Light specifically to angiogenic tumor vessels using a vascular targeting peptide (VTP) [53]. Scale bar, 25 μ m. (B) Vascular targeting of Light to RIP-Tag tumor vessels induces vessel normalization, high endothelial venules (HEVs), and tertiary lymph node structures (TLS) in a self-amplifying loop. Mechanistically, this can involve Light-triggered expression of inflammatory cytokines such as interleukin (Il)1 β , Il6, lymphotoxin (LT) α , tumor necrosis factor (Tnf) α , and the chemokine Ccl21 in macrophages (M ϕ), and subsequent recruitment of LT α -expressing CD4⁺ and CD8⁺ T cells. Both macrophages and T cells have been deemed essential for HEV/TLS induction [53]. EC, Endothelial cells. Created with ©BioRender.io. (C) Representative immunohistochemistry micrograph image depicting the formation of intratumoral TLS consisting of HEVs (MECA79, purple), B cells (B220, green), and T cells (CD3, red) that can occur following transfer of Light-stimulated macrophages into RIP-Tag mice bearing pancreatic neuroendocrine tumors, suggesting a key role for macrophages in triggering intratumoral TLS formation [53]. Scale bar, 50 μ m.

antibodies appeared to be required [36]. Activation of $LT\beta R$, the receptor for $LT\alpha$, $LT\beta$, and Light, induced HEVs, which in turn increased intratumoral T cell infiltration and sensitized resistant glioblastoma to anti-Vegf/anti-PD-L1 combination treatment [36]. Thus far, only few therapies have been shown to induce *bona fide* ectopic lymph nodes therapeutically; these include the treatment of mouse melanoma with antitumor antibodies fused to $LT\alpha$ [68], as well as treatment of pancreatic cancer patients with an attenuated, granulocyte-macrophage colony-stimulating factor-secreting, allogeneic, pancreatic tumor vaccine (GVAX), in combination with T reg depletion by low-dose cyclophosphamide [69]. Other approaches have tested vaccination of human papilloma virus (HPV)16-induced cervical cancer patients by targeting HPV16 E6/7 antigens [70], while others have aimed to treat pancreatic neuroendocrine mouse models with Light-VTP therapy [53], or anti-Vegf/anti-PD-L1 immunotherapy in combination with $LT\beta R$ stimulation via agonistic antibodies or Light-VTP, in mouse glioblastoma [36,71]. Increasing evidence suggests that combination therapies may induce a more functional or normalized vasculature and a critical threshold of effector T cells at the lesion site that can then induce HEVs and, presumably, render immune-enhancing therapies more effective. Future studies are warranted to investigate these possibilities.

Concluding Remarks

Some tumors, in particular those with high mutational load, such as melanoma and lung cancer [64], may spontaneously develop HEVs, as well as recruit and activate antitumor lymphocytes [72]. Controlling tumor growth in most cancers, however, requires escape from tumor-intrinsic immune suppression, for instance by depleting T regs or checkpoint blockade [65,39]. In fact, triple and quadruple combinations of immunotherapies are often required for immune-mediated destruction of advanced melanoma or pancreatic cancers in clinically relevant autochthonous mouse models [53,73]. The common denominator of successful immunotherapies is the attraction and function of sufficient intratumoral effector $CD4^+$ and $CD8^+$ T cells that can destroy the cancer. Recent exciting findings described in this review have demonstrated an unrecognized role of $CD4^+$ and/or $CD8^+$ T cells in vascular reprogramming and self-amplifying activation loops at the vascular wall. This role may be key in the design of more effective combination therapies that might increase the efficacies of immunotherapies such as anticancer vaccination or checkpoint inhibition. Thus, renewed interest has been sparked to better understand the potential of combined vascular and immune targeting strategies, such as anti-VEGF and immune checkpoint inhibition; indeed, clinical data from ongoing trials are highly anticipated [5]. Nevertheless, the field faces multiple challenges which include intrinsic tumor heterogeneity, the ultimate transient nature of stromal remodeling, as well as the lack of robust biomarkers that can determine vessel status before, during, and after therapy (see Outstanding Questions). For instance, the limitations of anti-VEGF therapy include short-lived normalization effects and induction of vessel death, which may trigger tumor resistance and relapse [74]. Whether transient stromal remodeling, when combined with T cell activation, will induce long-lasting antitumor effects remains to be determined. Moreover, therapies which induce high levels of intratumoral $IFN\gamma$, such as with anti-Vegf treatment, can also upregulate PD-L1, which can in turn lead to adaptive resistance as demonstrated in models of melanoma, pancreatic neuroendocrine, and breast cancers [36,37].

As a possible cause or consequence of antitumor immunity, HEV induction deserves further consideration when designing new immune combination therapies. Their therapeutic exploitation, however, requires a better understanding of the cellular players, chemokines, and cytokines involved in the generation of HEVs as well as of TLS in different cancer types. One might speculate that TLS-promoting factors may help to quickly expand local immune effector cells to a critical mass of therapeutic functionality. It is also possible that sustained

Outstanding Questions

What might be the most effective combination therapies that can simultaneously attract T cells, support transmigration, and facilitate T cell effector function in the eradication of solid tumors?

How durable is endothelial remodeling (activation, normalization, and HEV formation)?

Is vessel normalization a prerequisite for HEV induction?

How can endothelial remodeling be monitored clinically?

What are the respective roles of $CD4^+$ and $CD8^+$ effector T cells in vessel remodeling and tumor rejection?

What are the key T cell cytokines/chemokines that enable synergistic tumor blood vessel remodeling and HEV formation?

What are the roles of perivascular innate immune cells in HEV formation?

What is required to maximize a self-perpetuating immune-vascular loop before vessels are destroyed in an ongoing antitumor immune response?

Once vessels are destroyed in an ongoing antitumor immune response, what additional immune stimulation is required to minimize the risk of tumor relapse?

What is the impact of tumor blood vessel remodeling and HEV formation on metastasis?

vascular ‘preconditioning’ such as tumor vessel activation, normalization, or differentiation may be a prerequisite to maximizing T cell trafficking, function, and tumor cell elimination in a self-perpetuating loop, before stromal destruction can limit effector T cell infiltration. The next key steps will be to carefully dissect these potential mechanisms in solid tumor eradication.

Acknowledgements

This work was supported by the National Health and Medical Research Council (APP1042446, APP1122108, APP1141847), the Cancer Council of Western Australia and Woodside Energy (Fellowship to R.G.).

Disclaimer Statement

The authors declare no conflicts of interest.

References

- De Palma, M. *et al.* (2017) Microenvironmental regulation of tumour angiogenesis. *Nat. Rev. Cancer* 17, 457–474
- Johansson, A. *et al.* (2016) More than a scaffold: stromal modulation of tumor immunity. *Biochim. Biophys. Acta* 1865, 3–13
- Lanitis, E. *et al.* (2015) Targeting the tumor vasculature to enhance T cell activity. *Curr. Opin. Immunol.* 33, 55–63
- Rivera, L.B. and Bergers, G. (2015) Intertwined regulation of angiogenesis and immunity by myeloid cells. *Trends Immunol.* 36, 240–249
- Ott, P.A. *et al.* (2015) Inhibition of immune checkpoints and vascular endothelial growth factor as combination therapy for metastatic melanoma: an overview of rationale, preclinical evidence, and initial clinical data. *Front. Oncol.* 5, 202
- Jain, R.K. (2014) Antiangiogenesis strategies revisited: from starving tumors to alleviating hypoxia. *Cancer Cell* 26, 605–622
- Huang, Y. *et al.* (2012) Vascular normalizing doses of antiangiogenic treatment reprogram the immunosuppressive tumor microenvironment and enhance immunotherapy. *Proc. Natl. Acad. Sci. U. S. A.* 109, 17561–17566
- Vestweber, D. (2015) How leukocytes cross the vascular endothelium. *Nat. Rev. Immunol.* 15, 692–704
- Lee, M. *et al.* (2014) Transcriptional programs of lymphoid tissue capillary and high endothelium reveal control mechanisms for lymphocyte homing. *Nat. Immunol.* 15, 982–995
- Girard, J.P. *et al.* (2012) HEVs, lymphatics and homeostatic immune cell trafficking in lymph nodes. *Nat. Rev. Immunol.* 12, 762–773
- Pober, J.S. and Tselides, G. (2012) Participation of blood vessel cells in human adaptive immune responses. *Trends Immunol.* 33, 49–57
- Dieu-Nosjean, M.C. *et al.* (2014) Tertiary lymphoid structures in cancer and beyond. *Trends Immunol.* 35, 571–580
- Colbeck, E.J. *et al.* (2017) Tertiary lymphoid structures in cancer: drivers of antitumor immunity, immunosuppression, or bystander sentinels in disease? *Front. Immunol.* 8, 1830
- Ryschich, E. *et al.* (2002) Transformation of the microvascular system during multistage tumorigenesis. *Int. J. Cancer* 97, 719–725
- Fisher, D.T. *et al.* (2011) IL-6 trans-signaling licenses mouse and human tumor microvascular gateways for trafficking of cytotoxic T cells. *J. Clin. Invest.* 121, 3846–3859
- Dirkx, A.E. *et al.* (2003) Tumor angiogenesis modulates leukocyte-vessel wall interactions *in vivo* by reducing endothelial adhesion molecule expression. *Cancer Res.* 63, 2322–2329
- Hino, R. *et al.* (2010) Tumor cell expression of programmed cell death-1 ligand 1 is a prognostic factor for malignant melanoma. *Cancer* 116, 1757–1766
- Griffith, J.W. *et al.* (2014) Chemokines and chemokine receptors: positioning cells for host defense and immunity. *Annu. Rev. Immunol.* 32, 659–702
- Mikucki, M.E. *et al.* (2015) Non-redundant requirement for CXCR3 signalling during tumoricidal T-cell trafficking across tumour vascular checkpoints. *Nat. Commun.* 6, 7458
- Sistigu, A. *et al.* (2014) Cancer cell-autonomous contribution of type I interferon signaling to the efficacy of chemotherapy. *Nat. Med.* 20, 1301–1309
- Barreira da Silva, R. *et al.* (2015) Dipeptidylpeptidase 4 inhibition enhances lymphocyte trafficking, improving both naturally occurring tumor immunity and immunotherapy. *Nat. Immunol.* 16, 850–858
- Spranger, S. *et al.* (2015) Melanoma-intrinsic beta-catenin signalling prevents anti-tumour immunity. *Nature* 523, 231–235
- Moon, E.K. *et al.* (2011) Expression of a functional CCR2 receptor enhances tumor localization and tumor eradication by retargeted human T cells expressing a mesothelin-specific chimeric antibody receptor. *Clin. Cancer Res.* 17, 4719–4730
- Halama, N. *et al.* (2016) Tumoral immune cell exploitation in colorectal cancer metastases can be targeted effectively by anti-CCR5 therapy in cancer patients. *Cancer Cell* 29, 587–601
- Curiel, T.J. *et al.* (2004) Specific recruitment of regulatory T cells in ovarian carcinoma fosters immune privilege and predicts reduced survival. *Nat. Med.* 10, 942–949
- Facciabene, A. *et al.* (2011) Tumour hypoxia promotes tolerance and angiogenesis via CCL28 and T(reg) cells. *Nature* 475, 226–230
- Ganss, R. *et al.* (2002) Combination of T-cell therapy and trigger of inflammation induces remodeling of the vasculature and tumor eradication. *Cancer Res.* 62, 1462–1470
- Srivastava, M.K. *et al.* (2012) Myeloid suppressor cell depletion augments antitumor activity in lung cancer. *PLoS One* 7, e40677
- Romagnani, P. *et al.* (2004) CXC chemokines: the regulatory link between inflammation and angiogenesis. *Trends Immunol.* 25, 201–209
- Bouzin, C. *et al.* (2007) Effects of vascular endothelial growth factor on the lymphocyte-endothelium interactions: identification of caveolin-1 and nitric oxide as control points of endothelial cell anergy. *J. Immunol.* 178, 1505–1511
- Buckanovich, R.J. *et al.* (2008) Endothelin B receptor mediates the endothelial barrier to T cell homing to tumors and disables immune therapy. *Nat. Med.* 14, 28–36
- Motz, G.T. *et al.* (2014) Tumor endothelium FasL establishes a selective immune barrier promoting tolerance in tumors. *Nat. Med.* 20, 607–615
- Airas, L. *et al.* (2000) CD73 engagement promotes lymphocyte binding to endothelial cells via a lymphocyte function-associated antigen-1-dependent mechanism. *J. Immunol.* 165, 5411–5417
- Wang, L. *et al.* (2011) CD73 has distinct roles in nonhematopoietic and hematopoietic cells to promote tumor growth in mice. *J. Clin. Invest.* 121, 2371–2382
- Allard, B. *et al.* (2014) Anti-CD73 therapy impairs tumor angiogenesis. *Int. J. Cancer* 134, 1466–1473

36. Allen, E. *et al.* (2017) Combined antiangiogenic and anti-PD-L1 therapy stimulates tumor immunity through HEV formation. *Sci. Transl. Med.* 9, eaak9679
37. Schmittnaegel, M. *et al.* (2017) Dual angiopoietin-2 and VEGFA inhibition elicits antitumor immunity that is enhanced by PD-1 checkpoint blockade. *Sci. Transl. Med.* 9, eaak9670
38. Tumeah, P.C. *et al.* (2014) PD-1 blockade induces responses by inhibiting adaptive immune resistance. *Nature* 515, 568–571
39. Tang, H. *et al.* (2016) Facilitating T cell infiltration in tumor microenvironment overcomes resistance to PD-L1 blockade. *Cancer Cell* 29, 285–296
40. Klug, F. *et al.* (2013) Low-dose irradiation programs macrophage differentiation to an iNOS(+)/M1 phenotype that orchestrates effective T cell immunotherapy. *Cancer Cell* 24, 589–602
41. Sharabi, A.B. *et al.* (2015) Radiation and checkpoint blockade immunotherapy: radiosensitisation and potential mechanisms of synergy. *Lancet Oncol.* 16, e498–e509
42. Kang, J. *et al.* (2016) Current clinical trials testing the combination of immunotherapy with radiotherapy. *J. Immunother. Cancer* 4, 51
43. Garbi, N. *et al.* (2004) CpG motifs as proinflammatory factors render autochthonous tumors permissive for infiltration and destruction. *J. Immunol.* 172, 5861–5869
44. Sektioglu, I.M. *et al.* (2016) Macrophage-derived nitric oxide initiates T-cell diapedesis and tumor rejection. *Oncot Immunology* 5, e1204506
45. El Kebir, D. *et al.* (2009) Bacterial DNA activates endothelial cells and promotes neutrophil adherence through TLR9 signaling. *J. Immunol.* 182, 4386–4394
46. Demaria, O. *et al.* (2015) STING activation of tumor endothelial cells initiates spontaneous and therapeutic antitumor immunity. *Proc. Natl. Acad. Sci. U. S. A.* 112, 15408–15413
47. Johansson, A. *et al.* (2014) License for destruction: tumor-specific cytokine targeting. *Trends Mol. Med.* 20, 16–24
48. Facciabene, A. *et al.* (2017) Local endothelial complement activation reverses endothelial quiescence, enabling T-cell homing, and tumor control during T-cell immunotherapy. *Oncot Immunology* 6, e1326442
49. Bonavita, E. *et al.* (2015) PTX3 is an extrinsic oncosuppressor regulating complement-dependent inflammation in cancer. *Cell* 160, 700–714
50. Johansson, A. *et al.* (2012) Tumor-targeted TNF α stabilizes tumor vessels and enhances active immunotherapy. *Proc. Natl. Acad. Sci. U. S. A.* 109, 7841–7846
51. Johansson-Percival, A. *et al.* (2015) Intratumoral LIGHT restores pericyte contractile properties and vessel integrity. *Cell Rep.* 13, 2687–2698
52. Hamzah, J. *et al.* (2008) Vascular normalization in Rgs5-deficient tumours promotes immune destruction. *Nature* 453, 410–414
53. Johansson-Percival, A. *et al.* (2017) *De novo* induction of intratumoral lymphoid structures and vessel normalization enhances immunotherapy in resistant tumors. *Nat. Immunol.* 18, 1207–1217
54. Zhao, Y. *et al.* (2017) Targeting vascular endothelial-cadherin in tumor-associated blood vessels promotes T-cell-mediated immunotherapy. *Cancer Res.* 77, 4434–4447
55. Bradley, C.A. (2018) Checkpoint inhibitor combination sets the wheels in motion. *Nat. Rev. Urol.* Published online June 19, 2018. <http://dx.doi.org/10.1038/s41585-018-0043-8>
56. Tian, L. *et al.* (2017) Mutual regulation of tumour vessel normalization and immunostimulatory reprogramming. *Nature* 544, 250–254
57. Nakajima, C. *et al.* (2001) A role of interferon-gamma (IFN-gamma) in tumor immunity: T cells with the capacity to reject tumor cells are generated but fail to migrate to tumor sites in IFN-gamma-deficient mice. *Cancer Res.* 61, 3399–3405
58. Qin, Z. and Blankenstein, T. (2000) CD4⁺ T cell-mediated tumor rejection involves inhibition of angiogenesis that is dependent on IFN gamma receptor expression by nonhematopoietic cells. *Immunity* 12, 677–686
59. Kammertoens, T. *et al.* (2017) Tumour ischaemia by interferon-gamma resembles physiological blood vessel regression. *Nature* 545, 98–102
60. Schietinger, A. *et al.* (2013) Longitudinal confocal microscopy imaging of solid tumor destruction following adoptive T cell transfer. *Oncot Immunology* 2, e26677
61. Tauriello, D.V.F. *et al.* (2018) TGF β drives immune evasion in genetically reconstituted colon cancer metastasis. *Nature* 554, 538–543
62. Gasparri, A.M. *et al.* (2008) Critical role of indoleamine 2,3-dioxygenase in tumor resistance to repeated treatments with targeted IFN γ . *Mol. Cancer Ther.* 7, 3859–3866
63. Huang, Y. *et al.* (2013) Vascular normalization as an emerging strategy to enhance cancer immunotherapy. *Cancer Res.* 73, 2943–2948
64. Schumacher, T.N. and Schreiber, R.D. (2015) Neoantigens in cancer immunotherapy. *Science* 348, 69–74
65. Colbeck, E.J. *et al.* (2017) Treg depletion licenses T cell-driven HEV neogenesis and promotes tumor destruction. *Cancer Immunol. Res.* 5, 1005–1015
66. Hindley, J.P. *et al.* (2012) T-cell trafficking facilitated by high endothelial venules is required for tumor control after regulatory T-cell depletion. *Cancer Res.* 72, 5473–5482
67. Hiraoka, N. *et al.* (2015) Intratumoral tertiary lymphoid organ is a favourable prognosticator in patients with pancreatic cancer. *Br. J. Cancer* 112, 1782–1790
68. Schrama, D. *et al.* (2001) Targeting of lymphotoxin- α to the tumor elicits an efficient immune response associated with induction of peripheral lymphoid-like tissue. *Immunity* 14, 111–121
69. Lutz, E.R. *et al.* (2014) Immunotherapy converts nonimmunogenic pancreatic tumors into immunogenic foci of immune regulation. *Cancer Immunol. Res.* 2, 616–631
70. Maldonado, L. *et al.* (2014) Intramuscular therapeutic vaccination targeting HPV16 induces T cell responses that localize in mucosal lesions. *Sci. Transl. Med.* 6, 221ra13
71. He, B. *et al.* (2018) Vascular targeting of LIGHT normalizes blood vessels in primary brain cancer and induces intratumoural high endothelial venules. *J. Pathol.* 245, 209–221
72. Peske, J.D. *et al.* (2015) Effector lymphocyte-induced lymph node-like vasculature enables naive T-cell entry into tumours and enhanced anti-tumour immunity. *Nat. Commun.* 6, 7114
73. Moynihan, K.D. *et al.* (2016) Eradication of large established tumors in mice by combination immunotherapy that engages innate and adaptive immune responses. *Nat. Med.* 22, 1402–1410
74. Bergers, G. and Hanahan, D. (2008) Modes of resistance to antiangiogenic therapy. *Nat. Rev. Cancer* 8, 592–603
75. Gu-Trantien, C. *et al.* (2013) CD4(+) follicular helper T cell infiltration predicts breast cancer survival. *J. Clin. Invest.* 123, 2873–2892
76. Martinet, L. *et al.* (2013) High endothelial venule blood vessels for tumor-infiltrating lymphocytes are associated with lymphotoxin beta-producing dendritic cells in human breast cancer. *J. Immunol.* 191, 2001–2008
77. Gantsev, S.K. *et al.* (2013) The role of inflammatory chemokines in lymphoid neoorganogenesis in breast cancer. *Biomed. Pharmacother.* 67, 363–366
78. Martinet, L. *et al.* (2011) Human solid tumors contain high endothelial venules: association with T- and B-lymphocyte infiltration and favorable prognosis in breast cancer. *Cancer Res.* 71, 5678–5687
79. Bento, D.C. *et al.* (2015) High endothelial venules are rare in colorectal cancers but accumulate in extra-tumoral areas with disease progression. *Oncot Immunology* 4, e974374
80. Joshi, N.S. *et al.* (2015) Regulatory T cells in tumor-associated tertiary lymphoid structures suppress anti-tumor T cell responses. *Immunity* 43, 579–590

81. Hamzah, J. *et al.* (2009) Targeted liposomal delivery of TLR9 ligands activates spontaneous antitumor immunity in an autochthonous cancer model. *J. Immunol.* 183, 1091–1098
82. Hamzah, J. *et al.* (2008) Vascular targeting of anti-CD40 antibodies and IL-2 into autochthonous tumors enhances immunotherapy in mice. *J. Clin. Invest.* 118, 1691–1699
83. Calcinotto, A. *et al.* (2012) Targeting TNF-alpha to neoangiogenic vessels enhances lymphocyte infiltration in tumors and increases the therapeutic potential of immunotherapy. *J. Immunol.* 188, 2687–2694
84. Ganss, R. (2017) Cytokine therapy in the microenvironment: old players, new tricks. In *Cytokine Effector Functions in Tissues*, pp. 239–252, Elsevier



OUR NETWORK IS YOUR NETWORK

With Cell Press Webinars, our network is your network!


Cell Press Webinars give you access to hot topics in emerging research and the application of new technology.

Watch essential, need-to-know webcasts via live streaming or on demand from the comfort and convenience of your office, lab, or home.

Need-to-know topics, editorially curated

World-class presenters, experts in their field

Moderated by Cell Press editors



Powered by
people in the know.
Like you.

Tap into our network today!
Visit www.cell.com/webinars

CellPress
Webinars

Review

The Role of Type 1 Conventional Dendritic Cells in Cancer Immunity

Jan P. Böttcher^{1,*} and Caetano Reis e Sousa^{2,*}

Dendritic cells (DCs) are key orchestrators of immune responses. A specific DC subset, conventional type 1 DCs (cDC1s), has been recently associated with human cancer patient survival and, in preclinical models, is critical for the spontaneous rejection of immunogenic cancers and for the success of T cell–based immunotherapies. The unique role of cDC1 reflects the ability to initiate *de novo* T cell responses after migrating to tumor-draining lymph nodes, as well as to attract T cells, secrete cytokines, and present tumor antigens within the tumor microenvironment, enhancing local cytotoxic T cell function. Strategies aimed at increasing cDC1 abundance in tumors and enhancing their functionality provide attractive new avenues to boost anti-tumor immunity and overcome resistance to cancer immunotherapies.

DC Biology in Cancer

Conventional DCs (cDCs) are especially adept at presenting exogenous and endogenous antigens to T cells and regulating T cell proliferation, survival, and effector function. This unique function of cDCs is crucial in the context of cancer, where cDCs take up antigens from tumor cells and present them to T cells within the tumor microenvironment (TME) or after migration to tumor-draining lymph nodes.

cDCs in mice and humans express CD11c and MHC class II and can be divided into two distinct subsets, cDC1 and cDC2 [1,2], although additional subsets can be delineated in both mice and humans [3–5]. cDC1 depend on the transcription factors BATF3, IRF8, and ID2 for their development [5] and selectively express the chemokine receptor XCR1 and the C-type lectin receptor DNGR-1/CLEC9A [3,6–8]. Expression of the integrin α E (CD103) is also commonly used as an additional marker to identify cDC1 in mouse tumors, while BDCA3 is used for the same purpose in humans [9] (Box 1). cDC1sexcel at cross-presenting exogenous antigens (e.g., tumor antigens) to CD8⁺ T cells and are key cells for the generation of cytotoxic effector T cell responses. The importance of cDC1 in anti-tumor immunity is underscored by several studies with cDC1-deficient *Batf3*^{-/-} mice and other *in vivo* models of cDC1 depletion, which consistently display a loss of the ability to reject transplantable immunogenic tumors and are unable to support T cell–based immunotherapies such as adoptive T cell therapy or immune checkpoint blockade [10–14]. In the above-mentioned models, loss of BATF3-dependent cDC1 cannot be compensated by other DC subsets or through BATF3-independent cDC1 development, for example, through cytokine-mediated induction of BATF and BATF2 [15]. However, cDC1s appear redundant for the success of poly(I:C) therapy and anthracycline chemotherapy in some mouse tumor models, arguing that other cells can compensate for lack of cDC1 in certain instances [16,17].

The development of cDC2 depends on the transcription factors RELB, IRF4, and ZEB2 [2,5], although additional subtypes of cDC2 have been characterized, including one that selectively

Highlights

Conventional type 1 dendritic cells (cDC1s) are a specialized subset of DCs with a unique role in cancer immune control.

Rejection of immunogenic cancers and the success of T cell–based immunotherapies in preclinical models requires functional cDC1s.

In human cancer patients, cDC1 abundance in tumor tissue is associated with cancer patient survival and the responsiveness to immune checkpoint blockade.

The access of cDC1s to tumor tissue is tightly regulated and involves chemokine secretion from intratumoral lymphocytes such as natural killer cells.

Tumor-derived factors impair anti-tumor immunity by limiting cDC1 accumulation, survival, and function within the tumor microenvironment.

¹Institute of Molecular Immunology and Experimental Oncology, Klinikum rechts der Isar, Technische Universität München, Ismaningerstraße 22, 81675 München, Germany

²Immunobiology Laboratory, The Francis Crick Institute, 1 Midland Road, London NW1 1AT, UK

*Correspondence: j.boettcher@tum.de (J.P. Böttcher) and caetano@crick.ac.uk (C. Reis e Sousa).

Box 1. Human cDC1

In lymphoid and non-lymphoid organs, human cDC1s can be identified by BDCA3 expression and show a close relationship with mouse cDC1s at the gene expression level [9]. Similar to their murine counterparts, human cDC1s selectively express the C-type lectin receptor CLEC9A/DNGR-1 and XCR1, and this selective expression can be used in conjunction with BDCA3 expression to reliably identify these cells in human tissues. In addition to these phenotypic similarities, human and mouse cDC1s share many functional characteristics such as the efficient uptake and processing of dead cell-associated antigen for cross-presentation to CD8⁺ T cells and Toll-like receptor 3-induced production of IL-12 [67,68]. However, IL-12 production is not as restricted to cDC1s in humans as in mice and can also be observed in cDC2s upon appropriate stimulation [69,70].

Although human cDC1s only constitute a minority of myeloid cells in human tumors, similar to their murine counterparts, their presence in the TME is often associated with better survival of cancer patients [10,26,27]. Furthermore, the abundance of cDC1s in human melanoma positively correlates with the responsiveness of these cancer patients to anti-PD-1 therapy [28]. These recent findings suggest an important role for cDC1 in anticancer immunity in humans.

depends on KLF4 [18]. cDC2s are commonly distinguished from cDC1s by their preferential expression of CD11b and CD172a. However, these markers do not suffice to reliably identify cDC2s in inflamed tissues or tumors as their expression is shared with other CD11c⁺MHCII⁺ myeloid cells such as macrophages and monocyte-derived DCs, which differ from cDCs [19,20]. Whereas cDC1 can be accurately identified by selective expression of molecules such as DNGR-1 or XCR1, proteins uniquely expressed by cDC2 have not yet been identified, hindering the development of models for selective detection and/or depletion of cDC2s in tumors. This might be one reason why knowledge about the behavior of cDC2s in tumors and their role in anti-tumor immunity is still limited. It is often assumed that cDC2s are predominantly involved in antigen presentation on MHC class II to CD4T cells in tumor-draining lymph nodes, similar to their role in microbial infection [2].

In this review article, we discuss the unique role of cDC1 in cancer immune control, focusing on the mechanisms and molecular pathways that enable cDC1 to accumulate in tumors, orchestrate anti-tumor immunity after migration to lymph nodes, and support immunity within tumor tissue. We further indicate how different aspects of cDC1 function are inhibited by immunosuppressive factors present within the TME. We refrain from discussing the pathways that lead to DC activation such as the recognition of damage-associated molecular patterns from dying tumor cells, which are important for ensuring DC functionality but have received ample coverage in the recent past [21–23].

Access of DCs to Tumor Tissue

Compared to healthy tissue, cDC1s are under-represented in tumors [24] and constitute a small minority of intratumoral leukocytes in both mice and humans [10,11,25]. Despite their scarcity, the overall tumor content of cDC1s, as assessed by cDC1-specific signatures in gene expression data and/or by flow cytometric analysis, positively correlates with cancer patient survival across multiple cancers and is predictive of the responsiveness to anti-PD-1 immunotherapy in melanoma patients [10,26–28]. Consequently, elevating cDC1 numbers in tumors by expansion with cytokines or through recruitment with chemokines (see below) leads to accelerated anti-tumor immunity, even in absence of added stimuli to promote cDC1 activation [11,27].

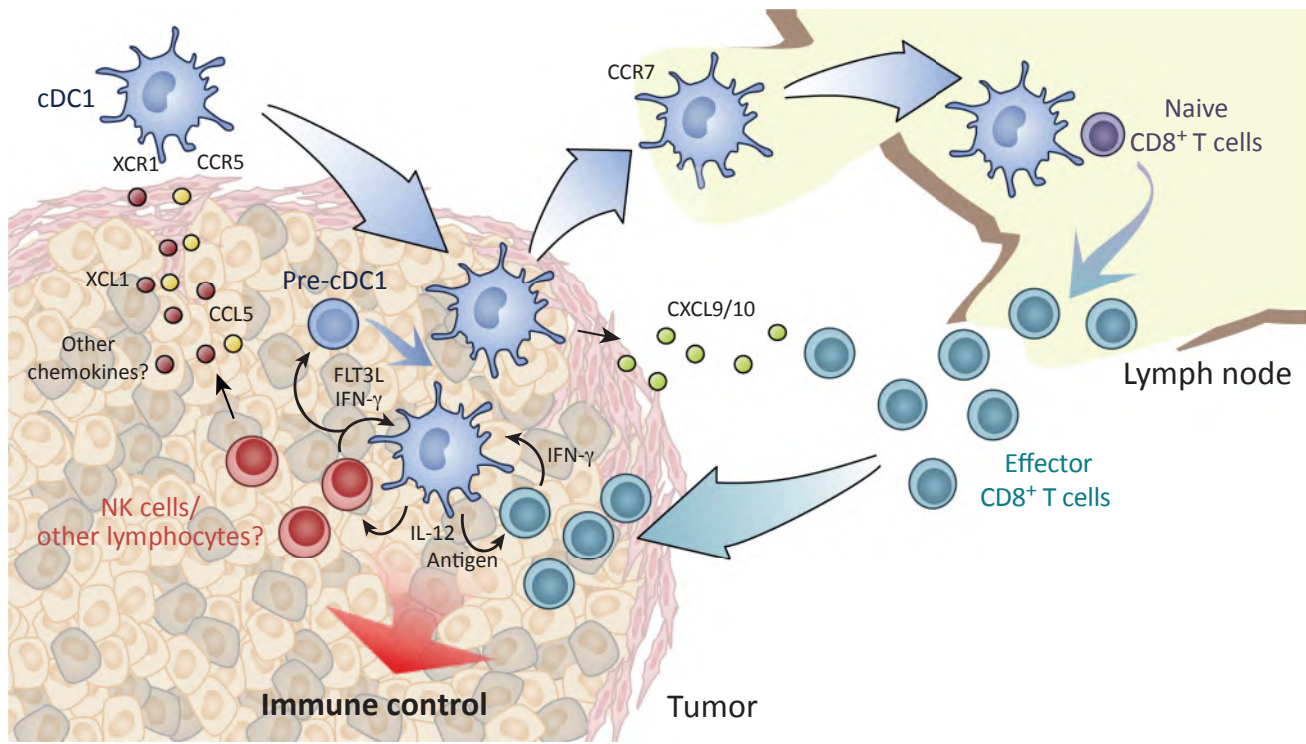
The mechanisms that determine cDC1 abundance in tumors can involve chemokine-mediated recruitment, as well as chemokine-dependent retention and positioning of cDC1s within the TME. A major source of chemokines is the cancer cells themselves, because they secrete

CXCL1, CCL2, and CCL20 to attract tumor-promoting immune cells such as monocytes, macrophages, regulatory T cells (T_{reg} cells), and T helper 22 cells [29,30]. Preferential production by tumor cells of chemokines that attract pro-tumorigenic immune cells might be one reason for the low cDC1 abundance observed in progressing tumors. Of note, absence of oncogenic signaling via the WNT/ β -catenin pathway in the murine $BRAF^{V600E}/PTEN^{-/-}$ melanoma model allows production of CCL4 by tumor cells and causes increased accumulation of cDC1s within the TME [13].

Besides CCL4, other chemokines can attract cDC1s into tumors. We recently investigated the accumulation of cDC1s in mouse transplantable tumors that are susceptible to cDC1-dependent immune control due to genetic ablation of the enzymes cyclooxygenase (COX)1 and COX2 in cancer cells [27,31]. In these COX-deficient tumors, the immune-suppressive prostanoid prostaglandin E_2 (PGE_2) is not produced, and cDC1s are recruited into the TME by the chemokines CCL5 and XCL1. Interestingly, those chemokines are not produced by the cancer cells but by natural killer (NK) cells that infiltrate tumors shortly after implantation [27]. NK cell-derived chemokines not only contribute to intratumoral cDC1 accumulation but also further regulate the local positioning of cDC1s within tumor tissue, allowing penetration of cDC1s into the TME and formation of NK cell/cDC1 clusters [27], an observation that was confirmed in an independent study [28]. Notably, in human cancer biopsies, the transcript levels of CCL5, XCL1, and its paralog XCL2 are associated with a cDC1-specific gene signature, suggesting a similar role for these chemokines in attracting cDC1s into human tumors [27]. The production of cDC1-recruiting chemokines by tumor NK cells therefore seems to be an important pathway regulating cDC1 accumulation within the TME (Figure 1).

Other cells such as $CD8^+$ T cells and innate lymphocytes [e.g., $\gamma\delta$ T cells, innate lymphoid cells (ILC1s)] are in principle able to produce both CCL5 and XCL1 and might contribute to cDC1 recruitment under certain circumstances or in other tumor contexts. In contrast to CCL5, which acts on the chemokine receptor CCR5 and can promote migration of tumor-promoting immune cells such as macrophages and T_{reg} cells [32,33], XCL1 acts as a ligand for XCR1 and acts on $XCR1^+$ cDC1s but not on other cells [7]. Local induction of XCL1 production in tumors, for example, by stimulation of intratumoral NK cells or targeted delivery of XCR1 ligands into tumors might therefore be an attractive strategy to attract cDC1s into the TME.

In addition to chemokine-mediated cDC1 recruitment and retention, cDC1 abundance within tumors is likely further regulated by the local availability of DC growth factors such as fms-like tyrosine kinase 3 ligand (FLT3L). Notably, NK cells were recently described as a key source of intratumoral FLT3L, which sustained the viability of cDC1s in the TME [28]. These data indicate that NK cells play a dual role in both cDC1 recruitment and positioning and in maintaining cDC1 longevity and functional competence [27,28] (Figure 1). Notably, FLT3L can also act on cDC precursors to favor cDC1 differentiation [34]. Consistent with that notion, treatment of mice with FLT3L leads to accumulation in tumors of $IRF8^+CD11c^+MHCI^+CD103^-$ cells that resemble precursors of cDC1 [11]. Intratumoral production of FLT3L by NK cells could therefore also facilitate local expansion of such precursors [28] (Figure 1). However, it is unlikely that all cDC1s in tumors originate from local expansion of recruited precursors. Indeed, fully differentiated cDC1 recruited from blood or surrounding tissue might be the predominant origin of intratumoral cDC1s that accumulate in response to XCL1 and CCL5 produced by tumor NK cells because cDC1 precursors express only low levels of transcripts for CCR5 and XCR1 [35] (Figure 1). Alternatively, the chemokines might be involved in prolonging intratumoral retention of cDC1s that differentiated locally from pre-cDCs, resulting in the observed net increase in cDC1 numbers.



Trends in Cancer

Figure 1. Orchestration of Cancer Immune Control by cDC1. Conventional type 1 dendritic cells (cDC1s) are recruited into the tumor microenvironment by chemokines such as XCL1 and CCL5, produced by intratumoral natural killer (NK) cells (and potentially other lymphocytes). NK cells further secrete the growth factor FLT3L, which supports the survival of cDC1s and might enhance local cDC1 differentiation from DC precursors. Within the tumor, cDC1s take up material from (dead?) tumor cells and are uniquely able to transport tumor antigens to tumor-draining lymph nodes for presentation to naive CD8⁺ T cells, priming cytotoxic effector CD8⁺ T cells. In addition, cDC1s within the tumor microenvironment produce the chemokines CXCL9/10 that can recruit CD8⁺ effector T cells into tumor tissue and can locally present tumor antigens to restimulate recruited T cells. Finally, the anti-tumor activity of T cells and NK cells within the tumor might further be boosted by cytokines made by cDC1, for example, interleukin-12 (IL-12), that, in turn, is amplified by T- and NK cell-derived cytokines such as interferon-γ (IFN-γ).

Priming of T Cells after Antigen Delivery to Tumor-Draining Lymph Nodes

De novo generation of cytotoxic effector CD8⁺ T cells specific for tumor antigens depends on cDCs cross-presenting tumor peptides on MHC class I molecules to naive antigen-specific T cells. Such T cell priming is thought to predominantly occur in tumor-draining lymph nodes, although some naive T cells might also be primed within the TME [36]. While tumor antigens can reach lymph nodes by themselves in certain experimental setups such as the injection of a high number of apoptotic tumor cells [37] or, naturally, during metastasis, priming of T cells in tumor-draining lymph nodes from progressively growing non-invasive tumors requires the delivery of tumor antigens to tumor-draining lymph nodes by migratory cDCs. Experiments with fluorescently labeled tumor cells demonstrated that although fluorescent material is efficiently taken up by different antigen-presenting cell populations within the TME, in tumor-draining lymph nodes fluorescence is predominantly detected in migratory CD103⁺ cDC1s [11,38]. It therefore seems that although tumor cDC2s also migrate to tumor-draining lymph nodes, only cDC1s are able to deliver intact tumor antigens to tumor-draining lymph nodes, a process that depends on the chemokine receptor CCR7 [11,38].

Within tumor-draining lymph nodes, CD103⁺ cDC1s transfer a fraction of fluorescently labeled material to other antigen-presenting cell populations, including resident CD8α⁺ cDC1s [38]

(Box 2). Despite this transfer, when isolated from tumor-draining lymph nodes and tested *ex vivo*, only migratory CD103⁺ cDC1s, but not lymph node-resident CD8 α ⁺ cDC1s, have the capacity to stimulate naive CD8⁺ T cells against tumor-associated model antigens [11,38]. From these studies, it seems that priming of naive CD8⁺ T cells in tumor-draining lymph nodes relies on CD103⁺ cDC1s, but not other cDCs. Consistent with this view, the lack of CD8⁺ T cell priming towards tumor antigens observed in BATF3-deficient mice appears to be due to the absence of migratory CD103⁺ cDC1s rather than loss of lymph-node resident CD8 α ⁺ cDC1s [12,39]. The unique ability of migratory cDC1s to cross-present tumor antigens to CD8⁺ T cells might be related to reduced antigen degradation in phagocytic compartments [40], as well as the ability of cDC1s to use DNGR-1 to shuttle material from dead cells into specialized endocytic compartments [41]. The latter can fuse with endoplasmic reticulum-derived vesicles that contain the MHC class I loading machinery [42], a process that can be mediated by the SEC22b SNARE [43]. The role of DNGR-1 and SEC22b in anti-tumor immunity is under investigation [44,45].

A Local Role for DCs within the TME

Investigating a role for cDC1s in tumors is complicated by the fact that the lack of cDC1s in *Batf3*^{-/-} mice or their inability to migrate to lymph nodes in *Ccr7*^{-/-} mice abrogates priming of tumor-specific CD8⁺ T cells [11,12]. Nevertheless, several recent studies suggest that cDC1 plays an important role in regulating anticancer immune responses locally within tumor tissue (Figure 1).

Within tumors, CD103⁺ cDC1 appears to be the main source of the chemokines CXCL9 and CXCL10, key for the recruitment of CXCR3⁺ effector T cells [46], and for facilitating T cell-mediated control of melanoma growth [14]. The cDC1-dependent guidance of effector T cells into tumors might be the reason why cDC1s are required for the responsiveness of cancer to adoptive T cell therapy [10]. In addition, production of CXCL9/10 might be important for positioning tumor-infiltrating T cells in cDC1-rich areas and facilitating local T cell restimulation, similar to the positioning of memory CD8⁺ T cells by CXCL9 in lymph nodes upon viral infection [47]. Of note, CXCL9 and CXCL10 expression in myeloid cells is not constitutive but requires exposure to type I interferon (IFN) or IFN- γ , suggesting a positive feedback loop whereby an influx of IFN- γ -producing CD8⁺ T cells into the TME could amplify cDC1-dependent recruitment of additional T cells.

The ability to acquire tumor material is not restricted to cDC1 but can be observed by several myeloid cell populations, including tumor-associated macrophages [10,11,48]. However, when analyzed *ex vivo*, tumor cDC1s are superior to other myeloid cells in stimulating T cell activation and proliferation, suggesting that they process ingested antigens more efficiently [10]. Furthermore, cDC1s produce high amounts of the cytokine interleukin (IL)-12 [10,25], which likely helps sustain the cytotoxic function of CD8⁺ effector T cells within the TME (Figure 1).

Box 2. cDC1 Subsets in Lymph Nodes

Two populations of cDC1s can be found in lymph nodes. Lymphoid-resident CD8 α ⁺ cDC1s develop locally from blood-borne precursors, while migratory CD103⁺ cDC1s enter via afferent lymphatics after migration from peripheral tissues or tumors. While these two cDC1 populations share similar gene expression signatures, and express cDC1-specific genes such as XCR1 and CLEC9A, migratory cDC1s in lymph nodes can be identified by higher expression of MHC class II. However, high levels of MHC class II expression can also be induced on CD8 α ⁺ cDC1s upon activation. In mice, only the selective expression of CD8 α and CD103 allows for reliable discrimination of the two cDC1 subsets in lymph nodes.

It seems likely that a stimulatory role for cDC1 in tumors is not restricted to T cells. Production of chemokines such as CXCL9 and CXCL10 might result in the recruitment of other CXCR3⁺ cells such as NK cells or ILC1 into tumors [49], which, by producing XCL1/2 and FLT3L facilitate close cell appositioning and promote reciprocal interactions. Local production of IL-12 by cDC1 supports NK cell production of IFN- γ and control of lung metastasis [50] and, in turn, IFN- γ potentiates IL-12 production by cDC1s [51]. One could envision that this two-way dialog extends to a three-partner conversation and that the local interaction between NK cells, cDC1s, and, eventually, T cells provides a localized cytokine milieu that favors anti-tumor immunity (Figure 1). Such interactions, if validated, have important implications for the design of NK cell and T cell-based immunotherapies.

The dynamics of cDC1 trafficking within tumors remains enigmatic, and it is currently not known whether all cDC1s that enter tumors will eventually leave and migrate to tumor-draining lymph nodes [38]. It might well be that some cDC1s establish residence in tumors and orchestrate local anti-tumor immunity by presenting tumor antigens to incoming T cells and stimulating NK and other innate immune cells, as stated above. It will be important to determine the half-life of cDC1s within tumors, especially of those cells that have acquired and processed tumor antigens for presentation to T cells, and the kinetics of cDC1 production of proinflammatory and immunomodulatory cytokines.

Impairment of cDC Function

During cancer development, tumor cells interact with surrounding cells to establish a local immunosuppressive milieu, allowing cancers to evade detection and destruction by the immune system [52]. Such an environment not only impairs tumor-specific T cells but also affects cDC1 biology, thereby also limiting anti-tumor immunity.

The exclusion of cDC1s from tumors is emerging as an important cancer immune evasion strategy. Low cDC1 abundance in tumors might result from reduced development of cDC1s, for example, through systemic suppression of DC development in the bone marrow [53] or by limiting the local production of FLT3L and other growth factors important for cDC1 differentiation, expansion, and survival [11,28]. In addition, the scarcity of tumor cDC1s might further ensue from suppression of chemokine-mediated recruitment of cDC1s into the TME. For example, we observed that PGE₂ produced by tumor cells acts on both NK cells and cDC1s to suppress production of cDC1 chemoattractants by the former and responsiveness to the chemokines by the latter [27]. As already mentioned, loss of production of CCL4 in β -catenin⁺ tumors might be responsible for reduced cDC1 recruitment [13]. Similarly, the loss of the tumor suppressor *TRP53* results in reduced production of CCL3, CCL4, and CCL5 by cancer cells [54], chemokines that potentially mediate cDC1 recruitment into tumors. It remains to be seen whether a shift in the chemokine profile towards cDC1-attracting chemokines can generally be induced by interference with oncogenic signaling in cancer cells.

Inhibitory factors present within the TME not only regulate cDC1 access to tumor tissue but also directly act on cDC1s by limiting their stimulatory activity. For example, in breast cancer the production of IL-10 by tumor-associated macrophages suppresses the production of IL-12 by cDC1s [25]. Similarly, cDC1s in PGE₂-producing BRAF^{V600E} melanoma display reduced IL-12 production and fail to express co-stimulatory molecules [31]. Furthermore, tumor-derived factors can induce the intracellular accumulation of oxidized lipids in cDC1s, resulting in impaired antigen cross-presentation to CD8⁺ T cells [55,56]. Other tumor-derived factors such as transforming growth factor β (TGF- β) might similarly affect the anti-tumor activity of cDC1s. *In vitro*, TGF- β can inhibit ability of myeloid cells to take up

antigen and secrete cytokines and chemokines, and blockade of TGF- β signaling has been shown to improve the efficacy of DC cancer vaccines [57,58]. However, a major target of TGF- β is the tumor stromal compartment [59], and it has yet to be established how TGF- β affects the cDC1 subset in tumors and the relevance of such suppression for anti-tumor immunity *in vivo*.

The activity of cDC1s in tumors might be further limited by signals from immune inhibitory receptors expressed on cDC1s. Although little is known about the relevance of PD-1 expression on cDCs, human cDC1s circulating in the blood of hepatocellular carcinoma patients show increased expression of that inhibitory receptor, suggesting that they might be susceptible to signaling in response to PD-L1 expressed on cells within the TME [60]. In the murine MMTV-PyMT breast cancer model, cDC1s do not display elevated PD-1 expression but highly express the immune inhibitory receptor TIM-3 [61]. Antibody-mediated blockade of TIM-3 or its ligand, galectin 9, increases CXCL9 production in cDC1s and results in cDC1-dependent immune control. While these findings suggest that TIM-3 signaling on cDC1s in breast cancer inhibits their ability to recruit CXCR3⁺ T cells into the TME, anti-TIM-3 treatment does not lead to an increase in intratumoral T cells [61], indicating additional effects that remain to be investigated.

With respect to the metabolic demands of immune cells, the TME constitutes a challenging environment with limited availability of oxygen and nutrients and increased concentration of metabolic products such as lactate due to aerobic glycolysis in proliferating cancer cells [62]. During their activation, DCs undergo substantial metabolic reprogramming to meet demands for protein synthesis and secretion, characterized by an increase in glucose uptake and enhanced glycolysis [63]. Although cDC1 metabolism has yet to be extensively studied, competition for glucose with other cells in the TME could dampen the ability of cDC1 to produce chemokines and cytokines in response to their activation in tumors, similar to the metabolic restriction imposed on effector T cells in tumors [64]. In addition, lactate has been shown to inhibit the secretion of cytokines by monocyte-derived DCs [65]. It is therefore possible that the high levels of lactate produced by tumor cells could impact on the production of chemokines and cytokines by tumor cDC1s *in vivo* [66]. Future studies will be necessary to elucidate the regulation of cDC1 metabolism in tumors and the impact of such regulation on their ability to orchestrate anti-tumor immunity.

Concluding Remarks

cDC1s are critically involved in the initiation of tumor-specific T cell responses in tumor-draining lymph nodes. However, recent evidence suggests a fundamental role for cDC1 in the regulation of cancer immunity and the immune cell composition within the tumor microenvironment, with important consequences for cancer immunotherapy. This local role involves the regulation of cytotoxic T cell recruitment and restimulation, but probably extends to other immune cell subsets within tumors, including NK cells. We still know very little about the biology of cDC1 in tumors, especially in human cancer patients. Future studies will help increase our knowledge of the multiple functions of DCs within the complex tumor microenvironment (see Outstanding Questions), from the acquisition of tumor antigens to local trafficking and communication with other immune cells. It will be important to further characterize the mechanisms by which different oncogenic signaling pathways, immunosuppressive factors secreted by tumor cells, and the special metabolic environment within tumors impact on the diverse aspects of cDC1 function. Strategies that aim to enhance the abundance and function of cDC1s in tumors may provide promising new ways to improve the responsiveness of cancer patients to immunotherapy.

Outstanding Questions

By which mechanisms and pathways do cDC1s regulate anti-tumor immunity within the tumor microenvironment and during immunotherapies such as immune checkpoint blockade?

Which mechanisms and local factors regulate cDC1 function within the microenvironment of tumors?

To what degree can cDC1 abundance in tumors serve as a predictive biomarker for the outcome of cancer immunotherapies?

Which strategies can be used to increase cDC1 numbers in tumors to enhance anti-tumor immunity and responsiveness to checkpoint blockade?

Are therapies targeting NK cells a promising approach to promote intratumoral cDC1 recruitment and survival?

References

- Guilliams, M. *et al.* (2014) Dendritic cells, monocytes and macrophages: a unified nomenclature based on ontogeny. *Nat. Rev. Immunol.* 14, 571–578
- Merad, M. *et al.* (2013) The dendritic cell lineage: ontogeny and function of dendritic cells and their subsets in the steady state and the inflamed setting. *Annu. Rev. Immunol.* 31, 563–604
- Villani, A.-C. *et al.* (2017) Single-cell RNA-seq reveals new types of human blood dendritic cells, monocytes, and progenitors. *Science* 356, eaah4573
- See, P. *et al.* (2017) Mapping the human DC lineage through the integration of high-dimensional techniques. *Science* 356, eaag3009
- Murphy, T.L. *et al.* (2016) Transcriptional control of dendritic cell development. *Annu. Rev. Immunol.* 34, 93–119
- Crozat, K. *et al.* (2011) Cutting edge: expression of XCR1 defines mouse lymphoid-tissue resident and migratory dendritic cells of the CD8⁺ type. *J. Immunol.* 187, 4411–4415
- Bachem, A. *et al.* (2012) Expression of XCR1 characterizes the Batf3-dependent lineage of dendritic cells capable of antigen cross-presentation. *Front. Immunol.* 3, 214
- Poulin, L.F. *et al.* (2012) DNGR-1 is a specific and universal marker of mouse and human Batf3-dependent dendritic cells in lymphoid and nonlymphoid tissues. *Blood* 119, 6052–6062
- Robbins, S.H. *et al.* (2008) Novel insights into the relationships between dendritic cell subsets in human and mouse revealed by genome-wide expression profiling. *Genome Biol.* 9, R17
- Broz, M.L. *et al.* (2014) Dissecting the tumor myeloid compartment reveals rare activating antigen-presenting cells critical for T cell immunity. *Cancer Cell* 26, 638–652
- Salmon, H. *et al.* (2016) Expansion and activation of CD103⁺ dendritic cell progenitors at the tumor site enhances tumor responses to therapeutic PD-L1 and BRAF inhibition. *Immunity* 44, 924–938
- Sánchez-Paulete, A.R. *et al.* (2016) Cancer Immunotherapy with immunomodulatory anti-CD137 and anti-PD-1 monoclonal antibodies requires BATF3-dependent dendritic cells. *Cancer Discov.* 6, 71–79
- Spranger, S. *et al.* (2015) Melanoma-intrinsic β -catenin signalling prevents anti-tumour immunity. *Nature* 523, 231–235
- Spranger, S. *et al.* (2017) Tumor-residing Batf3 dendritic cells are required for effector T cell trafficking and adoptive T cell therapy. *Cancer Cell* 31, 711–723.e4
- Tussiwand, R. *et al.* (2012) Compensatory dendritic cell development mediated by BATF-IRF interactions. *Nature* 490, 502–507
- Gilfillan, C.B. *et al.* (2018) Clec9A⁺ dendritic cells are not essential for anti-tumor CD8⁺ T cell responses induced by poly I:C immunotherapy. *J. Immunol.* 200, 2978–2986
- Ma, Y. *et al.* (2013) Anticancer chemotherapy-induced intratumoral recruitment and differentiation of antigen-presenting cells. *Immunity* 38, 729–741
- Tussiwand, R. *et al.* (2015) Klf4 expression in conventional dendritic cells is required for T helper 2 cell responses. *Immunity* 42, 916–928
- Laoui, D. *et al.* (2016) The tumour microenvironment harbours ontogenically distinct dendritic cell populations with opposing effects on tumour immunity. *Nat. Commun.* 7, 13720
- Briseño, C.G. *et al.* (2016) Distinct transcriptional programs control cross-priming in classical and monocyte-derived dendritic cells. *Cell Rep.* 15, 2462–2474
- Zelenay, S. and Reis e Sousa, C. (2013) Adaptive immunity after cell death. *Trends Immunol.* 34, 329–335
- Galluzzi, L. *et al.* (2017) Immunogenic cell death in cancer and infectious disease. *Nat. Rev. Immunol.* 17, 97–111
- Woo, S.-R. *et al.* (2015) Innate immune recognition of cancer. *Annu. Rev. Immunol.* 33, 445–474
- Lavin, Y. *et al.* (2017) Innate immune landscape in early lung adenocarcinoma by paired single-cell analyses. *Cell* 169, 750–765.e17
- Ruffell, B. *et al.* (2014) Macrophage IL-10 blocks CD8⁺ T cell-dependent responses to chemotherapy by suppressing IL-12 expression in intratumoral dendritic cells. *Cancer Cell* 26, 623–637
- Michea, P. *et al.* (2018) Adjustment of dendritic cells to the breast-cancer microenvironment is subset specific. *Nat. Immunol.* 19, 885–897
- Böttcher, J.P. *et al.* (2018) NK cells stimulate recruitment of cDC1 into the tumor microenvironment promoting cancer immune control. *Cell* 172, 1022–1037.e14
- Barry, K.C. *et al.* (2018) A natural killer-dendritic cell axis defines checkpoint therapy-responsive tumor microenvironments. *Nat. Med.* 27, 450
- Nagarsheth, N. *et al.* (2017) Chemokines in the cancer microenvironment and their relevance in cancer immunotherapy. *Nat. Rev. Immunol.* 17, 559–572
- Li, J. *et al.* (2018) Tumor cell-intrinsic factors underlie heterogeneity of immune cell infiltration and response to immunotherapy. *Immunity* 49, 178–193.e7
- Zelenay, S. *et al.* (2015) Cyclooxygenase-dependent tumor growth through evasion of immunity. *Cell* 162, 1257–1270
- Halama, N. *et al.* (2016) Tumoral immune cell exploitation in colorectal cancer metastases can be targeted effectively by anti-CCR5 therapy in cancer patients. *Cancer Cell* 29, 587–601
- Tan, M.C.B. *et al.* (2009) Disruption of CCR5-dependent homing of regulatory T cells inhibits tumor growth in a murine model of pancreatic cancer. *J. Immunol.* 182, 1746–1755
- Pulendran, B. *et al.* (1999) Distinct dendritic cell subsets differentially regulate the class of immune response *in vivo*. *Proc. Natl. Acad. Sci. U. S. A.* 96, 1036–1041
- Grajales-Reyes, G.E. *et al.* (2015) Batf3 maintains autoactivation of Irf8 for commitment of a CD8a⁺ conventional DC clonogenic progenitor. *Nat. Immunol.* 16, 708–717
- Thompson, E.D. *et al.* (2010) Tumor masses support naive T cell infiltration, activation, and differentiation into effectors. *J. Exp. Med.* 207, 1791–1804
- Asano, K. *et al.* (2011) CD169-Positive macrophages dominate anti-tumor immunity by crosspresenting dead cell-associated antigens. *Immunity* 34, 85–95
- Roberts, E.W. *et al.* (2016) Critical role for CD103(+)/CD141(+) dendritic cells bearing CCR7 for tumor antigen trafficking and priming of T cell immunity in melanoma. *Cancer Cell* 30, 324–336
- Hildner, K. *et al.* (2008) Batf3 deficiency reveals a critical role for CD8 α ⁺ dendritic cells in cytotoxic T cell immunity. *Science* 322, 1097–1100
- Savina, A. *et al.* (2009) The small GTPase Rac2 controls phagosomal alkalization and antigen crosspresentation selectively in CD8(+) dendritic cells. *Immunity* 30, 544–555
- Zelenay, S. *et al.* (2012) The dendritic cell receptor DNGR-1 controls endocytic handling of necrotic cell antigens to favor cross-priming of CTLs in virus-infected mice. *J. Clin. Invest.* 122, 1615–1627
- Guermonez, P. *et al.* (2003) ER-phagosome fusion defines an MHC class I cross-presentation compartment in dendritic cells. *Nature* 425, 397–402
- Cebrian, I. *et al.* (2011) Sec22b regulates phagosomal maturation and antigen crosspresentation by dendritic cells. *Cell* 147, 1355–1368
- Alloattii, A. *et al.* (2017) Critical role for Sec22b-dependent antigen cross-presentation in anti-tumor immunity. *J. Exp. Med.* 214, 2231–2241
- Wu, S.J. *et al.* (2017) A critical analysis of the role of SNARE protein SEC22B in antigen cross-presentation. *Cell Rep.* 19, 2645–2656
- Mikucki, M.E. *et al.* (2015) Non-redundant requirement for CXCR3 signalling during tumoricidal T-cell trafficking across tumour vascular checkpoints. *Nat. Commun.* 6, 7458
- Kastenmüller, W. *et al.* (2013) Peripheral prepositioning and local CXCL9 chemokine-mediated guidance orchestrate rapid memory CD8⁺ T cell responses in the lymph node. *Immunity* 38, 502–513

48. Engelhardt, J.J. *et al.* (2012) Migrating dendritic cells of the tumor microenvironment cross-present tumor antigens and stably engage tumor-specific T cells. *Cancer Cell* 21, 402–417
49. Wendel, M. *et al.* (2008) Natural killer cell accumulation in tumors is dependent on IFN-gamma and CXCR3 ligands. *Cancer Res.* 68, 8437–8445
50. Mittal, D. *et al.* (2017) Interleukin-12 from CD103⁺ Batf3-dependent dendritic cells required for NK-cell suppression of metastasis. *Cancer Immunol. Res.* 5, 1098–1108
51. Hochrein, H. *et al.* (2000) Interleukin (IL)-4 is a major regulatory cytokine governing bioactive IL-12 production by mouse and human dendritic cells. *J. Exp. Med.* 192, 823–833
52. Hanahan, D. and Weinberg, R.A. (2011) Hallmarks of cancer: the next generation. *Cell* 144, 646–674
53. Meyer, M.A. *et al.* (2018) Breast and pancreatic cancer interrupt IRF8-dependent dendritic cell development to overcome immune surveillance. *Nat. Commun.* 9, 1–19
54. Iannello, A. *et al.* (2013) p53-dependent chemokine production by senescent tumor cells supports NKG2D-dependent tumor elimination by natural killer cells. *J. Exp. Med.* 210, 2057–2069
55. Herber, D.L. *et al.* (2010) Lipid accumulation and dendritic cell dysfunction in cancer. *Nat. Med.* 16, 880–886
56. Veglia, F. *et al.* (2017) Lipid bodies containing oxidatively truncated lipids block antigen cross-presentation by dendritic cells in cancer. *Nat. Commun.* 8, 1–16
57. Kobie, J.J. *et al.* (2003) Transforming growth factor beta inhibits the antigen-presenting functions and anti-tumor activity of dendritic cell vaccines. *Cancer Res.* 63, 1860–1864
58. Hargadon, K.M. *et al.* (2016) Melanoma-derived factors alter the maturation and activation of differentiated tissue-resident dendritic cells. *Immunol. Cell Biol.* 94, 24–38
59. Mariathasan, S. *et al.* (2018) TGFβ attenuates tumour response to PD-L1 blockade by contributing to exclusion of T cells. *Nature* 554, 544–548
60. Lim, T.S. *et al.* (2016) PD-1 expression on dendritic cells suppresses CD8⁺ T cell function and anti-tumor immunity. *Oncotarget* 5, e1085146
61. de Mingo Pulido, Á. *et al.* (2018) TIM-3 regulates CD103⁺ dendritic cell function and response to chemotherapy in breast cancer. *Cancer Cell* 33, 60–74.e6
62. Buck, M.D. *et al.* (2017) Metabolic instruction of immunity. *Cell* 169, 570–586
63. Pearce, E.J. and Everts, B. (2015) Dendritic cell metabolism. *Nat. Rev. Immunol.* 15, 18–29
64. Chang, C.-H. *et al.* (2015) Metabolic competition in the tumor microenvironment is a driver of cancer progression. *Cell* 162, 1229–1241
65. Gottfried, E. *et al.* (2006) Tumor-derived lactic acid modulates dendritic cell activation and antigen expression. *Blood* 107, 2013–2021
66. Romero-Garcia, S. *et al.* (2016) Lactate contribution to the tumor microenvironment: mechanisms, effects on immune cells and therapeutic relevance. *Front. Immunol.* 7, 52
67. Jongbloed, S.L. *et al.* (2010) Human CD141⁺ (BDCA-3)⁺ dendritic cells (DCs) represent a unique myeloid DC subset that cross-presents necrotic cell antigens. *J. Exp. Med.* 207, 1247–1260
68. Bachem, A. *et al.* (2010) Superior antigen cross-presentation and XCR1 expression define human CD11c⁺CD141⁺ cells as homologues of mouse CD8⁺ dendritic cells. *J. Exp. Med.* 207, 1273–1281
69. Mittag, D. *et al.* (2011) Human dendritic cell subsets from spleen and blood are similar in phenotype and function but modified by donor health status. *J. Immunol.* 186, 6207–6217
70. Nizzoli, G. *et al.* (2013) Human CD1c⁺ dendritic cells secrete high levels of IL-12 and potently prime cytotoxic T-cell responses. *Blood* 122, 932–942

Complement C5a Fosters Squamous Carcinogenesis and Limits T Cell Response to Chemotherapy

Terry R. Medler,¹ Dhaarini Murugan,¹ Wesley Horton,² Sushil Kumar,¹ Tiziana Cotechini,¹ Alexandra M. Forsyth,¹ Patrick Leyshock,² Justin J. Leitenberger,³ Molly Kulesz-Martin,^{1,3,4} Adam A. Margolin,^{2,4} Zena Werb,⁵ and Lisa M. Coussens^{1,4,6,*}

¹Department of Cell, Developmental & Cancer Biology, Oregon Health & Science University, Knight Cancer Research Building Room 3030, 2720 SW Moody Avenue, #KC-CDCB, Portland, OR 97201-5042, USA

²Department of Biomedical Engineering, Program in Computational Biology, Oregon Health & Science University, Portland, OR 97239, USA

³Department of Dermatology, Oregon Health & Science University, Portland, OR 97239, USA

⁴Knight Cancer Institute, Oregon Health & Science University, Portland, OR 97239, USA

⁵Department of Anatomy, Helen Diller Family Comprehensive Cancer Center, Parker Immunotherapy Cancer Institute, University of California, San Francisco, CA 94143, USA

⁶Lead Contact

*Correspondence: cousseni@ohsu.edu

<https://doi.org/10.1016/j.ccell.2018.09.003>

SUMMARY

Complement is a critical component of humoral immunity implicated in cancer development; however, its biological contributions to tumorigenesis remain poorly understood. Using the K14-HPV16 transgenic mouse model of squamous carcinogenesis, we report that urokinase (uPA)⁺ macrophages regulate C3-independent release of C5a during premalignant progression, which in turn regulates protumorigenic properties of C5aR1⁺ mast cells and macrophages, including suppression of CD8⁺ T cell cytotoxicity. Therapeutic inhibition of C5aR1 via the peptide antagonist PMX-53 improved efficacy of paclitaxel chemotherapy associated with increased presence and cytotoxic properties of CXCR3⁺ effector memory CD8⁺ T cells in carcinomas, dependent on both macrophage transcriptional programming and IFN γ . Together, these data identify C5aR1-dependent signaling as an important immunomodulatory program in neoplastic tissue tractable for combinatorial cancer immunotherapy.

INTRODUCTION

As the co-dominant central mediator of humoral immunity, complement cascades are critical for recognition and elimination of pathogens and damaged cells, opsonization of pathogenic substances, and induction of anaphylactoid reactions (Schmidt et al., 2016). Acute generation of anaphylatoxins C3a, C4a, and C5a induces migration of phagocytes, degranulation of mast cells and granulocytes, and relaxation of smooth muscle cells in damaged tissues, whereas sustained complement acti-

vation instead fosters exacerbation of inflammatory pathologies (Ricklin et al., 2016). Because many of these characteristic features of tissue “damage” are also associated with chronic inflammation accompanying solid tumor development (Hanahan and Coussens, 2012; Hanahan and Weinberg, 2011; Mantovani et al., 2008), we hypothesized that complement components also functionally regulate aspects of de novo neoplastic progression.

The classical, lectin, and alternative pathways of complement activation represent primary mechanisms by which

Significance

Anaphylatoxins and the downstream pathways they regulate are emerging tractable targets for anticancer immunotherapy. Results presented herein identify uPA-expressing macrophages as critical regulators of C3-independent C5a generation in squamous cell carcinomas (SCCs) that sustain immunosuppressive tumor immune microenvironments (TiMEs). Therapeutic inhibition of C5aR1 in combination with chemotherapy fostered TiME reprogramming, resulting in CD8⁺ T cell-dependent antitumor immune responses correlating with decreased local and peripheral T cell receptor (TCR) β diversity. Intratumoral TCR β clonotypes were hyperexpanded and increasingly detected in matched peripherally expanded T cell populations, thereby implicating antigen-dependent peripheral priming in response to C5aR1 inhibition. These results reveal C5aR1-dependent signaling as a critical regulator of immunosuppressive TiMEs in SCCs that can be leveraged for CD8⁺ T cell-dependent antitumor immune responses.



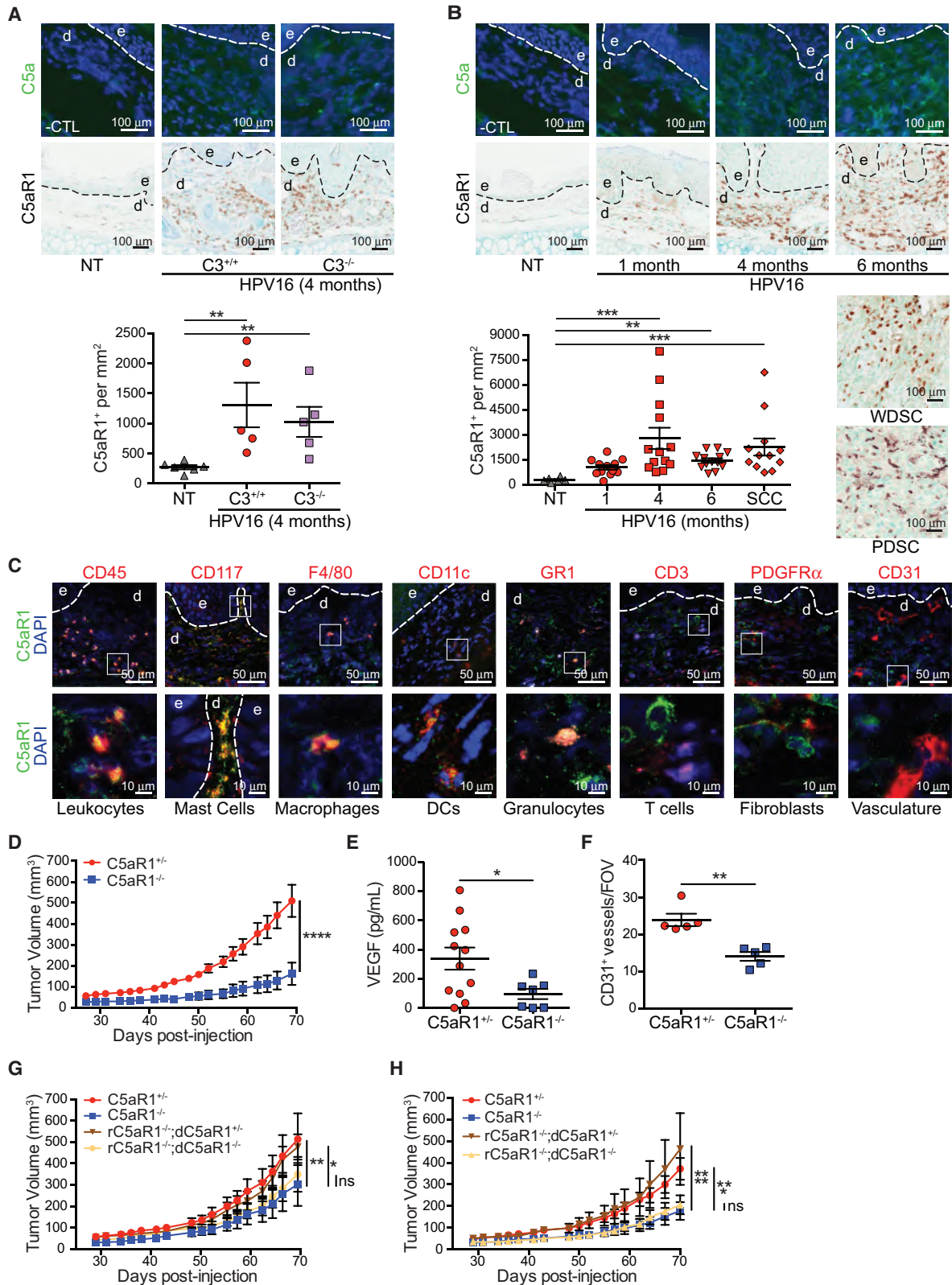


Figure 1. C5aR1⁺ Leukocytes Infiltrate Neoplastic Skin in HPV16 Mice

(A) Immunofluorescence (IF) detection of C5a (green, DAPI [blue]; top row), immunohistochemistry (IHC) of C5aR1 (brown; middle row), and quantification (bottom) of ear skin from nontransgenic (NT), and 4-month-old C3^{+/+} versus C3^{-/-} HPV16 mice. Representative images are shown.

(legend continued on next page)

complement-induced inflammation is initiated, although extrinsic proteases associated with coagulation and fibrinolytic pathways also directly activate anaphylatoxins irrespective of their individual convertases (Amara et al., 2008; Huber-Lang et al., 2006). The classical pathway involves complement proteins complexed with immunoglobulin (Ig)G or IgM antibodies that bind antigens, typically on microbial surfaces in the context of infection, where a proteolytic cascade promotes generation of anaphylatoxins C3a, and ultimately the terminal complement mediator C5a. The alternative pathway instead involves spontaneous hydrolysis of C3, also typically on microbial surfaces, which initiates alternative proteolytic cascades resulting in production of the C3 convertase C3bBb. While each of these pathways involves unique modes of initiation, they funnel to complement component C3 and generate similar effector molecules that initiate potent inflammatory responses in tissues.

We previously reported that B cells, humoral immunity, and immune complexes (ICs) containing complement components activate IgG receptor (Fc γ R) signaling pathways in infiltrating myeloid cells that foster neoplastic progression of squamous cell carcinomas (SCCs) and pancreatic adenocarcinomas (PDAs) (Affara et al., 2014; Andreu et al., 2010; de Visser et al., 2005; Gunderson et al., 2016; Schioppa et al., 2011). Since chronic activation of inflammatory pathways drives neoplastic progression of SCCs and PDAs, we hypothesized that generation of complement might also exert tumor-regulatory roles. While we previously reported that squamous carcinogenesis was independent of complement C3 (de Visser et al., 2004), herein we queried whether complement components downstream of C3 exerted tumor-regulatory roles and identified C5a and its receptor as functionally significant mediators of SCC progression.

RESULTS

Infiltration of C5aR1⁺ Leukocytes during Neoplastic Progression in Human Papilloma Virus Type 16 Mice

The K14-HPV16 (human papilloma virus type 16 [HPV16]) transgenic mouse model of squamous carcinogenesis is a well-characterized model of multi-stage epithelial carcinogenesis where mice express the HPV16 early region genes, expressed under control of a keratin 14 (K14) promoter/enhancer (Arbeit et al., 1994). Transgenic mice are born phenotypically normal; on the FVB/n background, by 1 month of age, 100% of mice develop cutaneous epidermal hyperplasia and progress to mild dysplasia by 4 months of age. By 6 months of age, mice develop high-grade dysplasias that can undergo malignant

conversion to invasive SCCs in ~50% of transgenic mice and metastasize to regional lymph nodes in ~30% of tumor-bearing animals (Coussens et al., 1996). Subsequent to benign hyperplasias of HPV16 mice, deposition of immunoglobulin G (IgG), C1q, and C3-containing ICs is observed that subsequently induces local recruitment of Fc γ R⁺ leukocytes that foster ongoing multi-stage carcinogenesis (Andreu et al., 2010; de Visser et al., 2005). Despite accumulation of ICs in premalignant dermal stroma, neoplastic progression is independent of C3 and the classical and alternative complement pathways (de Visser et al., 2004). Because fibrinolytic and coagulation cascade proteases can also generate C5a by C5 convertase-independent mechanisms (Amara et al., 2008; Huber-Lang et al., 2006), we reasoned that neoplastic tissues from both C3-proficient and C3-deficient HPV16 mice would be characterized by C5a accumulation. Indeed, HPV16/C3^{Tm1Crr/Tm1Crr} (HPV16/C3^{-/-}) mice exhibited abundant deposition of C5a, associated with increased presence of high-affinity C5a receptor (C5aR1)⁺ cells in stromal regions adjacent to premalignant dysplasias, similar to their C3-proficient littermates (Figure 1A). Deposition of C5a was a prominent feature of benign hyperplasias, as well as early and late dysplasias in HPV16 mice (1-, 4-, and 6-month-old mice, respectively), indicating C5a deposition is an early feature of squamous carcinogenesis (Figures 1B and S1A).

To exert biological functionality, C5a binds and activates C5aR1 or its alternative receptor C5L2. Immunostaining for C5aR1 revealed increased presence of C5aR1⁺ cells in dermal regions of neoplastic skin with highest concordance to C5a deposition in focal regions of high-grade dysplasia and maintained in well-differentiated SCCs (WDSCs) and poorly differentiated SCCs (PDSCs), respectively; (Figure 1B), while presence of C5L2⁺ cells was only modestly increased in a subset of high-grade dysplasias (Figure S1B). Co-immunofluorescent staining identified C5aR1⁺ cells as CD45⁺ leukocytes, including CD117⁺ mast cells, F4/80⁺ macrophages, CD11c⁺ dendritic cells (DCs), and Gr1⁺ granulocytes (Figure 1C). C5aR1 was not detected on CD31⁺ vasculature, platelet-derived growth factor receptor (PDGFR) α ⁺ cells (presumably dermal fibroblasts), or on CD3⁺ T cells (Figure 1C), consistent with results from flow cytometry (Figures S1C and S1D), which also identified C5aR1⁺- γ δ T cells and natural killer cells (Figure S1E).

C5aR1⁺ Leukocytes Mediate Squamous Cell Carcinogenesis

Because C5aR1⁺ leukocytes infiltrate premalignant skin of HPV16 mice, we evaluated whether its expression was

(B) IF detection of C5a (green, DAPI [blue]; top row), IHC of C5aR1 (brown middle row and side), and quantitation (bottom) from NT mice and canonical time points from HPV16 mice. Representative images are shown.

(C) Co-IF of C5aR1 (green) with indicated lineage markers in dysplastic ear skin from HPV16 mice. Representative images for each cell type are shown. Boxed areas on top are shown at higher magnification on bottom.

(D) PDSC5 tumor growth kinetics in C5aR1^{+/-} and C5aR1^{-/-} mice (n \geq 8 mice/group).

(E) Quantitation of VEGF protein in lysates by ELISA from SCCs in (D).

(F) Manual IHC analysis of CD31⁺ vessels from SCCs in (D).

(G and H) Growth kinetics of PDSC5 cells admixed with C5aR1^{+/-} or C5aR1^{-/-} BMMCs (G) or BMM Φ s (H) from donor (d) mice, implanted into syngeneic recipient (r) mice of indicated genotypes. Mice from two independent experiments depicted (BMMCs, n = 9–16; BMM Φ s n = 11–15 mice/group).

Data are represented as mean \pm SEM. *p < 0.05; **p < 0.01; ***p < 0.001; ****p < 0.0001. Significance determined by one-way (A and B) or two-way (D, G, and H) ANOVA with Bonferroni post test for multiple comparisons or by unpaired Student's t test with Welch's correction (E and F); ns = not significant. Each data point reflects an individual mouse. In (A)–(C), epidermal (e) and dermal (d) regions are indicated, with dotted lines reflecting epidermal-dermal interface. In (F), FOV = field of view. See also Figures S1 and S2.

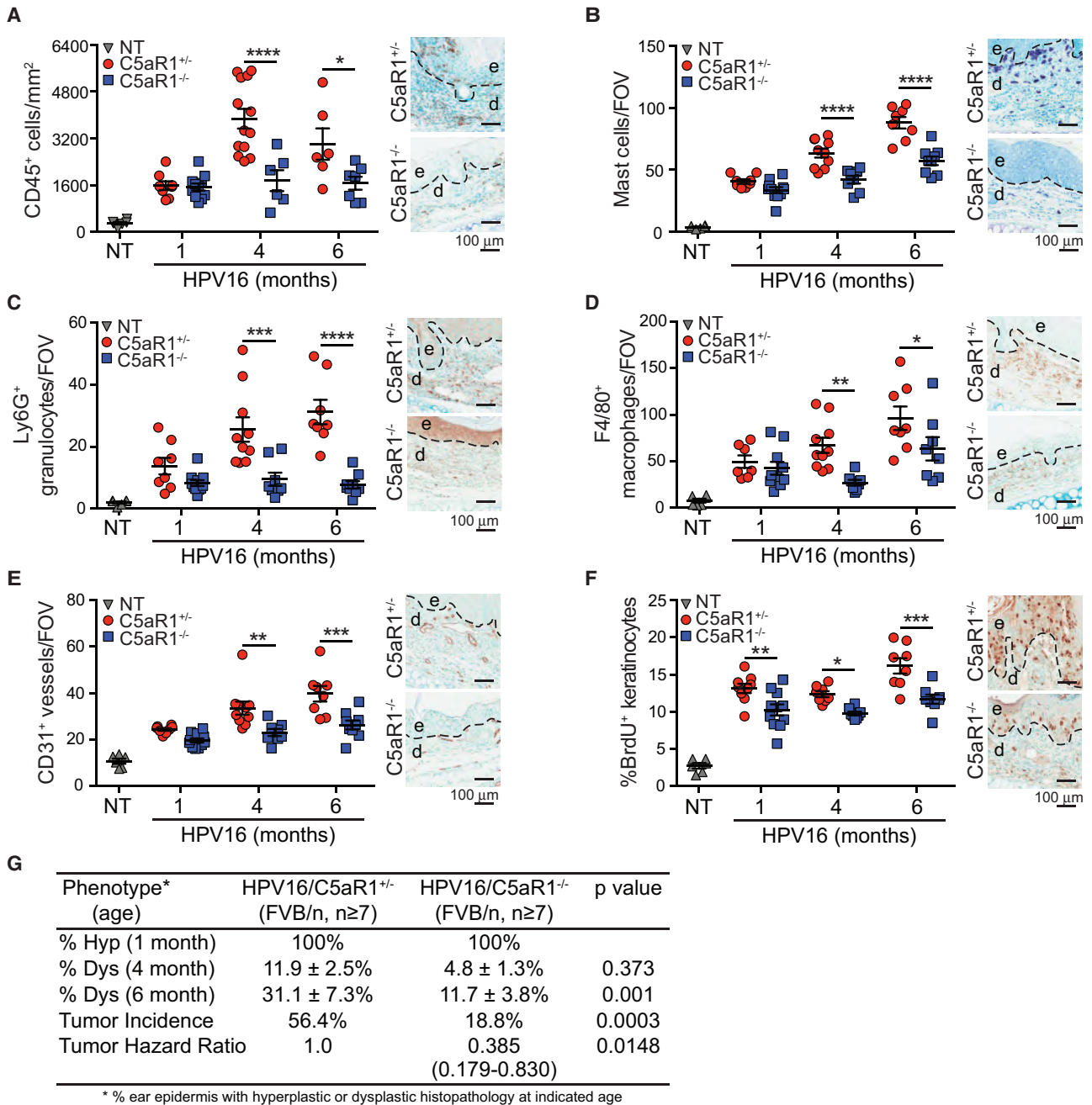


Figure 2. C5aR1 Expression Regulates Squamous Carcinogenesis in HPV16 Mice

(A–F) Automated (A) or manual (B–F) quantification of CD45⁺ cells (A), toluidine blue-stained mast cells (B), Ly6G⁺ granulocytes (C), F4/80⁺ macrophages (D), CD31⁺ vessels (E), and percentage of BrdU⁺ keratinocytes (F) in ear skin from HPV16/C5aR1^{+/-} and HPV16/C5aR1^{-/-} mice at 1, 4, and 6 months of age. Data points in graphs reflect independent mice, and micrographs on right are representative images from 6-month-old mice showing epidermal (e) and dermal (d) regions, and interface (dotted line).

(G) Percentage of ear skin area from indicated genotypes of HPV16 mice exhibiting hyperplasia (hyp; n = 8–11), dysplasia (dys; n = 8–9), and lifetime whole-body SCC incidence (HPV16/C5aR1^{+/-} n = 39 and HPV16/C5aR1^{-/-} n = 48), with significance determined by Chi-squared test, and hazard ratio determined by Kaplan-Meier analysis.

Significance determined by two-way ANOVA with Bonferroni post test for multiple comparisons unless otherwise indicated. Data represented as means ± SEM. *p < 0.05; **p < 0.01; ***p < 0.001; ****p < 0.0001. See also Figure S2.

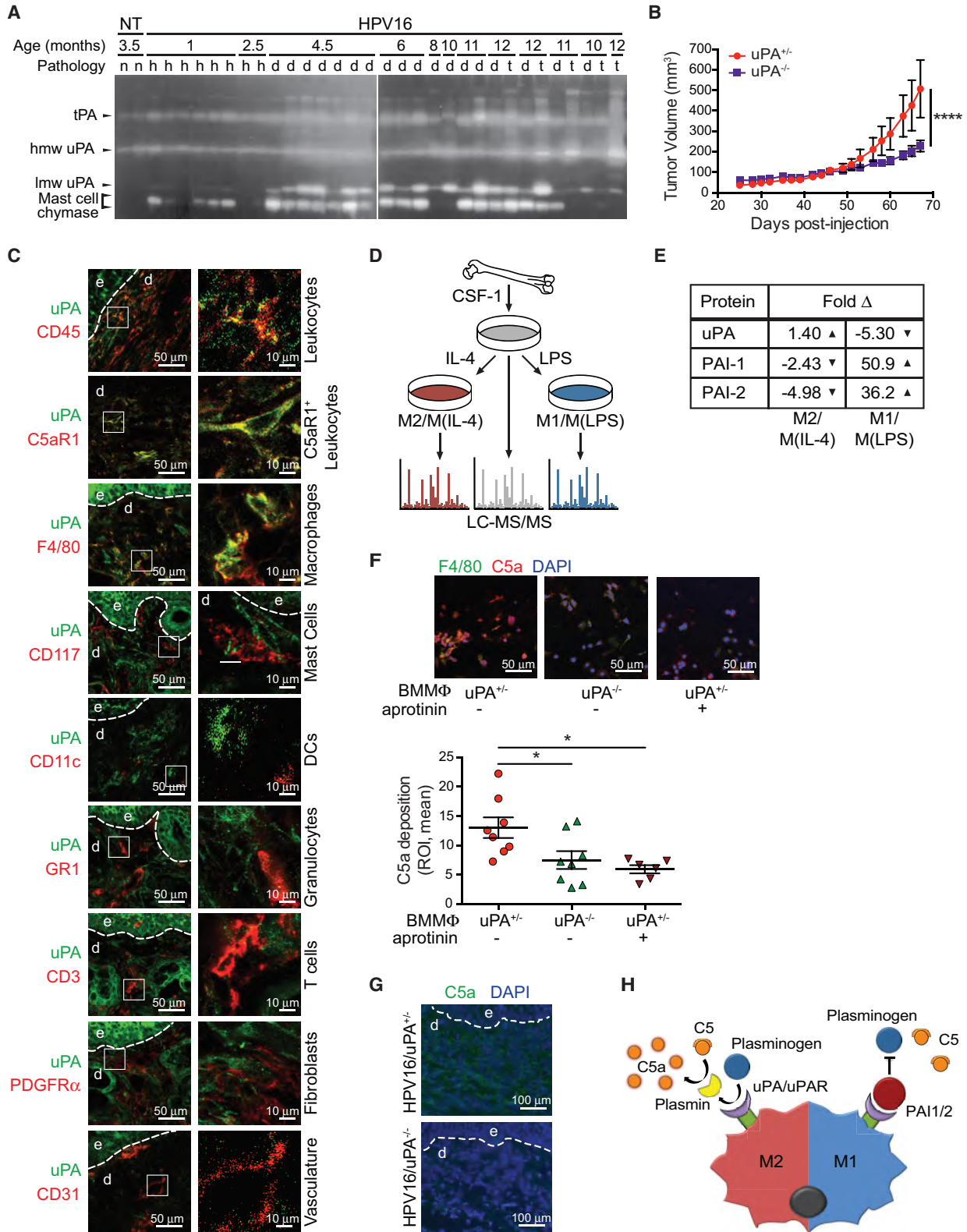


Figure 3. Urokinase Regulates Complement C5a Generation

(A) Casein/plasminogen zymogram of nontransgenic (n), hyperplastic (h), dysplastic (d), and SCC (t) tissue extracts at indicated ages. Protein identity based on molecular weight. lmw, low molecular weight; hmw, high molecular weight.

(legend continued on next page)

functionally significant with regards to orthotopic SCC growth. We assessed growth of two HPV16 SCC-derived cell lines, PDSC5 and WDSC1, derived from PDSCs and WDSCCs, respectively (Affara et al., 2014) following intradermal transplantation into *C5ar1^{tm1Cge/+}* (*C5aR1^{+/-}*) versus *C5aR1^{-/-}* syngeneic hosts. Growth of both PDSC5 and WDSC1 tumors was significantly growth restricted in *C5aR1*-deficient recipients (Figures 1D and S2A). End-stage SCCs in *C5aR1^{-/-}* mice exhibited significantly reduced levels of vascular endothelial growth factor (VEGF) (Figure 1E) and diminished density of CD31⁺ vasculature (Figure 1F).

Given that mast cells, macrophages, and granulocytes expressed the highest levels of *C5aR1* (Figures 1C and S1C) and our previous findings that cKIT⁺ mast cells and macrophages, but not granulocytes, regulate inflammation and angiogenesis in neoplastic tissue of HPV16 mice (Affara et al., 2014; Andreu et al., 2010; Coussens et al., 1999, 2000; de Visser et al., 2005), we asked whether these cell types were responsible for restricted tumor growth in *C5aR1^{-/-}* mice. We co-injected *C5aR1^{+/-}* versus *C5aR1^{-/-}* bone marrow-derived mast cells (BMMCs) or marrow-derived macrophages (BMMΦs) 1:1 with PDSC5 cells into syngeneic recipient *C5aR1^{-/-}* versus *C5aR1^{+/-}* mice to assess *C5aR1*-dependent regulation. Implantation of either *C5aR1^{+/-}* BMMCs or BMMΦs into *C5aR1^{-/-}* recipients restored tumor growth kinetics (Figures 1G and 1H) and characteristic CD31⁺ vascular density similar to *C5aR1^{+/-}* recipients (Figures S2B and S2C), whereas neither *C5aR1^{-/-}* BMMCs nor BMMΦs reinstated these characteristics. Admixed tumors grown in *C5aR1^{+/-}* recipients exhibited characteristic growth kinetics and vascular density (Figures S2D–S2G). Together, these data indicate that *C5aR1*-mediated effector programs in mast cells and macrophages are critical protumoral regulators of squamous carcinogenesis.

We next evaluated characteristic features of de novo premalignant and malignant progression to determine if *C5aR1*-dependent programs were similarly critical. We generated transgenic HPV16/*C5aR1^{-/-}* mice and quantitatively evaluated presence of CD45⁺ cells at canonical stages of neoplastic progression. This analysis revealed reduced leukocyte infiltration, including mast cells, Ly6G⁺ granulocytes, and F4/80⁺ macrophages, in premalignant skin of HPV16/*C5aR1^{-/-}* versus age-matched HPV16/*C5aR1^{+/-}* controls (Figures 2A–2D). Despite reduced presence of these cell types, overall leukocyte complexity remained unchanged (Figure S2H). Correlating with reduced leukocyte infiltration, density of CD31⁺ vasculature (Fig-

ure 2E), keratinocyte proliferation (Figure 2F), and development of focal dysplasia and SCC incidence (Figure 2G) were significantly reduced in HPV16/*C5aR1^{-/-}* mice compared with age-matched littermate controls. Together, these data indicate that *C5a* activation of *C5aR1*-expressing leukocytes is a co-dominant protumorigenic regulator of de novo squamous carcinogenesis.

C5a Generation in Neoplastic Tissue

Several members of the coagulation and fibrinolytic cascade generate *C5a* directly *in vitro*, including thrombin, plasmin, and factors IXa, Xa, and XIa (Amara et al., 2008; Huber-Lang et al., 2006), and since generation of *C5a* during squamous carcinogenesis was independent of C3 in HPV16 mice (de Visser et al., 2004), we hypothesized *C5a* regulation via one or another of these proteases. Of these, we identified plasmin as a likely candidate based on its activation by urokinase plasminogen activator (uPA), a serine protease highly expressed in numerous human solid tumors (Mekaway et al., 2014) and in HPV16 mice as revealed by casein-plasminogen zymography of skin lysates, where both high- and low-molecular-weight uPA increase concordantly with neoplastic progression (Figure 3A). Thus, we hypothesized that, if plasmin was a significant regulator of *C5a* release, then uPA-deficient mice would phenocopy *C5aR1* deficiency with regards to slowed tumor growth. To evaluate this, we orthotopically implanted PDSC5 cells into syngeneic uPA-proficient (*Plau^{tm1Mig/+}* [*uPA^{+/-}*]) and uPA^{-/-} mice and observed slowed orthotopic tumor growth in uPA-deficient hosts (Figure 3B). Because the implanted PDSC5 cells were uPA proficient (data not shown), this indicated that the relevant source of uPA was stromal. Using co-immunofluorescence, we found that macrophages represented a significant source of uPA in HPV16 dysplastic skin, whereas other stromal cell types yielded negligible uPA immunoreactivity (Figure 3C).

Since macrophages in neoplasms reflect a continuum of phenotypes regulated in part by their cytokine/chemokine milieu (Ruffell and Coussens, 2015), we asked whether plasminogen processing was a general property of macrophages, or, instead, a property unique to the continuum of M1-type or M2-type states (reviewed in Ruffell and Coussens, 2015). To assess this, we generated BMMΦs and subjected them to polarizing growth conditions using colony-stimulating factor (CSF)-1 plus interleukin (IL)-4 (M2/M(IL-4)-polarized), versus CSF1 plus lipopolysaccharide (LPS) (M1/M(LPS)-polarized), and subsequently examined their proteomes via liquid chromatography-tandem mass spectrometry (LC-MS/MS), compared with control

(B) SCC growth kinetics from PDSC5 cells, implanted in uPA^{+/-} versus uPA^{-/-} mice from two independent experiments (n ≥ 17 mice/group). Significance determined by two-way ANOVA with Bonferroni post test for multiple comparisons.

(C) Co-IF analysis of uPA (green) with indicated lineage markers in dysplastic ear skin from HPV16 mice. Representative images shown. Boxed areas on top are shown at higher magnification on right.

(D) Schematic of sample preparation for LC-MS/MS analysis.

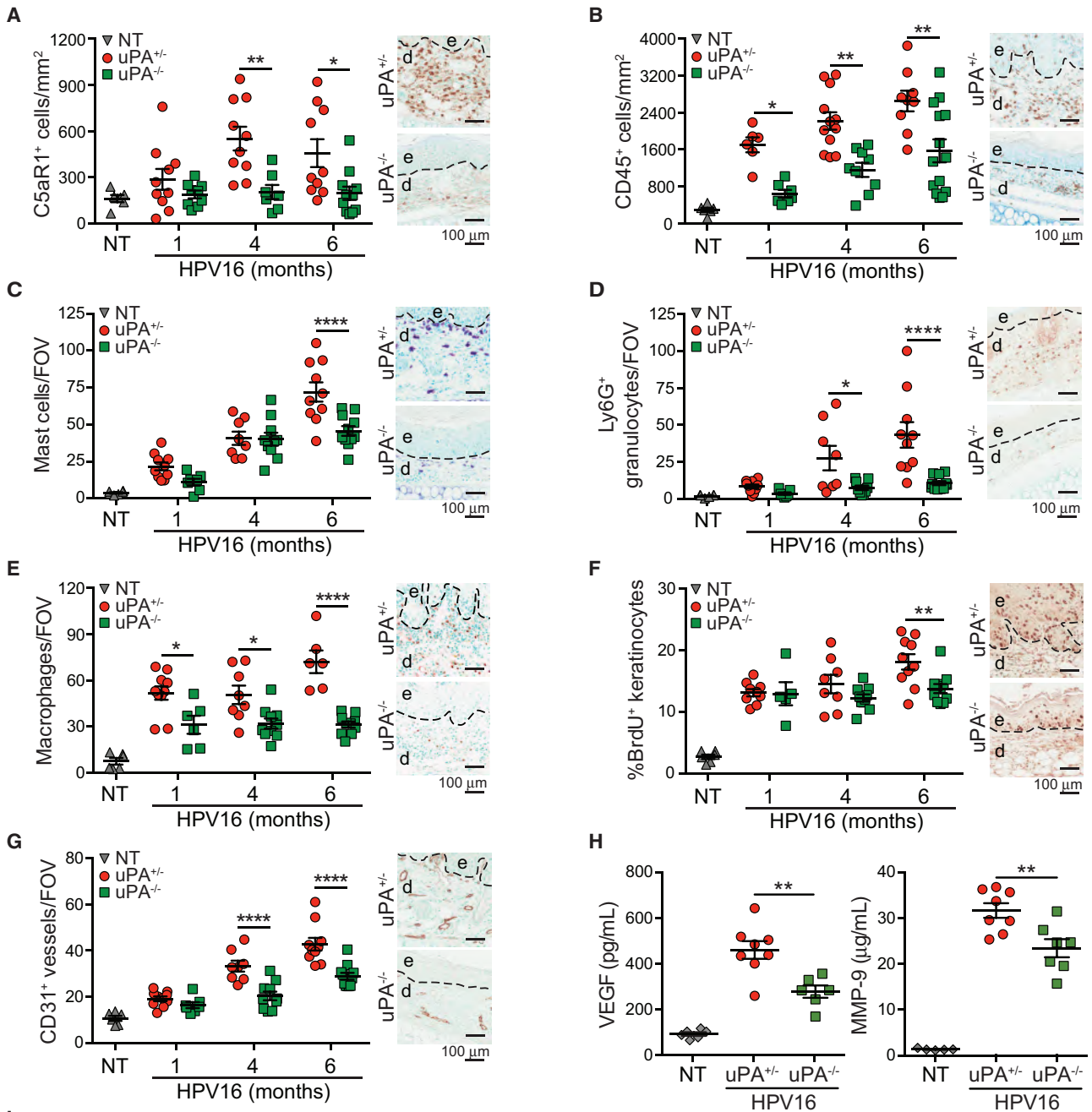
(E) Quantitation of fold change in protein levels of factors associated with plasminogen processing in M2/M(IL-4) and M1/M(LPS), compared with M0/M(CSF-1) macrophages.

(F) *In vitro* complement deposition assay of BMMΦs from uPA^{+/-} or uPA^{-/-} mice co-cultured with PDSC5 cells, IF stained for *C5a* (red) and F4/80 (green) (top), and quantified (bottom). Data points shown reflect two regions of interest per well with each experimental condition replicated in three to four wells, and the experiment repeated twice.

(G) IF staining of *C5a* (green) in tissue sections reflecting high-grade dysplasia from HPV16/uPA^{+/-} and HPV16/uPA^{-/-} mice. Representative images are shown.

(H) Model of complement activation. M2-type macrophages upregulate plasminogen processing to generate *C5a*, while M1-type macrophages produce negative regulators of plasminogen processing.

Data are represented as means ± SEM. *p < 0.05; **p < 0.01; ***p < 0.001; ****p < 0.0001. See also Figure S3.



Phenotype* (age)	HPV16/uPA ^{+/-} (FVB/n, n≥8)	HPV16/uPA ^{-/-} (FVB/n, n≥8)	p value
% Hyp (1 month)	100%	100%	
% Dys (4 month)	9.4 ± 2.0%	4.5 ± 1.9%	0.335
% Dys (6 month)	18.5 ± 3.2%	7.7 ± 2.4%	0.0009
Tumor Incidence	57.1%	10.1%	<0.0001
Tumor Hazard Ratio	1.0	0.273 (0.193-0.679)	0.0053

* % ear epidermis with hyperplastic or dysplastic histopathology at indicated age

(legend on next page)

CSF-1-stimulated BMMΦs (Figure 3D). LC-MS/MS revealed a modest increase in uPA (1.4-fold) with decreased expression of plasminogen activator inhibitor (PAI)-1 and -2 (2.43-fold and 4.98-fold, respectively) in M2/M(IL-4)-BMMΦs compared with CSF-1-stimulated controls (Figure 3E). In contrast, M1/M(LPS)-polarized macrophages exhibited a 5.3-fold decrease in uPA expression, in concert with 50.9- and 36.2-fold increased expression of PAI-1 and -2, respectively (Figure 3E), indicating that neoplasia-associated macrophages (M2-type) may facilitate plasminogen processing and C5a generation, in agreement with reports revealing macrophage-dependent generation of C5a by serine protease-dependent mechanisms (Huber-Lang et al., 2002). To examine this further, we exploited an *in vitro* complement activation assay by co-culturing BMMΦs from uPA^{+/-} versus uPA^{-/-} mice with PDSC5 cells and serum isolated from HPV16 mice, followed by C5a and F4/80 immunofluorescent staining and quantification. Although M(IL-4) uPA^{+/-} macrophages mediated robust C5a generation in a serine protease-dependent manner, M(IL-4) uPA^{-/-} macrophages exhibited significantly reduced C5a generation, comparable with aprotinin (a competitive serine protease inhibitor)-treated M(IL-4) uPA^{+/-} macrophages (Figure 3F). Using this same assay, we asked the degree to which C5a could be generated in serum depleted of either C3 or plasminogen and revealed C3-dependent aprotinin-sensitive and plasminogen-dependent aprotinin-insensitive C5a generation (Figure S3A), implicating both C3 and plasmin as regulators of C5a generation *in vitro*.

Since hallmark characteristics of neoplastic progression in HPV16 mice are C3 independent (de Visser et al., 2004), we next asked if downstream regulation of uPA represented a dominant mode of C5a generation *in vivo* and thus generated HPV16/*Plau*^{tm1Mlg/tm1Mlg} (HPV16/uPA^{-/-}) mice. We observed decreased C5a deposition in dermal stroma (Figure 3G) and skin lysates (Figure S3B) of HPV16/uPA^{-/-} mice, thus supporting a significant uPA-dependent mechanism for C5a generation *in vivo* (Figure 3H). Moreover, HPV16/uPA^{-/-} mice exhibited diminished recruitment of C5aR1⁺ cells (Figure 4A), and otherwise phenocopied HPV16/C5aR1^{-/-} mice with regards to canonical parameters of neoplastic progression, including reduced infiltration of CD45⁺ leukocytes, mast cells, Ly6G⁺ granulocytes, and F4/80⁺ macrophages (Figures 4B–4E); decreased BrdU⁺ keratinocyte proliferation (Figure 4F); reduced vascular density (Figure 4G); reduced levels of VEGF and matrix metalloproteinase (MMP)9 (Figure 4H); and reduced frequency of focal dysplasias and SCC incidence, with benign hyperplasias representing the most frequent terminal neoplastic phenotype (Figure 4I).

C5aR1⁺ Cells in Human SCCs

Since protumoral pathways downstream of C5aR1 signaling regulate squamous carcinogenesis in HPV16 mice, we asked if increased presence of C5aR1⁺ cells characterized human SCCs. We obtained human cutaneous SCCs (cSCC), vulvar SCCs, and head and neck SCCs (HNSCCs) and assessed presence of C5aR1⁺ cells compared with CD45⁺ cells. C5aR1⁺ cells were prominent features of each malignancy and were significantly increased compared with non-malignant homeostatic tissue (Figures 5A and 5B).

Vulvar SCCs are associated with high-risk HPV serotypes, as are a proportion of oropharyngeal SCCs, whereas cSCCs and other HNSCCs (laryngeal and oral cavity) typically are not. We observed that the increased presence of C5aR1⁺ cells was consistent across this spectrum of SCC subtypes (Figures 5B and 5C), indicating that C5aR1-associated inflammation reflects a general feature of squamous carcinomas. Accordingly, previously published HNSCC datasets similarly revealed increased expression of *C5AR1* and *PLAU* (uPA) (Figures 5D and 5E) compared with homeostatic buccal tissue. We also observed that coexpression of genes associated with *C5AR1* expression included *PLAU* and *PLAUR*, as well as other genes associated with mast cells (*MMP9*, but not *MMP2*) and macrophage recruitment or function (*CSF1R*, *ICAM1*, *CCL2*) (Figure 5F). *KRT17*, a gene associated with HNSCC, was moderately associated with C5aR1 expression, while *KRT13*, a gene lost in SCCs, negatively correlated with C5aR1 expression, with no association between *C5AR1* and *C3* expression (Figure 5F). To determine whether C5aR was associated with clinical outcomes, we assessed the Nature 2015 The Cancer Genome Atlas (TCGA) dataset for survival and found significantly increased survival for patients bearing *C5AR1*^{lo}*CD8A*^{hi} tumors compared with *C5AR1*^{hi}*CD8A*^{lo} tumors (Figure 5G), perhaps indicating that C5aR1-mediated inflammation influences CD8 T cell functionality and clinical outcomes.

C5a Inhibition Regulates Response to Chemotherapy in a CD8⁺ T Cell-Dependent Manner

Since genetic loss of C5aR1 significantly slowed SCC progression, we assessed whether C5aR1 might also represent a therapeutic target. To test this, PDSC5 cells were implanted intradermally into syngeneic hosts and grown to ~50–60 mm³, at which point Alzet pumps were subcutaneously implanted delivering PMX-53, a C5aR1 peptide antagonist (Finch et al., 1999). Mice were then treated with two cycles of paclitaxel (PTX). While neither PMX-53 nor PTX monotherapy significantly altered tumor growth kinetics, combination therapy was

Figure 4. uPA Deficiency Limits Neoplastic Progression and Phenocopies C5aR1 Deficiency in HPV16 Mice

(A–G) IHC and automated (A and B) or manual (C–G) quantitation of C5aR1⁺ cells (A), CD45⁺ leukocytes (B), toluidine blue-stained cells mast cells (C), Ly6G⁺ granulocytes (D), F4/80⁺ macrophages (E), percentage of BrdU⁺ keratinocytes (F), and CD31⁺ vessels (G) in tissue sections (ear) from HPV16/uPA^{+/-} and HPV16/uPA^{-/-} at 1, 4, and 6 months of age.

(H) VEGF and MMP9 levels in ear lysates determined by ELISA from 6-month-old HPV16/uPA^{+/-} and HPV16/uPA^{-/-} ears versus 4-month NT ear skin. Significance determined by unpaired Student's t test with Welch's correction.

(I) Percentage of ear skin area from indicated genotypes of HPV16 mice exhibiting hyperplasia (hyp; n = 6 or 7 mice per genotype), dysplasia (dys; n = 9–14 mice per genotype), and lifetime whole-body tumor incidence (HPV16/uPA^{+/-} n = 21, HPV16/uPA^{-/-} n = 203), with significance determined by Chi-squared test, and hazard ratio determined by Kaplan-Meier analysis.

For (A)–(H), data points reflect independent mice, and micrographs on right are representative images from 6-month-old mice. (A)–(E) and (G)–(H) show epidermal (e), dermal (d) regions, and interface (dotted line). Significance assessed by two-way ANOVA with Bonferroni post test for multiple comparisons unless otherwise indicated. Data represented as means ± SEM. *p < 0.05; **p < 0.01; ***p < 0.001; ****p < 0.0001.

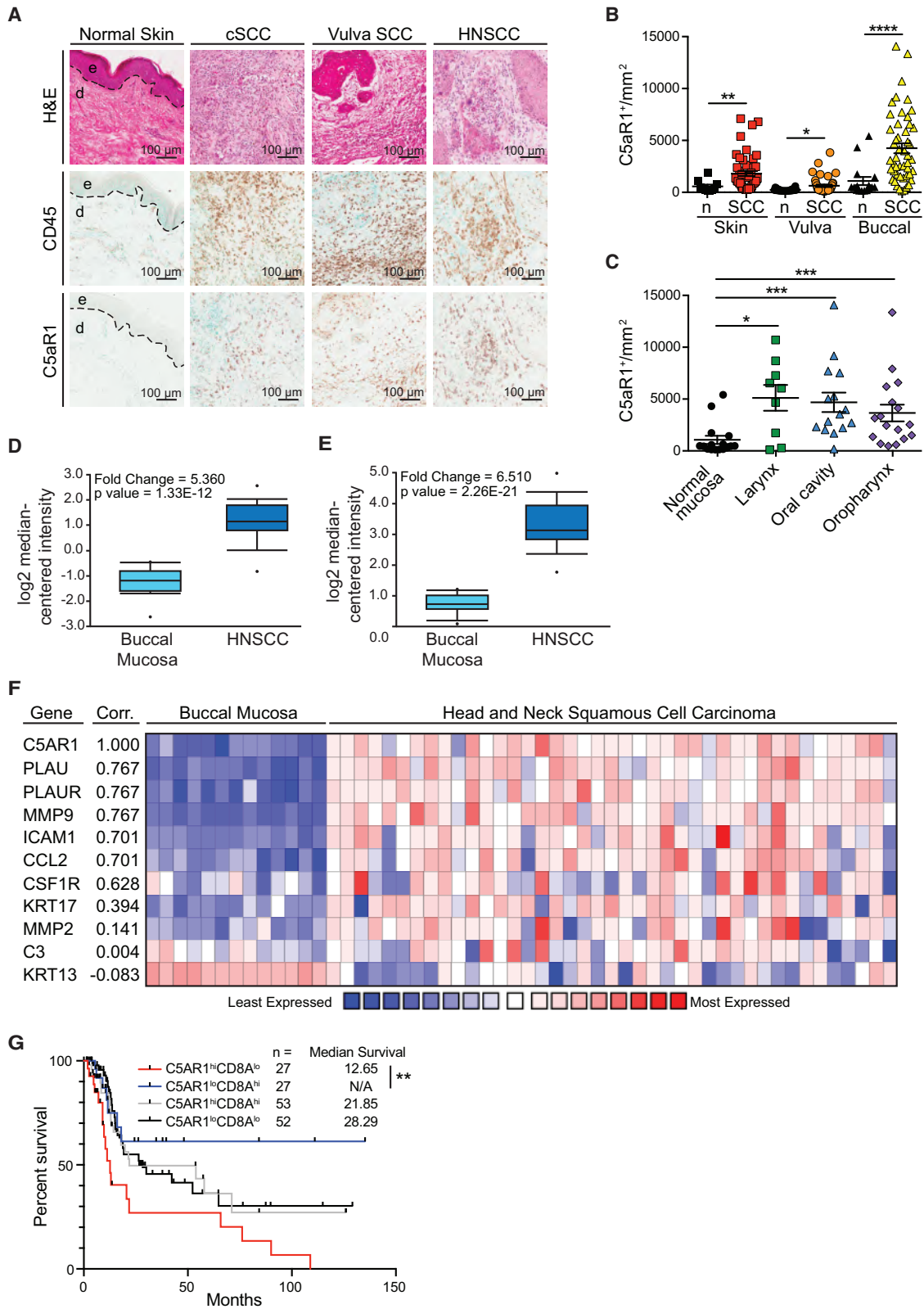


Figure 5. C5aR1 Infiltration Characterizes Human SCCs

(A) Representative histopathology of cutaneous SCC, vulva SCC, and HNSCC compared with healthy cutaneous skin. Panels depict representative H&E-stained tissue sections (top), and IHC staining for CD45 (middle) and C5aR1 (bottom) from serial sections.

(legend continued on next page)

synergistically effective in slowing SCC growth to end stage (Figure 6A).

To determine if SCCs remained responsive to combined therapy in a more advanced setting, we assessed SCC growth in mice given only the later cycle of PTX and observed a similar inhibition of SCC growth with combination therapy (Figure 6B). End-stage SCCs from combination-therapy-treated mice exhibited reduced CD31⁺ vasculature, increased presence of cleaved caspase-3⁺ cells, and a modest, albeit significant, decrease in proliferating cells (Figure 6C). Flow cytometric analysis of end-stage tumors revealed no significant changes in the major leukocyte populations between experimental groups (Figure S4A). Given this, we asked whether inhibition of C5aR1 instead induced a qualitative difference in signaling programs operative during tumor growth. To address this, we evaluated gene expression of end-stage tumors from the various experimental groups using NanoString Myeloid Innate Immunity Panel and Ingenuity Pathway Analysis (IPA) tools. We observed changes in mRNAs associated with DC maturation, NF- κ B and TREM1 signaling across all treatment groups, compared with untreated control tumors (Figure 6D). Moreover, we observed increased expression of mRNAs associated with T cell activation in SCCs from PTX and PMX-53/PTX-treated mice, as well as increased expression of genes associated with macrophage nitric oxide (NO) and reactive oxygen species (ROS) production in the PMX-53 treated group (Figure 6D).

Since C5aR1 is highly expressed by macrophages, and ROS and NO production are generally associated with T helper type 1 (T_H1)-type microenvironments, we asked whether macrophage polarization was altered in animals treated with PMX-53. We isolated macrophages from orthotopic SCC by fluorescence-activated cell sorting (FACS) and evaluated gene expression using NanoString PanCancer Immune Profiling Panel and IPA analysis to assess changes between PMX-53/PTX-treated animals compared with either PTX or PMX-53 monotherapy. Upstream analysis revealed that macrophages from SCCs of PMX-53/PTX-treated mice expressed gene signatures associated with LPS, IL-1 β , tumor necrosis factor (TNF), oncostatin M, and interferon (IFN) γ responses (Figure 6E). Network analysis revealed that SCC-derived macrophages from PMX-53/PTX versus PMX-53 groups expressed higher levels of several mRNAs associated with T_H1-type responses, including *S100a8*, *Tbk1*, *Tank*, *Cd274* (programmed death-ligand 1 [PD-L1]), as well as *Cxcl9* and *Cxcl11*, IFN γ -responsive chemokines notable for their ability to recruit CXCR3⁺ CD8⁺ T cells (Figure S4B). Increased levels of *Cxcl9* and *Cxcl11* were confirmed by qPCR (Figure S5A).

To assess the functional significance of these changes in regulating productive T cell responses, we depleted either CD8⁺ or

CD4⁺ T cells from PTX and PMX-53/PTX-treated mice bearing orthotopic SCCs and found that CD8⁺ T cells (Figure 6F), but not CD4⁺ T cells (Figure S5B), were required for efficacy of PMX-53/PTX therapy. Notably, CD31⁺ vascular density was restored to characteristic levels in CD8⁺ T cell-depleted (Figure S5C), but not in CD4⁺ T cell-depleted (Figure S5D), SCCs.

C5aR-Regulated Macrophage Programming Impacts CD8⁺ T Cell Recruitment and Effector Function

Because of the observed increase in CXCR3 ligands secreted by repolarized macrophages in SCCs of PMX-53/PTX-treated mice (Figures S4B and S5A), we assessed infiltration of CXCR3⁺ CD8⁺ T cells in SCCs and observed a significant increase in PMX-53/PTX-treated mice compared with other treatment groups (Figure 7A), while CCR5⁺ CD8⁺ T cells were unchanged (Figure S6A). Notably, CXCR3⁺CD8⁺ T cells were granzyme B⁺, indicative of their cytolytic capacity (Figure 7B). These data led us to ask whether (1) CXCR3 was necessary for therapeutic efficacy of PMX-53/PTX; (2) macrophages were responsible for CXCR3⁺ CD8⁺ T cell recruitment into PMX-53/PTX-treated SCCs; and (3) IFN γ was similarly required for therapeutic efficacy. While *in vivo* blockade of CXCR3 did not block overall CD8⁺ T cell presence in SCCs (Figure S6B), it abated CXCR3⁺ CD8⁺ T cell presence (Figure S6C), reversed efficacy of PMX-53/PTX therapy (Figure 7C), and restored characteristic SCC vascular density (Figure S6D). Reducing macrophage presence in SCCs via treatment of mice with a neutralizing monoclonal antibody (mAb) to CSF1 (Figure S6E) similarly reversed PMX-53/PTX efficacy (Figure 7D), coincident with reduced CXCR3⁺ CD8⁺ T cell presence (Figure 7E) and partially restored vascular density (Figure S6F). Similarly, blockade of IFN γ reversed therapeutic efficacy of PMX-53/PTX (Figure 7F).

Because PMX-53/PTX efficacy was dependent on CXCR3⁺ CD8⁺ T cells, we assessed the phenotype of CXCR3⁺CD8⁺ T cells and found the majority of these in all treatment groups to be CD44⁺CD62L⁻ (Figures 7G and S6G), indicative of an effector or effector memory subtype. We then assessed eomesodermin (EOMES) and programmed death-1 (PD-1) on CD44⁺CD62L⁻CXCR3⁺CD8⁺ T cells and found that the largest subgroup across all treatment groups was EOMES⁺PD-1⁻, which were also CD69⁻CD107a⁺Ki67^{+/-}KLRG1^{+/-} (Figure S7A), features characteristic of effector CD8⁺ T cells (Zehn and Wherry, 2015). We also noted a significantly decreased presence of EOMES⁺PD-1⁺ cells in SCCs of PMX-53/PTX-treated mice (Figure 7H) that were CD69⁻CD107a⁻Ki67⁻KLRG1⁻ (Figure S7B), indicative of an exhausted effector phenotype that was notably absent in PMX-53/PTX-treated SCCs (Figure 7H). In the PMX-53/PTX-treated SCCs, there was a modest increase in the proportion of EOMES⁻PD-1⁻ CD8⁺ T cells (Figure 7H) that

(B and C) Automated quantitation of C5aR1⁺ cells in tissue sections shown in (A) compared with normal counterparts, with significance determined by Mann-Whitney test.

(D and E) Relative expression of *C5AR1* (D) and *PLAU* (E) comparing normal buccal mucosa (n = 13) and HNSCC (n = 41) from the Ginos Head-Neck dataset in OncoPrint.

(F) Correlation (Corr.) between *C5AR1* and *PLAU*, *PLAU*, *MMP9*, *ICAM1*, *CCL2*, *CSF1R*, *KRT17*, *MMP2*, *C3*, and *KRT13* in the Ginos Head-Neck dataset using OncoPrint coexpression heatmaps. Correlation derived from the average linkage hierarchical clustering and data displayed as log₂ median-centered intensity with lowest expression in blue and highest expression in red.

(G) Overall survival of HNSCC patients from the Nature 2015 TCGA cohort based on HNSCC expression of *C5AR1* and *CD8A*. Significance determined by log rank analyses of each patient cohort.

Data represented as means \pm SEM. *p < 0.05; **p < 0.01; ***p < 0.001; ****p < 0.0001.

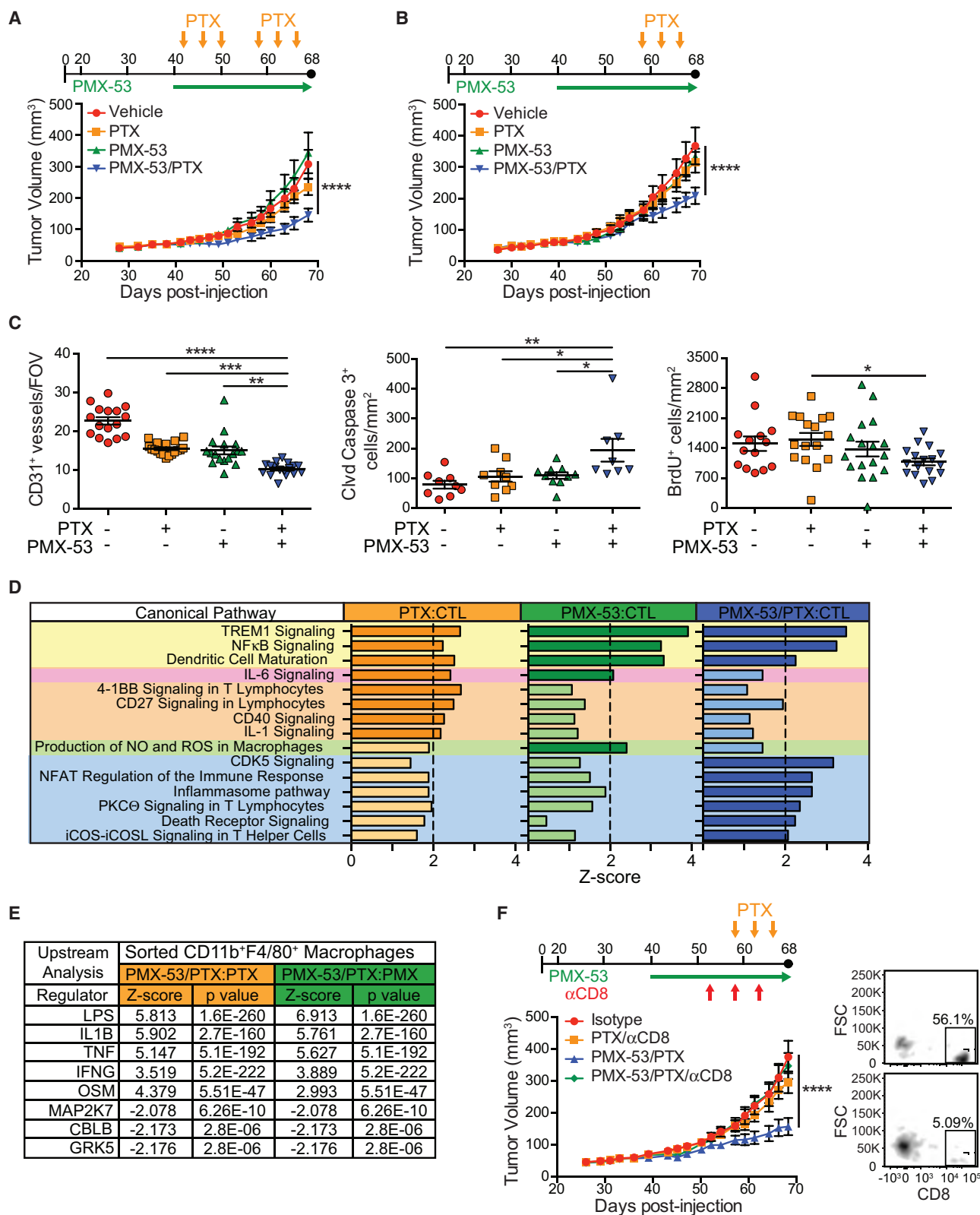


Figure 6. Therapeutic C5aR1 Blockade Sensitizes Established SCCs to Chemotherapy

(A and B) Dosing strategies (top) and PDSC5 growth kinetics (lower graph) in early- (A) or late-stage (B) SCCs. Average tumor volumes reflecting two independent experiments are shown: (A) $n = 12-15$ and (B) $n = 20-24$.

(legend continued on next page)

were CD69⁺CD107a⁺Ki67⁻KLRG1⁺ (Figure S7C), consistent with an effector memory phenotype. Analysis of FACS-isolated CD8⁺ T cells via NanoString PanCancer Immune Profiling Panel and IPA downstream analysis revealed that CD8⁺ T cells in the PMX-53/PTX group expressed a transcriptional profile indicative of an activated and migratory phenotype, compared with other groups (Figure 7I). Together, these data indicated that CXCR3⁺CD8⁺ T cells regulate response to chemotherapy by infiltrating SCCs in response to macrophage reprogramming associated with IFN γ . In support of this mechanism in human HNSCC, we observed a significant correlation between *CXCR3* and *CD8A*, *CXCL9*, *CXCL11*, *CD69*, *PRF1*, *GZMA*, and *GZMB* expression (Figure S7D).

PMX-53/PTX Expands Intratumoral High-Frequency T Cell Clones

To determine if expanded CD8⁺ T cell phenotypes reflect antigen-dependent expansion, we performed deep sequencing of the complementarity-determining region (CDR) 3 region of the T cell receptor (TCR) β chain in matched cardiac-perfused SCC lysates and peripheral blood mononuclear cells (PBMCs). Intratumoral diversity of TCR β sequences and the number of unique TCR β sequences were modestly decreased in SCCs by addition of PMX-53 to PTX (Figures 8A and 8B), accompanied by a modest expansion of the top 25 clones intratumorally (Figure 8C), though overall clonality and maximum clonal frequency were unchanged (Figures S8A and S8B), results that were mirrored in peripheral blood (Figures 8D–8F, S8C, and S8D). To understand how these modest clonal responses reflected varied clonal homeostasis (Nazarov et al., 2015), we assessed frequencies of rare (<10⁻⁵), small (10⁻⁵–10⁻⁴), medium (10⁻⁴–10⁻³), large (10⁻³–0.01), and hyperexpanded (>0.01) clones in SCCs and blood, represented as a fraction of the total population (=1.0). This revealed decreased presence of rare and medium populations, and concomitant increases in hyperexpanded populations in SCCs of PMX-53/PTX-treated mice (Figure 8G, top row), explaining decreased overall diversity (Figure 8A). Based on pairwise analysis of each population in SCCs and its clonotype overlap relative to blood, we observed decreased overlap of rare and small populations, in addition to increased overlap of hyperexpanded clones, revealing that high-frequency intratumoral clonotypes were increasingly found peripherally in PMX-53/PTX-treated mice (Figure 8H). Our interpretation of these data, given that the majority of

expanded CD8⁺ T cells in SCCs of PMX-53/PTX-treated SCCs were Ki67⁻, is that PMX-53/PTX therapy resulted in peripheral priming and expansion of antigen-specific clones that in turn traffic to SCCs, leading to the observed intratumoral high-frequency clonotypes detected in peripheral populations coinciding with decreased overall diversity of TCR β clonotypes both locally and peripherally.

DISCUSSION

Studies revealed herein indicate that signaling downstream of complement C5a represents a co-dominant regulator of cancer-associated chronic inflammation fostering hallmark characteristics of squamous carcinogenesis. The C3-independent nature of inflammation in HPV16 mice indicates that C5a generation can occur independent of classical, lectin, and alternative pathways when regulated downstream of uPA expressed by macrophages in neoplastic tissue. C5a binding to its high-affinity receptor (C5aR1) on infiltrating myeloid subsets activates protumorigenic and immunosuppressive bioactivities critical for neoplastic progression; HPV16 mice lacking either C5aR1 or uPA exhibited reduced neoplasia-associated inflammation, keratinocyte hyperproliferation, development of angiogenic vasculature, and reduced malignant progression to de novo SCC.

In homeostatic and acutely wounded tissues, precise control of complement activation is required to prevent unrestricted inflammation, anaphylactic shock, and exacerbation of pathologies or tissue damage (Ricklin et al., 2016); thus, it is not surprising that tumors co-opt this biological circuitry as a survival strategy (Reis et al., 2018). As such, components of complement have emerged as critical mediators of tumor progression (Afshar-Kharghan, 2017). In one of the first studies to reveal protumorigenic roles for complement, Markiewski et al. (2008) reported C5a promoted subcutaneous TC-1 cervical carcinoma growth by enhancing recruitment of T cell-suppressive myeloid cells. Sarcomas and mammary, ovarian, colon, and cutaneous carcinomas have also been reported to be regulated by C5a-mediated signaling, variably involving transforming growth factor (TGF) β , IL-10, and recruitment of T cell-suppressive macrophages responding to CCL2 (Bonavita et al., 2015; Reis et al., 2018). Although generation of C5a is C3 independent in HPV16 mice (de Visser et al., 2004), and instead is uPA and C5aR1 dependent, other tumor models report C3-dependent C5a generation, thereby underscoring the highly contextual nature

(C) Manual quantitation of CD31⁺ vessels and automated quantitation of cleaved (Clvd) caspase-3⁺ and BrdU⁺ cells in tissue sections from SCCs shown in (B). Each data point shown reflects an independent mouse.

(D) Canonical pathway analysis comparing indicated treatment groups using IPA. Gene expression of SCCs generated using the myeloid panel from NanoString. Significant differences (Z score > |2.0|, dark colors) indicate probability of association of gene expression from NanoString datasets with the indicated canonical pathways. Pathways shaded in yellow were increased in all groups compared with controls (CTL), while the pathway highlighted in pink was increased in PTX and PMX-53 compared with control. Pathways highlighted in orange, green, and blue were increased in PTX, PMX-53, and PMX-53/PTX compared with control, respectively. N = 9 mice/group.

(E) Upstream analysis comparing indicated treatment groups using IPA. Gene expression data from FACS-isolated CD11b⁺MHCII⁺F4/80⁺ macrophages using the PanCancer immune panel (NanoString). Upstream analyses predict upstream regulators significantly activated or inhibited (Z score > |2.0|). N = 3–5 mice/group.

(F) Dosing strategy (top) and growth kinetics (lower graph) of PDSC5-SCCs in syngeneic mice treated with PTX or PMX-53/PTX, and either isotype control (IgG2b) or α CD8 mAb. Shown are mice pooled from two independent experiments (n = 8–12 mice/group). At right is FACS plot showing percentage CD8⁺ cells (as a percentage of CD3⁺ cells) in tumors from control (top) versus CD8-depleted (bottom) mice.

Data represented as means \pm SEM. *p < 0.05; **p < 0.01; ***p < 0.001; ****p < 0.0001, with significance assessed by one-way (C) or two-way (A, B, and F) ANOVA with Bonferroni post test for multiple comparisons. See also Figures S4 and S5.

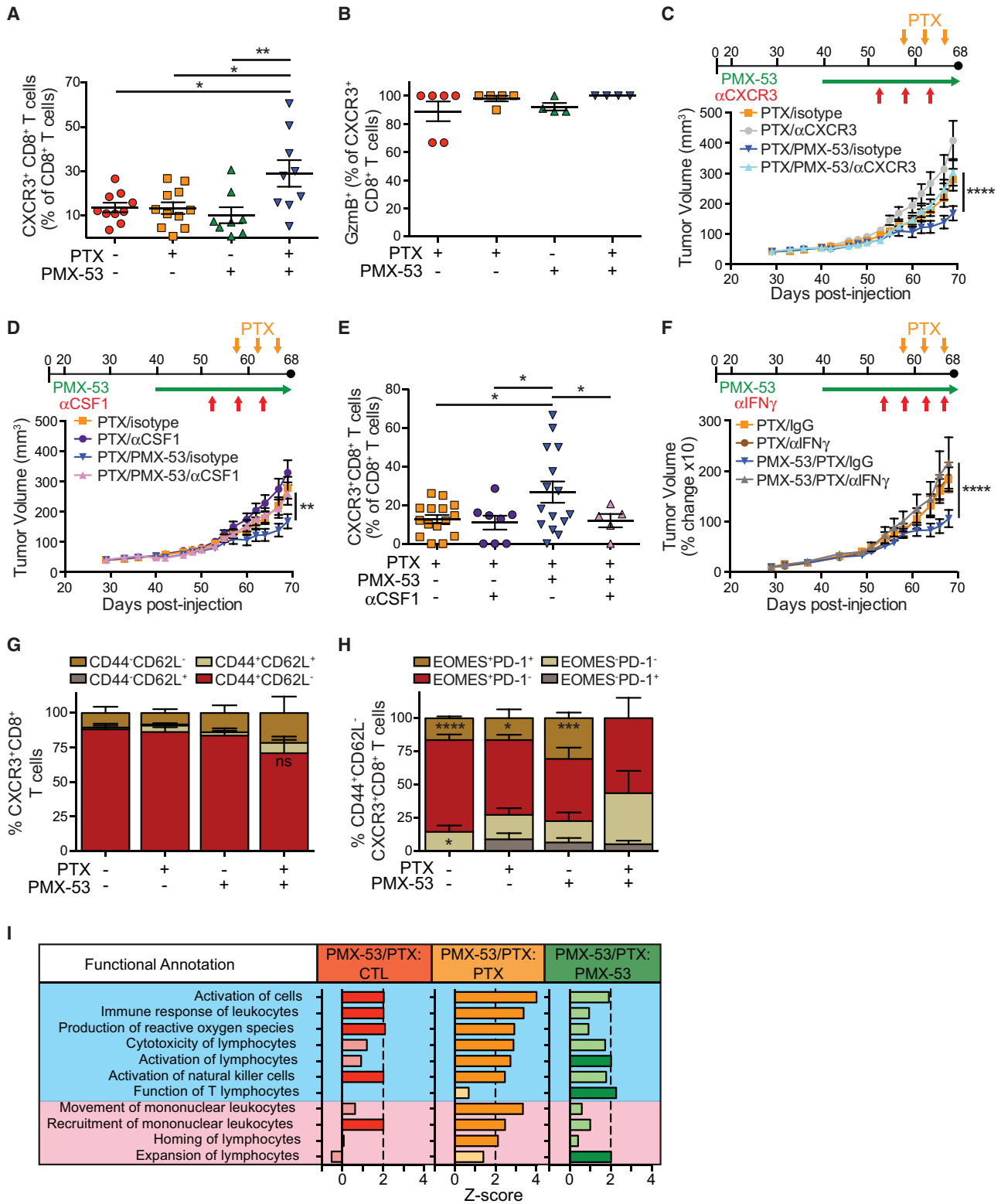


Figure 7. C5aR1 Inhibition of SCC Growth Is Dependent on Macrophage Recruitment of CXCR3⁺CD8⁺ T Cells

(A) Flow cytometric analysis assessing CXCR3⁺CD8⁺ T cells in end-stage SCCs from mice in treatment groups shown in Figure 6B.

(B) Granzyme B (GzmB) expression in CXCR3⁺CD8⁺ T cells in end-stage SCCs from indicated treatment groups from mice shown Figure 6B, assessed by flow cytometry.

(legend continued on next page)

of complement regulation in cancer development. Why the difference?

While it is entirely plausible that the dominant nature of HPV16 oncoproteins alters hemostasis and renders C5 susceptible to proteolysis by fibrinolytic proteases in HPV16/C3^{-/-} mice, it is also likely that mechanisms revealed herein reflect tumor evolution based on selective pressure. The coagulation and fibrinolytic systems regulate fibrin deposition and degradation, respectively. Leaky vasculature allows fibrinogen and circulating zymogens to enter tissue parenchyma. The fibrinolytic system, including tissue plasminogen activator (tPA), uPA, and plasmin, play important roles in regulating degradation of blood clots, regulation of wound healing, and promoting inflammation, likely in part by regulating complement activation (Foley, 2017). In contrast to the endothelial restricted nature of tPA, uPA is primarily localized to interstitia, where it activates plasmin in a fibrin-independent manner. In neoplastic tissue of HPV16 mice, stromal uPA localized to macrophages and regulated C5a generation, leading to enhanced inflammation and neoplastic progression. Macrophages are critical regulators of tissue repair and wound healing (Mantovani et al., 2013), and their expression of uPA has been implicated in skeletal muscle repair, cardiac fibrosis, atherosclerosis, and wound healing (Foley, 2017). uPA⁺ macrophages regulate plasmin processing and deposition, thereby facilitating localized generation of C3a and C5a, release of proinflammatory mediators, and phagocytosis of pathogens or apoptotic cells (Foley, 2017). The C3-independent nature of neoplastic progression in HPV16 mice, while certainly related to prominence of uPA⁺ macrophages regulating localized generation of C5a, could also be due to negative regulators of the complement interactome that rapidly degrade C3 or its downstream products, or in instances where negative regulators of C3 are rendered ineffective, such as when *PTX3* is methylated (Bonavita et al., 2015). Along these lines, we observed increased presence of PTX3⁺ cells during neoplastic progression (Figure S8E), thereby offering a plausible mechanism for the dispensable nature of C3 in this model.

Why might it be beneficial for a tumor to adapt and extrinsically activate complement C5a? During canonical complement activation, several factors upstream of C5 (C1q, C4b, and C3b and its degradation products iC3b and C3dg), function as opsonins regulating phagocytosis, antigen uptake, and cross-presentation by antigen-presenting cells (APCs), and aiding clearance of apoptotic cells (Schmidt et al., 2016). However, apoptotic ma-

ignant cells, in addition to releasing nucleic acids and other stress factors affecting APCs by toll-like receptor-mediated programs, can also be antigenic and would benefit by precluding opsonin generation. Human SCCs upregulate multiple negative regulators of complement that prevent C3 activation or instead increase degradation of opsonins, namely C3b and its cleavage product iC3b (Reis et al., 2018), which are also cleaved by plasmin and further reduce phagocytosis by macrophages (Foley et al., 2015). In HPV16 mice, plasmin generates C5a downstream of uPA and promotes neoplasia-associated inflammation, and likely also enables malignant keratinocytes to avoid decoration by opsonins and subsequent phagocytosis. Results of this are likely 2-fold: enhanced cell survival by virtue of factors secreted by recruited leukocytes responding to C5a, as well as lack of opsonization, reduced antigen uptake, and cross-presentation by APCs. It is therefore plausible that SCCs in HPV16 mice evolve to extrinsically activate complement C5a via the fibrinolytic and/or coagulation systems to promote cancer-associated inflammation while simultaneously evading immunosurveillance.

We observed that C5aR1^{-/-} mice exhibited decreased tumor incidence and reduced orthotopic tumor growth dependent on both macrophages and mast cells, similar to results observed in FcγR^{-/-} mice, likely reflecting regulation of redundant protumorigenic molecules (e.g., VEGF, TNFα, IL-10) affecting angiogenesis, tissue remodeling, immunosuppression, and tumor growth. Therapeutically, treatment of orthotopic SCCs with PMX-53 significantly improved response to paclitaxel involving gene expression networks linked to T_H1 transcriptional programming of macrophages associated with reduced vasculature density, increased keratinocyte cell death, and evidence of IFNγ- and CXCR3-dependent antitumor CD8⁺ T cell responses independent of CD4⁺ T cells.

As a result of macrophage-mediated T cell suppression, and likely chronic antigen exposure, CXCR3⁺ CD8⁺ T cells in SCCs manifest a dysfunctional phenotype characterized by PD-1⁺EOMES⁺ expression, reduced proliferation, and cell surface expression of the lysosomal marker CD107a, indicative of degranulation. In contrast, CD8⁺ T cells in SCCs from PMX-53/PTX-treated mice exhibited increased proportions of PD-1⁻EOMES⁻CXCR3⁺ CD8⁺ T cells, characterized as CD69⁻CD107a⁺Ki67⁻KLRG1⁺, indicative of effector memory cells. Effector memory CD8⁺ T cells expressing high levels of CXCR3 are thought to be long lived and associated with durable

(C) Dosing strategy (top) and PDSC5 growth kinetics (lower graph) in mice treated with PTX or PMX-53/PTX, and either isotype control (IgG2b) or αCXCR3 mAb. Shown are mice pooled from two independent experiments (n = 9–12 mice/group).

(D) Dosing strategy (top) and PDSC5 growth kinetics (lower graph) in mice treated with PTX or PMX-53/PTX, and either isotype control (IgG2b) or αCSF1 mAb. Shown are mice pooled from two independent experiments (n = 9–15 mice/group).

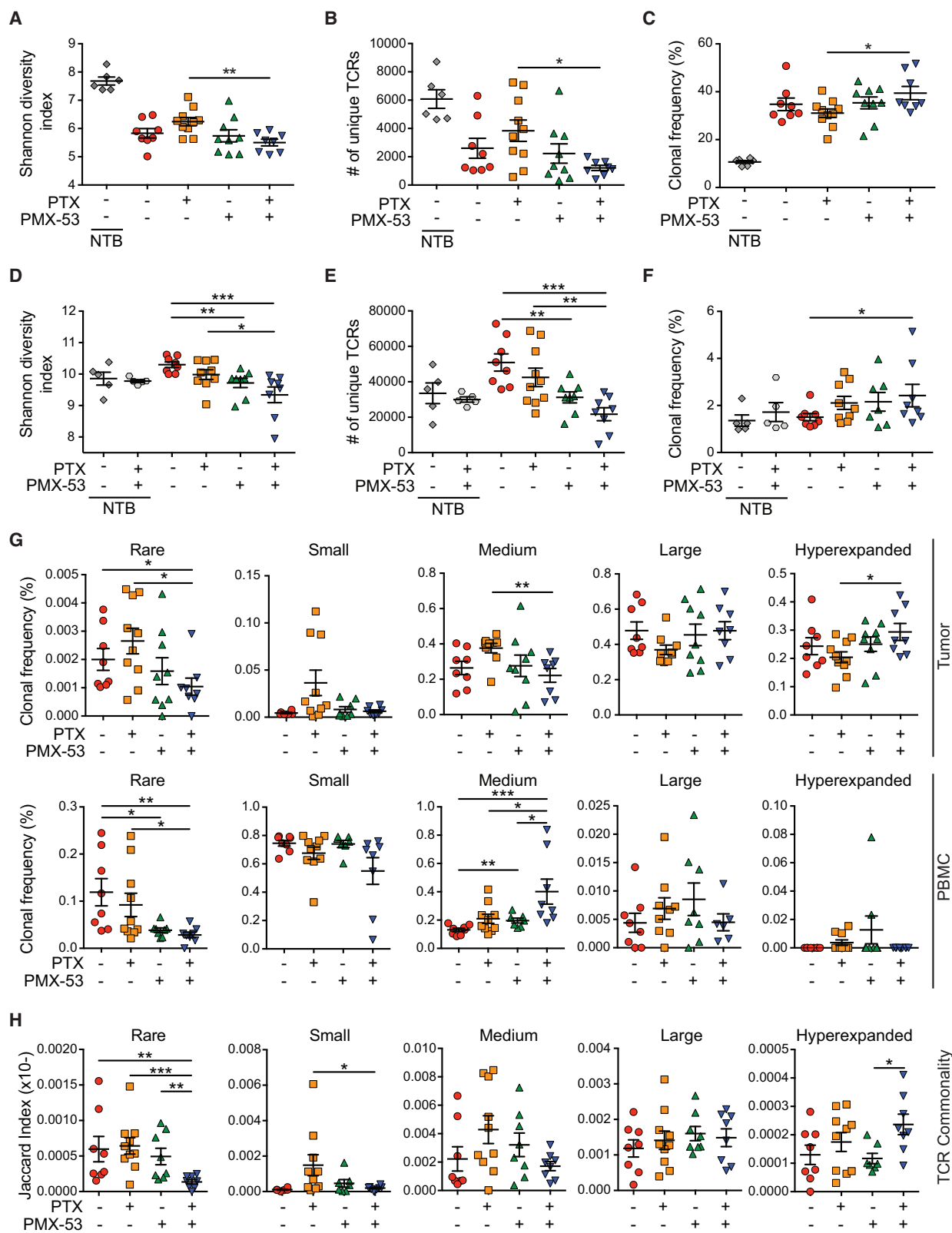
(E) Infiltration of CXCR3⁺ CD8⁺ T cells into end-stage SCCs in mice from Figure 7D and control groups from Figure 6B.

(F) Dosing strategy (top) and PDSC5 growth kinetics (lower graph) in mice treated with PTX or PMX-53/PTX, and either isotype control (IgG1) or αIFNγ mAb. Shown are percentage changes in SCCs in mice pooled from two independent experiments (n = 11–17 mice/group).

(G) CD44 and CD62L expression by flow cytometry on CXCR3⁺ CD8⁺ T cells in end-stage SCCs from mice in treatment groups shown in Figure 6B.

(H) EOMES and PD-1 by flow cytometry on CD44⁺CD62L⁻CXCR3⁺ CD8⁺ T cells infiltrating end-stage SCCs from mice in treatment groups shown in Figure 6B.

(I) Downstream effector pathway analysis comparing gene expression in FACS-isolated CD8⁺ T cells from indicated treatment groups (Figure 6B) using PanCancer immune panel (NanoString) and IPA. Significant differences (Z score > |2|) identify how indicated functions change based on differences in gene expression in the dataset. Functions listed in blue are indicative of activation, while functions in pink indicate movement or expansion. N = 3–5 mice/group. Data are represented as means ± SEM. *p < 0.05; **p < 0.01; ***p < 0.001; ****p < 0.0001, with significance determined by one-way (A, B, and E) or two-way (C, D, F) ANOVA with Bonferroni post test for multiple comparisons, or unpaired Student's t test with Welch's correction (G and H). In (A), (B), and (E), each data point reflects an individual mouse. See also Figures S6 and S7.



(legend on next page)

antitumor memory responses (Pages et al., 2005). CXCR3 is a chemokine receptor whose expression is increased following antigen stimulation of T_H1 - $CD4^+$ T cells and effector and subsets of memory $CD8^+$ T cells. These interactions enable T cell entry into inflamed tissues via $IFN\gamma$ -inducible ligands CXCL9, CXCL10, and CXCL11, expression of which correlates with $CD8^+$ T cell infiltration and outcomes (Mikucki et al., 2015). Herein, neoplasia-associated macrophages increased expression of CXCR3 ligands in response to $IFN\gamma$, which in turn enhanced recruitment of effector and effector memory $CD8^+$ T cells. This shift from a dysfunctional to a CXCR3⁺ effector memory $CD8^+$ T cell phenotype bolsters therapeutic efficacy, as depletion of macrophages or blockade of CXCR3 or $IFN\gamma$ reversed SCC growth kinetics in mice treated with PMX-53/PTX.

Analysis of TCR β sequences revealed that T cell clones were less diverse locally and peripherally, with high-frequency clones expanded in SCCs of PMX-53/PTX-treated mice. Because intratumoral $CD8^+$ T cells were largely Ki67⁻, and because there was high concordance with peripheral TCR sequences in PMX-53/PTX-treated groups as measured by the Jaccard index, we conclude that hyperexpanded T cell clones expanded in secondary lymphoid organs and subsequently were recruited to SCCs. While we anticipate these responses are likely antigen specific, we cannot rule out that a portion of therapeutic efficacy may be due to bystander T cell activation. Impacts of TCR β repertoire changes in PMX-53/PTX-treated mice are relevant given that patients with less diverse and more clonal TCR repertoires have improved therapeutic responses to α PD-1 therapy (Tumeh et al., 2014).

Taken together, results presented herein provide evidence that complement C5a and signaling pathways downstream of myeloid C5aR1 are early regulators of squamous carcinogenesis by promoting cancer-associated inflammation. Our pre-clinical data demonstrate that therapeutic inhibition of C5aR1, in combination with cytotoxic chemotherapy, results in transcriptional reprogramming of macrophages that not only affects angiogenic programs but also leads to recruitment of CXCR3⁺ cytotoxic $CD8^+$ T cells by $IFN\gamma$ -dependent mechanisms. Given that human SCCs are highly infiltrated with C5aR1⁺ cells, and that increased survival is observed in patients bearing C5AR1^{lo}CD8A^{hi} tumors, we assert that these malignancies may benefit from therapies targeting C5aR1 in conjunction with chemotherapy, with or without additional immunomodulating therapies.

STAR★METHODS

Detailed methods are provided in the online version of this paper and include the following:

- KEY RESOURCES TABLE
- CONTACT FOR REAGENT AND RESOURCE SHARING
- EXPERIMENTAL MODEL AND SUBJECT DETAILS
 - Human Studies
 - Animal Studies
- METHOD DETAILS
 - Bone Marrow-Derived Mast Cells and Macrophages
 - Immunohistochemistry
 - Immunofluorescence
 - Real-time PCR
 - Flow Cytometry and FACS
 - Complement Deposition Assay
 - ELISA
 - LC-MS/MS
 - Nanostring Profiling of Gene Expression
 - TCR β Deep Sequencing of Tumor and Blood
- QUANTIFICATION AND STATISTICAL ANALYSIS
- DATA AND SOFTWARE AVAILABILITY

SUPPLEMENTAL INFORMATION

Supplemental Information includes eight figures and can be found with this article online at <https://doi.org/10.1016/j.ccell.2018.09.003>.

ACKNOWLEDGMENTS

The authors thank the Knight Cancer Institute (P30 CA069533) Flow Cytometry, Advanced Light Microscopy, Bioinformatics, and OHSU Massively Parallel Sequencing shared resources. Human tissue specimens provided by the OHSU Department of Dermatology Molecular Profiling Tissue Resource Repository (IRB#10071). We are grateful to members of the Coussens Lab for critical discussions; to Ole Behrendtsen, Lia Kim, Miriam Marx, Shiv Shah, and Meghan Lavoie for technical assistance; to Justin Tibbitts and Teresa Beechwood for research regulatory oversight and animal husbandry; and to Drs. Leif Lund and Keld Dano for providing uPA^{-/-} mice. The authors acknowledge support from the American Cancer Society – Friends of Robert Kinas Postdoctoral Fellowship (PF-14-221-01-MPC), NIH/NCI Postdoctoral Training Grant (CA106195), the Cathy and Jim Rudd Career Development Award for Cancer Research, the Medical Research Foundation, and Drs. Gough and Crittenden for salary support during manuscript revision to T.R.M.; NIH/NCI (CA192405) to M.K.-M.; NIH/NCI (CA057621) to Z.W.; and the NIH/NCI (CA130980, CA155331, CA163123), a DOD BCRP Era of Hope Scholar

Figure 8. PMX-53/PTX Increases Hyperexpanded T Cell Clonotypes, Resulting in Decreased TCR β Diversity

(A–C) End-stage SCCs from mice shown in Figure 6A with specified treatments (n = 5–10 mice/group) were analyzed by deep sequencing of CDR3 regions of the TCR β chain to determine the Shannon diversity index reflecting the number of unique TCR β sequences and abundance of clonotypes (A), the total number of unique TCR β sequences (B), and the intratumoral frequency of top 25 TCR β clonotypes (C).

(D–F) Matched PBMCs from mice in (A)–(C) were analyzed by deep sequencing of CDR3 regions of the TCR β chain to determine the Shannon diversity index reflecting the number of unique TCR β sequences and abundance of clonotypes (D), the total number of unique TCR β sequences (E), and the intratumoral frequency of top 25 TCR β clonotypes (F).

(G) Alterations in clonal frequencies within the homeostatic space in SCCs (top) and PBMCs (bottom). Cumulative frequencies of rare (<10⁻⁵), small (10⁻⁵–10⁻⁴), medium (10⁻⁴–10⁻³), large (10⁻³–0.01), and hyperexpanded (>0.01) clones as a fraction of total TCR β repertoires are shown. Data presented are the sum of all clonal frequencies for each mouse and include all TCR β sequences with a detectable frequency count.

(H) Pairwise assessment of TCR clonotype sequence commonality between SCC and PBMCs. Each point represents the Jaccard overlap index between the various frequency subsets in tumor and matched PBMC sample.

Unless otherwise indicated, each data point reflects an independent mouse. Data are represented as means \pm SEM. *p < 0.05; **p < 0.01; ***p < 0.001 with statistical outliers removed using ROUT (robust regression and outlier removal) test (Q = 1) and significance determined by Mann-Whitney test. See also Figure S8.

Expansion Award (W81XWH-08-PRMRP-IIRA), the Susan G. Komen Foundation (KG110560), the Breast Cancer Research Foundation, the Brenden-Colson Center for Pancreatic Health, and a Stand Up To Cancer – Lustgarten Foundation Pancreatic Cancer Convergence Dream Team Translational Research Grant (SU2C-AACR-DT14-14) to L.M.C.

AUTHOR CONTRIBUTIONS

Conceptualization: T.R.M. and L.M.C.

Methodology: T.R.M., D.M., W.H., S.K., P.L., A.A.M. and L.M.C.

Formal Analysis: T.R.M., D.M., W.H., S.K., T.C., and A.M.F.

Resources: J.J.L., M.K.-M., Z.W., and L.M.C.

Writing – Original Draft: T.R.M. and D.M.

Writing – Review & Editing: Z.W. and L.M.C.

Visualization: T.R.M. and L.M.C.

Supervision: L.M.C.

Project Administration: L.M.C.

Funding Acquisition: T.R.M., M.K.-M., and L.M.C.

DECLARATION OF INTERESTS

The authors declare no financial conflicts of interests. L.M.C. declares that she is a paid consultant for Cell Signaling Technologies and received reagent support from NanoString Technologies. LMC is a member of the Scientific Advisory Boards of Syndax Pharmaceuticals, Inc. and CARMA Therapeutics.

Received: March 14, 2018

Revised: July 17, 2018

Accepted: September 5, 2018

Published: October 8, 2018

REFERENCES

- Affara, N.I., Ruffell, B., Medler, T.R., Gunderson, A.J., Johansson, M., Bornstein, S., Bergsland, E., Steinhoff, M., Li, Y., Gong, Q., et al. (2014). B cells regulate macrophage phenotype and response to chemotherapy in squamous carcinomas. *Cancer Cell* 25, 809–821.
- Afshar-Kharghan, V. (2017). The role of the complement system in cancer. *J. Clin. Invest.* 127, 780–789.
- Amara, U., Rittirsch, D., Flierl, M., Bruckner, U., Klos, A., Gebhard, F., Lambris, J.D., and Huber-Lang, M. (2008). Interaction between the coagulation and complement system. *Adv. Exp. Med. Biol.* 632, 71–79.
- Andreu, P., Johansson, M., Affara, N.I., Pucci, F., Tan, T., Junankar, S., Korets, L., Lam, J., Tawfik, D., DeNardo, D.G., et al. (2010). FcR γ activation regulates inflammation-associated squamous carcinogenesis. *Cancer Cell* 17, 121–134.
- Arbeit, J.M., Munger, K., Howley, P.M., and Hanahan, D. (1994). Progressive squamous epithelial neoplasia in K14-human papillomavirus type 16 transgenic mice. *J. Virol.* 68, 4358–4368.
- Arbeit, J.M., Olson, D.C., and Hanahan, D. (1996). Upregulation of fibroblast growth factors and their receptors during multi-stage epidermal carcinogenesis in K14-HPV16 transgenic mice. *Oncogene* 13, 1847–1857.
- Bolotin, D.A., Poslavsky, S., Mitrophanov, I., Shugay, M., Mamedov, I.Z., Putintseva, E.V., and Chudakov, D.M. (2015). MiXCR: software for comprehensive adaptive immunity profiling. *Nat. Methods* 12, 380–381.
- Bonavita, E., Gentile, S., Rubino, M., Maina, V., Papait, R., Kunderfranco, P., Greco, C., Feruglio, F., Molgora, M., Laface, I., et al. (2015). PTX3 is an extrinsic oncosuppressor regulating complement-dependent inflammation in cancer. *Cell* 160, 700–714.
- Carlson, C.S., Emerson, R.O., Sherwood, A.M., Desmarais, C., Chung, M.W., Parsons, J.M., Steen, M.S., LaMadrid-Herrmannsfeldt, M.A., Williamson, D.W., Livingston, R.J., et al. (2013). Using synthetic templates to design an unbiased multiplex PCR assay. *Nat. Commun.* 4, 2680.
- Carmeliet, P., Schoonjans, L., Kieckens, L., Ream, B., Degen, J., Bronson, R., De Vos, R., van den Oord, J.J., Collen, D., and Mulligan, R.C. (1994). Physiological consequences of loss of plasminogen activator gene function in mice. *Nature* 368, 419–424.
- Chen, X., Poncette, L., and Blankenstein, T. (2017). Human TCR-MHC coevolution after divergence from mice includes increased non-template-encoded CDR3 diversity. *J. Exp. Med.* 214, 3417–3433.
- Coussens, L.M., Hanahan, D., and Arbeit, J.M. (1996). Genetic predisposition and parameters of malignant progression in K14-HPV16 transgenic mice. *Am. J. Pathol.* 149, 1899–1917.
- Coussens, L.M., Raymond, W.W., Bergers, G., Laig-Webster, M., Behrendtsen, O., Werb, Z., Caughey, G.H., and Hanahan, D. (1999). Inflammatory mast cells up-regulate angiogenesis during squamous epithelial carcinogenesis. *Genes Dev.* 13, 1382–1397.
- Coussens, L.M., Tinkle, C.L., Hanahan, D., and Werb, Z. (2000). MMP-9 supplied by bone marrow-derived cells contributes to skin carcinogenesis. *Cell* 103, 481–490.
- Daniel, D., Meyer-Morse, N., Bergsland, E.K., Dehne, K., Coussens, L.M., and Hanahan, D. (2003). Immune enhancement of skin carcinogenesis by CD4+ T cells. *J. Exp. Med.* 197, 1017–1028.
- de Visser, K.E., Korets, L.V., and Coussens, L.M. (2004). Early neoplastic progression is complement independent. *Neoplasia* 6, 768–776.
- de Visser, K.E., Korets, L.V., and Coussens, L.M. (2005). De novo carcinogenesis promoted by chronic inflammation is B lymphocyte dependent. *Cancer Cell* 7, 411–423.
- Eichten, A., Hyun, W.C., and Coussens, L.M. (2007). Distinctive features of angiogenesis and lymphangiogenesis determine their functionality during de novo tumor development. *Cancer Res.* 67, 5211–5220.
- Faham, M., Zheng, J., Moorhead, M., Carlton, V.E., Stow, P., Coustan-Smith, E., Pui, C.H., and Campana, D. (2012). Deep-sequencing approach for minimal residual disease detection in acute lymphoblastic leukemia. *Blood* 120, 5173–5180.
- Finch, A.M., Wong, A.K., Paczkowski, N.J., Wadi, S.K., Craik, D.J., Fairlie, D.P., and Taylor, S.M. (1999). Low-molecular-weight peptidic and cyclic antagonists of the receptor for the complement factor C5a. *J. Med. Chem.* 42, 1965–1974.
- Foley, J.H. (2017). Plasmin(ogen) at the nexus of fibrinolysis, inflammation, and complement. *Semin. Thromb. Hemost.* 43, 135–142.
- Foley, J.H., Peterson, E.A., Lei, V., Wan, L.W., Krisinger, M.J., and Conway, E.M. (2015). Interplay between fibrinolysis and complement: plasmin cleavage of iC3b modulates immune responses. *J. Thromb. Haemost.* 13, 610–618.
- Gunderson, A.J., Kaneda, M.M., Tsujikawa, T., Nguyen, A.V., Affara, N.I., Ruffell, B., Gorjestani, S., Liudahl, S.M., Truitt, M., Olson, P., et al. (2016). Bruton tyrosine kinase-dependent immune cell cross-talk drives pancreas cancer. *Cancer Discov.* 6, 270–285.
- Hanahan, D., and Coussens, L.M. (2012). Accessories to the crime: functions of cells recruited to the tumor microenvironment. *Cancer Cell* 21, 309–322.
- Hanahan, D., and Weinberg, R.A. (2011). Hallmarks of cancer: the next generation. *Cell* 144, 646–674.
- Hopken, U.E., Lu, B., Gerard, N.P., and Gerard, C. (1996). The C5a chemoattractant receptor mediates mucosal defence to infection. *Nature* 383, 86–89.
- Huber-Lang, M., Sarma, J.V., Zetoune, F.S., Rittirsch, D., Neff, T.A., McGuire, S.R., Lambris, J.D., Warner, R.L., Flierl, M.A., Hoesel, L.M., et al. (2006). Generation of C5a in the absence of C3: a new complement activation pathway. *Nat. Med.* 12, 682–687.
- Huber-Lang, M., Younkin, E.M., Sarma, J.V., Riedemann, N., McGuire, S.R., Lu, K.T., Kunkel, R., Younger, J.G., Zetoune, F.S., and Ward, P.A. (2002). Generation of C5a by phagocytic cells. *Am. J. Pathol.* 161, 1849–1859.
- Junankar, S.R., Eichten, A., Kramer, A., de Visser, K.E., and Coussens, L.M. (2006). Analysis of immune cell infiltrates during squamous carcinoma development. *J. Investig. Dermatol. Symp. Proc.* 11, 36–43.
- Mantovani, A., Allavena, P., Sica, A., and Balkwill, F. (2008). Cancer-related inflammation. *Nature* 454, 436–444.
- Mantovani, A., Biswas, S.K., Galdiero, M.R., Sica, A., and Locati, M. (2013). Macrophage plasticity and polarization in tissue repair and remodelling. *J. Pathol.* 229, 176–185.

- Mirkiewski, M.M., DeAngelis, R.A., Benencia, F., Ricklin-Lichtsteiner, S.K., Koutoulaki, A., Gerard, C., Coukos, G., and Lambris, J.D. (2008). Modulation of the antitumor immune response by complement. *Nat. Immunol.* **9**, 1225–1235.
- Mekkawy, A.H., Pourgholami, M.H., and Morris, D.L. (2014). Involvement of urokinase-type plasminogen activator system in cancer: an overview. *Med. Res. Rev.* **34**, 918–956.
- Mikucki, M.E., Fisher, D.T., Matsuzaki, J., Skitzki, J.J., Gaulin, N.B., Muhitch, J.B., Ku, A.W., Frelinger, J.G., Odunsi, K., Gajewski, T.F., et al. (2015). Non-redundant requirement for CXCR3 signalling during tumoricidal T-cell trafficking across tumour vascular checkpoints. *Nat. Commun.* **6**, 7458.
- Nazarov, V.I., Pogorelyy, M.V., Komech, E.A., Zvyagin, I.V., Bolotin, D.A., Shugay, M., Chudakov, D.M., Lebedev, Y.B., and Mamedov, I.Z. (2015). tcR: an R package for T cell receptor repertoire advanced data analysis. *BMC Bioinformatics* **16**, 175.
- Pages, F., Berger, A., Camus, M., Sanchez-Cabo, F., Costes, A., Molidor, R., Mlecnik, B., Kirilovsky, A., Nilsson, M., Damotte, D., et al. (2005). Effector memory T cells, early metastasis, and survival in colorectal cancer. *N. Engl. J. Med.* **353**, 2654–2666.
- Reis, E.S., Mastellos, D.C., Ricklin, D., Mantovani, A., and Lambris, J.D. (2018). Complement in cancer: untangling an intricate relationship. *Nat. Rev. Immunol.* **18**, 5–18.
- Rhee, J.S., Diaz, R., Korets, L., Hodgson, J.G., and Coussens, L.M. (2004). TIMP-1 alters susceptibility to carcinogenesis. *Cancer Res.* **64**, 952–961.
- Ricklin, D., Reis, E.S., and Lambris, J.D. (2016). Complement in disease: a defence system turning offensive. *Nat. Rev. Nephrol.* **12**, 383–401.
- Robins, H.S., Campregher, P.V., Srivastava, S.K., Wachter, A., Turtle, C.J., Khsai, O., Riddell, S.R., Warren, E.H., and Carlson, C.S. (2009). Comprehensive assessment of T-cell receptor beta-chain diversity in alpha-beta T cells. *Blood* **114**, 4099–4107.
- Ruffell, B., and Coussens, L.M. (2015). Macrophages and therapeutic resistance in cancer. *Cancer Cell* **27**, 462–472.
- Schioppa, T., Moore, R., Thompson, R.G., Rosser, E.C., Kulbe, H., Nedospasov, S., Mauri, C., Coussens, L.M., and Balkwill, F.R. (2011). B regulatory cells and the tumor-promoting actions of TNF-alpha during squamous carcinogenesis. *Proc. Natl. Acad. Sci. USA* **108**, 10662–10667.
- Schmidt, C.Q., Lambris, J.D., and Ricklin, D. (2016). Protection of host cells by complement regulators. *Immunol. Rev.* **274**, 152–171.
- Tumeh, P.C., Harview, C.L., Yearley, J.H., Shintaku, I.P., Taylor, E.J., Robert, L., Chmielowski, B., Spasic, M., Henry, G., Ciobanu, V., et al. (2014). PD-1 blockade induces responses by inhibiting adaptive immune resistance. *Nature* **515**, 568–571.
- van Kempen, L.C., Rhee, J.S., Dehne, K., Lee, J., Edwards, D.R., and Coussens, L.M. (2002). Epithelial carcinogenesis: dynamic interplay between neoplastic cells and their microenvironment. *Differentiation* **70**, 610–623.
- Zehn, D., and Wherry, E.J. (2015). Immune memory and exhaustion: Clinically relevant lessons from the LCMV model. *Adv. Exp. Med. Biol.* **850**, 137–152.
- Zhang, J., Kobert, K., Flouri, T., and Stamatakis, A. (2014). PEAR: a fast and accurate Illumina Paired-End reAd mergeR. *Bioinformatics* **30**, 614–620.

Evolution of Metastases in Space and Time under Immune Selection

Mihaela Angelova,¹ Bernhard Mlecnik,^{1,2} Angela Vasaturo,¹ Gabriela Bindea,¹ Tessa Fredriksen,¹ Lucie Lafontaine,¹ Bénédicte Buttard,¹ Erwan Morgand,¹ Daniela Bruni,¹ Anne Jouret-Mourin,³ Catherine Hubert,³ Alex Kartheuser,³ Yves Humblet,³ Michele Ceccarelli,^{4,5} Najeeb Syed,⁶ Francesco M. Marincola,^{7,8} Davide Bedognetti,^{9,10} Marc Van den Eynde,^{1,3,10} and Jérôme Galon^{1,11,*}

¹INSERM, Laboratory of Integrative Cancer Immunology, Sorbonne Université, Sorbonne Paris Cité, Université Paris Descartes, Université Paris Diderot, Centre de Recherche des Cordeliers, 75006 Paris, France

²Inovarian, Paris, France

³Institut Roi Albert II, Department of Medical Oncology Cliniques universitaires St-Luc and Institut de Recherche Clinique et Experimentale (Pole MIRO), Université Catholique de Louvain, 1348 Brussels, Belgium

⁴Department of Science and Technology, Università degli Studi del Sannio, 82100, Benevento, Italy

⁵BIOGEM Istituto di Ricerche Genetiche "G. Salvatore," I-83031 Ariano Irpino, Italy

⁶Biomedical Informatics Division, Sidra Medicine, Doha, Qatar

⁷Refuge Biotechnologies Inc., Menlo Park, CA 94025, USA

⁸Office of the Chief Research Officer, Sidra Medicine, 26999 Doha, Qatar

⁹Tumor Biology, Immunology, and Therapy Section, Sidra Medicine, 26999 Doha, Qatar

¹⁰These authors contributed equally

¹¹Lead Contact

*Correspondence: jerome.galon@crc.jussieu.fr

<https://doi.org/10.1016/j.cell.2018.09.018>

SUMMARY

We examined how the immune microenvironment molds tumor evolution at different metastatic organs in a longitudinal dataset of colorectal cancer. Through multiplexed analyses, we showed that clonal evolution patterns during metastatic progression depend on the immune contexture at the metastatic site. Genetic evidence of neoantigen depletion was observed in the sites with high Immunoscore and spatial proximity between Ki67⁺ tumor cells and CD3⁺ cells. The immunoedited tumor clones were eliminated and did not recur, while progressing clones were immune privileged, despite the presence of tumor-infiltrating lymphocytes. Characterization of immune-privileged metastases revealed tumor-intrinsic and tumor-extrinsic mechanisms of escape. The lowest recurrence risk was associated with high Immunoscore, occurrence of immunoediting, and low tumor burden. We propose a parallel selection model of metastatic progression, where branched evolution could be traced back to immune-escaping clones. The findings could inform the understanding of cancer dissemination and the development of immunotherapeutics.

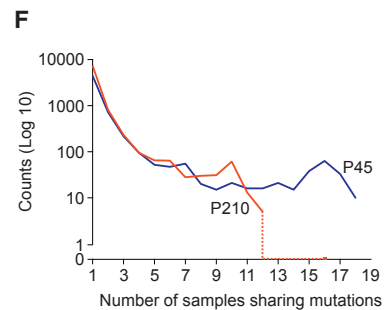
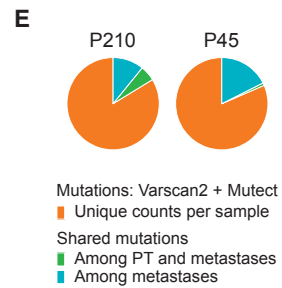
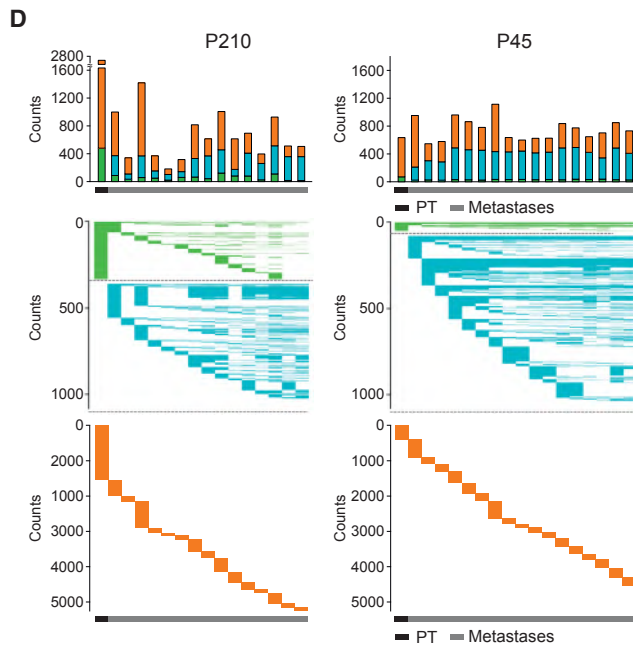
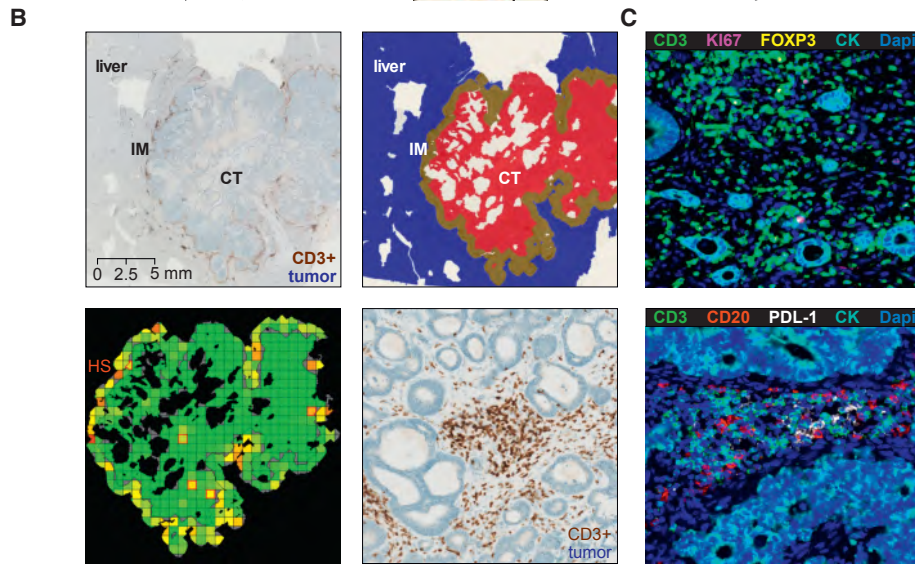
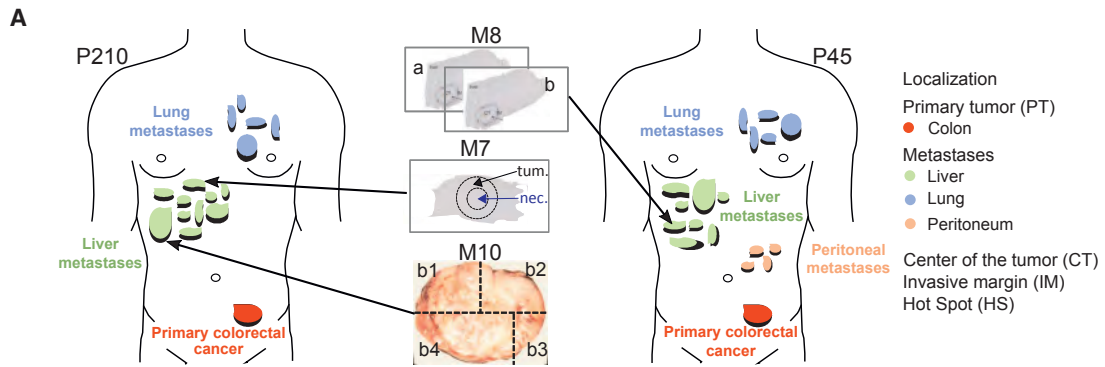
INTRODUCTION

One of the most renowned theories of tumor evolution in the past decades was formulated as an accumulation of driver mutations conferring successive steps of clonal expansion and selective advantage of specific tumor clones (Fearon

and Vogelstein, 1990). Alternatively, a big-bang model described tumor evolution as an initial single clone expansion that is rarely followed by subclonal outgrowth and selective sweeps (Sottoriva et al., 2015), which implies pervasiveness of the major driver mutations in all tumor cells and clonal robustness to the local microenvironment. More recently, a third model of tumor evolution described the accumulation of mutations under neutral evolutionary dynamics (Williams et al., 2016). Currently the most widely accepted, the branched evolution model posits multiple co-existing clonal expansions that diverge from a common ancestor and evolve in parallel (Gerlinger et al., 2012). These four theories reflect tumor cell-centric hypotheses.

Whereas some current models consider metastases to arise from cell-autonomous alterations in the cancer cell genome (Hunter et al., 2018), alternative views propose that metastatic traits are acquired through the exposure of cancer cells to paracrine signals (Langley and Fidler, 2007; Prendergast and Jaffee, 2007) and factors within the tumor microenvironment (Mlecnik et al., 2014). However, efforts to elucidate the role of the tumor microenvironment on the metastatic potential of tumor cells have been hindered by the vast diversity of infiltrating immune cells (Bindea et al., 2013), the extensive interactions between tumor cells and surrounding tissues (Labiano et al., 2015), and the elusive and dynamic nature of paracrine signals (Finn, 2008). Murine studies have shown that the immune system prevents the formation of distant metastasis by maintaining a state of dormancy in circulating tumor cells and potentially in tissue micrometastases (Koebel et al., 2007; Schreiber et al., 2011). In humans, our previous data demonstrated a major role of cytotoxic and memory T cells in predicting survival of cancer patients (Galon et al., 2006), in preventing early metastatic dissemination (Pagès et al.,





(legend on next page)

2005), and in protecting against seeding of distant metastasis (Mlecnik et al., 2016b).

Very few studies only recently have addressed the role of the immune system in metastatic heterogeneity (Jimenez-Sanchez et al., 2017; Zhang et al., 2018). However, the metastatic seeding and evolutionary clonal dynamics under immune pressure remain elusive in the absence of a longitudinal disease follow-up (Caswell and Swanton, 2017; Lloyd et al., 2016). An improved understanding of the processes leading to metastatic invasion and development is required to devise novel treatment paradigms for late-stage tumors.

We hypothesized that metastatic progression and clonal evolution of tumor cells underlie Darwinian selection of tumor clones mediated both by tumor-intrinsic characteristics as well as extrinsic immune pressure. Tumor cell variants having low immunogenicity and resistance to immune attack are thereby selected and proceed to the equilibrium phase, while highly immunogenic tumor clones are eradicated in the elimination phase. Indeed, the existence of cancer immunoeediting has been demonstrated both in mouse models (Matsushita et al., 2012) and in human primary tumors, for missense (Rooney et al., 2015) and frameshift mutations (Mlecnik et al., 2016a).

Here, we sought to determine how immune pressure shapes metastatic evolution based on 11-year-long spatiotemporal follow-up of metastatic colorectal cancer (CRC). We characterized the evolving metastatic genome and the immune microenvironment and then described the juncture of immune surveillance and escape and clonal seeding and progression. Herein we propose a parallel selection model of tumor evolution during the metastatic process depending on the strength and quality of the local immune response.

RESULTS

A Framework of Metastases Evolution under Immune Pressure

We closely examined a rare, longitudinal dataset of 31 metastases from two cases of stage IV CRC with exceptionally long survival. The progressive course of the metastatic diseases was followed by sampling spatiotemporally distinct sites, within and across metastases of two patients, P210 and P45 (Figure 1A). Accounting for a total of 36 samples, the fully resected primary tumors, synchronous, and metachronous metastases were characterized extensively at genomic level and with regards to the tumor microenvironment. This allowed the

evaluation of intra-metastasis, inter-metastasis, and inter-patient genomic and immune heterogeneity (Figure 1).

The immune microenvironment of the curatively resected metastases was first investigated using single-plex immunohistochemistry (IHC) staining and digital quantification for several immune markers of major lymphocytic lineages (Figure 1B). Three metrics were used to quantify the immune infiltrates: whole-slide immune cell densities (WS), densities of the three most-infiltrated tiles or hotspots (HSs), and the Immunoscore derived from the CD3⁺/CD8⁺ T cell densities in the center of the tumor (CT) and its invasive margin (IM). In addition, we charted the spatial distribution of the immune cells in the tumor microenvironment based on multispectral imaging with a 7-plex panel of immunofluorescent markers (Figure 1C).

Next, we performed whole-exome sequencing of matched blood samples, resected primary, and consecutive metastatic samples. The total number of somatic mutations (coding and non-coding) per sample ranged over one order of magnitude for patient P210 (221–2705), while a narrower and steadier distribution was observed for patient P45 (560–1130, Figure 1D). The mutational load was associated neither with metastasis location nor with therapeutic regimen. Strikingly, most of the coding mutations (>76%) were unique to one metastasis. Thus, both patients had high inter-metastatic genetic divergence, expressed by a small percentage of shared coding and non-coding mutations (18% in P210, 16% in P45, Figure 1E). Few mutations were found only in the primary tumor and in one metastasis ($n = 303$ [3.3%] in P210, $n = 23$ [0.3%] in P45). For each patient, we then plotted the frequency of mutational recurrence among the metastases, showing the number of point mutations that are unique for one sample or shared by 2, 3, 4, ..., n metastases (Figure 1F). There was no difference in the frequency of recurring mutations between the two patients (Figure 1F, two-sample Kolmogorov-Smirnov test, $p = 0.26$). Strikingly, no single mutation was shared in more than 12 metastases for P210 ($n = 17$ samples), whereas only 10 mutations, including missense (*GOLT1B*, *DIDO1*, *POLR1D*, *ZNF727*, *GRIN2A*, *NFATC2*), silent (*MOS*, *STK36*), splice-variant (*RAP*), and intronic (*PTGIS*), were shared among all ($n = 18$) metastases of P45.

The Metastatic Evolvogram Identified Multiple Routes of Dissemination in CRC

A phylogenetic tree was reconstructed based on the concordance of nonsilent point mutations among the primary and metastatic samples (Figure 2A), using the Parsimony Ratchet method (Murugaesu et al., 2015). Overall, the samples from the

Figure 1. Immunogenomic Characterization of Metastatic CRC Progression

(A) Anatomical map of biospecimen collection sites in two CRC patients, P210 and P45. Two consecutive slides were assayed from the metastasis M8 (a and b, P45). Multi-regional resection specimens were collected from a large necrotic area (M07n) and its surrounding tumor tissue in M07, as well as from one bulky metastasis, M10 (four sites b1–4, size 25 mm) in patient P210.

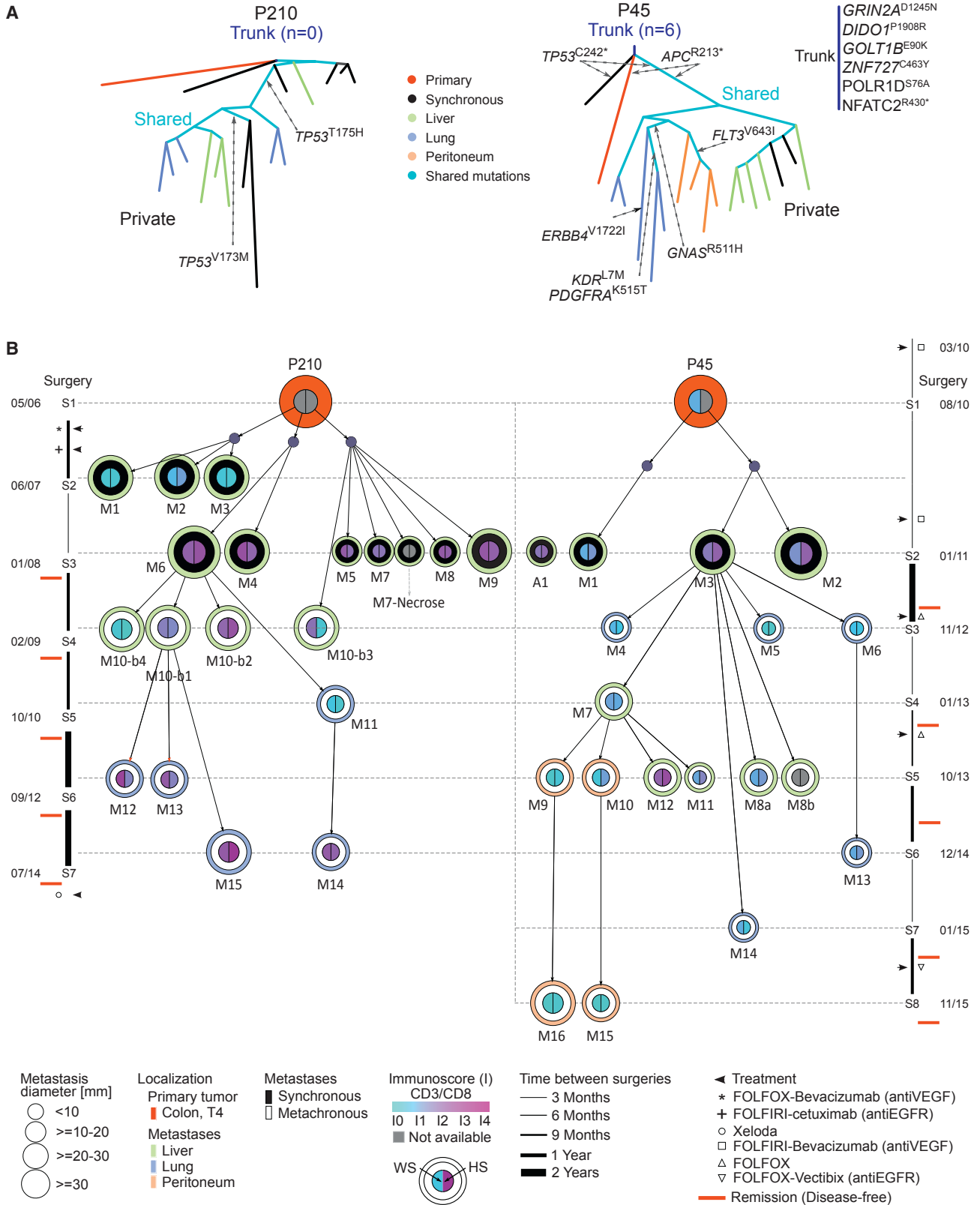
(B) Whole-slide digital scans with immunohistochemical staining of formalin-fixed paraffin-embedded cross-sections were annotated for the center of the tumor (CT), and the invasive margin (IM), and then separated into tiles for automated quantification of whole-slide (WS) and hotspot (HS) densities.

(C) Representative composite fluorescent images for seven biomarkers.

(D) The total number of coding and non-coding mutations is shown as stacked bars colored according to the recurrence status of the mutations: sample-specific mutations (orange), and mutations that recur in at least two samples, either including the primary tumor (green) or only metastases (blue). The clustered mutations were visualized so that the y axis tracks the cumulative order of each mutation (bottom).

(E) The Venn diagrams summarize the fractions of shared and unique mutations for each patient.

(F) Frequency of mutation recurrence during metastatic progression.



(legend on next page)

same metastatic location were phylogenetically closer and shared more mutations compared to anatomically separate metastases. In addition, previously known cancer driver genes were frequently located on the branches of shared mutations. Even so, there were no conserved early driver events still detectable for patient P210 (trunk = 0), regarding nonsilent point mutations, as well as copy-number variations (Figure S1A). Contrary to P210, in the patient P45, the trunk comprised six non-synonymous mutations without solid evidence for cancer-driving propensity in the literature span. *APC* and *TP53* harbored conserved, truncating mutations, previously described as some of the initial events in colorectal carcinogenesis (Gerstung et al., 2011).

We next inferred the origin of each metastasis based on the similarity of the coding mutation profiles. A parent-child relationship was defined by the highest Jaccard similarity coefficient. The routes of metastatic dissemination were then visualized with a tree representation of the metastases clade, from the time of diagnosis to the last follow-up (Figure 2B). In the patient P210, the tumor site M10-b3 was an integral part of the bulky metastasis M10, but it had a different origin than the remaining regions sampled from the same metastasis (M10-b1, -b2, and -b4), indicating that M10 was a result of multi-step colonization. Furthermore, there were indications of metastasis-to-metastasis spread within and across organ boundaries. Metastases could provoke seeding (1) in one or multiple instances of recurrence (e.g., M10-b1 and M11 in P210), (2) in the same time interval or at different time intervals (e.g., M7 and M3 in P45), (3) within the encompassing organ or at a distant anatomical site (e.g., M3 in P45). Of note, in both patients, only one of the synchronous metastases expanded the metastatic lineage; M06 in P210 had four recurrences at two different time points and two different locations, while M03 in P45 had six recurrence events, three times within 4.4 years at two distinct anatomical sites. These observations suggest that some metastases were more aggressive than others.

To compare aggressive and regressed metastases, we analyzed the tumor mutational spectrum, copy-number information, clonal composition and genealogy, and immunoeediting (observed/expected neoantigen rate). First, known patterns of chromosomal instability (CIN) with amplification of chromosomes 7, 13, 20, 8q, 17q, and deletion of chromosome 18, 8p, and 17p were found in multiple metastases (Figure 3A) (Mlecnik et al., 2016b). Overall, higher ploidy and higher chromosomal instability were observed in the patient P45 compared to P210 ($p = 0.009$ and $p = 0.001$, respectively, Mann-Whitney test). Interestingly, the primary tumors of both patients were near-diploid, but aneuploidy was frequently observed among their successive metastases (Figure S1B). Additional patterns over time were exhibited by decreasing mutation inter-metastasis heterogeneity

(IMH) (Figure S1C, not CNA IMH) and increasing immunoeediting scores (Figure S1D).

We followed the changes in genomic imprint also to reconstruct the tumor architecture of each sample and to track its clonal dynamic over time. The cellular prevalence of a given somatic mutation was estimated by integrating sequencing coverage with inferred parental copy numbers and estimated tumor purities (STAR Methods). Under the assumption that mutations at similar time points of the clonal phylogeny are present at similar cellular prevalence, a cross-sample Bayesian clustering approach was applied to infer tumor clones (Roth et al., 2014). For both patients, 12 different tumor clones that developed at a certain point over the follow-up timeline surpassed a clone detection threshold of 10% (Figure 3B). The metastases with similar clonal compositions were closely related anatomically, temporally, and phylogenetically.

To infer the hierarchy of the tumor clones, we further applied a genetic algorithm to the cellular frequencies and mutation clusters (Figure 3C; STAR Methods). The common clonal ancestor, i.e., the founder clone of the primary tumor was not detected, likely due to limited sampling of the primary tumors. However, the most persistent clones during disease progression were traceable back to the primary tumors. In both clinical scenarios, the origin of the synchronous metastases was subclonal. Rather than the major clone, minor subclones from the primary tumor fueled a sequence of recurrence events and (1) reinstated into dominant clones in metastatic samples (e.g., clone 2 in P210:M07–9, clone 1 in P45:M02–16) and (2) often co-evolved with new clones (P210:M10–15) or gave rise to new divergent clones (P210:M07n, P45:M11–12). Based on the reconstructed subclonal hierarchy, we found evidence of monophyletic dissemination, with both monoclonal (e.g., M07–9 in P210) and polyclonal (e.g., M01 in P45) seeding patterns (Figure S2C). In addition, polyphyly was tracked in both patients, having different subclones disseminated at different time points, and in separate organs (M06 of P210, M03 of P45).

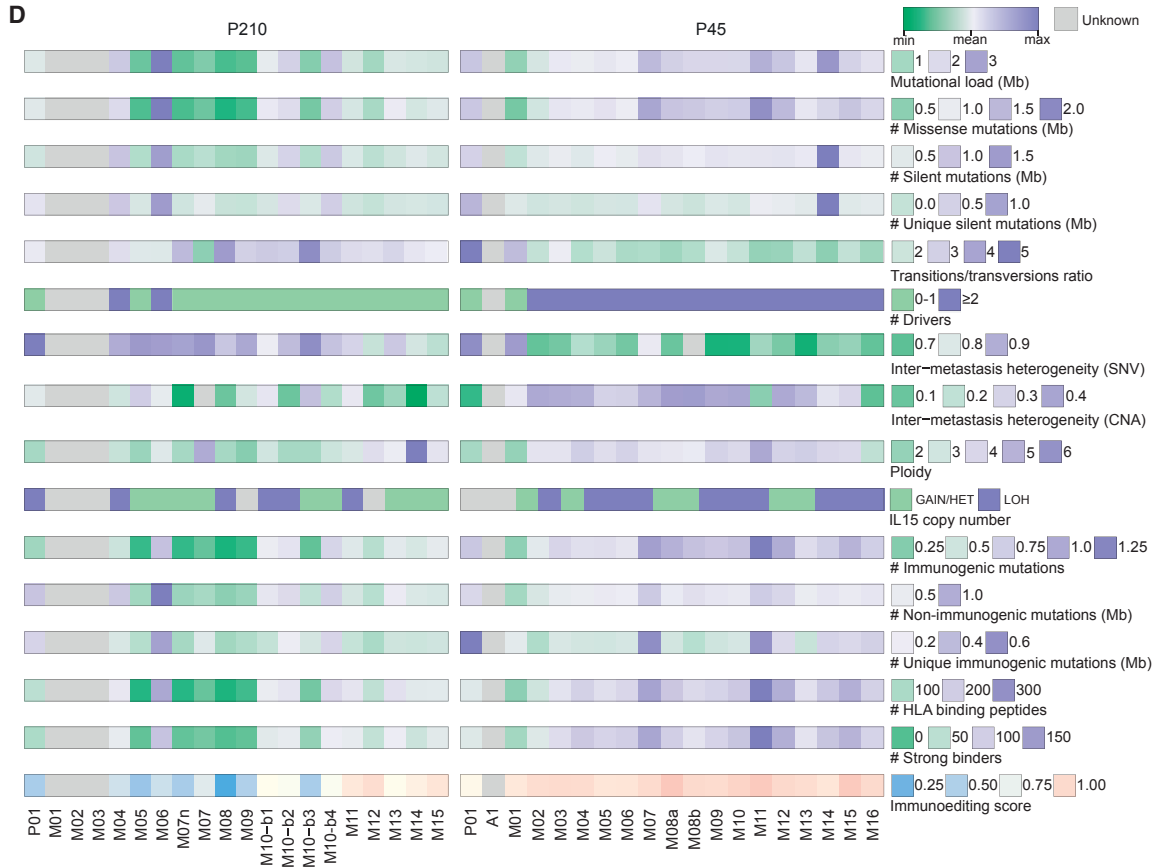
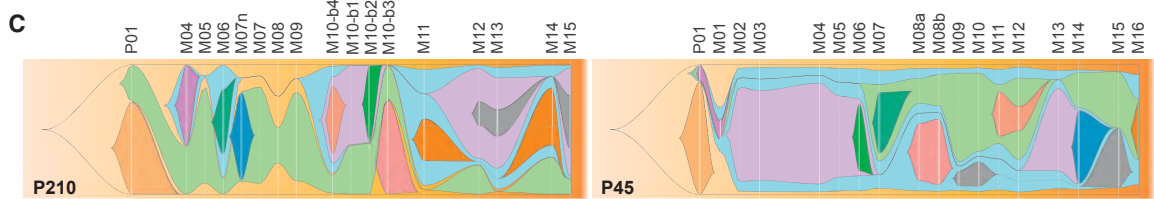
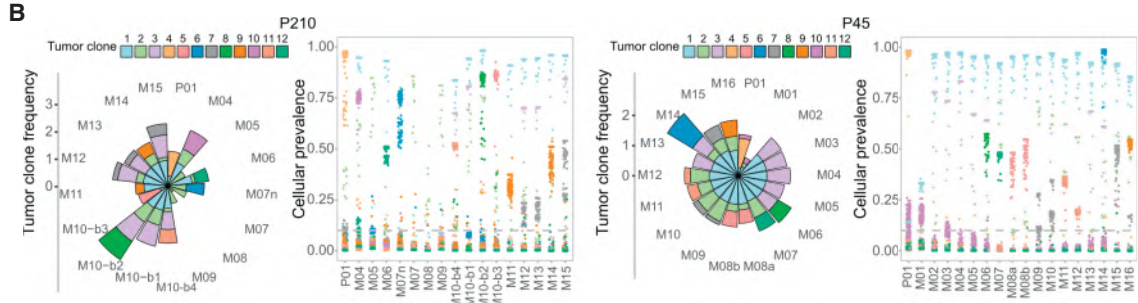
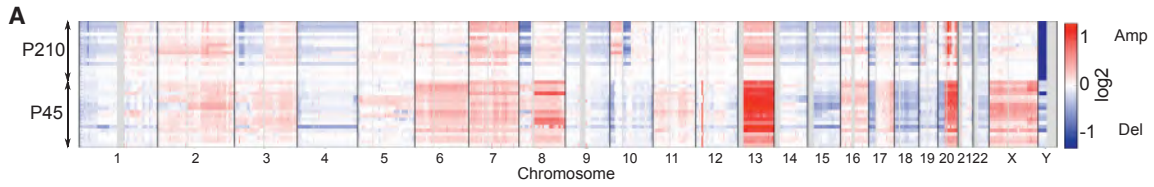
Despite the indications of a linear evolution model, there were elements of parallel evolution, such as the high level of genetic divergence between primary and metastatic tumors. Moreover, parallel evolution of *TP53* was observed for the metastasis M06, where two mutated loci were detected in two different clones, the persistent clone 1 and the eliminated clone 12 of patient P210. Ongoing evolution was manifested by unique tumor clones in several metastases (e.g., clone 8 in M06, P45, Figure S2C). Furthermore, the presence of different tumor clones in the spatially different samples of M10 in the patient P210 demonstrated intra-metastatic clonal heterogeneity.

Hence, the genomic structure of each tumor was elaborated by an extensive list of features (Figure 3D). First, different types of mutations correlated strongly with mutational burden

Figure 2. Chronological and Phylogenetic Representation of Metastatic Spread in Two CRC Patients

(A) A phylogenetic tree was constructed based on the mutational concordance among the matched primary and metastatic samples. The lengths of the branches were proportional to the number of nonsilent mutations. Highlighted are driver and trunk mutations.

(B) From the time of diagnosis (top) to the last follow-up time (bottom), each sample was plotted and annotated with a color code for location, Immunoscore (WS, HS), tumor size, and time lag from the primary malignancy (synchronous and metachronous). The time intervals between surgical interventions (represented by ranging line widths) and the treatment information are shown alongside each phylogenetic tree. The site of origin for each metastasis was determined based on the highest mutational concordance and represented by a link between each parent-child pair.



(legend on next page)

($\rho > 0.87$, $p < 0.001$, Table S1), while immunoediting showed a weaker correlation ($\rho = 0.49$, $p = 0.05$). Immunoscore and ploidy were not associated with mutational load (Table S1). Moreover, the two patients exhibited several differences on genomic level. The ratio of transitions and transversions was significantly higher in P210 compared to P45 ($p < 0.05$). In contrast, more epitopes, drivers, and mutations (missense, silent, immunogenic), higher ploidy, and immunoediting scores were found in P45 ($p < 0.05$). While the mutational IMH was higher in P210 compared to P45 ($p = 4e-05$), the copy-number IMH was lower ($p = 0.001$). Even more, major differences were found among the metastases of the same patient. Together, the metastatic evolvogram displayed clonal dynamics and heterogeneity, where some clones did not disseminate, while others persisted; thus, some metastases were able to colonize, whereas others didn't recur.

The Immune Microenvironment in Progressive Metastatic CRC

To elucidate the immune contexture, we interrogated tumor infiltrating lymphocytes (TILs) through single-plex IHC, multi-spectral imaging, and multiplex immune gene expression. Overall, the intra-patient variation of each phenotype was relatively large (Figure 4A). The most abundant immune phenotype in both patients were T cells within the invasive margin (IM, 334–3,218 cells/mm², median 1,494), which correlated with the single-plex IHC densities ($\rho = 0.74$, $p = 8e-6$, 268–3,473 cells/mm², median 1,895). The lowest densities were found for CD3⁺Ki67⁺ cells in the center of the tumor (CT, 0–14 cells/mm², median 0.06) and the invasive margin (0–95.7 cells/mm², median 0.77). Moreover, no differences in cell densities within the tumor tissue (CT) and only B cells in the stroma were significantly higher in P210 compared to P45. Similarly, higher Immunoscore values were measured among the metastases of P210 ($p = 0.005$, Mann-Whitney test). Interestingly, even some of the latest metastases had high Immunoscores (e.g., M14 and M15 in P210 at 8.1 years, and M12 in P45 at 3.2 years since diagnosis). Overall, there was no association between the Immunoscores of the parent and the child metastases.

To characterize the tumor microenvironment configuration, we examined the spatial patterns of every pair of cell phenotypes, using the topographic information derived for multispectral imaging. We measured the average mutual neighbor distance to describe potential interactions between each pair of cell phenotypes (Figure 4B). The shortest distances were observed for CD3 and CD3⁺Ki67⁺ in IM (4.7–18.2 μm , mean 10.2) and expectedly for CK⁺ (cytokeratin⁺) and

CK⁺Ki67⁺ in CT (5.3–48.1 μm , mean 13). We found little variation in mutual neighbor distances between the two patients. On average, there were no differences for any phenotype pair in CT, and only between PD-L1 and CD20 in IM there were shorter distances in the metastases of P210 (Figure 4B).

We then identified and quantified the clonotypes for T cell and B cell populations, using the raw exome sequencing data (Figure 4C). In both patients, we obtained a diverse pool of T cell receptor (TCR)- α sequences (P210 1–25, median 9.5; P45 1–19, median 5) and a lower number of B cell clonotypes (immunoglobulin K [IgK], 1–6, median 2). Rarely were the same TCR- α and TCR- β V-J recombinations shared among metastases, having V α 1-J α 33 from P210 as the most common ($n = 7$). Furthermore, the TCR- α diversity expressed as the number of different sequences of the complementarity-determining-region 3 (CDR3) strongly correlated with TIL densities and Immunoscore, as evaluated by single-plex and multiplex IHC, and immune gene expression (Figure S3).

Therefore, comparison between the patients showed little disparity with regards to averaged immune infiltrate densities and spatial distribution (Figures 4A and 4B). However, at the same time, there was a confounding diversity across spatially and temporally diverse tumor microenvironments of the same patient concerning their extent of immune infiltration and T cell repertoires.

Different Escape Mechanisms Delineated by Immune Status and Immunoediting

We evaluated the immunoediting score individually for each metastasis as the ratio of observed to expected immunogenic mutations per nonsilent mutation (Mlecnik et al., 2016a; Rooney et al., 2015) (Figure 5A; STAR Methods). A higher-than-expected immunogenic rate indicated absence/lack of immunoediting and immune tolerance (score > 0.8 , $n = 24$, Figure S4A). Several metastases displayed evidence of major immunoediting, i.e., a lower frequency of immunogenic mutations than expected (score ≤ 0.8 , $n = 7$). Furthermore, by plotting the immunoediting score (Yes/No) and the corresponding Immunoscore values (Hi/Lo), we defined four categories of metastases (HiYes, HiNo, LoYes, and LoNo, Figure 5A). Strikingly, none of the metastases corresponded to the group of low Immunoscore and immunoediting (LoYes). Supporting the notion that weak adaptive immunity is insufficient for immunoediting to occur, low Immunoscore and immunoediting were mutually exclusive (LoNo, $n = 18$). On the contrary, immunoediting was observed exclusively in metastases with inflamed T cell phenotype and high Immunoscore (HiYes, $n = 7$), and neoantigen depletion resulted from an active immune selection. Nevertheless, 54% of the

Figure 3. Evolving Genomic Profile with Metastatic Progression

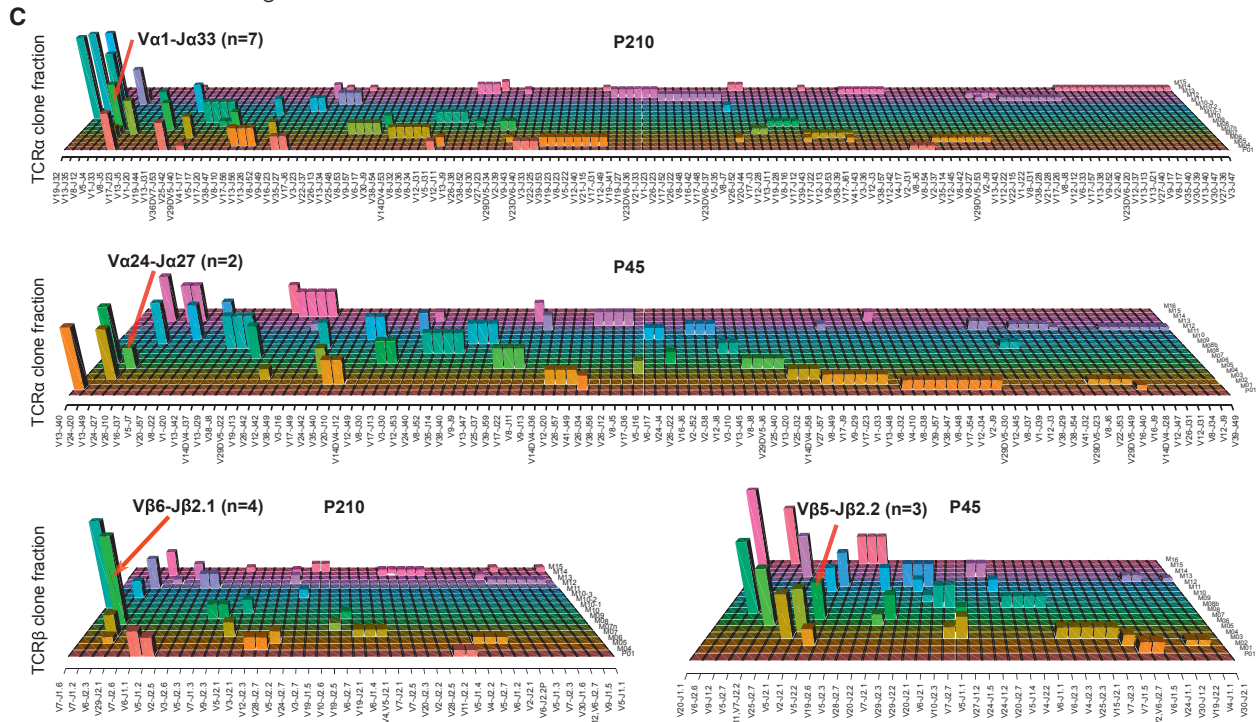
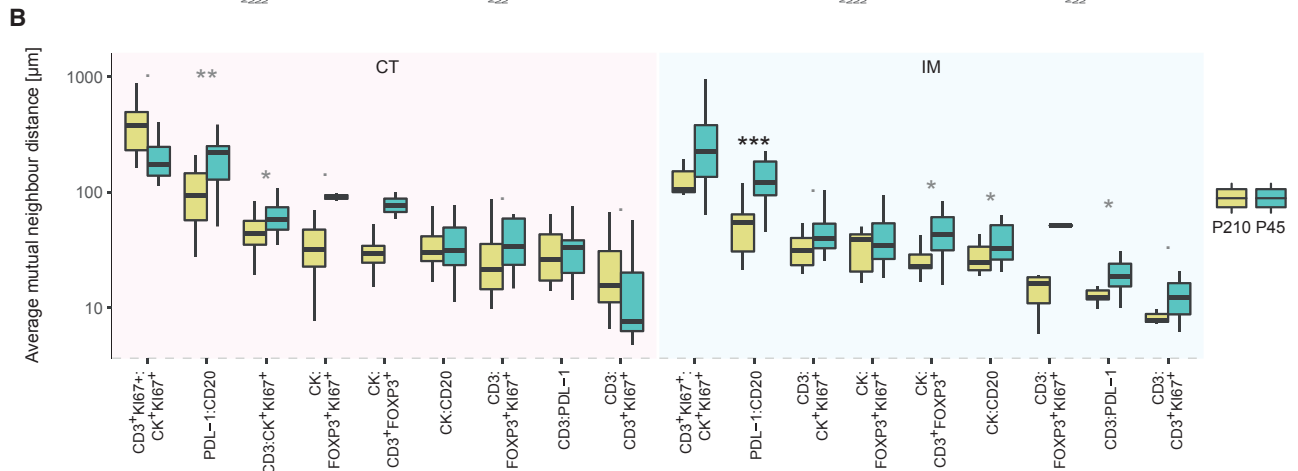
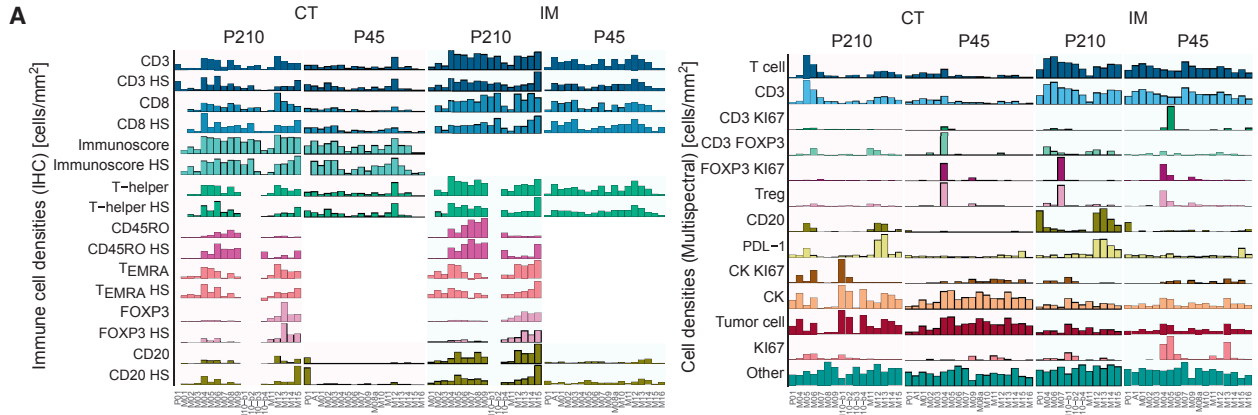
(A) Clustering of copy-number variations per chromosome derived from exome-sequencing data.

(B) Tumor clones were identified as clusters of mutations with similar cellular prevalence (STAR Methods). Each tumor clone was represented by its estimated clonal frequency (left) and the corresponding mutations (right).

(C) A tumor clone evolvogram along the study timeline of each patient. Clonal lineage inference analysis estimated the ancestral origin of each clone. The samples were ordered by detection time.

(D) A series of genomic parameters used to characterize each sample: mutations, chromosomal instability, inter-metastatic heterogeneity, immunogenicity, and immunoediting.

See Figures S1 and S2.



(legend on next page)

metastases with high Immunoscore were immunoedited. This result demonstrates that immune infiltration is necessary but not sufficient for immunoediting to occur and that immunoediting occurs in humans at the metastatic stage.

Interestingly, the metastases with low Immunoscore and no immunoediting were more prone to recurrence and gave rise to at least one child metastasis in 64% of the cases, as opposed to, only 8% of metastases with high Immunoscore ($p = 0.058$, Fisher's exact test). In six unedited metastases, there was a loss of heterozygosity (LOH) in at least one human leukocyte antigen (HLA) allele that could be attributed to lack of immunoediting in some metastases (Figures S1A and S1E). Moreover, unedited metastases were characterized by higher ploidy levels ($p = 0.55$, $p < 0.001$, Figure 5B). LOH in a chromosome 4 region containing the gene *IL15* was another tumor-intrinsic feature distinctive for the absence of both immune control and immunoediting (LoNo) (Fisher's exact test, $p = 0.05$, Hi versus Lo Immunoscore). On the contrary, the immunoedited metastases with high Immunoscore were differentiated by increased densities of memory T cells (CD45RO) and proliferating T cells (CD3⁺Ki67⁺), as well as higher mutation IMH (mlMH), compared to unedited metastases ($p < 0.05$) (Figure 5C). Furthermore, immunoediting had the strongest correlation with various T cell phenotypes associated with cytotoxicity, adhesion, Th1, Tfh, CD8 cells, the chemokine CCL2, cytokines, and immune checkpoints (Figure S3). Weaker and significant correlations could also be seen for neoantigen burden but not for coding mutations.

Identification of a group of metastases with no immunoediting in the presence of TILs (HiNo, $n = 6$) revealed several actions of tumor-extrinsic escape. Increased densities of FOXP3⁺ cells ($p \leq 0.02$, increase over HiYes: 442–527 cells/mm²) and PD-L1⁺ cells ($p \leq 0.01$, increase over HiYes: 11–41 cells/mm²) in CT and IM delineated the HiNo group (Figure 5C). Higher TCR- α diversity, as measured by the number of different clonotypes, could indicate absence or scarcity in T cell clonal expansion in this group (5.5-fold increase in HiNo versus HiYes, major and significant differences versus LoNo) (Figure 5D) (Jimenez-Sanchez et al., 2017).

Beyond immune cell densities, we also explored the spatial distribution of different cell phenotypes across whole-tumor resections. We measured mutual neighbor distances between each pair of cell phenotypes and calculated a cross-type cumulative distribution of the nearest neighbor distances, $G(r)$ (STAR Methods). We discerned differential spatial organization for CD3 T cells and proliferating tumor cells (CK⁺Ki67⁺) among the distinct Immunoscore-editing groups (Figure 5E). The spatial localization of proliferating tumor cells CK⁺Ki67⁺ and CD3⁺ T cells for representative metastases was illustrated with com-

posite fluorescent images (Figure 5F) and cumulative distributions of cross-type distances, $G(r)$ (Figure 5G). Indeed, the HiYes group had shorter average mutual neighbor distances between CD3⁺ and CK⁺Ki67⁺ cells (Figure 5H). Moreover, within HiYes metastases, on average one-half of the proliferating tumor cells in CT had a surrounding CD3⁺ cell(s) within a radius of 25 μ m (Figure 5H). Besides that, for the HiNo metastases, we found a higher percentage of T cells (CD3⁺) and tumor cells (CK⁺) that have the nearest PD-L1 within a radius of 25 μ m, in CT and IM, respectively. Therefore, beyond the quantitative immune characterization, the immune atlas revealed novel, potential tumor-extrinsic escape mechanisms. Thus, immunoedited metastases had high Immunoscore and a short distance between T cells and proliferating tumor cells, whereas non-immunoedited metastases had increased densities of FOXP3⁺ T cells, increased PD-L1 expression, and significant proximity of T cells to PD-L1⁺ cells.

Impact of Immunoscore and Immunoediting on Metastatic Disease Progression

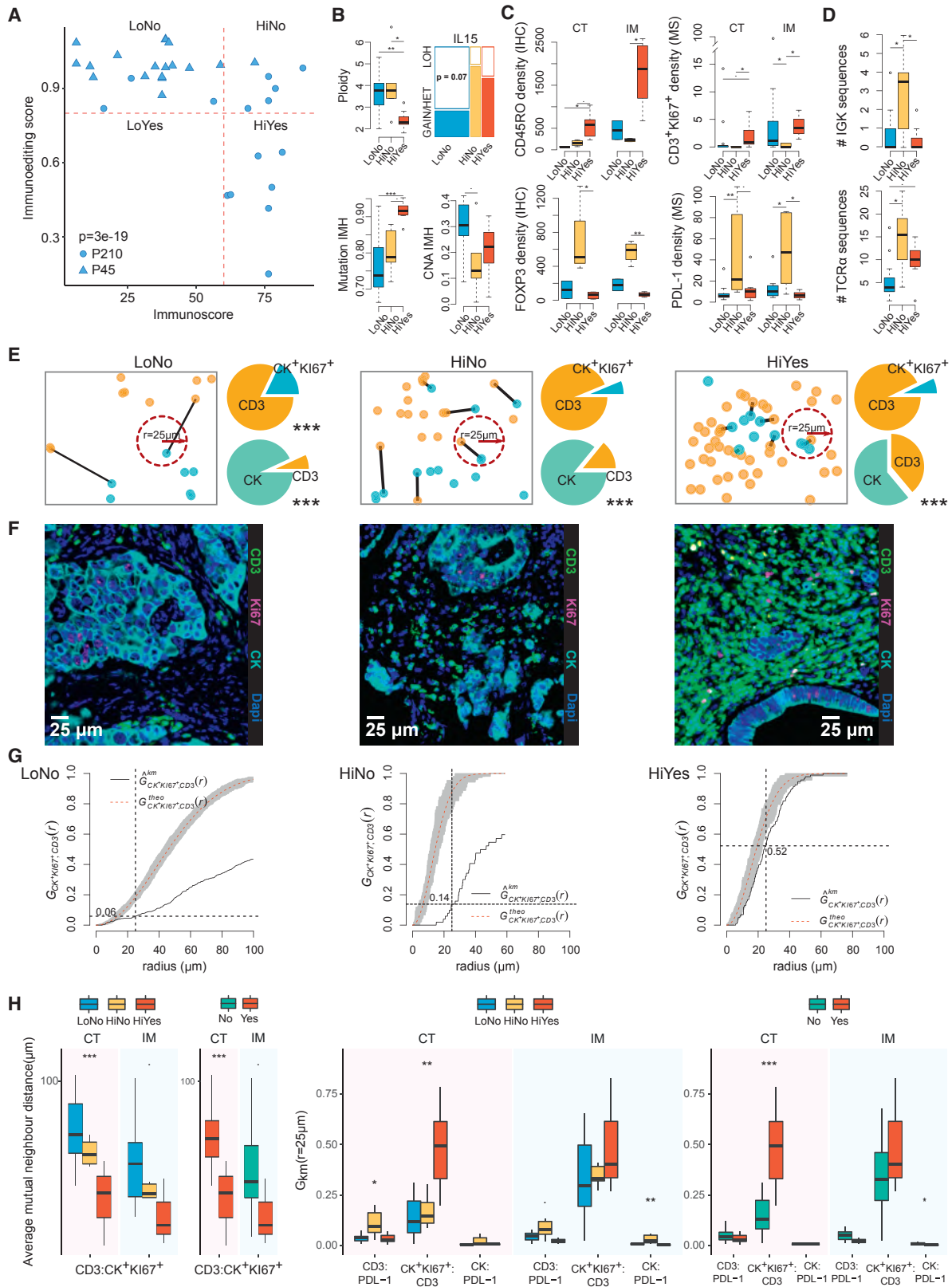
To understand the tumor characteristics related to its risk of recurrence, tumor clones were assigned into three groups depending on whether they had been transmitted to a child metastasis (persistent, eliminated, and early non-recurrent, STAR Methods). We compared the persistent and eliminated tumor clones by several genomic features, including the Dn/Ds score as an indicator of selective pressure on nonsilent mutations (Table S2). None of them was associated with the recurrence status of the tumor clones. Having observed above differential intra-metastatic immunogenicity, we calculated an immunoediting score for each tumor clone individually. Strikingly, immunoediting was more frequently found in eliminated tumor clones, whereas the absence of immunoediting was a feature of persistent clones (Fisher's exact test, $p = 9.7 \times 10^{-8}$) (Figure 6A). Notably, only one persistent clone, clone 2 from P45, presented with immunoediting. In fact, this clone had only one immunogenic mutation located within the gene *ZDHH11*, which had a negligible level of expression (median = 0.9 transcripts per million [TPM], interquartile range [IQR] = 1.3), according to public RNA sequencing (RNA-seq) of primary CRC ($n = 626$). Interestingly, the major clone (clone 4) was immunogenic, immunoedited, and eliminated, without reappearance in any consecutive metastases. Furthermore, immune selection separated persistent from eliminated clones (area under the curve [AUC] = 0.89, $p < 0.0001$) better than positive selection (Dn/Ds score, AUC = 0.59, $p = 0.52$) (Figure 6A; Table S2). Immunoediting was the best predictor of tumor clone recurrence (AUC = 0.89), having an even better performance without considering clone

Figure 4. The Immune Microenvironment in Consecutive Metastases

(A) Immune cell densities were measured by single-plex IHC (left) and multispectral fluorescent imaging with a 7-plex panel (right), separately for the CT and invasive margin (IM). On the multispectral analysis panel (right), T cell phenotypes combined CD3 single-positive, CD3⁺FoxP3⁺, and CD3⁺Ki67⁺, while CD3⁺ phenotype represented CD3 single-positive cells. The phenotype "Other" comprises cells negative for all investigated markers.

(B) The spatial distribution of the immune cells in the two patients, P210 and P45, was compared by the distances between mutually nearest cells. All possible phenotype pairs were tested, and the significant differences were highlighted in black at false discovery rate (FDR) <0.1, or gray otherwise (Wilcoxon rank-sum test, $p \leq 0.05$, Benjamini-Hochberg adjustment).

(C) TCR repertoire derived from raw exome-sequencing data. The identified pairs V α -J α and V β -J β genes were shown with their estimated TCR clonotype fractions (z axis) for each sample (y axis). The most commonly found TCR- α and TCR- β chains were highlighted for each patient.



(legend on next page)

2 of P45 (AUC = 0.98). Similar results were observed in an ovarian cancer case with metachronous metastasis (Figure S5).

Different clones from the same metastasis had different immunoediting scores (Figures S2B–S2D). Across different metastases, however, unedited clones remained unedited. Moreover, the core of the metastasis M07, populated with dying tumor cells and T cells, had one prevalent tumor clone, clone 6, which was not found in the invasive margin of the same metastasis (Figure S2B). We studied the immunogenicity of these mutations and found that clone 6 from the necrotic area was immunogenic, contrary to clone 2 in the invasive margin that had no immunogenic mutations. These observations provide evidence for differential immunogenic potential of tumor clones within one metastasis.

Finally, we asked which of the parameters that manifested mechanistic implications so far in our study could also have clinical relevance. We performed univariate analysis on a series of 22 clinical, genomic, immune, and spatial parameters (Table S3). We reasoned that each metastasis should be approached as a different disease/case, not only because of the large IMH but also because of their differential dissemination potential. The two best predictors of favorable clinical outcome were immunoediting (hazard ratio [HR] = 0.16, $p = 0.01$) and Immunoscore (HR = 0.13, $p = 0.03$, Figure 6B). Covariate selection on the significant parameters from the univariate analysis yielded the best multivariate regression model with four selected covariates (Figure 6C), one of which, the mutual neighbor distance between CK⁺Ki67⁺ and CD3⁺ cells in CT, was not significant in the multivariate model. According to the model, lower Immunoscore, absence of immunoediting, and higher metastasis burden had an adverse impact on recurrence-free survival. The relation between the immune system and tumor dissemination over time was evaluated by superimposing immunoediting and Immunoscore on the phylogenetic tree of metastases (Figure 6D). This illustrates the local control (smaller size) of the metastasis and the protective effect of Immunoscore in preventing recurrence. Thus, metastasis progression and time to recurrence were dependent upon mechanistically linked immune parameters (schematic abstract, Figure 6C).

We then generated a predictive time-to-event model of metastatic cancer evolution to estimate the probability of recurrence based on the selected covariates. The clinical outcome was considered until the last follow-up on January 2016, when both patients were in complete remission and disease free. The model

was built blindly to the clinical outcome after January 2016. Cumulative recurrence probabilities over time were calculated for each type of metastasis (Figure 6E). Thus, independently on time from detection (TFD), the metastases with the highest recurrence probability had a large size, low Immunoscore, and no immunoediting. Inversely, the lowest risk group comprised immunoedited metastases with high Immunoscore and small burden. The recurrence risk is particularly pronounced in the first 2 years since detection.

The estimates from the predictive model were then applied on each metastasis to quantify its probability to recur from the last follow-up onward (Figure 6F). According to the predicted outcome, almost all metastases from patient P210 have surpassed the time of recurrence risk, whereas for patient P45 there were several high-risk samples, particularly the latest metastases M15 and M16. The model predicted less than 35% probability for P210 to have a new recurrence event as of January 2018. Indeed, P210 is still in complete remission to date. In contrast, a high risk of relapse was estimated for P45. The two peritoneal metastases M15 and M16 have a probability of 95% to recur before January 2017, and a 99% recurrence probability before January 2018. In agreement with the model predictions, in April 2016 the patient P45 was diagnosed with a relapse, particularly with several unresectable metastatic lesions in the peritoneum and the liver.

Two independent validations were performed. First, we applied our prediction model a recently published case study of one ovarian cancer patient with 4 metachronous metastases (all resected simultaneously several years after their detection) (Jimenez-Sanchez et al., 2017) and predicted a high probability for a first recurrence (Figure S5). Second, assuming that progression is influenced by immune pressure in both metastatic and primary tumors, we analyzed primary CRC ($n = 132$) to predict the first event of metastatic dissemination. We observed an association between immunoediting and decreased risk of metachronous recurrence (Figures S6A–S6C). Moreover, our prediction model stratified low, intermediate, and high-risk tumors, which were confirmed to have significantly different recurrence rates (Figure S6D).

DISCUSSION

A critical step toward tailoring therapies for long-term disease-free survival is to decipher the resilience of certain clones and

Figure 5. Immunoscore and Immunoediting Delineate Distinct Escape Mechanisms

(A) Based on Immunoscore percentiles and immunoediting scores, the samples segregated into three groups: LoNo, HiNo, and HiYes.

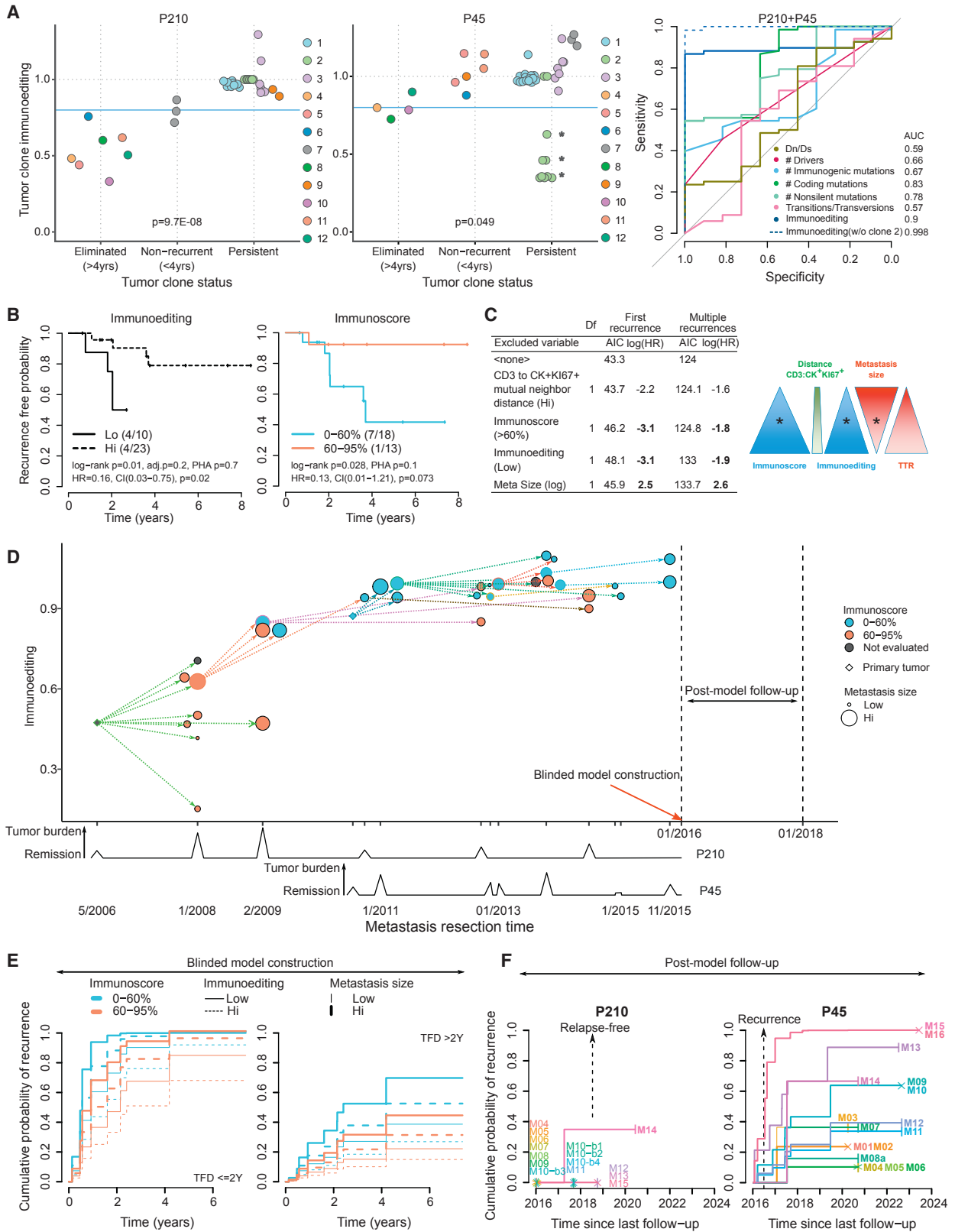
(B–D) They were differentiated by distinct genomic features (B), by immune cell densities of CD45RO, PD-L1, FOXP3, and CD3⁺Ki67⁺ (C), and by T and B cell diversity (D).

(E) Spatial organization patterns of T cells (orange) and proliferating tumor cells (blue, CK⁺Ki67⁺) in the tumor microenvironment. A connection between two points demonstrates mutually closest neighbors. The three-point patterns across LoNo, HiNo, and HiYes groups show decreasing mutual neighbor distances and lower segregation of CD3⁺ T cells and proliferating tumors cells. Pies show the percentage of CD3⁺ T cells next to proliferating (top) and non-proliferating tumor cells (bottom) observed in CT. Asterisks highlight significant differences in proportions between the sample groups.

(F) Representative composite fluorescent images showing spatial localization of proliferating tumor cells CK⁺Ki67⁺ (purple) and CD3⁺ T cells (green).

(G) Cumulative distributions of cross-type distance from CK⁺Ki67⁺ to the nearest CD3⁺ evaluated in an area with radius r . The theoretical curve, $G_{\text{theo}}(r)$ with its confidence envelopes illustrates random sample distribution.

(H) All cell phenotypes were compared pairwise by mutual neighbor distances and nearest-neighbor distance distribution functions (G_{km}) at 25 μm . Only significant associations were visualized (rank-based non-parametric test, post hoc multiple comparison, *** $p < 0.001$, ** $0.001 \geq p < 0.01$, * $0.01 \geq p < 0.05$). See Figure S3.



(legend on next page)

metastases. The tumor cells and its microenvironment communicate intricate fostering and restraining signals. Therefore, it is of utmost importance to understand metastasis evolution under immune pressure. Having a relatively large number of completely resected metastases per patient over an exceptionally long survival period (across more than 11 years), we investigated the drivers of recurrence and followed the evolutionary dynamics on matched spatiotemporally distinct genomes. We determined the origin of each metastasis and each clone and distinguished recurrent from non-recurrent metastases, as well as eliminated from persistent clones. Comparison of these metastases/clones revealed several findings on the power of the immune system in metastasis recurrence.

First, anatomically and temporally distinct metastatic sites exhibited different clinical responses, genomic architectures, and immune activities. Hence, each metastasis is a disease on its own and metastatic disease cannot be averaged per patient. Coexistence of different immune microenvironments in the same individual conforms to previous findings in multiple metastatic sites of ovarian cancer (Jimenez-Sanchez et al., 2017). In addition to that, here we observed distinct tumor-immune ecosystems in both space and time, remarkably, between parent and child metastases, and even within the same metastasis. The fact that neither a single biopsy nor one metastasis is sufficient to generalize the tumor setting poses daunting challenges for any clinical modality.

Second, we described the clonal evolvogram of metastatic progression. Understanding the trajectories of metastatic spread could be a powerful tool to estimate the risk of metastasis and could have profound implications for patient management (Turajlic and Swanton, 2016). We traced multiple routes of dissemination, including multistep colonization, polyphyly, and polyclonal seeding with genetic evidence for both linear and parallel progression, all within a single patient. However, whether a tumor clone is prone to dissemination remains an open question when considering genomics features solely. We could detect traits of tumor-intrinsic selective pressures over the disease course, such as recurrent inactivation of *TP53* and decreasing mutational IMH. Despite that, many tumor clones did not carry known driver mutations. Also, not a single driver or passenger mutation was present on all metastases in the patient P210.

Third, we therefore analyzed the immune microenvironment in relation to tumor clones through space and time. Several obser-

uations indicated that immunoeediting was imprinted in the metastatic genome. Of note, multiple lines of therapy were administered to the patients, but immunoeedited clones and metastases were observed independently of chemotherapy exposure and absence of immunoeediting could also be detected upon therapy response. We demonstrated a critical heterogeneity of clonal immunogenicity and immunoeediting within one metastasis. The immunoeediting score, rather than the mutational load, was associated exclusively with an active immune response, implying a predictive potential for immunotherapy. Even more, branched tumor evolution could be traced back to a failure in immune surveillance by immune-escaping clones. The eliminated clones were immunoeedited. The tumor clones that persisted and progressed were immune privileged, either unedited or non-immunogenic. This finding reveals for the first time the relationship between clonal seeding and immune surveillance and has significant implications for therapy. It shows that the persisting cells are identifiable and thereby therapeutically targetable. Targeting clonal neoantigens could prevent recurrence by aiming at the persistent, unedited tumor clones that retain immunogenic mutations. In support of this, a durable clinical benefit has been associated with T cell reactivity against clonal neoantigens previously observed in advanced non-small cell lung cancer (NSCLC) (McGranahan et al., 2016). Persistence of tumor clones without any immunogenic mutations urges the need for alternative strategies, such as perturbing the DNA mismatch repair machinery to induce genomic instability of tumor cells and increase the burden of neoantigens (Germano et al., 2017).

Fourth, while we could detect a potent immune activation and high Immunoscore even later in the disease timeline, the overall decreasing trend of immunoeediting over time implied acquisition of escape mechanisms. Indeed, aneuploidy was associated with absence of immunoeediting. Increasing evidence suggests that chromosomal instability can be an early driver event of metastasis (Wang et al., 2014) before the bulk of mutations are acquired, as it appears in the patient P45. This could result in a diluted concentration of neoantigens and a competitive advantage of self-peptides for antigen presentation, as recently hypothesized (Davoli et al., 2017). In this context, recruitment of surveilling immune cells would be silenced and accordingly immunoeediting would be undetectable (LoNo). Moreover, we identified unedited metastases with high immune infiltration (HiNo) that also had high ploidy. We believe that, in this case,

Figure 6. The Impact of the Immunoscore and Immunoeediting on Metastatic Recurrence

(A) The tumor clones were assigned into three groups depending on whether they recur (STAR Methods). Each clone is represented as one point, individually for each metastasis. The blue line was set at the cutoff value of 0.8 (see related Figures S2A and S4A). The performance of the immunoeediting score and additional mutational parameters in classifying the two recurrence groups is illustrated as receiver operating characteristic (ROC) curves and their respective AUC values. *Clone 2 in the patient P45 (green) has only one immunogenic mutation with negligible expression levels in primary CRC.

(B) Kaplan-Meier curves for univariate recurrence-free survival according to immunoeediting (left) and Immunoscore (right) (see related Table S3).

(C) The table lists the covariates selected for multivariate analysis out of several genomic, pathological, and immune features. Akaike information criterion (AIC) values were shown for each multivariate model excluding the corresponding variable. The hazard ratios (HRs) describe the final multivariate model, where either the first or multiple recurrence events were considered. Statistical significance was highlighted in bold, and a graphical summary of the model was illustrated.

(D) Superimposition of the three parameters associated with recurrence (immunoeediting, Immunoscore, tumor size) on the parent-child metastasis tree.

(E) A predictive model of metastasis recurrence was generated based on immunoeediting, Immunoscore, and metastasis size, assuming time-dependent probabilities (TFDs). The plot shows the cumulative probabilities of recurrence over time estimated for different parameters.

(F) The predictive model was applied to each sample to estimate its recurrence probability, starting from the last follow-up time (AIC, Akaike Information Criterion; PHA, proportional hazards assumption; CI, confidence intervals; TFD, time from detection; TTR, time to recurrence).

See Figures S2, S5, and S6.

chromosomal instability was a later event after the tumor cells were already loaded with neoantigens. Upon a sufficiently strong neoantigen signal, the immune cells could be recruited, but restrained by immunosuppression, resulting in undetectable immunoediting. Indeed, the absence of immunoediting in the presence of TILs (HiNo) revealed several escape mechanisms, including increased densities of immunosuppressive cells and segregation of immune from tumor cells. Thus, we propose that the immune contexture and metastasis immunoediting mirror the temporal order of chromosomal instability.

Finally, the absence of editing was an independent prognostic factor for recurrence, together with Immunoscore and metastasis size. We generated a predictive model of metastatic cancer evolution and correctly predicted the absence of metastatic recurrence risk for P210 and a high risk for P45. It will be important to further validate our findings longitudinally in a large independent cohort presenting with multiple metachronous metastases and long-term survival. However, we demonstrated the possibility to identify the metastases with the highest recurrence probability, so that the treatment could be adjusted according to their acquired escape mechanisms.

In conclusion, we showed evidence that the immune system influences tumor heterogeneity and sculpts clonal evolution. Our duality tumor-immunity model of human cancer metastases proposed that the development of tumor clones is linked to the intra-metastatic immune microenvironment via the immunoediting process. In contrast to the four existing tumor-cell centric models, we divulge here a parallel-multiverse immune selection model of tumor evolution during the metastatic process. These novel insights have several notable implications and may change the understanding of cancer evolution.

STAR★METHODS

Detailed methods are provided in the online version of this paper and include the following:

- KEY RESOURCES TABLE
- CONTACT FOR REAGENT AND RESOURCE SHARING
- EXPERIMENTAL MODEL AND SUBJECT DETAILS
 - Human subjects research
 - Distribution and availability of blood and tissue used in this study
- METHOD DETAILS
 - DNA Sequencing
 - IHC
 - Multispectral imaging
 - Multiplex immune gene expression
- QUANTIFICATION AND STATISTICAL ANALYSIS
 - Somatic variant detection
 - Driver mutations
 - Copy number estimation
 - Metastatic evolvogram
 - Inter-metastatic heterogeneity
 - HLA typing and mutation detection in HLA-I genes
 - Loss of heterozygosity in HLA class I genes
 - HLA-binding epitope prediction
 - Metastasis and clonal immunoediting

- Tumor clone immunoediting
- Permutation-based null model and immunoediting scores cutoff
- Tumor clone groups
- Dn/Ds selective pressure score
- T cell and B cell repertoire
- Multispectral imaging and second order spatial statistics
- Predictive model of metastasis evolution
- Statistics

SUPPLEMENTAL INFORMATION

Supplemental Information includes six figures and four tables and can be found with this article online at <https://doi.org/10.1016/j.cell.2018.09.018>.

ACKNOWLEDGMENTS

We thank Man Chun Leung for logistic and technical assistance with sequencing. This work was supported by grants from the National Cancer Institute of France (INCa), the Plan Cancer, the Cancerpole Ile de France, Institut National de la Santé et de la Recherche Médicale, France (INSERM), the Cancer research for personalized medicine (CARPEM), Paris Alliance of Cancer Research Institutes (PACRI), by ERAnet Transcan grant number TRANS201401218, the LabEx Immuno-oncology, Sidra Internal Funds, the Fondation St-Luc, and the CPTCR (Cliniques des Pathologies Tumorales du Colon et du Rectum) of the Cliniques Universitaires St-Luc.

AUTHOR CONTRIBUTIONS

Study Concept and Design, J.G. and M.A.; Data Acquisition, A.V., T.F., L.L., B.B., E.M., M.C., N.S., M.V.d.E.; Data Analysis and Interpretation, M.A., A.V., B.M., G.B., D.B., and J.G.; Manuscript – Draft, M.A. and J.G.; Manuscript – Critical Revision, B.M., A.V., G.B., T.F., L.L., B.B., E.M., D.B., A.J.-M., C.H., A.K., Y.H., D.B., F.M.M., and M.V.d.E.; Statistical Analysis, M.A., B.M., and G.B.; Technical Support, T.F., L.L., B.B., E.M., M.C., and N.S.; Material Support, A.J.-M., C.H., A.K., Y.H., D.B., and M.V.d.E.; Funding Acquisition, M.V.d.E., F.M.M., and J.G.; Study Supervision, J.G.

DECLARATION OF INTERESTS

Immunoscore is a registered trademark from INSERM. J.G. is co-founder and chairman of the scientific advisory board of HalioDx. J.G. and B.M. have patents associated with “in vitro method for the prognosis of progression of a cancer” (PCT/IB2006/003168, PCT/EP2013/062405).

Received: March 14, 2018

Revised: July 6, 2018

Accepted: September 11, 2018

Published: October 11, 2018

REFERENCES

- Bindea, G., Mlecnik, B., Tosolini, M., Kirilovsky, A., Waldner, M., Obenauf, A.C., Angell, H., Fredriksen, T., Lafontaine, L., Berger, A., et al. (2013). Spatio-temporal dynamics of intratumoral immune cells reveal the immune landscape in human cancer. *Immunity* 39, 782–795.
- Bolotin, D.A., Poslavsky, S., Mitrophanov, I., Shugay, M., Mamedov, I.Z., Putintseva, E.V., and Chudakov, D.M. (2015). MiXCR: software for comprehensive adaptive immunity profiling. *Nat Methods* 12, 380–381.
- Caswell, D.R., and Swanton, C. (2017). The role of tumour heterogeneity and clonal cooperativity in metastasis, immune evasion and clinical outcome. *BMC Med.* 15, 133.

- Davoli, T., Uno, H., Wooten, E.C., and Elledge, S.J. (2017). Tumor aneuploidy correlates with markers of immune evasion and with reduced response to immunotherapy. *Science* 355. Published online January 20, 2017. <https://doi.org/10.1126/science.aaf83399>.
- Fearon, E.R., and Vogelstein, B. (1990). A genetic model for colorectal tumorigenesis. *Cell* 61, 759–767.
- Finn, O.J. (2008). Cancer immunology. *N. Engl. J. Med.* 358, 2704–2715.
- Galon, J., Costes, A., Sanchez-Cabo, F., Kirilovsky, A., Mlecnik, B., Lagorce-Pagès, C., Tosolini, M., Camus, M., Berger, A., Wind, P., et al. (2006). Type, density, and location of immune cells within human colorectal tumors predict clinical outcome. *Science* 313, 1960–1964.
- Gerlinger, M., Rowan, A.J., Horswell, S., Math, M., Larkin, J., Endesfelder, D., Gronroos, E., Martinez, P., Matthews, N., Stewart, A., et al. (2012). Intratumor heterogeneity and branched evolution revealed by multiregion sequencing. *N. Engl. J. Med.* 366, 883–892.
- Germano, G., Lamba, S., Rospo, G., Barault, L., Magri, A., Maione, F., Russo, M., Crisafulli, G., Bartolini, A., Lerda, G., et al. (2017). Inactivation of DNA repair triggers neoantigen generation and impairs tumour growth. *Nature* 552, 116–120.
- Gerstung, M., Eriksson, N., Lin, J., Vogelstein, B., and Beerenwinkel, N. (2011). The temporal order of genetic and pathway alterations in tumorigenesis. *PLoS ONE* 6, e27136.
- Hunter, K.W., Amin, R., Deasy, S., Ha, N.H., and Wakefield, L. (2018). Genetic insights into the morass of metastatic heterogeneity. *Nat. Rev. Cancer* 18, 211–223.
- Jimenez-Sanchez, A., Memon, D., Pourpe, S., Veeraraghavan, H., Li, Y., Vargas, H.A., Gill, M.B., Park, K.J., Zivanovic, O., Konner, J., et al. (2017). Heterogeneous tumor-immune microenvironments among differentially growing metastases in an ovarian cancer patient. *Cell* 170, 927–938.
- Koebel, C.M., Vermi, W., Swann, J.B., Zerafa, N., Rodig, S.J., Old, L.J., Smyth, M.J., and Schreiber, R.D. (2007). Adaptive immunity maintains occult cancer in an equilibrium state. *Nature* 450, 903–907.
- Labiano, S., Palazon, A., and Melero, I. (2015). Immune response regulation in the tumor microenvironment by hypoxia. *Semin. Oncol.* 42, 378–386.
- Langley, R.R., and Fidler, I.J. (2007). Tumor cell-organ microenvironment interactions in the pathogenesis of cancer metastasis. *Endocr. Rev.* 28, 297–321.
- Lloyd, M.C., Cunningham, J.J., Bui, M.M., Gillies, R.J., Brown, J.S., and Gatehby, R.A. (2016). Darwinian dynamics of intratumoral heterogeneity: Not solely random mutations but also variable environmental selection forces. *Cancer Res.* 76, 3136–3144.
- Matsushita, H., Vesely, M.D., Koboldt, D.C., Rickert, C.G., Uppaluri, R., Magrini, V.J., Arthur, C.D., White, J.M., Chen, Y.S., Shea, L.K., et al. (2012). Cancer exome analysis reveals a T-cell-dependent mechanism of cancer immunoeediting. *Nature* 482, 400–404.
- McGranahan, N., Furness, A.J., Rosenthal, R., Ramskov, S., Lyngaa, R., Saini, S.K., Jamal-Hanjani, M., Wilson, G.A., Birkbak, N.J., Hiley, C.T., et al. (2016). Clonal neoantigens elicit T cell immunoreactivity and sensitivity to immune checkpoint blockade. *Science* 351, 1463–1469.
- McGranahan, N., Rosenthal, R., Hiley, C.T., Rowan, A.J., Watkins, T.B.K., Wilson, G.A., Birkbak, N.J., Veeriah, S., Van Loo, P., Herrero, J., et al. (2017). Allele-specific HLA loss and immune escape in lung cancer evolution. *Cell* 171, 1259–1271.
- Mlecnik, B., Bindea, G., Angell, H.K., Sasso, M.S., Obenauf, A.C., Fredriksen, T., Lafontaine, L., Bilocq, A.M., Kirilovsky, A., Tosolini, M., et al. (2014). Functional network pipeline reveals genetic determinants associated with in situ lymphocyte proliferation and survival of cancer patients. *Sci. Transl. Med.* 6, 228ra37.
- Mlecnik, B., Bindea, G., Angell, H.K., Maby, P., Angelova, M., Tougeron, D., Church, S.E., Lafontaine, L., Fischer, M., Fredriksen, T., et al. (2016a). Integrative analyses of colorectal cancer show immunoscore is a stronger predictor of patient survival than microsatellite instability. *Immunity* 44, 698–711.
- Mlecnik, B., Bindea, G., Kirilovsky, A., Angell, H.K., Obenauf, A.C., Tosolini, M., Church, S.E., Maby, P., Vasaturo, A., Angelova, M., et al. (2016b). The tumor microenvironment and Immunoscore are critical determinants of dissemination to distant metastasis. *Sci. Transl. Med.* 8, 327ra26.
- Mlecnik, B., Van den Eynde, M., Bindea, G., Church, S.E., Vasaturo, A., Fredriksen, T., Lafontaine, L., Haicheur, N., Marliot, F., Debetancourt, D., et al. (2018). Comprehensive intrametastatic immune quantification and major impact of immunoscore on survival. *J. Natl. Cancer Inst.* 110. Published online January 1, 2018. <https://doi.org/10.1093/jnci/djx123>.
- Murugaesu, N., Wilson, G.A., Birkbak, N.J., Watkins, T., McGranahan, N., Kumar, S., Abbassi-Ghadi, N., Salm, M., Mitter, R., Horswell, S., et al. (2015). Tracking the genomic evolution of esophageal adenocarcinoma through neoadjuvant chemotherapy. *Cancer Discov.* 5, 821–831.
- Pagès, F., Berger, A., Camus, M., Sanchez-Cabo, F., Costes, A., Molitor, R., Mlecnik, B., Kirilovsky, A., Nilsson, M., Damotte, D., et al. (2005). Effector memory T cells, early metastasis, and survival in colorectal cancer. *N. Engl. J. Med.* 353, 2654–2666.
- Prendergast, G.C., and Jaffee, E.M. (2007). Cancer immunologists and cancer biologists: Why we didn't talk then but need to now. *Cancer Res.* 67, 3500–3504.
- Rooney, M.S., Shukla, S.A., Wu, C.J., Getz, G., and Hacohen, N. (2015). Molecular and genetic properties of tumors associated with local immune cytolytic activity. *Cell* 160, 48–61.
- Roth, A., Khattra, J., Yap, D., Wan, A., Laks, E., Biele, J., Ha, G., Aparicio, S., Bouchard-Côté, A., and Shah, S.P. (2014). PyClone: Statistical inference of clonal population structure in cancer. *Nat. Methods* 11, 396–398.
- Schreiber, R.D., Old, L.J., and Smyth, M.J. (2011). Cancer immunoeediting: Integrating immunity's roles in cancer suppression and promotion. *Science* 331, 1565–1570.
- Schwarz, R.F., Trinh, A., Sipos, B., Brenton, J.D., Goldman, N., and Markowitz, F. (2014). Phylogenetic quantification of intra-tumour heterogeneity. *PLoS Comput. Biol.* 10, e1003535.
- Shukla, S.A., Rooney, M.S., Rajasagi, M., Tiao, G., Dixon, P.M., Lawrence, M.S., Stevens, J., Lane, W.J., Dellagatta, J.L., Steelman, S., et al. (2015). Comprehensive analysis of cancer-associated somatic mutations in class I HLA genes. *Nat. Biotechnol.* 33, 1152–1158.
- Sottoriva, A., Kang, H., Ma, Z., Graham, T.A., Salomon, M.P., Zhao, J., Marjoram, P., Siegmund, K., Press, M.F., Shibata, D., and Curtis, C. (2015). A Big Bang model of human colorectal tumor growth. *Nat. Genet.* 47, 209–216.
- Talevich, E., Shain, A.H., Botton, T., and Bastian, B.C. (2016). CNVkit: genome-wide copy number detection and visualization from targeted DNA sequencing. *PLoS Comput Biol* 12, e1004873.
- Turajlic, S., and Swanton, C. (2016). Metastasis as an evolutionary process. *Science* 352, 169–175.
- Wang, Y., Waters, J., Leung, M.L., Unruh, A., Roh, W., Shi, X., Chen, K., Scheet, P., Vattathil, S., Liang, H., et al. (2014). Clonal evolution in breast cancer revealed by single nucleus genome sequencing. *Nature* 512, 155–160.
- Williams, M.J., Werner, B., Barnes, C.P., Graham, T.A., and Sottoriva, A. (2016). Identification of neutral tumor evolution across cancer types. *Nat. Genet.* 48, 238–244.
- Zhang, A.W., McPherson, A., Milne, K., Kroeger, D.R., Hamilton, P.T., Miranda, A., Funnell, T., Little, N., de Souza, C.P.E., Laan, S., et al. (2018). Interfaces of malignant and immunologic clonal dynamics in ovarian cancer. *Cell* 173, 1755–1769.

Extrinsic Phagocyte-Dependent STING Signaling Dictates the Immunogenicity of Dying Cells

Jeonghyun Ahn,¹ Tianli Xia,¹ Ailem Rabasa Capote,¹ Dillon Betancourt,¹ and Glen N. Barber^{1,2,*}

¹Department of Cell Biology, The University of Miami Miller School of Medicine, University of Miami, 511 Papanicolaou Building, 1550 NW 10th Avenue, Miami, FL 33136, USA

²Lead Contact

*Correspondence: gbarber@med.miami.edu

<https://doi.org/10.1016/j.ccell.2018.03.027>

SUMMARY

The ability of dying cells to activate antigen-presenting cells (APCs) is carefully controlled to avoid unwarranted inflammatory responses. Here, we show that engulfed cells containing cytosolic double-stranded DNA species (viral or synthetic) or cyclic di-nucleotides (CDNs) are able to stimulate APCs via extrinsic STING (stimulator of interferon genes) signaling, to promote antigen cross-presentation. In the absence of STING agonists, dying cells were ineffectual in the stimulation of APCs *in trans*. Cytosolic STING activators, including CDNs, constitute cellular danger-associated molecular patterns (DAMPs) only generated by viral infection or following DNA damage events that rendered tumor cells highly immunogenic. Our data shed insight into the molecular mechanisms that drive appropriate anti-tumor adaptive immune responses, while averting harmful autoinflammatory disease, and provide a therapeutic strategy for cancer treatment.

INTRODUCTION

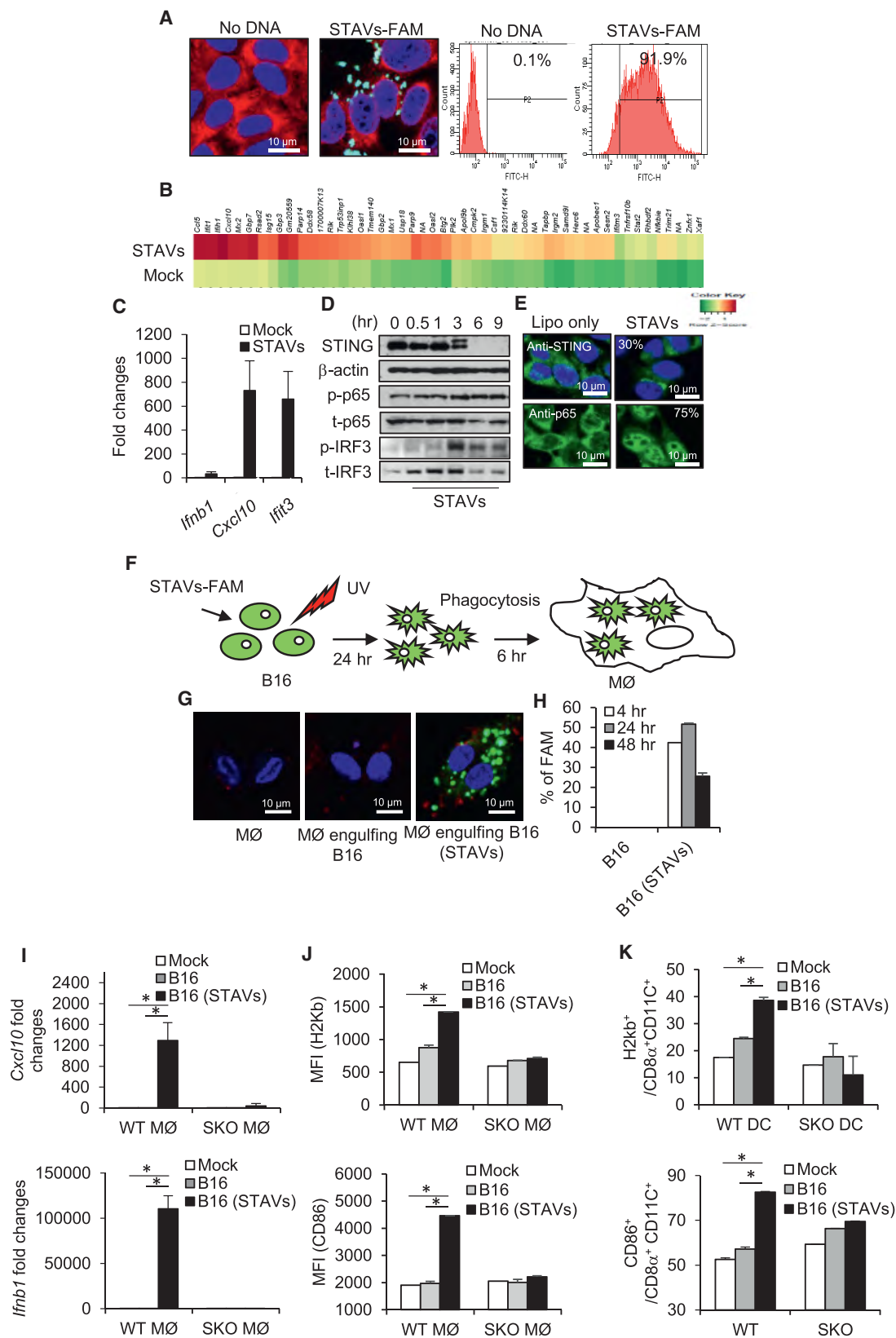
The generation of T cells that recognize specific antigens presented on tumor cells constitutes an important host defense response that has evolved to eliminate the development of cancer (Gajewski et al., 2013). The mechanisms underlying the stimulation of antigen-presenting cells (APCs) and the priming of tumor-specific T cells remain to be clarified but are thought to involve the generation of immune stimulatory type I interferon (IFN) and other cytokines (Diamond et al., 2011; Fuertes et al., 2011; Ma et al., 2013; Marichal et al., 2011; Zitvogel et al., 2015). Generally, non-tumorigenic cells undergoing apoptosis avoid activating APCs, an event that would otherwise cause lethal autoinflammatory disease due to chronic cytokine production (Ahn and Barber, 2014; Kawane et al., 2001; Nagata et al., 2003). By likely adopting comparable processes, tumor cells are also able to avoid the activation of APCs and thus the subsequent spontaneous generation of anti-tumor T cells. In contrast, microbial-infected cells are potentially able to activate APCs

following engulfment and can robustly generate anti-pathogen T cells (Belz et al., 2004; Smith et al., 2003). While DNA from engulfed cells is known to play a key role in stimulating APCs (Ahn et al., 2012), how phagocytes differentiate between an apoptotic/tumorigenic cell and an infected cell, all of which harbor considerable amounts of cellular DNA, remains to be fully determined.

The innate immune pathways governing the stimulation of cytokine production involve STING (stimulator of interferon genes) signaling within phagocytes such as CD8 α ⁺ dendritic cells (Barber, 2015; Corrales et al., 2015; Deng et al., 2014; Woo et al., 2014). STING directly senses cyclic di-nucleotides (CDNs), including c-di-GMP or c-di-AMP secreted by invading intracellular bacteria or cyclic-GMP-AMP (cGAMP) generated by the cellular synthase, cyclic GMP-AMP synthase (cGAS) following association with cytosolic double-stranded DNA (dsDNA) species such as microbial DNA, or even self-DNA (Ablasser et al., 2013; Barber, 2014). Generally, the cytosol of the cell is free of DNA, since it would aggravate STING-dependent cytokine

Significance

Tumor cells are notoriously non-immunogenic and acquire properties that enable them to evade the immunosurveillance system. Here, we demonstrate that defects in cytosolic DNA-activated innate immune signaling pathways, controlled by STING, enable pre-cancerous cells to escape DNA damage-mediated cytokine production. We further demonstrate that tumor cells additionally avoid aggravating antigen-presenting cells (APCs) by efficiently simulating regular dying cells, which following phagocytosis are prevented from initiating autoinflammatory responses. However, dying tumor cells containing exogenous cytosolic DNA, viral DNA, or cyclic di-nucleotides (CDNs) potentially activate APCs *in trans* through extrinsic STING signaling to generate cytotoxic T lymphocyte activity. Our data provide an explanation as to how tumor cells avoid triggering immune responses and provide a therapeutic strategy to stimulate anti-tumor immunity.



(legend on next page)

production, an event that can lead to lethal autoinflammatory disease. For example, self-DNA leaked from the nucleus of cells, following cell division or following DNA damage, is prevented from activating STING signaling by the exonuclease DNase III (Trex1) (Ahn et al., 2014a). Consequently, defects in Trex1 function lead to severe autoinflammatory disease due to undigested self-DNA triggering STING activity. In addition, following the engulfment of apoptotic cells, phagocyte-dependent DNase II plays a critical role in digesting the DNA within the dead cell to prevent it from activating STING signaling extrinsically (Ahn et al., 2012). Loss of DNase II function is embryonic lethal in murine models due to high-level cytokine production being instigated by overactive STING activity.

Thus, the eradication of apoptotic cells is designed to avoid invoking an inflammatory event. Dying cells are generally poor activators of phagocytes and immunologically indolent due to the nuclear compartmentalized genomic DNA being degraded by host DNases to prevent the intrinsic and extrinsic activation of STING. Given this, we thus postulated that apoptotic cells containing cytosolic dsDNA species or CDNs could potentially stimulate APCs, via extrinsic STING signaling, to promote the cross-presentation of antigen. Plausibly, cytosolic STING activators, including CDNs, constitute potent cellular danger-associated molecular patterns (DAMPs) only generated by viral infection or following DNA damage events, which can render apoptotic and tumorigenic cells immunogenic and able to facilitate anti-tumor T cell activity. Our goals were to gain further insight into the molecular mechanisms that drive appropriate adaptive immune responses, while averting harmful autoinflammatory disease and possibly providing effective therapeutic strategies for the treatment of cancer.

RESULTS

STING-Dependent Adjuvants (STAVs) Can Stimulate the Activation of Macrophages in a STING-Dependent Manner

To further investigate the importance of STING in facilitating adaptive immune responses, we generated a variety of DNA-dependent nucleic acids and examined their ability to activate STING signaling. We noted that transfected cytosolic dsDNA, modified on the 5' end to help prevent exonuclease degradation, greater than approximately 30 bp in murine cells (murine embry-

onic fibroblasts [MEFs] or 70 bp in human cells (human telomerase reverse transcriptase immortalized cell lines [hTERT] and primary human macrophages) were required for the efficient activation of STING (Figures S1A–S1I). The effects following transfection appeared to be largely independent of sequence specificity, and both AT- or GC-rich structures were readily able to trigger STING activity. As a result of these endeavors, an AT-rich STING activating dsDNA ligand of 90 bp with modified 5' ends (referred to as STING-dependent adjuvants [STAVs]) was used for further study. Following the transfection of a variety of cells, including murine B16 cells, we noted that the majority of the STAVs remained in the cytosol of the cell in as-yet undefined cellular compartments (Figure 1A). Quantitation studies indicated that the cytosolic STAVs constituted approximately 1% of the total cellular DNA content (Figure S1J).

To evaluate the importance of STING signaling in the stimulation of APCs following cellular engulfment, we transfected B16 cells with STAVs, routinely obtaining greater than 90% transfection efficiency (Figure 1A), and confirmed that B16 cells exhibited cytosolic DNA-dependent STING signaling as determined by observing an increase in cytokine production, including Cxcl10 (Figures 1B and 1C and Table S1). This event coincided with an increase in STING and IRF3 phosphorylation (Figures 1D and S1K) and STING and nuclear factor κ B (NF- κ B) (p65) trafficking (Figure 1E). Cytokine levels were noted to be elevated in the presence of STAVs compared with unmodified dsDNA or cGAMP, perhaps due to being protected from host DNases (Figure S2). This was performed since we have previously noted that numerous types of cancer cells appear defective in STING signaling, perhaps to avoid the DNA damage-mediated cytokine production that can occur via intrinsic STING signaling, which likely alerts the immune system to the vicinity of the damaged cell (Xia et al., 2016a, 2016b). We next fed UV-treated STAVs-containing cells to phagocytes (murine bone marrow-derived macrophages [BMDMs] from wild-type [WT] or *Sting* knockout [SKO]) *in vitro* (Figure 1F). UV irradiation triggered both annexin V and propidium iodide (PI)-positive cell staining in greater than 90% of the cells, with the cells retaining STAVs for up to 24 hr (>90%) (Figures S3A and S3B). Approximately 50% of the macrophages consistently engulfed the cells, as determined using B16 cells transfected with fluorescently labeled STAVs (Figures 1F–1H and S3C). B16 cells containing STAVs robustly induced the production of cytokines in macrophages, which

Figure 1. Activation of Macrophages by Exogenous Cytosolic DNA (STAVs) in Engulfed Apoptotic Cells

- (A) Confocal analysis and flow cytometry analysis of B16 OVA cells (B16) transfected with FAM-labeled STAVs (green). DAPI (blue), and anti-calreticulin (red) as counter staining; bar represents 10 μ m.
- (B) Gene array analysis of B16 cells transfected with 3 μ g/mL of STAVs for 6 hr. Highest variable inflammation-related genes are shown.
- (C) qRT-PCR analysis of *Irfn1*, *Cxcl10*, and *Irf3* in B16 OVA cells same as in (B).
- (D) Western blot analysis of STING, p65, and IRF3 in B16 cells transfected with 3 μ g/mL STAVs and incubated for time courses as indicated.
- (E) Immunofluorescent microscopy analysis using anti-STING and anti-p65 in B16 cells at 3 hr after transfection of STAVs (3 μ g/mL); bar represents 10 μ m.
- (F) Schematic representation of the phagocytosis of B16 cells by macrophages. B16 cells were transfected by 3 μ g/mL of STAVs for 3 hr and irradiated by UV (120 mJ/cm). The irradiated B16 cells were fed to macrophages (M ϕ) at 24 hr after UV irradiation.
- (G and H) Confocal microscopy analysis (G) and flow cytometry analysis (H) in macrophages following cellular engulfment of B16 cells transfected with FAM-labeled STAVs.
- (I) qRT-PCR analysis of *Cxcl10* and *Irfn1* in WT and SKO macrophages (WT M ϕ and SKO M ϕ) following engulfment of B16 cells in presence or absence of STAVs.
- (J) Flow cytometry for H-2Kb and CD86 on macrophages following phagocytosis of B16 cells.
- (K) Flow cytometry for CD86 and H-2Kb on CD8 α^+ CD11c $^+$ dendritic cells following phagocytosis of B16 cells containing STAVs. Data are representative of at least three independent experiments. DC, dendritic cell.
- Error bars indicate mean \pm SD. * p < 0.05; Student's t test. See also Figures S1–S3 and Table S1.

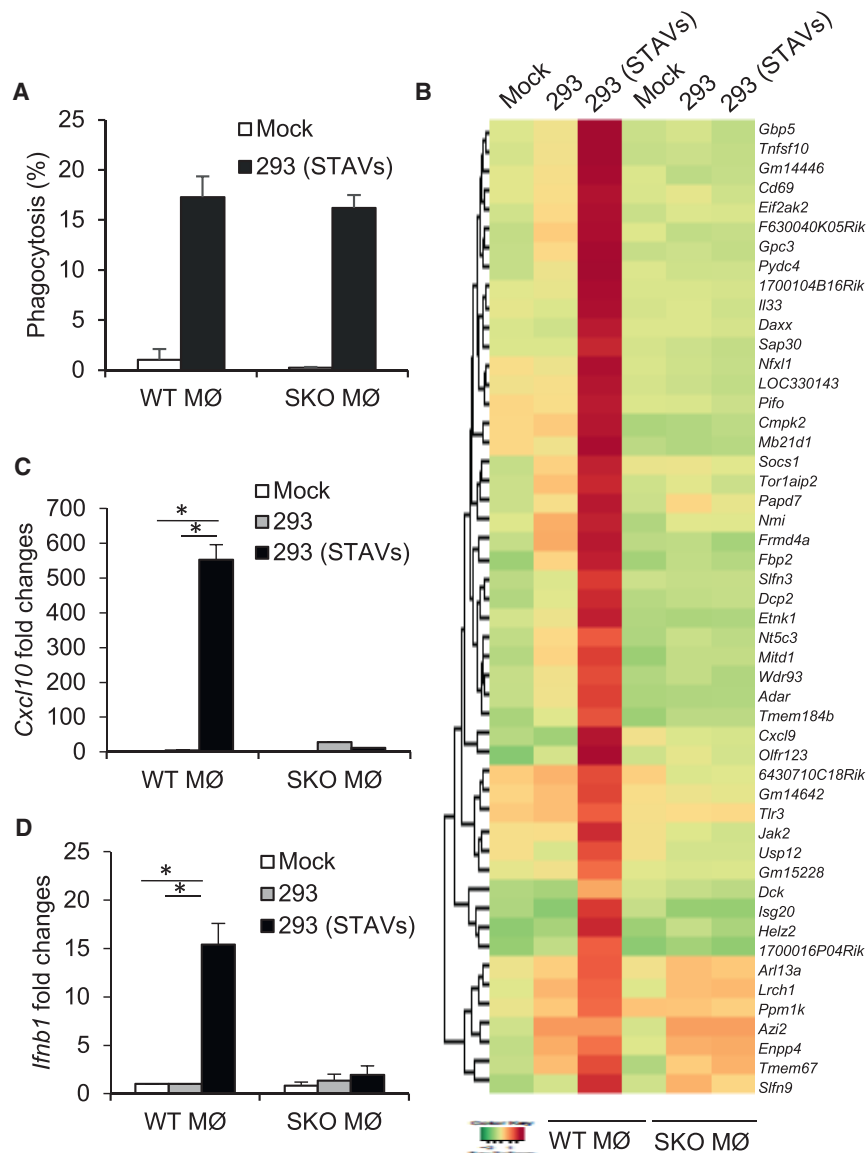


Figure 2. Extrinsic STING Signaling-Dependent Gene Expression in Macrophages

(A) Flow cytometry analysis in macrophages following cellular engulfment of UV-irradiated HEK293 cells (293) transfected with FAM-labeled STAVs.

(B) Gene array analysis of WT and SKO macrophages following engulfment of irradiated 293 cells with/without STAVs. Highest variable inflammation-related genes are shown.

(C and D) qRT-PCR analysis of *Cxcl10* (C) and *Ifnb1* (D), the same as in (A). Data are representative of at least three independent experiments.

Error bars indicate mean \pm SD. * $p < 0.05$; Student's t test. See also Table S2.

The Stimulation of Engulfing Macrophages Can Occur *In Trans* by Cytosolic DNA Promoting STING Signaling in Macrophages

It is possible that the transfected cytosolic DNA could stimulate intrinsic STING signaling within the treated cell and facilitate the production of immunoregulatory cytokines that may provoke APC activation. Thus, we treated MEFs that lacked STING or cGAS with STAVs and confirmed that both STING and cGAS were required to produce cytokines such as type I IFN in the presence of cytosolic DNA (Figures 3A and 3B). UV-treated MEFs were then incubated with macrophages to ascertain the latter's activation (Figure 3C). Our results again indicated that only apoptotic cells containing cytosolic DNA were able to activate macrophages (Figures 3D and 3E). Indeed, MEFs lacking cGAS or STING, transfected with STAVs, remained able to activate APCs, indicating that STING-dependent cytokine produc-

tion within the engulfed cell was not essential for macrophage activation *in vitro* (Figures 3A, 3D, 3E, and S4A). A similar effect was observed following the phagocytosis of B16 Sting knockout (B16-SKO) and B16 cGAS knockout (B16-cGASKO) generated by CRISPR (clustered regularly interspaced short palindromic repeats) technology (Figure S4B). These data suggest that exogenous cytosolic DNA, but not indigenous cellular DNA, is responsible for the stimulation of the APCs, including macrophages. To complement these studies, we transfected STAVs into human 293T cells that lack both cGAS and STING. Unlike normal human hTERT cells, 293T cells are consequently unable to produce type I IFN in response to STAVs (Figures 3F and S4C). We then incubated STAV-treated 293T cells with murine macrophages and observed that only 293T cells containing STAVs were able to stimulate cytokine production in engulfing macrophages (Figures 3G and 3H). This effect was dependent on STING signaling in the macrophages (Figures 3G and 3H).

was dependent on extrinsic STING signaling within the macrophages (Figures 1I and 1J). However, UV-treated B16 cells alone or B16 cells containing poly(I:C) failed to stimulate the macrophages, as verified by measuring *Cxcl10*, type I IFN, macrophage maturation marker (CD86), and MHC class I (H-2Kb) (Figures 1I, 1J, and S3D). Irradiated B16 cells harboring STAVs were also observed to activate dendritic cells (murine bone marrow-derived dendritic cells [BMDCs]) as verified by upregulation of the maturation markers CD86 and H-2Kb (Figure 1K). We confirmed that cells containing STAVs undergoing alternate forms of cell death, such as initiated by cisplatin or hydrogen peroxide, also induced the production of cytokines in macrophages (Figures S3E and S3F). A similar effect was observed following the phagocytosis of HEK293 cells containing STAVs (Figure 2 and Table S2). These data indicated that exogenous cytosolic DNA species present in engulfed apoptotic cells can potentially stimulate the activation of macrophages *in trans* in a STING-dependent manner.

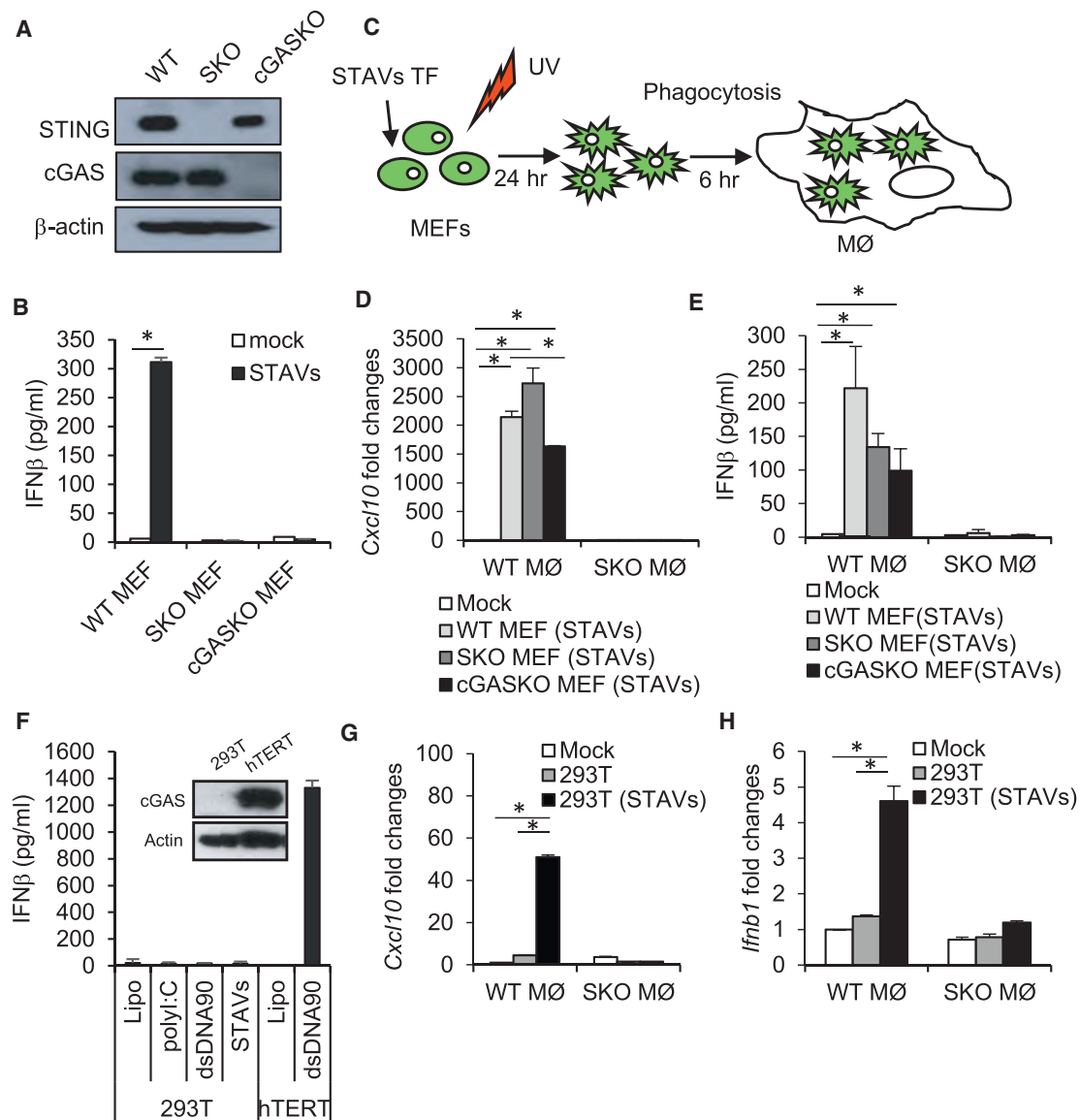


Figure 3. Macrophage Stimulation *In Trans* by Cytosolic DNA

(A) Western blot analysis of STING and cGAS in MEFs.

(B) ELISA analysis of IFN β in WT, SKO, and cGAS knockout (cGASKO) transfected with 3 μ g/mL STAVs.

(C) Schematic representation of the phagocytosis of MEFs by macrophages.

(D and E) qRT-PCR analysis of *Cxcl10* (D) and *Ifnb1* (E) in WT and SKO macrophages following engulfment of UV-irradiated WT, SKO, and cGASKO MEFs with 3 μ g/mL STAVs.

(F) ELISA analysis of IFN β in 293T and hTERT cells transfected with STAVs.

(G and H) qRT-PCR analysis of *Cxcl10* (G) and *Ifnb1* (H) in WT and SKO macrophages following engulfment of UV-irradiated 293T cells with or without STAVs. Data are representative of at least three independent experiments.

Error bars indicate mean \pm SD. * $p < 0.05$; Student's *t* test. See also Figure S4.

CDNs in Engulfed Cells Can *Trans*-Activate STING Signaling in Macrophages

To extend our studies, we next further examined the importance of extrinsic STING signaling within the engulfing APC. To accomplish this, we treated B16 cells with STAVs and fed them to murine macrophages lacking cGAS or STING. This analysis surprisingly indicated that macrophages lacking cGAS or TLR9, but not STING, were readily able to be activated by B16 cells con-

taining STAVs (Figures 4A and S4B). Thus, STING, but not cGAS, is essential for the activation of APCs following cellular engulfment. This event was also noted to not require TLR9 (Figure 4A). These data suggest that STAVs within the UV-treated cell could be binding to an alternate DNA-binding STING activating molecule within the APCs or conversely that CDNs were being generated within the B16 cell by cGAS, which are able to activate STING signaling extrinsically within the APC, *in trans*.

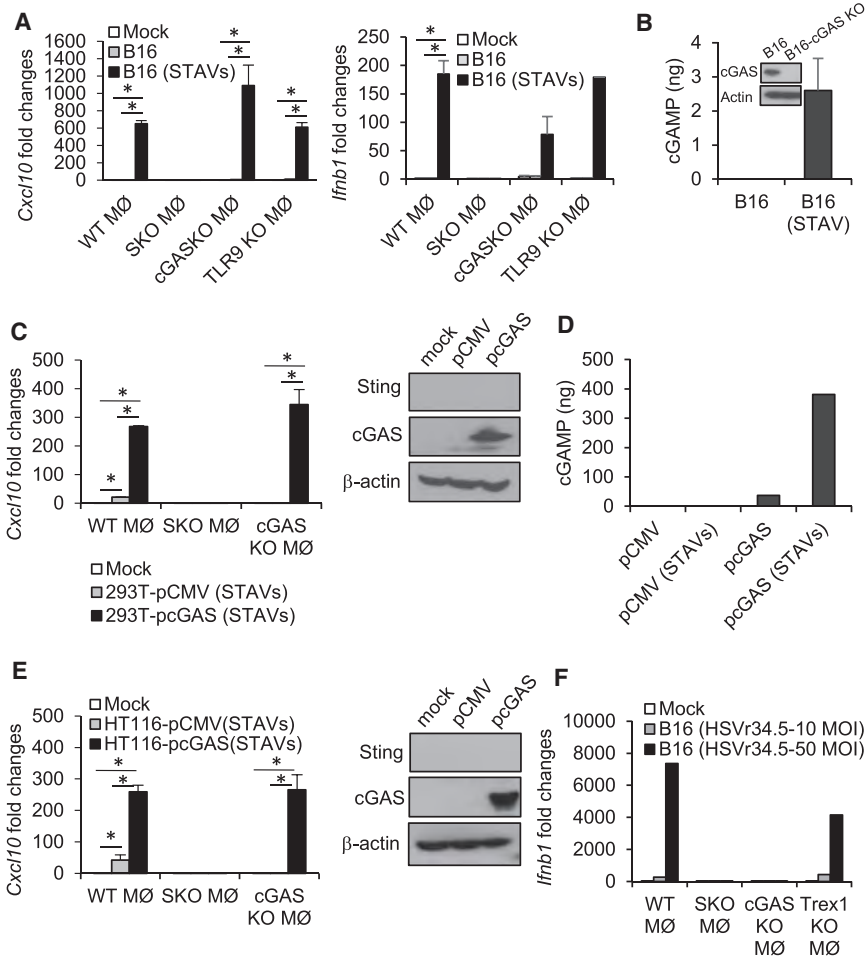


Figure 4. Extrinsic Activation of the cGAS/STING Axis in Macrophages

(A) qRT-PCR analysis of *Cxcl10* and *Ifnb1* in WT, SKO, cGASKO, and TLR9 knockout (KO) macrophages following engulfment of UV-irradiated B16 cells in presence of 3 μ g/mL of STAVs or absence. (B) cGAS expression by western blot and cGAMP amount by a hybrid mass spectrometer in B16 cells. B16-cGASKO cells were used as negative control for WB.

(C) qRT-PCR analysis of *Cxcl10* in WT, SKO, and cGASKO macrophages following engulfment of UV-irradiated 293T cells containing 3 μ g/mL STAVs. The 293T cells were reconstituted with pcGAS or pcMV as control vector.

(D) Measurement of cGAMP levels by a hybrid mass spectrometer in 293T cells as in (C).

(E) qRT-PCR analysis of *Cxcl10* in WT, SKO, and cGASKO macrophages following engulfment of UV-irradiated HT116 cells containing STAVs. The HT116 cells were reconstituted with pcGAS or pcMV as control vector.

(F) qRT-PCR analysis of *Ifnb1* in WT, SKO, cGASKO, and Trex1 KO macrophages following engulfment of B16 cells infected with HSV γ 34.5. The HT116 cells were reconstituted with pcGAS or pcMV as control vector.

Error bars indicate mean \pm SD. * p < 0.05, Student's t test. See also Figure S4.

Our analysis indeed indicated that cGAS was expressed in B16 cells and could generate CDNs in the presence of cytosolic DNA, as determined by mass spectrometry (Figure 4B). Next, we transfected 293T cells that lack cGAS or STING with STAVs. Unlike B16 or MEFs cells, 293T cells cannot generate CDNs (Figures 3F and S4D). We had previously confirmed that 293T cells containing cytosolic DNA (STAVs) were able to modestly stimulate WT macrophages but not macrophages that lacked STING (Figures 3G and 3H). We further observed that macrophages lacking cGAS were similarly unable to be activated by 293T cells containing STAVs, since the STAVs are probably unable to activate cGAS-generated CDNs production within the APC to activate STING signaling (Figure 4C). To extend this study, we therefore reconstituted 293T cells with a plasmid expressing cGAS. This experiment indicated that 293T cells expressing cGAS could readily generate CDNs, as determined by mass spectrometry, and that these intrinsic CDN-containing cells could activate STING signaling in macrophages, *in trans* (Figures 4C, 4D, S4E, and S4F). These results were confirmed using a human colon cancer cell line that similarly lacks cGAS (HT116) (Figures 4E and S4G). cGAS-lacking cells containing STAVs were also observed to activate cGAS-lacking phagocytes less than WT or SKO phagocytes, again suggesting that CDNs are stimulatory *in trans* (Figure S4B).

To complement this study, we evaluated the importance of STING signaling in phagocyte activation in relation to other forms of cell death and cytosolic DNA species. Our data indicated that the DNA virus HSV1 (γ 34.5) functioned similarly to transfected STAVs following infection of B16 cells. That is, only engulfed viral-infected cells, and not uninfected cells, could activate macrophages. Further, this event similarly occurred in a cGAS/STING-dependent manner (Figure 4F). We next evaluated whether STING signaling was important for the immunogenic effects not only of DNA virus-infected cells but also of chemotherapeutic drugs (cisplatin) (Galluzzi et al., 2015; Pfirschke et al., 2016). We have previously shown that cisplatin-induced DNA damage can activate intrinsic STING signaling (Ahn et al., 2014b). B16 cells heterologously expressing cGAS were treated with cisplatin or UV or γ irradiation, the results of which indicated the release of host nuclear DNA into the cytosol, which colocalized with cGAS (Figure S5A) (Ahn et al., 2014b; Harding et al., 2017; Mackenzie et al., 2017). STAVs were also confirmed as co-localizing with cGAS (Figure S5B). We observed that cisplatin treatment could generate CDNs in a cGAS-specific manner similar to UV or γ irradiation (Figure S5C). Engulfed cisplatin-treated B16 cells were observed to stimulate phagocyte activity as determined by measuring the upregulation of H-2Kb and cytokines such as *Cxcl10* (Figures S5D and S5E). Finally, mice treated with cisplatin were able to generate enhanced CD8⁺ T cell activity to subcutaneously growing B16 tumors that was dependent on STING signaling (Figure S5F). Our analysis would suggest that, in addition to UV and γ irradiation, DNA virus-infected cells and

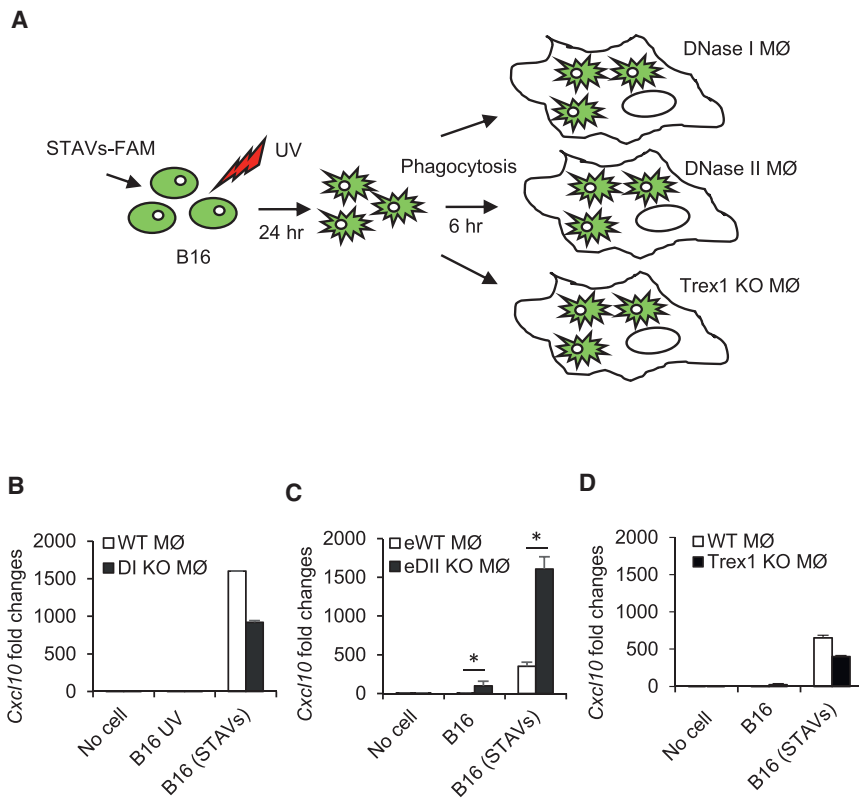


Figure 5. Apoptotic Cells Containing STAVs Escape Degradation by DNase II

(A) Schematic representation of the phagocytosis of B16 cells by DNase I, DNase II, or Trex1 KO macrophages. B16 cells were transfected by STAVs for 3 hr and irradiated by UV (120 mJ/cm). The irradiated B16 cells were fed to three different genotypes of macrophages (MØ) at 24 hr after UV irradiation.

(B–D) qRT-PCR analysis of *Cxcl10* in DNase I KO (B), DNase II KO (C), and Trex1 KO (D) macrophages at 6 hr following engulfment of B16 cells containing STAVs. B16 UV, UV-irradiated; B16 (STAVs), transfected with STAVs; DI KO, DNase I KO; eWT, WT embryo; eDII KO, DNase II KO embryo.

Error bars indicate mean \pm SD. * $p < 0.05$; Student's *t* test.

alternate forms of DNA damage that generates cytosolic DNA species can stimulate immune activity through extrinsic STING-dependent signaling in phagocytes. Collectively, our data indicate that STAVs transfected into cells can extrinsically activate the cGAS/STING axis in phagocytes. Second, STAVs and other cytosolic DNA species generated from DNA damage events can generate CDNs within the treated cell, which can also act *in trans* to stimulate extrinsic STING signaling in APCs. Further, reconstitution of cGAS, for example within a tumor cell, can generate CDNs that are able to similarly act *in trans* to stimulate the activation of phagocytes via STING. Finally, host macrophages can distinguish between a viral-infected and uninfected dying cells predominantly through cGAS/STING detection of viral cytoplasmic DNA, analogous to STAVs.

Apoptotic Cells Containing STAVs Escape Degradation by DNase II and Stimulate Extrinsic cGAS/STING Signaling

Our data thus indicate that cytosolic DNA (STAVs) or CDNs can activate APCs, directly or indirectly, and facilitate antigen cross-presentation (Figures S6A–S6D). It remained unclear why cytosolic DNA (STAVs) and not indigenous cellular DNA is able to stimulate APCs *in trans*. However, nuclear DNA, and plausibly mtDNA, undergoes degradation during the apoptotic process. The responsible nucleases within the nuclei that cleave genomic DNA between nucleosomes involves CAD (caspase-activated DNase) (McIlroy et al., 2000; Nagata et al., 2003). Thus, fragments of nuclear DNA sufficient to activate STING signaling may not be generated or escape into the cytosol. Following engulfment by macrophages, the remainder of the DNA is

likely degraded by additional DNases (DNase II) within the lysosomal compartment of APCs (Ahn et al., 2012; Kawane et al., 2001). It is thus plausible that cytosolic DNA species (STAVs or viral DNA) escape cellular degradation within the apoptotic cell and following engulfment in APCs is more readily available to escape the lysosomal compartment and stimulate extrinsic cGAS/STING signaling in the APC. To explore this further, we retrieved macrophages from mice lacking DNase I (Figures 5A and 5B), II (Figures 5A and 5C), or III (Trex1) (Figures 5A and 5D) and fed them B16 cells containing or lacking STAVs. Our data again indicated that apoptotic cells poorly activate normal macrophages, perhaps explaining why tumor cells are generally non-immunogenic. However, APCs lacking DNase II, but not DNase I or DNase III, exhibited an increase in cytokine production following the engulfment by untreated apoptotic cells (Figures 5 and S6E). This event was greatly augmented in STAVs-containing cells (Figure 5). These data confirm that DNases such as CAD efficiently degrade self-DNA within apoptotic cells to help prevent the activation of macrophages (Nagata and Tanaka, 2017). However, DNase II in APCs predominantly ensures that any engulfed apoptotic DNA that escapes degradation is broken down in lysosomal compartments into non-STING-activating nucleotides. Significantly, cells containing cytosolic DNA (STAVs) or cytoplasmic viral DNA likely escape degradation in the apoptotic cell and are able to stimulate extrinsic cGAS/STING signaling in the APCs, prior to degradation by DNase II.

STAVs Induce Anti-tumor Immunity Involving the Generation of Cytotoxic T Cell Activity

Our data indicate that cells have devised efficient ways to eliminate the lethal possibility of self-DNA activating innate immune sensor pathways such as those governed by STING (Ahn et al., 2012, 2014a). Likely, tumor cells also utilize this process to remain immunologically indolent. To determine whether STAVs could render tumor cells immunogenic *in vivo*, we intratumorally inoculated B16 OVA melanoma cells containing or lacking

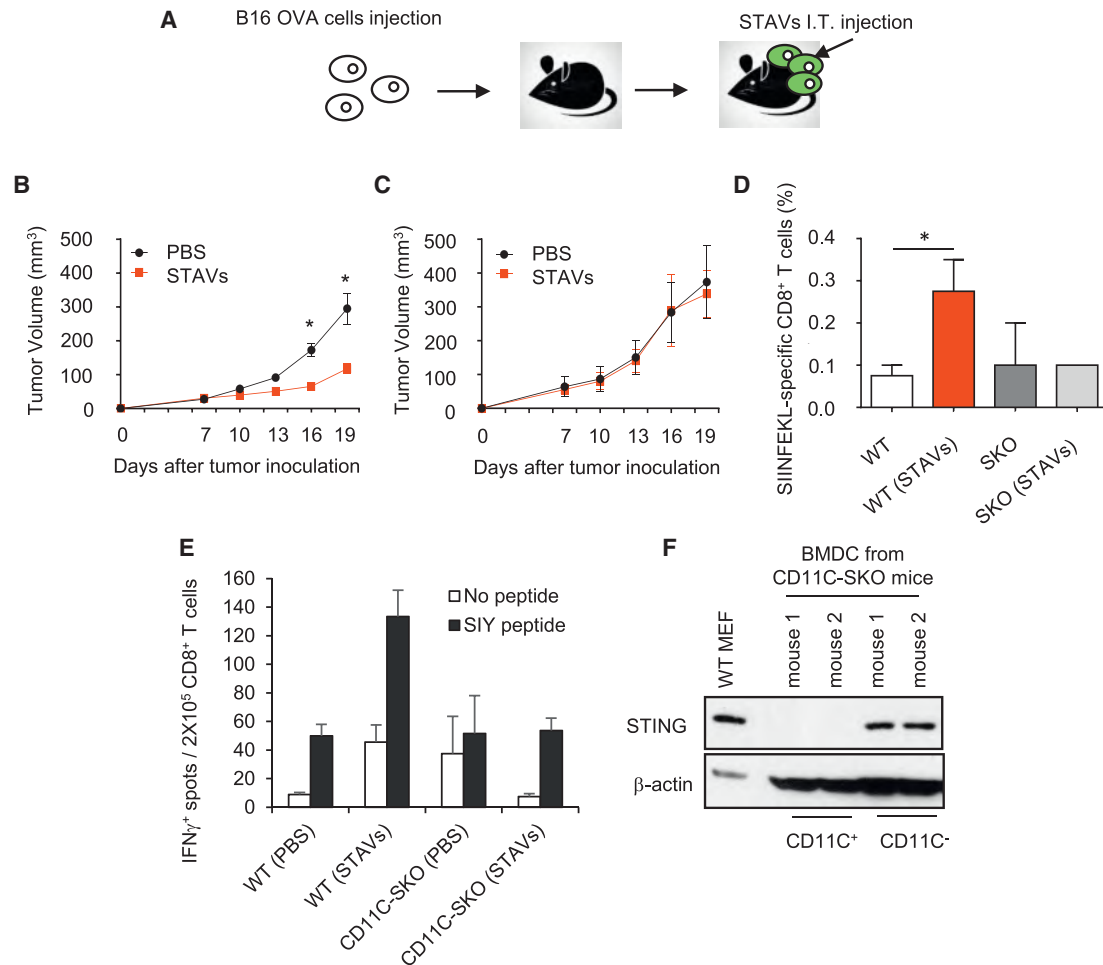


Figure 6. Anti-Tumor Activity of STAVs in B16 OVA Melanoma-Bearing Mice

(A) Schematic representation of intratumoral injection of STAVs in B16 OVA melanoma-bearing mice. The mice were subcutaneously injected with B16 OVA cells on the flank. 10 μ g of STAVs was injected intratumorally (I.T.) every 3 days.

(B and C) Tumor volumes from WT (n = 7/group) (B) and SKO mice (n = 7/group) (C) were measured on the indicated days.

(D) Frequency of OVA-specific CD8⁺ T cells in the spleen from WT (n = 4/group) and SKO (n = 4/group) mice injected with STAV or PBS as control.

(E) IFN γ ELISPOT assay in CD8⁺ T cells from WT or CD11C-cre; *Sting*^{loxP} (CD11C-SKO) mice. The mice were subcutaneously injected with B16-SIY cells on the flank. 10 μ g of STAVs was injected intratumorally (I.T.) every 3 days. CD8⁺ T cell priming was evaluated by IFN γ ELISPOT.

(F) STING expression in CD11C⁺ BMDCs from the CD11C-SKO mice. CD11C⁺ cells were selected by CD11C microbeads (CD11C⁺), lysed, and analyzed for STING expression by western blot. The unlabeled cell fraction was used as a control (CD11C⁻).

Error bars indicate mean \pm SD. *p < 0.05; Student's t test. See also Figure S6.

STAVs into immunocompetent C57BL/6J mice (Figure 6A). We observed that B16 OVA cells treated with STAVs exhibited less growth compared with mice inoculated with untreated cells (Figure 6B). In addition, the STAV-containing cells did not exert any anti-tumor activity in the absence of STING in the recipient mice (Figure 6C). The ability of the STAVs to inhibit tumor growth involved the generation of anti-tumor CTL to the tumor, as determined by measuring anti-SIINFEKL-specific CD8⁺ T cells (Figure 6D). To start to evaluate the importance of dendritic cells in this process, we utilized C57/BL6 syngeneic mice lacking STING in CD11c⁺ cells (CD11C-SKO). B16 SIY cells (expressing the peptide SIYRYRYGL) were inoculated into the flanks of syngeneic C57/BL6 CD11C-SKO mice. After 9 days, STAVs were injected intratumorally. CD8⁺ T cells were isolated from splenocytes and analyzed by enzyme-linked ImmunoSpot (ELISPOT) to eval-

uate anti-tumor T cell responses. This analysis indicated that mice lacking STING specifically in CD11c⁺ dendritic cells generated less anti-tumor T cell activity compared with WT mice, thus implying a key role for STING signaling in T cell priming and these subsets of APCs (Figures 6E and 6F). Further, our data would indicate that tumor cells containing STAVs could be potent stimulators of anti-tumor immunity.

STAV-Containing Cells Provide an Effective Immunotherapeutic Cell-Based Therapy Against Melanoma Metastasis

To additionally evaluate whether STAV-containing cells were able to generate immune responses in murine models, B16 cells were loaded with STAVs, irradiated, and used to immunize C57BL/6J mice (Figure 7A). This study indicated that

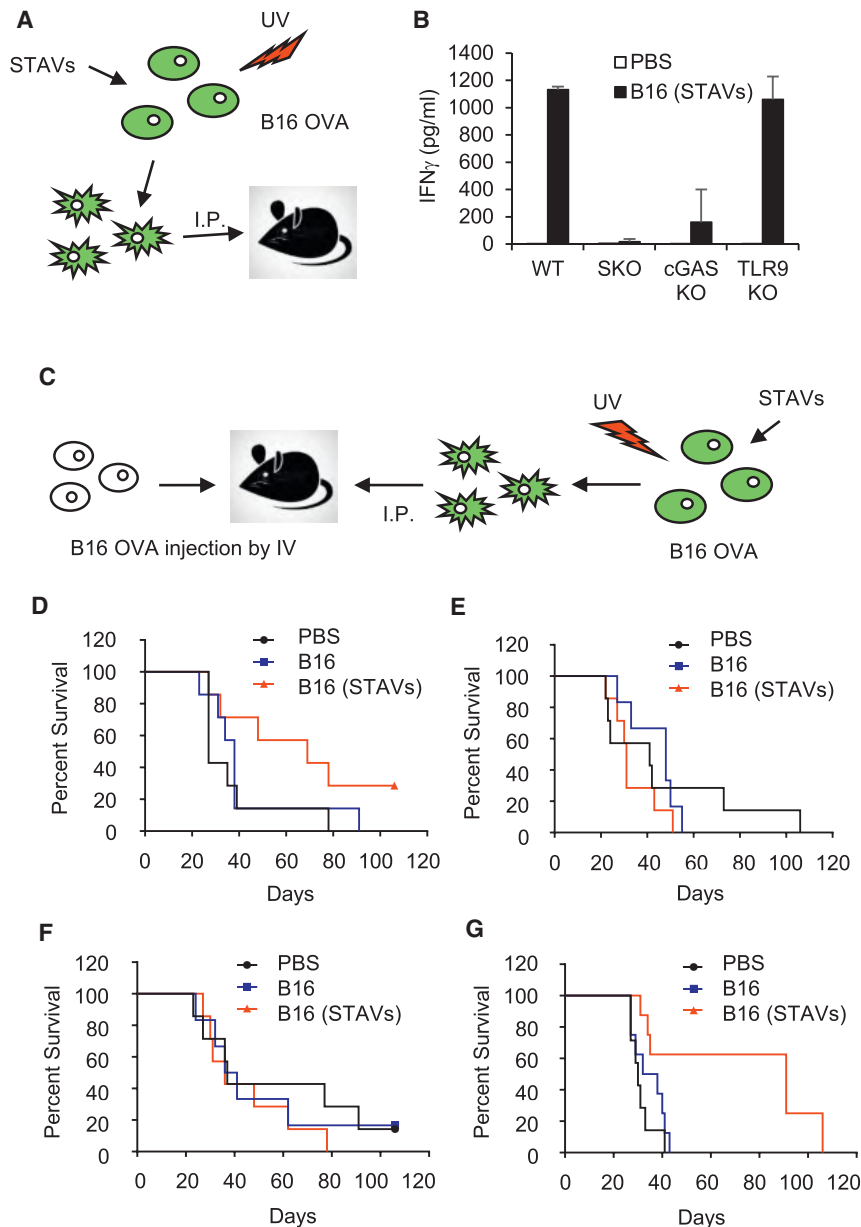


Figure 7. Protection of Lung Metastasis by B16 OVA Requires STING

(A) Schematic representation of dead cell immunization. B16 OVA cells were transfected by STAVs for 3 hr and irradiated by UV (120 mJ/cm). After 24 hr, WT, SKO, TLR9 KO, and cGASKO mice were intraperitoneally (I.P.) injected with irradiated B16 cells with/without STAV, twice every week.

(B) IFN γ measurement in splenocytes from WT, SKO, TLR9 KO, and cGASKO mice at 7 days after the second immunization. Error bars indicate mean \pm SD.

(C) Schematic representation of post-vaccination for B16 OVA-mediated lung metastasis. WT, TLR9KO, SKO, and cGASKO mice were intravenously (IV) injected with B16 OVA cells (5×10^4 cells/mouse). On days 1, 3, 7, and 14, the mice were I.P injected with UV-irradiated B16 OVA cells (1×10^6 cells/mouse) with STAVs.

(D–G) Survival rates from WT ($p = 0.0429$, $n = 7$ /group) (D), SKO ($p = 0.2616$, $n = 7$ /group) (E), cGASKO ($p = 0.4075$, $n = 7$ /group) (F), and TLR9KO ($p = 0.0012$, $n = 7$ /group) (G) mice were monitored. PBS, control group treated with PBS; B16, post-vaccinated group with UV-irradiated B16 cells; B16 (STAVs), post-vaccinated group with UV-irradiated B16 cells with STAVs. p values are based on log rank tests, with $p < 0.05$ considered statistically significant.

See also Figure S7.

STAVs-containing cells were competent to stimulate CD8 $^+$ T cell priming and the generation of type II IFN, a further indicator of CTL activity (Figures 7B and S7A–S7C). STAVs-dependent type II IFN production was dependent on STING and partially dependent on cGAS, but not TLR9. These data would indicate that tumor cells containing STAVs could be potent stimulators of anti-tumor immunity, through STING signaling.

To examine this further, we inoculated C57BL/6J mice with B16 OVA melanoma cells, intravenously, which induces metastatic disease. We subsequently vaccinated the tumor-bearing mice with B16 OVA cells loaded with STAVs (Figure 7C). We found that the B16 OVA tumors killed the majority of mice within 40 days in WT mice (Figure 7D). However, mice treated with B16 OVA STAVs had a median life of 70 days, with 40% of the mice alive after 100 days (Figure 7D). Mice lacking STING (Figure 7E)

or cGAS (Figure 7F), but not TLR9 (Figure 7G), however, succumbed to lethal disease similar to WT mice, indicating the importance of STING signaling in combatting cancer metastasis (Figures 7E–7G). Finally, we tested whether the blockade of the immunosuppressive receptor programmed cell death-1 (PD-1) could enhance the anti-tumor activity of STAVs-containing tumor cells. We thus vaccinated tumor-bearing mice with B16 OVA cells loaded with STAVs, in the presence or absence of anti-PD-1 antibody. We observed that survival rates significantly increased in mice treated with both anti-PD-1 and STAVs-containing cells (Figure S7D). These data indicate that anti-PD-1 could improve the therapeutic efficacy of STAVs. To confirm our anti-tumor strategy, we used another syngeneic tumor model, namely BALB/c mice bearing STAV-treated or -untreated TS/A (breast adenocarcinoma)-Luc cells. Similarly, we observed that mice carrying metastatic TS/A survived longer when treated with TS/A-luc cells loaded with STAVs (Figures S7E and S7F). Significantly fewer luciferase-expressing metastatic TS/A cells were detected in the STAV-treated mice, using *in vivo* imaging systems (Figure S7G). The immunized mice with TS/A (STAVs) were re-challenged with TS/A cells in the flank of the mice 153 days after the first exposure of the metastatic tumor. Tumor growth in the immunized mice with TS/A (STAVs) was clearly shown to be significantly reduced or prevented entirely (Figure S7H). Thus, cells

containing STAVs may provide an effective immunotherapeutic cell-based therapy for the treatment of cancer.

DISCUSSION

STING signaling has become a key mechanism for stimulating innate and adaptive immune responses following detection of DNA species in the cytosol. Generally, STING functions as a sensor to detect microbial invasion, although leaked self-DNA generated following DNA damage events or cell division can also trigger STING activity and cytokine production (Barber, 2015). These responses would presumably alert the immune system to the damaged area, with the cells being eliminated by phagocytosis. However, overactive STING activity is now known to cause lethal autoinflammatory disease (Ahn and Barber, 2014; Barber, 2015; Liu et al., 2014; Nagata and Tanaka, 2017). Thus, STING signaling is rigidly controlled to avoid autoimmune malaise. Indeed, defects in cellular DNases that are accountable for degrading cytosolic self-DNA species are responsible for instigating severe autoinflammatory disease caused via STING signaling (Ahn et al., 2012, 2014a; Rodero and Crow, 2016).

Our data demonstrate that cytosolic dsDNA species present within a dying cell can activate extrinsic STING signaling in phagocytes likely following association with cGAS, which would generate CDNs. It is likely that the cytosolic DNA species avoid being degraded by nuclear DNases, responsible for degrading genomic DNA. Such cytosolic species appear significantly more capable of activating STING in phagocytes, as a result of avoiding being degraded within the dying cell and/or by phagocytes following engulfment. DNase-resistant cytosolic species were thus more competent at activating STING *in trans*. In addition, CDNs generated from an infected or damaged cell are able to directly activate STING-dependent signaling in APCs *in trans*, to trigger immune responses, the cross-presentation of antigen, and the generation of T cells. CDNs are only generated following DNA-damaging events or after infection, and are thus effective DAMPs. CDNs generated within a dying cell are also predominantly resistant to the activity of DNases within the engulfed phagocyte, unlike susceptible cellular DNA, which makes them highly efficient at stimulating extrinsic STING signaling, although they are likely susceptible to other forms of negative regulation. It is likely that tumorigenic cells closely mimic normal cells undergoing cell death and avoid triggering STING signaling. Thus, tumorigenic cells are predominantly non-immunogenic.

We suggest that intrinsic STING signaling is likely important within a stressed cell (DNA damage or microbial infection) to alert APCs to the damaged region, while the extrinsic STING signaling component within phagocytes is critical for the production of cytokines such as type I IFN that facilitate cross-presentation events. Since self-DNA from the apoptotic/tumor cell is efficiently degraded to prevent autoinflammatory events, tumor cells are, as a consequence, immunologically indolent (Nagata and Tanaka, 2017). Our data indicate that CD8 α^+ CD11C $^+$ APCs play a key role in facilitating STING-dependent T cell priming (Belz et al., 2004). However, macrophage (CD11b $^+$) cells may also play a role and are presently under investigation. Our data also indicate that numerous tumor cells exhibit defective STING signaling through loss of cGAS and/or STING (Xia et al., 2016a, 2016b). This would presumably enable the DNA-damaged cells

to avoid alerting the immune system for elimination. However, our analyses also indicate that, by suppressing CDN production, a tumor cell or infected cell would also additionally evade the activation of the APC itself, *in trans*. Our data further indicate that reconstitution of CDNs and STING signaling may not only alert the immune system to the tumor cell but also stimulate the adaptive immune responses by activating phagocytes *in trans*. It has been suggested that certain forms of cell death are more immunostimulatory than other types (Deng et al., 2014; Dou et al., 2017; Galluzzi et al., 2015; Harding et al., 2017; Kono and Rock, 2008; Pfirschke et al., 2016; Russell and Peng, 2017; Yatim et al., 2017). However, a variety of studies have shown that the immunomodulatory effects are modest and generally most dying cells are relatively non-immunogenic, to avoid autoinflammation, as described (Nagata and Tanaka, 2017; Woo et al., 2014). Our data indicate that STAVs, viral, or DNA damage generated self-dsDNA species within a dying cell, or CDNs can greatly enhance the immunogenicity of tumor cells. The use of STAVs to treat cancer, either directly into tumors or carried inside tumor cells, or as vaccine adjuvants may provide powerful anti-tumor therapies. Moreover, the generation of CDNs within a tumor cell may also provide a valid approach to stimulate anti-tumor T cell responses. It is possible to consider that loss of cGAS (CDNs) and/or STING in tumors may help explain resistance to radiation treatment, which exerts its anti-tumor effects in part through the stimulation of STING-dependent immune responses (Harding et al., 2017; Mackenzie et al., 2017). Thus loss of STING may help explain resistance not only to radiation treatment but also to the immunological benefits of chemotherapy. Suppression of STING signaling may also help explain mechanisms of DNA-virus-mediated oncolysis. Activators of STING signaling (STAVs) may be useful for the immunotreatment of cancer following intratumoral inoculation, similar to strategies using CDNs (Woo et al., 2014). Alternatively, or in combination, tumor cells loaded with STAVs may also be a potent mechanism for stimulating anti-tumor T cell responses. Reconstitution of cGAS-STING signaling in cancer cells may increase the efficacy of a diversity of immuno-oncology-related tumor treatments in addition to the use of checkpoint inhibitors (Rivera Vargas et al., 2017). Indeed, it is plausible that complementary treatments consisting of a variety of methods to augment STING signaling may have significant benefits for the treatment of cancer. Finally, our data provide a plausible explanation for how phagocytes are able to distinguish between an uninfected versus a microbial-infected cell.

STAR★METHODS

Detailed methods are provided in the online version of this paper and include the following:

- KEY RESOURCES TABLE
- CONTACT FOR REAGENT AND RESOURCE SHARING
- EXPERIMENTAL MODEL AND SUBJECT DETAILS
 - Mice
 - In Vivo Tumor Models
 - Cell Lines
 - Primary Cell Cultures
- METHOD DETAILS

- STING-Dependent Adjuvants (STAVs)
- In Vitro Phagocytosis
- Gene Array Analysis
- Quantitative Real-Time PCR (qPCR)
- Cell Death Induction and Analysis
- Transfection Efficiency
- Antigen Presentation Assay
- Immunofluorescence Staining
- Liquid Chromatography Mass Spectrometry (LC-MS) Analysis
- In Vivo Imaging of Mice
- OVA Specific CD8⁺ T Cell Analysis and Ifn γ ELISA
- IFN γ ELISPOT Assay
- DimerX Analysis
- QUANTIFICATION AND STATISTICAL ANALYSES
- DATA AND SOFTWARE AVAILABILITY

SUPPLEMENTAL INFORMATION

Supplemental Information includes seven figures and three tables and can be found with this article online at <https://doi.org/10.1016/j.ccell.2018.03.027>.

ACKNOWLEDGMENTS

We thank Ms. Delia Gutman and Ms. Auristela Rivera for mouse maintaining and genotyping; Dr. Hyeilim Park for assisting with flow cytometry analysis; Dr. Eli Gilboa for providing B16 OVA cells; Dr. Ralph R. Weichselbaum at University of Chicago for providing B16 SIY cells; Biostatistics & Bioinformatics Shared Resource at Sylvester Comprehensive Cancer Center for gene array analysis; Dr. Larry Sallans at University of Cincinnati for mass spectrometry analysis. This study was supported by an NIH grant (5R01AI079336-10).

AUTHOR CONTRIBUTIONS

J.A. carried out the majority of experiments and data analysis; T.X. participated in designing STAVs and mass spectrometry analysis; A.R.C. performed flow cytometry analysis and helped with animal experiments; D.B. performed BALB/c metastasis experiments; and G.N.B. wrote the manuscript and supervised the study.

DECLARATION OF INTERESTS

The authors have a patent related to this work. Application number: 15/120,694/ Undergoing Examination.

Received: June 28, 2017
 Revised: January 4, 2018
 Accepted: March 28, 2018
 Published: April 26, 2018

REFERENCES

Ablasser, A., Goldeck, M., Cavlar, T., Deimling, T., Witte, G., Rohl, I., Hopfner, K.P., Ludwig, J., and Hornung, V. (2013). cGAS produces a 2'-5'-linked cyclic dinucleotide second messenger that activates STING. *Nature* **498**, 380–384.

Ahn, J., and Barber, G.N. (2014). Self-DNA, STING-dependent signaling and the origins of autoinflammatory disease. *Curr. Opin. Immunol.* **31**, 121–126.

Ahn, J., Gutman, D., Saijo, S., and Barber, G.N. (2012). STING manifests self DNA-dependent inflammatory disease. *Proc. Natl. Acad. Sci. USA* **109**, 19386–19391.

Ahn, J., Ruiz, P., and Barber, G.N. (2014a). Intrinsic self-DNA triggers inflammatory disease dependent on STING. *J. Immunol.* **193**, 4634–4642.

Ahn, J., Xia, T., Konno, H., Konno, K., Ruiz, P., and Barber, G.N. (2014b). Inflammation-driven carcinogenesis is mediated through STING. *Nat. Commun.* **5**, 5166.

Barber, G.N. (2014). STING-dependent cytosolic DNA sensing pathways. *Trends Immunol.* **35**, 88–93.

Barber, G.N. (2015). STING: infection, inflammation and cancer. *Nat. Rev. Immunol.* **15**, 760–770.

Belz, G.T., Smith, C.M., Eichner, D., Shortman, K., Karupiah, G., Carbone, F.R., and Heath, W.R. (2004). Cutting edge: conventional CD8 alpha+ dendritic cells are generally involved in priming CTL immunity to viruses. *J. Immunol.* **172**, 1996–2000.

Corrales, L., Glickman, L.H., McWhirter, S.M., Kanne, D.B., Sivick, K.E., Katibah, G.E., Woo, S.R., Lemmens, E., Banda, T., Leong, J.J., et al. (2015). Direct activation of STING in the tumor microenvironment leads to potent and systemic tumor regression and immunity. *Cell Rep.* **11**, 1018–1030.

Deng, L., Liang, H., Xu, M., Yang, X., Burnette, B., Arina, A., Li, X.D., Mauceri, H., Beckett, M., Darga, T., et al. (2014). STING-dependent cytosolic DNA sensing promotes radiation-induced type I interferon-dependent antitumor immunity in immunogenic tumors. *Immunity* **41**, 843–852.

Diamond, M.S., Kinder, M., Matsushita, H., Mashayekhi, M., Dunn, G.P., Archambault, J.M., Lee, H., Arthur, C.D., White, J.M., Kalinke, U., et al. (2011). Type I interferon is selectively required by dendritic cells for immune rejection of tumors. *J. Exp. Med.* **208**, 1989–2003.

Dou, Z., Ghosh, K., Vizioli, M.G., Zhu, J., Sen, P., Wangenstein, K.J., Simithy, J., Lan, Y., Lin, Y., Zhou, Z., et al. (2017). Cytoplasmic chromatin triggers inflammation in senescence and cancer. *Nature* **550**, 402–406.

Fuertes, M.B., Kacha, A.K., Kline, J., Woo, S.R., Kranz, D.M., Murphy, K.M., and Gajewski, T.F. (2011). Host type I IFN signals are required for antitumor CD8+ T cell responses through CD8[alpha]+ dendritic cells. *J. Exp. Med.* **208**, 2005–2016.

Gajewski, T.F., Schreiber, H., and Fu, Y.X. (2013). Innate and adaptive immune cells in the tumor microenvironment. *Nat. Immunol.* **14**, 1014–1022.

Galluzzi, L., Buqué, A., Kepp, O., Zitvogel, L., and Kroemer, G. (2015). Immunological effects of conventional chemotherapy and targeted anticancer agents. *Cancer Cell* **28**, 690–714.

Gao, D., Li, T., Li, X.D., Chen, X., Li, Q.Z., Wight-Carter, M., and Chen, Z.J. (2015). Activation of cyclic GMP-AMP synthase by self-DNA causes autoimmune diseases. *Proc. Natl. Acad. Sci. USA* **112**, 5699–5705.

Harding, S.M., Benci, J.L., Irianto, J., Discher, D.E., Minn, A.J., and Greenberg, R.A. (2017). Mitotic progression following DNA damage enables pattern recognition within micronuclei. *Nature* **548**, 466–470.

Heiber, J.F., and Barber, G.N. (2011). Vesicular stomatitis virus expressing tumor suppressor p53 is a highly attenuated, potent oncolytic agent. *J. Virol.* **85**, 10440–10450.

Ishikawa, H., and Barber, G.N. (2008). STING is an endoplasmic reticulum adaptor that facilitates innate immune signalling. *Nature* **455**, 674–678.

Ishikawa, H., Ma, Z., and Barber, G.N. (2009). STING regulates intracellular DNA-mediated, type I interferon-dependent innate immunity. *Nature* **461**, 788–792.

Kawane, K., Fukuyama, H., Kondoh, G., Takeda, J., Ohsawa, Y., Uchiyama, Y., and Nagata, S. (2001). Requirement of DNase II for definitive erythropoiesis in the mouse fetal liver. *Science* **292**, 1546–1549.

Kono, H., and Rock, K.L. (2008). How dying cells alert the immune system to danger. *Nat. Rev. Immunol.* **8**, 279–289.

Liu, Y., Jesus, A.A., Marrero, B., Yang, D., Ramsey, S.E., Sanchez, G.A.M., Tenbrock, K., Wittkowski, H., Jones, O.Y., Kuehn, H.S., et al. (2014). Activated STING in a vascular and pulmonary syndrome. *N. Engl. J. Med.* **371**, 507–518.

Ma, Y., Adjemian, S., Mattarollo, S.R., Yamazaki, T., Aymeric, L., Yang, H., Portela Catani, J.P., Hannani, D., Duret, H., Steegh, K., et al. (2013). Anticancer chemotherapy-induced intratumoral recruitment and differentiation of antigen-presenting cells. *Immunity* **38**, 729–741.

Mackenzie, K.J., Carroll, P., Martin, C.A., Murina, O., Fluteau, A., Simpson, D.J., Olova, N., Sutcliffe, H., Rainger, J.K., Leitch, A., et al. (2017). cGAS surveillance of micronuclei links genome instability to innate immunity. *Nature* **548**, 461–465.

- Marichal, T., Ohata, K., Bedoret, D., Mesnil, C., Sabatel, C., Kobiyama, K., Lekeux, P., Coban, C., Akira, S., Ishii, K.J., et al. (2011). DNA released from dying host cells mediates aluminum adjuvant activity. *Nat. Med.* *17*, 996–1002.
- McIlroy, D., Tanaka, M., Sakahira, H., Fukuyama, H., Suzuki, M., Yamamura, K., Ohsawa, Y., Uchiyama, Y., and Nagata, S. (2000). An auxiliary mode of apoptotic DNA fragmentation provided by phagocytes. *Genes Dev.* *14*, 549–558.
- Nagata, S., Nagase, H., Kawane, K., Mukae, N., and Fukuyama, H. (2003). Degradation of chromosomal DNA during apoptosis. *Cell Death Differ.* *10*, 108–116.
- Nagata, S., and Tanaka, M. (2017). Programmed cell death and the immune system. *Nat. Rev. Immunol.* *17*, 333–340.
- Pfirschke, C., Engblom, C., Rickelt, S., Cortez-Retamozo, V., Garris, C., Pucci, F., Yamazaki, T., Poirier-Colame, V., Newton, A., Redouane, Y., et al. (2016). Immunogenic chemotherapy sensitizes tumors to checkpoint blockade therapy. *Immunity* *44*, 343–354.
- Rivera Vargas, T., Benoit-Lizon, I., and Apetoh, L. (2017). Rationale for stimulator of interferon genes-targeted cancer immunotherapy. *Eur. J. Cancer* *75*, 86–97.
- Rodero, M.P., and Crow, Y.J. (2016). Type I interferon-mediated monogenic autoinflammation: the type I interferonopathies, a conceptual overview. *J. Exp. Med.* *213*, 2527–2538.
- Russell, S.J., and Peng, K.W. (2017). Oncolytic virotherapy: a contest between apples and oranges. *Mol. Ther.* *25*, 1107–1116.
- Smith, C.M., Belz, G.T., Wilson, N.S., Villadangos, J.A., Shortman, K., Carbone, F.R., and Heath, W.R. (2003). Cutting edge: conventional CD8 alpha+ dendritic cells are preferentially involved in CTL priming after footpad infection with herpes simplex virus-1. *J. Immunol.* *170*, 4437–4440.
- Woo, S.R., Fuertes, M.B., Corrales, L., Spranger, S., Furdyna, M.J., Leung, M.Y., Duggan, R., Wang, Y., Barber, G.N., Fitzgerald, K.A., et al. (2014). STING-dependent cytosolic DNA sensing mediates innate immune recognition of immunogenic tumors. *Immunity* *41*, 830–842.
- Xia, T., Konno, H., Ahn, J., and Barber, G.N. (2016a). Deregulation of STING signaling in colorectal carcinoma constrains DNA damage responses and correlates with tumorigenesis. *Cell Rep.* *14*, 282–297.
- Xia, T., Konno, H., and Barber, G.N. (2016b). Recurrent loss of STING signaling in melanoma correlates with susceptibility to viral oncolysis. *Cancer Res.* *76*, 6747–6759.
- Yatim, N., Cullen, S., and Albert, M.L. (2017). Dying cells actively regulate adaptive immune responses. *Nat. Rev. Immunol.* *17*, 262–275.
- Zitvogel, L., Galluzzi, L., Kepp, O., Smyth, M.J., and Kroemer, G. (2015). Type I interferons in anticancer immunity. *Nat. Rev. Immunol.* *15*, 405–414.

Fibrinogen-like Protein 1 Is a Major Immune Inhibitory Ligand of LAG-3

Jun Wang,¹ Miguel F. Sanmamed,¹ Ila Datar,² Tina Tianjiao Su,¹ Lan Ji,¹ Jingwei Sun,¹ Ling Chen,³ Yusheng Chen,⁴ Gefeng Zhu,¹ Weiwei Yin,⁵ Linghua Zheng,¹ Ting Zhou,¹ Ti Badri,¹ Sheng Yao,¹ Shu Zhu,¹ Agedi Boto,^{1,2} Mario Sznol,⁶ Ignacio Melero,⁷ Dario A.A. Vignali,^{8,9} Kurt Schalper,² and Lieping Chen^{1,3,6,10,*}

¹Department of Immunobiology, Yale University, New Haven, CT 06511, USA

²Department of Pathology, Yale University, New Haven, CT 06510, USA

³Immunotherapy Institute, Fujian Medical University, Fuzhou, Fujian 350108, China

⁴Provincial Clinical Medical College, Fujian Medical University, Fuzhou, Fujian 350108, China

⁵Key Laboratory for Biomedical Engineering of Ministry of Education, College of Biomedical Engineering and Instrument Science, Zhejiang University, Hangzhou 310027, China

⁶Department of Medicine (Medical Oncology), Yale University, New Haven, CT 06510, USA

⁷Department of Immunology and Immunotherapy, University of Navarra, Pamplona 31008, Spain

⁸Department of Immunology, University of Pittsburgh, Pittsburgh, PA 15213, USA

⁹Tumor Microenvironment Center, UPMC Hillman Cancer Center, Pittsburgh, PA 15232, USA

¹⁰Lead Contact

*Correspondence: lieping.chen@yale.edu

<https://doi.org/10.1016/j.cell.2018.11.010>

SUMMARY

Lymphocyte-activation gene 3 (LAG-3) is an immune inhibitory receptor, with major histocompatibility complex class II (MHC-II) as a canonical ligand. However, it remains controversial whether MHC-II is solely responsible for the inhibitory function of LAG-3. Here, we demonstrate that fibrinogen-like protein 1 (FGL1), a liver-secreted protein, is a major LAG-3 functional ligand independent from MHC-II. FGL1 inhibits antigen-specific T cell activation, and ablation of FGL1 in mice promotes T cell immunity. Blockade of the FGL1-LAG-3 interaction by monoclonal antibodies stimulates tumor immunity and is therapeutic against established mouse tumors in a receptor-ligand inter-dependent manner. FGL1 is highly produced by human cancer cells, and elevated FGL1 in the plasma of cancer patients is associated with a poor prognosis and resistance to anti-PD-1/B7-H1 therapy. Our findings reveal an immune evasion mechanism and have implications for the design of cancer immunotherapy.

INTRODUCTION

Lymphocyte-activation gene 3 (LAG-3, CD223) is a transmembrane protein primarily found on activated T cells (Anderson et al., 2016; Andrews et al., 2017; Triebel et al., 1990). LAG-3 protein consists of four extracellular immunoglobulin (Ig)-like domains (D1–D4) with high homology to CD4 (Triebel et al., 1990). LAG-3 expression can be upregulated by interleukin (IL)-2 and IL-12 on activated T cells (Annunziato et al., 1996, 1997; Bruniquel et al., 1998), where it mainly functions as a receptor that delivers inhibitory signals (Huard et al., 1994, 1996;

Workman et al., 2002a). LAG-3 negatively regulates the proliferation, activation, effector function, and homeostasis of both CD8⁺ and CD4⁺ T cells, as shown in LAG-3 knockout mice and antibody studies (Huard et al., 1994; Workman et al., 2002a, 2002b, 2004; Workman and Vignali, 2003, 2005). LAG-3 may represent an “exhaustion” marker for CD8⁺ T cells similar to PD-1 in response to repetitive antigen stimulation in chronic viral infections or cancers (Blackburn et al., 2009; Chihara et al., 2018; Grosso et al., 2007, 2009; Matsuzaki et al., 2010; Williams et al., 2017). Additionally, LAG-3 is also constitutively expressed on a subset of regulatory T cells and contributes to their suppressive function (Camisaschi et al., 2010; Gagliani et al., 2013; Huang et al., 2004). Currently, monoclonal antibodies (mAbs) that block the interaction of LAG-3 with its canonical ligand, MHC-II, are being evaluated for their antitumor activity in clinical trials (Anderson et al., 2016; Ascierto et al., 2017; Rotte et al., 2018).

The major ligand that mediates the immune suppressive functions of LAG-3, however, remains controversial. Initial studies by Baixeras et al. (1992) showed an interaction between MHC-II and LAG-3 via a cell-cell adhesion assay, which was further extended by studies indicating LAG-3 fusion protein binding to MHC-II⁺ B cell lines (Huard et al., 1995, 1996). However, there is a lack of direct evidence for the protein-protein interaction between LAG-3 and MHC-II. MHC-II was proposed to interact with LAG-3 through the residues on the membrane-distal, top face of the LAG-3 D1 domain (Huard et al., 1997). Functionally, the MHC-II-CD4 interaction supported helper T cell activation, while overexpression of LAG-3 downregulated antigen-dependent CD4⁺ T cell responses *in vitro* (Workman and Vignali, 2003). However, several mAbs that do not block the binding of LAG-3 to MHC-II nonetheless promoted T cell functions. For example, C9B7W, a specific mAb against the murine LAG-3 D2 domain, enhanced the proliferation and effector functions of T cells *in vitro* and *in vivo* (Workman et al., 2002b, 2004; Workman and Vignali, 2005). This antibody also increased the accumulation and effector function of tumor-specific CD8⁺ T cells in



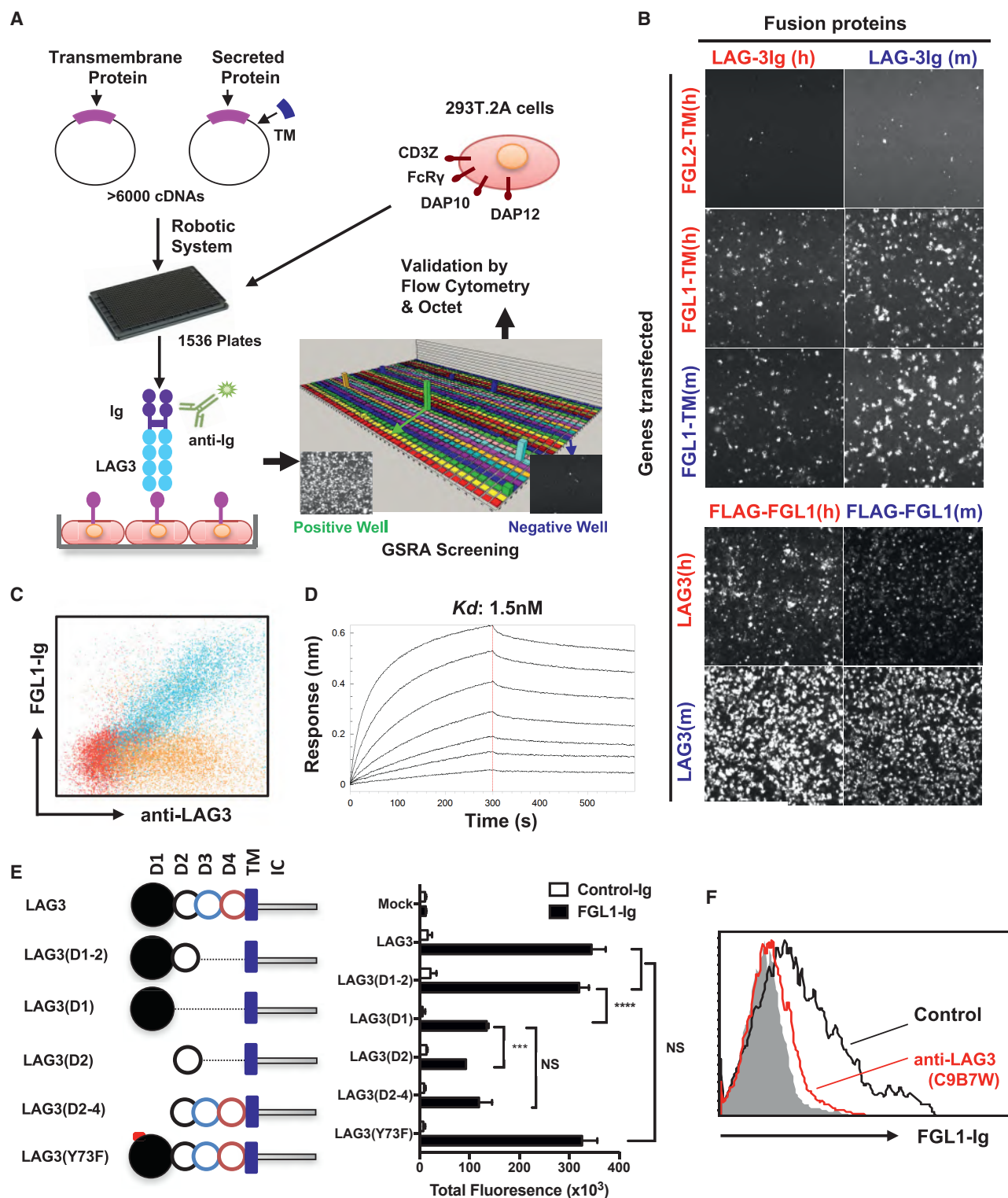


Figure 1. Identification of FGL1 as a Binding Partner of LAG-3 in the GSRA System

(A) Schematic representation of the GSRA system. Individual plasmids of genes encoding both transmembrane and secreted proteins were transfected into 293T.2A cells (see STAR Methods and Table S1) in 1,536-well plates. LAG-3-Ig as well as fluorescence labeled anti-Fc mAb were added into each well for rapid detection of LAG-3-Ig binding. Human Fc receptors served as internal positive controls within each plate. Positive hits were confirmed by flow cytometry or Octet bio-layer interferometry. TM, transmembrane domain.

(legend continued on next page)

several tumor models (Grosso et al., 2007; Woo et al., 2012). The effects of C9B7W mAb on T cells are largely similar, if not identical, to those produced by LAG-3 genetic deficiency (Woo et al., 2012; Workman and Vignali, 2005). A recent study also showed that anti-LAG-3 mAb that do not block MHC-II binding could still stimulate T cell activation and anti-tumor activity (Cemerski et al., 2015). Given that LAG-3 also suppresses the function of CD8⁺ T cells and natural killer (NK) cells, which do not interact with MHC-II (Anderson et al., 2016), these studies raise the possibility that the immunological functions of LAG-3 might be mediated via an unknown ligand.

Here, we report that fibrinogen-like protein 1 (FGL1) is a major functional ligand of LAG-3. FGL1 belongs to the fibrinogen family with high amino acid homology to the carboxyl terminus of the fibrinogen beta- and gamma-subunits, but it does not have the characteristic platelet-binding site, cross-linking region, and thrombin-sensitive site necessary for fibrin clot formation (Yamamoto et al., 1993). Under normal physiological conditions, FGL1 protein is primarily secreted from hepatocytes and contributes to its mitogenic and metabolic functions (Demchev et al., 2013; Hara et al., 2001; Li et al., 2010; Liu and Ukomadu, 2008; Yamamoto et al., 1993; Yan et al., 2002). The immunological function of FGL1, however, remains unknown. Our results demonstrate that FGL1 is a major inhibitory ligand for LAG-3, revealing a new mechanism of immune evasion.

RESULTS

FGL1 Is an MHC Class II-Independent High-Affinity Ligand of LAG-3

We employed our genome-scale receptor array (GSRA) technology to search for LAG-3 binding protein(s) using an immunoglobulin (Ig) Fc-tagged LAG-3 extracellular domain fusion protein (LAG-3-Ig) (Figure 1A). The GSRA is a semi-automatic gene expression and detection system for rapidly identifying protein-protein interactions, which has been modified from our previous report (Yao et al., 2011). In this updated system, individual human cDNA encoding transmembrane and secreted proteins (upon addition of a transmembrane domain) were overexpressed on the surface of 293T cells. Several adaptor genes were also expressed in 293T (293T.2A cells) to facilitate protein expression on the cell surface (Figure 1A). An Ig-tagged protein of interest can then be screened for interaction(s) using the

GSRA system in a high throughput fashion by the mix-and-read laser scanning macro-confocal fluorescent plate reader. The current version of the GSRA contains over 90% of annotated genes encoding human transmembrane (~5,600) and secreted (~1,000) proteins (Table S1). FGL1 was identified as a major binding protein for LAG-3-Ig in the GSRA system (Figures 1B and S1A). The FGL1-LAG-3 interaction is conserved across species in both human and mouse (Figure 1B). This interaction was further validated by flow cytometry, as indicated by a linear association between FGL1-Ig and anti-LAG-3 staining on LAG-3⁺ cells (Figure 1C). The FGL1-LAG-3 interaction was shown to have a K_d value of ~1.5 nM by Octet bio-layer interferometry analysis (Figure 1D). Using an SEC650 size exclusion column, the purified recombinant FLAG-tagged FGL1 (FLAG-FGL1) showed an oligomeric state (peak 1-2) and a dimeric peak (peak 3) (Figure S1B), which was validated via size exclusion chromatography with multi-angle light scattering analysis (SEC-MALS, data not shown). We observed stronger binding of the oligomeric forms of FLAG-FGL1 (peak 1-2) than the dimeric form (peak 3) to immobilized LAG-3-Ig in the Octet analysis (Figure S1C). In addition, the slow disassociation rate hints at a stable interaction between FGL1 and LAG-3 in both human and mouse (Figures 1D and S1D). FGL2, a homolog of FGL1 previously implicated in Treg functions (Shevach, 2009), as well as other fibrinogen domain-containing family members such as angiopoietin-related proteins, did not bind LAG-3 (Figure 1B and data not shown), indicating that the FGL1-LAG-3 interaction is highly specific.

FGL1 is composed of a coil-coil domain (CCD) and a fibrinogen-like domain (FD) (Yamamoto et al., 1993). Through domain deletion studies, we demonstrated that the FD, but not CCD, is responsible for LAG-3 binding (Figure S1E). The LAG-3 protein consists of four Ig-like extracellular domains, D1–D4 (Huard et al., 1997; Triebel et al., 1990) (Figure 1E, left). The deletion of the D3–D4 domain in LAG-3 did not affect FGL1 binding, while either D1 or D2 alone partially decreased the binding (Figure 1E, right), suggesting that both D1 and D2 contribute to the FGL1-LAG-3 interaction. A single point mutation (Y73F) in the C' strand of LAG-3 D1 domain was previously shown to disrupt MHC-II binding (Huard et al., 1997; Workman et al., 2002a). However, this mutation did not affect FGL1-Ig binding (Figure 1E, right), indicating that the FGL1-LAG-3 interaction is non-redundant with MHC-II-LAG-3 binding. Furthermore, pre-incubation of

(B) Image of the FGL1-LAG-3 interaction in GSRA system. 293T.2A cells were transfected with human (h) or mouse (m) FGL1-TM or full-length LAG-3 as indicated on the y axis. Human FGL2-TM was included as a negative control. The indicated fusion proteins shown on the x axis were added to the culture to evaluate binding to the transfectants by the cellular detection system (CDS).

(C) Representative flow cytometry dot plot of FGL1-Ig binding to mouse LAG-3⁺ 293T.2A (blue) or mock cells (red). Control Ig binding to mouse LAG-3⁺ 293T.2A is also shown (brown).

(D) Representative Octet sensorgrams showing various amounts of FLAG-tagged mouse FGL1 (starting from 10 μg/mL, 2-fold serial dilutions) binding to immobilized mouse LAG-3-Ig.

(E) Schematic representation of constructs coding full-length mouse LAG-3, LAG-3 Y73F mutant, or LAG-3 with different extracellular domain deletions (left). LAG-3 full-length protein consists of four extracellular Ig domains (D1–D4), the transmembrane domain (TM), and intracellular domain (IC) (left). Quantification of FGL1-Ig binding to 293T.2A cells transfected to express LAG-3 with domain deletion/mutation (right). Data were analyzed by CDS software and presented as the mean ± SEM. ***p < 0.001, ****p < 0.0001, NS, not significant by Student's t test.

(F) FGL1-Ig binding to mouse LAG-3⁺ 293T.2A cells in the presence of control mAb (black line) or anti-LAG-3 (red line) by flow cytometry. Cells stained with control Ig (shadow) served as a negative control.

All data are representative of at least two independent experiments.

See also Figure S1.

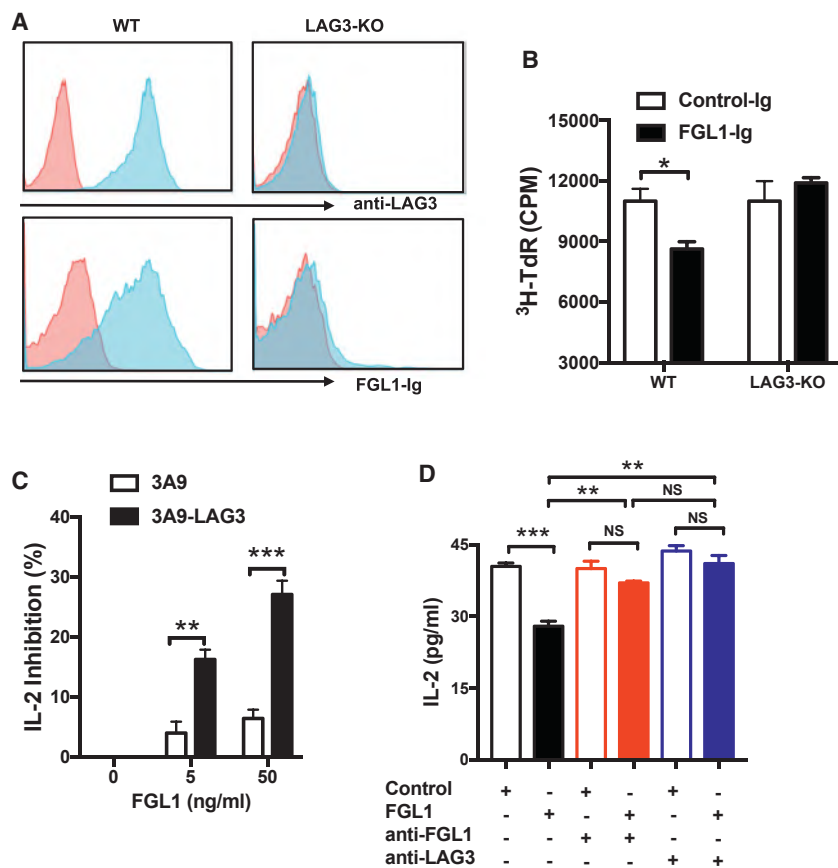


Figure 2. FGL1 Mediates LAG-3-Dependent T Cell Suppression

(A) Splenic T cells from WT or LAG-3-KO mice were activated by immobilized anti-CD3 mAb for 24 hr, stained with anti-LAG-3 mAb or FGL1-Ig fusion protein (blue) or control antibody/Ig (red), and analyzed by flow cytometry.

(B) Splenic T cells from WT or LAG-3-KO mice were activated by immobilized anti-CD3 mAb at suboptimal concentration in the presence of soluble FGL1-Ig or control-Ig (5 μ g/mL) for 3 days before the addition of 3 H-dTR. Thymidine incorporation of proliferated T cells was analyzed 16 hr later.

(C) The 3A9-LAG-3 or parental 3A9 mouse T cell hybridoma cells were co-cultured with LK35.2 B cell line in CellGenix serum free medium in the presence of HEL peptide and the indicated concentrations of FLAG-tagged FGL1. Shown is the normalized % of inhibition on the IL-2 levels in the supernatant at 24 hr normalized to levels with 0 ng/mL FGL1.

(D) The 3A9-LAG-3 mouse T cell hybridoma cells were co-cultured with LK35.2 B cell line in the presence of HEL peptide, FLAG tagged FGL1 (50 ng/mL), anti-FGL1, or anti-LAG-3 mAb (1 μ g/mL). Shown are the IL-2 levels in the supernatant at 24 hr.

Data are representative of at least two independent experiments and are presented as the mean \pm SEM. * p < 0.05, ** p < 0.01; *** p < 0.001, NS, not significant by Student's t test.

See also Figure S2.

LAG-3⁺ 293T cells with C9B7W, an anti-LAG-3 mAb that binds the LAG-3 D2 domain without blocking the FGL1-MHC-II interaction (Andrews et al., 2017; Cemerski et al., 2015; Workman et al., 2002b), led to complete abrogation of FGL1-LAG-3 binding (Figure 1F). Finally, LAG-3⁺ cells stained with MHC-II (I-A^b) fusion protein did not show a significant decrease in binding even in the presence of a 100-fold excess of FGL1-Ig (Figure S1F). Taken together, our results indicate that FGL1 interacts with LAG-3 in an MHC-II-independent manner, and this interaction involves the FGL1 fibrinogen-like domain and the LAG-3 D1-D2 domain.

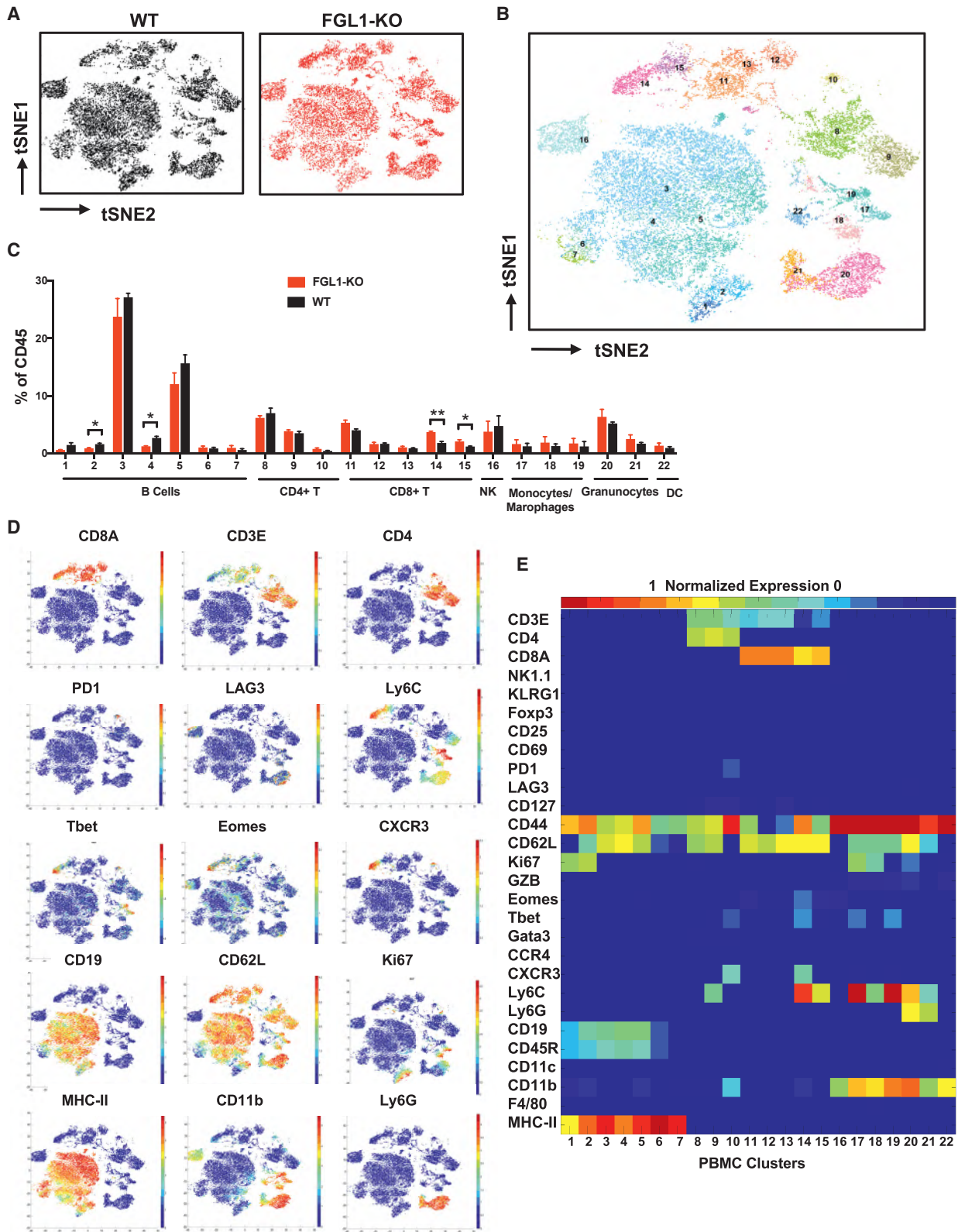
FGL1 Inhibits Antigen-Mediated T Cell Responses via LAG-3 *In Vitro* and *In Vivo*

LAG-3 is not found on resting T cells other than a subset of Tregs but can be upregulated under various antigen stimulation conditions (Baixeras et al., 1992; Triebel et al., 1990; Workman et al., 2002b). FGL1-Ig fusion protein did not bind resting T cells that express minimal LAG-3 levels (data not shown), although it did bind activated T cells from wild-type (WT) but not from LAG-3-KO mice, as determined via flow cytometry analysis (Figure 2A). Inclusion of FGL1-Ig partially suppressed WT splenic T cell proliferation under suboptimal anti-CD3 stimulation, but this suppression was diminished using LAG-3-KO splenocytes (Figure 2B), indicating that the suppressive effect of FGL1-Ig is dependent on LAG-3. Similarly, FGL1 better suppressed the

antigen-specific induction of IL-2 from a murine LAG-3 overexpressing 3A9 T cell line (3A9-LAG-3) in a dose-dependent fashion compared to the parental 3A9 cell line with low endogenous LAG-3 expression (Figure 2C). We generated a mAb specific for mouse FGL1 (clone 177R4) that blocks FGL1-Ig binding to LAG-3⁺ 293T cells in a similar manner to anti-LAG-3 mAb C9B7W (Figures S2A and S2B). Both mAbs abrogated the suppression of FGL1 on IL-2 production from 3A9-LAG-3 cells (Figure 2D). Upon CD8⁺ OT-1 transgenic T cell transfer into syngeneic mice and subsequent immunization with chicken ovalbumin peptide antigen, administration of anti-FGL1 mAb 177R4 significantly promoted antigen-specific OT-1 T cell activation in a manner similar to anti-LAG-3 mAb, as determined by increased plasma levels of tumor necrosis factor alpha (TNF- α) and interferon (IFN)- γ (Figures S2C and S2D). Thus, our results support that FGL1 is an inhibitory ligand of LAG-3.

Fgl1-Deficient Mice Slowly Develop Spontaneous Autoimmune Symptoms

We generated a *Fgl1* gene knockout mouse strain (FGL1-KO) on the C57BL/6 background using an agouti color gene modified mouse ESC line (JM8) (Pettitt et al., 2009). In WT mice, *Fgl1* mRNA was detected in the liver but not in other organs or hematopoietic cells (Figure S3A). Soluble FGL1 was also detected in mouse blood (Figure S3B) as previously reported (Liu and Ukomadu, 2008). In contrast, FGL1 was not detected in the plasma or liver of FGL1-KO mice via specific sandwich ELISA and western blot analysis, respectively (Figures S3B and S3C).



(legend on next page)

FGL1-KO mice have an overall normal appearance, organ size, and litters, indicating that FGL1 does not globally affect the development and growth of mice. However, up to 40% (8/20) of FGL1-KO mice developed spontaneous dermatitis at the age of 8 months or older, showing lymphocyte infiltration in the dermis (Figures S3D and S3E). At 14–16 months of age, 5/8 female, but not male mice, had elevated levels of anti-double-stranded DNA autoantibodies in their plasma compared to WT mice (Figure S3F). These findings are consistent with the role of FGL1 as an immune suppressive molecule. To evaluate overall changes in the immune system of this KO strain, we profiled mouse peripheral blood cells by mass cytometry (CyTOF), a single cell high dimensional analysis tool using 32 metal-conjugated mAbs to determine immune cell lineages as well as functional molecules. A recently described unsupervised clustering method named x-shift was also employed (Samusik et al., 2016). Analysis of the total CD45⁺ hematopoietic cells revealed 22 distinct cell type or subsets (clusters), with small but significant increases in central memory-like CD8⁺ T cells subsets (cluster 14–15, CD44⁺ CD62L⁺ Ly6C⁺ CD127^{med} Tbet⁺ Eomes⁺) and decreases in two B cell subsets (cluster 2 and 4) (Figures 3A–3E). All other clusters were similar in FGL1-KO compared to WT mice (Figures 3A–3E). There were no major differences in T cells or myeloid cell subsets in peripheral lymphoid tissues including the spleen or liver (data not shown).

These findings indicate that endogenous FGL1 does not affect mouse development and growth, although it may participate in regulating autoimmunity and immune homeostasis in aged mice.

Fgl1 Silencing Promotes T Cell Immunity against Tumor Growth in Mouse Models

FGL1-KO and LAG-3-KO mice were inoculated subcutaneously (s.c.) with syngeneic murine MC38 colon cancer cells. Similar to LAG-3-KO mice, FGL1-KO mice showed significantly slower tumor growth in comparison to WT mice (Figure 4A). Whereas all of the WT mice reached an endpoint (average mean tumor diameter of 15 mm) within 60 days, ~50% of FGL1-KO or LAG-3-KO mice were tumor-free beyond 200 days upon MC38 inoculation (Figure 4B). Similarly, both anti-FGL1 and anti-LAG-3 mAbs significantly controlled tumor growth of established MC38 murine colon (Figure 4C) and Hepa1-6 murine liver cell lines inoculated s.c. in syngeneic C57BL/6 mice (Figure S4A). In contrast, the anti-FGL1 and anti-LAG-3 mAb antitumor effect was abrogated in Rag1-KO C57BL/6 mice, which are devoid of T and B cells (Figure 4D). Consistent with these findings, depletion of either CD8⁺ or CD4⁺ T cells by specific mAbs completely eliminated the anti-tumor effect of both anti-FGL1 and anti-LAG-3 mAb in the MC38 tumor model, indicating that the anti-tumor effect of these mAbs is dependent on both CD8⁺ and CD4⁺ T cells (Figure S4B).

To exclude the possibility that additional ligands for LAG-3 are functionally redundant to FGL1 and contribute to the anti-tumor effect of the anti-LAG-3 mAb, we tested the effect of anti-LAG-3 mAb in FGL1-KO mice. While the anti-LAG-3 mAb suppressed MC38 tumor growth in WT mice, this anti-tumor effect was completely eliminated in FGL1-KO mice (Figure 4E). The effect of anti-FGL1 was also dependent on LAG-3, as this mAb did not have additive effects on tumor growth in LAG-3-KO mice (Figure 4F). Therefore, the anti-tumor effect of anti-FGL1 mAb is dependent on LAG-3, whereas the effect of anti-LAG-3 relies on FGL1 but not MHC-II or other LAG-3 ligands. Altogether, our findings support FGL1 as a major ligand for LAG-3 to induce T cell suppressive function and immune evasion.

The deficiency of FGL1 significantly reduced MC38 tumor growth while spleen size and the number of lymphocytes in either tumor-draining or non-tumor-draining lymph nodes remained similar (Figure S4C). Analysis of tumor-infiltrating leukocytes (TIL) in tumors excised on day 17 from FGL1-KO and WT mice by mass cytometry revealed a significant increase of CD45⁺ leukocytes in FGL1-KO tumors (Figure S4D). In 22 clusters across CD45⁺ cells (Figures 5A and 5B), we found a significant expansion of CD44⁺ CD62L⁻ PD-1⁺ Gata3⁺ effector memory-like CD4⁺ TIL (cluster 2 and 3), as well as CD44⁺ Ly6C⁺ memory-like CD8⁺ (DeLong et al., 2018; Pihlgren et al., 1996; Walunas et al., 1995) TIL populations (clusters 8–10) in FGL1-KO tumors (Figures 5B–5E). In contrast, Treg (cluster 1), NK (cluster 11), or B cells (cluster 14) did not change significantly (Figures 5B–5E). Interestingly, a natural killer T (NKT) population (cluster 12) was highly expanded in the FGL1-KO tumors, in comparison with a significant decrease of F4/80⁺ CD11b⁺ MHC-II⁺ CD11c^{med} tumor-associated macrophages (cluster 15) (Figures 5C–5E). Confirming this data, we also observed a significant increase in the absolute number of leukocytes (CD45⁺ cells), CD8⁺, and CD4⁺ TIL per mg of tumor tissues in mice treated with anti-FGL1 or anti-LAG-3 mAbs compared to control treated mice (Figure S4E). Furthermore, there was a significant increase in activation or functional markers, such as CD69, Ly6C, granzyme B (GZB), CD4, and FAS, in CD4⁺ or CD8⁺ TIL from anti-FGL1 or anti-LAG-3 treated mice (Figure S4F). Our results indicate that silencing the FGL1-LAG-3 interaction by either genetic knockout or antibody blockade promotes tumor immunity by stimulating T cell expansion and activation preferentially in the tumor microenvironment.

FGL1 Is Upregulated in Human Cancers

FGL1 mRNA and protein expression is largely limited to the liver and pancreas of human normal tissues according to the BioGPS tissue microarray database and proteome analysis (Kim et al., 2014) (Figure S5A). Meta-analysis of the OncoPrint databases revealed the upregulation of *FGL1* mRNA in human solid tumors including lung cancer, prostate cancer, melanoma, and

Figure 3. Immune Cell Phenotyping of FGL1-KO Mice

- (A) Density t-SNE plots of an equal number of CD45⁺ compartment in the peripheral blood from WT and FGL1-KO mice (n = 3).
 (B) t-SNE plot of CD45⁺ compartment overlaid with color-coded clusters.
 (C) Frequency of clusters grouped by indicated immune cell subsets. Data were shown as the mean ± SEM. *p < 0.05; **p < 0.01 by unpaired t test.
 (D) t-SNE plot of CD45⁺ compartment overlaid with the expression of selected markers.
 (E) Heatmap displaying normalized marker expression of each immune cluster.
 See also Figure S3.

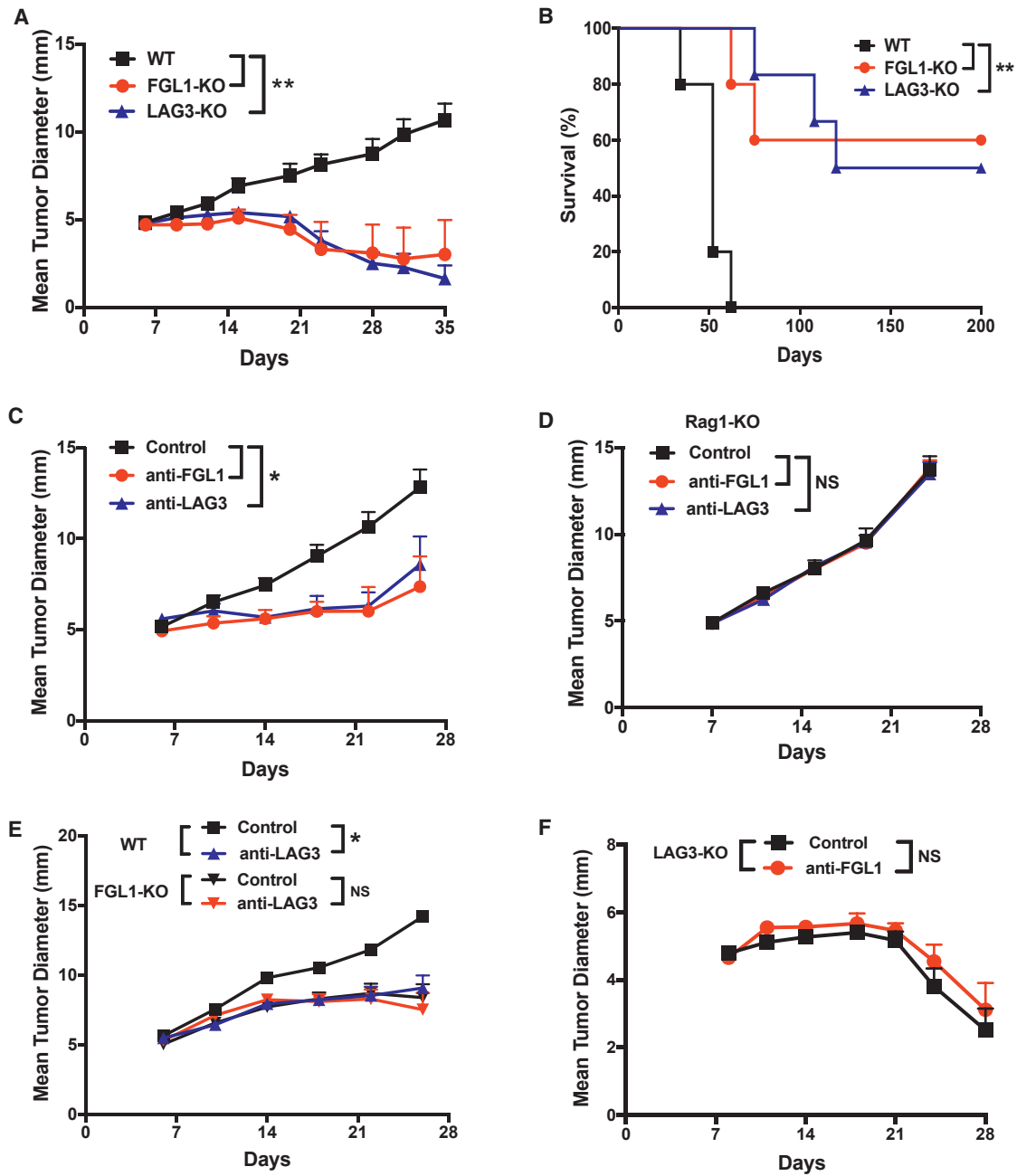


Figure 4. Ablation of the FGL1-LAG-3 Interaction Inhibits Tumor Growth in Mouse Models

(A and B) FGL1-KO, LAG-3-KO, or WT littermates were inoculated with MC38 cells (0.5×10^6 /mouse). The mean tumor diameters (A) and survival (B) of mice in each group ($n = 6$) are shown.

(C and D) B6 (C) or Rag1-KO (D) mice were inoculated with MC38 cells (0.5×10^6 /mouse) at day 0 and treated with anti-FGL1, anti-LAG-3, or control mAbs every 4 days from day 6 to day 18. The mean tumor diameters in each group ($n = 6$) are shown.

(E) WT or FGL1-KO mice were inoculated with MC38 cells and were treated with anti-LAG-3 or control mAb as in (C). The mean tumor diameters in each group ($n = 6-8$) are shown.

(F) LAG-3-KO mice were inoculated with MC38 cells and were treated with anti-FGL1 ($n = 8$) or control mAb ($n = 7$) as in (C). The mean tumor diameters in each group are shown.

Data were representative of at least two independent experiments and are shown as the mean \pm SEM. * $p < 0.05$; ** $p < 0.01$; NS, not significant. (A) and (C-F) by two-way ANOVA; (B) by log-rank test.

See also Figure S4.

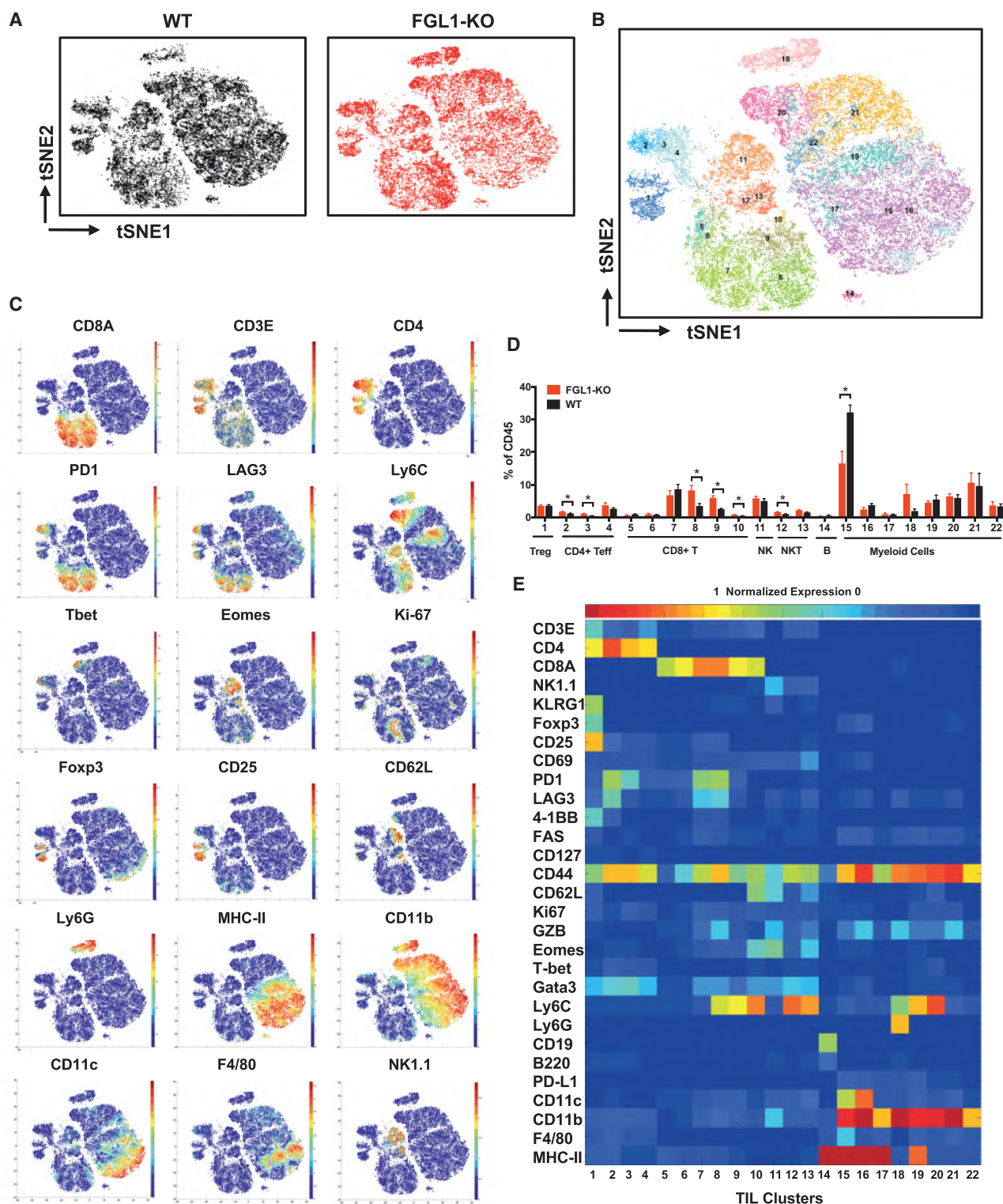


Figure 5. Expansion of Tumor-Infiltrating T Cell Populations in FGL1-KO Mice

(A) Density t-SNE plots of an equal number of CD45⁺ MC38 tumor-infiltrating leukocytes in WT (n = 4) and FGL1-KO (n = 5) mice. Size of unsupervised clusters denotes the relative number of cells in that grouping.

(B) t-SNE plot of tumor infiltrating leukocytes overlaid with color-coded clusters.

(legend continued on next page)

colorectal cancer compared to normal tissues, with the highest percentage of upregulation (8/23, or 35%) in lung cancer datasets, while its expression appeared to be downregulated in pancreas, liver, and head and neck cancers (Figure S5B). Furthermore, *FGL1* is one of the most upregulated genes in The Cancer Genome Atlas (TCGA) database for lung adenocarcinoma (Figure S5C; Table S2). *FGL1* is also significantly upregulated in prostate or breast cancer but is downregulated in liver cancer within this database (Figure S5C).

We established a multiplex quantitative immunofluorescence (QIF) assay to detect FGL1 protein expression on cells and tissues. In addition, a quantitative sandwich ELISA was also established to detect secreted FGL1 in human plasma (see STAR Methods). A 293T line constitutively expressing FGL1 and human tissue samples were utilized to standardize the assay in FFPE preparations and establish the signal detection threshold (Figure S6A). As expected, levels of FGL1 protein were highest in a cell line transfected to express the *FGL1* gene (Figure S6A) and human liver (data not shown), but low or undetectable in mock-transfected cells (Figure S6A) or samples from human testis and skeletal muscle (data not shown). We then evaluated the localized expression of FGL1 in 275 non-small cell lung carcinomas (NSCLC) presented in tissue microarray format (cohort #1, from Yale University, also see Table S3) by simultaneous staining of FGL1 and pan-cytokeratin using multiplex QIF staining. In NSCLC, FGL1 protein was found localized in tumor cells (the pan-cytokeratin-positive) with minimal expression in the stromal compartment (the pan-cytokeratin-negative) (Figure 6A) and no expression in paired normal lung tissues (Figure S6B). Tissue FGL1 levels showed a continuous distribution in this cohort and ~15% of specimens from NSCLC patients showed elevated expression (Figure 6B) which was associated with a significantly decreased 5-year overall survival (Figure 6C). Interestingly, there was no association between FGL1 and B7-H1 (PD-L1) expression levels, but high FGL1 in tumor tissue was significantly associated with high LAG-3 levels (Figure S6C). In addition, we also found significantly higher plasma FGL1 levels in NSCLC patients compared to healthy donors in two independent cohorts (see also Table S3): cohort #2 (n = 18) from University of Navarra, Pamplona, Spain (Figure 6D) and cohort #3 (n = 56) from Fujian Medical University, Fuzhou, China (Figure S6D). Of note, there was no difference in plasma FGL1 levels among NSCLC patients with or without metastasis as well as liver injury (Figure S6E). Furthermore, in cohort #2, we found a positive association of tumor FGL1 QIF scores and plasma FGL1 levels (data not shown). Our findings indicate that FGL1 is upregulated in human cancers, especially in NSCLC.

High Plasma FGL1 Is Associated with Poor Outcomes in Patients with Anti-PD Therapy

To test if FGL1 acts independently from the B7-H1-PD-1 pathway to suppress tumor immunity, we evaluated the associ-

ation between the baseline plasma FGL1 levels and the efficacy of the B7-H1-PD-1 blockade therapy (anti-PD therapy) in metastatic NSCLC patients. In cohort #2 (see also Tables S3 and S4), we found that higher plasma FGL1 levels were associated with worse overall survival in NSCLC patients treated with anti-PD therapy (hazard ratio [HR] = 6.8, 95% confidence interval [CI] = 1.1–42 and p value = 0.04) (Figure 6E). Similar results were observed in an independent cohort (cohort #4, from Yale University, see also Tables S3 and S4) of metastatic melanoma patients (n = 21) treated with anti-PD-1 mAbs (HR = 7.9; 95% CI = 2.2–27.4 and p value <0.001) (Figure 6F). Our results suggest that the FGL1-LAG-3 interaction is independent from the B7-H1-PD-1 pathway and could potentially contribute to the resistance of anti-PD therapy in human cancers.

We further tested the role of the anti-FGL1 or anti-LAG-3 in the presence of the B7-H1-PD-1 pathway blockade using the MC38 tumor model. Mice were inoculated s.c. with MC38, and established tumors at day 6 were treated with the mAbs. When applied individually, anti-FGL1, anti-LAG-3, or anti-B7-H1 mAb slowed tumor growth and minimally prolonged survival (Figure 6G). However, anti-FGL1 or anti-LAG-3 mAb in combination with anti-B7-H1 mAb significantly improved survival (Figure 6G) and decreased tumor burden (Figure 6H) compared to single mAb treatment. A significant proportion of mice (>30% of mice) treated with the combination therapy were free of tumor for over 150 days (Figure 6G). Our results suggest that the FGL1-LAG-3 pathway is an independent tumor immune evasion mechanism, and blockade of this interaction may synergize with anti-PD therapy.

DISCUSSION

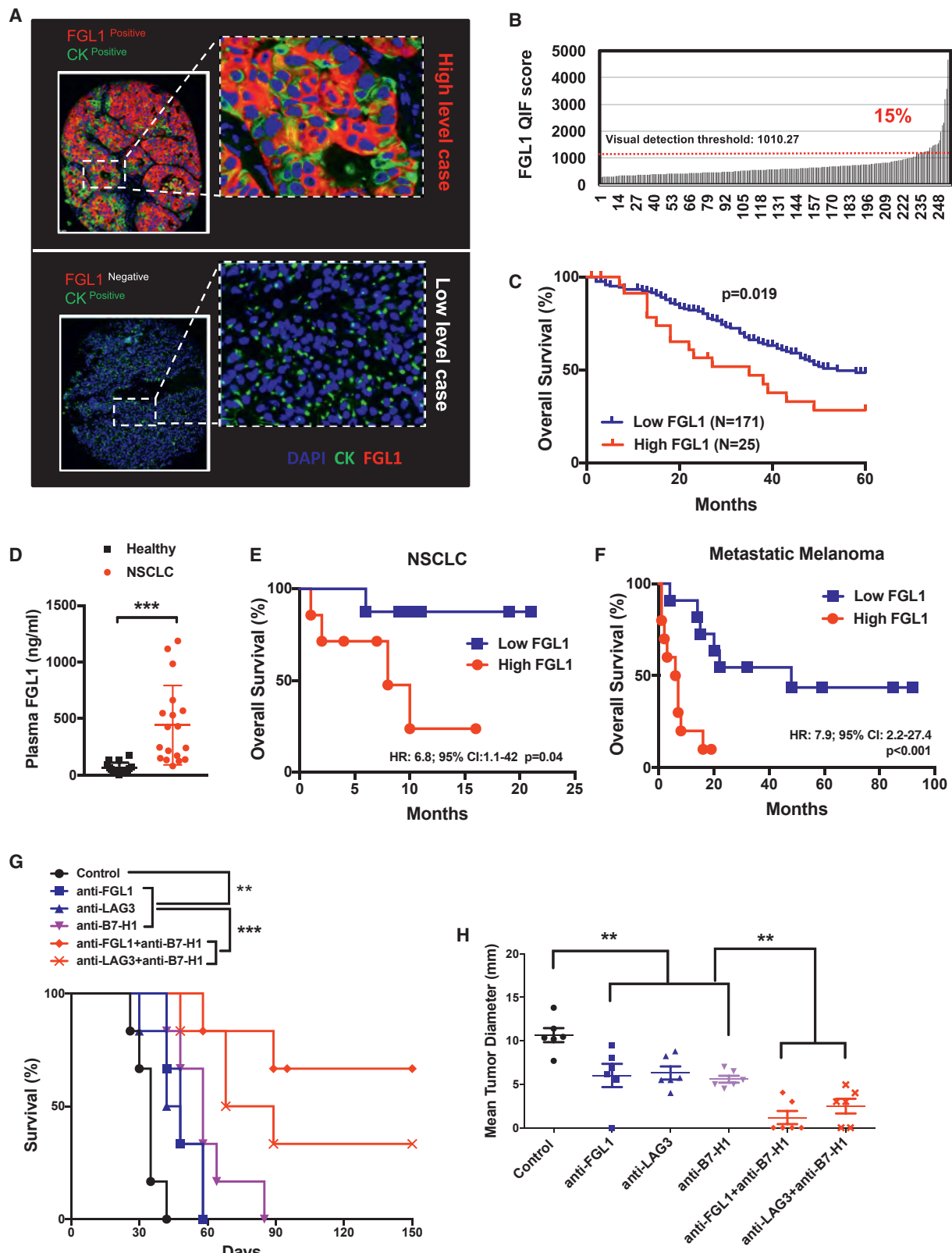
In this study, we have identified and characterized FGL1 as a major ligand of LAG-3 that is responsible for its T cell inhibitory function in a receptor-ligand interdependent manner both *in vitro* and *in vivo*. Genetic ablation or mAbs blocking the FGL1-LAG-3 interaction enhanced T cell responses and promoted anti-tumor immunity. With limited expression in the majority of normal tissues, FGL1 is upregulated in several human cancers and is associated with a poor prognosis and therapeutic outcome. Together, our findings support the FGL1-LAG-3 pathway as an immune escape mechanism and a potential target for cancer immunotherapy.

Physiological functions of FGL1 are not well understood. Soluble FGL1 protein can be detected in the blood plasma of healthy donors at the ng/mL level, while *FGL1* mRNA can only be detected in liver and pancreas across a large panel of normal tissues (Figure S5A), suggesting that FGL1 may be produced by the liver and/or pancreas and subsequently released into the bloodstream. In addition to the reported function in hepatocyte regeneration and metabolism, our findings reveal for the first time a prominent role of FGL1 in the negative regulation of

(C) t-SNE plot of tumor infiltrating leukocytes overlaid with the expression of selected markers.

(D) Frequency of clusters grouped by indicated immune cell subsets. Data were shown as the mean \pm SEM. *p < 0.05 by unpaired t test.

(E) Heatmap displaying normalized marker expression of each immune cluster. See also Figure S4.



(legend on next page)

inflammatory immune responses. FGL1-KO mice spontaneously developed several autoimmune symptoms including dermatitis and anti-dsDNA autoantibodies (Figures S3D–S3F). However, these symptoms developed only in the aged but not in newborn or young adult mice, indicating that endogenous FGL1 is not a major regulator for self-tolerance but may suppress environmentally induced inflammation. Interestingly, liver is considered an immune-privileged organ, as allogeneic liver transplants can survive longer without immune suppressive agents (Horst et al., 2016). The underlying mechanism for this immune privilege, however, is largely unknown. We did not observe significant liver inflammation in aged FGL1-KO mice (data not shown), perhaps due to a lack of LAG-3 expression on resting T cells in the liver. While FGL1 may play a local role in maintaining the tolerogenic environment of the liver, its secretion as a soluble factor allows for potential cross-talk between the liver and other peripheral tissues that may help fine-tune systemic inflammation. This normal physiological function of FGL1 may be hijacked by several solid tumors that increase FGL1 expression to suppress local anti-tumor immunity. In this context, immune evasion may be mediated by high levels of FGL1 in the tumor microenvironment through the interaction with LAG-3 specifically expressed on tumor-infiltrating T cells. Our results in mouse tumor models indicate a preferential activation of T cell immunity in the tumor microenvironment upon FGL1-LAG-3 blockade while the effect of this blockade in systemic immune suppression is minimal (unpublished data), suggesting a major role for FGL1 in immune suppression of the tumor microenvironment.

Our results support FGL1 as a major ligand for the T cell inhibitory function of LAG-3. First, FGL1-LAG-3 represents a high-affinity interaction that is specific and physiological, as indicated by fusion protein binding experiments involving primary T cells from WT or *Lag3*-deficient mice. Second, FGL1 mAb has similar effects to anti-LAG-3 on the stimulation of T cell responses and antitumor effect in our *in vitro* and *in vivo* experiments. Furthermore, anti-FGL1 mAb has no antitumor effect in LAG-3-deficient mice while anti-LAG-3 mAb likewise loses efficacy in *Fgl1*-deficient mice. Finally, our preliminary studies indicate that adult *Fgl1*-deficient mice are also prone to the induction of autoimmune diseases (unpublished data), a phenotype similar to LAG-3-deficient mice (Bettini et al., 2011; Woo et al., 2012).

To date, at least four different proteins have been reported to interact with LAG-3 including MHC-II, galectin-3, LSECtin, and α -synuclein. Galectin-3 and LSECtin have potential roles in T cell regulation, while α -synuclein is possibly involved in the neurological function of LAG-3 (Kouo et al., 2015; Mao et al., 2016; Xu et al., 2014). The interaction modality of galectin-3 and LSECtin to LAG-3 are less known, but both molecules have previously been shown to have several other binding partners (Kizuka et al., 2015; Li et al., 2009; Liu et al., 2004; Stillman et al., 2006; Tang et al., 2010). It remains to be shown whether their roles in the suppression of T cell-responses and antitumor immunity are dependent on LAG-3. Although MHC-II is the first identified ligand for LAG-3, the detailed biochemistry and affinity of this interaction is still unclear. Given that FGL1 does not compete with MHC-II for LAG-3 binding (Figure S1F), this opens the possibility for the existence of a FGL1-MHC-II-LAG-3 trimolecular complex—open questions include the signaling outcome of FGL1 versus MHC-II upon interaction with LAG-3 and how this complex could contribute to T cell suppression. A detailed stoichiometry analysis may be required to understand how soluble FGL1 triggers cell surface LAG-3 to transmit signals for T cell suppression, which is currently unknown. We found that FGL1 could form oligomers, and these oligomeric forms of FGL1 bound to LAG-3 much better than the dimeric form (Figures S1B and S1C), implicating that oligomeric FGL1 may be required for T cell suppression. The presence of native oligomeric FGL1 may also explain our results in the Octet assay showing a high-affinity interaction of purified soluble FGL1 with LAG-3. Thus, increased avidity of FGL1, most likely through oligomerization, but potentially through other mechanisms such as attachments to the extracellular matrix, may facilitate its interaction with LAG-3 *in vivo*. Currently, several MHC-II blocking anti-LAG-3 mAbs are being evaluated in clinical trials for the treatment of advanced human cancer. Preliminary data of these trials showed minimal or modest effect as a single agent (Ascierto and McArthur, 2017; Ascierto et al., 2017). Based on our findings, a possible interpretation for the clinical results could be that these mAbs block the MHC-II-LAG-3 interaction but do not block FGL1-LAG-3 binding. Thus, these mAbs may still allow FGL1 to transmit inhibitory signals to LAG-3, leading to an incomplete blockade of LAG-3-mediated immune suppression. Our findings warrant careful re-evaluation of

Figure 6. Upregulated FGL1 in Human Cancers Is Associated with a Poor Prognosis

(A) Representative immunofluorescence staining of FGL1, DAPI (for nuclear counterstain), and pan-cytokeratin (CK) in FGL1-positive or -negative NSCLC cancer sections.

(B and C) FGL1 expression as indicated by quantitative immunofluorescence (QIF) staining in NSCLC cancer tissues from cohort #1 (see also Table S3).

(B) Distribution of FGL1 expression and (C) association of high or low FGL1 expression with overall survival of the patients. The QIF visual detection threshold (1010.27) was used as a cutoff as indicated by dotted line in (B).

(D) The baseline plasma FGL1 levels were determined by ELISA in cohort #2 (see also Table S3) of NSCLC cancer patients ($n = 18$) and healthy donors ($n = 16$). Data were presented as the mean \pm SEM. *** $p < 0.001$ by Student's *t* test.

(E and F) Kaplan-Meier plots of overall survival stratified by median baseline plasma FGL1 levels in NSCLC (cut-point: 336.5 ng/mL) and melanoma (cut-point: 114 ng/mL) patients treated with single-agent anti-PD-1 therapy in NSCLC (D, cohort #2, $n = 18$) and melanoma (E, cohort #4, $n = 21$). See also Tables S3 and S4.

(G and H) B6 mice were inoculated s.c. with MC38 cells (0.5×10^6 /mouse) at day 0, followed by the treatment with anti-FGL1, anti-LAG-3, or control mAb ($n = 6$ per group) every 4 days from day 6 to day 18. In some groups, mice were also treated with a single dose of anti-B7-H1 (10B5) at day 6.

(G) Survival of the mice is shown. Survival analysis was conducted by log-rank test, ** $p < 0.01$; *** $p < 0.001$. The presented data is representative of at least two independent experiments.

(H) Tumor sizes are shown as the mean tumor diameter \pm SEM at day 22. ** $p < 0.01$ by Student's *t* test.

See also Figures S5 and S6 and Table S2.

therapeutic strategies that aim to block the immune inhibitory function of LAG-3.

Our findings support that the FGL1-LAG-3 pathway maybe an important immune evasion mechanism and could contribute to current cancer immunotherapy efforts for several reasons. Our studies indicate that FGL1 is a major ligand for LAG-3 to suppress T cell responses and constitute a new target for immune modulation. Furthermore, upregulation of FGL1 on tumor cells but not in normal tissues (Figure S5) may allow for a highly tumor-selective targeting of antibody therapy. In addition, tumor model studies using FGL1-KO mice demonstrate that FGL1 has a potent immune suppressive effect on anti-tumor immunity that is dependent on LAG-3. FGL1-LAG-3 interaction may also affect the generation of memory T cells as shown by our CyTOF data of increased memory-like CD4⁺ and CD8⁺ T cells in TILs from FGL1 KO mice during tumor growth (Figure 5) and an association of low FGL1 level with long-term survival of cancer patients upon anti-PD therapy (Figure 6E and 6F). Moreover, FGL1 may be a potential biomarker to predict the outcome of anti-PD therapy, since high plasma FGL1 levels are associated with a worse response to anti-PD therapy in NSCLC and melanoma patients (Figures 6E and 6F). Lastly, FGL1 blockade also synergizes with anti-B7-H1 blockade in animal models (Figures 6G and 6H), suggesting that FGL1 and anti-PD dual-blockade may be an alternative treatment for patients who are resistant to anti-PD therapy. In summary, our findings identify a functional interaction of the LAG-3 pathway and reveal a possible mechanism that tumors may employ for immune evasion, with important implications for developing next generation cancer immunotherapies.

STAR★METHODS

Detailed methods are provided in the online version of this paper and include the following:

- KEY RESOURCES TABLE
- CONTACT FOR REAGENT AND RESOURCE SHARING
- EXPERIMENTAL MODEL AND SUBJECT DETAILS
 - Mice
 - Plasmids, fusion proteins and antibodies
 - Human subjects
- METHOD DETAILS
 - The genome-scale receptor array system
 - Protein-protein interaction analysis
 - T cell function assays
 - Syngeneic mouse tumor models
 - Mouse tissue digestion
 - Mass cytometry sample preparation
 - Mass cytometry sample acquisition
 - Quantitative multiplex immunofluorescence
 - Measurement of plasma FGL1 levels
- QUANTIFICATION AND STATISTICAL ANALYSIS
 - Mass cytometry data analysis
 - Tissue fluorescence measurement and scoring
 - Bioinformatics and statistics
- DATA AND SOFTWARE AVAILABILITY

SUPPLEMENTAL INFORMATION

Supplemental Information includes six figures and four tables and can be found with this article online at <https://doi.org/10.1016/j.cell.2018.11.010>.

ACKNOWLEDGMENTS

We thank Beth Cadugan for editing the manuscript, Jun Zhao for data analysis, and other members in the laboratories of Yale for helpful discussions and technical assistance as well as Drs. Tim Zheng, Anne Vogt, Birgit Fogal, Timothy Fenn, Sven Mostboeck, Karl-Heinz Heider, and David Blair from Boehringer Ingelheim for their helpful discussion. This research was supported partially by NIH (P30 CA16359 and P50 CA196530), sponsored research funding from Boehringer Ingelheim, and an endowment from United Technologies Corporation to Lieping Chen. M.F.S. is supported by a Miguel Servet contract from Instituto de Salud Carlos III, Fondo de Investigación Sanitaria (Spain). D.A.A.V. is supported by NIH (P01 AI108545) and NCI Comprehensive Cancer Center Support CORE (P30 CA047904).

AUTHOR CONTRIBUTIONS

Conceptualization, J.W., M.F.S., and Lieping Chen; Methodology, J.W., M.F.S., I.D., T.T.S., L.J., Ling Chen, J.S., S.Y., and G.Z.; Software, J.W., M.F.S., T.T.S., I.D., W.Y., T.Z., and S.Z.; Formal Analysis, J.W., M.F.S., T.T.S., I.D., W.Y., A.B., and Ling Chen; Investigation, J.W., M.F.S., T.T.S., L.J., I.D., Ling Chen, J.S., and T.B.; Resources, L.Z., T.Z., S.Y., M.S., I.M., D.A.A.V., Y.C., K.S., and Lieping Chen; Writing – Original Draft, J.W. and Lieping Chen; Writing – Review & Editing, J.W., Lieping Chen, T.T.S., M.F.S., D.A.A.V., M.S., I.M., and K.S.; Visualization, J.W., M.F.S., and Lieping Chen; Supervision, Lieping Chen; Project Administration, J.W. and Lieping Chen.; Funding Acquisition, Lieping Chen.

DECLARATION OF INTERESTS

Lieping Chen is a consultant or advisory board member and receives consulting fees from Pfizer, Vcanbio, and GenomiCare; is a scientific founder of NextCure and TAYU Biotech; and has sponsored research grants from Boehringer Ingelheim and NextCure. There is a patent application pending related to this work.

Received: June 28, 2018

Revised: October 13, 2018

Accepted: November 9, 2018

Published: December 20, 2018

REFERENCES

- Anderson, A.C., Joller, N., and Kuchroo, V.K. (2016). Lag-3, Tim-3, and TIGIT: co-inhibitory receptors with specialized functions in immune regulation. *Immunity* 44, 989–1004.
- Andrews, L.P., Marciscano, A.E., Drake, C.G., and Vignali, D.A. (2017). LAG3 (CD223) as a cancer immunotherapy target. *Immunol. Rev.* 276, 80–96.
- Annunziato, F., Manetti, R., Tomasévic, I., Guidizi, M.G., Biagiotti, R., Giannò, V., Germano, P., Mavilia, C., Maggi, E., and Romagnani, S. (1996). Expression and release of LAG-3-encoded protein by human CD4⁺ T cells are associated with IFN- γ production. *FASEB J.* 10, 769–776.
- Annunziato, F., Manetti, R., Cosmi, L., Galli, G., Heusser, C.H., Romagnani, S., and Maggi, E. (1997). Opposite role for interleukin-4 and interferon- γ on CD30 and lymphocyte activation gene-3 (LAG-3) expression by activated naive T cells. *Eur. J. Immunol.* 27, 2239–2244.
- Ascierto, P.A., and McArthur, G.A. (2017). Checkpoint inhibitors in melanoma and early phase development in solid tumors: what's the future? *J. Transl. Med.* 15, 173.
- Ascierto, P.A., Melero, I., Bhatia, S., Bono, P., Sanborn, R.E., Lipson, E.J., Callahan, M.K., Gajewski, T., Gomez-Roca, C.A., Hodi, F.S., et al. (2017). Initial efficacy of anti-lymphocyte activation gene-3 (anti-LAG-3; BMS-986016) in

- combination with nivolumab (nivo) in pts with melanoma (MEL) previously treated with anti-PD-1/PD-L1 therapy. *J. Clin. Oncol.* **35**, 9520.
- Baixeras, E., Huard, B., Miossec, C., Jitsukawa, S., Martin, M., Hercend, T., Auffray, C., Triebel, F., and Piatier-Tonneau, D. (1992). Characterization of the lymphocyte activation gene 3-encoded protein. A new ligand for human leukocyte antigen class II antigens. *J. Exp. Med.* **176**, 327–337.
- Bettini, M., Szymczak-Workman, A.L., Forbes, K., Castellaw, A.H., Selby, M., Pan, X., Drake, C.G., Korman, A.J., and Vignali, D.A. (2011). Cutting edge: accelerated autoimmune diabetes in the absence of LAG-3. *J. Immunol.* **187**, 3493–3498.
- Blackburn, S.D., Shin, H., Haining, W.N., Zou, T., Workman, C.J., Polley, A., Betts, M.R., Freeman, G.J., Vignali, D.A., and Wherry, E.J. (2009). Coregulation of CD8+ T cell exhaustion by multiple inhibitory receptors during chronic viral infection. *Nat. Immunol.* **10**, 29–37.
- Bruniquel, D., Borie, N., Hannier, S., and Triebel, F. (1998). Regulation of expression of the human lymphocyte activation gene-3 (LAG-3) molecule, a ligand for MHC class II. *Immunogenetics* **48**, 116–124.
- Camisaschi, C., Casati, C., Rini, F., Perego, M., De Filippo, A., Triebel, F., Parmiani, G., Belli, F., Rivoltini, L., and Castelli, C. (2010). LAG-3 expression defines a subset of CD4(+)CD25(high)Foxp3(+) regulatory T cells that are expanded at tumor sites. *J. Immunol.* **184**, 6545–6551.
- Cemerski, S., Zhao, S., Chenard, M., Laskey, J., Cui, L., Shukla, R., et al. (2015). T cell activation and anti-tumor efficacy of anti-LAG-3 antibodies is independent of LAG-3 – MHCII blocking capacity. *J. Immunother. Cancer* **3** (Suppl 2), 183.
- Chapoval, A.I., Ni, J., Lau, J.S., Wilcox, R.A., Flies, D.B., Liu, D., Dong, H., Sica, G.L., Zhu, G., Tamada, K., and Chen, L. (2001). B7-H3: a costimulatory molecule for T cell activation and IFN-gamma production. *Nat. Immunol.* **2**, 269–274.
- Chen, L., Ashe, S., Brady, W.A., Hellström, I., Hellström, K.E., Ledbetter, J.A., McGowan, P., and Linsley, P.S. (1992). Costimulation of antitumor immunity by the B7 counterreceptor for the T lymphocyte molecules CD28 and CTLA-4. *Cell* **71**, 1093–1102.
- Chen, L., McGowan, P., Ashe, S., Johnston, J., Li, Y., Hellström, I., and Hellström, K.E. (1994). Tumor immunogenicity determines the effect of B7 costimulation on T cell-mediated tumor immunity. *J. Exp. Med.* **179**, 523–532.
- Chihara, N., Madi, A., Kondo, T., Zhang, H., Acharya, N., Singer, M., Nyman, J., Marjanovic, N.D., Kowalczyk, M.S., Wang, C., et al. (2018). Induction and transcriptional regulation of the co-inhibitory gene module in T cells. *Nature* **558**, 454–459.
- DeLong, J.H., Hall, A.O., Konradt, C., Coppock, G.M., Park, J., Harms Pritchard, G., and Hunter, C.A. (2018). Cytokine- and TCR-mediated regulation of T cell expression of Ly6C and Sca-1. *J. Immunol.* **200**, 1761–1770.
- Demchev, V., Malana, G., Vangala, D., Stoll, J., Desai, A., Kang, H.W., Li, Y., Nayeib-Hashemi, H., Niepel, M., Cohen, D.E., and Ukomadu, C. (2013). Targeted deletion of fibrinogen like protein 1 reveals a novel role in energy substrate utilization. *PLoS ONE* **8**, e58084.
- Dong, H., Strome, S.E., Salomao, D.R., Tamura, H., Hirano, F., Flies, D.B., Roche, P.C., Lu, J., Zhu, G., Tamada, K., et al. (2002). Tumor-associated B7-H1 promotes T-cell apoptosis: a potential mechanism of immune evasion. *Nat. Med.* **8**, 793–800.
- Gagliani, N., Magnani, C.F., Huber, S., Gianolini, M.E., Pala, M., Licona-Limon, P., Guo, B., Herbert, D.R., Bulfone, A., Trentini, F., et al. (2013). Coexpression of CD49b and LAG-3 identifies human and mouse T regulatory type 1 cells. *Nat. Med.* **19**, 739–746.
- Grosso, J.F., Kelleher, C.C., Harris, T.J., Maris, C.H., Hipkiss, E.L., De Marzo, A., Anders, R., Netto, G., Getnet, D., Bruno, T.C., et al. (2007). LAG-3 regulates CD8+ T cell accumulation and effector function in murine self- and tumor-tolerance systems. *J. Clin. Invest.* **117**, 3383–3392.
- Grosso, J.F., Goldberg, M.V., Getnet, D., Bruno, T.C., Yen, H.R., Pyle, K.J., Hipkiss, E., Vignali, D.A., Pardoll, D.M., and Drake, C.G. (2009). Functionally distinct LAG-3 and PD-1 subsets on activated and chronically stimulated CD8 T cells. *J. Immunol.* **182**, 6659–6669.
- Hara, H., Yoshimura, H., Uchida, S., Toyoda, Y., Aoki, M., Sakai, Y., Morimoto, S., and Shiokawa, K. (2001). Molecular cloning and functional expression analysis of a cDNA for human hepassocin, a liver-specific protein with hepatocyte mitogenic activity. *Biochim. Biophys. Acta* **1520**, 45–53.
- Hirano, F., Kaneko, K., Tamura, H., Dong, H., Wang, S., Ichikawa, M., Rietz, C., Flies, D.B., Lau, J.S., Zhu, G., et al. (2005). Blockade of B7-H1 and PD-1 by monoclonal antibodies potentiates cancer therapeutic immunity. *Cancer Res.* **65**, 1089–1096.
- Horst, A.K., Neumann, K., Diehl, L., and Tiegs, G. (2016). Modulation of liver tolerance by conventional and nonconventional antigen-presenting cells and regulatory immune cells. *Cell. Mol. Immunol.* **13**, 277–292.
- Huang, C.T., Workman, C.J., Flies, D., Pan, X., Marson, A.L., Zhou, G., Hipkiss, E.L., Ravi, S., Kowalski, J., Levitsky, H.I., et al. (2004). Role of LAG-3 in regulatory T cells. *Immunity* **21**, 503–513.
- Huard, B., Tournier, M., Hercend, T., Triebel, F., and Faure, F. (1994). Lymphocyte-activation gene 3/major histocompatibility complex class II interaction modulates the antigenic response of CD4+ T lymphocytes. *Eur. J. Immunol.* **24**, 3216–3221.
- Huard, B., Prigent, P., Tournier, M., Bruniquel, D., and Triebel, F. (1995). CD4/major histocompatibility complex class II interaction analyzed with CD4- and lymphocyte activation gene-3 (LAG-3)-Ig fusion proteins. *Eur. J. Immunol.* **25**, 2718–2721.
- Huard, B., Prigent, P., Pagès, F., Bruniquel, D., and Triebel, F. (1996). T cell major histocompatibility complex class II molecules down-regulate CD4+ T cell clone responses following LAG-3 binding. *Eur. J. Immunol.* **26**, 1180–1186.
- Huard, B., Mastrangeli, R., Prigent, P., Bruniquel, D., Donini, S., El-Tayar, N., Maigret, B., Dréano, M., and Triebel, F. (1997). Characterization of the major histocompatibility complex class II binding site on LAG-3 protein. *Proc. Natl. Acad. Sci. USA* **94**, 5744–5749.
- Kim, M.S., Pinto, S.M., Getnet, D., Nirujogi, R.S., Manda, S.S., Chaerkady, R., Madugundu, A.K., Kelkar, D.S., Isserlin, R., Jain, S., et al. (2014). A draft map of the human proteome. *Nature* **509**, 575–581.
- Kizuka, Y., Kitazume, S., Sato, K., and Taniguchi, N. (2015). Clec4g (LSECtin) interacts with BACE1 and suppresses A β generation. *FEBS Lett.* **589**, 1418–1422.
- Kouo, T., Huang, L., Pucsek, A.B., Cao, M., Solt, S., Armstrong, T., and Jaffee, E. (2015). Galectin-3 shapes antitumor immune responses by suppressing CD8+ T cells via LAG-3 and inhibiting expansion of plasmacytoid dendritic cells. *Cancer Immunol. Res.* **3**, 412–423.
- Li, Y., Hao, B., Kuai, X., Xing, G., Yang, J., Chen, J., Tang, L., Zhang, L., and He, F. (2009). C-type lectin LSECtin interacts with DC-SIGNR and is involved in hepatitis C virus binding. *Mol. Cell. Biochem.* **327**, 183–190.
- Li, C.Y., Cao, C.Z., Xu, W.X., Cao, M.M., Yang, F., Dong, L., Yu, M., Zhan, Y.Q., Gao, Y.B., Li, W., et al. (2010). Recombinant human hepassocin stimulates proliferation of hepatocytes in vivo and improves survival in rats with fulminant hepatic failure. *Gut* **59**, 817–826.
- Liu, Z., and Ukomadu, C. (2008). Fibrinogen-like protein 1, a hepatocyte derived protein is an acute phase reactant. *Biochem. Biophys. Res. Commun.* **365**, 729–734.
- Liu, W., Tang, L., Zhang, G., Wei, H., Cui, Y., Guo, L., Gou, Z., Chen, X., Jiang, D., Zhu, Y., et al. (2004). Characterization of a novel C-type lectin-like gene, LSECtin: demonstration of carbohydrate binding and expression in sinusoidal endothelial cells of liver and lymph node. *J. Biol. Chem.* **279**, 18748–18758.
- Mao, X., Ou, M.T., Karuppagounder, S.S., Kam, T.I., Yin, X., Xiong, Y., Ge, P., Umanah, G.E., Brahmachari, S., Shin, J.H., et al. (2016). Pathological α -synuclein transmission initiated by binding lymphocyte-activation gene 3. *Science* **353**, aah3374.
- Matsuzaki, J., Grnjatic, S., Mhawech-Fauceglia, P., Beck, A., Miller, A., Tsuji, T., Eppolito, C., Qian, F., Lele, S., Shrikant, P., et al. (2010). Tumor-infiltrating NY-ESO-1-specific CD8+ T cells are negatively regulated by LAG-3 and PD-1 in human ovarian cancer. *Proc. Natl. Acad. Sci. USA* **107**, 7875–7880.

- Pettitt, S.J., Liang, Q., Rairdan, X.Y., Moran, J.L., Prosser, H.M., Beier, D.R., Lloyd, K.C., Bradley, A., and Skarnes, W.C. (2009). Agouti C57BL/6N embryonic stem cells for mouse genetic resources. *Nat. Methods* 6, 493–495.
- Pihlgren, M., Dubois, P.M., Tomkowiak, M., Sjögren, T., and Marvel, J. (1996). Resting memory CD8+ T cells are hyperreactive to antigenic challenge in vitro. *J. Exp. Med.* 184, 2141–2151.
- Rotte, A., Jin, J.Y., and Lemaire, V. (2018). Mechanistic overview of immune checkpoints to support the rational design of their combinations in cancer immunotherapy. *Ann. Oncol.* 29, 71–83.
- Samusik, N., Good, Z., Spitzer, M.H., Davis, K.L., and Nolan, G.P. (2016). Automated mapping of phenotype space with single-cell data. *Nat. Methods* 13, 493–496.
- Schalper, K.A., Brown, J., Carvajal-Hausdorf, D., McLaughlin, J., Velcheti, V., Syrigos, K.N., Herbst, R.S., and Rimm, D.L. (2015). Objective measurement and clinical significance of TILs in non-small cell lung cancer. *J. Natl. Cancer Inst.* 107, dju435.
- Shevach, E.M. (2009). Mechanisms of foxp3+ T regulatory cell-mediated suppression. *Immunity* 30, 636–645.
- Sica, G.L., Choi, I.H., Zhu, G., Tamada, K., Wang, S.D., Tamura, H., Chapoval, A.I., Flies, D.B., Bajorath, J., and Chen, L. (2003). B7-H4, a molecule of the B7 family, negatively regulates T cell immunity. *Immunity* 18, 849–861.
- Stillman, B.N., Hsu, D.K., Pang, M., Brewer, C.F., Johnson, P., Liu, F.T., and Baum, L.G. (2006). Galectin-3 and galectin-1 bind distinct cell surface glycoprotein receptors to induce T cell death. *J. Immunol.* 176, 778–789.
- Tang, L., Yang, J., Tang, X., Ying, W., Qian, X., and He, F. (2010). The DC-SIGN family member LSECtin is a novel ligand of CD44 on activated T cells. *Eur. J. Immunol.* 40, 1185–1191.
- Triebel, F., Jitsukawa, S., Baixeras, E., Roman-Roman, S., Genevee, C., Viegas-Pequignot, E., and Hercend, T. (1990). LAG-3, a novel lymphocyte activation gene closely related to CD4. *J. Exp. Med.* 171, 1393–1405.
- van der Maaten, L., and Hinton, G. (2008). Visualizing data using t-SNE. *J. Mach. Learn. Res.* 9, 2579–2605.
- Walunas, T.L., Bruce, D.S., Dustin, L., Loh, D.Y., and Bluestone, J.A. (1995). Ly-6C is a marker of memory CD8+ T cells. *J. Immunol.* 155, 1873–1883.
- Williams, J.B., Horton, B.L., Zheng, Y., Duan, Y., Powell, J.D., and Gajewski, T.F. (2017). The EGR2 targets LAG-3 and 4-1BB describe and regulate dysfunctional antigen-specific CD8+ T cells in the tumor microenvironment. *J. Exp. Med.* 214, 381–400.
- Woo, S.R., Turnis, M.E., Goldberg, M.V., Bankoti, J., Selby, M., Nirschl, C.J., Bettini, M.L., Gravano, D.M., Vogel, P., Liu, C.L., et al. (2012). Immune inhibitory molecules LAG-3 and PD-1 synergistically regulate T-cell function to promote tumoral immune escape. *Cancer Res.* 72, 917–927.
- Workman, C.J., and Vignali, D.A. (2003). The CD4-related molecule, LAG-3 (CD223), regulates the expansion of activated T cells. *Eur. J. Immunol.* 33, 970–979.
- Workman, C.J., and Vignali, D.A. (2005). Negative regulation of T cell homeostasis by lymphocyte activation gene-3 (CD223). *J. Immunol.* 174, 688–695.
- Workman, C.J., Dugger, K.J., and Vignali, D.A. (2002a). Cutting edge: molecular analysis of the negative regulatory function of lymphocyte activation gene-3. *J. Immunol.* 169, 5392–5395.
- Workman, C.J., Rice, D.S., Dugger, K.J., Kurschner, C., and Vignali, D.A. (2002b). Phenotypic analysis of the murine CD4-related glycoprotein, CD223 (LAG-3). *Eur. J. Immunol.* 32, 2255–2263.
- Workman, C.J., Cauley, L.S., Kim, I.J., Blackman, M.A., Woodland, D.L., and Vignali, D.A. (2004). Lymphocyte activation gene-3 (CD223) regulates the size of the expanding T cell population following antigen activation in vivo. *J. Immunol.* 172, 5450–5455.
- Xu, F., Liu, J., Liu, D., Liu, B., Wang, M., Hu, Z., Du, X., Tang, L., and He, F. (2014). LSECtin expressed on melanoma cells promotes tumor progression by inhibiting antitumor T-cell responses. *Cancer Res.* 74, 3418–3428.
- Yamamoto, T., Gotoh, M., Sasaki, H., Terada, M., Kitajima, M., and Hirohashi, S. (1993). Molecular cloning and initial characterization of a novel fibrinogen-related gene, HFREP-1. *Biochem. Biophys. Res. Commun.* 193, 681–687.
- Yan, J., Ying, H., Gu, F., He, J., Li, Y.L., Liu, H.M., and Xu, Y.H. (2002). Cloning and characterization of a mouse liver-specific gene mrfep-1, up-regulated in liver regeneration. *Cell Res.* 12, 353–361.
- Yao, S., Zhu, Y., Zhu, G., Augustine, M., Zheng, L., Goode, D.J., Broadwater, M., Ruff, W., Flies, S., Xu, H., et al. (2011). B7-h2 is a costimulatory ligand for CD28 in human. *Immunity* 34, 729–740.

The Lineage-Defining Transcription Factors SOX2 and NKX2-1 Determine Lung Cancer Cell Fate and Shape the Tumor Immune Microenvironment

Gurkan Mollaoglu,¹ Alex Jones,² Sarah J. Wait,¹ Anandaroop Mukhopadhyay,¹ Sangmin Jeong,¹ Rahul Arya,¹ Soledad A. Camolotto,² Timothy L. Mosbrugger,³ Chris J. Stubben,³ Christopher J. Conley,³ Arjun Bhutkar,⁴ Jeffery M. Vahrenkamp,¹ Kristofer C. Berrett,¹ Melissa H. Cessna,⁵ Thomas E. Lane,² Benjamin L. Witt,^{2,6} Mohamed E. Salama,^{2,6} Jason Gertz,¹ Kevin B. Jones,^{1,7} Eric L. Snyder,^{1,2} and Trudy G. Oliver^{1,8,*}

¹Department of Oncological Sciences, Huntsman Cancer Institute, University of Utah, Salt Lake City, UT 84112, USA

²Department of Pathology, University of Utah, Salt Lake City, UT 84112, USA

³Huntsman Cancer Institute, Bioinformatics Shared Resource, Salt Lake City, UT 84112, USA

⁴David H. Koch Institute for Integrative Cancer Research, Massachusetts Institute of Technology, Cambridge, MA 02139, USA

⁵Intermountain Biorepository, Intermountain Healthcare, Salt Lake City, UT 84111, USA

⁶ARUP Laboratories at University of Utah, Salt Lake City, UT 84108, USA

⁷Department of Orthopaedics, University of Utah, Salt Lake City, UT 84112, USA

⁸Lead Contact

*Correspondence: trudy.oliver@hci.utah.edu

<https://doi.org/10.1016/j.immuni.2018.09.020>

SUMMARY

The major types of non-small-cell lung cancer (NSCLC)—squamous cell carcinoma and adenocarcinoma—have distinct immune microenvironments. We developed a genetic model of squamous NSCLC on the basis of overexpression of the transcription factor *Sox2*, which specifies lung basal cell fate, and loss of the tumor suppressor *Lkb1* (SL mice). SL tumors recapitulated gene-expression and immune-infiltrate features of human squamous NSCLC; such features included enrichment of tumor-associated neutrophils (TANs) and decreased expression of NKX2-1, a transcriptional regulator that specifies alveolar cell fate. In *Kras*-driven adenocarcinomas, mis-expression of *Sox2* or loss of *Nkx2-1* led to TAN recruitment. TAN recruitment involved SOX2-mediated production of the chemokine CXCL5. Deletion of *Nkx2-1* in SL mice (SNL) revealed that NKX2-1 suppresses SOX2-driven squamous tumorigenesis by repressing adeno-to-squamous transdifferentiation. Depletion of TANs in SNL mice reduced squamous tumors, suggesting that TANs foster squamous cell fate. Thus, lineage-defining transcription factors determine the tumor immune microenvironment, which in turn might impact the nature of the tumor.

INTRODUCTION

Non-small-cell lung cancer (NSCLC) represents approximately 85% of all lung cancers and predominantly comprises lung squamous-cell carcinoma (LSCC) and adenocarcinoma (LADC). LSCC and LADC can be distinguished by their histopathology, biomarkers, patterns of gene expression, genomic alterations, and

response to therapy (Campbell et al., 2016; Langer et al., 2016). Adenosquamous carcinoma is a less common NSCLC variant defined by the presence of both LADC and LSCC components. Recently, it has been shown that LADC and LSCC have differences in the immune microenvironment (Kargl et al., 2017; Nagaraj et al., 2017; Xu et al., 2014). This is clinically relevant because advances in immunotherapy have led to the approval of immune checkpoint inhibitors for NSCLC (Ribas and Wolchok, 2018). Immunotherapy response is impacted by the complex and dynamic interactions among multiple immune cell types and cancer cells in the tumor immune microenvironment (TIME) (Pitt et al., 2016). It is important to decipher the function of cells in the TIME to better understand the role of the immune system in tumor initiation and progression and to fully exploit the potential of immunotherapy.

Neutrophils are among the first responders to infection and tissue damage (Powell and Huttenlocher, 2016). Neutrophils are present in the TIME of most solid tumors and can contribute to tumor progression by promoting cell growth, angiogenesis, metastasis, and immune evasion, although they can play anti-tumor roles as well (Coffelt et al., 2016; Powell and Huttenlocher, 2016). A pan-cancer study of 25 malignancies, including NSCLC, showed that neutrophil abundance in the TIME is a leading predictor of a poor outcome (Gentles et al., 2015). Similarly, a high neutrophil-to-lymphocyte ratio is associated with poor prognosis in many solid tumors, including NSCLC (Templeton et al., 2014). Mice that bear activating mutations in *Kras* and that are deficient for the tumor suppressor *Lkb1* (*Kras*^{LSL-G12D/+}; *Lkb1*^{fl/fl} [KL mice]) harbor a spectrum of NSCLC histologies, and tumor-associated neutrophils (TANs) in this model demonstrate pro-tumor features (Koyama et al., 2016; Nagaraj et al., 2017).

Neutrophils are more abundant in human LSCC than in LADC, whereas macrophages are more abundant in LADC (Eruslanov et al., 2014; Kargl et al., 2017). TAN enrichment in LSCC is also observed in genetically engineered mouse models (GEMMs); LSCCs in *Lkb1*^{fl/fl}; *Pten*^{fl/fl} (LP) and *Sox2*^{LSL/LSL}; *Pten*^{fl/fl}; *Cdkn2ab*^{fl/fl} (*Sox2PC*) mice have more neutrophils but fewer macrophages than LADC GEMMs (Ferone et al., 2016; Xu



et al., 2014). Similarly, adenosquamous tumors in KL mice have more TANs and fewer macrophages than adenocarcinomas in the same genetic model (Nagaraj et al., 2017). On the basis of this result, it was hypothesized that squamous histological classification (i.e., histotype) rather than genetic alterations (i.e., genotype) determine the immune contexture (Nagaraj et al., 2017). Tumor histology and genetic alterations are intimately linked in NSCLC, so it is difficult to tease apart whether histotype or genotype is the most important determinant of the TIME. A significant subset of lung tumors (so-called “not otherwise specified” tumors) is difficult to classify histologically, and both tumor heterogeneity and plasticity, including changes in tumor subtype in response to targeted therapy, occur in the clinical setting. Therefore, it is important to determine whether and how histotype and/or genotype dictate the immune microenvironment. Specifically, it remains unknown which factors promote the difference in TAN levels between LSCC and LADC.

During development, the transcription factors SOX2 and NKX2-1 exhibit opposing patterns of expression within the primitive foregut and embryonic lung (Morrissey and Hogan, 2010). Likewise, in the adult lung, SOX2 amounts are highest in the proximal airways, whereas NKX2-1 amounts are highest in type 2 pneumocytes of the alveoli. In the normal lung, SOX2 promotes proliferation and maintains stem and basal cell identity, whereas NKX2-1 specifies alveolar cell identity. SOX2 and NKX2-1 exhibit opposing patterns of expression in the two major subtypes of NSCLC as well. SOX2 is amplified in ~21% and overexpressed in >80% of LSCCs, whereas it is rarely expressed in LADC (Campbell et al., 2016). In contrast, NKX2-1 is amplified in ~10% and highly expressed in 70%–80% of LADC and is rarely expressed in LSCC (Campbell et al., 2016). LADC shares features with normal alveolar cells where NKX2-1 is normally expressed, whereas LSCC shares features of basal cells where SOX2 is normally expressed. SOX2 is thus considered a lineage-specific oncogene because it drives multiple squamous cancers, including lung cancer, and directs tumor type toward a basal-cell fate (Bass et al., 2009; Ferone et al., 2016; Lu et al., 2010; Mukhopadhyay et al., 2014). On the other hand, the impact of NKX2-1 in LADC appears to be context dependent. NKX2-1 is considered to be a lineage-specific oncogene in adenocarcinoma when it is amplified or highly expressed (Tanaka et al., 2007). However, a subset of adenocarcinomas is NKX2-1 negative, and these tumors are associated with poor prognosis relative to NKX2-1⁺ adenocarcinomas. Furthermore, loss of NKX2-1 accelerates *Kras* mutant lung adenocarcinoma in mice and alters their cell fate, suggesting that NKX2-1 has lineage-specific tumor suppressor functions as well. Here, we developed and employed multiple GEMMs to elucidate the role of lung-cancer lineage specifiers SOX2 and NKX2-1 in tumor cell fate and neutrophil recruitment.

RESULTS

Murine SOX2-Driven Lung Squamous Tumors Recapitulate Human Pathology

Our previous work demonstrated that lentiviral *Sox2* overexpression combined with *Lkb1* deletion promotes LSCC (Mukhopadhyay et al., 2014). To create a genetic model, we generated mice with a *Lox-Stop-Lox-Sox2-IRES-GFP* cassette in the

Rosa26 locus (*Rosa26*^{LSL-Sox2-IRES-GFP}) and crossed them to *Lkb1*^{fl/fl} mice to yield *Rosa26*^{LSL-Sox2-IRES-GFP};*Lkb1*^{fl/fl} (SL) mice (Figure S1A). To confirm that the *Sox2* allele functions properly, we isolated mouse embryonic fibroblasts (MEFs) from *Sox2*^{LSL/+};*Lkb1*^{fl/fl} and *Sox2*^{LSL/LSL};*Lkb1*^{fl/fl} mice (Figure S1B). GFP and SOX2 expression were induced in MEFs infected with adenoviruses that express Cre recombinase under the control of a CMV promoter (Ad5-CMV-Cre), and *Sox2* homozygous cells expressed both proteins at higher levels than heterozygous cells (Figures S1C and S1D).

Next, we infected homozygous and heterozygous SL mice, LP mice, and *Kras*^{LSL-G12D/+};*Trp53*^{fl/fl} (KP) mice with Ad5-CMV-Cre by using intranasal inhalation. Although heterozygous SL mice had not developed tumors one year after infection, homozygous SL mice developed tumors after an average of 11 months, comparable to the latency of other LSCC GEMMs (Ferone et al., 2016; Xu et al., 2014) (Figures S1E and S1F). Tumor penetrance was higher in SL mice than Lenti-*Sox2*-Cre-infected *Lkb1*^{fl/fl} mice (71% versus 40%) and slightly higher than that of LP mice (60%) (Figure S1G). SL mice developed one or a few tumors, in similarity to the LP model (Figure S1H), and were GFP positive as revealed by whole-mount microscopy (Figure S1I). The vast majority (>90%) of tumors in the SL mice were classified as squamous by two board-certified pathologists (B.L.W. and E.L.S.), whereas smaller LADCs were rarely detected in the same animals (Figure 1A and Figure S1J). With flattened and keratinized cells and desmoplastic stroma, SL tumors exhibited characteristic features of squamous tumors and were similar to human LSCC and murine LP tumors (Figure 1A). SL tumors were positive for two established LSCC biomarkers, KRT5 and DNp63 (Figures 1B–1D).

Mutations in components of the PI3K-AKT-mTOR pathway result in activation of this signaling axis in ~47% of LSCCs (Campbell et al., 2016). LKB1 functions as a tumor suppressor through its negative regulation of the mTOR pathway. *LKB1* loss-of-function alterations are relatively infrequent in human LSCC but are found in a significant fraction of adenosquamous tumors (Zhang et al., 2017). We assessed mouse and human LSCC for phosphorylated 4EBP1 (p4EBP1), an established marker of mTOR pathway activation. SL tumors were positive for SOX2 and p4EBP1 at protein amounts similar to those of LP and human LSCC (Figures 1E–1G). KP adenocarcinomas were negative for SOX2 and had low to no detectable p4EBP1. IHC analysis of 43 human LSCCs demonstrated that 58% of samples were positive for p4EBP1 and that 93% were positive for SOX2 (58% were positive for both), suggesting that murine SL tumors resemble a significant fraction of human LSCCs (Figures 1H and 1I). Together, these results demonstrate that the combination of SOX2 overexpression and mTOR pathway activation, frequent characteristics of human LSCC, promotes LSCC tumorigenesis.

Murine SOX2-Driven Lung Squamous Tumors Recapitulate the Molecular Phenotype of Human LSCC

To determine whether SL tumors recapitulate the molecular features of human LSCC, we compared gene expression profiles of SL, LP, and KP mouse tumors to normal adult mouse lung and human LSCC by RNA sequencing (RNA-seq). Cross-species analysis of differentially expressed genes demonstrated

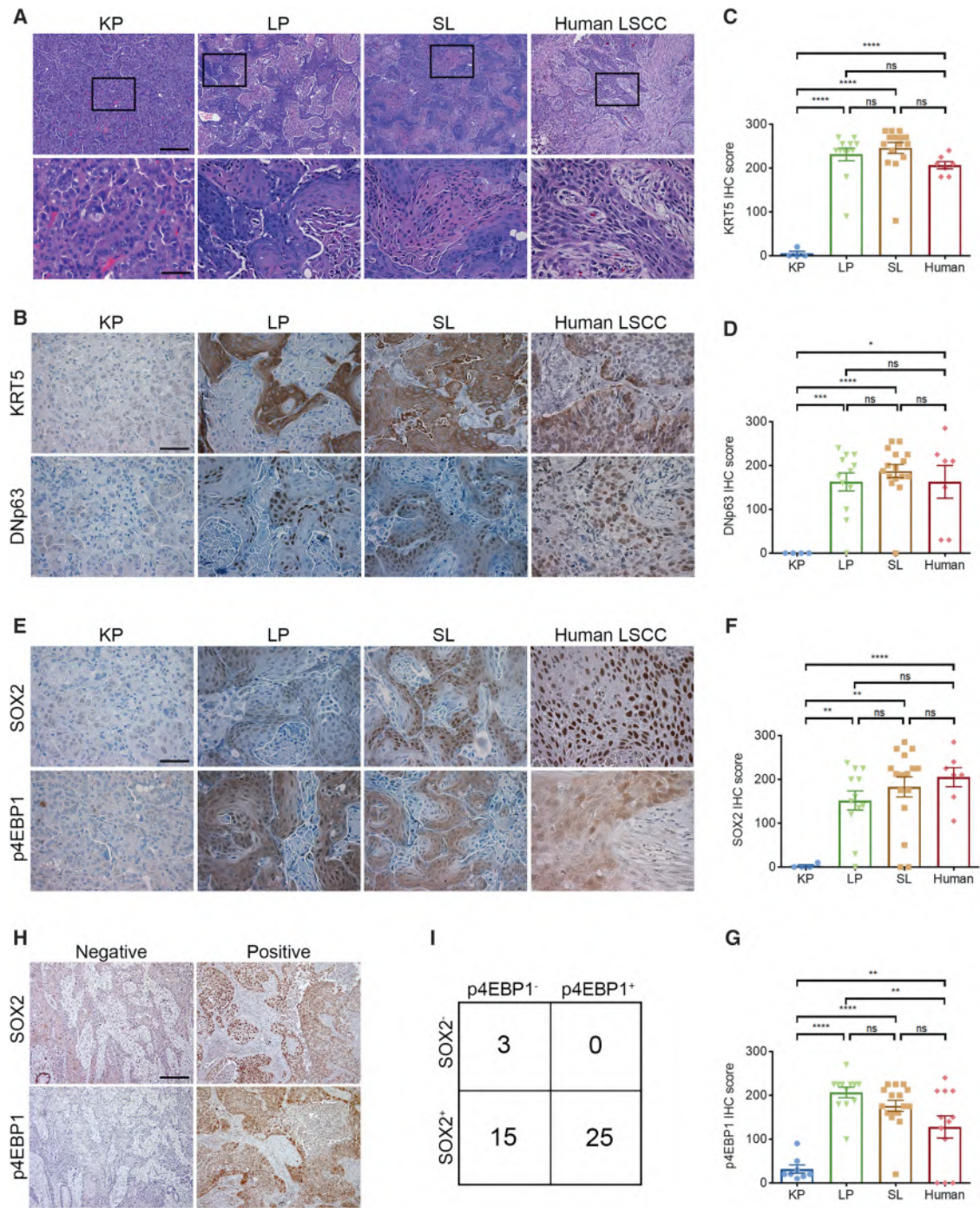


Figure 1. Murine SOX2-Driven Lung Squamous Tumors Recapitulate Human Pathology

(A) Representative H&E images from indicated GEMM tumors and human LSCC. Scale bars represent 200 μ m in the top row and 50 μ m in the bottom row. Boxes on the upper panel indicate areas shown in higher magnification on the lower panel.

(B–D) Immunohistochemistry (IHC) for KRT5 and DNP63 in indicated mouse and human tumor types (B) and IHC quantification of KRT5 (C) and DNP63 (D). The scale bar represents 50 μ m.

(E–G) IHC for SOX2 and p4EBP1 in indicated mouse and human tumor types (E) and IHC quantification of SOX2 (F) and p4EBP1 (G). The scale bar represents 50 μ m.

(H and I) IHC for SOX2 and p4EBP1 in a panel of 43 human LSCCs (H) and a contingency table for binary staining results (I). The scale bar represents 50 μ m.

Error bars indicate mean \pm SEM. Two-tailed unpaired t tests, ****p < 0.0001, ***p < 0.001, **p < 0.01, *p < 0.05, ns = not significant. In (C), (D), (F), and (G), each dot represents one tumor from 3–8 mice per genotype and six patient tumors. See also Figure S1.

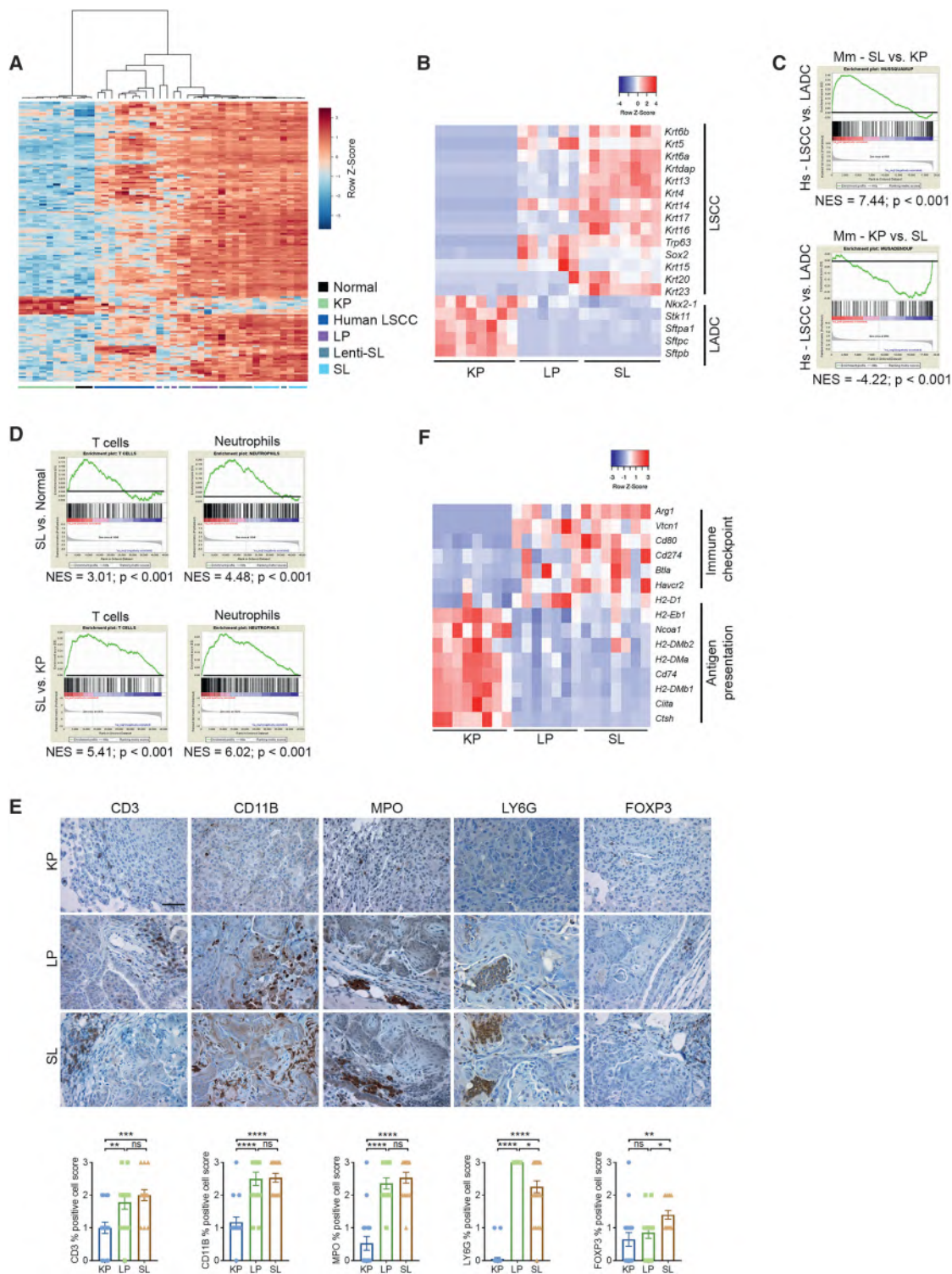


Figure 2. Mouse Lung Tumors Recapitulate Molecular Phenotype and Tumor Immune Microenvironment of Human Tumors

(A) Heatmap and hierarchical clustering of GEMM lung tumors, normal mouse lung tissue, and human LSCCs based on signature of differentially expressed transcripts from RNA-seq analysis (see Star Methods).

(B) Gene expression heatmap for lung squamous and adenocarcinoma marker genes comparing SL, LP, and KP tumors. $p < 0.01$ $\text{Log}_2\text{FC} > 1$ as a cutoff.

(C) GSEA from mouse (Mm) SL versus KP (top) and KP versus SL (bottom) tumors with normalized enrichment scores and p values for human (Hs) LSCC versus LADC gene signatures generated from TCGA data.

(legend continued on next page)

similarities among SL, LP, and human LSCC (Figure 2A). Mouse and human squamous tumors aligned more closely in a semi-supervised clustering analysis and were distinct from KP adenocarcinomas and normal lung tissue. Expression of squamous biomarkers such as *Krt5*, *Krt14*, and other cytokeratin genes, as well as *Trp63* and *Sox2*, was significantly increased in SL tumors, whereas expression of adenocarcinoma markers such as *Nkx2-1*, *Sftpc*, and other surfactant genes was decreased (Figure 2B). Gene-set enrichment analysis (GSEA) of human LSCC compared to LADC derived from The Cancer Genome Atlas (TCGA) revealed a significant positive enrichment for genes expressed in SL or LP versus KP tumors (Figure 2C and Figure S2A). There was a significant depletion of adenocarcinoma-enriched genes in SL and LP versus KP tumors (Figures 2C and S2A). Ingenuity pathway analysis (IPA) of differentially expressed genes in SL versus KP tumors identified human and mouse “embryonic stem cell pluripotency” pathways (Figure S2B). By GSEA, SL tumors and human LSCCs were enriched for gene sets, including genes in the DNP63 pathway, lung-stem-cell markers (Vaughan et al., 2015; Zuo et al., 2015), and tracheal basal-cell-surface markers (Van de Laar et al., 2014) (Figure S2C and Tables S2 and S3). Together, these findings suggest that SL tumors strongly recapitulate human LSCCs at the molecular level.

Mouse Lung Tumors Recapitulate the Human Tumor Immune Microenvironment with Elevated Quantities of Tumor-Associated Neutrophils

IPA identified “granulocyte adhesion and diapedesis” among the top enriched pathways in SL versus KP tumors (Figure S2B). It also identified multiple immune-related pathways, including those involving specific immune cell types, cytokines, and transcription factors as key upstream regulators (Figures S2D and S2E), as significantly enriched in SL tumors, as compared to KP tumors. The comparison of all significantly enriched pathways in human LSCC versus LADC (Campbell et al., 2016) and in SL versus KP tumors demonstrated that there is a high degree of overlap of immune-related pathways between mouse and human LSCC (Figure S2F). GSEA also suggested that SL tumors are enriched for gene signatures of immune cells in lymphoid, myeloid, and macrophage lineages (Figure S2G). Compared to normal lung tissue and KP tumors, SL tumors had a significant positive enrichment for T cell, neutrophil, and TAN gene sets (Figure 2D and Figure S2H). Consistent with TAN enrichment in squamous tumors, we found that multiple upstream molecules associated with neutrophil recruitment and “N2” pro-tumor function were enriched in SL tumors (Figure S2D). Together, these findings suggested that LSCC and LADC have significantly different TIMEs.

In order to better understand the LSCC TIME, we analyzed the abundance of T cells in murine tumors. IHC for CD3 demonstrated significantly greater T cell infiltration in SL and LP tumors

compared to KP adenocarcinomas (Figure 2E). High neutrophil infiltration in SL tumors was evident on H&E evaluation by a pathologist (E.L.S.) (Figure S2I) and was confirmed by IHC analysis of neutrophil markers CD11B, MPO, and LY6G (Figure 2E). Neutrophils were found in extravascular clusters located throughout the TIME; these clusters were found at the periphery and within the tumor, often immediately adjacent to the carcinoma cells. Because squamous tumors were apparently growing in this inflammatory and T-cell-rich microenvironment, we postulated that the cancer cells might employ immune evasion mechanisms. We found that FOXP3⁺ regulatory T (Treg) cells were enriched in SL tumors compared to LP and KP tumors (Figure 2E). SL tumors also displayed increased expression of genes encoding multiple immunosuppressive molecules such as *Arg1*, *Vtcn1*, *Cd80*, *Btla*, *Havcr2*, and *Cd274 (Pd-I1)*, as measured by RNA-seq; some of these molecules have increased gene expression in LP squamous tumors (Xu et al., 2014) (Figure 2F). SL tumors showed reduced expression of major histocompatibility complex (MHC) genes (Figure 2F), suggesting reduced antigen presentation as a potential immune evasion mechanism active in these tumors. Collectively, SL squamous tumors display some hallmarks of an immunosuppressive TIME, for example enrichment of Treg cells and TANs. This does not rule out the possibility that adenocarcinoma also harbors an immunosuppressive TIME, albeit potentially through distinct mechanisms.

SOX2 Promotes Tumor-Associated Neutrophil Recruitment in the Absence of Squamous Transdifferentiation

Recent studies suggest that elevated TANs in LSCC might be due to a squamous histotype as opposed to a genetic phenomenon (Nagaraj et al., 2017). It is challenging to decouple the function of SOX2 from its role in “squamousness” because SOX2 can promote squamous differentiation (Bass et al., 2009; Lu et al., 2010; Mukhopadhyay et al., 2014). To tease apart these functions, we overexpressed SOX2 in the KP adenocarcinoma model to determine whether SOX2 can alter tumor histotype and/or TAN levels. KP mice were infected with Lenti-Sox2-Cre or control Lenti-GFP-Cre viruses (Figure 3A), and lungs were harvested four months later. Lenti-GFP-Cre-infected KP tumors (KPG) were GFP positive (Figure 3B), as expected. We analyzed serial sections by IHC for squamous and neutrophil markers in matched individual tumors. In Lenti-Sox2-Cre-infected KP animals (KPS), SOX2 overexpression was observed in many but not all tumors, indicating an occasional uncoupling of SOX2 expression from Cre-mediated recombination (Figures 3C and 3D). All KPS tumors exhibited adenocarcinoma histology regardless of the amount of SOX2 (Figure 3B). Neither SOX2⁺ nor SOX2⁻ tumors in KPS lungs expressed squamous biomarkers DNP63 or KRT5 (Figures 3C, 3E, and 3F), suggesting that

(D) GSEA from mouse SL versus normal lung tissue (top) and SL versus KP tumors (bottom) are shown along with normalized enrichment scores and p values for T cell and neutrophil gene signatures.

(E) IHC for immune cell markers (CD3, T cells; FOXP3, Tregs; CD11B, MPO, LY6G, neutrophils) in indicated GEMM tumors (top), and IHC quantification (bottom). The scale bar represents 50 μ m. Error bars indicate mean \pm SEM. Two-tailed unpaired t tests, ****p < 0.0001, ***p < 0.001, **p < 0.01, *p < 0.05, ns = not significant. Each dot represents one tumor from three to seven mice per genotype.

(F) Heatmap representing selected immune-related genes differentially expressed in SL, LP, and KP tumors. p < 0.01 and Log2FC > 1 were used as a cutoff. See also Figure S2 and Table S1.

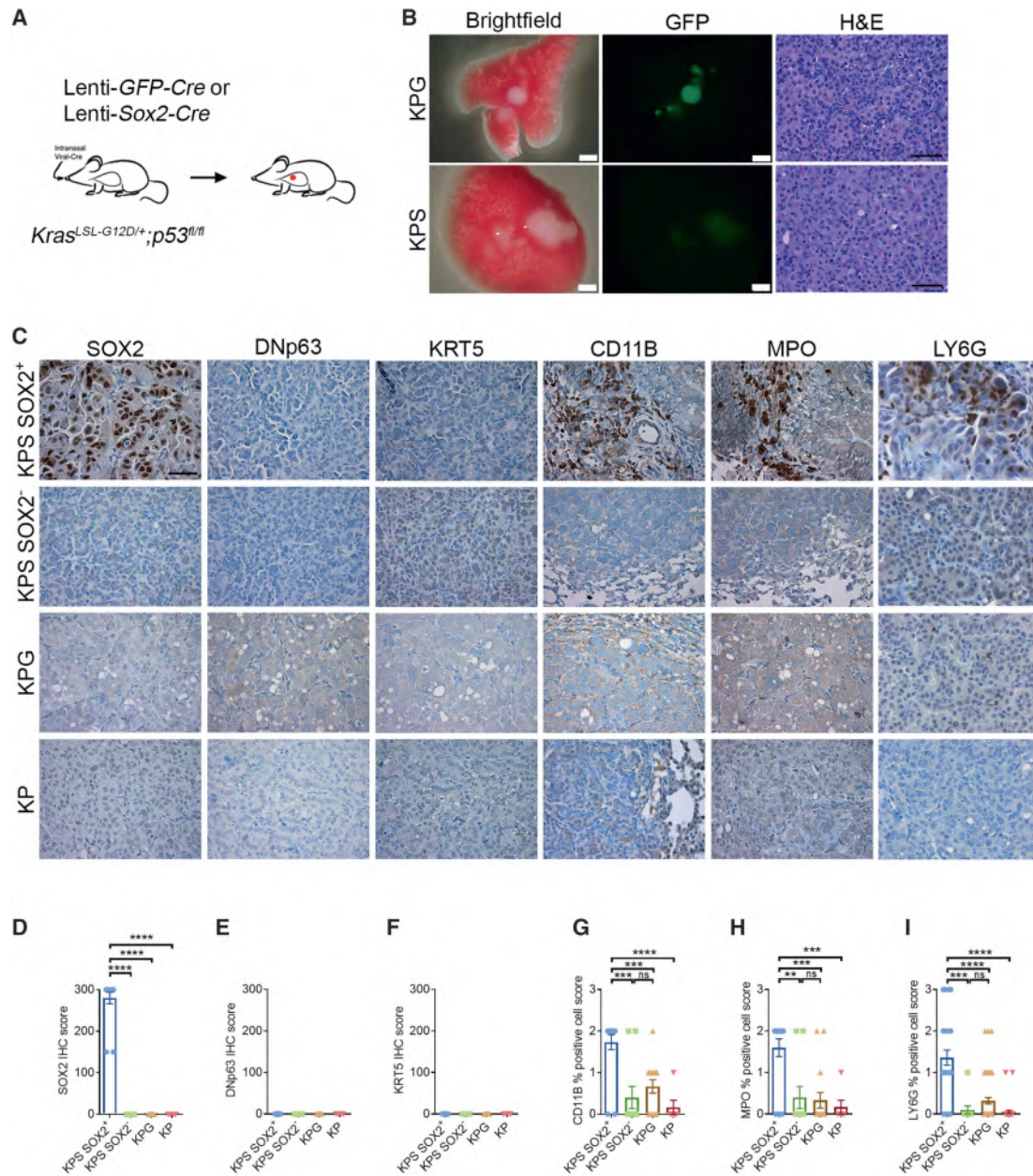


Figure 3. SOX2 Promotes Tumor-Associated Neutrophil Recruitment in the Absence of Squamous Transdifferentiation

(A) Schematic representation of lentiviral *Sox2* or *Gfp* overexpression in KP mice.

(B) Representative whole-mount brightfield (left), fluorescence (middle) and H&E-stained histology (right) images from indicated GEMM tumors. Scale bars represent 200 μ m for brightfield and fluorescence images; 50 μ m for H&E images.

(C–I) Representative IHC (C) and IHC quantification for SOX2 (D), DNP63 (E), KRT5 (F), CD11B (G), MPO (H), or LY6G (I) in indicated tumor models. The scale bar represents 50 μ m. Error bars indicate mean \pm SEM. Two-tailed unpaired t tests, **** p < 0.0001, *** p < 0.001, ** p < 0.01, ns = not significant. In (D)–(I), each dot represents one tumor from three to five mice per genotype.

SOX2 is not sufficient to promote squamous fate in this context. However, we observed elevated TAN quantities specifically in SOX2⁺ KPS tumors but not in control SOX2⁻ KPS, KPG, or KP tumors (Figures 3C and 3G–3I). On the basis of analyses of individual SOX2⁺ and SOX2⁻ tumors within the same lungs, TAN recruitment appeared not to be due to a systemic effect of increased TANs throughout the entire lung but rather to be localized to specific tumors expressing SOX2. Together, these data

suggest that SOX2 is sufficient to promote TAN recruitment independently of tumor histotype.

SOX2 Suppresses NKX2-1 Activity and NKX2-1 Loss Promotes TAN Recruitment in the Absence of Squamous Histotype

Next, we aimed to understand the mechanisms of TAN recruitment by SOX2 in a histotype-independent manner. During lung

development, SOX2 and NKX2-1 exhibit inverse patterns of expression at multiple stages. In the course of investigating KPS tumors, we observed that NKX2-1 amounts were significantly decreased in SOX2⁺ KPS tumors compared to SOX2⁻ KPS and KP tumors (Figures 4A and 4B). Consistent with the reduction in NKX2-1 amounts, SOX2⁺ KPS tumors had significantly lower protein amounts of SPC (an established NKX2-1 target gene product) than did control tumors (Figures 4A and 4C). SL and LP tumors, both of which have high SOX2 expression, also had subtly but significantly lower protein amounts of NKX2-1 than did KP adenocarcinomas (Figures 4D and 4E). Lower levels of NKX2-1 were due to reduced intensity (evident by comparisons of NKX2-1 amounts in tumor cells to those in neighboring alveolar cells) rather than a reduction in the number of tumor cells expressing NKX2-1 (Figures S3A and S3B). In squamous tumors, SPC protein amounts were significantly reduced, further suggesting suppressed NKX2-1 activity in cells with high amounts of SOX2 (Figures 4D and 4F). Consistently, IPA identified NKX2-1 inhibition as a top upstream regulator in SL tumors compared to KP tumors (Figure 4G). Together this suggests that SOX2 promotes a reduction in NKX2-1 amounts and/or activity. Although the mechanism of regulation is unclear, chromatin immunoprecipitation-RNA sequencing (ChIP-seq) analyses suggested that SOX2 and NKX2-1 can each bind their own promoters, and SOX2 might weakly bind the *Nkx2-1* promoter (Figure S3C). Furthermore, inducible SOX2 expression can repress NKX2-1 amounts in four of five human lung cancer cell lines examined (Figure S3D).

Because SOX2 promotes TAN recruitment and leads to decreased NKX2-1 activity, we tested whether NKX2-1 plays a role in TAN recruitment. We employed *Kras*^{FSF-G12D/+}; *Trp53*^{Frr/Frr}; *Rosa26*^{FSF-CreERT2}; *Nkx2-1*^{fl/fl} (KPN) mice, where *Nkx2-1* can be temporally deleted in the KP adenocarcinoma model. We infected KPN mice with Ad5-CMV-Flp to initiate tumorigenesis, and 6 weeks after infection, we treated them with vehicle or tamoxifen to cause *Nkx2-1* deletion. Four weeks after tamoxifen treatment, we harvested tumors for IHC analysis. KPN tumors exhibited a significant reduction in NKX2-1 and SPC expression in comparison to KP tumors, exhibited a mucinous adenocarcinoma histology (Figures 4H-4J) consistent with our prior studies (Snyder et al., 2013), and did not express SOX2 (Figures 4H and 4K). However, *Nkx2-1* deletion in KPN adenocarcinomas resulted in significantly elevated quantities of TANs (Figures 4H and 4L-4N and Figure S3E). Together, these results demonstrate that NKX2-1 suppresses TAN recruitment independently of SOX2 induction or squamous histotype.

SOX2 and NKX2-1 Inversely Regulate the Neutrophil Chemoattractant *Cxcl5*

We sought to define the mechanisms by which SOX2 and NKX2-1 regulate neutrophil recruitment. GSEA suggested that SL tumors are positively enriched for cytokine and chemokine signatures in comparison to KP tumors (Figure S4A). Expression of neutrophil-recruitment-associated genes such as *Cxcl2*, *Cxcl3*, *Cxcl5*, and *Pppb* (*Cxcl7*) was greater in SL and LP tumors than in KP tumors (Figure 5A). We employed an unbiased comprehensive approach to determine whether SOX2 and NKX2-1 converge on the regulation of any of these chemokines. First, we identified SOX2 binding sites in the genomes of LP tu-

mors and KPS cell lines by ChIP-seq. We chose LP tumors because they represent a neutrophil-rich squamous tumor with physiological levels of SOX2 expression, and we used KPS samples because they recapitulate SOX2 function in TAN recruitment independently of squamous histotype. To generate a similar dataset for NKX2-1 targets, we used published NKX2-1 ChIP-seq data from K adenocarcinomas and gene expression data comparing K and *Kras*^{LSL-G12D/+}; *Nkx2-1*^{fl/fl} (KN) tumors (Snyder et al., 2013). ChIP-seq analyses identified SOX2 and NKX2-1 binding motifs that were similar to those identified in previously published studies (Maeda et al., 2012; Watanabe et al., 2014) (Figure S4B). SOX2 and NKX2-1 bound some of the same genes, whereas each factor also bound unique targets (Figure 5B). We integrated ChIP-seq and gene expression data for each dataset to identify genes that were bound by and transcriptionally activated or suppressed by SOX2 and NKX2-1. Genes that were transcriptionally regulated by both SOX2 and NKX2-1 were mostly regulated inversely (Figure 5C), such that SOX2-induced genes were repressed by NKX2-1 and such that NKX2-1-induced genes were suppressed by SOX2. In contrast, many fewer genes were induced (or repressed) by both SOX2 and NKX2-1. These data suggest that SOX2 and NKX2-1 have unique genomic targets and inversely regulate transcription of many genes in lung cancer.

SOX2 promotes TAN accumulation, whereas NKX2-1 inhibits neutrophil accumulation in tumors, so we focused on genes that were induced by SOX2 and/or repressed by NKX2-1. *Cxcl5* was the only known neutrophil chemoattractant gene bound by either transcription factor in this category. Binding sites for both SOX2 and NKX2-1 could be identified in the promoter and first exon of *Cxcl5* (Figure 5D). *Cxcl5* mRNA expression was significantly elevated in SL and LP tumors compared to KP tumors and normal lung tissue, as well as in KN versus K tumors (Figure S4C). *CXCL6*, the human ortholog of mouse *Cxcl5* (Figures S4D and S4E), was significantly elevated in human LSCC compared to LADC (Campbell et al., 2016) (Figure S4C). *CXCL6* was one of only two CXCR2 ligands that significantly correlated with a squamous subtype and high SOX2 and low *NKX2-1* expression in a large collection of human NSCLC samples from TCGA (Figure 5E and Figures S4C and S4F).

Consistent with the gene expression data, SOX2⁺ KPS tumors and KPN tumors had significantly higher CXCL5 protein levels than control SOX2⁻ KPS, KPG, and KP tumors (Figures 5F and 5G). Moreover, SL and LP squamous tumors had high levels of CXCL5, whereas KP adenocarcinomas completely lacked it. Together, these findings suggest that SOX2 and NKX2-1 inversely regulate *Cxcl5* expression. To further test this, we overexpressed SOX2 in a panel of human lung cancer cell lines. Exogenous SOX2 was sufficient to induce CXCL6 in five of six cell lines (Figure S4G). In contrast, altering NKX2-1 amounts by overexpression or CRISPR-mediated loss was not sufficient to alter CXCL5 or CXCL6 levels *in vitro* (Figures S4H and S4I). Thus, it appears that NKX2-1 regulation of CXCL6 differs *in vitro* in human cells compared to mouse tumors.

To determine whether CXCL5 expression is sufficient to promote neutrophil recruitment, we infected KP mice with Lenti-Cxcl5-Cre or Lenti-GFP-Cre viruses and analyzed lungs 3-4 months after infection. Reminiscent of our observations with Lenti-Sox2-Cre, there was an occasional uncoupling of

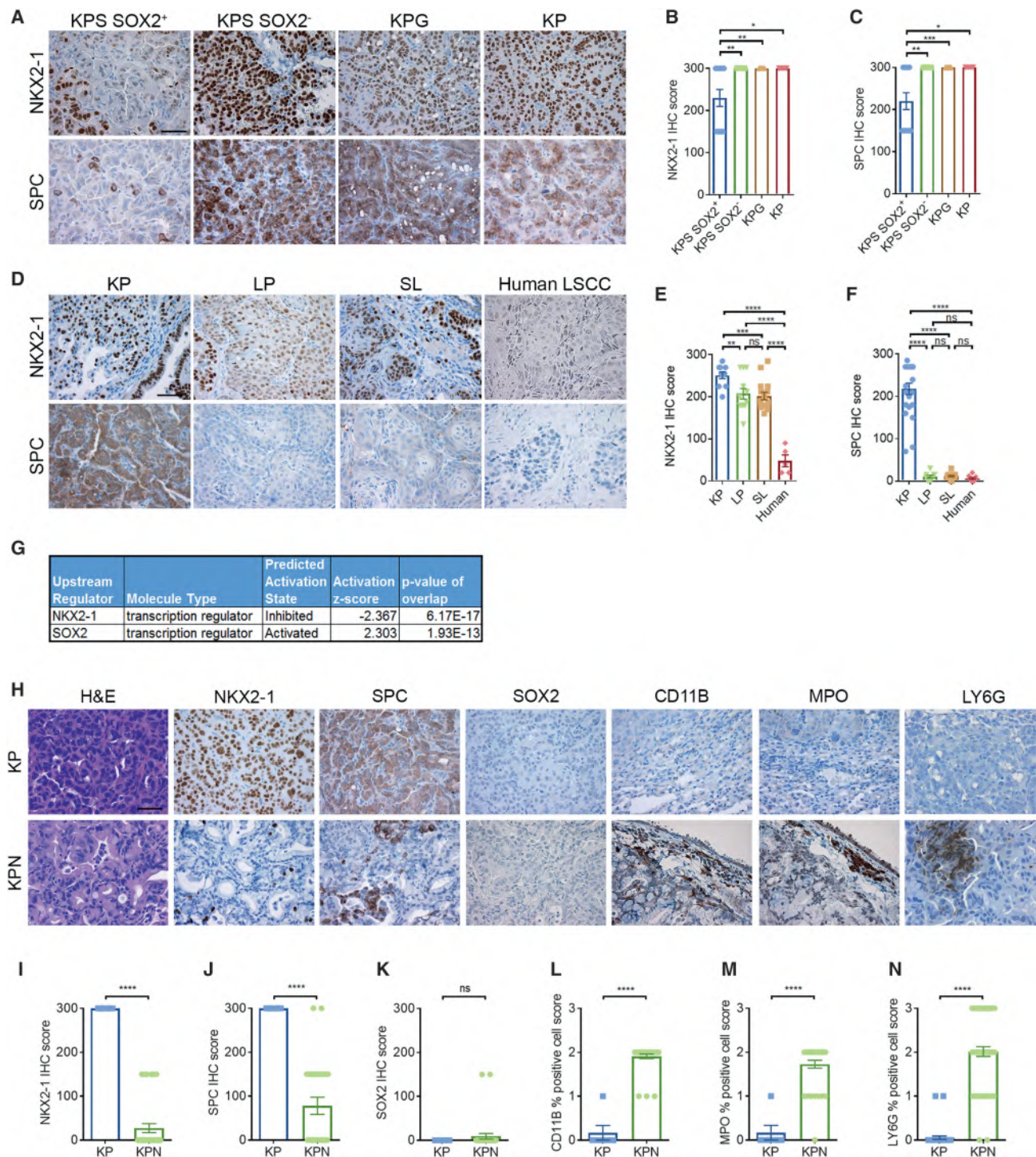
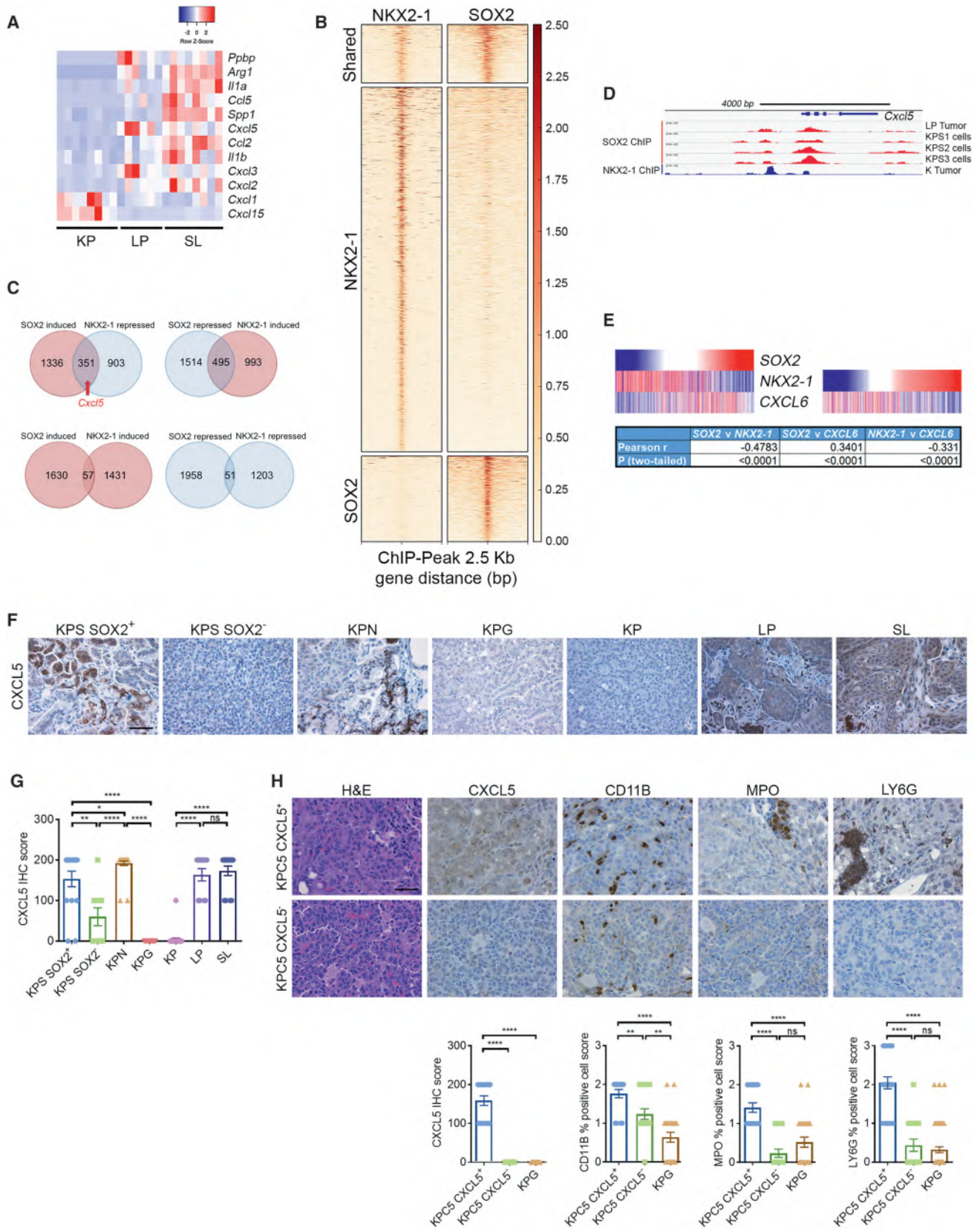


Figure 4. SOX2 Suppresses NKX2-1 Activity and NKX2-1 Loss Promotes TAN Recruitment in the Absence of Squamous Histotype

(A–C) IHC for NKX2-1 and SPC in indicated mouse tumor genotypes (A) and IHC quantification of NKX2-1 (B) and SPC (C). (D–F) IHC for NKX2-1 and SPC in indicated mouse and human tumors (D) and IHC quantification of NKX2-1 (E) and SPC (F). (G) IPA upstream-regulator analysis of RNA-seq data identify SOX2 and NKX2-1; activation z scores and p values are shown for SL versus KP tumors. (H–N) Representative IHC (H) and IHC quantification for NKX2-1 (I), SPC (J), SOX2 (K), CD11B (L), MPO (M), and LY6G (N) in indicated tumor models. Scale bars represent 50 μ m. Error bars indicate mean \pm SEM. Two-tailed unpaired t tests, **** p < 0.0001, *** p < 0.001, ** p < 0.01, * p < 0.05, ns = not significant. (B, C, E, F, and I–N) Each dot represents one tumor from three to eight mice per genotype and 6 patient LSCC tumors. See also Figure S3.



(legend on next page)

Cre and CXCL5 expression; some tumors lacked high CXCL5 expression (Figure 5H). KP-CXCL5⁺ (KPC5) tumors demonstrated high expression of CXCL5 and a significant increase in TAN accumulation (Figure 5H). When tumors with and without CXCL5 were detected near each other in the KPS or KPC5 models, only CXCL5⁺ tumors harbored neutrophils—suggesting that CXCL5's impact on neutrophil recruitment is relatively local (Figure S4J). These data demonstrate that tumor-derived CXCL5 expression is sufficient to promote TAN accumulation in lung cancer.

Loss of NKX2-1 Dramatically Accelerates Squamous Lung Tumorigenesis

To better understand the functions of SOX2 and NKX2-1, we performed pathway analyses by using Enrichr on genomic targets that were transcriptionally regulated *in vivo* (Figure 5C and Table S4). SOX2 induced expression of its own target genes, as well as genes bound by the transcriptional regulators TP63 and NFE2L2, which are known oncogenic transcription factors in LSCC (Campbell et al., 2016). SOX2-induced genes included those related to squamous cell fate (*Krt6a* and *Krt19*), ciliated cell fate (*Foxj1*), and the TP63 target gene (*Perp*) (Table S4 and Figure S5A). SOX2-repressed genes overlapped with genes bound by chromatin regulators, including EZH2, which is enriched in squamous lung tumors (Zhang et al., 2017). SOX2-repressed genes included gastric- and liver-fate regulators such as *Hnf4a*, *Foxa2*, and *Vil1* (Maeda et al., 2012). In contrast, NKX2-1 positively regulated genes involved in lung and alveolar cell fate; such genes included *Sftpa1*, *Sftpb*, and *Sftpc*. NKX2-1 inhibited expression of genes involved in gastrointestinal differentiation, consistent with our previous findings (Snyder et al., 2013). NKX2-1-repressed genes overlapped with known SOX2 genomic targets, as well as gastrointestinal-cell-fate genes, including *Foxa1*, *Perp*, *Lgals2*, *Lgals4*, *Krt20*, *Vil1*, *Cdh17*, and the mucous metaplasia gene, *Spdef* (Figure S5A and Table S4).

SL tumors have reduced but not completely absent NKX2-1 expression, whereas human LSCCs tend to be completely negative (Figure 4E). Given that NKX2-1 repressed the expression of genes that are induced by SOX2, we speculated that complete loss of NKX2-1 might facilitate SOX2-driven tumorigenesis. To address this hypothesis, we generated *Rosa26*^{LSL-Sox2-IRES-GFP}; *Nkx2-1*^{fl/fl}; *Lkb1*^{fl/fl} (SNL) mice. We infected SNL and SL mice with Ad5-CMV-Cre by using intratracheal inhalation and monitored mice for tumor formation via microCT imaging. We observed tumors in SNL mice as early as 8 weeks after tumor

initiation (Figure S5B). We then subjected a large cohort of mice to histopathologic review 16 weeks after infection. All SNL mice (n = 10) harbored multifocal neoplasia, including mucinous adenocarcinomas and adenosquamous and squamous cell carcinomas (Figures 6A and 6B and Figure S5C). In contrast, only one SL mouse (n = 25) harbored a single LSCC at this time point. In SNL mice, both mucinous and squamous components expressed SOX2 and GFP and lacked NKX2-1 (Figure 6B and Figure S5D). SOX2 intensity was heterogeneous in the squamous lesions, and basal-like cells expressed higher protein amounts than more highly keratinized tumor cells. SOX2 amounts were uniformly high in adenocarcinoma components, in concordance with a similar observation in KL mice (Zhang et al., 2017). DNp63 and KRT5 were robustly expressed in the squamous components of the SNL tumors and were absent in the mucinous adenocarcinoma cells, which instead expressed gastric-differentiation markers, including HNF4A, LGALS4, and CTSE (Figure 6B and Figure S5D). This is consistent with our previous work showing that NKX2-1 loss leads to activation of a gastric-differentiation program in LADC (Snyder et al., 2013).

Adenocarcinomas arising in KL mice undergo transdifferentiation to a squamous differentiation state over time (Li et al., 2015). To determine whether a similar phenomenon occurs in SNL mice, we analyzed lung tumors 4, 8, and 12 weeks after infection. At four weeks, we identified multifocal mucinous adenocarcinoma in the lungs of all mice (n = 6), whereas we found DNp63⁺ tumor cells only in a minority (33%) of mice (Figure 6C). The proportion of mice with DNp63⁺ tumor cells increased over time, such that by 12 weeks after infection DNp63⁺ tumor cells could be identified in the lungs of all SNL mice. The relative quantity of DNp63⁺ tumors in each mouse increased over time as well (Figure 6D). Taken together, these data show that loss of NKX2-1 dramatically accelerates tumorigenesis driven by SOX2 and loss of LKB1. These data suggest that alteration of these three genes induces mostly if not entirely mucinous adenocarcinoma lesions that undergo transdifferentiation to LSCC over time.

We sought to utilize this LSCC model to further investigate TAN regulation. TANs were abundant in all SNL tumors, regardless of histotype, although squamous tumors had subtly but significantly higher quantities of CD11B- and LY6G-positive cells (Figures 6E and 6F). Flow cytometry from SNL and KP tumors confirmed that squamous tumors exhibit increased TANs but fewer macrophages than do adenocarcinomas (Figures 6G and 6H and Figures S5E and S5F). SNL tumors with squamous and adenocarcinoma histotypes both exhibited high CXCL5

Figure 5. SOX2 and NKX2-1 Inversely Regulate Neutrophil Chemoattractant *Cxcl5*

- (A) Gene expression heatmap for genes implicated in neutrophil recruitment in SL, LP, and KP tumors. $p < 0.01$ and $\text{Log}_2\text{FC} > 1$ were used as a cutoff.
- (B) ChIP-seq heatmap view of genome-wide binding sites of SOX2 (LP tumors and KPS cells) and NKX2-1 [K tumors (Snyder et al., 2013)].
- (C) Venn diagrams indicating the total number of genes that are direct genomic targets of SOX2 and NKX2-1; the directionality of transcriptional regulation is shown. ChIP-seq data were integrated with RNA-seq data (SL versus KP tumors) and exon array data (KN versus K tumors) to define directionality of transcriptional regulation. $p < 0.05$ $\text{Log}_2\text{FC} > 1$ as a cutoff.
- (D) ChIP analysis of SOX2 and NKX2-1 genomic binding at the *Cxcl5* locus in the indicated samples.
- (E) Gene expression heatmaps for SOX2, *NKX2-1* and *CXCL6* in the TCGA lung cancer dataset (n = 1,129). Patient samples are sorted on the basis of SOX2 (left) or NKX2-1 (right) expression levels. Pearson correlation coefficient and two-tailed p values for each correlation gene pair is listed in a table (bottom). Data are visualized by UCSC Xena Browser.
- (F and G) IHC for CXCL5 in indicated GEMM lung tumors (F) and IHC quantification (G).
- (H) Representative H&E images and IHC for CXCL5, CD11B, MPO, and LY6G in indicated mouse tumors (top) and IHC quantification (bottom). The scale bars represent 50 μm . Error bars indicate mean \pm SEM. Two-tailed unpaired t tests, **** $p < 0.0001$, ** $p < 0.01$, * $p < 0.05$, ns = not significant. In (G) and (H), each dot represents one tumor from three to six mice per genotype. See also Figure S4 and Table S4.

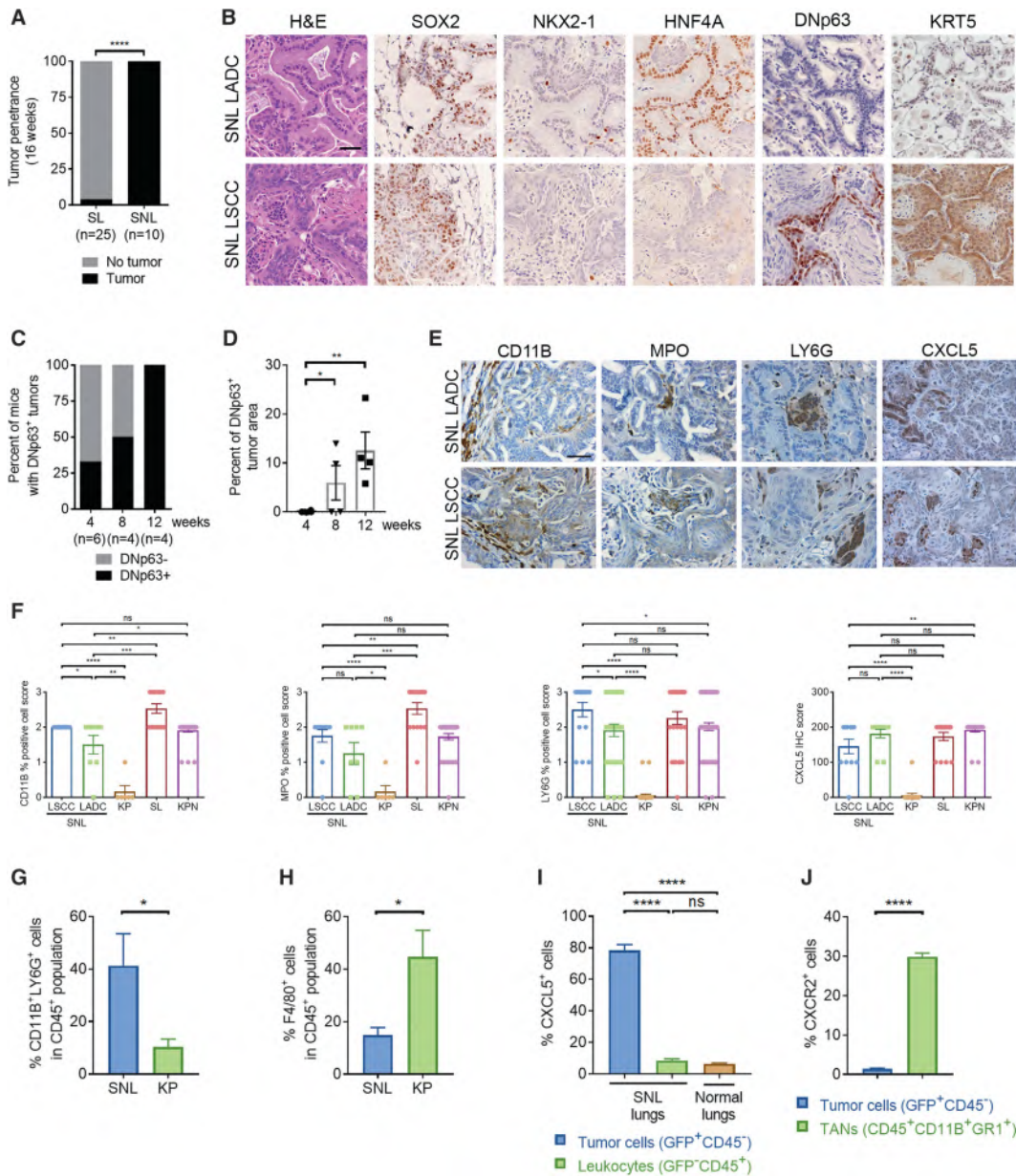


Figure 6. Loss of NKX2-1 Dramatically Accelerates Squamous Lung Tumorigenesis

(A) Proportion of SL (n = 25) versus SNL (n = 10) mice with squamous carcinoma 16 weeks after infection with Ad5-CMV-Cre. Fisher’s exact test (two-tailed), ****p < 0.0001.

(B) Representative images of H&E and IHC for SOX2, NKX2-1, HNF4A, DNP63, and KRT5 in LADC and LSCC tumors in the SNL model 16 weeks after infection.

(C) Percent of mice with DNP63⁺ tumors in SNL mice 4 (n = 6 mice), 8 (n = 4), and 12 (n = 4) weeks after infection.

(D) Percent of DNP63⁺ tumor area over total tumor area in SNL mice 4 (n = 6 mice), 8 (n = 4), and 12 (n = 4) weeks after infection. Mann-Whitney U tests, **p < 0.01, *p < 0.05. Each dot represents one mouse.

(E and F) Representative IHC for CD11B, MPO, LY6G, and CXCL5 in LADC and LSCC in the SNL model (E) and IHC quantification (F). KP, SL, and KPN quantification data are replicated from various other figures for ease of comparison. Each dot represents one tumor from four mice per group.

(G) Quantification of flow-cytometry data for CD11B⁺LY6G⁺ neutrophils as a percentage of leukocytes (CD45⁺) in SNL versus KP lungs (n = 4–6 samples per group).

(H) Quantification of flow-cytometry data for F4/80⁺ macrophages as a percentage of leukocytes (CD45⁺) in SNL versus KP lungs (n = 6–7 samples per group).

(I) Quantification of flow-cytometry data for CXCL5⁺ cancer cells (GFP⁺CD45⁻) and leukocytes (GFP⁺CD45⁺) in SNL versus normal lungs (n = 4–5 samples per group).

(J) Quantification of flow-cytometry data for CXCR2⁺ cancer cells (GFP⁺CD45⁻) and TANs (CD45⁺CD11B⁺GR1⁺) in SNL lungs (n = 8 samples per group).

Scale bars represent 50 μm. Error bars indicate mean ± SEM. Two-tailed unpaired t tests, ****p < 0.0001, ***p < 0.001, **p < 0.01, *p < 0.05, ns = not significant. See also Figure S5.

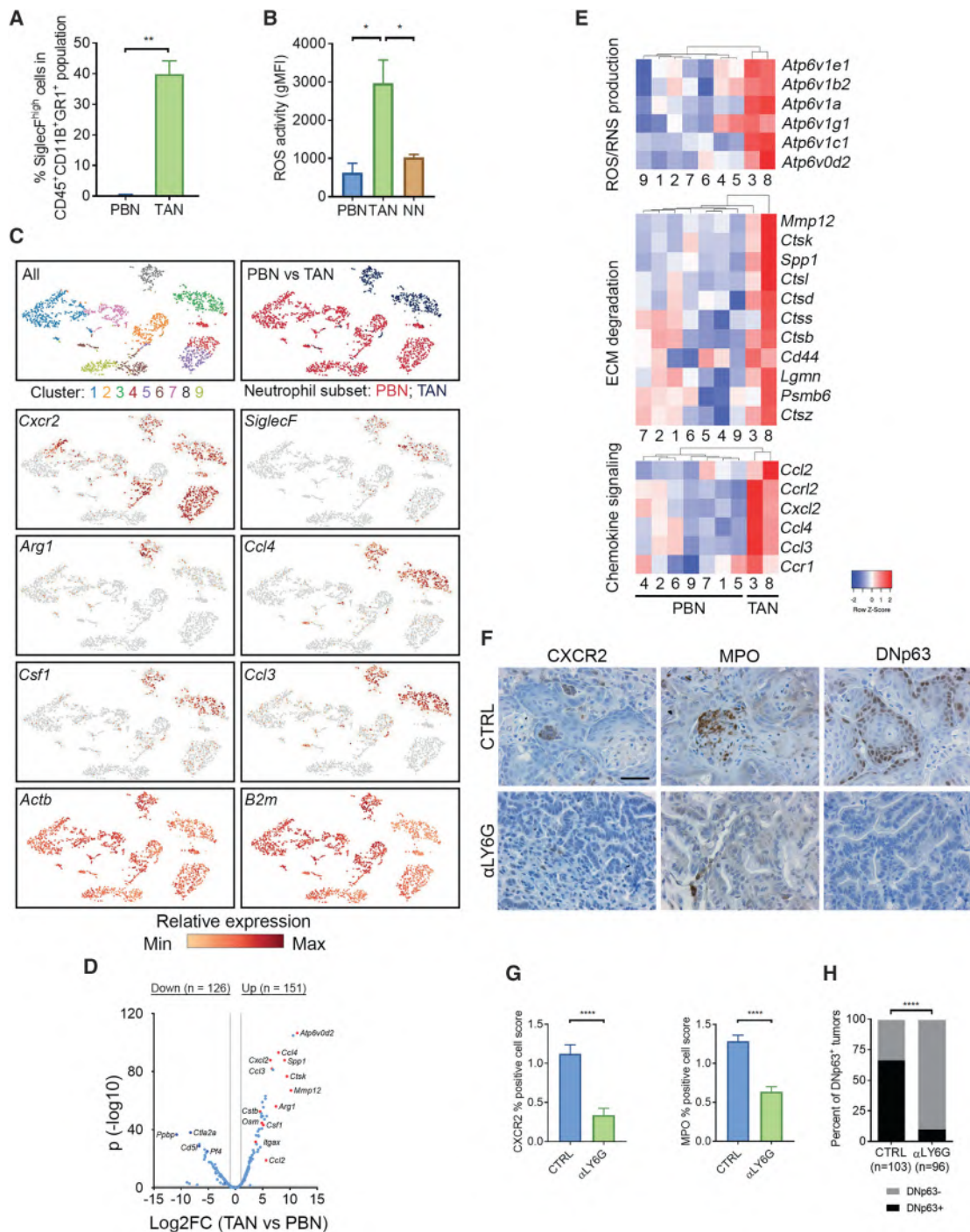


Figure 7. TANs are Distinct from Peripheral-Blood Neutrophils with Pro-tumor Features

(A) Quantification of flow-cytometry data for SiglecF^{high} cells as a percentage of neutrophils (CD45⁺CD11B⁺GR1⁺) in SNL lung tumors (n = 8) versus peripheral-blood neutrophils (PBNs) from SNL tumor-bearing mice (n = 2).

(B) Quantification of flow-cytometry data as geometric mean fluorescence intensity (gMFI) for ROS activity in PBNs, normal lung neutrophils (NNs), and tumor-associated neutrophils (TANs) (n = 4–8 samples per group from n = 2 mice each).

(C) tSNE plots of scRNA-seq data demonstrate all cell clusters (top left), PBN versus TAN cells (top right), and relative expression levels of selected genes (other panels). Flow-sorted samples were pooled from blood or lung tumors of SNL mice (n = 2 each).

(D) Volcano plot showing differential gene expression of scRNA-seq data comparing TANs and PBNs. p < 0.05 and Log₂FC > 1 were used as a cutoff (denoted by gray lines parallel to X and Y axes). Selected genes are highlighted (red).

(legend continued on next page)

protein amounts (Figures 6E and 6F). Furthermore, ~80% of SNL tumor cells expressed CXCL5, whereas < 10% of CD45⁺ immune cells from tumor-bearing or normal lungs expressed CXCL5 (Figure 6I and Figure S5G). TANs within both SNL LADC and LSCC tumor regions expressed CXCR2, the receptor for CXCL5 (Figures 6J and Figures S5H and S5I). Together, these findings suggest that CXCL5-expressing tumor cells recruit CXCR2⁺ neutrophils through a paracrine mechanism. They further suggest that TAN recruitment to tumors is determined by transcriptional regulators that specify cell fate.

TANs Exhibit Pro-tumor Features and Promote Squamous Tumors

To further characterize TANs in this model, we sorted CD45⁺ CD11B⁺GR1⁺ cells and examined their cytology (Figure S6A). Many TANs exhibited a circular banding phenotype reminiscent of N2 TANs (Fridlender et al., 2009). We analyzed CD45⁺ CD11B⁺GR1⁺ cells from tumor-bearing lungs and the blood of SNL animals for the recently identified N2 marker SiglecF (Engblom et al., 2017). Approximately 40% of TANs, but not peripheral blood neutrophils (PBNs), expressed SiglecF (Figure 7A and Figure S6B). SiglecF⁺ neutrophils exhibit multiple pro-tumor functions, including increased reactive oxygen species (ROS) production and the ability to foster tumor progression (Engblom et al., 2017). To determine whether SNL TANs exhibit pro-tumor functions, we measured the ability of normal neutrophils (NNs) from healthy control lungs, PBNs, and TANs to produce intracellular ROS. TANs exhibited significantly more ROS than both NNs and PBNs by ~3- to 4-fold (Figure 7B and Figure S6C).

Because TANs exhibited cytological heterogeneity and only a subset expressed SiglecF, we sought to explore TAN heterogeneity by using single-cell RNA-seq (scRNA-seq). We sorted CD45⁺CD11B⁺LY6G⁺ cells from the peripheral blood of tumor-bearing SNL animals (i.e., PBNs) or lung tumors (i.e., TANs) from the same animals (Figure S6D). We used the Chromium drop-seq platform (10x Genomics) to obtain transcriptomes from PBNs (n = 1744 cells) or TANs (n = 519 cells). We visualized chromium-derived transcriptional profiles by using t-distributed stochastic neighbor embedding (tSNE) (van der Maaten and Hinton, 2008). Cell Ranger clustering called nine distinct clusters, seven within the PBNs and two among the TANs (Figure 7C). *Cxcr2* and house-keeping genes *Actb* and *B2m* were expressed in most clusters, regardless of the source of neutrophil. Although clusters 8 and 9 were negative for *Cxcr2*, they expressed *S100a8/9*, suggesting that these cells were also neutrophils (Figure S6E). Consistent with the flow-cytometry data, *SiglecF* expression was largely confined to the TAN clusters (Figure 7C). GSEA revealed enrichment of the SiglecF-high versus SiglecF-low neutrophil gene signature (Engblom et al., 2017) in the SNL TAN population (Figure S6F). Furthermore, many N2-neutro-

phil-associated genes, such as *Arg1*, *Ccl3*, *Ccl4* and *Csf1*, had significantly increased expression in TANs versus PBNs (Figures 7C and 7D). Pathway analyses using Enrichr on differentially expressed genes among TANs versus PBNs (Figure 7D and Table S5) revealed that TANs had increased expression of genes involved in ROS and reactive nitrogen species (RNS) production, extracellular matrix (ECM) degradation, and N2-related chemokine signaling (Figure 7E). Neutrophil degranulation genes were differentially expressed among PBNs and TANs, and PBNs were enriched for pathways related to “positive regulation of the immune system” (Figures S6E and S6G). Together, these data suggest that LSCC TANs are a heterogeneous population in which at least some cells exhibit gene expression and functional activities ascribed to N2 TANs.

Finally, we sought to determine the function of TANs in the SNL model by using a neutrophil-depletion strategy (Fridlender et al., 2009; Steele et al., 2016). SNL mice were treated with control or anti-LY6G antibody for three weeks, after which tumor-bearing lungs were harvested. TANs were significantly reduced in anti-LY6G-treated animals as determined by IHC analyses (Figures 7F and 7G). The lungs of neutrophil-depleted animals had fewer squamous tumors upon inspection of H&E-stained sections. Consistent with this observation, neutrophil-depleted lungs had significantly fewer DNp63⁺ tumors than did controls (Figures 7F and 7H). These findings suggest that TANs promote squamous tumorigenesis and might directly or indirectly impact tumor-cell fate in this transdifferentiation model. Altogether, these data suggest that lineage-specifier genes impact the tumor immune microenvironment, and the immune microenvironment in turn might impact tumor phenotype.

DISCUSSION

A distinctive feature of the LSCC TIME compared to that of LADC is the enrichment of neutrophils. Multiple LSCC mouse models (LP, Sox2PC, and now SL and SNL) display elevated neutrophils in comparison to LADC GEMMs (KP and K). It was previously postulated that histotype determines the TIME in NSCLC. Abundant keratinization in squamous tumors, for example, can molecularly resemble a persistent wound accompanied by aberrant inflammation. On the other hand, a growing body of evidence suggests that cancer-cell-intrinsic factors also impact the TIME (Bezzi et al., 2018; Li et al., 2018). STAT3 and NF-κB signaling have roles in inflammation and are elevated in LSCC compared to LADC (Mukhopadhyay et al., 2014; Xiao et al., 2013). A recent finding that *Egfr*- and *Kras*-driven LADC mouse tumors have distinct lymphocyte compositions also suggests that oncogenic drivers might dictate the TIME (Busch et al., 2016). Our findings here reveal tumor-intrinsic mechanisms whereby lineage-specific tumor drivers (SOX2 and NKX2-1) inversely regulate TAN accumulation.

(E) Gene expression heatmaps for genes implicated in ROS and RNS production; extracellular matrix (ECM) degradation and cysteine endopeptidase activity; and chemokine signaling. Gene sets were derived from Enrichr analyses. Cell cluster numbers are labeled below each column identified in Figure 7C. $p < 0.05$ and $\text{Log}_2\text{FC} > 1$ were used as a cutoff.

(F–H) Representative images of IHC for CXCR2, MPO, and DNp63 in SNL mice treated with anti-LY6G antibody versus anti-IgG1 control antibody thrice weekly for 3–4 weeks (n = 8 mice per group) (F) and IHC quantification for CXCR2 and MPO (G) and DNp63 (H).

The scale bar represents 50 μm. In (A), (B), and (G), error bars indicate mean ± SEM; two-tailed unpaired t tests, ****p < 0.0001, **p < 0.005, *p < 0.05. (H) Fisher’s exact test (two-tailed), ****p < 0.0001. See also Figure S6 and Table S5.

Multiple chemokines can act upon the CXCR2 neutrophil receptor to induce neutrophil chemotaxis (Zlotnik and Yoshie, 2012). *Cxcl3*, *-5*, and *-7* have greater expression in SL and LP tumors than in KP and K tumors. Although the exact mechanism of transcriptional regulation requires further study, unbiased ChIP and RNA-seq data from GEMM tumors revealed that *Cxcl5* is a direct genomic target of SOX2 and NKX2-1. We found that SOX2 overexpression or NKX2-1 loss is sufficient to induce CXCL5 in tumor cells *in vivo*, and tumor-associated CXCL5 is sufficient to recruit TANs. It is likely that other neutrophil recruitment chemokines are indirectly regulated in these lung-cancer subtypes and might also be sufficient for TAN recruitment. Future studies employing *Cxcl5* genetic deletion and/or antibody-mediated CXCL5 depletion will be necessary to determine whether CXCL5 is required for TAN recruitment. Our data suggest CXCL5 regulation is governed by lineage specifiers rather than tumor histotype because we observe CXCL5 expression and TAN influx in adenocarcinomas when either SOX2 or NKX2-1 is altered. These data are consistent with previous studies in KL mice, where TANs are enriched in LSCCs as opposed to LADCs. In the KL model, SOX2 and CXCL5 expression levels are both increased, whereas NKX2-1 levels are decreased during adeno-to-squamous transdifferentiation (Nagaraj et al., 2017; Zhang et al., 2017), consistent with the mechanisms proposed here. *CXCL6*, the human ortholog of mouse *Cxcl5*, is positively correlated with SOX2 and negatively correlated with *NKX2-1* expression in human NSCLC, suggesting the mechanisms described here most likely function in human tumors.

Importantly, we found that NKX2-1, which has pro- and anti-oncogenic activities in LADC, is a tumor suppressor in LSCC. In SL and LP mice, the peripheral location of squamous tumors and the detection of smaller adenosquamous lesions at early time points hinted that these tumors originate from distal lung epithelium. Studies in *Sox2PC* mice showed that in addition to basal cells, club cells and alveolar type 2 cells can give rise to squamous tumors (Ferone et al., 2016). SOX2 overexpression (either genetically or naturally acquired during tumorigenesis) is common to all three squamous GEMMs. NKX2-1 levels are reduced in squamous GEMMs but are not entirely absent, in contrast to complete NKX2-1 loss in human LSCC. These findings suggest that squamous tumors in GEMMs are primarily initiated in distal epithelium and transdifferentiate to squamous fate over time, perhaps during their long latency. It seems likely that all LSCCs must downregulate NKX2-1 to adopt a squamous fate, whether they arise from basal cells in the proximal airway or in the distal lung, where peripheral-type LSCCs arise. Consistent with this hypothesis, *Nkx2-1* deletion significantly accelerated LSCC development, and there was evidence of transdifferentiation. ChIP and RNA-seq data suggested that NKX2-1 repressed known SOX2 target genes, so we speculate that this provides a mechanism by which NKX2-1 loss facilitates SOX2-driven transformation. An independent study recently found that *Sox2* expression and *Nkx2-1* deletion in the mouse lung (i.e., SN) cooperate to promote squamous lung cancer and that NKX2-1 loss alters SOX2 occupancy in the genome (Tata et al., 2018). Similar to our observations in SNL mice, SN cells in that study might transdifferentiate in organoid cultures, including in the absence of stromal cells. If confirmed *in vivo*, this might suggest

that neutrophils promote squamous tumorigenesis but are not required for transdifferentiation. Future studies should address how SN and SNL tumor development might differ in terms of latency, tumor-cell fate, and the TIME. Although the Tata et al. study did not investigate the TIME, our data predict that SN tumors will have elevated CXCL5 and TANs, as in SNL mice. Tata et al. suggest that airway cells are more permissive than alveolar cells for squamous transformation, so additional studies are warranted to determine how the cell of origin impacts tumor cell fate upon *Nkx2-1* loss.

Our scRNA-seq data suggest that TANs are fundamentally different from PBNs and acquire pro-tumor features such as increased ROS activity and elevated expression of genes that block T cell activity and promote ECM degradation. Because the scRNA-seq data presented here are limited to small numbers of cells, fully deciphering the molecular and functional heterogeneity among TANs will require further studies. The neutrophil depletion experiments demonstrated that TANs preferentially promote squamous tumors. This observation is intriguing because it suggests a bidirectional crosstalk between tumor cells and immune cells. The underlying mechanism by which TANs impact tumor cell fate remains elusive because TANs might either create a favorable TIME for preexisting squamous cancer cells over adenocarcinoma cells or accelerate adeno-to-squamous transdifferentiation. Because ROS and hypoxia can promote adeno-to-squamous transdifferentiation (Han et al., 2014; Li et al., 2015) and both are induced by neutrophils (Campbell et al., 2014; Coffelt et al., 2016), future studies should test the role of TAN-induced ROS and hypoxia in this phenomenon.

Multiple studies have indicated that relapsed LADC after targeted therapy or chemotherapy can transition to LSCC, although the mechanisms are still poorly understood (Hou et al., 2016). Understanding the heterogeneity and plasticity of the TIME and how tumor genotype shapes the TIME is crucial for effective therapy. Here we find that the genetic mechanisms that regulate adeno-to-squamous transdifferentiation also shape the TIME and that, in turn, immune cells can impact tumor phenotype. Future studies are warranted for determining how TANs and other immune cell types evolve during tumor transdifferentiation and how these fluctuations might affect response to immunotherapy.

STAR★METHODS

Detailed methods are provided in the online version of this paper and include the following:

- KEY RESOURCES TABLE
- CONTACT FOR REAGENT AND RESOURCES SHARING
- EXPERIMENTAL MODELS AND SUBJECT DETAILS
 - Mice
 - MEFs
 - Human Cell Lines
 - Human Lung Cancer Tissue
- METHOD DETAILS
 - MicroCT Imaging
 - *Ex vivo* Imaging
 - Lentivirus Production

- Immunohistochemistry
- Immunoblot
- RNA Isolation and RNA-Sequencing
- Chromatin Immunoprecipitation Sequencing (ChIP-seq)
- Flow Cytometry
- Single Cell RNA-Sequencing
- Evaluation of Neutrophil Morphology
- *Ex vivo* ROS Activity
- Neutrophil Depletion
- Bioinformatic Analyses
- QUANTIFICATION AND STATISTICAL ANALYSIS
- DATA AND SOFTWARE AVAILABILITY
 - Data Resources

SUPPLEMENTAL INFORMATION

Supplemental Information includes six figures and five tables and is available with this article online at <https://doi.org/10.1016/j.immuni.2018.09.020>.

ACKNOWLEDGMENTS

We thank the T. Jacks laboratory for lentiviral constructs and KP mice and M. Van Brocklin for HEK293T reporter cells. Thanks to excellent core facilities, specifically to J. O'Shea, B. Anderson, and K. Gligorich for histological services; J. Marvin for flow cytometry; and B. Dalley for bioinformatics support. We are grateful to members of the Oliver, Snyder, and McMahon laboratories for technical assistance and feedback; specifically, we thank P. Ballieu, D. Hansen, R. Olsen, and R. Dahlgren. We acknowledge support from the National Cancer Institute (NCI) of the National Institutes of Health (NIH) under award P30CA042014 awarded to Huntsman Cancer Institute for the use of core facilities, including the Biorepository and Molecular Pathology, High-Throughput Genomics and Bioinformatics Analysis, and Flow Cytometry Shared Resources, and we acknowledge internal funding from the Immunology, Inflammation, and Infectious Diseases Initiative. G.M. is supported by the NIH NCI (F99CA223015). E.L.S. holds a Career Award for Medical Scientists from the Burroughs Wellcome Fund and the NIH (R01CA212415). T.G.O. was supported in part by the Damon Runyon Cancer Research Foundation (DRR-26-13), American Cancer Society (Research Scholar Award no. RSG-13-300-01-TBG) and the NIH NCI (R01CA187457).

AUTHOR CONTRIBUTIONS

Conceptualization, G.M., E.L.S., T.E.L., T.G.O.; Methodology, G.M., A.J., A.M., K.B.J., E.L.S., T.G.O.; Formal Analysis, G.M., A.J., T.L.M., A.B., C.S., C.J.C., J.M.V., J.G., M.E.S., E.L.S., T.G.O.; Investigation, G.M., A.J., A.M., K.C.B., D.H., S.A.C., R.A., S.J., S.J.W., S.C., B.L.W., J.G., M.E.S., K.B.J., E.L.S., T.G.O.; Pathology, B.L.W., M.E.S., E.L.S.; Resources, M.H.C.; Data Curation, -; Writing – Original Draft, G.M. & T.G.O.; Writing – Review & Editing, G.M., E.L.S., T.G.O.; Visualization, G.M., T.G.O.; Supervision, E.L.S., T.G.O.; Project Administration, E.L.S., T.G.O.; Funding Acquisition, G.M., E.L.S., T.E.L., T.G.O.

DECLARATION OF INTERESTS

The authors declare no competing interests.

Received: July 12, 2018

Revised: August 16, 2018

Accepted: September 25, 2018

Published: October 16, 2018

REFERENCES

Asselin-Labat, M.-L., and Filby, C.E. (2012). Adult lung stem cells and their contribution to lung tumorigenesis. *Open Biol.* 2, 120094.

Bass, A.J., Watanabe, H., Mermel, C.H., Yu, S., Perner, S., Verhaak, R.G., Kim, S.Y., Wardwell, L., Tamayo, P., Gat-Viks, I., et al. (2009). SOX2 is an amplified lineage-survival oncogene in lung and esophageal squamous cell carcinomas. *Nat. Genet.* 41, 1238–1242.

Bezzi, M., Seitzer, N., Ishikawa, T., Reschke, M., Chen, M., Wang, G., Mitchell, C., Ng, C., Katon, J., Lunardi, A., et al. (2018). Diverse genetic-driven immune landscapes dictate tumor progression through distinct mechanisms. *Nat. Med.* 24, 165–175.

Busch, S.E., Hanke, M.L., Kargl, J., Metz, H.E., MacPherson, D., and Houghton, A.M. (2016). Lung cancer subtypes generate unique immune responses. *J. Immunol.* 197, 4493–4503.

Campbell, E.L., Bruyninckx, W.J., Kelly, C.J., Glover, L.E., McNamee, E.N., Bowers, B.E., Bayless, A.J., Scully, M., Saeedi, B.J., Golden-Mason, L., et al. (2014). Transmigrating neutrophils shape the mucosal microenvironment through localized oxygen depletion to influence resolution of inflammation. *Immunity* 40, 66–77.

Campbell, J.D., Alexandrov, A., Kim, J., Wala, J., Berger, A.H., Pedamallu, C.S., Shukla, S.A., Guo, G., Brooks, A.N., Murray, B.A., et al.; Cancer Genome Atlas Research Network (2016). Distinct patterns of somatic genome alterations in lung adenocarcinomas and squamous cell carcinomas. *Nat. Genet.* 48, 607–616.

Coffelt, S.B., Wellenstein, M.D., and de Visser, K.E. (2016). Neutrophils in cancer: neutral no more. *Nat. Rev. Cancer* 16, 431–446.

Engblom, C., Pfirschke, C., Zilionis, R., Da Silva Martins, J., Bos, S.A., Courties, G., Rickelt, S., Severe, N., Baryawno, N., Faget, J., et al. (2017). Osteoblasts remotely supply lung tumors with cancer-promoting Siglec^F^{high} neutrophils. *Science* 358, 15081.

Eruslanov, E.B., Bhojnarwal, P.S., Quatromoni, J.G., Stephen, T.L., Ranganathan, A., Deshpande, C., Akimova, T., Vachani, A., Litzky, L., Hancock, W.W., et al. (2014). Tumor-associated neutrophils stimulate T cell responses in early-stage human lung cancer. *J. Clin. Invest.* 124, 5466–5480.

Ferone, G., Song, J.-Y., Sutherland, K.D., Bhaskaran, R., Monkhorst, K., Lambooi, J.-P., Proost, N., Gargiulo, G., and Berns, A. (2016). SOX2 is the determining oncogenic switch in promoting lung squamous cell carcinoma from different cells of origin. *Cancer Cell* 30, 519–532.

Fridlender, Z.G., Sun, J., Kim, S., Kapoor, V., Cheng, G., Ling, L., Worthen, G.S., and Albelda, S.M. (2009). Polarization of tumor-associated neutrophil phenotype by TGF- β : “N1” versus “N2” TAN. *Cancer Cell* 16, 183–194.

Fridlender, Z.G., Sun, J., Mishalian, I., Singhal, S., Cheng, G., Kapoor, V., Horng, W., Fridlender, G., Bayuh, R., Worthen, G.S., and Albelda, S.M. (2012). Transcriptomic analysis comparing tumor-associated neutrophils with granulocytic myeloid-derived suppressor cells and normal neutrophils. *PLoS ONE* 7, e31524.

Gentles, A.J., Newman, A.M., Liu, C.L., Bratman, S.V., Feng, W., Kim, D., Nair, V.S., Xu, Y., Khuong, A., Hoang, C.D., et al. (2015). The prognostic landscape of genes and infiltrating immune cells across human cancers. *Nat. Med.* 21, 938–945.

Han, X., Li, F., Fang, Z., Gao, Y., Li, F., Fang, R., Yao, S., Sun, Y., Li, L., Zhang, W., et al. (2014). Transdifferentiation of lung adenocarcinoma in mice with Lkb1 deficiency to squamous cell carcinoma. *Nat. Commun.* 5, 3261.

Hou, S., Han, X., and Ji, H. (2016). Squamous transition of lung adenocarcinoma and drug resistance. *Trends Cancer* 2, 463–466.

Jackson, E.L., Willis, N., Mercer, K., Bronson, R.T., Crowley, D., Montoya, R., Jacks, T., and Tuveson, D.A. (2001). Analysis of lung tumor initiation and progression using conditional expression of oncogenic K-ras. *Genes Dev.* 15, 3243–3248.

Jonkers, J., Meuwissen, R., van der Gulden, H., Peterse, H., van der Valk, M., and Berns, A. (2001). Synergistic tumor suppressor activity of BRCA2 and p53 in a conditional mouse model for breast cancer. *Nat. Genet.* 29, 418–425.

Kargl, J., Busch, S.E., Yang, G.H.Y., Kim, K.-H., Hanke, M.L., Metz, H.E., Hubbard, J.J., Lee, S.M., Madtes, D.K., McIntosh, M.W., and Houghton, A.M. (2017). Neutrophils dominate the immune cell composition in non-small cell lung cancer. *Nat. Commun.* 8, 14381.

- Kim, C.F.B., Jackson, E.L., Woolfenden, A.E., Lawrence, S., Babar, I., Vogel, S., Crowley, D., Bronson, R.T., and Jacks, T. (2005). Identification of bronchioalveolar stem cells in normal lung and lung cancer. *Cell* **121**, 823–835.
- Koyama, S., Akbay, E.A., Li, Y.Y., Aref, A.R., Skoulidis, F., Herter-Sprue, G.S., Buczkowski, K.A., Liu, Y., Awad, M.M., Denning, W.L., et al. (2016). STK11/LKB1 deficiency promotes neutrophil recruitment and proinflammatory cytokine production to suppress T-cell activity in the lung tumor microenvironment. *Cancer Res.* **76**, 999–1008.
- Kusakabe, T., Kawaguchi, A., Hoshi, N., Kawaguchi, R., Hoshi, S., and Kimura, S. (2006). Thyroid-specific enhancer-binding protein/NKX2.1 is required for the maintenance of ordered architecture and function of the differentiated thyroid. *Mol. Endocrinol.* **20**, 1796–1809.
- Langer, C.J., Obasaju, C., Bunn, P., Bonomi, P., Gandara, D., Hirsch, F.R., Kim, E.S., Natale, R.B., Novello, S., Paz-Ares, L., et al. (2016). Incremental innovation and progress in advanced squamous cell lung cancer: Current status and future impact of treatment. *J. Thorac. Oncol.* **11**, 2066–2081.
- Lee, C.-L., Moding, E.J., Huang, X., Li, Y., Woodlief, L.Z., Rodrigues, R.C., Ma, Y., and Kirsch, D.G. (2012). Generation of primary tumors with Flp recombination in FRT-flanked p53 mice. *Dis. Model. Mech.* **5**, 397–402.
- Li, F., Han, X., Li, F., Wang, R., Wang, H., Gao, Y., Wang, X., Fang, Z., Zhang, W., Yao, S., et al. (2015). LKB1 inactivation elicits a redox imbalance to modulate non-small cell lung cancer plasticity and therapeutic response. *Cancer Cell* **27**, 698–711.
- Li, J., Byrne, K.T., Yan, F., Yamazoe, T., Chen, Z., Baslan, T., Richman, L.P., Lin, J.H., Sun, Y.H., Rech, A.J., et al. (2018). Tumor cell-intrinsic factors underlie heterogeneity of immune cell infiltration and response to immunotherapy. *Immunity* **49**, 178–193.e7.
- Lu, Y., Futtner, C., Rock, J.R., Xu, X., Whitworth, W., Hogan, B.L.M., and Onaitis, M.W. (2010). Evidence that SOX2 overexpression is oncogenic in the lung. *PLoS ONE* **5**, e11022.
- Maeda, Y., Tsuchiya, T., Hao, H., Tompkins, D.H., Xu, Y., Mucenski, M.L., Du, L., Keiser, A.R., Fukazawa, T., Naomoto, Y., et al. (2012). Kras(G12D) and Nkx2-1 haploinsufficiency induce mucinous adenocarcinoma of the lung. *J. Clin. Invest.* **122**, 4388–4400.
- Morrissey, E.E., and Hogan, B.L.M. (2010). Preparing for the first breath: genetic and cellular mechanisms in lung development. *Dev. Cell* **18**, 8–23.
- Mukhopadhyay, A., Berrett, K.C., Kc, U., Clair, P.M., Pop, S.M., Carr, S.R., Witt, B.L., and Oliver, T.G. (2014). Sox2 cooperates with Lkb1 loss in a mouse model of squamous cell lung cancer. *Cell Rep.* **8**, 40–49.
- Nagaraj, A.S., Lahtela, J., Hemmes, A., Pellinen, T., Blom, S., Devlin, J.R., Salmenkivi, K., Kallioniemi, O., Mäyränpää, M.I., Närhi, K., and Verschuren, E.W. (2017). Cell of origin links histotype spectrum to immune microenvironment diversity in non-small-cell lung cancer driven by mutant Kras and loss of Lkb1. *Cell Rep.* **18**, 673–684.
- Palmer, C., Diehn, M., Alizadeh, A.A., and Brown, P.O. (2006). Cell-type specific gene expression profiles of leukocytes in human peripheral blood. *BMC Genomics* **7**, 115.
- Papagiannakopoulos, T., Bauer, M.R., Davidson, S.M., Heimann, M., Subbaraj, L., Bhutkar, A., Bartlebaugh, J., Vander Heiden, M.G., and Jacks, T. (2016). Circadian rhythm disruption promotes lung tumorigenesis. *Cell Metab.* **24**, 324–331.
- Pitt, J.M., Vétizou, M., Daillère, R., Roberti, M.P., Yamazaki, T., Routy, B., Lepage, P., Boneca, I.G., Chamaillard, M., Kroemer, G., and Zitvogel, L. (2016). Resistance mechanisms to immune-checkpoint blockade in cancer: Tumor-intrinsic and -extrinsic factors. *Immunity* **44**, 1255–1269.
- Powell, D.R., and Huttenlocher, A. (2016). Neutrophils in the tumor microenvironment. *Trends Immunol.* **37**, 41–52.
- Ribas, A., and Wolchok, J.D. (2018). Cancer immunotherapy using checkpoint blockade. *Science* **359**, 1350–1355.
- Schönhuber, N., Seidler, B., Schuck, K., Veltkamp, C., Schachtler, C., Zukowska, M., Eser, S., Feyerabend, T.B., Paul, M.C., Eser, P., et al. (2014). A next-generation dual-recombinase system for time- and host-specific targeting of pancreatic cancer. *Nat. Med.* **20**, 1340–1347.
- Segura, E., Touzot, M., Bohineust, A., Cappuccio, A., Chiochia, G., Hosmalin, A., Dalod, M., Soumelis, V., and Amigorena, S. (2013). Human inflammatory dendritic cells induce Th17 cell differentiation. *Immunity* **38**, 336–348.
- Snyder, E.L., Watanabe, H., Magendantz, M., Hoersch, S., Chen, T.A., Wang, D.G., Crowley, D., Whittaker, C.A., Meyerson, M., Kimura, S., and Jacks, T. (2013). Nkx2-1 represses a latent gastric differentiation program in lung adenocarcinoma. *Mol. Cell* **50**, 185–199.
- Steele, C.W., Karim, S.A., Leach, J.D.G., Bailey, P., Upstill-Goddard, R., Rishi, L., Foth, M., Bryson, S., McDaid, K., Wilson, Z., et al. (2016). CXCR2 inhibition profoundly suppresses metastases and augments immunotherapy in pancreatic ductal adenocarcinoma. *Cancer Cell* **29**, 832–845.
- Stewart, S.A., Dykxhoorn, D.M., Palliser, D., Mizuno, H., Yu, E.Y., An, D.S., Sabatini, D.M., Chen, I.S.Y., Hahn, W.C., Sharp, P.A., et al. (2003). Lentivirus-delivered stable gene silencing by RNAi in primary cells. *RNA* **9**, 493–501.
- Tanaka, H., Yanagisawa, K., Shinjo, K., Taguchi, A., Maeno, K., Tomida, S., Shimada, Y., Osada, H., Kosaka, T., Matsubara, H., et al. (2007). Lineage-specific dependency of lung adenocarcinomas on the lung development regulator TTF-1. *Cancer Res.* **67**, 6007–6011.
- Tata, P.R., Chow, R.D., Saladi, S.V., Tata, A., Konkimalla, A., Bara, A., Montoro, D., Hariri, L.P., Shih, A.R., Mino-Kenudson, M., et al. (2018). Developmental history provides a roadmap for the emergence of tumor plasticity. *Dev. Cell* **44**, 679–693.e5.
- Templeton, A.J., McNamara, M.G., Šeruga, B., Vera-Badillo, F.E., Aneja, P., Ocaña, A., Leibowitz-Amit, R., Sonpavde, G., Knox, J.J., Tran, B., et al. (2014). Prognostic role of neutrophil-to-lymphocyte ratio in solid tumors: a systematic review and meta-analysis. *J. Natl. Cancer Inst.* **106**, dju124.
- Van de Laar, E., Clifford, M., Hasenoeder, S., Kim, B.R., Wang, D., Lee, S., Paterson, J., Vu, N.M., Waddell, T.K., Keshavjee, S., et al. (2014). Cell surface marker profiling of human tracheal basal cells reveals distinct subpopulations, identifies MST1/MSP as a mitogenic signal, and identifies new biomarkers for lung squamous cell carcinomas. *Respir. Res.* **15**, 160.
- van der Maaten, L., and Hinton, G. (2008). Visualizing data using t-SNE. *J. Mach. Learn. Res.* **9**, 2579–2605.
- Vaughan, A.E., Brumwell, A.N., Xi, Y., Gotts, J.E., Brownfield, D.G., Treutlein, B., Tan, K., Tan, V., Liu, F.C., Looney, M.R., et al. (2015). Lineage-negative progenitors mobilize to regenerate lung epithelium after major injury. *Nature* **517**, 621–625.
- Watanabe, H., Ma, Q., Peng, S., Adelmant, G., Swain, D., Song, W., Fox, C., Francis, J.M., Pedamallu, C.S., DeLuca, D.S., et al. (2014). SOX2 and p63 colocalize at genetic loci in squamous cell carcinomas. *J. Clin. Invest.* **124**, 1636–1645.
- Xiao, Z., Jiang, Q., Willette-Brown, J., Xi, S., Zhu, F., Burkett, S., Back, T., Song, N.Y., Datla, M., Sun, Z., et al. (2013). The pivotal role of IKK α in the development of spontaneous lung squamous cell carcinomas. *Cancer Cell* **23**, 527–540.
- Xu, C., Fillmore, C.M., Koyama, S., Wu, H., Zhao, Y., Chen, Z., Herter-Sprue, G.S., Akbay, E.A., Tchaicha, J.H., Altobelli, A., et al. (2014). Loss of Lkb1 and Pten leads to lung squamous cell carcinoma with elevated PD-L1 expression. *Cancer Cell* **25**, 590–604.
- Young, N.P., Crowley, D., and Jacks, T. (2011). Uncoupling cancer mutations reveals critical timing of p53 loss in sarcomagenesis. *Cancer Res.* **71**, 4040–4047.
- Zhang, H., Fillmore Brainson, C., Koyama, S., Redig, A.J., Chen, T., Li, S., Gupta, M., Garcia-de-Alba, C., Paschini, M., Herter-Sprue, G.S., et al. (2017). Lkb1 inactivation drives lung cancer lineage switching governed by Polycomb Repressive Complex 2. *Nat. Commun.* **8**, 14922.
- Zheng, H., Ying, H., Yan, H., Kimmelman, A.C., Hiller, D.J., Chen, A.-J.J., Perry, S.R., Tonon, G., Chu, G.C., Ding, Z., et al. (2008). p53 and Pten control neural and glioma stem/progenitor cell renewal and differentiation. *Nature* **455**, 1129–1133.
- Zlotnik, A., and Yoshie, O. (2012). The chemokine superfamily revisited. *Immunity* **36**, 705–716.
- Zuo, W., Zhang, T., Wu, D.Z., Guan, S.P., Liew, A.-A., Yamamoto, Y., Wang, X., Lim, S.J., Vincent, M., Lessard, M., et al. (2015). p63(+)Krt5(+) distal airway stem cells are essential for lung regeneration. *Nature* **517**, 616–620.

Mitophagy in Intestinal Epithelial Cells Triggers Adaptive Immunity during Tumorigenesis

Paul K. Ziegler,^{1,2} Julia Bollrath,¹ Charles K. Pallangyo,¹ Takaji Matsutani,³ Özge Canli,¹ Tiago De Oliveira,¹ Michaela A. Diamanti,¹ Nina Müller,¹ Jaba Gamrekashvili,⁴ Tracy Putoczki,⁵ David Horst,⁶ Arun K. Mankan,¹ Meryem G. Öner,⁷ Susanna Müller,⁷ Josef Müller-Höcker,⁷ Thomas Kirchner,^{7,8} Julia Slotta-Huspenina,⁹ M. Mark Taketo,¹⁰ Thomas Reinheckel,^{8,11} Stefan Dröse,¹² Andrew C. Larner,¹³ Winfried S. Wels,^{1,8} Matthias Ernst,¹⁴ Tim F. Greten,¹⁵ Melek C. Arkan,^{1,8,16} Thomas Korn,¹⁷ Dagmar Wirth,^{18,19} and Florian R. Greten^{1,8,20,*}

¹Institute for Tumor Biology and Experimental Therapy, Georg-Speyer-Haus, 60596 Frankfurt am, Germany

²Institute of Pathology, Frankfurt University Hospital, 60590 Frankfurt, Germany

³R&D Department, Repertoire Genesis Incorporation, Ibaraki, Osaka 567-0085, Japan

⁴Department of Nephrology, Medical School Hannover, 30625 Hannover, Germany

⁵Walter and Eliza Hall Institute of Medical Research, Melbourne VIC, Australia

⁶Institute of Pathology, Charité- Universitätsmedizin Berlin, 10117 Berlin, Germany

⁷Institute of Pathology, Ludwig-Maximilians-University, 80337 Munich, Germany

⁸German Cancer Consortium (DKTK) and German Cancer Research Center (DKFZ), 69120 Heidelberg, Germany

⁹Institute of Pathology of the Technical University Munich, 81675 Munich, Germany

¹⁰Division of Experimental Therapeutics, Graduate School of Medicine, Kyoto University, Kyoto 606-8501, Japan

¹¹Institute of Molecular Medicine and Cell Research, Faculty of Medicine, Albert-Ludwigs-University Freiburg, 79104 Freiburg, Germany

¹²Department of Anesthesiology, Frankfurt University Hospital, 60590 Frankfurt am, Germany

¹³Department of Biochemistry and Molecular Biology, and Massey Cancer Center, Virginia Commonwealth University, Richmond, VA 23298, USA

¹⁴Olivia Newton-John Cancer Research Institute, La Trobe University School of Cancer Medicine, Heidelberg VIC 3084, Australia

¹⁵National Institutes of Health, National Cancer Institute, Medical Oncology Branch, Bethesda, MD 20892, USA

¹⁶Institute of Biochemistry II, Goethe University School of Medicine, 60590 Frankfurt am, Germany

¹⁷Department of Neurology, Klinikum rechts der Isar, Technical University Munich, 81675 Munich, Germany

¹⁸Model Systems for Infection and Immunity, Helmholtz Centre for Infection Research, Inhoffenstr. 7, 38124 Braunschweig, Germany

¹⁹Experimental Hematology, Hannover Medical School, Carl-Neuberg-Str. 1, 30625 Hannover, Germany

²⁰Lead Contact

*Correspondence: greten@gsh.uni-frankfurt.de

<https://doi.org/10.1016/j.cell.2018.05.028>

SUMMARY

In colorectal cancer patients, a high density of cytotoxic CD8⁺ T cells in tumors is associated with better prognosis. Using a Stat3 loss-of-function approach in two wnt/ β -catenin-dependent autochthonous models of sporadic intestinal tumorigenesis, we unravel a complex intracellular process in intestinal epithelial cells (IECs) that controls the induction of a CD8⁺ T cell based adaptive immune response. Elevated mitophagy in IECs causes iron(II)-accumulation in epithelial lysosomes, in turn, triggering lysosomal membrane permeabilization. Subsequent release of proteases into the cytoplasm augments MHC class I presentation and activation of CD8⁺ T cells via cross-dressing of dendritic cells. Thus, our findings highlight a so-far-unrecognized link between mitochondrial function, lysosomal integrity, and MHC class I presentation in IECs and suggest that therapies triggering mitophagy or inducing LMP in IECs may prove successful in shifting the balance toward anti-tumor immunity in colorectal cancer.

INTRODUCTION

Colorectal cancer (CRC) belongs to a group of the most commonly diagnosed cancers in both men and women in the Western world (Siegel et al., 2016). Activating mutations in the Wnt pathway that mostly affect *APC* or *CTNNB1* are found in the majority of cases; however, apart from these, only a small number of additional genes are significantly mutated (Cancer Genome Atlas, 2012). Instead, colorectal carcinogenesis depends on the close interaction of mutated tumor cells with their microenvironment (Grivnenkov et al., 2010). The presence of tumor-infiltrating T cells and, in particular, CD8⁺ T cells and increased interferon-gamma (IFN γ) expression has prognostic relevance and is associated with prolonged survival, whereas a T helper 17 (Th17) T-cell-dominated immune response is associated with a worse outcome (Fridman et al., 2012). While the clinical correlation between T cell infiltration and prognosis is undisputed and has led to the development of an immune score that can be employed to predict survival of CRC patients (Fridman et al., 2012), less is known about the underlying cellular and molecular mechanisms that drive T cell polarization during intestinal carcinogenesis.

Activation of the transcription factor STAT3 has been documented in a wide range of tumors, including CRC (Bollrath and Greten, 2009). Multiple pathways, including receptor

engagement by interleukin-6 (IL-6) family members, G-protein-coupled receptors, Toll-like receptors, and microRNAs, have been identified to activate JAK-STAT3 signaling in tumor cells and infiltrating immune cells (Yu et al., 2014). This results in Y705 phosphorylation of STAT3 and nuclear translocation of STAT3 to drive transcription of genes involved in cell-cycle regulation, cell survival, cell migration, and, importantly, immunosuppression. In addition to phosphorylation of the Y705 residue of STAT3, phosphorylation can occur at serine-727 (S727) as a result of receptor engagement by various growth factors, such as epidermal growth factor (EGF), and signals that are transduced via the ERK-, p38-, JNK-, or PKC δ -pathways (Decker and Kovarik, 2000). Apart from STAT3's classical role as a transcription factor, non-canonical STAT3-dependent functions also have been proposed (Demaria et al., 2014; Gough et al., 2009; Wegrzyn et al., 2009).

Autophagy represents an intracellular degradation process that encloses ubiquitinated proteins in vesicles termed "autophagosomes," which subsequently fuse with lysosomes (Levine and Kroemer, 2008). Besides its role as a response mechanism to cellular stress (e.g., during nutrient deprivation), autophagy also serves as the specific degradation mechanism of aged and/or damaged mitochondria, a process known as "mitophagy." The kinase PINK1 binds to mitochondria with decreased membrane potential, the driving force of mitochondrial respiration, and thereby marks these to degradation via the autophagosomal-lysosomal pathway (Youle and Narendra, 2011). Mitochondria are rich in iron-containing macromolecules; therefore, mitophagy, which leads to transfer of mitochondrial proteins into lysosomes, can contribute to lysosomal iron content, which is critical for their resistance to reactive oxygen species (Terman et al., 2010).

The adaptive immune system relies on the presentation of cellular antigens by other cells on their surface via major histocompatibility complex (MHC) molecules. Whereas MHC class II molecules are present only on specialized antigen-presenting cells (mainly dendritic cells, DCs), MHC class I molecules are present on virtually all cells of mammalian organisms and can be recognized by CD8⁺ T cells. To bind to nascent MHC molecules, antigens have to be transported into the endoplasmic reticulum (ER) by the transmembrane transport system transporter associated with antigen presentation (TAP).

In addition to a large body of evidence indicating that the proteasome is the origin of most antigens presented via MHC class I molecules, some evidence indicates that other proteases can contribute to antigen processing (Cruz et al., 2017; Münz, 2016; Rock et al., 2010). Most notably, the lysosomal protease cathepsin S has been found to facilitate antigen generation in DCs in the endosomal-lysosomal compartment before being presented by MHC class I molecules (Hari et al., 2015; Shen et al., 2004). In addition, in intestinal epithelial cells (IECs) as well as bone-marrow-derived antigen-presenting cells, cathepsin S is involved in antigen-presentation by MHC class II molecules, whereas cathepsin L is required for this in thymic cortical epithelial cells (Beers et al., 2005; Nakagawa et al., 1998).

Apart from the ability of DCs to present peptide antigens from their cytoplasm, these cells are also involved in the uptake and processing of extracellular antigens with MHC class I molecules to CD8⁺ T cells by cross presentation (Cruz et al., 2017).

Recently, it was noted that, in addition to foreign protein, DCs can also take up complete antigen-MHC class I (and II) complexes and present them to T cells, a process termed "cross-dressing" (Nakayama, 2015). This process has been implicated in anti-tumor immunity as well as anti-viral host defense (Nakayama, 2015).

RESULTS

Loss of Stat3 in IECs Prevents Sporadic Tumorigenesis and Causes Infiltration of CD8⁺ T Cells during Tumor Initiation

Stat3^{fllox} and *Stat3^{ΔIEC}* mice were subjected to 6 weekly injections of the somatic mutagen azoxymethane (AOM) and tumor development was examined 18 weeks later. While AOM induces oncogenic point mutations in β -catenin and led to development of tubular adenomas in the colons of 100% of *Stat3*-proficient (*Stat3^{fllox}*) animals, tumor formation was completely abolished in mice where *Stat3* was deleted in IECs (Figures 1A–1C). Strikingly, the absence of *Stat3* also prevented formation of pre-neoplastic foci which still occurred in these mice when challenged with AOM in the context of chronic inflammation during CAC (Bollrath et al., 2009), suggesting the complete loss of mutagenized *Stat3*-deficient IECs during initiation of sporadic tumorigenesis. Histological examination of AOM challenged *Stat3^{ΔIEC}* mice revealed a pronounced accumulation of lamina propria CD3⁺ T cells when compared to *Stat3^{fllox}* controls (Figures 1D–1F). T cell accumulation in *Stat3^{ΔIEC}* mice was preceded by an elevated number of CD11c⁺, but not F4/80⁺ or Gr1⁺, cells (Figure 1H) and increased *Il12* mRNA expression (Figure 1I) in the colonic lamina propria at an early time point in the model when first pre-neoplastic aberrant crypt foci (ACF) were detectable in both genotypes (Figure 1G; data not shown). This raised the possibility that AOM exposure triggered an adaptive immune response against mutagenized cell in *Stat3^{ΔIEC}* mice, thereby preventing their subsequent outgrowth into macroscopic colonic tumors. This finding is in line with a recent report demonstrating that CD8⁺ T cells can be stimulated by retinoic acid *in vivo* and, in doing so, can contribute to controlling AOM/DSS-induced tumor growth (Bhattacharya et al., 2016).

To distinguish whether an underlying mechanism is dependent on the mutagenic effect of AOM in IECs or the influence of mutated IECs on their cellular environment, we utilized *villin-creER^{T2}/Ctnnb^{loxEx3/WT}* mice, termed " β -cat^{c.a.}," as a defined genetic model for oncogenic activation of the wnt pathway. This model confers IEC-specific and tamoxifen-induced expression of an exon-3-deleted—and thereby stabilized form of— β -catenin. Accordingly, β -cat^{c.a.} mice mimic the AOM-induced missense mutation in exon 3 of *Ctnnb* that results in stabilization of the corresponding protein and aberrant activation of the wnt/ β -catenin pathway (Greten et al., 2004) observed in >80% of human colorectal cancer (CRC) (Cancer Genome Atlas, 2012). Mice expressing stabilized β -catenin are characterized by rapid expansion of proliferative intestinal crypt stem cells and loss of absorptive enterocytes causing death of β -cat^{c.a.} mice within ~4 weeks after oral tamoxifen application (Schwitalla et al., 2013). IEC-specific expression of the serine 727- and tyrosine 705-phosphorylated form of *Stat3* indicated marked *Stat3*

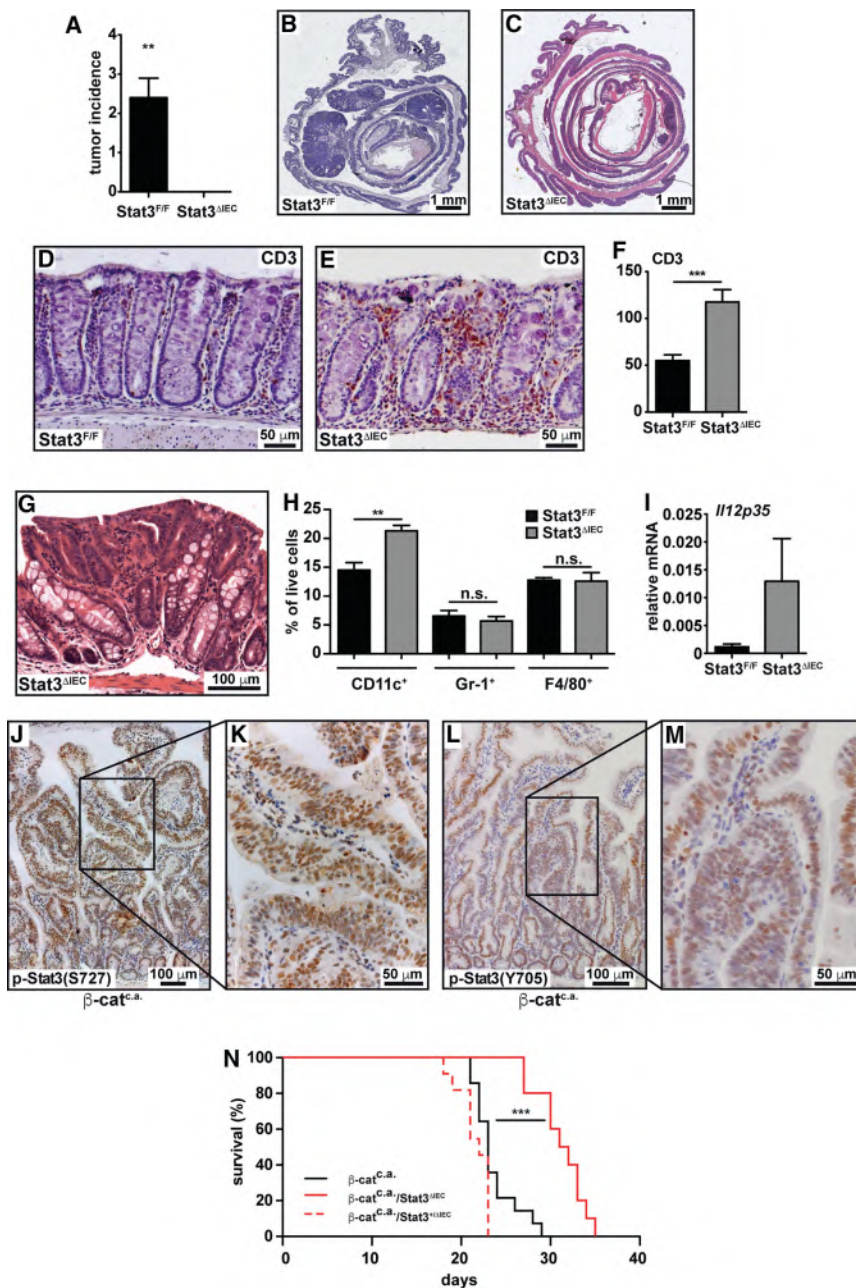


Figure 1. Loss of Stat3 in IEC Blocks Initiation of Sporadic Intestinal Tumorigenesis

(A) Tumor incidence in *Stat3^{F/F}* (n = 10) and *Stat3^{ΔIEC}* (n = 9) mice 18 weeks after initial AOM challenge. Data are mean ± SEM, **p < 0.01 by one-sample t test.

(B–E) Representative H&E-stained sections (B and C) and CD3 immunohistochemistry (IHC) (D and E) of AOM-challenged colons. Scale bars, 1 mm (B and C) and 50 μm (D and E).

(F) Quantification of infiltrating CD3⁺ T cells in colonic non-tumor areas. Data are mean ± SEM, ***p < 0.001 by Student's t test.

(G) Representative H&E-stained colonic aberrant crypt focus from a *Stat3^{ΔIEC}* mouse 8 weeks after the first AOM injection. Scale bar, 100 μm.

(H) Flow cytometric analysis of different myeloid cell subpopulations in colonic lamina propria of *Stat3^{F/F}* and *Stat3^{ΔIEC}* mice 1 week after the last AOM injection. Data are mean ± SEM; n = 5 per genotype; **p < 0.01 by Student's t test.

(I) Relative mRNA expression 1 week after the last AOM injection. Data are mean ± SEM; n = 5 per genotype.

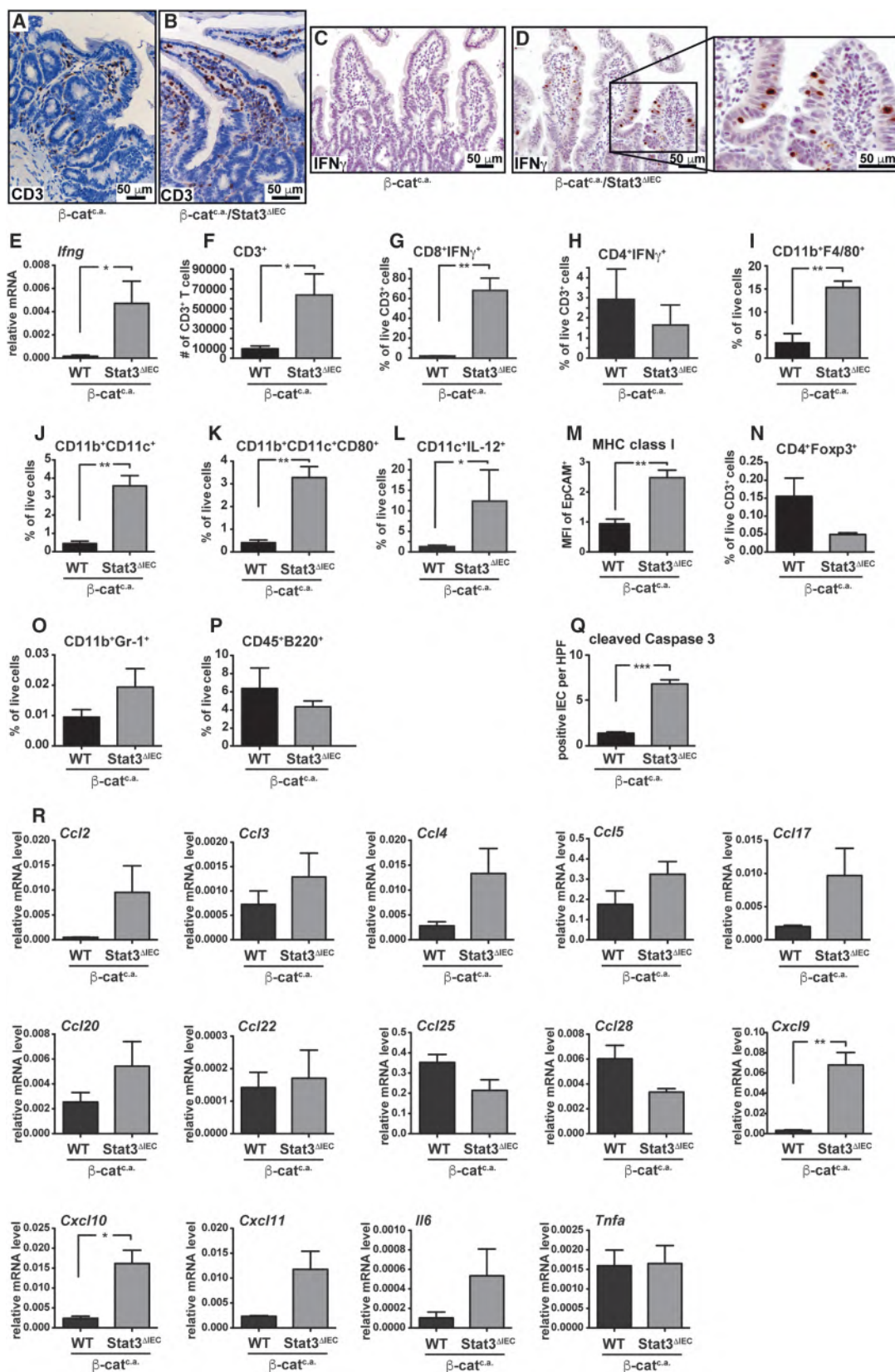
(J–M) IHC of p-Stat3^{S727} (J and K) and p-Stat3^{Y705} (L and M) in *β-cat^{c.a.}* mice. Scale bars, 100 μm (J and L) and 50 μm (K and M).

(N) Survival of *β-cat^{c.a.}* (n = 15), *β-cat^{c.a.}/Stat3^{ΔIEC}* (n = 10) and *β-cat^{c.a.}/Stat3^{+ΔIEC}* mice (n = 11). ***p < 0.001 by log-rank test. See also Figure S1.

of CD3⁺ cells, similar to our observations in AOM-challenged *Stat3^{ΔIEC}* mice, as well as a high number of IFNγ-expressing infiltrating intraepithelial lymphocytes (Figures 2A–2D). Real-Time PCR confirmed elevated *Il12p35* expression in the mucosa of *β-cat^{c.a.}/Stat3^{ΔIEC}* mice when compared to their Stat3 proficient counterparts (Figure 2E). These findings were further corroborated by fluorescence-activated cell sorting (FACS) analysis, which revealed a marked increase of CD3⁺ T cells in the lamina propria of *β-cat^{c.a.}/Stat3^{ΔIEC}* mice and CD8⁺ cells of the αβ lineage, rather than CD4⁺ T cells as the main source of IFNγ

activation in transformed crypts of *β-cat^{c.a.}* mice (Figures 1J–1M). By contrast, IEC-restricted homozygous ablation of Stat3 significantly prolonged survival of the corresponding *β-cat^{c.a.}/Stat3^{ΔIEC}* mice (median survival of *β-cat^{c.a.}* mice 23 days versus 31 days in *β-cat^{c.a.}/Stat3^{ΔIEC}* mice; median survival of heterozygous *β-cat^{c.a.}/Stat3^{+ΔIEC}* mice: 22 days; n ≥ 10; p < 0.001) (Figure 1N). We did not detect any evidence for improved differentiation or changes in proliferation of Stat3-deficient *β-cat^{c.a.}* IECs (Figures S1A–S1H), yet a higher villus/crypt ratio indicated a block in crypt expansion in *β-cat^{c.a.}/Stat3^{ΔIEC}* mice compared to Stat3-proficient controls (Figure S1G). Moreover, *β-cat^{c.a.}/Stat3^{ΔIEC}* mice were characterized by a marked accumulation

(Figures 2F–2H; data not shown). This was accompanied by a significantly increased number of cleaved caspase3-positive apoptotic IECs in *β-cat^{c.a.}/Stat3^{ΔIEC}* mice (Figure 2Q), supporting cytotoxic activity of CD8⁺ T cells. Furthermore, *β-cat^{c.a.}/Stat3^{ΔIEC}* mice showed an elevated frequency of CD11b⁺F4/80⁺ macrophages (Figure 2I), activated CD11b⁺/CD11c⁺ dendritic cells (DC) that expressed CD80 and IL-12 (Figures 2J–2L), and elevated expression of MHC class I in EpCAM⁺ IECs (Figure 2M). In contrast, other notable immune cell populations were unchanged (Figures 2N–2P). In addition, we could detect a number of T cell related chemokines, most notably the IFNγ-inducible chemokines CXCL-9, CXCL-10, and



(legend on next page)

CXCL-11, to be upregulated in Stat3-deficient IECs during tumorigenesis (Figure 2R). Collectively, these data suggest that loss of Stat3 in IECs triggered an adaptive immune response leading to IEC death, which delayed expansion of β -catenin mutant crypt cells associated with prolonged survival of β -cat^{c.a.}/*Stat3* ^{Δ IEC} mice.

Prolonged Survival of β -Cat^{c.a.}/*Stat3* ^{Δ IEC} Mice Depends on Presence of CD8⁺ T Cells and IFN γ

Genetically modified mouse models are usually not very immunogenic and do not express many neo-antigens because of their low mutational burden. Therefore, we aimed to confirm a T cell contribution to this model and sequenced TCR α - and β -chain CDR3 regions in sorted CD8⁺ T cells from intestinal mucosa of β -cat^{c.a.} and β -cat^{c.a.}/*Stat3* ^{Δ IEC} mice. Indeed, loss of Stat3 in β -catenin mutant IECs led to clonal expansion of CD8⁺ T cells (Figure 3A) and less diverse T cell receptors (TCRs) (Figures 3B, 3C, and S2A–S2H). These findings are in line with an enhanced antigen-dependent immune response in these mice. This was further corroborated when we introduced a model antigen by employing ROSAOVA mice that contain an immunogenic peptide from ovalbumin (ova, amino acids [aa] 246–353) flanked by inversely oriented loxP sites and targeted into the ubiquitously active ROSA26 locus (Sandhu et al., 2011). ROSAOVA mice were crossed with both β -cat^{c.a.} mice (β -cat^{c.a.}/*OVA*^{IEC}) as well as β -cat^{c.a.}/*Stat3* ^{Δ IEC} mice (β -cat^{c.a.}/*Stat3* ^{Δ IEC}/*OVA*^{IEC}) and resultant offspring were treated with tamoxifen. Expectedly, flow cytometry on day 15 using a K^b/OVA (SIINFEKL) pentamer confirmed a significantly increased number of SIINFEKL-specific CD8⁺ T cells in the intestinal mucosa in β -cat^{c.a.}/*Stat3* ^{Δ IEC}/*OVA*^{IEC} mice (Figure 3D). Moreover, staining of IECs using the 25-D1.16 monoclonal antibody that specifically reacts with ovalbumin-derived peptide SIINFEKL bound to H-2K^b of MHC class I revealed increased binding on Stat3-deficient IECs, confirming enhanced antigen processing in IECs from β -cat^{c.a.}/*Stat3* ^{Δ IEC}/*OVA*^{IEC} mice (Figure 3E). Similarly, the number of SIINFEKL-specific CD8⁺ T cells was elevated in AOM-challenged *Stat3* ^{Δ IEC}/*OVA*^{IEC} mice when compared to *OVA*^{IEC} mice (Figure 3F).

To functionally confirm that the survival advantage of β -cat^{c.a.}/*Stat3* ^{Δ IEC} mice was indeed dependent on the observed adaptive immune response rather than on IEC-specific cell autonomous effects such as proliferation, we either depleted CD8⁺ T cells using a neutralizing antibody or CD11c⁺ DCs using CD11c-DTR mice (Jung et al., 2002). Expectedly, antibody-mediated loss of CD8⁺ T cells or diphtheria toxin-induced ablation of CD11c⁺ DCs reduced survival of β -cat^{c.a.}/*Stat3* ^{Δ IEC} mice (median survival

24 days in CD8⁺ T cell or CD11c⁺ DCs depleted β -cat^{c.a.}/*Stat3* ^{Δ IEC} animals, Figure 3G and 3H). A comparable reduction of survival was also observed in β -cat^{c.a.}/*Stat3* ^{Δ IEC}/*Irfng*^{-/-} compound mutants, with a median survival of 23 days (Figure 3I). Collectively, these data strongly suggest that IEC-specific Stat3 activation precludes the generation of an effective CD8⁺ T cell-dependent immune response during the tumor initiation phase.

CD8⁺ T Cell Activation Is a Consequence of Lysosomal Membrane Permeabilization

Having established the consequence of Stat3 deficiency in IECs during intestinal tumor initiation, we aimed to identify the responsible mechanism that prevented CD11c⁺ DC and T cell activation. In fully malignant murine colon cancer cells or B16 melanoma cells expression of dominant negative Stat3 increases expression of pro-inflammatory cytokines, including tumor necrosis factor alpha (TNF- α), IL-6, CCL5, CXCL10, and IFN β , which triggers CD8⁺ T cell activation (Wang et al., 2004). Surprisingly, we did not observe marked expression differences for these cytokines and chemokines between primary IECs of Stat3 wild-type (WT) β -cat^{c.a.} and Stat3-deficient β -cat^{c.a.}/*Stat3* ^{Δ IEC} mice 3 days after the first tamoxifen application (Figure S3A). Instead, careful histomorphological examination revealed enlarged lysosomal structures in IECs of β -cat^{c.a.}/*Stat3* ^{Δ IEC} mice when stained for LAMP2 (Figures 4A and 4B), which prompted us to examine lysosomal function. Lysosomal membrane permeabilization (LMP) in response to the acute cellular stress commonly elicited in mutagenized cells, leads to the release of cathepsins from lysosomes into the cytosol (Boya and Kroemer, 2008). While total expression of cathepsins S, L, and B and of the lysosomal protease inhibitor cystatin C remained unaffected in IECs of β -cat^{c.a.}/*Stat3* ^{Δ IEC} mice (Figures S3B and S3C), proteases accumulated in cytoplasmic fractions of these cells presumably in response to increased release from lysosomes (Figures 4C–4E). Importantly, administration of the membrane permeable pan-cysteine protease inhibitor E64d prevented upregulation of *Irfng* gene expression in both β -cat^{c.a.} and β -cat^{c.a.}/*Stat3* ^{Δ IEC} mice (Figure 4F), as well as IEC apoptosis (Figure S3D), supporting the notion that lysosomal proteases play an important role in CD8⁺ T cell activation. To examine whether LMP was essential in this context and whether such immune cell activation could also be elicited in Stat3-proficient IECs, we treated β -cat^{c.a.} mice with chloroquine, a well-known inducer of LMP (Boya et al., 2003). Indeed, chloroquine triggered release of cathepsins from lysosomes in β -catenin mutant IECs (Figure 4G) and caused accumulation of CD3⁺ T cells in the lamina propria of β -cat^{c.a.} mice (Figures 4H and 4I) as well as

Figure 2. *Stat3* ^{Δ IEC} Mice Are Characterized by Increased Accumulation of CD8⁺/IFN γ ⁺ T Cells in the Intestine upon Activation of wnt Signaling

(A–D) IHC of CD3 (A and B) and IFN γ (C and D) 15 days after starting tamoxifen.

(E) Relative *Irfng* mRNA expression in small intestinal mucosa of β -cat^{c.a.} and β -cat^{c.a.}/*Stat3* ^{Δ IEC} mice on day 15; n = 6/genotype.

(F) Quantification of infiltrating CD3⁺ T cells.

(G–L) Flow cytometric analysis of IFN γ in CD8⁺ (G) and CD4⁺ (H) T cells, CD11b⁺F4/80⁺ (I) and CD11b⁺CD11c⁺ (J) cells as well as CD80 (K) and IL-12 (L) in CD11c⁺ cells on day 15; n = 3/genotype.

(M) Surface expression (mean fluorescence intensity, MFI) of MHC class I 3 days after first tamoxifen; n = 4/genotype.

(N–P) Flow cytometric analysis of CD4⁺Foxp3⁺ (N), CD11b⁺Gr1⁺ (O), and CD45⁺B220⁺ (P) cells on day 15; n = 3/genotype.

(Q) Number of cleaved caspase 3-pos. IEC; n = 4/genotype; \geq 20 high-power fields (HPF)/animal.

(R) Relative gene expression of the indicated cytokines or chemokines in IECs on day 15; n = 3/genotype.

In (E)–(R), data are mean \pm SEM. Scale bars, 50 μ m. *p < 0.05, **p < 0.01 by Student's t test.

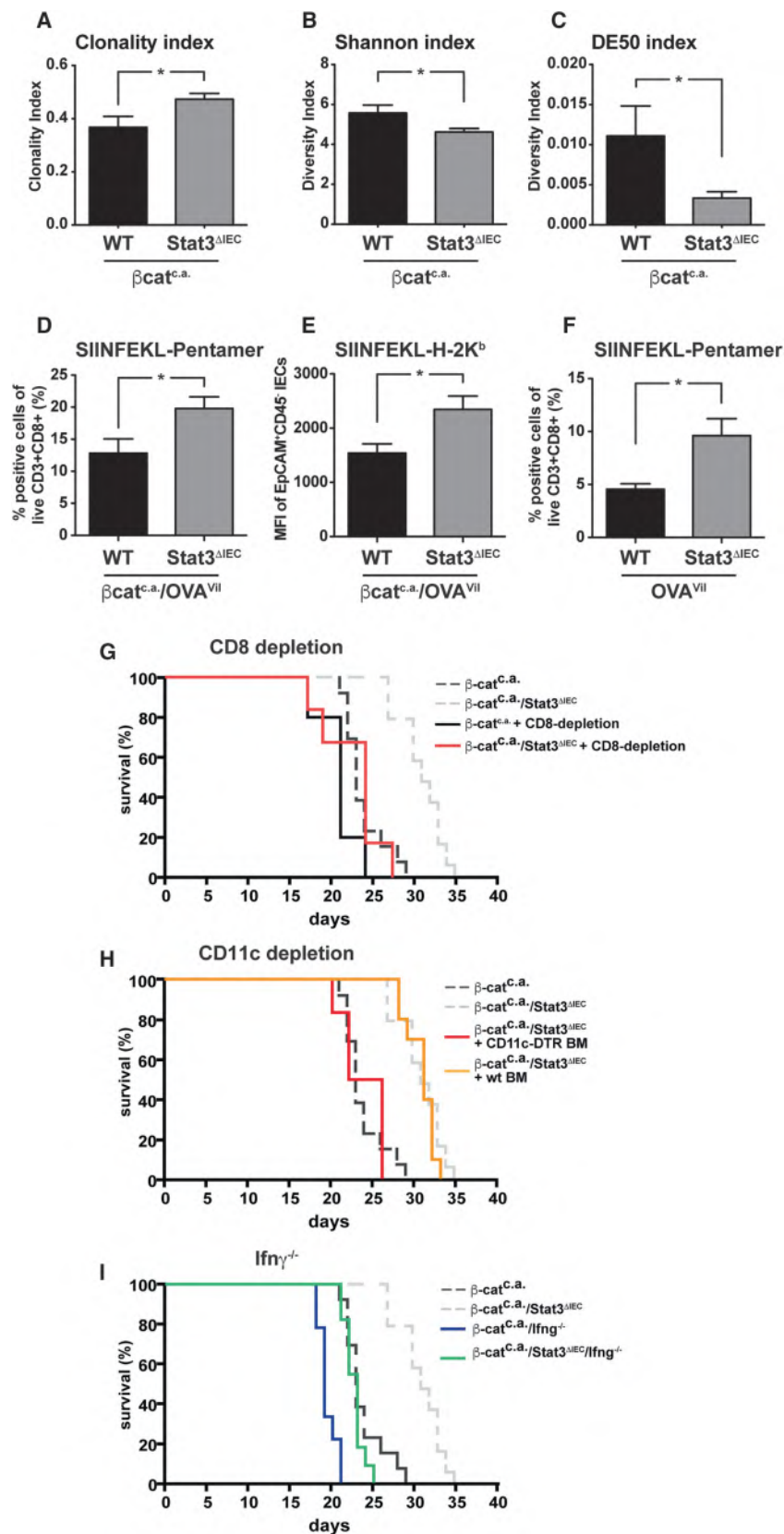


Figure 3. Suppression of Intestinal Tumor Initiation in Stat3^{ΔIEC} Mice Depends on CD8⁺/IFN γ ⁺ T Cells

(A–C) Statistical analysis for clonality (A) and diversity of T cell receptor (TCR α and TCR β) (B and C) in sorted mucosal CD8⁺ T cells on day 15; n = 3 and 4/genotype, respectively; *p < 0.05 by Mann-Whitney U test. (D and E) Flow cytometric quantification of SIINFEKL-MHC pentamer binding CD3⁺CD8⁺ T cells (D) in mucosa and surface expression of SIINFEKL-binding MHC class I on IEC (E) on day 15. n = 5 mice/genotype.

(F) Flow cytometric quantification of SIINFEKL-MHC pentamer binding CD3⁺CD8⁺ T cells in AOM-challenged mice (week 18); n \geq 4/genotype.

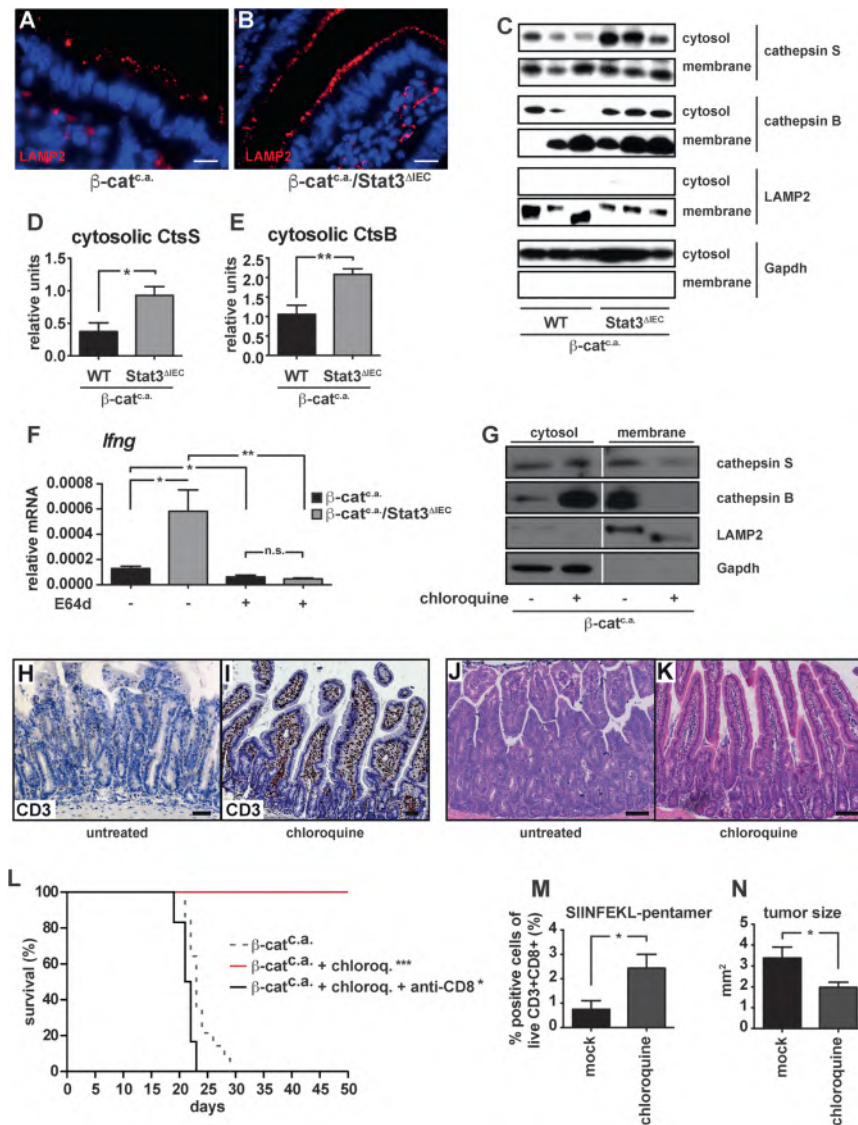
(G) Survival of β -cat^{c.a.} and β -cat^{c.a.}/Stat3^{ΔIEC} mice injected with CD8⁺ T-cell-depleting antibody; n \geq 5/genotype.

(H) Survival of β -cat^{c.a.}/Stat3^{ΔIEC} mice that had been transplanted with bone marrow (BM) from CD11c-DTR (n = 6) or wild-type (WT) mice (n = 6) 8 weeks before tamoxifen administration and diphtheria toxin injection to deplete CD11c⁺ cells.

(I) Survival of β -cat^{c.a.}/Ifn γ ^{-/-} (n = 9) and β -cat^{c.a.}/Stat3^{ΔIEC}/Ifn γ ^{-/-} mice (n = 11).

*p < 0.05 by Student's t test (D–F). The dashed gray lines in (A)–(C) represent survival curves of untreated β -cat^{c.a.} and β -cat^{c.a.}/Stat3^{ΔIEC} mice as reproduced from Figure 1N for better comparison.

In (A)–(F), data are mean \pm SEM. See also Figure S2.



upregulation of *lfn* mRNA (Figure S3E). Furthermore, cleaved caspase-3⁺ apoptotic IECs were markedly increased in chloroquine-treated β -cat^{c.a.} mice (Figure S3F) in line with a cytotoxic T cell activation. Consequently, chloroquine prevented expansion of β -catenin mutant crypts and death of β -cat^{c.a.} mice in a CD8⁺ T-cell-dependent manner (Figures 4J–4L and S3G). In agreement with this notion, we could observe an increased number of SIINFEKL-specific CD8⁺ T cells in the intestinal mucosa AOM-challenged OVA^{IEC} mice (Figure 4M). Consequently, chloroquine treatment over a period of 4 weeks reduced tumor load of established AOM-induced adenomas in WT mice (Figure 4N), strongly supporting the stimulation of an anti-tumor immune response upon LMP induction.

To further examine the link between LMP in IECs and CD8⁺ T cell recruitment, we established an *ex vivo* co-culture system. The system comprises an ovalbumin-expressing murine (C57BL/6) colon carcinoma cell line (OVA-CMT93) stably expressing a Stat3 miRNA or a scrambled control (OVA-CMT^{Stat3KD}

or OVA-CMT^{scr}, respectively) that were co-cultured together with splenocytes from OT-I transgenic mice harboring a T cell receptor (TCR) that recognizes the ovalbumin-derived peptide (SIINFEKL) on cytotoxic T cells. The level of T cell activation was measured by the release of IFN γ by OT-I cells (Figure 5A). After confirmation of successful Stat3 knockdown (KD) (Figure 5B), we verified increased LMP upon stimulation with H₂O₂ in OVA-CMT^{Stat3KD} cells by flow cytometric monitoring of the reduction in acidophilic acridine orange staining (Figure 5C). While unchallenged OVA-CMT^{Stat3KD} or OVA-CMT^{scr} cells resulted in similar OT-I T cell activation, induction of LMP in tumor cells by H₂O₂-treatment prior to their co-culture with OT-I splenocytes significantly elevated IFN γ production (Figure 5D). Similar to the *in vivo* situation and consistent with a higher degree of LMP, IFN γ release by OT-I cells was greatly enhanced when Stat3 was absent from ovalbumin expressing tumor cells and markedly reduced upon treatment of OVA-CMT^{Stat3KD} with the pan-cysteine protease inhibitor E64d (Figure 5E), further

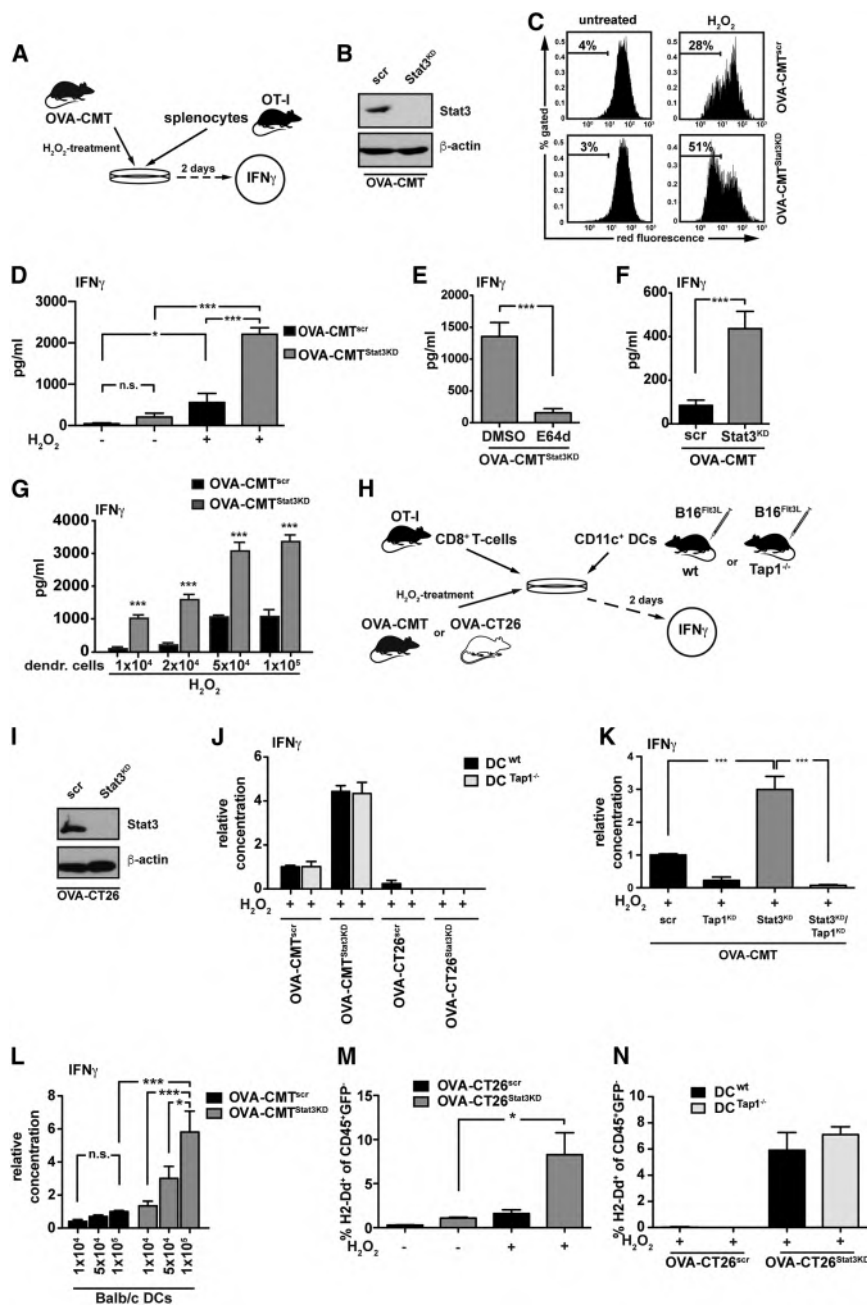


Figure 5. T Cell Activation by Antigen-Expressing Tumor Cells Is Enhanced by LMP and DC Cross-Dressing In Vitro

For a Figure360 author presentation of Figure 5, see the figure legend at <https://10.1016/j.cell.2018.05.028>.

(A) Experimental setup of co-culture experiment. (B) Immunoblot analysis of STAT3. (C) Representative flow cytometric analysis of acridine-orange-stained OVA-CMT^{scr} and OVA-CMT^{Stat3KD} cells.

(D) $IFN\gamma$ released by OT-I splenocytes after co-culture with OVA-CMT^{scr} or OVA-CMT^{Stat3KD} cells for 2 days; n = 6 from 2 independent experiments. (E) $IFN\gamma$ released by OT-I splenocytes that had been co-cultured for 2 days with E64d-pre-treated OVA-CMT^{Stat3KD} cells; n = 6 from 2 independent experiments. Note that protease inhibitor was present during H_2O_2 stimulation but absent during co-culture with OT-I cells.

(F) $IFN\gamma$ released by CD8⁺ OT-I T cells co-cultured for 2 days with H_2O_2 -pre-treated OVA-CMT^{scr} or OVA-CMT^{Stat3KD} cells; n = 6 from 2 independent experiments.

(G) $IFN\gamma$ released by CD8⁺ OT-I T cells co-cultured with H_2O_2 -pre-treated OVA-CMT^{scr} or OVA-CMT^{Stat3KD} cells; n ≥ 3 from 2 independent experiments.

(H) Experimental setup of co-culture experiments. (I) Immunoblot analysis of STAT3.

(J) $IFN\gamma$ released by OT-I T cells co-cultured with WT or Tap1^{-/-} CD11c⁺ DCs and with H_2O_2 -stimulated OVA-CMT or OVA-CT26 cells; n = 6 from 2 independent experiments.

(K) $IFN\gamma$ released by OT-I splenocytes after co-culture with H_2O_2 -stimulated OVA-CMT cells with knockdown of Tap1 and/or Stat3; n = 6 from 2 independent experiments. ***p < 0.001 by Student's t test.

(L) $IFN\gamma$ released by CD8⁺ OT-I T cells co-cultured with OVA-CMT^{scr} or OVA-CMT^{Stat3KD} cells and DCs from BALB/c donors as indicated; n = 12 from 4 independent experiments. *p < 0.05, ***p < 0.001 by one-way ANOVA.

(M) Quantification of H2-D^d on splenocytes from WT C57BL/6 donor mice co-cultured with OVA-CT26^{scr} or OVA-CT26^{Stat3KD} cells pre-treated as indicated; n = 6 from 2 independent experiments. *p < 0.05 by Student's t test.

(N) Quantification of H2-D^d on splenocytes from WT or Tap1^{-/-} C57BL/6 donor mice co-cultured with H_2O_2 pretreated OVA-CT26^{scr} or OVA-CT26^{Stat3KD} cells; n = 6 from two independent experiments.

*p < 0.05, ***p < 0.001 by Student's t test (D–G). In (D)–(G) and (J)–(N), data are mean ± SEM. See also Figure S4.

supporting the notion that LMP-dependent protease release may be involved in antigen processing in epithelial cells. Indeed, when H_2O_2 challenged OVA-CMT^{Stat3KD} or OVA-CMT^{scr} cells were co-cultured with MACS-purified OT-I CD8⁺ T cells in the absence of CD11c⁺ DCs, this was sufficient to elicit $IFN\gamma$ secretion (Figure 5F), yet $IFN\gamma$ production was greatly enhanced when increasing numbers of CD11c⁺ DCs were added (Figure 5G) suggesting the transfer and presentation of MHC class I mole-

cules via cross-dressing (Nakayama, 2015) rather than cross-presentation. To examine this possibility, we co-cultured ovalbumin-expressing CT26 colon tumor cells of BALB/c origin (OVA-CT26^{Stat3KD} and OVA-CT26^{scr}) or haplo-identical OVA-CMT^{Stat3KD} and OVA-CMT^{scr} together with C57BL/6-derived DCs from WT or Tap1-deficient mice along with OT-I CD8 T cells (Figure 5H). In the presence of BALB/c CT26 cells no OT-I T cell activation could be observed regardless of

Figure360

whether or not CT26 cells had been pre-treated with H₂O₂. Instead, T cell activation was only triggered by OVA-CMT cells, yet absence of Tap1 in DCs did not affect IFN γ release (Figure 5J), supporting the notion that T cell activation occurred independently of cross presentation. In contrast, knockdown of Tap1 in tumor cells prevented IFN γ production by OT-I cells (Figures 5K and S4A), providing further evidence that antigen-processing can occur directly in tumor cells. This was further supported when addition of DCs derived from BALB/c mice enhanced the stimulation of OT-I T cells in a dose-dependent manner when cultured together with OVA-CMT^{Stat3KD} cells but not with OVA-CMT^{scr} cells (Figure 5L). Moreover, when we co-cultured BALB/c CT26 cells with C57BL/6 splenocytes, we could detect the presence of the BALB/c MHC class I allele D^d on C57BL/6 DCs. The MHC transfer was enhanced by H₂O₂ pre-treatment of tumor cells, which, again, occurred independent of Tap1 expression in DCs (Figures 5M and 5N). Collectively, these results further strongly supported our hypothesis that Stat3-deficient tumor cells can directly process antigens in a LMP-dependent manner and cross-dress DCs to induce an effective CD8⁺ T cell response.

Previously, it had been suggested that cathepsin S is engaged in MHC class II-mediated antigen presentation in IECs *in vivo*, whereas cathepsin L enables this in thymic cortical epithelial cells (Beers et al., 2005; Nakagawa et al., 1998; Shen et al., 2004). To functionally examine whether cathepsin S, cathepsin L, or alternative cathepsins might be responsible for MHC-class-I-mediated antigen presentation in Stat3-deficient tumor cells, we individually knocked down expression of single cathepsins B, D, F, H, L or S in OVA-CMT^{Stat3KD} cells and examined IFN γ release by OT-I T cells upon H₂O₂ treatment prior to the co-culture. Indeed, reduced expression of either cathepsin S or cathepsin L OVA-CMT^{Stat3KD} cells markedly reduced IFN γ release, while knockdown of the other cathepsins did not (Figure S4B). To confirm the contribution of cathepsin S and cathepsin L to the observed phenotype in Stat3-deficient/ β -catenin mutant IECs *in vivo*, we crossed *Ctss*^{-/-} whole-body mutants to β -*cat*^{c.a./Stat3 Δ IEC} animals. Surprisingly, the loss of cathepsin S in the corresponding *Ctss*^{-/-}/ β -*cat*^{c.a./Stat3 Δ IEC} mice did not affect *Irfng* expression on day 15. Similarly, IECs restricted deletion of cathepsin L (*Ctll* ^{Δ IEC/ β -*cat*^{c.a./Stat3 Δ IEC}) and even simultaneous loss of cathepsin S and L neither prevented IFN γ upregulation (Figure S4C) nor affected LMP in intestinal epithelia of *Ctss*^{-/-}/*Ctll* ^{Δ IEC/ β -*cat*^{c.a./Stat3 Δ IEC} mice (Figure S4D). Importantly, we could not detect reduced protease activity in IECs of these mice when using the cathepsin substrate z-Leu-Arg-AMC (Figure S4E), indicating that *in vivo* the absence of cathepsin S and L could be compensated by other cysteine proteases as suggested in a murine pancreatic neuroendocrine tumor model (Akkari et al., 2016).}}

Enhanced Mitophagy Leads to Iron(II) Accumulation in Lysosomes, thereby Triggering the Fenton Reaction

Next, we aimed to address the mechanism causing LMP. LMP can be triggered by various stimuli, the most common being ROS-mediated lysosomal destabilization in the event of intralysosomal iron(II) accumulation (Boya and Kroemer, 2008). During the Fenton reaction iron(II) catalyzes the conversion of H₂O₂ into highly reactive hydroxyl and hydroperoxyl radicals (Winterbourn,

1995). Oncogenic wnt activation triggers ROS production in IECs (Myant et al., 2013), and, using the fluorescent Fe²⁺-specific probe IP-1 (Au-Yeung et al., 2013), we confirmed enhanced iron(II) accumulation in Stat3-deficient CMT93 cells (Figures 6A–6D). The signal of the iron probe IP-1 co-localized with LysoTracker fluorescence, confirming lysosomes as the predominant intracellular site of iron(II) accumulation in OVA-CMT cells (Figures S5A–S5F). However, we were not able to detect significant alterations in expression of genes coding for proteins involved in iron uptake (Figure S5G). Instead, we observed an increased presence of components of the mitochondrial oxidative phosphorylation system (COXII) in lysosomes of OVA-CMT^{Stat3KD} cells (Figures 6E–6H, S5H, and S5I). This was suggestive of enhanced mitophagy, a process selectively eliminating damaged or excessive mitochondria by the autophagic pathway as the transfer of iron-containing electron transporting complexes to lysosomes results in intralysosomal iron(II) accumulation (Terman et al., 2006; Youle and Narendra, 2011). Interestingly, serine-phosphorylated Stat3 had been suggested to be involved in mitochondrial function to preserve oxidative phosphorylation in cardiac and nerve cells as well as RAS-transformed tumor cells (Gough et al., 2009; Wegrzyn et al., 2009). However, a transcriptionally constitutive active Stat3 (Stat3C) induces a metabolic switch toward aerobic glycolysis (Demaria et al., 2010) in a Hif1 α -dependent manner, thereby eliciting the Warburg effect commonly described in cancers (Warburg et al., 1924). In Stat3-deficient CMT93 cells we observed an increased basal and maximal oxygen consumption rate, decreased glucose-uptake and increased ATP levels (Figures 6I–6L and S5J), suggesting enhanced oxidative phosphorylation. In line with this notion, OVA-CMT^{Stat3KD} cells proliferated significantly more in carbohydrate-deficient medium, or in the presence of the glycolysis inhibitors bromopyruvate or deoxyglucose, or when cultured in galactose, which all require mitochondrial activity to yield a positive energy balance but proliferated indifferently in the presence of glucose (Figure S5K). Staining with MitoTracker indicated an elevated number of mitochondria in OVA-CMT^{Stat3KD} cells while at the same time the mitochondrial membrane potential was decreased in a larger proportion of these cells (Figures 6M and 6N). Collectively, these data suggested a higher turnover of mitochondria in Stat3-deficient cells, which was supported by flow cytometry after labeling OVA-CMT^{scr} and OVA-CMT^{Stat3KD} cells with Mito-Timer (Hernandez et al., 2013) (Figure 6O). To confirm that LMP induction was dependent on mitochondrial Stat3, we triggered LMP in Stat3-deficient fibroblasts by H₂O₂ treatment. Retroviral reconstitution of *Stat3*^{-/-} cells with either WT Stat3, a mitochondrial-targeted version of Stat3 (MLS-Stat3), a dominant negative tyrosine-to-phenylalanine mutant (MLS-Stat3Y705F), or a DNA binding mutant (MLS-Stat3E434A/435A) all prevented increased LMP. Because the additional inactivation of the S727 phosphorylation site (MLS-Stat3Y705F/S727A) blocked induction of LMP to a lesser extent than the other mutants, we speculate LMP was prevented by S727 phosphorylated Stat3 in mitochondria rather than Stat3-dependent transcription (Figure 6P). Accordingly, expression levels of Stat3-dependent genes involved in glycolysis or mitochondrial respiration (Demaria et al., 2010) were not markedly changed in OVA-CMT^{Stat3KD} cells (Figure S5L).

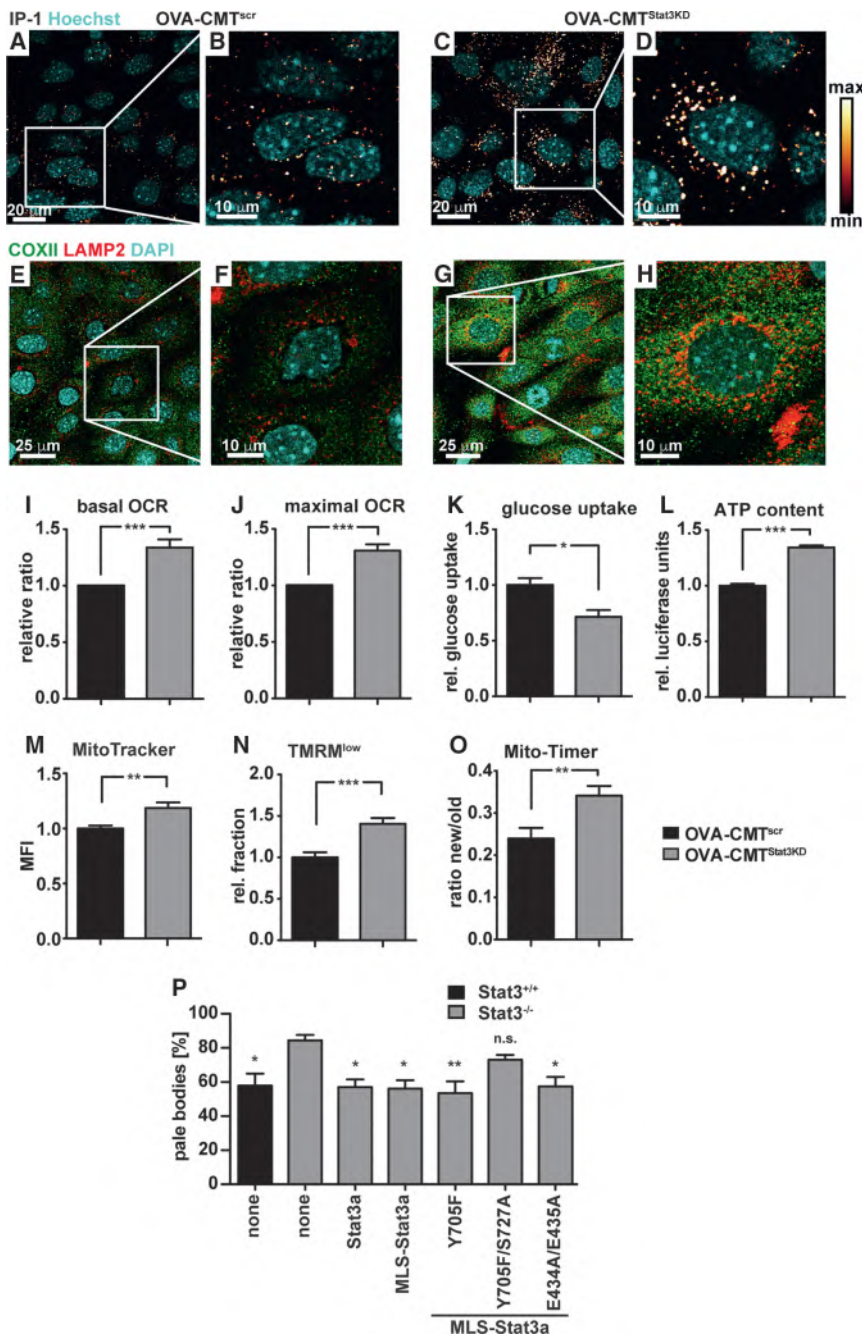


Figure 6. Stat3 Deficiency Induces Mitophagy and Increased Lysosomal Iron Load

(A–D) Confocal live cell microscopy of the fluorescent Fe²⁺-specific probe IP-1 in OVA-CMT^{scr} (A and B) or OVA-CMT^{Stat3KD} (C and D) cells. LUT as depicted on the right-hand side.

(E–H) Mitophagy in OVA-CMT^{scr} (E and F) and OVA-CMT^{Stat3KD} (G and H) was visualized by co-staining for the mitochondrial protein COXII (green) and the lysosomal membrane protein LAMP2 (red). (I and J) Respirometry of intact cells. Basal rate was measured after an initial stabilization time (position a in Figure S5J) (I) and the maximal rate after addition of a saturating amount of FCCP (positions b and c for OVA-CMT^{scr} and OVA-CMT^{Stat3KD}, respectively, in Figure S5J) (J); n = 10 from 10 independent experiments.

(K) Relative glucose uptake over 12 hr; n = 7 from 2 independent experiments.

(L) ATP content as measured by luciferase activity; n = 12 from 4 independent experiments.

(M) MFI of cells incubated with MitoTracker; n = 11 from 3 independent experiments.

(N) Relative fraction of cells showing low TMRM staining; n = 9 from 3 independent experiments.

(O) Ratio of cells showing green or red fluorescence of MitoTimer, indicating new or old mitochondria, respectively; n = 18 from 3 independent experiments.

(P) Relative amount of pale bodies in MEFs reconstituted with the indicated variant of Stat3a after treatment with H₂O₂; n = 7 of 3 independent experiments, *p < 0.05, **p < 0.001 by one-way ANOVA against not-reconstituted Stat3^{-/-} MEFs. *p < 0.05, **p < 0.01, ***p < 0.001 by Student's t test (J–O).

In (I)–(P), data are mean ± SEM. See also Figure S5.

(Figures S6I–S6M), and prevented IFN γ production in the OT-I co-culture system (Figure 7B). Moreover, pre-treatment of CMT93-cells with antimycin A or rotenone, which inhibit complex III and I of the respiratory chain, respectively, induce mitophagy (Fang et al., 2014) and increase the lysosomal iron(II) load (Figures S6N–S6P), thus sensitizing CMT93 cells to H₂O₂-induced LMP, which could be prevented by DFO (Figure S6Q).

In line with improved oxidative phosphorylation in Stat3-deficient CMT cells in culture, in IECs of β -cat^{c.a./Stat3 Δ IEC} we also detected elevated citrate synthase activity and an increased NAD⁺/NADH ratio (Figures 7C and 7D). Expression of genes controlling glycolysis was unchanged (Figure S6R) and immunofluorescent staining indicated the presence of COXII in lysosomes of β -cat^{c.a./Stat3 Δ IEC} IECs (Figures 7E–7H). Electron microscopy confirmed morphological changes in mitochondrial ultrastructure, such as cristaelysis (Figures S6S and S6T) and immunoblot analysis revealed elevated activation of Drp1 in β -cat^{c.a./Stat3 Δ IEC} IECs (Figure 7I). Furthermore, conversion of LC3-I to LC3-II in β -cat^{c.a./Stat3 Δ IEC}

To confirm the functional relevance of intralysosomal iron(II) accumulation for enhanced LMP in OVA-CMT^{Stat3KD} cells, we treated CMT cells with the iron chelator deferoxamine (DFO) prior to the H₂O₂ challenge, and this was indeed sufficient to prevent LMP (Figures 7A and S6A–S6H). The direct involvement of mitophagy in lysosomal iron accumulation, as well as T cell activation, was demonstrated by the finding, that RNAi-mediated gene knockdown of Pink1, a kinase responsible for the degradation of damaged mitochondria in the Pink1-Parkin pathway, in OVA-CMT^{Stat3KD} cells markedly reduced lysosomal iron levels

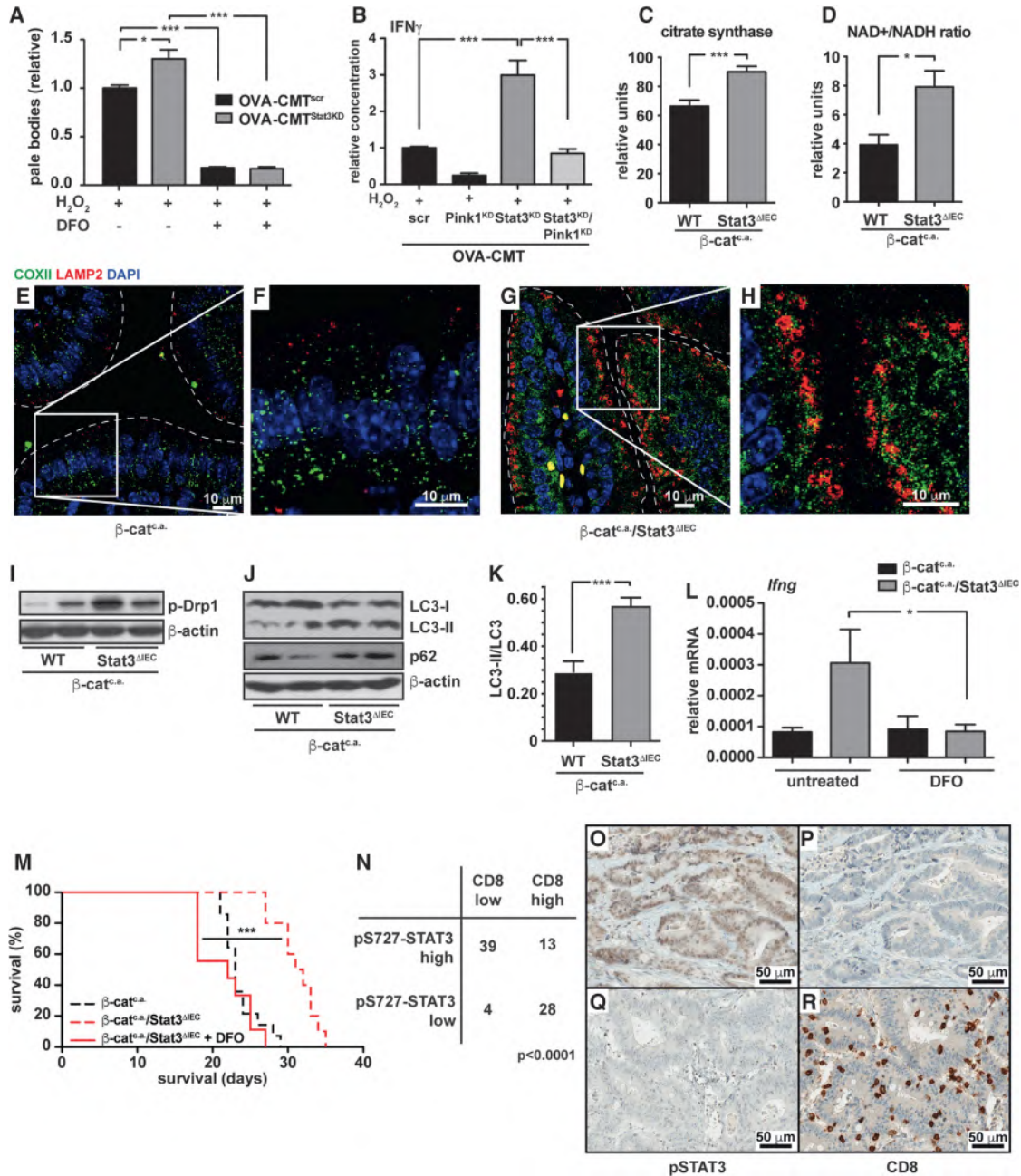


Figure 7. Lysosomal Iron Enhances Anti-tumor Immune Reaction In Vivo

(A) Relative fraction of OVA-CMT^{scr} and OVA-CMT^{Stat3^{KD}} cells with low red acridine orange fluorescence (pale bodies); n = 4 of two independent experiments. (B) IFN_γ released by OT-1 splenocytes after co-culture with H₂O₂ stimulated OVA-CMT cells with knockdown of Pink1 and/or Stat3; n = 6 from 2 independent experiments. (C) Citrate synthase activity in mitochondrial isolates of IECs of β -cat^{c.a.} and β -cat^{c.a.}/Stat3^{ΔIEC} 3 days after the start of tamoxifen. Samples were normalized to total protein content and measured in triplicates of 6 mice each. (D) NAD⁺/NADH-ratio in β -cat^{c.a.} and β -cat^{c.a.}/Stat3^{ΔIEC} mice on day 3; n ≥ 4/genotype. (E–H) Co-staining for the mitochondrial protein COXII (green) and the lysosomal membrane protein LAMP2 (red) in β -cat^{c.a.} (E and F) and β -cat^{c.a.}/Stat3^{ΔIEC} (G and H) mice on day 3. (I) Immunoblot analysis of phospho-Drp1 protein in lysates of IECs of β -cat^{c.a.} and β -cat^{c.a.}/Stat3^{ΔIEC} mice on day 3. (J and K) Immunoblot analysis of LC3 and p62 (J) and quantification of LC3-II/LC3 conversion ratio (K) in β -cat^{c.a.} and β -cat^{c.a.}/Stat3^{ΔIEC} mice on day 15. (L) Relative *Ifng*-mRNA in β -cat^{c.a.} and β -cat^{c.a.}/Stat3^{ΔIEC} mice treated with the iron-chelator DFO (400 mg/kg bodyweight) or control; n ≥ 5/genotype. (M) Survival of β -cat^{c.a.}/Stat3^{ΔIEC} mice (n = 9) treated with DFO. Dashed lines have been reproduced from Figure 1N for better comparison. ***p < 0.001 by log-rank test. (N) Immunohistochemistry for pS727-STAT3 and CD8 in β -cat^{c.a.} and β -cat^{c.a.}/Stat3^{ΔIEC} mice. p < 0.0001. (O–R) Immunohistochemistry for pSTAT3 (O, Q) and CD8 (P, R) in β -cat^{c.a.} (O, P) and β -cat^{c.a.}/Stat3^{ΔIEC} (Q, R) mice.

(legend continued on next page)

IECs was elevated, suggesting enhanced autophagosome formation, yet simultaneous accumulation of p62 suggested decreased autophagic flux (Figures 7J and 7K) in agreement with induction of mitophagy but impaired lysosomal function. Importantly, DFO administration to $\beta\text{-cat}^{\text{c.a.}}$ and $\beta\text{-cat}^{\text{c.a.}}/\text{Stat3}^{\Delta\text{IEC}}$ mice prevented *Irfng* upregulation in $\beta\text{-cat}^{\text{c.a.}}/\text{Stat3}^{\Delta\text{IEC}}$ mice (Figure 7L) and prevented prolonged survival of $\beta\text{-cat}^{\text{c.a.}}/\text{Stat3}^{\Delta\text{IEC}}$ mice (Figure 7M), thus further supporting the notion that accumulation of intralysosomal iron(II) was essential for the observed anti-tumor cell immune phenotype in these animals. In contrast, pharmacological suppression of autophagy using either 3-methyladenine or genetic ablation of *Atg7* did not prevent $\text{IFN}\gamma$ upregulation in lamina propria of $\beta\text{-cat}^{\text{c.a.}}/\text{Stat3}^{\Delta\text{IEC}}$ mice but, instead, increased it even further (Figures S6U and S6V).

A newly established immune score based on the presence of different T cell subsets can efficiently predict tumor recurrence in CRC patients (Fridman et al., 2012). In particular the presence of CD8^+ T cells and high $\text{IFN}\gamma$ expression are associated with a better prognosis. Therefore, we examined whether STAT3 activation was involved in this phenomenon. Indeed, when we analyzed CRC biopsies, we found a significant inverse correlation between the accumulation of S727-phosphorylated STAT3 in tumor epithelia and the frequency of infiltrating CD8^+ T cells (Figures 7N–7R) suggesting that STAT3 may also be functionally involved in the suppression of CD8^+ T cell recruitment in human CRC.

DISCUSSION

Here, we have identified a so far unrecognized complex multi-step process linking altered mitochondrial function and antigen presentation in IECs. By triggering mitophagy and increasing the amount of intralysosomal ferrous iron lysosomes are sensitized for the induction of LMP via the Fenton reaction. As a consequence cathepsins are released into the cytoplasm, enabling antigen processing directly in IECs. While we have discovered this connection in the context of Stat3 deletion, this mechanism is not strictly Stat3-dependent considering that LMP can be pharmacologically induced by chloroquine in a Stat3 WT background, thus suggesting a previously unrecognized role for lysosomes in regulating the immunogenicity of malignant transformed epithelial cells. Knockdown of both cathepsin S and cathepsin L could prevent OT-I T cell activation *ex vivo*, yet the absence of cathepsin S and cathepsin L could be compensated by other proteases *in vivo*. This suggests that not only one single cathepsin is involved in antigen presentation in IECs but also several proteases have the capacity to process the relevant antigen *in vivo*. Nevertheless, our data underscore the importance of LMP in IECs for CD8^+ T cell activation since prevention of LMP by iron chelation was equally effective in suppressing $\text{IFN}\gamma$ upregulation as blockade of protease activity using E64d. Whether only the release of cathepsins to the cytoplasm or also cell death of IECs, which is usually associated with

LMP induction (Boya and Kroemer, 2008), contributes to enhanced T cell activation still has to be determined.

Our data support the concept of cross-dressing (Nakayama, 2015) and suggest that the capacity of DCs to cross present is not essential for T cell activation in this scenario. Most likely, however, DCs are still required to provide essential co-stimulatory signals and indeed *in vivo* proper T cell activation by cross-dressing depends on the presence of DCs (Cerovic et al., 2015). Interestingly, chloroquine-induced LMP in $\beta\text{-cat}^{\text{c.a.}}$ mice IECs extended survival more efficiently than loss of Stat3 in IECs. Chloroquine can enhance human CD8^+ T cell responses against soluble antigens by inhibiting endosomal acidification in DCs (Accapezzato et al., 2005). Therefore, we cannot rule out that apart from affecting LMP in IECs some of the substantial tumor suppression is mediated by chloroquine's ability to influence endosomes in DCs as well.

In addition to controlling the transcription of a wide range of genes involved in cell proliferation and survival (Bollrath and Greten, 2009), Stat3 has been suggested to confer transcription-independent functions including the regulation of mitochondrial activity (Meier and Larner, 2014). Indeed, mitochondrial Stat3 has been associated with decreased ETC activity, mainly complexes I, II, and V (Gough et al., 2009; Wegrzyn et al., 2009). Further studies showed that Stat3 deficiency decreased activity in complexes III and IV (Meier and Larner, 2014). In contrast, a constitutively active form of Stat3 (Stat3-C) supports a shift from oxidative phosphorylation toward glycolysis (Warburg effect) in mouse embryonic fibroblasts (MEFs) (Demaria et al., 2010). That the latter phenotype is at least in part dependent on Y705 phosphorylation and nuclear functions of Stat3 highlights the pleiotropic role of Stat3 in mitochondrial activity and illustrates that actions of Stat3 in the mitochondria greatly vary between types of cells and experimental systems. The relative contribution of mitochondrial Stat3 to a given response probably most likely depends on the relative contribution of nuclear Stat3 in the particular context. Cancer-cell-generated lactate is now considered a critical immune suppressive metabolite and reducing lactate production by blocking glycolysis or direct inhibition of LDH-A has been suggested to restore physiological T cell function (Choi et al., 2013). Our data suggest that in addition to inhibiting lactate production enhanced oxidative phosphorylation may trigger mitophagy, which would stimulate antigen processing thus further contributing to improved intestinal tumor suppressive immune function. Interestingly, the mitochondrial phenotype of Stat3-deficient cells comprising more mitochondria and enhanced oxidative phosphorylation does not match those typically of cells undergoing mitophagy. However, the fact that knockdown of Pink1 prevents LMP and CD8^+ T cell activation strongly supports a contribution of mitophagy even though also mitophagy-independent functions of PINK1 have been described (Matheoud et al., 2016). Thus, it will be of great interest to define the exact molecular

(N) Correlation of pS727-STAT3 expression and presence of CD8^+ T cells in human colorectal cancer (CRC, N = 84; χ^2 test, $p < 0.0001$).

(O–R) Representative immunohistochemical analysis of pS727-STAT3 (O and Q) and CD8 (P and R) in human CRC. Scale bars, 50 μm .

See also Figure S6.

* $p < 0.05$, *** $p < 0.001$ by Student's t test (A–D). In (A)–(D) and (J)–(L), data are mean \pm SEM.

alterations in Stat3-deficient mitochondria causing this particular phenotype.

Our findings may provide the basis for novel therapeutic strategies that exploit anti-tumor immunity in CRC patients. These could encompass therapies interfering with mitochondrial function, thereby triggering mitophagy and the release of LMP-inducing compounds. Compounds directed against Stat3 or presumably its upstream Jak tyrosine kinases or chloroquine might be good candidates to examine in this context.

STAR★METHODS

Detailed methods are provided in the online version of this paper and include the following:

- KEY RESOURCES TABLE
- CONTACT FOR REAGENT AND RESOURCE SHARING
- EXPERIMENTAL MODEL AND SUBJECT DETAILS
 - Mice
 - Human Samples
- METHOD DETAILS
 - *In vivo* analyses
 - Protein Analysis and Immunohistochemistry
 - Isolation and analysis of lamina propria cells
 - Cell culture and T cell activation assay
 - Metabolic analyses
 - RNA Analysis
 - NGS-based TCR repertoire analysis
- QUANTIFICATION AND STATISTICAL ANALYSIS

SUPPLEMENTAL INFORMATION

Supplemental Information includes six figures and one table and can be found with this article online at <https://doi.org/10.1016/j.cell.2018.05.028>.

ACKNOWLEDGMENTS

We thank Kerstin Burmeister, Saskia Ettl, Kathleen Mohs, Hana Kunkel, Christin Danneil, Natalia Delis, and Eva Rudolf for technical assistance, as well as the Histology and Flow Cytometry Core Facilities at the Georg-Speyer-Haus. We are grateful to Johanna Joyce and Masaaki Komatsu for generously providing *Ctss*^{-/-} and floxed *Atg7* mice, respectively, and we thank Chris Chang for generously providing IP-1. The plasmid pTRE-Tight-MitoTimer was a kind gift from Roberta Gottlieb (Addgene plasmid # 50547), DEC205-OVA was a kind gift from Anne Krug, and pES.1-2(M2N)_p was kindly provided by Rainer Loew. We gratefully acknowledge the TUM-MRI-Tissue Biobank at the Department of Pathology, Klinikum rechts der Isar, and the Victorian Cancer Biobank for providing colon cancer specimens. We would like to thank Lisa Sevenich, Firouzeh Korangy, Ari Waisman, and Thomas Blankenstein for helpful discussions. This work was supported in part by the LOEWE Center for Cell and Gene Therapy Frankfurt (CGT, III L 4-518/17.004) and institutional funds from the Georg-Speyer-Haus, as well as grants from the Deutsche Forschungsgemeinschaft (DFG) (SFB 850 Project B7 to T.R.; Gr1916/5-1, FOR2438 Gr1916/11-1, SFB 815, 1177, and 1292 to F.R.G.).

AUTHOR CONTRIBUTIONS

Conceptualization, P.K.Z., J.B., W.S.W., M.C.A., T.K., and F.R.G.; Methodology, P.K.Z., J.B., and F.R.G.; Investigation, P.K.Z., J.B., C.K.P., T.M., Ö.C., T.D., M.A.D., N.M., J.G., D.H., A.K.M., M.G.Ö., S.M., J.M.-H., and S.D.; Resources, T.P., J.S.-H., M.M.T., T.R., A.C.L., M.E., T.F.G., and D.W.; Writing-Original Draft, P.K.Z. and F.R.G.; Writing Review & Editing, P.K.Z. and

F.R.G.; Visualization P.K.Z. and F.R.G.; Supervision T.K., W.S.W., and F.R.G.; and Funding Acquisition, F.R.G.

DECLARATION OF INTERESTS

The authors declare no competing interests.

Received: March 6, 2018

Revised: April 3, 2018

Accepted: May 14, 2018

Published: June 14, 2018

REFERENCES

- Accapezzato, D., Visco, V., Francavilla, V., Molette, C., Donato, T., Paroli, M., Mondelli, M.U., Doria, M., Torrisi, M.R., and Barnaba, V. (2005). Chloroquine enhances human CD8⁺ T cell responses against soluble antigens in vivo. *J. Exp. Med.* *202*, 817–828.
- Akkari, L., Gocheva, V., Quick, M.L., Kester, J.C., Spencer, A.K., Garfall, A.L., Bowman, R.L., and Joyce, J.A. (2016). Combined deletion of cathepsin protease family members reveals compensatory mechanisms in cancer. *Genes Dev.* *30*, 220–232.
- Au-Yeung, H.Y., Chan, J., Chantarojsiri, T., and Chang, C.J. (2013). Molecular imaging of labile iron(II) pools in living cells with a turn-on fluorescent probe. *J. Am. Chem. Soc.* *135*, 15165–15173.
- Beers, C., Burich, A., Kleijmeer, M.J., Griffith, J.M., Wong, P., and Rudensky, A.Y. (2005). Cathepsin S controls MHC class II-mediated antigen presentation by epithelial cells in vivo. *J. Immunol.* *174*, 1205–1212.
- Bhattacharya, N., Yuan, R., Prestwood, T.R., Penny, H.L., DiMaio, M.A., Reticker-Flynn, N.E., Krois, C.R., Kenkel, J.A., Pham, T.D., Carmi, Y., et al. (2016). Normalizing microbiota-induced retinoic acid deficiency stimulates protective CD8⁺ T cell-mediated immunity in colorectal cancer. *Immunity* *45*, 641–655.
- Bollrath, J., and Greten, F.R. (2009). IKK/NF- κ B and STAT3 pathways: central signalling hubs in inflammation-mediated tumour promotion and metastasis. *EMBO Rep.* *10*, 1314–1319.
- Bollrath, J., Pheesse, T.J., von Burstin, V.A., Putoczki, T., Bennecke, M., Bateman, T., Nebelsiek, T., Lundgren-May, T., Canli, O., Schwitalla, S., et al. (2009). gp130-mediated Stat3 activation in enterocytes regulates cell survival and cell-cycle progression during colitis-associated tumorigenesis. *Cancer Cell* *15*, 91–102.
- Boya, P., and Kroemer, G. (2008). Lysosomal membrane permeabilization in cell death. *Oncogene* *27*, 6434–6451.
- Boya, P., Gonzalez-Polo, R.A., Poncet, D., Andreau, K., Vieira, H.L., Roumier, T., Perfettini, J.L., and Kroemer, G. (2003). Mitochondrial membrane permeabilization is a critical step of lysosome-initiated apoptosis induced by hydroxychloroquine. *Oncogene* *22*, 3927–3936.
- Cancer Genome Atlas, N.; Cancer Genome Atlas Network (2012). Comprehensive molecular characterization of human colon and rectal cancer. *Nature* *487*, 330–337.
- Cerovic, V., Houston, S.A., Westlund, J., Utraiainen, L., Davison, E.S., Scott, C.L., Bain, C.C., Joeris, T., Agace, W.W., Kroczeck, R.A., et al. (2015). Lymph-borne CD8 α ⁺ dendritic cells are uniquely able to cross-prime CD8⁺ T cells with antigen acquired from intestinal epithelial cells. *Mucosal Immunol.* *8*, 38–48.
- Choi, S.Y., Collins, C.C., Gout, P.W., and Wang, Y. (2013). Cancer-generated lactic acid: a regulatory, immunosuppressive metabolite? *J. Pathol.* *230*, 350–355.
- Cruz, F.M., Colbert, J.D., Merino, E., Kriegsman, B.A., and Rock, K.L. (2017). The biology and underlying mechanisms of cross-presentation of exogenous antigens on MHC-I molecules. *Annu. Rev. Immunol.* *35*, 149–176.
- Decker, T., and Kovarik, P. (2000). Serine phosphorylation of STATs. *Oncogene* *19*, 2628–2637.
- Demaria, M., Giorgi, C., Lebedzinska, M., Esposito, G., D'Angeli, L., Bartoli, A., Gough, D.J., Turkson, J., Levy, D.E., Watson, C.J., et al. (2010).

- A STAT3-mediated metabolic switch is involved in tumour transformation and STAT3 addiction. *Aging (Albany N.Y.)* 2, 823–842.
- Demaria, M., Camporeale, A., and Poli, V. (2014). STAT3 and metabolism: how many ways to use a single molecule? *Int. J. Cancer* 135, 1997–2003.
- elMarjou, F., Janssen, K.P., Chang, B.H., Li, M., Hindie, V., Chan, L., Louvard, D., Chambon, P., Metzger, D., and Robine, S. (2004). Tissue-specific and inducible Cre-mediated recombination in the gut epithelium. *Genesis* 39, 186–193.
- Fang, E.F., Scheibye-Knudsen, M., Brace, L.E., Kassahun, H., SenGupta, T., Nilsen, H., Mitchell, J.R., Croteau, D.L., and Bohr, V.A. (2014). Defective mitophagy in XPA via PARP-1 hyperactivation and NAD(+)/SIRT1 reduction. *Cell* 157, 882–896.
- Fridman, W.H., Pages, F., Sautes-Fridman, C., and Galon, J. (2012). The immune contexture in human tumours: impact on clinical outcome. *Nat. Rev. Cancer* 12, 298–306.
- Gamrekelashvili, J., Krüger, C., von Wasielewski, R., Hoffmann, M., Huster, K.M., Busch, D.H., Manns, M.P., Korangy, F., and Greten, T.F. (2007). Necrotic tumor cell death in vivo impairs tumor-specific immune responses. *J. Immunol.* 178, 1573–1580.
- Gough, D.J., Corlett, A., Schlessinger, K., Wegrzyn, J., Lerner, A.C., and Levy, D.E. (2009). Mitochondrial STAT3 supports Ras-dependent oncogenic transformation. *Science* 324, 1713–1716.
- Greten, F.R., Eckmann, L., Greten, T.F., Park, J.M., Li, Z.W., Egan, L.J., Kagnoff, M.F., and Karin, M. (2004). IKKbeta links inflammation and tumorigenesis in a mouse model of colitis-associated cancer. *Cell* 118, 285–296.
- Grivnenkov, S.I., Greten, F.R., and Karin, M. (2010). Immunity, inflammation, and cancer. *Cell* 140, 883–899.
- Harada, N., Tamai, Y., Ishikawa, T., Sauer, B., Takaku, K., Oshima, M., and Taketo, M.M. (1999). Intestinal polyposis in mice with a dominant stable mutation of the beta-catenin gene. *EMBO J.* 18, 5931–5942.
- Hari, A., Ganguly, A., Mu, L., Davis, S.P., Stenner, M.D., Lam, R., Munro, F., Namet, I., Alghamdi, E., Fürstehaupt, T., et al. (2015). Redirecting soluble antigen for MHC class I cross-presentation during phagocytosis. *Eur. J. Immunol.* 45, 383–395.
- Hernandez, G., Thornton, C., Stotland, A., Lui, D., Sin, J., Ramil, J., Magee, N., Andres, A., Quarato, G., Carreira, R.S., et al. (2013). MitoTimer: a novel tool for monitoring mitochondrial turnover. *Autophagy* 9, 1852–1861.
- Jung, S., Unutmaz, D., Wong, P., Sano, G., De los Santos, K., Sparwasser, T., Wu, S., Vuthoori, S., Ko, K., Zavala, F., et al. (2002). In vivo depletion of CD11c+ dendritic cells abrogates priming of CD8+ T cells by exogenous cell-associated antigens. *Immunity* 17, 211–220.
- Komatsu, M., Waguri, S., Ueno, T., Iwata, J., Murata, S., Tanida, I., Ezaki, J., Mizushima, N., Ohsumi, Y., Uchiyama, Y., et al. (2005). Impairment of starvation-induced and constitutive autophagy in Atg7-deficient mice. *J. Cell Biol.* 169, 425–434.
- Levine, B., and Kroemer, G. (2008). Autophagy in the pathogenesis of disease. *Cell* 132, 27–42.
- Loschko, J., Heink, S., Hackl, D., Dudziak, D., Reindl, W., Korn, T., and Krug, A.B. (2011). Antigen targeting to plasmacytoid dendritic cells via Siglec-H inhibits Th cell-dependent autoimmunity. *J. Immunol.* 187, 6346–6356.
- Mach, N., Gillissen, S., Wilson, S.B., Sheehan, C., Mihm, M., and Dranoff, G. (2000). Differences in dendritic cells stimulated in vivo by tumors engineered to secrete granulocyte-macrophage colony-stimulating factor or Flt3-ligand. *Cancer Res.* 60, 3239–3246.
- Matheoud, D., Sugiura, A., Bellemare-Pelletier, A., Laplante, A., Rondeau, C., Chemali, M., Fazel, A., Bergeron, J.J., Trudeau, L.E., Burelle, Y., et al. (2016). Parkinson's disease-related proteins PINK1 and Parkin repress mitochondrial antigen presentation. *Cell* 166, 314–327.
- Meier, J.A., and Lerner, A.C. (2014). Toward a new STAtE: the role of STATs in mitochondrial function. *Semin. Immunol.* 26, 20–28.
- Münz, C. (2016). Autophagy beyond intracellular MHC class II antigen presentation. *Trends Immunol.* 37, 755–763.
- Myant, K.B., Cammareri, P., McGhee, E.J., Ridgway, R.A., Huels, D.J., Cordero, J.B., Schwitalla, S., Kalna, G., Ogg, E.L., Athineos, D., et al. (2013). ROS production and NF- κ B activation triggered by RAC1 facilitate WNT-driven intestinal stem cell proliferation and colorectal cancer initiation. *Cell Stem Cell* 12, 761–773.
- Nakagawa, T., Roth, W., Wong, P., Nelson, A., Farr, A., Deussing, J., Villadangos, J.A., Ploegh, H., Peters, C., and Rudensky, A.Y. (1998). Cathepsin L: critical role in li degradation and CD4 T cell selection in the thymus. *Science* 280, 450–453.
- Nakayama, M. (2015). Antigen presentation by MHC-dressed cells. *Front. Immunol.* 5, 672.
- Rock, K.L., Farfán-Arribas, D.J., and Shen, L. (2010). Proteases in MHC class I presentation and cross-presentation. *J. Immunol.* 184, 9–15.
- Sandhu, U., Cebula, M., Behme, S., Riemer, P., Wodarczyk, C., Metzger, D., Reimann, J., Schirbeck, R., Hauser, H., and Wirth, D. (2011). Strict control of transgene expression in a mouse model for sensitive biological applications based on RMCE compatible ES cells. *Nucleic Acids Res.* 39, e1.
- Schwitalla, S., Fingerle, A.A., Cammareri, P., Nebelsiek, T., Göktuna, S.I., Ziegler, P.K., Canli, O., Heijmans, J., Huels, D.J., Moreaux, G., et al. (2013). Intestinal tumorigenesis initiated by dedifferentiation and acquisition of stem-cell-like properties. *Cell* 152, 25–38.
- Shen, L., Sigal, L.J., Boes, M., and Rock, K.L. (2004). Important role of cathepsin S in generating peptides for TAP-independent MHC class I cross-presentation in vivo. *Immunity* 21, 155–165.
- Shi, G.P., Villadangos, J.A., Dranoff, G., Small, C., Gu, L., Haley, K.J., Riese, R., Ploegh, H.L., and Chapman, H.A. (1999). Cathepsin S required for normal MHC class II peptide loading and germinal center development. *Immunity* 10, 197–206.
- Siegel, R.L., Miller, K.D., and Jemal, A. (2016). Cancer statistics, 2016. *CA Cancer J. Clin.* 66, 7–30.
- Takeda, K., Kaisho, T., Yoshida, N., Takeda, J., Kishimoto, T., and Akira, S. (1998). Stat3 activation is responsible for IL-6-dependent T cell proliferation through preventing apoptosis: generation and characterization of T cell-specific Stat3-deficient mice. *J. Immunol.* 161, 4652–4660.
- Terman, A., Kurz, T., Gustafsson, B., and Brunk, U.T. (2006). Lysosomal labilization. *IUBMB Life* 58, 531–539.
- Terman, A., Kurz, T., Navratil, M., Arriaga, E.A., and Brunk, U.T. (2010). Mitochondrial turnover and aging of long-lived postmitotic cells: the mitochondrial-lysosomal axis theory of aging. *Antioxid. Redox Signal.* 12, 503–535.
- Tholen, M., Hillebrand, L.E., Tholen, S., Sedelmeier, O., Arnold, S.J., and Reinheckel, T. (2014). Out-of-frame start codons prevent translation of truncated nucleocytoplasmic cathepsin L in vivo. *Nat. Commun.* 5, 4931.
- Urlinger, S., Baron, U., Thellmann, M., Hasan, M.T., Bujard, H., and Hillen, W. (2000). Exploring the sequence space for tetracycline-dependent transcriptional activators: novel mutations yield expanded range and sensitivity. *Proc. Natl. Acad. Sci. USA* 97, 7963–7968.
- Wang, T., Niu, G., Kortylewski, M., Burdelya, L., Shain, K., Zhang, S., Bhattacharya, R., Gabrilovich, D., Heller, R., Coppola, D., et al. (2004). Regulation of the innate and adaptive immune responses by Stat-3 signaling in tumor cells. *Nat. Med.* 10, 48–54.
- Warburg, O., Poesner, K., and Negelein, E. (1924). On the metabolism of carcinoma cells. *Biochem. Z.* 9, 309–344.
- Wegrzyn, J., Potla, R., Chwae, Y.J., Sepuri, N.B., Zhang, Q., Koeck, T., Derecka, M., Szczepanek, K., Szelag, M., Gornicka, A., et al. (2009). Function of mitochondrial Stat3 in cellular respiration. *Science* 323, 793–797.
- Winterbourn, C.C. (1995). Toxicity of iron and hydrogen peroxide: the Fenton reaction. *Toxicol. Lett.* 82–83, 969–974.
- Youle, R.J., and Narendra, D.P. (2011). Mechanisms of mitophagy. *Nat. Rev. Mol. Cell Biol.* 12, 9–14.
- Yu, H., Lee, H., Herrmann, A., Buettner, R., and Jove, R. (2014). Revisiting STAT3 signalling in cancer: new and unexpected biological functions. *Nat. Rev. Cancer* 14, 736–746.

The Immune Landscape of Cancer

Vésteinn Thorsson,^{1,36,*} David L. Gibbs,^{1,35} Scott D. Brown,² Denise Wolf,³ Dante S. Bortone,⁴ Tai-Hsien Ou Yang,⁵ Eduard Porta-Pardo,^{6,7} Galen F. Gao,⁸ Christopher L. Plaisier,^{1,9} James A. Eddy,¹⁰ Elad Ziv,¹¹ Aedin C. Culhane,¹² Evan O. Paull,¹³ I.K. Ashok Sivakumar,¹⁴ Andrew J. Gentles,¹⁵ Raunaq Malhotra,¹⁶ Farshad Farshidfar,¹⁷ Antonio Colaprico,¹⁸ Joel S. Parker,⁴ Lisle E. Mose,⁴ Nam Sy Vo,¹⁹ Jianfang Liu,²⁰ Yuexin Liu,¹⁹ Janet Rader,²¹ Varsha Dhankani,¹ Sheila M. Reynolds,¹ Reanne Bowlby,² Andrea Califano,¹³ Andrew D. Cherniack,⁸ Dimitris Anastassiou,⁵ Davide Bedognetti,²² Arvind Rao,¹⁹ Ken Chen,¹⁹ Alexander Krasnitz,²³ Hai Hu,²⁰ Tathiane M. Malta,^{24,25} Houtan Noushmehr,^{24,25} Chandra Sekhar Pedomallu,²⁶ Susan Bullman,²⁶ Akinyemi I. Ojesina,²⁷

(Author list continued on next page)

¹Institute for Systems Biology, 401 Terry Ave N, Seattle, WA 98109, USA

²Canada's Michael Smith Genome Sciences Centre, BC Cancer Agency, Vancouver, BC V5Z 4S6, Canada

³University of California, San Francisco, Box 0808, 2340 Sutter Street, S433, San Francisco, CA 94115, USA

⁴Lineberger Comprehensive Cancer Center, Curriculum in Bioinformatics and Computational Biology, University of North Carolina, 125 Mason Farm Road, Chapel Hill, NC 27599-7295, USA

⁵Department of Systems Biology and Department of Electrical Engineering, Columbia University, New York, NY 10027, USA

⁶Barcelona Supercomputing Centre, c/Jordi Girona, 29, 08034 Barcelona, Spain

⁷SBP Medical Discovery Institute, La Jolla, CA 92037, USA

⁸The Eli and Edythe L. Broad Institute of Massachusetts Institute of Technology and Harvard University, Cambridge, MA 02142, USA

⁹School of Biological and Health Systems Engineering, Arizona State University, Tempe, AZ 85281, USA

¹⁰Sage Bionetworks, 2901 Third Ave, Suite 330, Seattle, WA 98121, USA

¹¹Department of Medicine, Institute for Human Genetics, Helen Diller Family Comprehensive Cancer Center, University of California, San Francisco, 1450 3rd St, San Francisco, CA 94143, USA

¹²Department of Biostatistics and Computational Biology, Dana-Farber Cancer Institute, Boston, MA 02215, USA

¹³Irving Cancer Research Center, Room 913, 1130 St. Nicholas Avenue, New York, NY 10032, USA

¹⁴Department of Computer Science, Institute for Computational Medicine; Johns Hopkins University, Baltimore, MD 21218, USA

¹⁵Departments of Medicine and Biomedical Data Science, Stanford University, Stanford, CA 94305, USA

¹⁶Seven Bridges Genomics, Cambridge, MA 02142, USA

¹⁷Department of Oncology, University of Calgary, Calgary, AB T2N 4N1, Canada

¹⁸Universite libre de Bruxelles (ULB), Computer Science Department, Faculty of Sciences, Boulevard du Triomphe - CP212, 1050 Bruxelles, Belgium

¹⁹Department of Bioinformatics and Computational Biology, The University of Texas MD Anderson Cancer Center, Houston, TX 77030, USA

²⁰Chan Soon-Shiong Institute of Molecular Medicine at Windber, Windber, PA 15963, USA

²¹Medical College of Wisconsin, 9200 Wisconsin Avenue, Milwaukee, WI 53226 USA

²²Division of Translational Medicine, Research Branch, Sidra Medical and Research Center, PO Box 26999, Doha, Qatar

²³Simons Center for Quantitative Biology, Cold Spring Harbor Laboratory, 1 Bungtown Road, Cold Spring Harbor, NY 11724, USA

(Affiliations continued on next page)

SUMMARY

We performed an extensive immunogenomic analysis of more than 10,000 tumors comprising 33 diverse cancer types by utilizing data compiled by TCGA. Across cancer types, we identified six immune subtypes—wound healing, IFN- γ dominant, inflammatory, lymphocyte depleted, immunologically quiet, and TGF- β dominant—characterized by differences in macrophage or lymphocyte signatures, Th1:Th2 cell ratio, extent of intratumoral heterogeneity, aneuploidy, extent of neoantigen load, overall cell proliferation, expression of immunomodulatory genes, and prognosis. Specific driver mutations correlated with lower (*CTNNB1*, *NRAS*, or *IDH1*) or higher (*BRAF*, *TP53*, or *CASP8*) leukocyte levels across all cancers. Multiple control modalities of the intracellular and extracellular networks (tran-

scription, microRNAs, copy number, and epigenetic processes) were involved in tumor-immune cell interactions, both across and within immune subtypes. Our immunogenomics pipeline to characterize these heterogeneous tumors and the resulting data are intended to serve as a resource for future targeted studies to further advance the field.

INTRODUCTION

The Cancer Genome Atlas (TCGA) has profoundly illuminated the genomic landscape of human malignancy. Genomic and transcriptomic data derived from bulk tumor samples have been used to study the tumor microenvironment (TME), and measures of immune infiltration define molecular subtypes of ovarian, melanoma, and pancreatic cancer (Bailey et al., 2016; The Cancer Genome Atlas Network, 2015; The Cancer Genome Atlas



Andrew Lamb,¹⁰ Wanding Zhou,²⁸ Hui Shen,²⁸ Toni K. Choueiri,²⁶ John N. Weinstein,¹⁹ Justin Guinney,¹⁰ Joel Saltz,²⁹ Robert A. Holt,² Charles E. Rabkin,³⁰ The Cancer Genome Atlas Research Network, Alexander J. Lazar,³¹ Jonathan S. Serody,³² Elizabeth G. Demicco,^{33,35} Mary L. Disis,^{34,35} Benjamin G. Vincent,^{4,*} and Ilya Shmulevich^{1,*}

²⁴Department of Neurosurgery, Henry Ford Hospital, Detroit, MI 48202, USA

²⁵Department of Genetics, Ribeirao Preto Medical School, University of São Paulo, São Paulo, Brazil

²⁶Department of Medical Oncology, Dana-Farber Cancer Institute, Boston, MA 02215, USA

²⁷University of Alabama at Birmingham, Birmingham, AL 35294, USA

²⁸Center for Epigenetics, Van Andel Research Institute, Grand Rapids, MI 49503, USA

²⁹Department of Biomedical Informatics, Stony Brook Medicine, 100 Nicolls Rd, Stony Brook, NY 11794, USA

³⁰Division of Cancer Epidemiology and Genetics, National Cancer Institute, 9609 Medical Center Dr., Bethesda, MD 20892, USA

³¹Departments of Pathology, Genomics Medicine and Translational Molecular Pathology, The University of Texas MD Anderson Cancer Center, 1515 Holcombe Blvd-Unit 85, Houston, TX 77030, USA

³²Department of Medicine and Microbiology and Lineberger Comprehensive Cancer Center, 125 Mason Farm Road, Chapel Hill, NC 27599-7295, USA

³³Mount Sinai Hospital, Department of Pathology and Laboratory Medicine, 600 University Ave., Toronto, ON M5G 1X5, Canada

³⁴UW Medicine Cancer Vaccine Institute, 850 Republican Street, Brotman Building, 2nd Floor, Room 221, Box 358050, University of Washington, Seattle, WA 98109-4714, USA

³⁵These authors contributed equally

³⁶Lead Author

*Correspondence: vesteinn.thorsson@systemsbiology.org (V.T.), benjamin.vincent@unchealth.unc.edu (B.G.V.), ilya.shmulevich@systemsbiology.org (I.S.)

<https://doi.org/10.1016/j.immuni.2018.03.023>

Research Network, 2011) and immune gene expression in other tumors varies by molecular subtype (Iglesia et al., 2016). Characterization of the immune microenvironment using gene expression signatures, T cell receptor (TCR), and B cell receptor (BCR) repertoire, and analyses to identify neo-antigenic immune targets provide a wealth of information in many cancer types and have prognostic value (Bindea et al., 2013; Brown et al., 2014, 2015; Charoentong et al., 2017; Gentles et al., 2015; Iglesia et al., 2016; Li et al., 2016; Porta-Pardo and Godzik, 2016; Rooney et al., 2015).

Contemporaneous with the work of TCGA, cancer immunotherapy has revolutionized cancer care. Antibodies against CTLA-4, PD-1, and PD-L1 are effective in treating a variety of malignancies. However, the biology of the immune microenvironment driving these responses is incompletely understood (Hugo et al., 2016; McGranahan et al., 2016) but is critical to the design of immunotherapy treatment strategies.

We integrated major immunogenomics methods to characterize the immune tumor microenvironment (TME) across 33 cancers analyzed by TCGA, applying methods for the assessment of total lymphocytic infiltrate (from genomic and H&E image data), immune cell fractions from deconvolution analysis of mRNA-seq data, immune gene expression signatures, neoantigen prediction, TCR and BCR repertoire inference, viral RNA expression, and somatic DNA alterations (Table S1). Transcriptional regulatory networks and extracellular communication networks that may govern the TME were found, as were possible germline determinants of TME features, and prognostic models were developed.

Through this approach, we identified and characterized six immune subtypes spanning multiple tumor types, with potential therapeutic and prognostic implications for cancer management. All data and results are provided in Supplemental Tables, at the NCI Genomic Data Commons (GDC, <https://portal.gdc.cancer.gov>), and though the Cancer Research Institute *iAtlas* portal for interactive exploration and visualization (<http://www.cri-iatlas.org>), and are intended to serve as a resource for future studies in the field of immunogenomics.

RESULTS

Analytic Pipeline

To characterize the immune response to cancer in all TCGA tumor samples, identify common immune subtypes, and evaluate whether tumor-extrinsic features can predict outcomes, we analyzed the TME across the landscape of all TCGA tumor samples. First, source datasets from all 33 TCGA cancer types and six molecular platforms (mRNA, microRNA, and exome sequencing; DNA methylation-, copy number-, and reverse-phase protein arrays) were harmonized by the PanCanAtlas consortium for uniform quality control, batch effect correction, normalization, mutation calling, and curation of survival data (Ellrott et al., 2018; Liu et al., 2018). We then performed a series of analyses, which we summarize here and describe in detail in the ensuing manuscript sections as noted within parentheses. We first compiled published tumor immune expression signatures and scored these across all non-hematologic TCGA cancer types. Meta-analysis of subsequent cluster analysis identified characteristic immunooncologic gene signatures, which were then used to cluster TCGA tumor types into six groups, or subtypes (described in Immune Subtypes in Cancer). Leukocyte proportion and cell type were then defined from DNA methylation, mRNA, and image analysis (see Composition of the Tumor Immune Infiltrate). Survival modeling was performed to assess how immune subtypes associate with patient prognosis (see Prognostic Associations of Tumor Immune Response Measures). Neoantigen prediction and viral RNA expression (see Survey of Immunogenicity), TCR and BCR repertoire inference (see The Adaptive Immune Receptor Repertoire in Cancer), and immunomodulator (IM) expression and regulation (see Regulation of Immunomodulators) were characterized in the context of TCGA tumor types, TCGA-defined molecular subtypes, and these six immune subtypes, so as to assess the relationship between factors affecting immunogenicity and immune infiltrate. In order to assess the degree to which specific underlying somatic alterations (pathways, copy-number

alterations, and driver mutations) may drive the composition of the TME, we identified which alterations correlate with modified immune infiltrate (see Immune Response Correlates of Somatic Variation). We likewise asked whether gender and ancestry predispose individuals to particular tumor immune responses (see Immune Response Correlates of Demographic and Germline Variation). Finally, we sought to identify the underlying intracellular regulatory networks governing the immune response to tumors, as well as the extracellular communication networks involved in establishing the particular immune milieu of the TME (see Networks Modulating Tumoral Immune Response).

Immune Subtypes in Cancer

To characterize intratumoral immune states, we scored 160 immune expression signatures and used cluster analysis to identify modules of immune signature sets (Figure 1A, top). Five immune expression signatures—macrophages/monocytes (Beck et al., 2009), overall lymphocyte infiltration (dominated by T and B cells) (Calabro et al., 2009), TGF- β response (Teschendorff et al., 2010), IFN- γ response (Wolf et al., 2014), and wound healing (Chang et al., 2004)—which robustly reproduced co-clustering of these immune signature sets, were selected to perform cluster analysis of all 30 non-hematologic cancer types (Figures 1A middle, and S1A). The six resulting clusters “Immune Subtypes,” C1–C6 (with 2,416, 2,591, 2,397, 1,157, 385, and 180 cases, respectively) were characterized by a distinct distribution of scores over the five representative signatures (Figure 1A, bottom) and showed distinct immune signatures based on the dominant sample characteristics of their tumor samples (Figures 1B and 1C). Immune subtypes spanned anatomical location and tumor type, while individual tumor types and TCGA subtypes (Figures 1D and S1B–S1D) varied substantially in their proportion of immune subtypes.

C1 (wound healing) had elevated expression of angiogenic genes, a high proliferation rate (Figure 1C), and a Th2 cell bias to the adaptive immune infiltrate. Colorectal cancer (COAD [colon adenocarcinoma], READ [rectum adenocarcinoma]) and lung squamous cell carcinoma (LUSC) were rich in C1, as were breast invasive carcinoma (BRCA) luminal A (Figures S1C and S1D), head and neck squamous cell carcinoma (HNSC) classical, and the chromosomally unstable (CIN) gastrointestinal subtype.

C2 (IFN- γ dominant) had the highest M1/M2 macrophage polarization (Figure S2A, mean ratio = 0.52, $p < 10^{-149}$, Wilcoxon test relative to next-highest), a strong CD8 signal and, together with C6, the greatest TCR diversity. C2 also showed a high proliferation rate, which may override an evolving type I immune response, and was comprised of highly mutated BRCA, gastric, ovarian (OV), HNSC, and cervical tumors (CESC).

C3 (inflammatory) was defined by elevated Th17 and Th1 genes (Figure 1C, both $p < 10^{-23}$), low to moderate tumor cell proliferation, and, along with C5, lower levels of aneuploidy and overall somatic copy number alterations than the other subtypes. C3 was enriched in most kidney, prostate adenocarcinoma (PRAD), pancreatic adenocarcinoma (PAAD), and papillary thyroid carcinomas (THCA).

C4 (lymphocyte depleted) was enriched in particular subtypes of adrenocortical carcinoma (ACC), pheochromocytoma and paraganglioma (PCPG), liver hepatocellular carcinoma (LIHC),

and gliomas, and displayed a more prominent macrophage signature (Figure 2A), with Th1 suppressed and a high M2 response (Figure S2A).

C5 (immunologically quiet), consisted mostly of brain lower-grade gliomas (LGG) (Figures 1D and S1B), exhibited the lowest lymphocyte ($p < 10^{-17}$) and highest macrophage ($p < 10^{-7}$) responses (Figure 2A), dominated by M2 macrophages (Figure S2A). Glioma subtypes (Ceccarelli et al., 2016) CpG island methylator phenotype-high (CIMP-H), the 1p/19q codeletion subtype and pilocytic astrocytoma-like (PA-like) were prevalent in C5, with remaining subtypes enriched in C4. *IDH* mutations were enriched in C5 over C4 (80% of *IDH* mutations, $p < 2 \times 10^{-16}$, Fisher’s exact test), suggesting an association of *IDH* mutations with favorable immune composition. Indeed, *IDH* mutations associate with TME composition (Venteicher et al., 2017) and decrease leukocyte chemotaxis, leading to fewer tumor-associated immune cells and better outcome (Amankulor et al., 2017).

Finally, C6 (TGF- β dominant), which was a small group of mixed tumors not dominant in any one TCGA subtype, displayed the highest TGF- β signature ($p < 10^{-34}$) and a high lymphocytic infiltrate with an even distribution of type I and type II T cells.

These six categories represent features of the TME that largely cut across traditional cancer classifications to create groupings and suggest certain treatment approaches may be independent of histologic type. For a complete list of the TCGA cancer type abbreviations, please see <https://gdc.cancer.gov/resources-tcga-users/tcga-code-tables/tcga-study-abbreviations>.

Composition of the Tumor Immune Infiltrate

Leukocyte fraction (LF) varied substantially across immune subtypes (Figure 1C) and tumor types (Figure 2B). Tumors within the top third LF included cancers most responsive to immune checkpoint inhibitors, such as lung adenocarcinoma (LUAD), LUSC, cutaneous melanoma (SKCM), HNSC, and kidney renal clear cell carcinoma (KIRC), and in particular, the LUSC.secretory, LUAD.6, bladder urothelial carcinoma (BLCA.4), kidney renal papillary cell carcinoma (KIRP.C2a), and HNSCC mesenchymal subtypes. Uveal melanoma (UVM) and ACC had very low LF. Glioma subtypes displayed a greater range in LF than other tumors, which may reflect the presence or absence of microglia.

The leukocyte proportion of tumor stromal fraction, ρ , varied across tumor types and immune subtypes (Figures 2C and S2B), ranging from >90% in SKCM to <10% in stroma-rich tumors such as PAAD, PRAD, and LGG. Some tumors, e.g., BRCA, showed variation within annotated or immune subtypes. In BRCA, C1 has the lowest ρ ($\rho^{C1} = 0.44$) while $\rho^{C2} = 0.61$ was 37% higher ($p < 0.001$) (Figure S2B), and there were likewise differences between luminal A and basal BRCA ($\rho^{LumA} = 0.45$ and $\rho^{Basal} = 0.67$ [$p < 0.001$]). For LGG, $\rho^{C5} = 0.28$ ($p < 0.001$), whereas $\rho^{C3} = 0.48$ and $\rho^{C4} = 0.50$ ($p < 0.001$) (Figure S2B), and in READ, $\rho^{CIN} = 0.40$ and $\rho^{MSI} = 0.78$ ($p < 0.001$).

The spatial fraction of tumor regions with tumor-infiltrating lymphocytes (TILs), estimated by analysis of digitized TCGA H&E-stained slides (Saltz et al., 2018), varied by immune subtype, with C2 the highest ($p < 10^{-16}$, Figure 2D). Image estimates correlated modestly with molecular estimates of lymphocyte proportion (Figures S2C and S2D), in part because the molecular

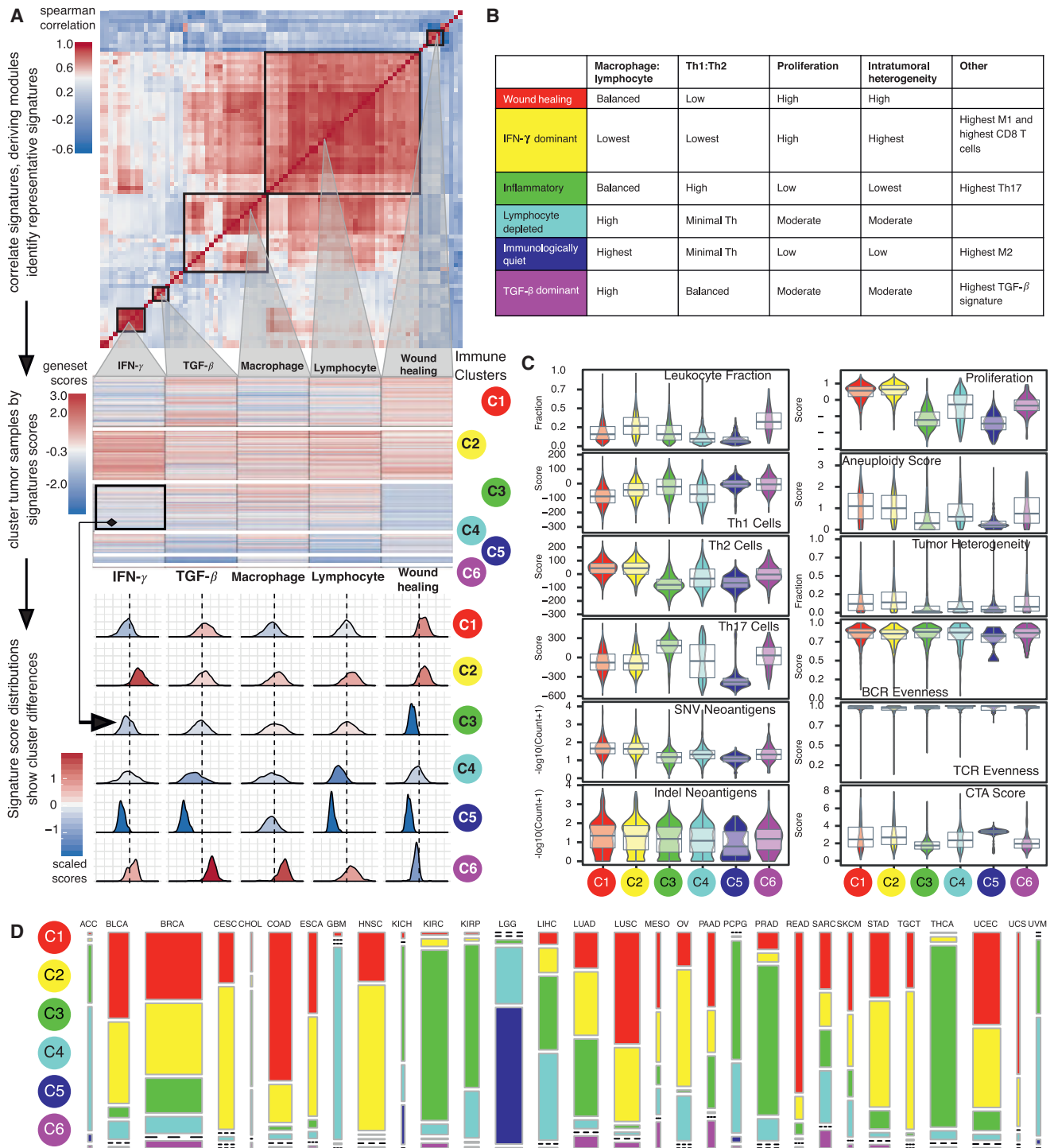


Figure 1. Immune Subtypes in Cancer

(A) Expression signature modules and identification of immune subtypes. Top: Consensus clustering of the pairwise correlation of cancer immune gene expression signature scores (rows and columns). Five modules of shared associations are indicated by boxes. Middle: Representative gene expression signatures from each module (columns), which robustly reproduced module clustering, were used to cluster TCGA tumor samples (rows), resulting in six immune subtypes C1–C6 (colored circles). Bottom: Distributions of signature scores within the six subtypes (rows), with dashed line indicating the median.

(B) Key characteristics of immune subtypes.

(C) Values of key immune characteristics by immune subtype.

(D) Distribution of immune subtypes within TCGA tumors. The proportion of samples belonging to each immune subtype is shown, with colors as in (A). Bar width reflects the number of tumor samples.

See also Figure S1 and Table S1.

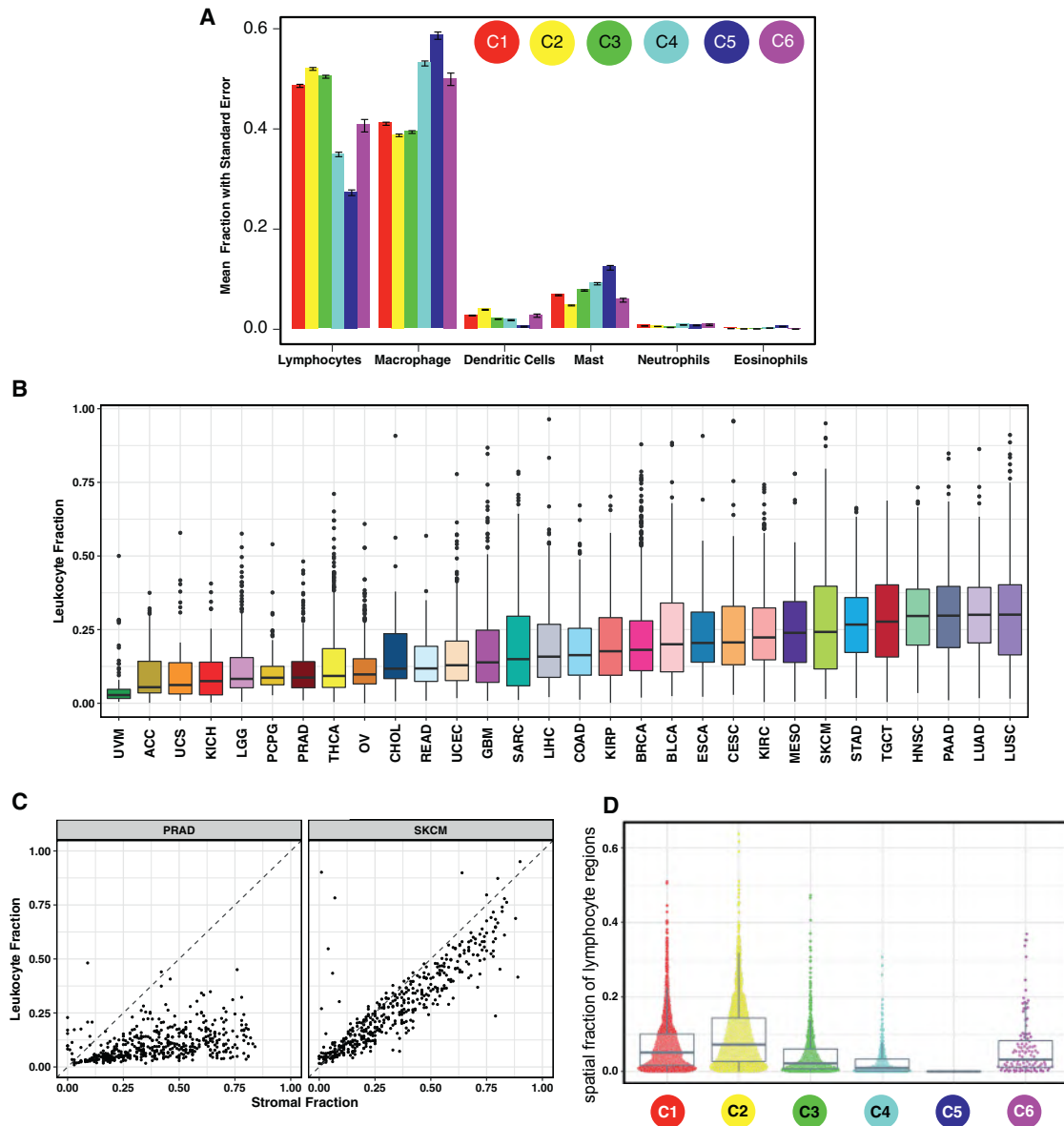


Figure 2. Composition of the Tumor Immune Infiltrate

(A) The proportion of major classes of immune cells (from CIBERSORT) within the leukocyte compartment for different immune subtypes. Error bars show the standard error of the mean.

(B) Leukocyte fraction (LF) within TCGA tumor types, ordered by median.

(C) LF (y axis) versus non-tumor stromal cellular fraction in the TME (x axes) for two representative TCGA tumor types: PRAD, (low LF relative to stromal content) and SKCM (high leukocyte fraction in the stroma). Dots represent individual tumor samples.

(D) The spatial fraction of lymphocyte regions in tissue was estimated using machine learning on digital pathology H&E images (see also Saltz et al., 2018).

estimate is more similar to cell count, while spatial TIL is a fraction of the area. The relative similarity of the estimates of lymphocytic content between two radically different methodologies reinforces the robustness of individual methods.

Prognostic Associations of Tumor Immune Response Measures

Immune subtypes associated with overall survival (OS) and progression-free interval (PFI) (Figures 3A and S3A). C3 had the best prognosis (OS HR 0.628, $p = 2.34 \times 10^{-8}$ relative to

C1, adjusted for tumor type), while C2 and C1 had less favorable outcomes despite having a substantial immune component. The more mixed-signature subtypes, C4 and C6, had the least favorable outcome. Functional orientation of the TME for tumor and immune subtypes was measured using the concordance index (CI) (Pencina and D’Agostino, 2004) and found to have context-dependent prognostic impact (Figures 3B, 3C and S3B). Higher lymphocyte signature associated with improved outcome in C1 and C2. An increased value of any of the five signatures led to worse outcome in C3 (Figure 3B), perhaps

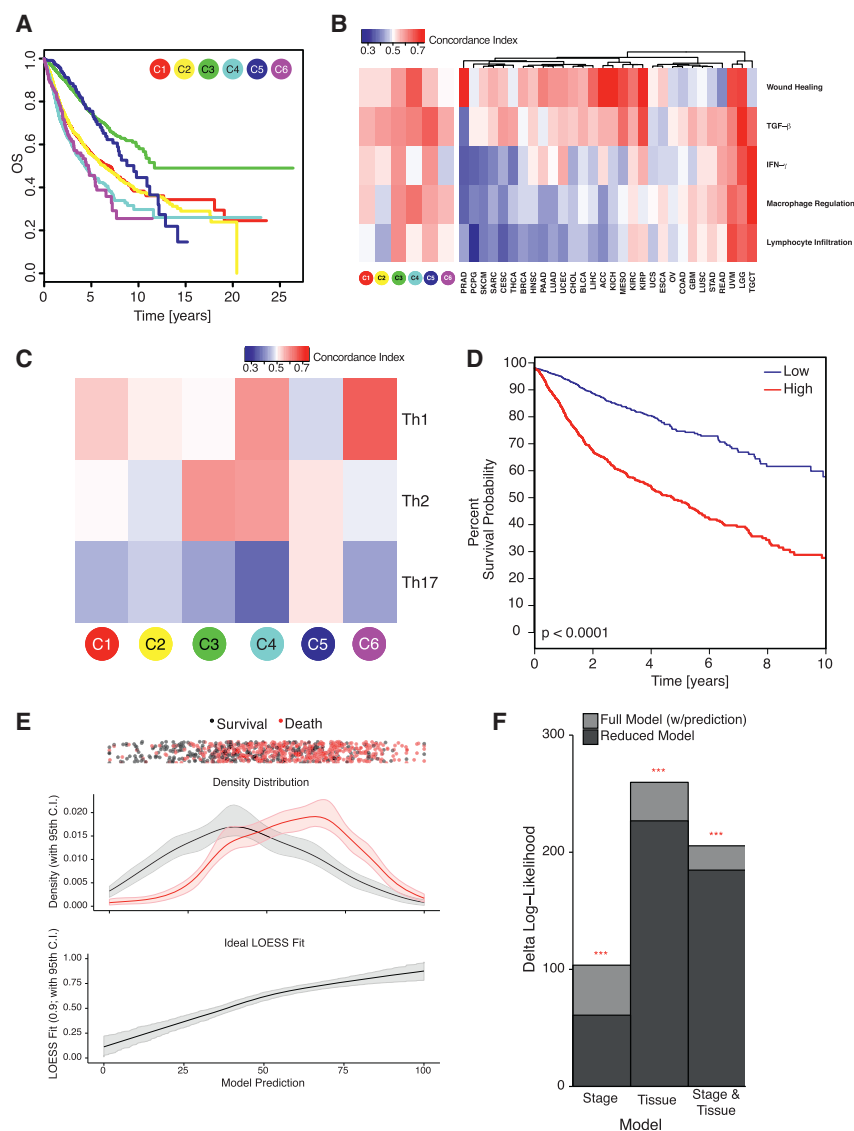


Figure 3. Immune Response and Prognostics

(A) Overall survival (OS) by immune subtype.

(B) Concordance index (CI) for five characteristic immune expression signature scores (Figure 1A) in relation to OS, for immune subtypes and TCGA tumor types. Red denotes higher and blue lower risk, with an increase in the signature score.

(C) CI for T helper cell scores in relation to OS within immune subtypes.

(D) Risk stratification from elastic net modeling of immune features. Tumor samples were divided into discovery and validation sets, and an elastic net model was optimized on the discovery set using immune gene signatures, TCR/BCR richness, and neoantigen counts. Kaplan-Meier plot shows the high (red) and low (blue) risk groups from this model as applied to the validation set, $p < 0.0001$ (*G-rho* family of tests, Harrington and Fleming).

(E) Prediction versus outcome from elastic net model in validation set data (from D). Top: Patient outcomes for each sample (black, survival; red, death) plotted with vertical jitter, along the sample's model prediction (x axis). Middle: Fractional density of the outcomes plotted against their model predictions. Confidence intervals were generated by bootstrapping with replacement. Bottom: LOESS fit of the actual outcomes against the model predictions; narrow confidence bands confirm good prediction accuracy.

(F) CoxPH models of stage and tumor type ("Tissue") with (full model) or without (reduced model) the validation set predictions of the elastic net model were compared; the full model significantly outperformed the reduced model in all comparisons ($p < 0.001$; false discovery rate (FDR) BH-corrected). See also Figure S3.

reflecting a balanced immune response. While increased Th17 cells generally led to improved OS, Th1 associated with worse OS across most immune subtypes, and Th2 orientation had mixed effects (Figure 3C). Tumor types displayed two behaviors relative to immune orientation (Figures 3B, OS; S3B, PFI). In the first group including SKCM and CESC, activation of immune pathways was generally associated with better outcome, while in the other, the opposite was seen. The relative abundance of individual immune cell types had complex associations that differed between tumor types (Figures S3C and S3D). These analyses extend beyond mere determination of lymphocyte presence to suggest testable properties that correlate with patient outcome in different tumor types and immune contexts.

We obtained and validated a survival model using elastic-net Cox proportional hazards (CoxPH) modeling with cross-validation. Low- and high-score tumors displayed significant survival differences in the validation set (Figure 3D), with good prediction accuracy (Figure 3E). Incorporating immune features into Cox models fit with tumor type, stage, and tumor type + stage

macrophages most strongly associated with improved OS (Figure S3E), while wound healing, macrophage regulation, and TGF- β associated with worse OS, recapitulating survival associations in immune subtypes. Within tumor types, the prognostic implications of immune subtypes seen in univariate analyses were largely maintained, with C3 correlating with better OS in six tumor types and C4 with poor OS in three cancer types (Figure S3F).

Immune Response Correlates of Somatic Variation

The immune infiltrate was related to measures of DNA damage, including copy number variation (CNV) burden (both in terms of number of segments and fraction of genome alterations), aneuploidy, loss of heterozygosity (LOH), homologous recombination deficiency (HRD), and intratumor heterogeneity (ITH) (Figure 4A). LF correlated negatively with CNV segment burden, with strongest correlation in C6 and C2, and positively with aneuploidy, LOH, HRD, and mutation load, particularly in C3. These results suggest a differential effect of multiple smaller,

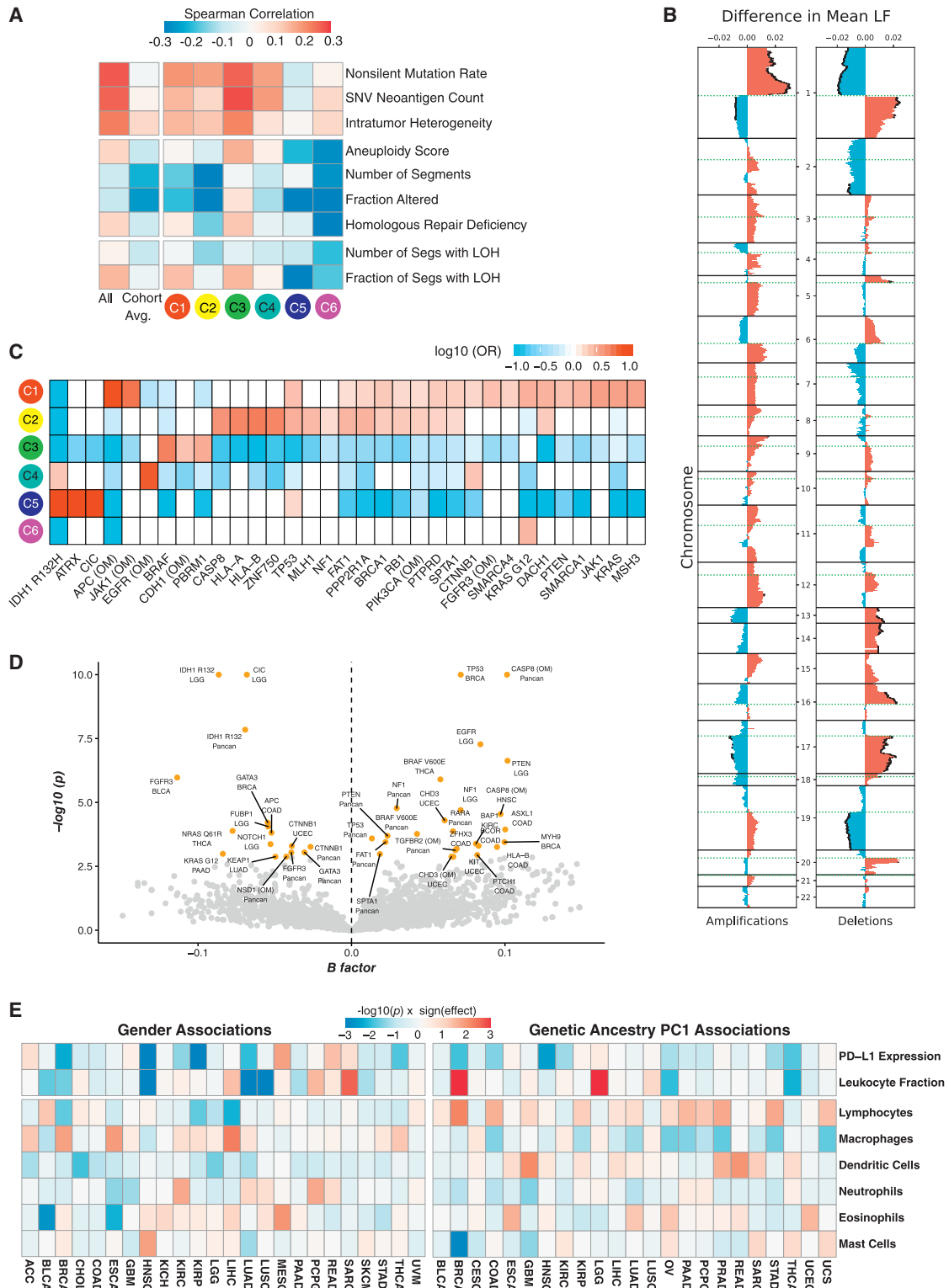


Figure 4. Immune Response and Genome State

(A) Correlation of DNA damage measures (rows) with LF. From left to right: all TCGA tumors; averaged over tumor type; grouped by immune subtype.

(B) LF association with copy number (CN) alterations. Left: Differences between observed and expected mean LF in tumors with amplifications, by genomic region. Significant (FDR < 0.01) differences in mean LF are marked with black caps on the profiles. Right: Same, for deletions.

(legend continued on next page)

focal copy number events versus larger events on immune infiltration in certain immune subtypes.

Specific SCNAs affected LF and immune composition (Figures 4B and S4A). Chromosome 1p (including *TNFRS9* and *VTCN1*) amplification associated with higher LF, while its deletion did the opposite. 19q deletion (including *TGFB1*) also correlated with lower LF, consistent with the role of TGF- β in immune cell recruitment (Bierie and Moses, 2010). Amplification of chr2, 20q, and 22q (including *CTLA4*, *CD40*, and *ADORA2*, respectively), and deletions of 5q, 9p, and chr19 (including *IL13* and *IL4*, *IFNA1* and *IFNA2*, and *ICAM1*, respectively) associated with changes in macrophage polarity (Figure S4A). IL-13 influences macrophage polarization (Mantovani et al., 2005), implying a possible basis for our observation that IL-13 deletions associated with altered M0 macrophage fractions.

Increased ITH associates with worse clinical outcomes or lower efficacy of IM therapy in a number of cancer types (McGranahan et al., 2016; Morris et al., 2016). ITH correlated (Spearman, Benjamini-Hochberg [BH]-adjusted $p < 0.05$) with total LF in nine tumor types (LUAD, BRCA, KIRC, HNSC, GBM [glioblastoma multiforme], OV, BLCA, SKCM, and READ; data not shown) and with individual relative immune cell fractions in many tumor types (Figure S4B). ITH was highest in C1 and C2 ($p < 10^{-229}$ relative to all others) and lowest in C3 ($p = 3 \times 10^{-5}$, Figure 1C), possibly supporting the link between lower ITH and improved survival.

We correlated mutations in 299 cancer driver genes with immune subtypes and found 33 significant associations ($q < 0.1$) (Figure 4C, Table S2). C1 was enriched in mutations in driver genes, such as *TP53*, *PIK3CA*, *PTEN*, or *KRAS*. C2 was enriched in many of these genes, as well as *HLA-A* and *B* and *CASP8*, which could be immune-evading mechanisms (Rooney et al., 2015). C3 was enriched in *BRAF*, *CDH1*, and *PBRM1* mutations, a finding of note since patients with *PBRM1* mutations respond particularly well to IM therapy (Miao et al., 2018). C4 was enriched in *CTNNB1*, *EGFR*, and *IDH1* mutations. C5 was enriched in *IDH1*, *ATRX*, and *CIC*, consistent with its predominance of LGG samples. C6 was only enriched in *KRAS* G12 mutations. Mutations in 23 driver genes associated with increased LF either in specific tumor types or across them, including *TP53*, *HLA-B*, *BRAF*, *PTEN*, *NF1*, *APC*, and *CASP8*. Twelve other events were associated with lower LF, including the *IDH1* R132H mutation, *GATA3*, *KRAS*, *NRAS*, *CTNNB1*, and *NOTCH1* (Figure 4D).

Since driver mutations in the same pathway had opposing correlations with LF (e.g., *BRAF*, *KRAS*, *NRAS*), we considered the overall effect of somatic alterations (mutations and SCNAs) on eight oncogenic signaling pathways. PI3K, NOTCH, and RTK/RAS pathway disruptions showed variable, tumor type-specific effects on immune factors, while TGF- β pathway disruptions

more consistently associated with lower LF (most prominently in C2 and C6; Figure S4C), higher eosinophils (C2), and increased macrophages. However, in C3, TGF- β pathway disruption associated with higher LF and M1 macrophages and lower memory B cells, helper T cells, and M0 macrophages. Thus, TGF- β pathway disruption has context-dependent effects on LF but may promote increased macrophages, particularly M1. Higher M1/M2 ratio, in turn, may reiterate the local pro-inflammatory state in these patients.

Immune Response Correlates of Demographic and Germline Variation

Immune cell content and expression of *PD-L1* varied by gender and genetic ancestry (Figures 4E and S4D). *PD-L1* expression was greater ($p < 0.05$, Kruskal-Wallis test, unadjusted) in women than in men in HNSC, KIRC, LUAD, THCA, and KIRP (Figure S4E), while mesothelioma (MESO) showed an opposite trend. *PD-L1* expression was lower in individuals of predicted African ancestry (overall $p = 5 \times 10^{-6}$). This association was consistent across most cancer types and was significant ($p < 0.05$, unadjusted) in BRCA, COAD, HNSC (Figure S4F), and THCA. No single *cis*-eQTL significantly correlated with *PD-L1* expression, although the SNP rs822337, approximately 1 kb upstream of *CD274* transcription start, correlated weakly ($p = 0.074$; 1.3×10^{-4} unadjusted; Figure S4G). Lymphocyte fractions tended to be lower in people of Asian ancestry, particularly in UCEC (uterine corpus endometrial carcinoma) and BLCA (Figure S4H). The significance of these demographic associations remains unclear but provides hypotheses for the efficacy of checkpoint inhibitor therapy based on genetic ancestry.

Survey of Immunogenicity

Peptides predicted to bind with MHC proteins (pMHCs) and induce antitumor adaptive immunity were identified from SNV and indel mutations. The number of pMHCs (neoantigen load) varied between immune subtypes (Figure 1C), correlated positively with LF in most immune subtypes (Figure S4I), and trended positive in most TCGA tumor subtypes, with some negative correlation seen among GI subtypes, and differential trending seen among individual LUAD, LUSC, OV, and KIRP subtypes (Figure S4J). Neoantigen load also associated with higher content of CD8 T cells, M1 macrophages, and CD4 memory T cells, and lower Treg, mast, dendritic, and memory B cells in multiple tumor types (Figure S4K).

Most SNV-derived peptides which bind to MHC were each found in the context of a single MHC allele (89.9%). Single mutations generate 99.8% of unique pMHCs while 0.2% result from distinct mutations in different genetic loci yielding identical peptides (Figure 5A). The most frequently observed pMHCs

(C) Enrichment and depletion of mutations in driver genes and oncogenic mutations (OM) within immune subtypes, displayed as fold enrichment. Significance was evaluated by the Cochran-Mantel-Haenszel χ^2 test, to account for cancer type (white, no significant association).

(D) Volcano plot showing driver genes and OMs associated with changes in LF, across all tumors ("Pancan") and within specific tumor types as indicated. x axis: Multivariate correlation with LF (B-factor), taking into account tumor type and number of missense mutations. Values > 0 represent positive correlation with LF and vice versa; y axis: $-\log_{10}(p)$. Significant events ($FDR < 0.1$; $p < 0.003$) are in orange, others in gray.

(E) Left: Degree of association between gender for eight selected immune characteristics (rows) within TCGA tumor types (columns). Blue denotes a higher value in women than in men, and red the opposite. Right: Degree of association between the immune characteristics and the first principal component of genetic ancestry in TCGA participants (PC1), reflecting degree of African ancestry. Blue reflects lower values in individuals of African descent. See also Figure S4 and Table S2.

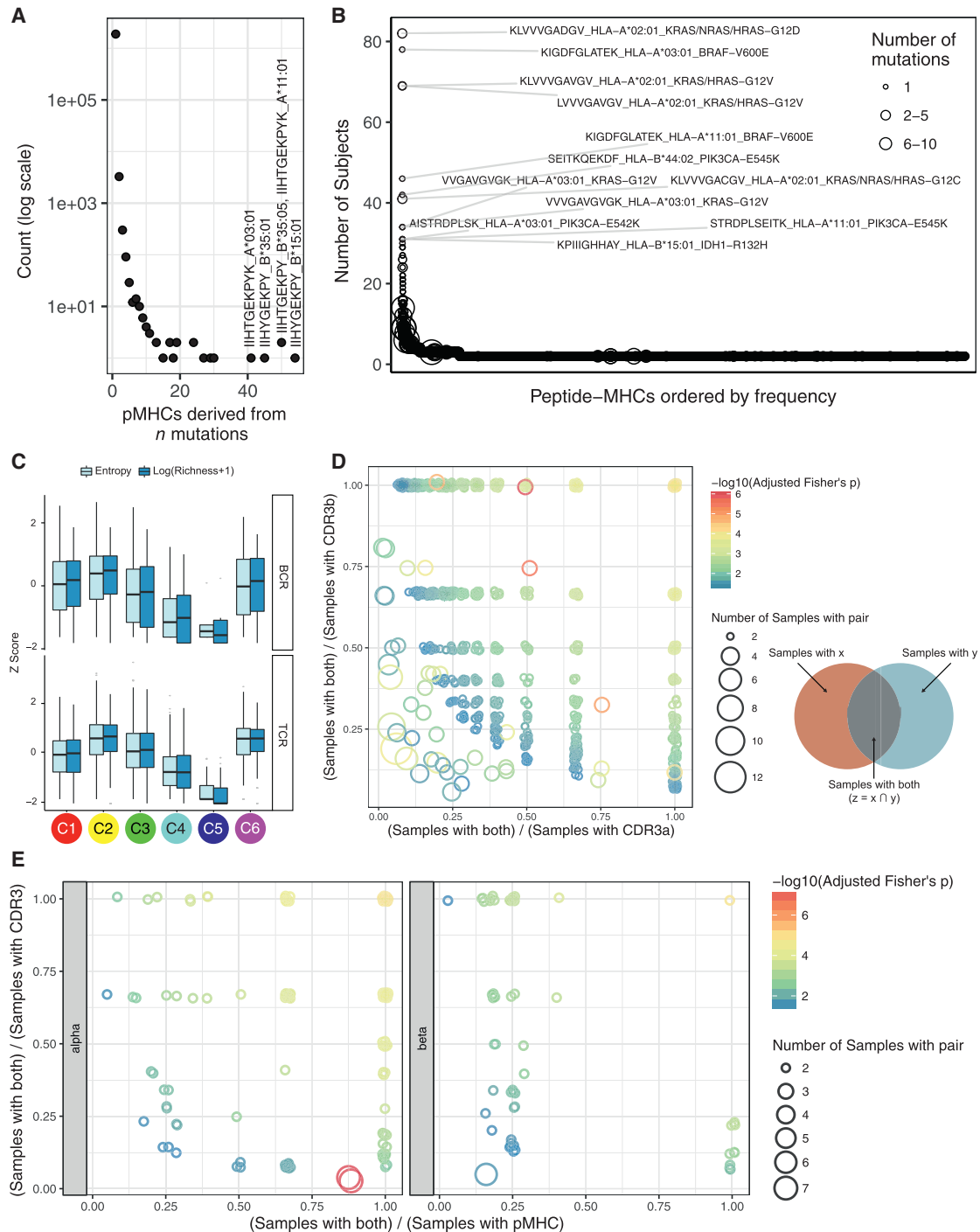


Figure 5. The Tumor-Immune Interface

(A) Distribution of the number of pMHCs associated with number of mutations; the 4 pMHCs derived from > 40 mutations are labeled.
 (B) Numbers of tumors expressing shared pMHCs. The known cancer genes from which the most frequent pMHCs in the population are derived are indicated.
 (C) BCR (top) and TCR (bottom) diversity measured by Shannon entropy and species richness, logarithmically transformed, and expressed as Z-scores, for immune subtypes.
 (D and E) Co-occurrence of CDR3a-CDR3b (D) and pMHC-CDR3 pairs (E) as a surrogate marker for shared T cell responses. Pairs found in at least two samples and meeting statistical significance are plotted, with jitter. x and y axes indicate how exclusive the pair members are: pairs in the top right typically co-occur, whereas along the axes each member is more often found separately. Size of the circle indicates how many samples that pair was found in.
 See also Figure S5 and Tables S3, S4, and S5.

were from recurrently mutated genes (*BRAF*, *IDH1*, *KRAS*, and *PIKC3A* for SNVs, *TP53* and *RNF43* for indels) (Figure 5B, Tables S3 and S4). In BRCA and LIHC, worse PFI was associated with higher neoantigen load, while BLCA and UCEC showed the opposite effect (Figure S5A). For most tumors, however, there were no clear associations between predicted pMHC count and survival. Within immune subtypes (Figure S5B), higher neoantigen load was associated with improved PFI in C1 and C2 and worse PFI in C3, C4, and C5. These results suggest that neoantigen load provides more prognostic information within immune subtypes than based on tissue of origin, emphasizing the importance of overall immune signaling in responding to tumor neoantigens.

Cancer testis antigens (CTA) overall expression, and that of individual CTAs, varied by immune subtype with C5 having the highest ($p < 10^{-13}$) and C3 the lowest ($p = 10^{-4}$) expression values (Figure 1C). *CEP55*, *TTK*, and *PBK* were broadly expressed across immune subtypes, with enrichment in C1 and C2. C5 demonstrated high expression of multiple CTAs, illustrating that CTA expression alone is insufficient to elicit an intratumoral immune response.

We found human papilloma virus (HPV) in 6.2% of cases, mainly in CESC, GBM, HNSC, and KIRC, whereas hepatitis B virus (HBV) and Epstein-Barr virus (EBV) were mainly found in LIHC and STAD (stomach adenocarcinoma), respectively. In a regression model of all tumors, high load of each virus type associated with immune features (Figure S5C, cancer-type adjusted). High EBV content associated strongly with high *CTLA4* and *CD274* expression and low B cell signatures. High HPV levels associated with increased proliferation and Th2 cells but low macrophage content. In contrast, high HBV levels associated with Th17 signal and $\gamma\delta$ T cell content. These findings highlight the diverse effect of different viruses on the immune response in different cancer types.

Our findings suggest that pMHC burden and viral content impact immune cell composition, while CTAs have inconsistent effects on the immune response. Moreover, the effect of pMHC load on prognosis is disease specific and influenced by immune subtype.

The Adaptive Immune Receptor Repertoire in Cancer

Antigen-specific TCR and BCR repertoires are critical for recognition of pathogens and malignant cells and may reflect a robust anti-tumor response comprising a large number of antigen-specific adaptive immune cells that have undergone clonal expansion and effector differentiation.

We evaluated TCR α and β and immunoglobulin heavy and light chain repertoires from RNA-seq. Mean TCR diversity values differed by immune subtype, with the highest diversity in C6 and C2 ($p < 10^{-183}$, Wilcoxon, relative to all other subtypes; Figure 5C) and by tumor type (Figure S5D, lower panel). We saw recurrent TCR sequences across multiple samples (Figure S5E, Table S5), suggesting a common, but not necessarily cancer-related, antigen (the top recurrent TCRs include known mucosal associated invariant T cell sequences). We assessed co-occurrence of complementarity determining region 3 (CDR3) α and β chains, in order to determine the frequency of patients with identical TCRs (a surrogate marker for shared T cell responses). We identified 2,812 α - β pairs present in at least 2 tumors ($p \leq 0.05$, Fisher's

exact test with Bonferroni correction; Figure 5D and Table S5). Likewise, testing for co-occurrence of specific SNV pMHC-CDR3 pairs across all patients identified 206 pMHC-CDR3 α pairs and 196 pMHC-CDR3 β pairs (Figure 5E, Table S5). Thus, a minority of these patients appear to share T cell responses, possibly mediated by public antigens. That said, there is relatively little pMHC and TCR sharing among tumors, highlighting the large degree of diversity in TILs.

Higher TCR diversity only correlated with improved PFI in a few tumor types (BLCA, COAD, LIHC, and UCEC) (Figure S5F). Therefore, it may be more important for the immune system to mount a robust response against only a few antigens, than a diverse response against many different antigens.

The pattern of immunoglobulin heavy chain diversity was similar to that of TCR diversity (Figures 5C and S5D), with tumors showing significant variance in IgH repertoire diversity, suggesting differential B cell recruitment and/or clonal expansion within the tumor types.

Regulation of Immunomodulators

IMs are critical for cancer immunotherapy with numerous IM agonists and antagonists being evaluated in clinical oncology (Tang et al., 2018). To advance this research, understanding of their expression and modes of control in different states of the TME is needed. We examined IM gene expression, SCNAs, and expression control via epigenetic and miRNA mechanisms.

Gene expression of IMs (Table S6, Figure 6A) varied across immune subtypes, and IM expression largely segregated tumors by immune subtypes (Figure S6A), perhaps indicative of their role in shaping the TME. Genes with the greatest differences between subtypes (Figures 6B and S6B) included *CXCL10* (BH-adjusted $p < 10^{-5}$), most highly expressed in C2 (consistent with its known interferon inducibility) and *EDNRB* (BH-adjusted $p < 10^{-5}$), most highly expressed in the immunologically quiet C5. DNA methylation of many IM genes, e.g., *CD40* (Figure 6C), *IL10*, and *IDO1*, inversely correlated with gene expression, suggesting epigenetic silencing. 294 miRNAs were implicated as possible regulators of IM gene expression; among these, several associated with IMs in multiple subtypes (Figure S6C) including immune inhibitors (*EDNRB*, *PD-L1*, and *VEGFA*) and activators (*CD28* and *TNFRSF9*). The immune activator *BTN3A1* was one of the most commonly co-regulated IMs from the SYGNAL-PanImmune network (below). Negative correlations between *miR-17* and *BTN3A1*, *PDCD1LG2*, and *CD274* may relate to the role of this miRNA in maturation and activation of cells into effector or memory subsets (Liang et al., 2015).

Copy-number alterations affected multiple IMs and varied across immune subtypes. C1 and C2 showed both frequent amplification and deletion of IM genes, consistent with their greater genomic instability, while subtypes C3 and C5 generally showed fewer alterations in IM genes. In particular, IMs *SLAMF7*, *SELP*, *TNFSF4* (*OX40L*), *IL10*, and *CD40* were amplified less frequently in C5 relative to all samples, while *TGFB1*, *KIR2DL1*, and *KIR2DL3* deletions were enriched in C5 (Figure 6D), consistent with our observation of lower immune infiltration with *TGFB1* deletion (Figure S4A). *CD40* was most frequently amplified in C1 (Figure 6D) (Fisher's exact $p < 10^{-10}$ for all comparisons mentioned). Overall, these marked differences in IM copy

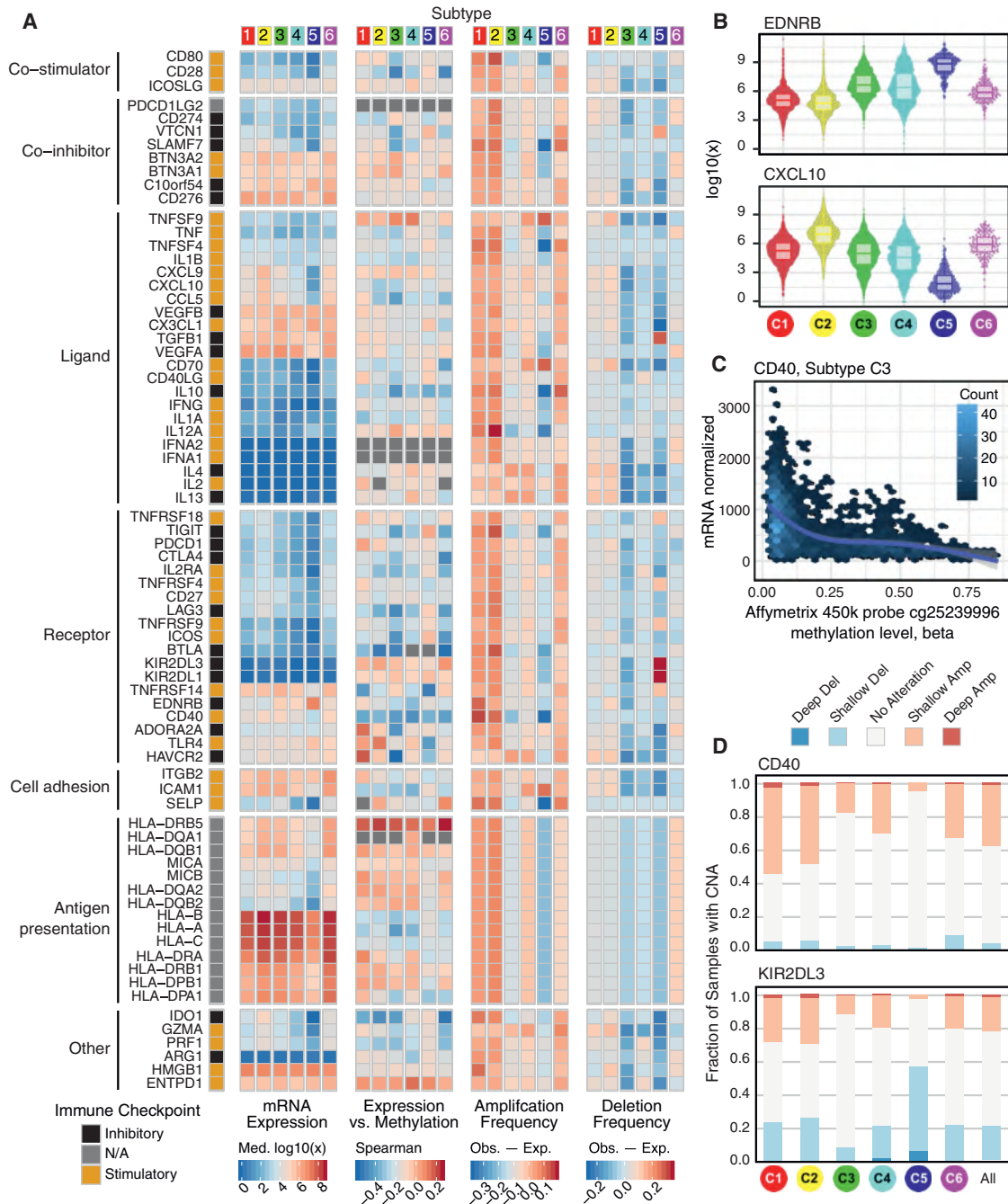


Figure 6. Regulation of Immunomodulators

(A) From left to right: mRNA expression (median normalized expression levels); expression versus methylation (gene expression correlation with DNA-methylation beta-value); amplification frequency (the difference between the fraction of samples in which an IM is amplified in a particular subtype and the amplification fraction in all samples); and the deletion frequency (as amplifications) for 75 IM genes by immune subtype.

(B) Distribution of log-transformed expression levels for IM genes with largest differences across subtypes (by Kruskal-Wallis test).

(C) *CD40* expression is inversely correlated to methylation levels (Affymetrix 450K probe cg25239996, 125 bases upstream of *CD40* TSS) in C3. Each point represents a tumor sample, and color indicates point density.

(D) Proportion of samples in each immune subtype with copy number alterations in *CD40* (top) and *KIR2DL3* (bottom). The “All” column shows the overall proportion (8,461 tumors).

See also Figure S6 and Table S6.

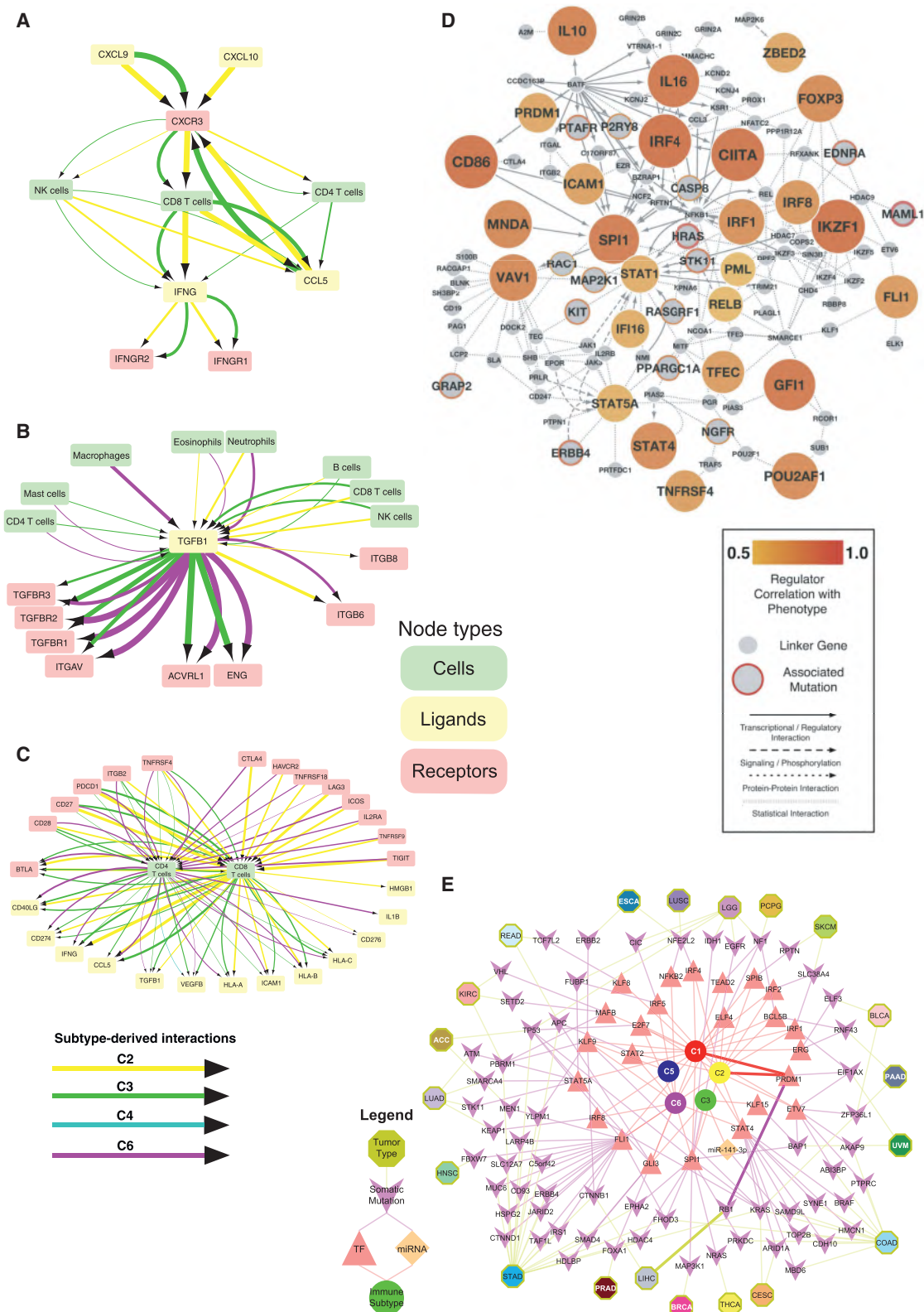


Figure 7. Predicted Networks Modulating the Immune Response to Tumors

TME estimates and tumor cell characteristics were combined with available data on possible physical, signaling, and regulatory interactions to predict cellular and molecular interactions involved in tumoral immune responses.

(legend continued on next page)

number may be reflective of more direct modulation of the TME by cancer cells.

Among IMs under investigation for cancer therapy, expression of *VISTA* is relatively high in all tumor types and highest in MESO; *BTLA* expression is high in C4 and C5; *HAVCR2* (*TIM-3*) shows evidence of differential silencing among immune subtypes; and *IDO1* is amplified, mostly in C1. The observed differences in regulation of IMs might have implications for therapeutic development and combination immune therapies, and the multiple mechanisms at play in evoking them further highlights their biological importance.

Networks Modulating Tumoral Immune Response

The immune response is determined by the collective states of *intracellular* molecular networks in tumor, immune, and other stromal cells and the *extracellular* network encompassing direct interaction among cells and communication via soluble proteins such as cytokines to mediate interactions among those cells.

Beginning with a large network of extracellular interactions known from other sources, we identified which of those met a specified precondition for interaction, namely that both interaction partners are consistently present within samples in an immune subtype, according to our TME estimates. We focused the network on IMs. Networks in C2 and C3 had abundant CD8 T cells, while C3, C4, and C6 were enriched in CD4 T cells.

A small sub-network (Figure 7A), focused around IFN- γ , illustrates some subtype-specific associations. In both C2 and C3, CD4 T cells, CD8 T cells, and NK cells correlated with expression of *IFNG* and *CCL5*, a potent chemoattractant. A second sub-network (Figure 7B), centered on TGF- β , was found in the C2, C3, and C6 networks. Across subtypes, different cell types were associated with abundant expression of *TGFB1*: CD4 T cells and mast cells in C3 and C6, macrophages in C6, neutrophils and eosinophils in C2 and C6, and B cells, NK cells, and

CD8 T cells in C2 and C3. The receptors known to bind TGF- β likewise were subtype specific and may help mediate the TGF- β -driven infiltrates, with *TGFB1R1*, 2, and 3 found only in the C3 and C6 networks. These results largely echo findings seen in our TGF- β pathway analysis (Figure S4C), which examined the effects of intracellular, rather than extracellular, signaling disruption on immune TME composition across immune subtypes. Finally, a third cytokine subnetwork illustrates variation in T cell ligands and receptors across immune subtypes (Figure 7C). CD4 and CD8 receptors fell into two groups, those found in C2, C3, and C6 networks, such as *PDCD1*, and those absent in C3, such as *IL2RA* and *LAG3*. Some T cell-associated ligands were subtype specific, such as *CD276* (C2, C6), *IL1B* (C6), and *VEGFB* (C4).

The derived extracellular networks reflect the properties of immune subtypes in terms of cellular propensities and immune pathway activation noted earlier (Figures 1B, 1C, 2A, and S2A), but also place those properties in the context of possible interactions in the TME that may play a role in sculpting those same properties. The particular associations observed among IMs within distinct subtypes may be important for identifying directions for therapy.

We next used two complementary approaches, master regulators (MRs) and SYGNAL, to synthesize a pan-cancer transcriptional regulatory network describing the interactions linking genomic events to transcriptional regulators to downstream target genes, and finally to immune infiltration and patient survival. In both approaches, somatic alterations were used as anchors to infer regulatory relationships, in that they can act as a root cause of the “downstream” transcriptional changes mediated through transcription factors (TFs) and miRNAs.

This resulted in two transcriptional networks. The first one, MR-PanImmune, consisted of 26 MRs that acted as hubs associated with observed gene expression and LF, connected with 15 putative upstream driver events (Figure 7D). The second

(A) Immune subtype-specific extracellular communication network involving IFN- γ (*IFNG*, bottom of the diagram), whose expression is concordant with that of its cognate receptors *IFNGR1* and *IFNGR2* (bottom right and left, respectively), in C2 and C3 (yellow and green arrows, respectively); line thickness indicates strength of association). NK cells (left), which are known to secrete IFN- γ , could be producing IFN- γ in C2 and C3, as the NK cellular fraction is concordant with *IFNG* expression in both. *CXCR3* is known to be expressed on NK cells and has concordant levels, but only in C3 (green arrow). This is a subnetwork within a larger network constructed by similarly combining annotations of known interactions between ligands, receptors, and particular immune cells types, with evidence for concordance of those components.

(B) TGF- β subnetwork. Magenta: C6.

(C) T cell subnetwork.

(D) Master Regulator (MR)-Pan-Immune Network. The network diagram shows 26 MR “hubs” (filled orange) significantly associated with 15 upstream driver events (orange rings), along with proteins linking the two. The lineage factor *VAV1* (on left) is inferred to be a MR by combining predicted protein activity with data on gene expression, protein interactions, and somatic alterations. *VAV1* activity correlates with LF (degree of correlation depicted as degree of orange). Mutations in *HRAS* (center of network) are statistically associated with changes in LF. The *HRAS* and *VAV1* proteins are in close proximity on a large network of known protein-protein interactions (not shown), as both can lead to activation of protein MAP2K1, (as shown connecting with dotted lines). Mutations in *HRAS* are associated ($p < 0.05$) with *VAV1* activity, and their link through documented protein interactions implies that *HRAS* could directly modulate the activity of *VAV1*. In the diagram, the size of MR nodes represents their ranked activity. Smaller nodes with red borders represent mutated and/or copy-number altered genes statistically associated with one or more MR and LF, with the thickness of the border representing the number of associated MRs; small gray nodes are “linker” proteins.

(E) Regulators of immune subtypes from SYGNAL-PanImmune Network. Tumor types (octagons) linked through mutations (purple chevrons) to transcription factors (TFs, red triangles) and miRNAs (orange diamonds) that actively regulate the expression of IMs in biclusters associated with a single immune subtype (circles). The network describes predicted causal and mechanistic regulatory relationships linking tumor types through their somatic mutations (yellow edges) which causally modulate the activity of TFs and/or miRNAs (purple edges), which in turn regulate genes (not shown) whose expression is associated with an immune subtype (red edges). For example, *RB1* mutations in LIHC (5% of patients) have significant evidence for causally modulating the activity of *PRDM1* which in turn regulates genes associated (causal model at least 3 times as likely as alternative models and p value < 0.05) with C1 and C2. Interactions for this path are bolded.

one, SYGNAL-PanImmune, comprised 171 biclusters enriched in IMs and associated with LF.

Seven TFs were shared between the MR- and SYGNAL-PanImmune networks, a significant overlap ($p = 4.8 \times 10^{-10}$, Fisher's exact test): *PRDM1*, *SPI1*, *FLI1*, *IRF4*, *IRF8*, *STAT4*, and *STAT5A*. Additional MRs included the hematopoietic lineage specific factor *IKZF1*, which may reflect variation in immune cell content, and known IMs, such as *IFNG*, *IL16*, *CD86*, and *TNFRSF4*. The regulators in SYGNAL-PanImmune were inferred to regulate a total of 27 IM genes (Figure S7C). The top two most commonly co-regulated IMs from SYGNAL-PanImmune, *BTN3A1* and *BTN3A2*, are of particular interest as they modulate the activation of T cells (Cubillos-Ruiz et al., 2010) and have antibody-based immunotherapies (Benyamine et al., 2016; Legut et al., 2015).

Somatic alterations in *AKAP9*, *HRAS*, *KRAS*, and *PREX2* were inferred to modulate the activity of IMs according to both the MR- and SYGNAL-PanImmune, a significant overlap ($p = 1.6 \times 10^{-7}$, Fisher's exact test). In MR-PanImmune, *MAML1* and *HRAS* had the highest number of statistical interactions with 26 MRs. This analysis identified complex roles for the RAS-signaling pathway (Figure 7D) specifically through connections to lineage factor *VAV1* (implicated in multiple human cancers), potentially mediated by *MAP2K1*. Similarly, *MAML1*, hypothesized to mediate cross-talk across pathways in cancer (McElhinny et al., 2008), was associated ($p \leq 0.05$) with multiple MRs, including *STAT1*, *STAT4*, *CIITA*, *SPI1*, *TNFRSF4*, *CD86*, *VAV1*, *IKZF1*, and *IL16*.

In SYGNAL-PanImmune, some regulators of IMs, but not upstream somatic mutations, were shared between tumor types, including *STAT4*, which regulated *BTN3A1* and *BTN3A2* in both LUSC and UCEC, secondary to implied causal mutations *TP53* and *ARHGAP35*, respectively. Conversely, causal mutations shared across tumor types may associate with different tumor-specific downstream regulators. *TP53* was a causal mutation in UCEC acting through *IRF7* to regulate many of the same IMs as was seen in LUSC. These differences in causal relationships arise because the different cell types giving rise to each tumor type affect oncogenic paths.

We identified the putative regulators of immune gene expression within immune subtypes (Figure 7E). In these predictions, C1-associated biclusters were regulated by *ERG*, *KLF8*, *MAFB*, *STAT5A*, and *TEAD2*. C1 and C2 shared regulation by *BCL5B*, *ETV7*, *IRF1*, *IRF2*, *IRF4*, *PRDM1*, and *SPIB*, consistent with IFN- γ signaling predominance in these subtypes. C3 was regulated by *KLF15* and *miR-141-3p*. C6-associated biclusters were regulated by *NFKB2*. C1, C2, and C6 shared regulation by *STAT2* and *STAT4*, implying shared regulation by important immune TF families, such as STAT and IRF, but also differential employment of subunits and family members by the immune milieu.

In SYGNAL-PanImmune, the increased expression of biclusters enriched with IMs from KIRC, LGG, LUSC, and READ was associated with worse patient survival (CoxPH BH adjusted p value ≤ 0.05). Conversely, the increased expression of biclusters enriched with IMs from SKCM, containing *CCL5*, *CXCL9*, *CXCL10*, *HAVCR2*, *PRF1*, and MHC class II genes, were associated with improved patient survival (BH-adjusted $p \leq 0.05$).

DISCUSSION

We report an extensive evaluation of immunogenomic features in more than 10,000 tumors from 33 cancer types. Data and results are available as Supplemental Tables, at NCI GDC, and interactively at the CRI iAtlas portal, which is being configured to accept new immunogenomics datasets and feature calculations as they come available, including those derived from immunotherapy clinical trials, to develop as a "living resource" for the immunogenomics community. Meta-analysis of consensus expression clustering revealed immune subtypes spanning multiple tumor types and characterized by a dominance of either macrophage or lymphocyte signatures, T-helper phenotype, extent of intratumoral heterogeneity, and proliferative activity. All tumor samples were assessed for immune content by multiple methods. These include the estimation of immune cell fractions from deconvolution of gene expression and DNA methylation data, prediction of neoantigen-MHC pairs from mutations and HLA-typing, and evaluation of BCR and TCR repertoire from RNA-sequencing data. Immune content was compared among immune and cancer subtypes, and somatic alterations were identified that correlate with changes in the TME. Finally, predictions were made of regulatory networks that could influence the TME, and intracellular communication networks in the TME, based on integrating known interactions and observed associations. Immunogenomic features were predictive of outcome, with OS and PFI differing between immune subtypes both within and across cancer types.

C4 and C6 subtypes conferred the worst prognosis on their constituent tumors and displayed composite signatures reflecting a macrophage dominated, low lymphocytic infiltrate, with high M2 macrophage content, consistent with an immunosuppressed TME for which a poor outcome would be expected. In contrast, tumors included in the two subtypes displaying a type I immune response, C2 and C3, had the most favorable prognosis, consistent with studies suggesting a dominant type I immune response is needed for cancer control (Galon et al., 2013). In addition, C3 demonstrated the most pronounced Th17 signature, in agreement with a recent systematic review suggesting that Th17 expression is generally associated with improved cancer survival (Punt et al., 2015). C2 was IFN- γ dominant and showed a less favorable survival despite having the highest lymphocytic infiltrate, a CD8 T cell-associated signature, and highest M1 content, suggesting a robust anti-tumor immune response. One explanation for this discrepancy is the aggressiveness of both the tumor types and specific cases within C2 relative to C3. C2 showed the highest proliferation signature and ITH while C3 was the lowest in both those categories. It may be that the immune response simply could not control the rapid growth of tumors comprising C2. A second hypothesis is that tumors in C2 are those that have already been remodeled by the existing robust type I infiltrate and have escaped immune recognition. While signatures biased toward interferon-mediated viral sensing and antigen presentation genes were often associated with higher survival, interferon signatures without increased antigen presentation showed an opposite association. Loss of genes associated with antigen processing and presentation is often found in tumors that have been immune edited. In contrast to the potential immune

editing of C2, C3 may represent immunologic control of disease, that is, immune equilibrium.

Possible impact of somatic alterations on immune response was seen. For example, *KRAS* mutations were enriched in C1 and but infrequent in C5, suggesting that mutations in driver oncogenes alter pathways that affect immune cells. Driver mutations such as *TP53*, by inducing genomic instability, may alter the immune landscape via the generation of neoantigens. Our findings confirmed previous work showing that mutations in *BRAF* (Ilieva et al., 2014) enhance the immune infiltrate while those in *IDH1* diminish it (Amankulor et al., 2017). Further work is needed to determine the functional aspects of these associations.

Tumor-specific neoantigens are thought to be key targets of anti-tumor immunity and are associated with improved OS and response to immune checkpoint inhibition in multiple tumor types (Brown et al., 2014). We found OS correlated with pMHC number in only a limited number of tumors, with no clear association in most tumors, including several responsive to immune checkpoint inhibitor therapy. There are some caveats to this finding. The current predictors are highly sensitive but poorly specific for neoantigen identification, and our approach did not include neoantigens from introns or spliced variants. Moreover, it is not possible to fully determine the ability to process and present an epitope or the specific T cell repertoire in each tumor, which impacts the ability to generate a neoantigen response. It is also possible that the role of neoantigens may vary with tumor type, as supported by our per-tumor results.

Integrative methods predicted tumor-intrinsic and tumor-extrinsic regulation in, of, and by the TME and yielded information on specific modes of intracellular and extracellular control, the latter reflecting the network of cellular communication among immune cells in the TME. The resulting network was rich in structure, with mast cells, neutrophils, CD4 T cells, NK cells, B cells, eosinophils, macrophages, and CD8 T cells figuring prominently. The cellular communication network highlighted the role of key receptor and ligands such as *TGFB1*, *CXCL10*, and *CXCR3* and receptor-ligand pairs, such as the *CCL5-CCR5* axis, and illustrated how immune cell interactions may differ depending on the immune system context, manifested in the immune subtype.

Predicted intracellular networks implied that seven immune-related TFs (including interferon and STAT-family transcription factors) may play an active role in transcriptional events related to leukocyte infiltration, and that mutations in six genes (including Ras-family proteins) may influence immune infiltration. Across tumor types, the TFs and miRNAs regulating the expression of IMs tended to be shared, while somatic mutations modulating those regulatory factors tended to differ. This suggests that therapies targeting regulatory factors upstream of IMs should be considered and that they may have a broader impact across tumor types than therapies focusing on somatic mutations. Of note, in these approaches, it is not always possible to fully ascertain whether some particular interaction acts in the tumor, immune, or stromal cell compartments, but this could be improved on by incorporating additional cell-type-specific knowledge. Shared elements of intra- and extracellular network models should also be explored, with particular regard to the IMs and cytokines in both.

There are important caveats to using TCGA data. First, survival event rates and follow-up durations differ across the tumor types. Second, for most tumor types, samples with less than 60% tumor cell nuclei by pathologist review were excluded from study, thus potentially removing the most immune-infiltrated tumors from analysis. The degree to which this biases the results, relative to the general population of cancer patients, is difficult to ascertain. Our analyses were also limited by restriction to data from genome-wide molecular assays, in the absence of targeted classical cellular immunology assays for confirming cell phenotype distribution, as those types of data have not been collected from TCGA patients.

In summary, six stable and reproducible immune subtypes were found to encompass nearly all human malignancies. These subtypes were associated with prognosis, genetic, and immune modulatory alterations that may shape the specific types of immune environments we have observed. With our increasing understanding that the tumor immune environment plays an important role in prognosis as well as response to therapy, the definition of the immune subtype of a tumor may play a critical role in the predicting disease outcome as opposed to relying solely on features specific to individual cancer types.

STAR★METHODS

Detailed methods are provided in the online version of this paper and include the following:

- KEY RESOURCES TABLE
- CONTACT FOR REAGENT AND RESOURCE SHARING
- EXPERIMENTAL MODEL AND SUBJECT DETAILS
 - Human Subjects
 - Sample Inclusion Criteria
- METHOD DETAILS
 - Clinical and Molecular Data
 - Immune Subtype Identification
 - Leukocyte and Stromal Fractions
 - Immune Cellular Fraction Estimates
 - Prognostic Correlations of Immune Phenotypes
 - Copy Number and DNA Damage Scores
 - Genomic Correlations with Immune Phenotypes
 - Genetic Ancestry
 - Identification of Neoantigens
 - Genomic Viral Content Analysis
 - T- and B- Cell Receptor Analysis
 - Immunomodulator Identification and Analysis
 - The Cell-to-Cell Communication Network
 - Master Regulators of Immune Genes
 - SYstems Genetics Network Analysis
- QUANTIFICATION AND STATISTICAL ANALYSIS
- SOFTWARE AND DATA AVAILABILITY

SUPPLEMENTAL INFORMATION

Supplemental Information includes seven figures and six tables and can be found with this article online at <https://doi.org/10.1016/j.immuni.2018.03.023>.

ACKNOWLEDGMENTS

We are grateful to all the patients and families who contributed to this study. We also thank the Office of Cancer Genomics at the NCI for organizational and logistical support of this study. The high-throughput analyses in this study were performed on the Institute for Systems Biology-Cancer Genomics Cloud (ISB-CGC) under contract number HHSN261201400007C and on the Seven Bridges Cancer Genomics Cloud under contract HHSN261201400008C, with federal funds from the National Cancer Institute, NIH, Department of Health and Human Services. Funding from the Cancer Research Institute is gratefully acknowledged, as is support from NCI through U54 HG003273, U54 HG003067, U54 HG003079, U24 CA143799, U24 CA143835, U24 CA143840, U24 CA143843, U24 CA143845, U24 CA143848, U24 CA143858, U24 CA143866, U24 CA143867, U24 CA143882, U24 CA143883, U24 CA144025, and P30 CA016672. The study was supported by W81XWH-12-2-0050, HU0001-16-2-0004 from the US Department of Defense through the Henry M. Jackson Foundation for the Advancement of Military Medicine. We thank Peter Hammerman and Yasin Şenbabaoglu for contributions in early phases of this work.

AUTHOR CONTRIBUTIONS

Analysis, Computation, and Software: V.T., D.L.G., S.D.B., D.W., D.S.B., T.O.Y., E.P.-P., G.F.G., C.L.P., J.A.E., E.Z., A.C.C., E.O.P., I.K.A.S., A.J.G., R.M., F.F., A. Colaprico, J.S.P., L.E.M., N.S.V., J.L., Y.L., V.D., S.M.R., R.B., A.D.C., D.B., A.R., A.K., H.H., T.M.M., H.N., C.S.P., S.B., A.I.O., A.L., W.Z., J.G., J.S., B.G.V. Supervision: J.R., A. Califano, D.A., K.C., H.S., T.K.C., J.N.W., J.G., R.A.H., B.G.V., I.S. Writing: V.T., D.L.G., S.D.B., D.W., D.S.B., T.O.Y., E.P.-P., G.F.G., C.L.P., E.Z., A.C.C., E.O.P., I.K.A.S., A.J.G., R.M., F.F., A. Colaprico, N.S.V., H.H., T.M.M., H.N., J.S., C.E.R., A.J.L., J.S.S., E.G.D., M.L.D., B.G.V., I.S.

DECLARATION OF INTERESTS

Michael Seiler, Peter G. Smith, Ping Zhu, Silvia Buonamici, and Lihua Yu are employees of H3 Biomedicine, Inc. Parts of this work are the subject of a patent application: WO2017040526 titled "Splice variants associated with neomorphic sf3b1 mutants." Shouyoung Peng, Anant A. Agrawal, James Palacino, and Teng Teng are employees of H3 Biomedicine, Inc. Andrew D. Cherniack, Ashton C. Berger, and Galen F. Gao receive research support from Bayer Pharmaceuticals. Gordon B. Mills serves on the External Scientific Review Board of AstraZeneca. Anil Sood is on the Scientific Advisory Board for Kiyatec and is a shareholder in BioPath. Jonathan S. Serody receives funding from Merck, Inc. Kyle R. Covington is an employee of Castle Biosciences, Inc. Preethi H. Gunaratne is founder, CSO, and shareholder of NextmiRNA Therapeutics. Christina Yau is a part-time employee/consultant at NantOmics. Franz X. Schaub is an employee and shareholder of SEngine Precision Medicine, Inc. Carla Grandori is an employee, founder, and shareholder of SEngine Precision Medicine, Inc. Robert N. Eisenman is a member of the Scientific Advisory Boards and shareholder of Shenogen Pharma and Kronos Bio. Daniel J. Weisenberger is a consultant for Zymo Research Corporation. Joshua M. Stuart is the founder of Five3 Genomics and shareholder of NantOmics. Marc T. Goodman receives research support from Merck, Inc. Andrew J. Gentles is a consultant for Cibermed. Charles M. Perou is an equity stock holder, consultant, and Board of Directors member of BioClassifier and GeneCentric Diagnostics and is also listed as an inventor on patent applications on the Breast PAM50 and Lung Cancer Subtyping assays. Matthew Meyerson receives research support from Bayer Pharmaceuticals; is an equity holder in, consultant for, and Scientific Advisory Board chair for Origimed; and is an inventor of a patent for EGFR mutation diagnosis in lung cancer, licensed to LabCorp. Eduard Porta-Pardo is an inventor of a patent for domainXplorer. Han Liang is a shareholder and scientific advisor of Precision Scientific and Eagle Nebula. Da Yang is an inventor on a pending patent application describing the use of antisense oligonucleotides against specific lncRNA sequence as diagnostic and therapeutic tools. Yonghong Xiao was an employee and shareholder of TESARO, Inc. Bin Feng is an employee and shareholder of TESARO, Inc. Carter Van Waes received research funding for the study of IAP inhibitor ASTX660 through a Cooperative Agreement between NIDCD, NIH, and Astex

Pharmaceuticals. Raunaq Malhotra is an employee and shareholder of Seven Bridges, Inc. Peter W. Laird serves on the Scientific Advisory Board for AnchorDx. Joel Tepper is a consultant at EMD Serono. Kenneth Wang serves on the Advisory Board for Boston Scientific, Microtech, and Olympus. Andrea Califano is a founder, shareholder, and advisory board member of Darwin-Health, Inc. and a shareholder and advisory board member of Tempus, Inc. Toni K. Choueiri serves as needed on advisory boards for Bristol-Myers Squibb, Merck, and Roche. Lawrence Kwong receives research support from Array BioPharma. Sharon E. Plon is a member of the Scientific Advisory Board for Baylor Genetics Laboratory. Beth Y. Karlan serves on the Advisory Board of Invitae.

Received: July 21, 2017

Revised: January 23, 2018

Accepted: March 21, 2018

Published: April 5, 2018

REFERENCES

- Agarwal, V., Bell, G.W., Nam, J.W., and Bartel, D.P. (2015). Predicting effective microRNA target sites in mammalian mRNAs. *eLife* 4, <https://doi.org/10.7554/eLife.05005>.
- Alvarez, M.J., Shen, Y., Giorgi, F.M., Lachmann, A., Ding, B.B., Ye, B.H., and Califano, A. (2016). Functional characterization of somatic mutations in cancer using network-based inference of protein activity. *Nat. Genet.* 48, 838–847.
- Amankulor, N.M., Kim, Y., Arora, S., Kargl, J., Szulzewsky, F., Hanke, M., Margineantu, D.H., Rao, A., Bolouri, H., Delrow, J., et al. (2017). Mutant IDH1 regulates the tumor-associated immune system in gliomas. *Genes Dev.* 31, 774–786.
- Aten, J.E., Fuller, T.F., Lusic, A.J., and Horvath, S. (2008). Using genetic markers to orient the edges in quantitative trait networks: the NEO software. *BMC Syst. Biol.* 2, 34.
- Bailey, T.L., Boden, M., Buske, F.A., Frith, M., Grant, C.E., Clementi, L., Ren, J., Li, W.W., and Noble, W.S. (2009). MEME SUITE: tools for motif discovery and searching. *Nucleic Acids Res.* 37, W202–208.
- Bailey, P., Chang, D.K., Nones, K., Johns, A.L., Patch, A.M., Gingras, M.C., Miller, D.K., Christ, A.N., Bruxner, T.J., Quinn, M.C., et al. (2016). Genomic analyses identify molecular subtypes of pancreatic cancer. *Nature* 531, 47–52.
- Barbie, D.A., Tamayo, P., Boehm, J.S., Kim, S.Y., Moody, S.E., Dunn, I.F., Schinzel, A.C., Sandy, P., Meylan, E., Scholl, C., et al. (2009). Systematic RNA interference reveals that oncogenic KRAS-driven cancers require TBK1. *Nature* 462, 108–112.
- Beck, A.H., Espinosa, I., Edris, B., Li, R., Montgomery, K., Zhu, S., Varma, S., Marinelli, R.J., van de Rijn, M., and West, R.B. (2009). The macrophage colony-stimulating factor 1 response signature in breast carcinoma. *Clin. Cancer Res.* 15, 778–787.
- Bedognetti, D., Hendrickx, W., Ceccarelli, M., Miller, L.D., and Seliger, B. (2016). Disentangling the relationship between tumor genetic programs and immune responsiveness. *Curr. Opin. Immunol.* 39, 150–158.
- Benyamine, A., Le Roy, A., Mamessier, E., Gertner-Dardenne, J., Castanier, C., Orlanducci, F., Pouyet, L., Goubard, A., Collette, Y., Vey, N., et al. (2016). BTN3A molecules considerably improve Vgamma9Vdelta2T cells-based immunotherapy in acute myeloid leukemia. *Immunology* 5, e1146843.
- Bierie, B., and Moses, H.L. (2010). Transforming growth factor beta (TGF-beta) and inflammation in cancer. *Cytokine Growth Factor Rev.* 21, 49–59.
- Bindea, G., Mlecnik, B., Tosolini, M., Kirilovsky, A., Waldner, M., Obenaus, A.C., Angell, H., Fredriksen, T., Lafontaine, L., Berger, A., et al. (2013). Spatiotemporal dynamics of intratumoral immune cells reveal the immune landscape in human cancer. *Immunity* 39, 782–795.
- Bolotin, D.A., Shugay, M., Mamedov, I.Z., Putintseva, E.V., Turchaninova, M.A., Zvyagin, I.V., Britanova, O.V., and Chudakov, D.M. (2013). MITCR: software for T-cell receptor sequencing data analysis. *Nat. Methods* 10, 813–814.
- Bray, N.L., Pimentel, H., Melsted, P., and Pachter, L. (2016). Near-optimal probabilistic RNA-seq quantification. *Nat. Biotechnol.* 34, 525–527.

- Brown, S.D., Warren, R.L., Gibb, E.A., Martin, S.D., Spinelli, J.J., Nelson, B.H., and Holt, R.A. (2014). Neo-antigens predicted by tumor genome meta-analysis correlate with increased patient survival. *Genome Res.* **24**, 743–750.
- Brown, S.D., Raeburn, L.A., and Holt, R.A. (2015). Profiling tissue-resident T cell repertoires by RNA sequencing. *Genome Med.* **7**, 125.
- Calabro, A., Beissbarth, T., Kuner, R., Stojanov, M., Benner, A., Asslaber, M., Ploner, F., Zatloukal, K., Samonigg, H., Poustka, A., et al. (2009). Effects of infiltrating lymphocytes and estrogen receptor on gene expression and prognosis in breast cancer. *Breast Cancer Res. Treat.* **116**, 69–77.
- Carter, S.L., Cibulskis, K., Helman, E., McKenna, A., Shen, H., Zack, T., Laird, P.W., Onofrio, R.C., Winckler, W., Weir, B.A., et al. (2012). Absolute quantification of somatic DNA alterations in human cancer. *Nat. Biotechnol.* **30**, 413–421.
- Ceccarelli, M., Barthel, F.P., Malta, T.M., Sabedot, T.S., Salama, S.R., Murray, B.A., Morozova, O., Newton, Y., Radenbaugh, A., Pagnotta, S.M., et al. (2016). Molecular profiling reveals biologically discrete subsets and pathways of progression in diffuse glioma. *Cell* **164**, 550–563.
- Chang, H.Y., Sneddon, J.B., Alizadeh, A.A., Sood, R., West, R.B., Montgomery, K., Chi, J.T., van de Rijn, M., Botstein, D., and Brown, P.O. (2004). Gene expression signature of fibroblast serum response predicts human cancer progression: similarities between tumors and wounds. *PLoS Biol.* **2**, E7.
- Charoentong, P., Finotello, F., Angelova, M., Mayer, C., Efremova, M., Rieder, D., Hackl, H., and Trajanoski, Z. (2017). Pan-cancer immunogenomic analyses reveal genotype-immunophenotype relationships and predictors of response to checkpoint blockade. *Cell Rep.* **18**, 248–262.
- Chen, J.C., Alvarez, M.J., Talos, F., Dhruv, H., Rieckhof, G.E., Iyer, A., Diefes, K.L., Aldape, K., Berens, M., Shen, M.M., et al. (2014). Identification of causal genetic drivers of human disease through systems-level analysis of regulatory networks. *Cell* **159**, 402–414.
- Cheng, W.Y., Ou Yang, T.H., and Anastassiou, D. (2013a). Biomolecular events in cancer revealed by attractor metagenes. *PLoS Comput. Biol.* **9**, e1002920.
- Cheng, W.Y., Ou Yang, T.H., and Anastassiou, D. (2013b). Development of a prognostic model for breast cancer survival in an open challenge environment. *Sci. Transl. Med.* **5**, 181ra150.
- Chu, J., Sadeghi, S., Raymond, A., Jackman, S.D., Nip, K.M., Mar, R., Mohamadi, H., Butterfield, Y.S., Robertson, A.G., and Birol, I. (2014). BioBloom tools: fast, accurate and memory-efficient host species sequence screening using bloom filters. *Bioinformatics* **30**, 3402–3404.
- Colaprico, A., Silva, T.C., Olsen, C., Garofano, L., Cava, C., Garolini, D., Sabedot, T.S., Malta, T.M., Pagnotta, S.M., Castiglioni, I., et al. (2016). TCGAAbioblinks: an R/Bioconductor package for integrative analysis of TCGA data. *Nucleic Acids Res.* **44**, e71.
- Cubillos-Ruiz, J.R., Martinez, D., Scarlett, U.K., Rutkowski, M.R., Nesbeth, Y.C., Composeco-Jacobs, A.L., and Conejo-Garcia, J.R. (2010). CD277 is a negative co-stimulatory molecule universally expressed by ovarian cancer microenvironmental cells. *Oncotarget* **1**, 329–338.
- Dobin, A., Davis, C.A., Schlesinger, F., Drenkow, J., Zaleski, C., Jha, S., Batut, P., Chaisson, M., and Gingeras, T.R. (2013). STAR: ultrafast universal RNA-seq aligner. *Bioinformatics* **29**, 15–21.
- Drake, J.M., Paull, E.O., Graham, N.A., Lee, J.K., Smith, B.A., Titz, B., Stoyanova, T., Faltermeier, C.M., Uzunangelov, V., Carlin, D.E., et al. (2016). Phosphoproteome integration reveals patient-specific networks in prostate cancer. *Cell* **166**, 1041–1054.
- Ellrott, K., Bailey, M.H., Saksena, G., Covington, K.R., Kandath, C., Stewart, C., Hess, J., Ma, S., McLellan, M., Sofia, H.J., et al. (2018). Scalable open science approach for mutation calling of tumor exomes using multiple genomic pipelines. *Cell Syst.* **6**, <https://doi.org/10.1016/j.cels.2018.03.002>.
- Friedman, J., Hastie, T., and Tibshirani, R. (2010). Regularization paths for generalized linear models via coordinate descent. *J. Stat. Softw.* **33**, 1–22.
- Galon, J., Angell, H.K., Bedognetti, D., and Marincola, F.M. (2013). The continuum of cancer immunosurveillance: prognostic, predictive, and mechanistic signatures. *Immunity* **39**, 11–26.
- Gentles, A.J., Newman, A.M., Liu, C.L., Bratman, S.V., Feng, W., Kim, D., Nair, V.S., Xu, Y., Khuong, A., Hoang, C.D., et al. (2015). The prognostic landscape of genes and infiltrating immune cells across human cancers. *Nat. Med.* **21**, 938–945.
- Godec, J., Tan, Y., Liberzon, A., Tamayo, P., Bhattacharya, S., Butte, A.J., Mesirov, J.P., and Haining, W.N. (2016). Compendium of immune signatures identifies conserved and species-specific biology in response to inflammation. *Immunity* **44**, 194–206.
- Gusenleitner, D., Howe, E.A., Bentink, S., Quackenbush, J., and Culhane, A.C. (2012). iBBiG: iterative binary bi-clustering of gene sets. *Bioinformatics* **28**, 2484–2492.
- Hanahan, D., and Weinberg, R.A. (2011). Hallmarks of cancer: the next generation. *Cell* **144**, 646–674.
- Hänzelmann, S., Castelo, R., and Guinney, J. (2013). GSEA: gene set variation analysis for microarray and RNA-seq data. *BMC Bioinformatics* **14**, 7.
- Harrow, J., Frankish, A., Gonzalez, J.M., Tapanari, E., Diekhans, M., Kokocinski, F., Aken, B.L., Barrell, D., Zadissa, A., Searle, S., et al. (2012). GENCODE: the reference human genome annotation for The ENCODE Project. *Genome Res.* **22**, 1760–1774.
- Hendrickx, W., Simeone, I., Anjum, S., Mokrab, Y., Bertucci, F., Finetti, P., Curigliano, G., Seliger, B., Cerulo, L., Tomei, S., et al. (2017). Identification of genetic determinants of breast cancer immune phenotypes by integrative genome-scale analysis. *Oncology* **6**, e1253654.
- Hornik, K. (2005). A CLUE for CLUSTER ensembles. *J. Stat. Softw.* **14**, 1–25.
- Hugo, W., Zaretsky, J.M., Sun, L., Song, C., Moreno, B.H., Hu-Lieskovan, S., Berent-Maoz, B., Pang, J., Chmielowski, B., Cherry, G., et al. (2016). Genomic and transcriptomic features of response to anti-PD-1 therapy in metastatic melanoma. *Cell* **165**, 35–44.
- Hundal, J., Carreno, B.M., Petti, A.A., Linette, G.P., Griffith, O.L., Mardis, E.R., and Griffith, M. (2016). pVAC-Seq: A genome-guided in silico approach to identifying tumor neoantigens. *Genome Med.* **8**, 11.
- Iglesia, M.D., Parker, J.S., Hoadley, K.A., Serody, J.S., Perou, C.M., and Vincent, B.G. (2016). Genomic analysis of immune cell infiltrates across 11 tumor types. *J. Natl. Cancer Inst.* **108**, <https://doi.org/10.1093/jnci/djw144>.
- Ilieva, K.M., Correa, I., Josephs, D.H., Karagiannis, P., Egbuniwe, I.U., Cafferkey, M.J., Spicer, J.F., Harries, M., Nestle, F.O., Lacy, K.E., et al. (2014). Effects of BRAF mutations and BRAF inhibition on immune responses to melanoma. *Mol. Cancer Ther.* **13**, 2769–2783.
- Kertesz, M., Iovino, N., Unnerstall, U., Gaul, U., and Segal, E. (2007). The role of site accessibility in microRNA target recognition. *Nat. Genet.* **39**, 1278–1284.
- Khurana, E., Fu, Y., Chen, J., and Gerstein, M. (2013). Interpretation of genomic variants using a unified biological network approach. *PLoS Comput. Biol.* **9**, e1002886.
- Knijnenburg, T., Wang, L., Zimmermann, M., Chambwe, N., Gao, G., Cherniack, A., Fan, H., Shen, H., Way, G., Greene, C., et al. (2018). Genomic and molecular landscape of DNA damage repair deficiency across The Cancer Genome Atlas. *Cell Rep.* **23**, <https://doi.org/10.1016/j.celrep.2018.03.076>.
- Langfelder, P., and Horvath, S. (2007). Eigengene networks for studying the relationships between co-expression modules. *BMC Syst. Biol.* **1**, 54.
- Langfelder, P., and Horvath, S. (2008). WGCNA: an R package for weighted correlation network analysis. *BMC Bioinformatics* **9**, 559.
- Lefranc, M.P., Giudicelli, V., Ginestoux, C., Jabado-Michaloud, J., Folch, G., Bellahcene, F., Wu, Y., Gemrot, E., Brochet, X., Lane, J., et al. (2009). IMGT, the international ImMunoGeneTics information system. *Nucleic Acids Res.* **37**, D1006–D1012.
- Legut, M., Cole, D.K., and Sewell, A.K. (2015). The promise of gammadelta T cells and the gammadelta T cell receptor for cancer immunotherapy. *Cell. Mol. Immunol.* **12**, 656–668.
- Li, B., and Dewey, C.N. (2011). RSEM: accurate transcript quantification from RNA-Seq data with or without a reference genome. *BMC Bioinformatics* **12**, 323.
- Li, H., and Durbin, R. (2009). Fast and accurate short read alignment with Burrows-Wheeler transform. *Bioinformatics* **25**, 1754–1760.

- Li, M.X., Yeung, J.M., Cherny, S.S., and Sham, P.C. (2012). Evaluating the effective numbers of independent tests and significant p-value thresholds in commercial genotyping arrays and public imputation reference datasets. *Hum. Genet.* *131*, 747–756.
- Li, B., Severson, E., Pignon, J.C., Zhao, H., Li, T., Novak, J., Jiang, P., Shen, H., Aster, J.C., Rodig, S., et al. (2016). Comprehensive analyses of tumor immunity: implications for cancer immunotherapy. *Genome Biol.* *17*, 174.
- Liang, Y., Pan, H.F., and Ye, D.Q. (2015). microRNAs function in CD8+T cell biology. *J. Leukoc. Biol.* *97*, 487–497.
- Liu, J., Lichtenberg, T., Hoadley, K.A., Poisson, L.M., Lazar, A.J., Cherniack, A.D., Kovatich, A.J., Benz, C.C., Levine, D.A., Lee, A.V., et al. (2018). An Integrated TCGA Pan-Cancer Clinical Data Resource to drive high quality survival outcome analytics. *Cell* *173*, <https://doi.org/10.1016/j.cell.2018.02.052>.
- Mantovani, A., Sica, A., and Locati, M. (2005). Macrophage polarization comes of age. *Immunity* *23*, 344–346.
- Margolin, A.A., Nemenman, I., Basso, K., Wiggins, C., Stolovitzky, G., Dalla Favera, R., and Califano, A. (2006). ARACNE: an algorithm for the reconstruction of gene regulatory networks in a mammalian cellular context. *BMC Bioinformatics* *7* (Suppl 1), S7.
- McCarthy, S., Das, S., Kretschmar, W., Delaneau, O., Wood, A.R., Teumer, A., Kang, H.M., Fuchsberger, C., Danecek, P., Sharp, K., et al. (2016). A reference panel of 64,976 haplotypes for genotype imputation. *Nat. Genet.* *48*, 1279–1283.
- McElhinny, A.S., Li, J.L., and Wu, L. (2008). Mastermind-like transcriptional co-activators: emerging roles in regulating cross talk among multiple signaling pathways. *Oncogene* *27*, 5138–5147.
- McGranahan, N., Furness, A.J., Rosenthal, R., Ramskov, S., Lyngaa, R., Saini, S.K., Jamal-Hanjani, M., Wilson, G.A., Birkbak, N.J., Hiley, C.T., et al. (2016). Clonal neoantigens elicit T cell immunoreactivity and sensitivity to immune checkpoint blockade. *Science* *351*, 1463–1469.
- McLaren, W., Gil, L., Hunt, S.E., Riat, H.S., Ritchie, G.R., Thormann, A., Flicek, P., and Cunningham, F. (2016). The Ensembl Variant Effect Predictor. *Genome Biol.* *17*, 122.
- Mermel, C.H., Schumacher, S.E., Hill, B., Meyerson, M.L., Beroukhi, R., and Getz, G. (2011). GISTIC2.0 facilitates sensitive and confident localization of the targets of focal somatic copy-number alteration in human cancers. *Genome Biol.* *12*, R41.
- Miao, D., Margolis, C.A., Gao, W., Voss, M.H., Li, W., Martini, D.J., Norton, C., Bosse, D., Wankowicz, S.M., Cullen, D., et al. (2018). Genomic correlates of response to immune checkpoint therapies in clear cell renal cell carcinoma. *Science* *359*, 801–806.
- Morris, L.G., Riaz, N., Desrichard, A., Senbabaoglu, Y., Hakimi, A.A., Makarov, V., Reis-Filho, J.S., and Chan, T.A. (2016). Pan-cancer analysis of intratumor heterogeneity as a prognostic determinant of survival. *Oncotarget* *7*, 10051–10063.
- Mose, L.E., Selitsky, S.R., Bixby, L.M., Marron, D.L., Iglesia, M.D., Serody, J.S., Perou, C.M., Vincent, B.G., and Parker, J.S. (2016). Assembly-based inference of B-cell receptor repertoires from short read RNA sequencing data with VDJer. *Bioinformatics* *32*, 3729–3734.
- Newman, A.M., Liu, C.L., Green, M.R., Gentles, A.J., Feng, W., Xu, Y., Hoang, C.D., Diehn, M., and Alizadeh, A.A. (2015). Robust enumeration of cell subsets from tissue expression profiles. *Nat. Methods* *12*, 453–457.
- Nielsen, M., and Andreatta, M. (2016). NetMHCpan-3.0; improved prediction of binding to MHC class I molecules integrating information from multiple receptor and peptide length datasets. *Genome Med.* *8*, 33.
- Paull, E.O., Carlin, D.E., Niepel, M., Sorger, P.K., Haussler, D., and Stuart, J.M. (2013). Discovering causal pathways linking genomic events to transcriptional states using Tied Diffusion Through Interacting Events (TieDIE). *Bioinformatics* *29*, 2757–2764.
- Pavesi, G., and Pesole, G. (2006). Using Weeder for the discovery of conserved transcription factor binding sites. *Curr Protoc Bioinformatics Chapter 2*. Unit 2 11.
- Pencina, M.J., and D'Agostino, R.B. (2004). Overall C as a measure of discrimination in survival analysis: model specific population value and confidence interval estimation. *Stat. Med.* *23*, 2109–2123.
- Plaisier, C.L., Horvath, S., Huertas-Vazquez, A., Cruz-Bautista, I., Herrera, M.F., Tusie-Luna, T., Aguilar-Salinas, C., and Pajukanta, P. (2009). A systems genetics approach implicates USF1, FADS3, and other causal candidate genes for familial combined hyperlipidemia. *PLoS Genet.* *5*, e1000642.
- Plaisier, C.L., Pan, M., and Baliga, N.S. (2012). A miRNA-regulatory network explains how dysregulated miRNAs perturb oncogenic processes across diverse cancers. *Genome Res.* *22*, 2302–2314.
- Plaisier, C.L., O'Brien, S., Bernard, B., Reynolds, S., Simon, Z., Toledo, C.M., Ding, Y., Reiss, D.J., Paddison, P.J., and Baliga, N.S. (2016). Causal mechanistic regulatory network for glioblastoma deciphered using systems genetics network analysis. *Cell Syst.* *3*, 172–186.
- Porta-Pardo, E., and Godzik, A. (2016). Mutation drivers of immunological responses to cancer. *Cancer Immunol. Res.* *4*, 789–798.
- Price, A.L., Patterson, N.J., Plenge, R.M., Weinblatt, M.E., Shadick, N.A., and Reich, D. (2006). Principal components analysis corrects for stratification in genome-wide association studies. *Nat. Genet.* *38*, 904–909.
- Punt, S., Langenhoff, J.M., Putter, H., Fleuren, G.J., Gorter, A., and Jordanova, E.S. (2015). The correlations between IL-17 vs. Th17 cells and cancer patient survival: a systematic review. *Oncolimmunology* *4*, e984547.
- Ramilowski, J.A., Goldberg, T., Harshbarger, J., Kloppmann, E., Lizio, M., Satagopam, V.P., Itoh, M., Kawaji, H., Carninci, P., Rost, B., et al. (2015). A draft network of ligand-receptor-mediated multicellular signalling in human. *Nat. Commun.* *6*, 7866.
- Reiss, D.J., Plaisier, C.L., Wu, W.J., and Baliga, N.S. (2015). cMonkey2: Automated, systematic, integrated detection of co-regulated gene modules for any organism. *Nucleic Acids Res.* *43*, e87.
- Rooney, M.S., Shukla, S.A., Wu, C.J., Getz, G., and Hacohen, N. (2015). Molecular and genetic properties of tumors associated with local immune cytolytic activity. *Cell* *160*, 48–61.
- Saltz, J.H., Gupta, R., Hou, L., Kurc, T., Singh, P., Nguyen, V., Samarasinghe, D., Shroyer, K.R., Zhao, T., Batiste, R., et al. (2018). Spatial organization and molecular correlation of tumor infiltrating lymphocytes using deep learning on pathology images. *Cell Rep.* *23*, <https://doi.org/10.1016/j.celrep.2018.03.086>.
- Sanchez-Vega, F., Mina, M., Armenia, J., Chatila, W.K., Luna, A., La, K., Dimitriadou, S., Liu, D.L., Kantheti, H.S., Saghafein, S., et al. (2018). Oncogenic signaling pathways in The Cancer Genome Atlas. *Cell* *173*.
- Scrucca, L., Fop, M., Murphy, T.B., and Raftery, A.E. (2016). mclust 5: clustering, classification and density estimation using Gaussian finite mixture models. *R J.* *8*, 289–317.
- Senbabaoglu, Y., Gejman, R.S., Winer, A.G., Liu, M., Van Allen, E.M., de Velasco, G., Miao, D., Ostrovskaya, I., Drill, E., Luna, A., et al. (2016). Tumor immune microenvironment characterization in clear cell renal cell carcinoma identifies prognostic and immunotherapeutically relevant messenger RNA signatures. *Genome Biol.* *17*, 231.
- Shukla, S.A., Rooney, M.S., Rajasagi, M., Tiao, G., Dixon, P.M., Lawrence, M.S., Stevens, J., Lane, W.J., Dellagatta, J.L., Steelman, S., et al. (2015). Comprehensive analysis of cancer-associated somatic mutations in class I HLA genes. *Nat. Biotechnol.* *33*, 1152–1158.
- Silva, T.C., Colaprico, A., Olsen, C., D'Angelo, F., Bontempi, G., Ceccarelli, M., and Noshmeh, H. (2016). TCGA Workflow: Analyze cancer genomics and epigenomics data using Bioconductor packages. *F1000Res.* *5*, 1542.
- Siragusa, E., Weese, D., and Reinert, K. (2013). Fast and accurate read mapping with approximate seeds and multiple backtracking. *Nucleic Acids Res.* *41*, e78.
- Subramanian, A., Tamayo, P., Mootha, V.K., Mukherjee, S., Ebert, B.L., Gillette, M.A., Paulovich, A., Pomeroy, S.L., Golub, T.R., Lander, E.S., and Mesirov, J.P. (2005). Gene set enrichment analysis: a knowledge-based approach for interpreting genome-wide expression profiles. *Proc. Natl. Acad. Sci. USA* *102*, 15545–15550.

- Szolek, A., Schubert, B., Mohr, C., Sturm, M., Feldhahn, M., and Kohlbacher, O. (2014). OptiType: precision HLA typing from next-generation sequencing data. *Bioinformatics* *30*, 3310–3316.
- Tang, J., Shalabi, A., and Hubbard-Lucey, V.M. (2018). Comprehensive analysis of the clinical immuno-oncology landscape. *Ann. Oncol.* *29*, 84–91.
- Tatlow, P.J., and Piccolo, S.R. (2016). A cloud-based workflow to quantify transcript-expression levels in public cancer compendia. *Sci. Rep.* *6*, 39259.
- Taylor, A.M., Shih, J., Ha, G., Gao, G.F., Zhang, X., Berger, A.C., Schumacher, S.E., Wang, C., Hu, H., Liu, J., et al. (2018). Genomic and functional approaches to understanding cancer aneuploidy. *Cancer Cell* *33*, <https://doi.org/10.1016/j.ccell.2018.03.007>.
- Teschendorff, A.E., Gomez, S., Arenas, A., El-Ashry, D., Schmidt, M., Gehrman, M., and Caldas, C. (2010). Improved prognostic classification of breast cancer defined by antagonistic activation patterns of immune response pathway modules. *BMC Cancer* *10*, 604.
- The Cancer Genome Atlas Network (2015). Genomic classification of cutaneous melanoma. *Cell* *161*, 1681–1696.
- The Cancer Genome Atlas Research Network (2011). Integrated genomic analyses of ovarian carcinoma. *Nature* *474*, 609–615.
- Tibshirani, R., and Walther, G. (2005). Cluster validation by prediction strength. *J. Comput. Graph. Stat.* *14*, 511–528.
- Venteicher, A.S., Tirosh, I., Hebert, C., Yizhak, K., Neftel, C., Filbin, M.G., Hovestadt, V., Escalante, L.E., Shaw, M.L., Rodman, C., et al. (2017). Decoupling genetics, lineages, and microenvironment in IDH-mutant gliomas by single-cell RNA-seq. *Science* *355*, <https://doi.org/10.1126/science.aai8478>.
- Wingender, E., Schoeps, T., and Donitz, J. (2013). TFClass: an expandable hierarchical classification of human transcription factors. *Nucleic Acids Res.* *41*, D165–D170.
- Wolf, D.M., Lenburg, M.E., Yau, C., Boudreau, A., and van 't Veer, L.J. (2014). Gene co-expression modules as clinically relevant hallmarks of breast cancer diversity. *PLoS ONE* *9*, e88309.
- Zack, T.I., Schumacher, S.E., Carter, S.L., Cherniack, A.D., Saksena, G., Tabak, B., Lawrence, M.S., Zhsng, C.Z., Wala, J., Mermel, C.H., et al. (2013). Pan-cancer patterns of somatic copy number alteration. *Nat. Genet.* *45*, 1134–1140.
- Zhang, Q.C., Petrey, D., Deng, L., Qiang, L., Shi, Y., Thu, C.A., Bisikirska, B., Lefebvre, C., Accili, D., Hunter, T., et al. (2012). Structure-based prediction of protein-protein interactions on a genome-wide scale. *Nature* *490*, 556–560.

INSIGHTS DRIVE DRUG DISCOVERY

Are you keeping pace with peer-reviewed research that will affect the future of therapeutics? Are you up to speed on the latest trends, delivery mechanisms, and policies?



Research Arc is a new multi-faceted, multi-format resource for R&D professionals that draws on the vast collection of top-tier life science review journals published by Cell Press. It's the perfect companion for anyone in the biopharmaceutical community looking for targeted scientific insights that mirror the trajectory of drug development.

It's curated by experts and presented in a highly visual format that is easy to scan and digest. Access to new Research Arc content is unrestricted for the first 60 days. To stay up to date, all you have to do is register. What are you waiting for?

cell.com/research-arc



2.0

Listened. Learned.

Introducing Sneak Peek 2.0

We heard you. Now it's even easier to preview Cell Press papers under review. Improved search? Done. Want to read the abstract without having to register? No problem. See a paper you want to cite? Go for it.

**Go on, satisfy your curiosity.
Check out Sneak Peek 2.0 today!
Visit www.cell.com/sneakpeek**

CellPress

Sneak Peek

A PREVIEW OF PAPERS UNDER REVIEW

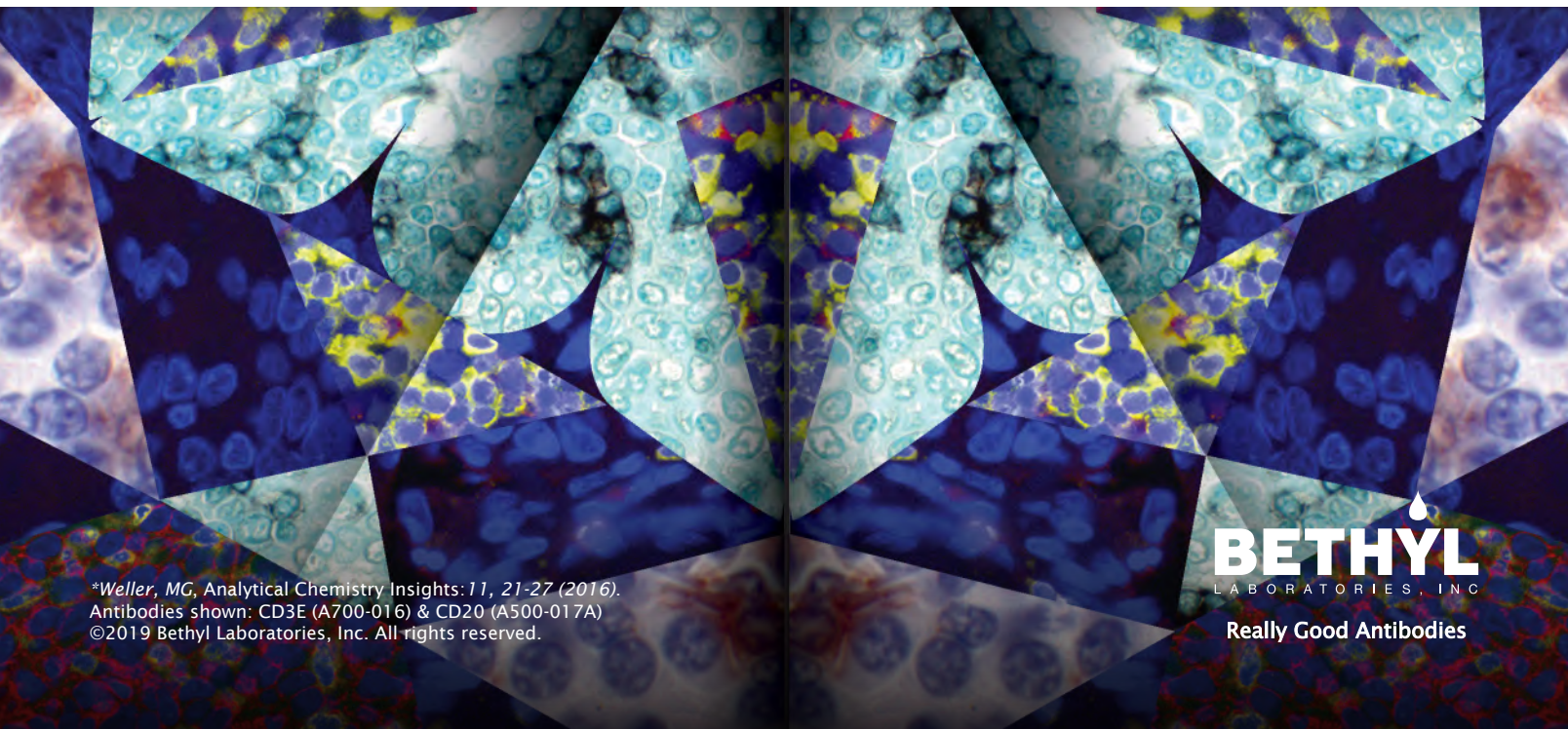


Radiant reproducibility

Get results you can rely on with antibodies that
are 100% guaranteed to work

The best discoveries take determination, dedication and reliable antibody tools. Yet, nearly 50% of all antibodies fail.* Backed by more than 45 years of experience in manufacturing and validation, you can trust every antibody from Bethyl. From catalog and custom polyclonal and recombinant rabbit monoclonal antibodies, to ELISA kits and sets, we have the solutions you need to take it to the next level. Work with Bethyl to bring your discovery into full focus.

See our data at [bethyl.com/breakthrough](https://www.bethyl.com/breakthrough)



*Weller, MG, Analytical Chemistry Insights: 11, 21-27 (2016).
Antibodies shown: CD3E (A700-016) & CD20 (A500-017A)
©2019 Bethyl Laboratories, Inc. All rights reserved.

BETHYL
LABORATORIES, INC

Really Good Antibodies

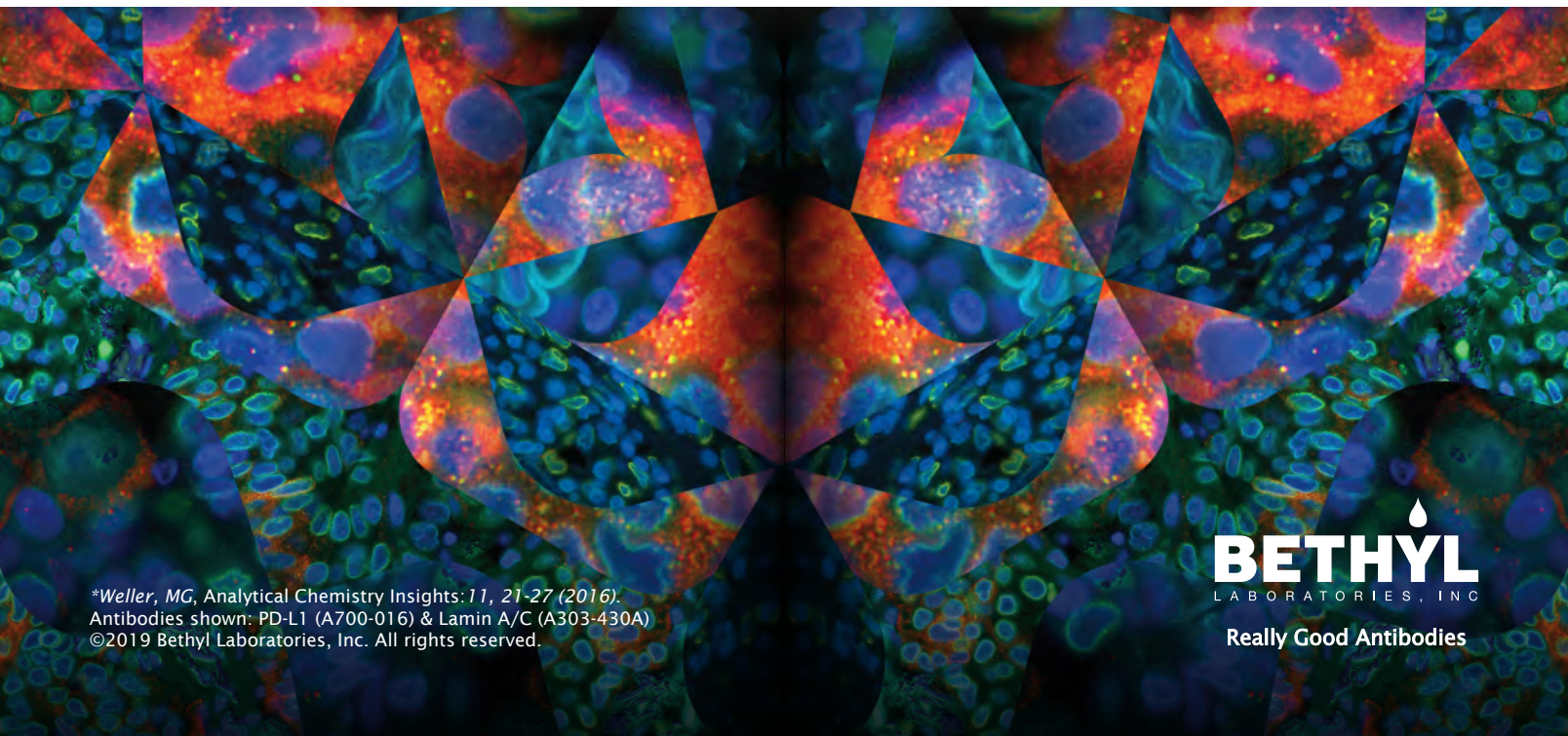


Brilliant visualization

See the difference to make big breakthroughs
in your tumor microenvironment research

In the world of next generation immuno-oncology research, having confidence in your immunoassay results is vital. Unfortunately, 75% of antibodies in today's market are non-specific or simply do not work at all.* That's why at Bethyl, we manufacture and validate every antibody on-site to ensure target specificity and sensitivity. More than 10,000 independent citations over the past 15 years have proven that our antibodies will function as designed in your assay — and we offer a 100% guarantee. Work with Bethyl to bring your discovery into full focus.

See our data at bethyl.com/immuno-oncology



*Weller, MG, Analytical Chemistry Insights: 11, 21-27 (2016).
Antibodies shown: PD-L1 (A700-016) & Lamin A/C (A303-430A)
©2019 Bethyl Laboratories, Inc. All rights reserved.

**BETHYL**
LABORATORIES, INC

Really Good Antibodies